

Identification of immunotherapy-related biomarkers for gynecological cancers

Edited by

Jinhui Liu, Shaohua Xu and Jianguang Ji

Published in

Frontiers in Oncology



FRONTIERS EBOOK COPYRIGHT STATEMENT

The copyright in the text of individual articles in this ebook is the property of their respective authors or their respective institutions or funders. The copyright in graphics and images within each article may be subject to copyright of other parties. In both cases this is subject to a license granted to Frontiers.

The compilation of articles constituting this ebook is the property of Frontiers.

Each article within this ebook, and the ebook itself, are published under the most recent version of the Creative Commons CC-BY licence. The version current at the date of publication of this ebook is CC-BY 4.0. If the CC-BY licence is updated, the licence granted by Frontiers is automatically updated to the new version.

When exercising any right under the CC-BY licence, Frontiers must be attributed as the original publisher of the article or ebook, as applicable.

Authors have the responsibility of ensuring that any graphics or other materials which are the property of others may be included in the CC-BY licence, but this should be checked before relying on the CC-BY licence to reproduce those materials. Any copyright notices relating to those materials must be complied with.

Copyright and source acknowledgement notices may not be removed and must be displayed in any copy, derivative work or partial copy which includes the elements in question.

All copyright, and all rights therein, are protected by national and international copyright laws. The above represents a summary only. For further information please read Frontiers' Conditions for Website Use and Copyright Statement, and the applicable CC-BY licence.

ISSN 1664-8714
ISBN 978-2-83251-733-8
DOI 10.3389/978-2-83251-733-8

About Frontiers

Frontiers is more than just an open access publisher of scholarly articles: it is a pioneering approach to the world of academia, radically improving the way scholarly research is managed. The grand vision of Frontiers is a world where all people have an equal opportunity to seek, share and generate knowledge. Frontiers provides immediate and permanent online open access to all its publications, but this alone is not enough to realize our grand goals.

Frontiers journal series

The Frontiers journal series is a multi-tier and interdisciplinary set of open-access, online journals, promising a paradigm shift from the current review, selection and dissemination processes in academic publishing. All Frontiers journals are driven by researchers for researchers; therefore, they constitute a service to the scholarly community. At the same time, the *Frontiers journal series* operates on a revolutionary invention, the tiered publishing system, initially addressing specific communities of scholars, and gradually climbing up to broader public understanding, thus serving the interests of the lay society, too.

Dedication to quality

Each Frontiers article is a landmark of the highest quality, thanks to genuinely collaborative interactions between authors and review editors, who include some of the world's best academicians. Research must be certified by peers before entering a stream of knowledge that may eventually reach the public - and shape society; therefore, Frontiers only applies the most rigorous and unbiased reviews. Frontiers revolutionizes research publishing by freely delivering the most outstanding research, evaluated with no bias from both the academic and social point of view. By applying the most advanced information technologies, Frontiers is catapulting scholarly publishing into a new generation.

What are Frontiers Research Topics?

Frontiers Research Topics are very popular trademarks of the *Frontiers journals series*: they are collections of at least ten articles, all centered on a particular subject. With their unique mix of varied contributions from Original Research to Review Articles, Frontiers Research Topics unify the most influential researchers, the latest key findings and historical advances in a hot research area.

Find out more on how to host your own Frontiers Research Topic or contribute to one as an author by contacting the Frontiers editorial office: frontiersin.org/about/contact

Identification of immunotherapy-related biomarkers for gynecological cancers

Topic editors

Jinhui Liu — Nanjing Medical University, China

Shaohua Xu — Tongji University, China

Jianguang Ji — Lund University, Sweden

Citation

Liu, J., Xu, S., Ji, J., eds. (2023). *Identification of immunotherapy-related biomarkers for gynecological cancers*. Lausanne: Frontiers Media SA.
doi: 10.3389/978-2-83251-733-8

Table of contents

- 05 **Inflammation-Related LncRNAs Signature for Prognosis and Immune Response Evaluation in Uterine Corpus Endometrial Carcinoma**
Hongmei Gu, Jiahang Song, Yizhang Chen, Yichun Wang, Xiaofang Tan and Hongyu Zhao
- 22 **Advances in the Application of Radionuclide-Labeled HER2 Affibody for the Diagnosis and Treatment of Ovarian Cancer**
Xianwen Hu, Dandan Li, Yujie Fu, Jiashen Zheng, Zelong Feng, Jiong Cai and Pan Wang
- 35 **Controversial Role of the Immune Checkpoint OX40L Expression on Platelets in Breast Cancer Progression**
Susanne M. Rittig, Martina S. Lutz, Kim L. Clar, Yanjun Zhou, Korbinian N. Kropp, André Koch, Andreas D. Hartkopf, Martina Hinterleitner, Lars Zender, Helmut R. Salih, Stefanie Maurer and Clemens Hinterleitner
- 45 **The IFN- γ -related long non-coding RNA signature predicts prognosis and indicates immune microenvironment infiltration in uterine corpus endometrial carcinoma**
Chunyan Gu, Chen Lin, Zheng Zhu, Li Hu, Fengxu Wang, Xuehai Wang, Junpu Ruan, Xinyuan Zhao and Sen Huang
- 60 **Estradiol mediates the interaction of LINC01541 and miR-429 to promote angiogenesis of G1/G2 endometrioid adenocarcinoma *in-vitro*: A pilot study**
Dan Qiao, Xiaoduo Qin, Haiyan Yang, Xuanton Liu, Libing Liu, Sufen Liu and Zhongzhi Jia
- 72 **Molecular subtypes, clinical significance, and tumor immune landscape of angiogenesis-related genes in ovarian cancer**
Haixia Tang, Jingsong Shan, Juan Liu, Xuehai Wang, Fengxu Wang, Suping Han, Xinyuan Zhao and Jinxiu Wang
- 88 **Single cell sequencing analysis and transcriptome analysis constructed the liquid-liquid phase separation(LLPS)-related prognostic model for endometrial cancer**
Jiayang Wang, Fei Meng and Fei Mao
- 100 **Identification and validation of a novel necroptosis-related prognostic signature in cervical squamous cell carcinoma and endocervical adenocarcinoma**
Weiyu Zhang, Wujun Cao, Zhuting Tong, Qinqin Jin, Xiya Jiang, Yinting Yang, Hui Yao, Guo Chen, Wei Gao, Yuting Zhu and Shuguang Zhou
- 117 **Reclassification of endometrial cancer and identification of key genes based on neural-related genes**
Fan Chen, Tiansheng Qin, Yigan Zhang, Linzhen Wei, Yamei Dang, Peixia Liu and Weilin Jin

- 137 **Identification of bromodomain-containing proteins prognostic value and expression significance based on a genomic landscape analysis of ovarian serous cystadenocarcinoma**
Juan Zhang, Yan Li, Ting-yu Fan, Dan Liu, Wen-da Zou, Hui Li and Yu-kun Li
- 157 **High rate of epidermal growth factor receptor-mutated primary lung cancer in patients with primary breast cancer**
Tianyu Zeng, Hai Xu, Yincheng Liu, Chunxiao Sun, Fan Yang, Yan Liang, Xiang Huang, Ziyi Fu, Wei Li and Yongmei Yin
- 166 **Identification of CD8+ T cell infiltration-related genes and their prognostic values in cervical cancer**
Xiaopeng Shen, Chunguang Wang, Meng Li, Sufen Wang, Yun Zhao, Zhongxian Liu and Guoping Zhu
- 183 **Integrated bioinformatics analysis and experimental validation reveals fatty acid metabolism-related prognostic signature and immune responses for uterine corpus endometrial carcinoma**
Chenrui Guo, Yan He, Leiming Chen, Yuan Li, Yajun Wang, Yunlei Bao, Ni Zeng, Feng Jiang, Hang Zhou and Le Zhang
- 196 **Prognostic biomarker MCP-4 triggers epithelial-mesenchymal transition *via* the p38 MAPK pathway in ovarian cancer**
Siting Li, Yuexin Hu, Ouxuan Liu, Xiao Li and Bei Lin



Inflammation-Related LncRNAs Signature for Prognosis and Immune Response Evaluation in Uterine Corpus Endometrial Carcinoma

Hongmei Gu^{1†}, Jiahang Song^{2†}, Yizhang Chen^{3†}, Yichun Wang^{4†}, Xiaofang Tan^{5*} and Hongyu Zhao^{1*}

OPEN ACCESS

Edited by:

Shaohua Xu,
Tongji University, China

Reviewed by:

Feng Xu,
Shantou University, China
Wei Shenyu,
Zhejiang Chinese Medical University,
China

*Correspondence:

Hongyu Zhao
z_hy07@126.com
Xiaofang Tan
txf15@163.com

[†]These authors have contributed
equally to this work

Specialty section:

This article was submitted to
Gynecological Oncology,
a section of the journal
Frontiers in Oncology

Received: 19 April 2022

Accepted: 05 May 2022

Published: 02 June 2022

Citation:

Gu H, Song J, Chen Y, Wang Y, Tan X
and Zhao H (2022) Inflammation-
Related LncRNAs Signature for
Prognosis and Immune Response
Evaluation in Uterine Corpus
Endometrial Carcinoma.
Front. Oncol. 12:923641.
doi: 10.3389/fonc.2022.923641

¹ Department of Radiotherapy Oncology, Affiliated Hospital of Nantong University, Nantong, China, ² Department of Radiation Oncology, The First Affiliated Hospital of Nanjing Medical University, Nanjing, China, ³ Department of Oncology, The First Affiliated Hospital of Nanjing Medical University, Nanjing, China, ⁴ Department of Urology, The First Affiliated Hospital of Nanjing Medical University, Nanjing, China, ⁵ Affiliated Maternity and Child Health Care Hospital of Nantong University, Nantong, China

Backgrounds: Uterine corpus endometrial carcinoma (UCEC) is one of the greatest threats on the female reproductive system. The aim of this study is to explore the inflammation-related LncRNA (IRLs) signature predicting the clinical outcomes and response of UCEC patients to immunotherapy and chemotherapy.

Methods: Consensus clustering analysis was employed to determine inflammation-related subtype. Cox regression methods were used to unearth potential prognostic IRLs and set up a risk model. The prognostic value of the prognostic model was calculated by the Kaplan-Meier method, receiver operating characteristic (ROC) curves, and univariate and multivariate analyses. Differential abundance of immune cell infiltration, expression levels of immunomodulators, the status of tumor mutation burden (TMB), the response to immune checkpoint inhibitors (ICIs), drug sensitivity, and functional enrichment in different risk groups were also explored. Finally, we used quantitative real-time PCR (qRT-PCR) to confirm the expression patterns of model IRLs in clinical specimens.

Results: All UCEC cases were divided into two clusters (C1 = 454) and (C2 = 57) which had significant differences in prognosis and immune status. Five hub IRLs were selected to develop an IRL prognostic signature (IRLPS) which had value in forecasting the clinical outcome of UCEC patients. Biological processes related to tumor and immune response were screened. Function enrichment algorithm showed tumor signaling pathways (ERBB signaling, TGF- β signaling, and Wnt signaling) were remarkably activated in high-risk group scores. In addition, the high-risk group had a higher infiltration level of M2 macrophages and lower TMB value, suggesting patients with high risk were prone to a immunosuppressive status. Furthermore, we determined several potential molecular drugs for UCEC.

Conclusion: We successfully identified a novel molecular subtype and inflammation-related prognostic model for UCEC. Our constructed risk signature can be employed to assess the survival of UCEC patients and offer a valuable reference for clinical treatment regimens.

Keywords: UCEC, inflammation, tumor microenvironment, prognostic signature, immunotherapy, TCGA

INTRODUCTION

UCEC ranks the fourth most common in cancer incidence among females around the world (1), with unfavorable cure rate and high mortality (2). UCEC patients diagnosed in later stage have a significantly higher rate of recurrence and complications, leading to a bleak prognosis (3, 4). Traditional surgical resection, chemotherapy, and radiotherapy have been developed and have undergone constant evolution, but the overall survival (OS) has seen no significant improvement. Therefore, gaining new insight into the tumorigenesis process, pathological nature, and therapeutical agent of UCEC is vital in fighting this deadly disease.

Inflammation has a predominant effect on the immune system, creating a microenvironment conducive to cellular transformation and the spread of invasive diseases (5, 6). Research evidence shows that inflammation can also affect the occurrence and progression of cancer, *via* various pathways like oxidative stress, interleukin secretion, and pro-inflammatory transcription factors (7). Cumulative evidence also suggests epigenetics modifications like DNA methylation, histone modification, remodeling of chromatin, and regulation *via* non-coding RNAs can modulate the balance of inflammation and accelerate the tumorigenesis process (8). lncRNAs are a novel kind of RNA that can regulate cellular signaling pathways in UCEC (9). For example, lncRNA NEAT1 is found to drive endometrial cancer progression by targeting the oncogene STAT3 (10). Similarly, Wang et al. reported another lncRNA NR2F1-AS1 is able to assist miR-363 to target SOX4, thus increasing the risk of endometrial cancer (11). Considerable research has shown the role of inflammatory pathways in cancer is regulated by a number of lncRNAs. Hu et al. disclosed that upregulation of lncRNA XLOC-000647 can inhibit the expression of NLRP3 inflammatory vesicles, which in turn suppresses the metastasis of pancreatic cancer cells (12). In breast cancer, lncRNA NKILA was proven to interact directly with NF- κ B to mediate inflammatory pathways and thereby inhibit tumor metastasis (13).

The TME supports the intricate process of tumorigenesis by modulating various functionally interlinked cells and non-cellular components (14, 15). Numerous previous studies have reported modulation function of immune and inflammatory cells on UCEC cells. These factors woven together provide a welcoming host for the UCEC cells, and greatly enhance their

capability to replicate, invade, and resist drugs. Previous research has discovered numerous potential hallmark signals and proteins. For example, the overexpression of CXCL12/CXCR4 is reported to be correlated with unfavorable prognosis in UCEC patients (16). Utilizing the ESTIMATE and CIBERSORT algorithms, Xu et al. discovered that cell-cell chemokine receptor 2 (CCR2) can facilitate the recruitment of monocytes and macrophages into the TME, affecting the prognosis of UCEC patients. On the other hand, MSI status implies the existence of high-level TIL-infiltration, taking mismatch repair defect into consideration. Prognostic effects of biomarkers varies on molecular subtypes: In p53-mutant UCEC, Treg is an independent prognostic factor, while in NSMP, WHO-grading has unreplaceable prognostic value (17). Cumulating evidence implies additional factors are needed to drive the tumorigenesis process apart from merely genetic mutations, and the microenvironment-derived factors may be exactly the missing puzzle piece. However, the precise mechanism and molecular signal remains disputed, and calls for additional research. Any new insight into the nature of TME can potentially improve the precision of prognosis prediction or reveal promising therapeutic targets.

In this project, we determined a novel molecular subtype and a risk signature based on IRLs which were tightly correlated with survival outcome of UCEC cases. Moreover, our proposed risk model can reflect the immune status and evaluate the benefits of immunotherapy and chemotherapy.

METHODS

Data Acquisition

Transcriptome and RNA-seq data of UCEC patients were retrieved from the TCGA database (<https://portal.gdc.cancer.gov/>) and the transcriptome data files were in “FPKM” format. Five hundred eleven UCEC patients with clinicopathological information were used for analysis. The exclusion criteria were set as follows (1): histologic diagnosis is not UCEC (2); samples without completed clinical data; and (3) survival time of less than 30 days. In total, 511 UCEC patients were randomly divided equally into the training cohort (256 patients) and a validation cohort (255 patients) by utilizing the caret R package. Detailed annotation of the tumor samples complete with clinical and pathological information can be found in **Table S1** ($P > 0.05$, Chi squared test).

Determination of the IRLs

The list of 200 inflammation-related genes was acquired from the GSEA database (<http://www.gsea-msigdb.org>). We screened the

Abbreviations: UCEC, Uterine corpus endometrial carcinoma; TCGA, The cancer genome atlas; IRLs, inflammation-related lncRNA; TMB, tumor mutation burden; ICIs, immune checkpoint inhibitors; GO, Gene ontology; KEGG, Kyoto encyclopedia of genes and genomes; GSEA, Gene set enrichment analysis; OS, Overall survival; IRLPS, IRLs prognostic signature.

IRLs by Pearson's correlation analysis, and 636 IRLs were identified. The process applied the criteria of $|\text{Pearson } R| > 0.5$ and $p < 0.001$.

Gene Set Enrichment Analysis

The training set was applied to establish the IRLPS, and validation of aforementioned model is made using the testing set and entire set. Completed with survival data retrieved from TCGA, we explored the prognosis value of IRLs, and univariate Cox regression was used to filter 27 prognostic IRLs. The next step was to understand the biological processes that these IRLs are involved in. The "ConsensusClusterPlus" package was used to divide UCEC patients into groups based on clinical outcome and pathological classifications (18). Then, gene set enrichment analysis (GSEA) was used to determine which process or pathway made a difference in the outcome (19, 20). KEGG can identify predefined gene sets activated or deactivated, p-value were determined by performing 5000 permutations according to the gene set. A pathway with a p-value < 0.05 was considered as significant.

Estimating of Tumor-Infiltrating Immune Cells

CIBERSORT was employed to calculate the abundance of 22 types of immune-related tumor-infiltrating cells in all samples (21). The proportion of data generated will be used for further analysis. ESTIMATE algorithm was used to screen each sample, computing the proportion of immune and stromal components in the TME (22); the immune score and stromal score are results of these algorithms. The ESTIMATE score is determined by combining immune score and stromal score. The value of these scores has a positive connection with the proportion of stromal, immune, and the sum of the first two, respectively. With the "GSVA" package in R, we calculated the abundance of 16 immune cells in the microenvironment, represented by the infiltration scores, and the activities of 13 immune-related pathways between the high-risk and low-risk groups *via* single-sample gene set enrichment analysis (ssGSEA) (23).

Establishment of the IRLPS

To build our risk model, we chose the LASSO Cox regression to generate the optimal choice of coefficients and variants that constitutes the risk score equation (24). A 10-fold cross validation with minimum criteria was applied to optimize the signature. The remaining non-zero features were utilized to build the final model. LASSO regression was conducted with the R package "glmnet" (25). Generated from LASSO, these coefficients made up our risk score equation:

$$\text{risk score} = \sum_{i=1}^n \text{coefficient}_i * \text{expression level of IRL}_i$$

Acquisition of Clinical Specimens

The 32 specimens (16 tumor samples and 16 normal samples) used for quantitative PCR assay were acquired from 16 consenting patients at Maternity and Child Health Care

Hospital of Nantong University. Our research protocol was approved by the Ethics Committee for Clinical Research of the Maternity and Child Health Care Hospital of Nantong University. All research was conducted in strict adherence to the Declaration of Helsinki.

RNA Extraction and Quantitative Real-Time Quantitative PCR (RT-qPCR) Analysis

The total RNA was extracted from the aforementioned 32 samples using TRIzol reagent (Thermo Fisher Scientific, Waltham, MA, USA), and then evaluated for RNA structure integrity using the Agilent Bioanalyzer 2100 (Agilent Technologies, Santa Clara, CA, USA) with the RNA 6000 Nano Kit. By utilizing the High-Capacity cDNA Reverse Transcription Kit (Thermo Fisher Scientific), we therefore synthesized complementary single-stranded DNA and then performed the real-time quantitative analysis by the SYBR Green PCR Kit (Thermo Fisher Scientific). The relative transcription level was assessed with the $2^{-\Delta\Delta C_t}$ method, C_t represents the cycle threshold of each IRL. All programs and procedures were conducted on the basis of the instructions offered by the manufacturer. Primer sequences that were used can be found in Table S2.

Validation of the IRLPS

Now that we have this risk score to forecast the OS of UCEC patients, the next step was validation of our model. Again, our patients were assigned to groups assigned by the median risk score, and then we checked whether there was a statistical difference in OS between groups. The accuracy of IRLPS was presented in the form of receiver operating characteristic (ROC) curve and the area under the ROC curve (AUC value), generated by using R package "survivalROC" (26). The model was then validated with the testing data set and entire set, its effectiveness was measured by ROC curve, compared with clinical or pathological criteria alone and combined as a risk indicator. The Kaplan-Meier analysis was performed with the "survival" package (27). The risk curve and scatter plot were generated to illustrate the risk score and survival status of each sample. The heatmap indicated the expression profiles of the signature in the two groups. Principal components analysis (PCA) was applied to dimensionality reduction (28). In order to identify independence of IRLPS, we employed both univariate and multivariate Cox regression analyses. To further verify the prediction power of our risk score, we performed stratified analysis by clinical classifications. We built the nomogram on the basis of the outcomes of multivariate Cox regression to predicting 1-, 3-, and 5-year survival probability through "rms" package (29). The calibration figures represent the consistency of our prediction with reality.

Mutation Analysis

Patient characteristics and their sequencing status were retrieved from TCGA. The forest plots give visual hints of the 20 most frequent mutated genes, made by the R package "maftools" (30). Additionally, the stemness of tumor cells in each endometrial

carcinoma sample was determined by one-class logistic regression, represented by the stemlike indices (31).

Immunophenoscore Analysis

Derived by z-scores of iconic genes related to immunogenicity, immunophenoscore (IPS) is a representation of a sample's overall immunogenicity. The IPSs of UCEC patients were extracted from the Cancer Immunome Atlas (TCIA) (32) (<https://tcia.at/home>). Based on four main classes of genes (PD1, PD-L1, PD-L2, CTLA-4), MSI was generated by machine learning in an unbiased manner. Together, IPS and MSI give an overview of the immunophenotype.

Chemotherapy Response and Drug Sensitivity Analysis

The response of UCEC patients to therapeutic agents, whether chemotherapy or small molecular agents, were found in a public database called Genomics of Drug Sensitivity in Cancer (GDSC; <https://www.cancerrxgene.org>). The half-maximal inhibitory concentration (IC50) was taken as an index to measure the sensitivity (33). Up to 60 different cancer cell lines that originated from nine different cancers were made available as per request *via* the CellMiner interface (<https://discover.nci.nih.gov/cellminer>) (34, 35). Correlation between the expression of

previously mentioned genes with prognostic value and drug sensitivity were explored using Pearson correlation analysis.

Statistical Analysis

All the analyses were processed using R software (version 4.1.0) (36). Student's t-test was applied to perform the group comparisons between subgroups separately. To uncover potentially significant differences in OS between risk score defined groups, Kaplan-Meier analysis and log-rank tests were used. The correlation of the risk score generated by our model with stemness score, stromal score, immune score, and drug sensitivity was tested by Spearman or Pearson correlation analysis. a p-value < 0.05 is considered significant.

RESULTS

Data Acquisition and Generation of Differential Expressed lncRNAs

The total workflow of this research is shown in **Figure 1**. In short, we first retrieved transcriptome and clinical data of the UCEC patients from the TCGA database, and inflammation-related gene sets from the GSEA database. Combining them, we subsequently used Pearson correlation analysis to screen 636 lncRNAs to find

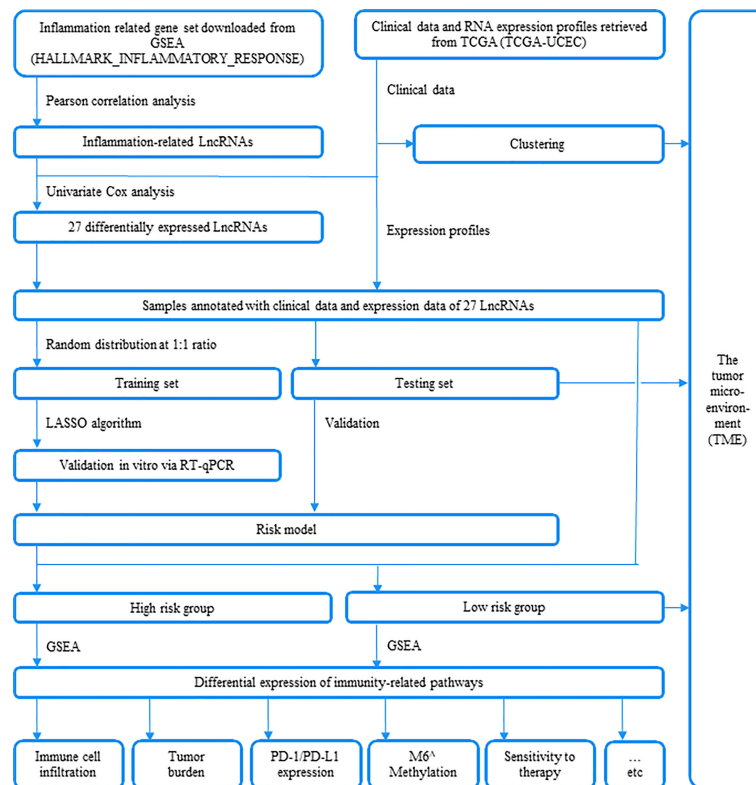


FIGURE 1 | An outline of this research is depicted in this plot.

those most closely correlated with prognosis. Twenty-seven lncRNAs were identified as prognostic *via* univariate Cox regression (Table S3). The expression levels of 27 IRLs in UCEC and normal tissues were evident (Figures 2A, B).

Identification of Inflammation Molecular Subtype in UCEC

To determine the inflammation-associated subtype, all UCEC cases were subject to consensus clustering method based on 27 IRLs. Figures S1A, S1B show the respective cumulative distribution function (CDF) of consensus clusters ranging from $k = 2$ to 9 and the corresponding area under curve. As is shown, $k = 2$ is the choice to divide the UCEC patient in order to reach maximum consensus within clusters (Figures S1A, B). Tracking plots for $k = 2$ to $k = 10$ is exhibited in Figure S1C, and relative change in area under CDFG curve is demonstrated in Figure S1D. According to the expression levels of the 27 IRLs, 511 UCEC patients were clustered into cluster 1 ($n_1 = 454$) and

cluster 2 ($n_2 = 57$). As suggested by Figure 2C, patients in cluster2 presented a dismal outcome compared to those in cluster 1 ($p < 0.001$). We then assessed the correlation between clusters and clinical parameters of UCEC patients. (Figures 2D–H).

Immune Activity Analysis of Molecular Subtype

Expression of PD-1 and CTLA-4 were compared between tumor and normal tissue samples in UCEC patients. Our result revealed that the expression of PD-1 and CTLA-4 in UCEC tissues was upregulated ($P < 0.001$, Figures 3A, B) compared to their normal counterparts. In regard to the consensus clusters, we observed the higher expression of PD-1 and CTLA-4 in cluster 1 (Figures 3C, D). In addition, the expression of two immune checkpoints was positively related to the expression levels of FAM66C, UNQ6494, AC078883.1, AP002761.4, FMR1-IT1, LINC01126, AC244517.7, and AC244517.1 (Figures 3E, F).

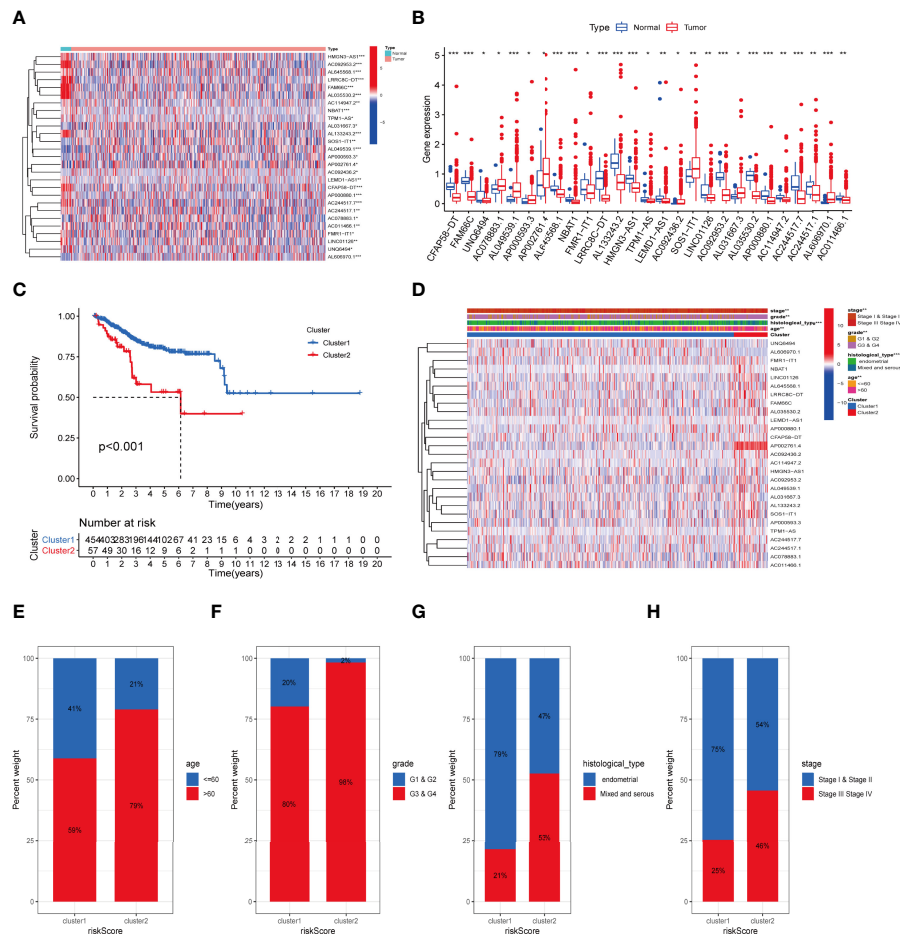


FIGURE 2 | The association between the transcription level of IRLs and clinicopathological and prognostic features of the UCEC patients. (A, B) The transcription levels of 27 differentially expressed IRLs between the tumor and normal samples were visualized by heatmap and boxplot. (C) The overall survival of UCEC patients in the two clusters was calculated by Kaplan-Meier curves. (D) The transcription levels of 27 differentially expressed IRLs between the two clusters with clinical features were shown in heatmap. (E–H) The ratio of different age (E), grade (F), histological type (G), and stage (H) in the groups. * $P < 0.05$, ** $P < 0.01$, *** $P < 0.001$.

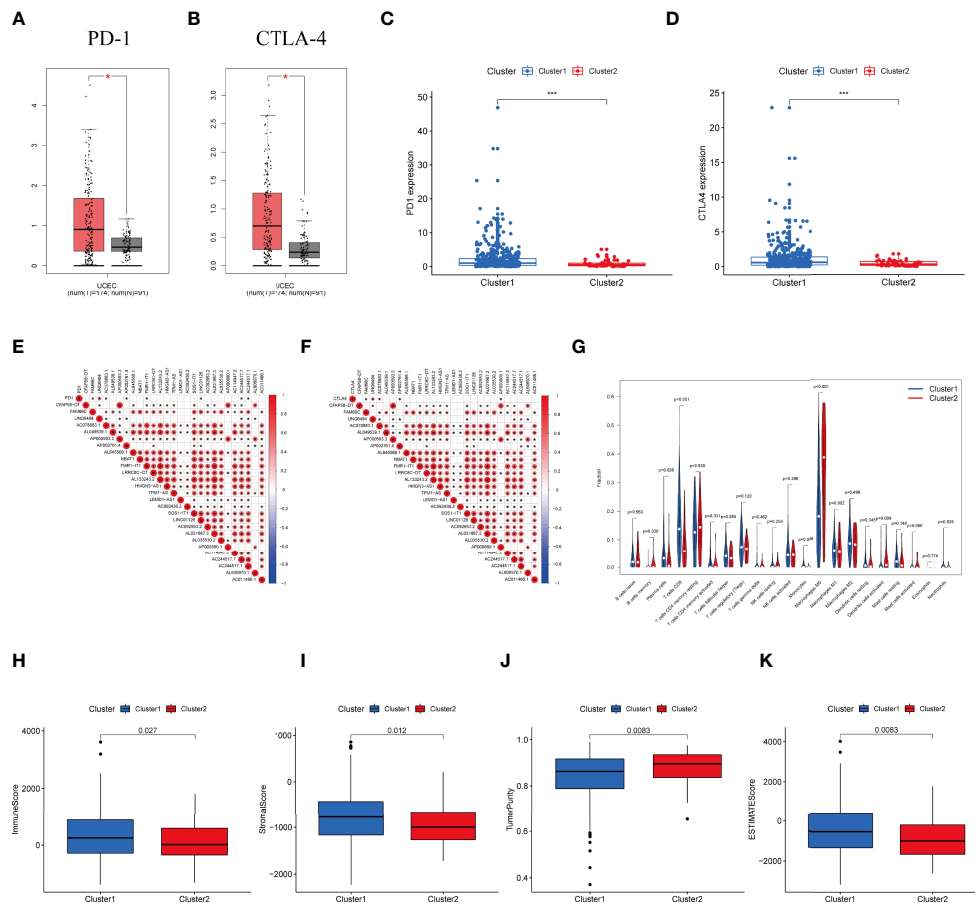


FIGURE 3 | Differential expression profile of immune checkpoint related genes and TME components between clusters. **(A)** The expression of PD-1 in normal and UCEC tissues. **(B)** The expression of CTLA-4 in normal and UCEC samples. **(C)** The expression level of PD-1 in the clusters. **(D)** The expression level of CTLA-4 in the clusters. **(E)** The correlation of the transcription levels of IRLs and PD-L1, red circle means positive relationship. **(F)** The correlation of the transcription levels of IRLs and CTLA-4, red circle means positive correlation. **(G)** The infiltrating levels of 21 immune cell types in two clusters. **(H–K)** The **(H)** Immunescore, **(I)** Stromascore, **(J)** Tumor purity score, and **(K)** ESTIMATEScore in cluster 1 and cluster 2. * $P < 0.05$, *** $P < 0.001$.

The differential infiltration of 22 immunocytes between the two clusters is shown in **Figure 3G**.

Moreover, we assessed the immune microenvironment value of the UCEC samples. The results suggested that cluster 1 displayed a higher immune microenvironment score, whereas cluster 2 had the higher level of tumor purity (**Figures 3H–K**). Meanwhile, GSEA was employed to detect the TME phenotype of the two clusters. We found that immune-related pathways were mainly enriched in cluster 2. The results reveal that the top 10 pathways enriched in cluster 1, while cancer-associated pathways were activated in cluster 2 (**Figure S2A**).

Establishment of Prognostic Signatures Based on IRL

In the training dataset, univariate Cox regression was first used to filter 27 prognostic IRLs. Then we employed LASSO algorithm to remove overfitting genes and selected five lncRNAs to create a signature (**Figure S3**), including HMGN3-AS1, LEMD1-AS1, AP000880.1, AC244517.1, and AC011466.1. The complete

formula was as below: Risk score = $(0.286 \times \text{HMGN3-AS1}) + (0.065 \times \text{LEMD1-AS1}) + (0.854 \times \text{AP000880.1}) + (0.048 \times \text{AC244517.1}) + (0.600 \times \text{AC011466.1})$. Next, the expression pattern of five hub markers between tumor and normal specimens was confirmed. Both five lncRNAs were downregulated in tumor tissues based on TCGA-UCEC dataset (**Figure S4A–E**). We further examined the expression level of five lncRNAs in clinical samples. The results indicated that only AP000880.1 and AC244517.1 showed the expression difference between two groups (**Figure S4F–J**).

Subsequently, UCEC patients were divided into high-risk and low-risk groups. PCA analysis shows satisfying separation efficacy in the training, testing group, and entire cohort (**Figures S5A–C**). Sankey diagram presented the association among cluster, risk score, and survival outcome of UCEC cases (**Figures S5D**).

Then we validated this model in the test set and entire set. In the training set, Kaplan-Meier curves uncovered the significant difference of prognosis between two high groups (**Figures 4A**). The AUC value of 1-, 3-, and 5-year OS were 0.725, 0.780, and

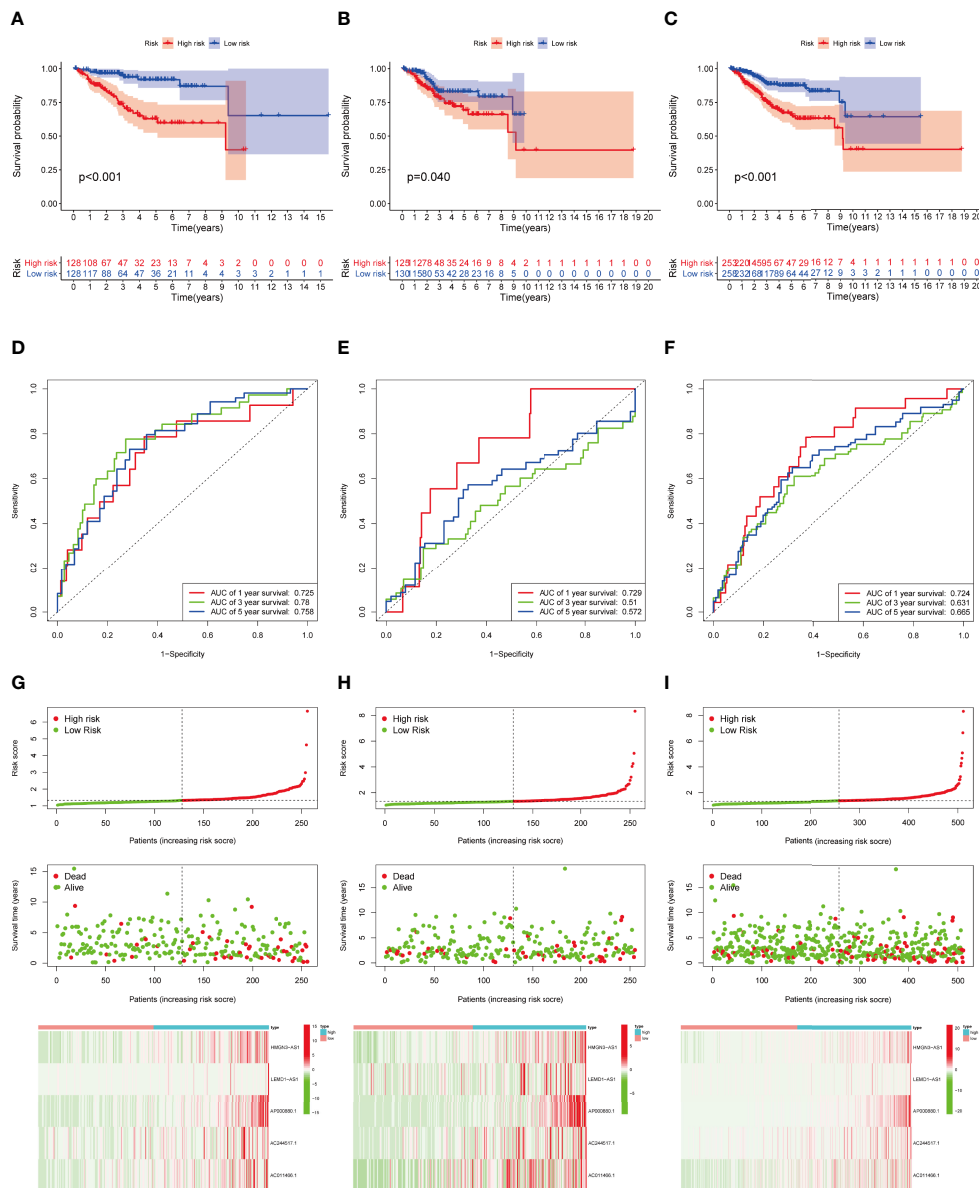


FIGURE 4 | Construction and validation of IRLPS. (A–C) Survival analysis for patients in the (A) training, (B) testing, and (C) entire cohort. (D–F) ROC curves measuring the predictability of the signature in the (D) training set, (E) testing set, and (F) entire cohort. (G–I) Distribution of risk score, survival status, and heatmap of the transcription levels of five prognostic signatures in the (G) training set, (H) testing set, and (I) entire cohort.

0.758, respectively (Figure 4D). The performance of model was shown in Figure 4G. At the same time, the test set and entire set were utilized to confirm our proposed signature (Figure 4).

In addition, we explored the predictive ability of the model based on subgroup analysis. Figure 5 reveals that signature showed the favorable power in age and stage subgroups. Furthermore, we plotted a heatmap as an overview of the relationship between clinical features and risk score (Figure 5I). The risk score was significantly different between some clinical factors including age, grade, histological type, immune subtype, immunescore, stage, and cluster (Figures 5J–P).

Development of a Prognosis Nomogram

As uncovered by Cox regression analysis, our constructed signature was proven to be an independent factor in training, testing, and entire sets, respectively (Table S4). Previous work has already explored the prognostic value of lncRNAs in UCEC, and yielded promising results (37, 38). In this research, risk score based on IRLs (IRLPS) is more superior in prognostic accuracy compared to its predecessors (Figure 6A). Next, we conducted the univariate and multivariate methods and found that the histological type and stage are also independent prognostic factors in UCEC (Figure 6B). We then compared our model

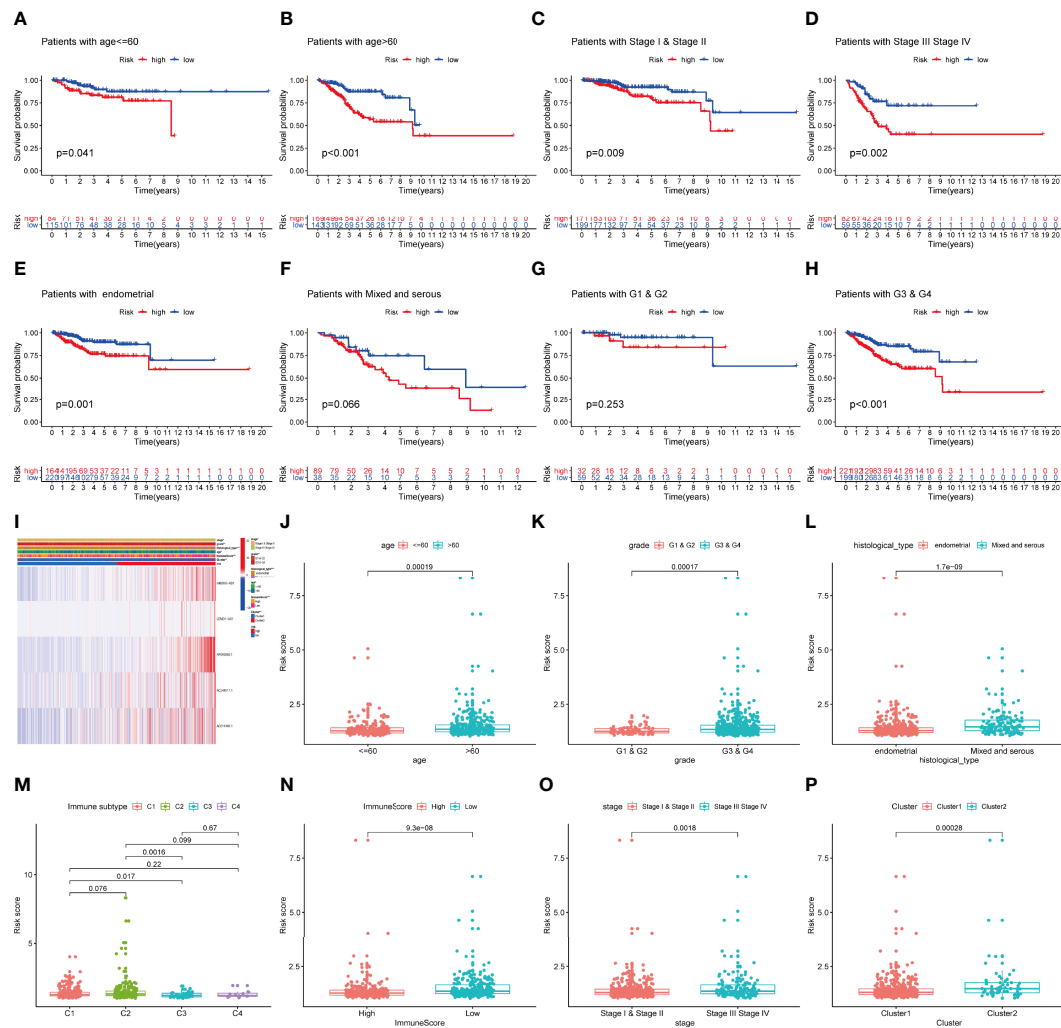


FIGURE 5 | The prognostic value of IRLPS in stratified patient groups, and correlation of IRLPS with clinicopathological features and immunoscore. IRLPS showed satisfactory prediction performance in patients regardless of (A, B) age and (C, D) stage, (E, F) histological type and (G, H) grade. (I) Heatmap and clinical features of the groups. (J–P) Distribution of IRLPS stratified by (J) age, (K) grade, (L) histological type, (N) immunological subtype, (M) Immunescore, (O) tumor stage and (P) cluster. * $P < 0.05$, ** $P < 0.01$ *** $P < 0.001$.

and clinical characteristics in pursuit of greater efficacy for predicting clinical outcome (Figure 6C) and observed that taking clinical factors into consideration presented higher AUC value. To further expand the forecasting ability, we established a nomogram by combining risk score and other clinical traits (Figure 6D). Each of them is mapped to a bar representing range of value they contribute to prognostic risk. To test the sensitivity and specificity of the nomogram, we established calibration curves, which implies there was a close fit between the prognosis and real curves (Figures 6E–G).

GSEA Enrichment of Risk Model

GSEA revealed the top five active pathways in the high-risk group including cell cycle, endometrial cancer, ERBB signaling pathway, TGF- β signaling pathway, and WNT signaling pathway

(Figure 7A), while the low-risk group included allograft rejection, autoimmune thyroid disease, graft versus host disease, intestinal immune network for IgA production, and primary immunodeficiency (Figure 7B).

Immune Landscape Between Two Risk Groups

Considering that the IRLPS were associated with the immune-related pathway, we detected the immune status of two subgroups. Firstly, we noticed that the low-risk patients had a higher TME score than the high-risk patients (Figures 7C, E, G). Also, correlation analysis verified the above results (Figures 7D, F, H). Subsequently, the immune landscape of the two risk groups was mirrored by Figure 8A. The relationship between five model lncRNAs and immune cell infiltration was further

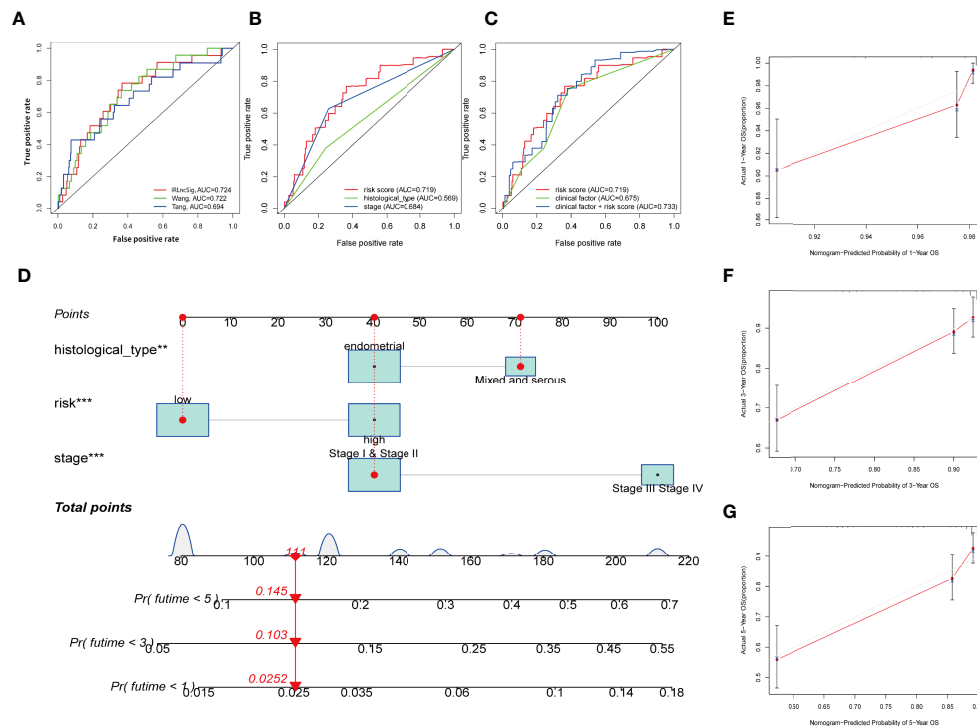


FIGURE 6 | Establishing the IRLPS based on risk score and clinical factors, and validating it in calibration plot. **(A)** ROC plot indicates that IRLPS is superior in predicting the prognosis in UCEC patients than previous works. **(B)** IRLPS is also more superior in prediction accuracy than histological type or tumor stage alone. **(C)** Combining IRLPS with clinical factors is better yet. **(D)** A nomogram to illustrate the IRLPS, a risk model to predict endometrial carcinoma patient prognosis basing on aforementioned IRLPS, and clinical factors. **(E–G)** Calibration curves showing the favorable performance of nomogram. ** $P < 0.01$ *** $P < 0.001$.

analyzed (Figure 8B). Correlation method showed that the infiltration levels of B cells and Macrophages M2 were positively associated with risk score, while risk score had a negative correlation with the proportions of monocytes, activated NK cells, and CD8 T cells (Figures 8C–H).

ssGSEA also presented the similar immune status of all patients (Figure 8I). Additionally, we found that the high-risk group had lower immune activity, which might be a potential explanation for the dismal outcome of cases with high risk (Figure 8J). Previous reports have demonstrated that patients with poor immune activity tend to have worse prognosis (39–41).

RNA stemness score (RNAss) is an effect index representing tumor stemness (42). All three types of stemness-related indicators uncovered that the high-risk group had a higher tumor stemness (Figures 8K–M).

Immunotherapy Response Analysis of IRLPS

Considering the crucial role of immune checkpoints in immunotherapy, we collected 27 immune checkpoint genes (ICGs), including CD44, TNFRSF9, CD27, TNFRSF18, CTLA4, CD244, ICOS, CD48, NRP1, CD276, TIGIT, TNFSF9, PDCD1, HAVCR2, TNFSF14, TMIGD2, CD70, TNFRSF14, CD40LG, LGALS9, TNFRSF4, and LAIR1. The results suggested that most immune checkpoints were highly expressed in the low-risk group

(Figure 9A). The relationship between six classical immune checkpoints and risk score are shown in Figure 9B. Meanwhile, we observed that high risk score was positively correlated with the expression levels of CTLA-4, HAVCR-2, and PD1 (Figures 9C–F). Moreover, IPS algorithm was employed to determine the immunogenicity of the two groups. Four types of IPS-related scores were lower in the high-risk group (Figures 9G–J).

The comparison in the expression of m6A-related markers between the two groups indicated that the expressions of all markers were significant except for FTO, YTHDC2, and ALKBH5 (Figure S6A). Mismatched repair genes (MRGs) have long been established as predictors for immunotherapy benefits (43, 44). Here, we found that four MRGs (MSH2, MSH6, PMS2, and MLH1) were highly expressed in the high-risk group.

TMB Analysis of the IRLPS

TMB level was yet another factor that can't be ignored in predicting the response to immunotherapy. Here, we examined both subgroups and compared their TMB levels. Figures 10A, B show that the TMB was negatively related to risk score. Subsequently, the patients were assigned into unique clusters in terms of the TMB value. Survival analysis showed that the high-TMB group displayed a favorable outcome (Figure 10C, $p < 0.001$). Furthermore, we noticed that patients with low TMB

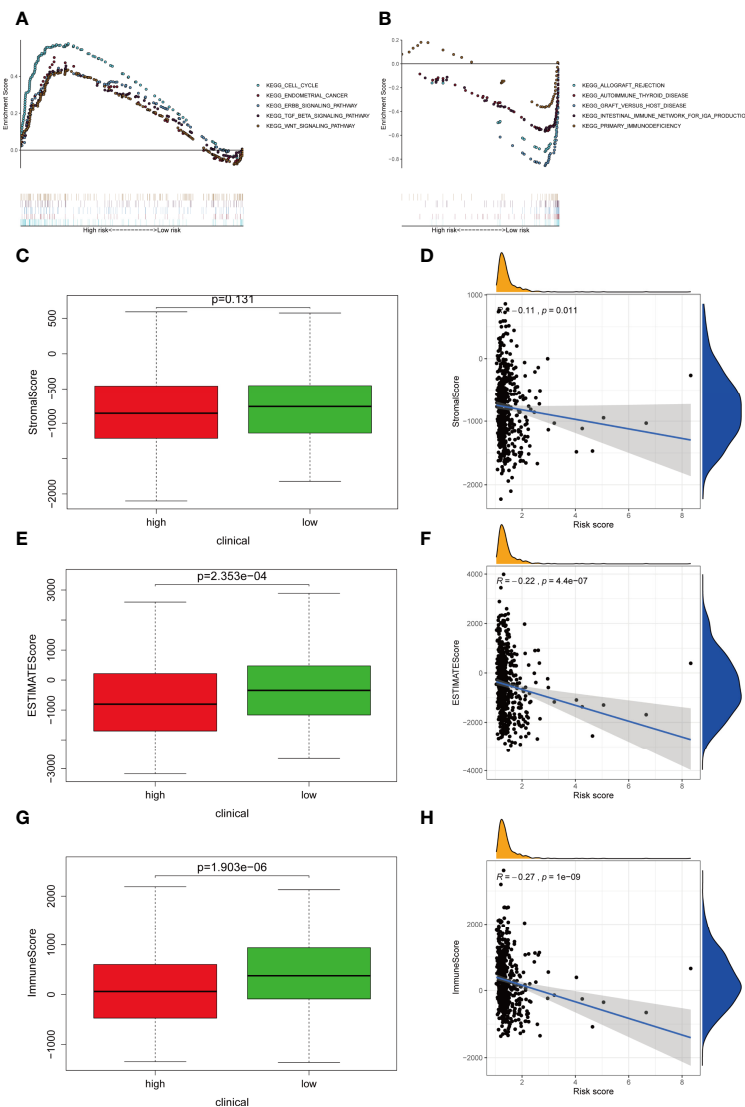


FIGURE 7 | Differentially activated pathways and immune infiltration between the groups. **(A, B)** Multiple GSEA analysis was conducted to predict the potential functions and pathways involved in **(A)** high-risk and **(B)** low-risk groups. **(C, D)** Stromal score does not differ significantly between the groups. However, correlation analysis implies significant relationship between stromal score and IRLPS. **(E, F)** ESTIMATE score differs significantly between the groups, and correlation analysis implies a significant relationship between ESTIMATE score and IRLPS. **(G, H)** Immunescore differs significantly between the groups, and correlation analysis implies a significant relationship between Immunescore and IRLPS risk score.

as well as a high-risk score showed the worst clinical outcomes (**Figure 10D**, $p < 0.001$).

An overview of somatic variants provides an insight into the scatter patterns of the top 20 most frequently mutated genes. The mutational landscapes presented that the top 20 mutated genes were the same in both groups, led by PTEN, PIK3CA, and ARID1A (**Figures 10E, F**). In this case, we also evaluated the MSI of UCEC patients. As is shown in **Figure 10G**, the prevalence of high instability of microsatellites (MSI-H) was higher in the low-risk group (38% vs. 27%), while the prevalence of stable microsatellites (MSS) was higher in the high-risk group (**Figures 10G, H**). This implies a negative

correlation between microsatellite instability and IRLPS risk score.

Chemotherapy Response Analysis of IRLPS

To select potential chemotherapeutics for UCEC patients, we calculated the IC₅₀ of three common chemotherapeutic drugs in two groups and assessed the correlation between IRLs and chemotherapeutic drugs. The results showed that etoposide and doxorubicin had higher IC₅₀ in the low-risk group (**Figures 11A–C**). Five model lncRNAs were closely related to the sensitivity of chemotherapeutic drugs ($P < 0.05$) (**Figure 11D**).

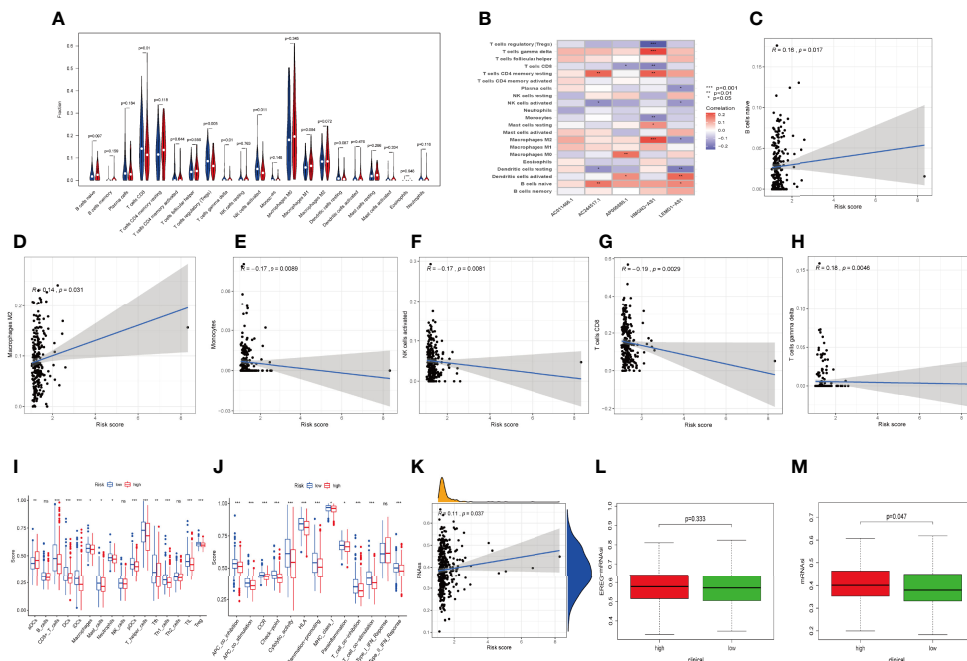


FIGURE 8 | Relationships between IRLPS and different aspects in the immune microenvironment, including infiltration abundances and activation status of immune cells and cell stemness. **(A)** Violin plot depicts 21 immune cell types that is differently distributed in high and low risk IRLPS risk score groups. **(B)** The correlation of IRLs expression and infiltration abundance of immune cells, visualized by heatmap. **(C–H)** The correlation of 6 immune cell types with the 5 IRLs in our risk signature. **(I, J)** ssGSEA reveals significant difference in **(I)** immune cell abundance and **(J)** activation of immune processes between the groups. **(K)** Correlation analysis implies significant relationship in cancer cell stemness represented by methylation of RNA (RNAs) with risk score. **(L)** No significant difference in epigenetic mRNA stemlike indices (EREG mRNAs) between the groups. **(M)** The mRNA based stemlike indices (mRNAs) is significantly different in the groups. * $P < 0.05$, ** $P < 0.01$, *** $P < 0.001$, ns indicates no statistical difference.

DISCUSSION

UCEC is among the most encountered threat to the female reproductive system. As for now, the therapy in clinical use is based on the clinical staging system, which is far from satisfactory, partly because it neglects the heterogeneity of UCEC patients and interactions in the TME (45).

Numerous reports have suggested that the inflammatory chemokine ligand/receptor axis promotes UCEC proliferation, progression, and metastasis (46). The inflammation process play an indispensable role in the progression and metastasis phase (47). Sorted by TME profiling signatures, the solid tumor is classified into three types, the T cell inflamed, the “desert,” and the “excluded” phenotype (48). The context of this specified immune landscape is closely associated with response to immunotherapy. Therefore, understanding the extent to which the tumor is inflamed is of vital significance, and should be the starting point of effective immunotherapy. Currently, there is no widely recognized indicator of inflammation activity on the epigenetics level. Our work is aimed to contribute to a more comprehensive and decisive means to predict and optimize the efficacy of immunotherapy.

The risk signature constructed in our study is a reliable and robust marker to predict the survival outcome of UCEC patients. Besides this, the signature was robustly associated with immune infiltration levels, TMB scores, and chemo-sensitivity. Our

research further investigates the role of LRLs in the tumor microenvironment, pharmaceutical landscape, and prognostic prediction in UCEC, providing a novel insight for future research and clinical practice.

In this research, we first determined a novel inflammation-associated subtype for UCEC. All patients were classified into two clusters which had significant differences in both prognosis and immune activity, suggesting the tremendous clinical potency of this molecular subtype. As is elucidated above, the transcription profile of IRLs is tightly correlated with immune cells infiltration, tumor purities, and immune status. In short, they are closely connected with the immune landscape of UCEC. Accumulating evidence suggests a crucial role of TME in assessing prognosis of several tumors (49). Therefore, we came up with the idea to use IRLs as a risk signature to forecast the clinical outcome of UCEC patients.

The full profile of IRLs transcription is not a practical tool for clinical use, due to the availability of full transcriptome sequencing. This process also generates excessive data, which is almost impossible for care providers to analyze in clinical settings. Consequently, we performed the LASSO regression to set up an IRLs-based signature which consisted of five key IRLs. Moreover, our proposed IRLPS showed a superior precision to its predecessors (37, 38). To achieve better performance of IRLPS, we further constructed a nomogram by integrating risk

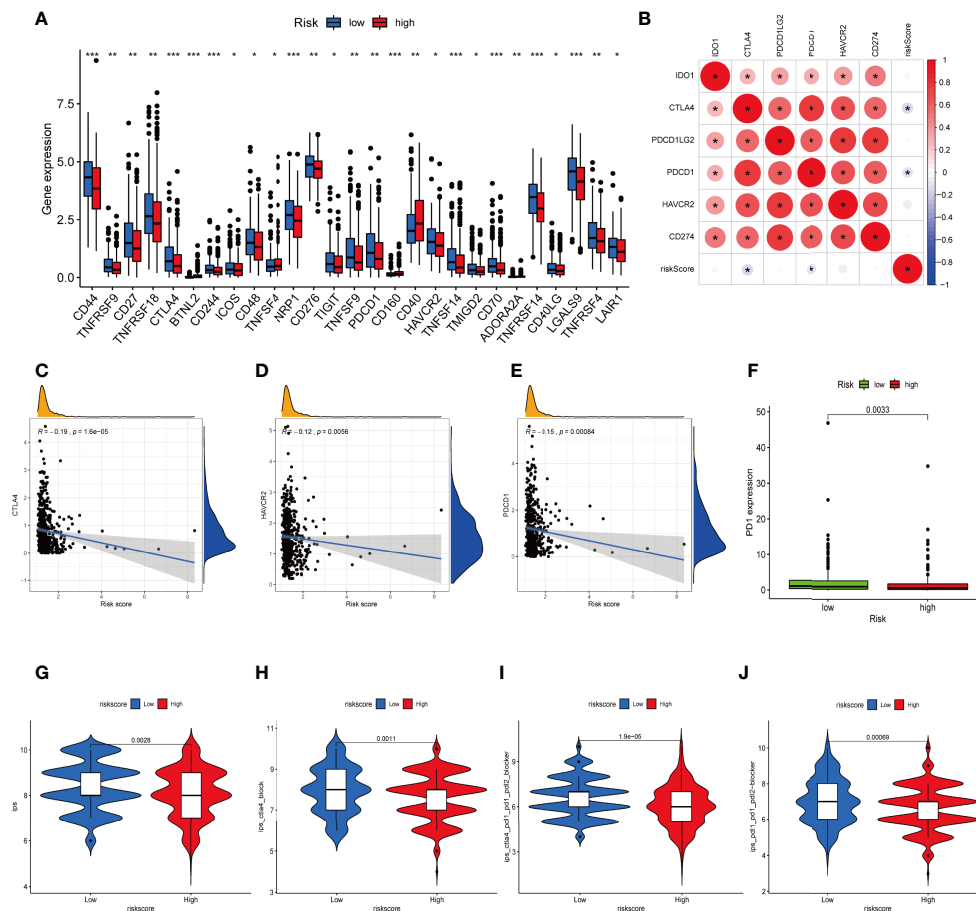


FIGURE 9 | Difference in ICGs expression in the two IRLPS groups. **(A)** The boxplot shows the correlation of ICGs and risk score. **(B)** Correlation between expression of ICGs and IRLPS. **(C-E)** Correlation analysis reveals expression levels of ICGs **(C)** CTLA-4, **(D)** HAVCR-2, and **(E)** PDCD1 are negatively related to IRLPS risk score. **(F)** Boxplot illustrates significantly higher expression of ICG PD-1 in the IRLPS low-risk group than in the high-risk group. **(G-J)** IPS scoring reveals **(G)** IPS, **(H)** IPS-CTLA4, **(I)** IPS-CTLA-4/PD-L1/PD-1/PD-L2, and **(J)** IPS-PD-L1/PD-1/PD-L2 scores were all significantly higher in the low-risk group. * $P < 0.05$; ** $P < 0.01$; *** $P < 0.001$.

score and other clinical factors. Calibration curves showed the nomogram had favorable ability for survival assessment. Next, GSEA analysis indicated that ERBB signaling, TGF- β signaling, and Wnt signaling were enriched in the high-risk group, suggesting patients with high risk tend to have a pro-tumor effect. It is believed that the intracellular accumulation of β -catenin is a marker for the activation of the classical Wnt signaling pathway, so any mutation genes resulting in the accumulation of β -catenin will activate the classical Wnt signaling pathway. Wnt signaling pathway, one of the main factors inducing the occurrence of cancer metastasis, could upregulate the expression of Slug, Snail, and Twist and block the expression of E-cadherin, causing the lack of epithelial polarity and connection (50). Almost 40% of UCEC cases exhibit abnormal activation of the Wnt/ β -catenin pathway. It has been shown that CT-NNB1 mutations leading to activation of the Wnt signaling pathway are bound up with high-grade UCEC in young women (51). As suggested by Chen et al.,

inhibition of MRP4 could block the viability and survival of endometrial tumors by targeting Wnt/ β -catenin pathway (52).

In our established IRLPS, five model IRLs (HMGN3-AS1, LEMD1-AS1, AP000880.1, AC244517.1, and AC011466.1) were deeply involved in the pathological processes of UCEC. HMGN3 is involved in glucose transportation in cells (53), DNA binding, protein binding (54), and chromatin organization (55). LEMD is found to promote proliferation in gastric cancer *via* activating the PI3K/Akt signaling pathway (56), and is also found to be active in tumorigenesis in colorectal cancer (57) and prostate cancer (58). AP000880.1 is possibly related to TTC12 and NCAM1 gene, which in turn plays an important role in the initiation of leukemia (59, 60). AC244517.1 is associated with the PCDH16 family gene, which regulates protocadherin, and is responsible for cell-to-cell adhesion (55) and synaptic transmission (61). AC011466.1 is associated with ZSWIM9, CARD8, PLA2G4C, and LIG1 gene. In research by Linder et al. in 2020, CARD8 can promote T cell proptosis *via* the

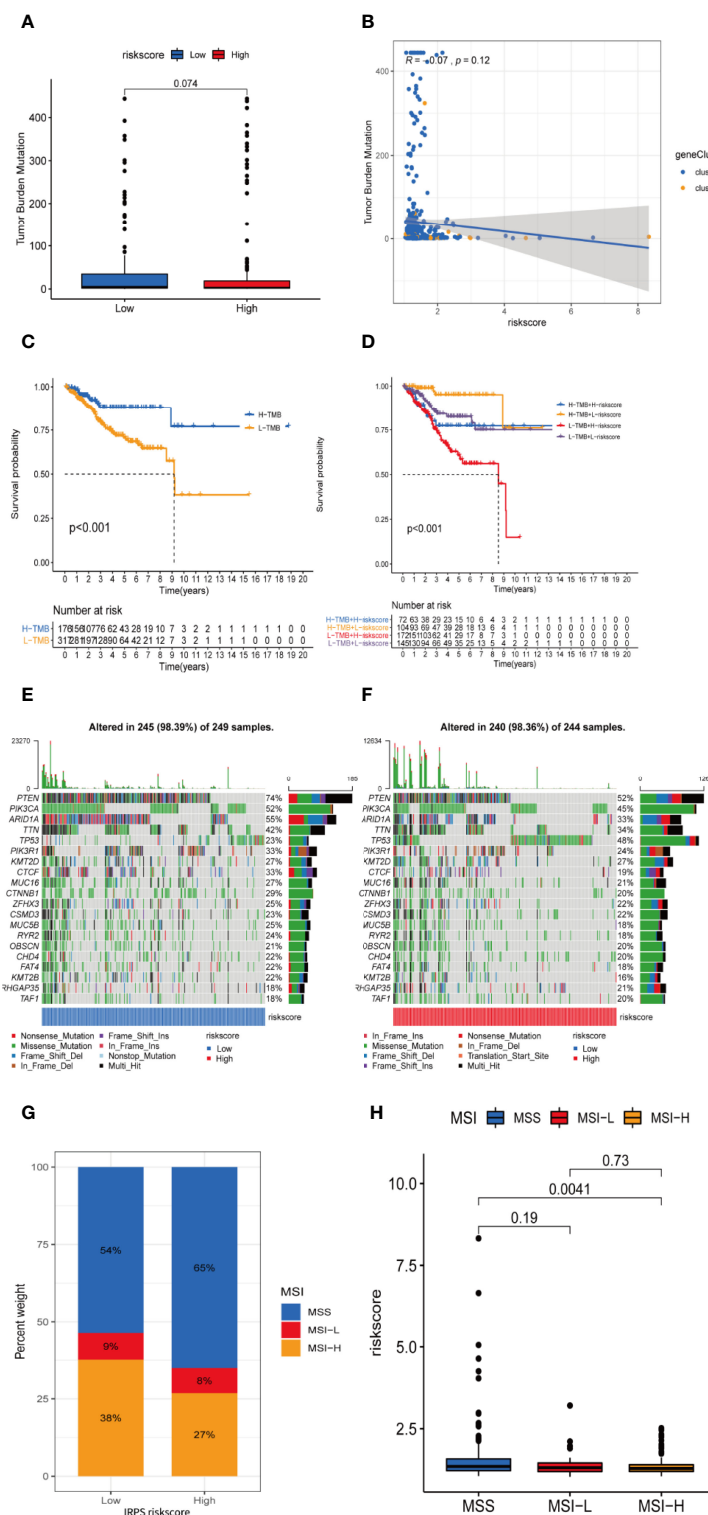


FIGURE 10 | TMB and microsatellite instability are negatively correlated to IRLPS risk score, and can contribute to more significant prognostic discrimination combined with risk score. **(A)** Boxplot shows higher TMB in the low-risk group. **(B)** Correlation analysis implies TMB is potentially negatively related to IRLPS risk score. **(C)** Kaplan-Meier analysis indicates unfavorable outcome for low TMB patients. **(D)** Patients with lower TMB and higher risk score have significantly more pessimistic outcomes. **(E, F)** Mutation profile in **(E)** low and **(F)** high risk score groups. **(G)** IRLPS high-risk group has higher proportion of MSS and lower proportion of MSI-H. **(H)** Divided by microsatellite status, the MSI-H group has significantly lower risk score.

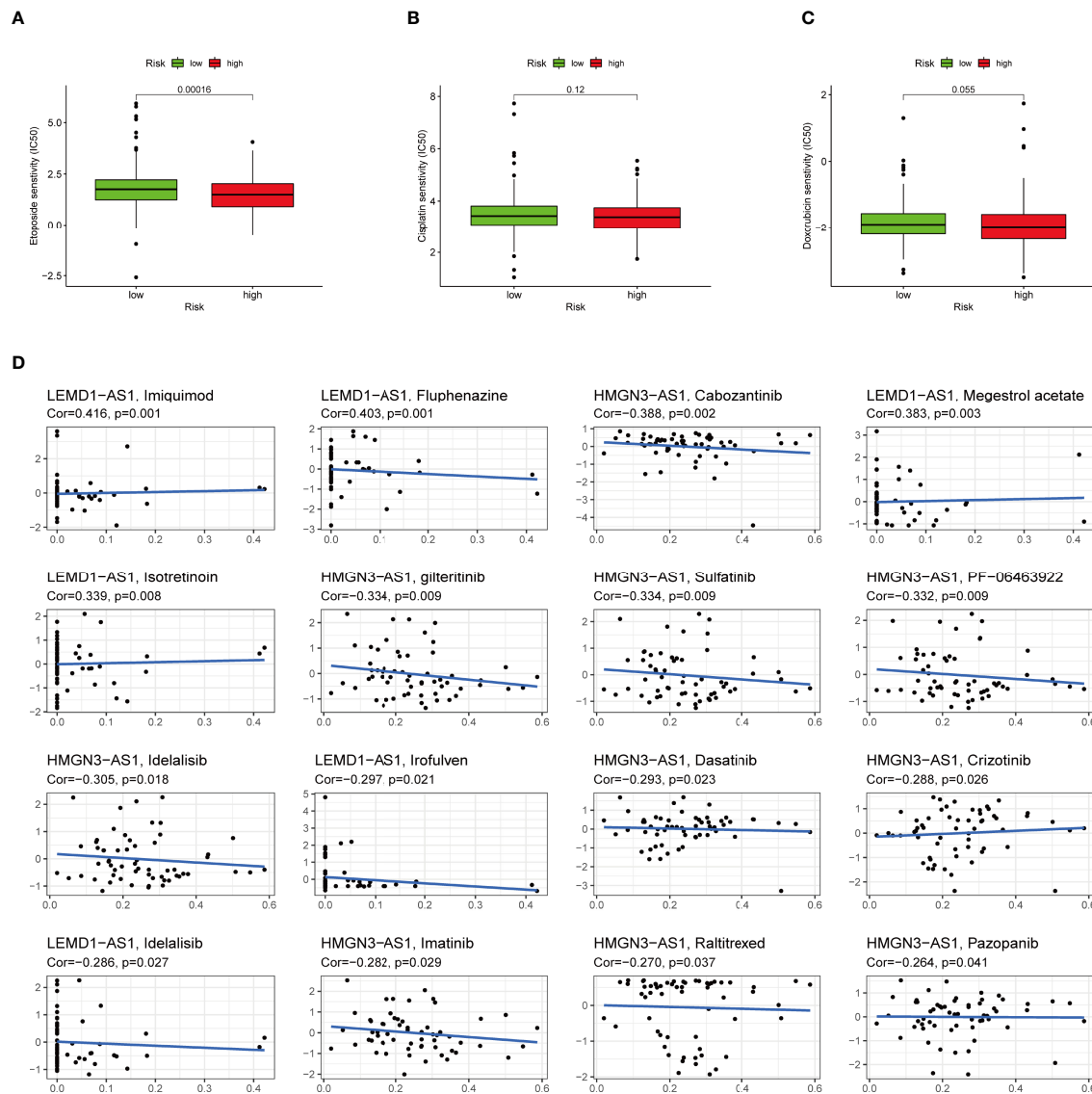


FIGURE 11 | High-risk group is generally less sensitive to chemotherapy and several potential small molecule therapeutical agents targeting the IRLs. (A–C) Correlation of risk score clustering and chemotherapy response. Response to (A) etoposide, (B) cisplatin, and (C) doxorubicin is generally less significant in high-risk patients. (D) Several small molecular agents are found to be able to counter the expression of these IRLs.

CARD8-caspase-1-GSDMD axis (62). LIG1 has already seen comprehensive research, and its role in DNA ligase activity (63) and DNA repair (64, 65) is well established. Li et al. reported in a meta-analysis that included 10 studies with a total of 4012 lung cancer cases and 5629 healthy controls that upregulated expression of LIG1 is related to the increased risk of lung cancer (66). However, due to the limited clinical samples, the results of the PCR were not completely consistent with the bioinformatics analysis. Tumor is a complicated disease induced by multigene, since the interaction of genes contribute to the complexity of tumor regulatory mechanisms.

As a current research hotspot, immune activity plays a central part in tumor development. Our model can successfully

demonstrate the capability of mirroring immune status and evaluating the benefits of immunotherapy. By depicting the immune landscape of two risk groups, we observed that risk score exhibited a negative correlation with immunescore which is an indicator of immune activity in TME, suggesting high-risk patients were prone to an immunosuppressive status. CIBERSORT disclosed that M2 macrophages were greatly enriched in the high-risk group. As a type of immunosuppressive immunocyte, M2 macrophages have been proven to be closely bound up with poor patient outcome of UCEC, which is in agreement with the results predicted by our IRLPS.

ICI is currently an effective treatment which could strengthen immune activity of the human body by blocking immune escape

of tumors. We found that four classical immune checkpoints were lowly expressed in the IRLPS-high group, suggesting patients may hardly benefit from ICI therapy. Also, four IPS-related scores were lower in the high-risk group, indicating unsatisfactory immune efficacy of UCEC. TMB is another favorable indicator for evaluating outcomes of immunotherapy and high TMB tends to forecast a poor prognosis. We demonstrated that TMB value was significantly higher in the IRLPS-high group. All the above results suggest that our model can predict the benefit of immunotherapy for UCEC patients and offer a valuable reference for individualized treatment.

In addition to immunotherapy, we sought to determine the association between risk score and the effectiveness of common chemotherapeutic agents in managing UCEC. We found that the high-risk group had lower IC50 of etoposide and doxorubicin. This means that patients with high IRLPS might benefit from these two drugs. Apart from the conventional drugs, we also explored several promising small molecule agents such as imiquimod, fluphenazine, and cabozantinib which can interact with model IRLs. Imiquimod is an aminoquinoline immune modulator that induces interferon production and activates innate immune cells *via* TLR-7, and thus initiates apoptotic and autophagic cell death (67–69). Fluphenazine is a potent antipsychotic drug, dating back to its discovery in the 1950s, exerting its effect by blocking dopamine receptors (70). Cabozantinib is a tyrosine kinase inhibitor, known for inhibiting VEGFR, MET, and AXL, already in clinical use against multiple kinds of malignancies like hepatocellular carcinoma (71), sarcoma (72), and renal-cell carcinoma (73).

This research still has several limitations. First, the clinical and expression data we used for our research are mainly TCGA-based, and thus limited in sample size, patients race, and ethnicity, which should be validated in larger and localized sets of examples. Second, our analysis is based on our choosing of the algorithm, and although we spared no effort in tuning and optimization, there will still be a certain amount of bias in our model. Third, the link we observed between IRL transcription and TME is correlational, not causal. Further investigation *in vivo* is needed to confirm the interaction of IRLs with other components of TME.

CONCLUSION

In this study, we identified a novel inflammation-related subtype of UCEC. On the basis of five hub prognostic IRLs (HMGN3-AS1, LEMD1-AS1, AP000880.1, AC244517.1, and AC011466.1), a robust risk signature was created which could serve as an independent clinical factor for UCEC. Our nominated signature cannot only mirror the immune landscape and assess immunotherapy response for UCEC cases, but also provide valuable chemotherapeutic strategies for individualized treatment.

REFERENCES

1. Sorosky JL. Endometrial Cancer. *Obstet Gynecol* (2012) 120(2 Part 1):383–97. doi: 10.1097/AOG.0b013e3182605bf1

DATA AVAILABILITY STATEMENT

The original contributions presented in the study are included in the article/**Supplementary Material**. Further inquiries can be directed to the corresponding authors.

AUTHOR CONTRIBUTIONS

HZ and XT visualized the study and took part in the study design and performance. HG, JS, YC, and YW conducted the manuscript writing and bioinformatics analysis. All authors read and approved the final manuscript.

ACKNOWLEDGMENTS

We would like to thank the researchers and study participants for their contributions.

SUPPLEMENTARY MATERIAL

The Supplementary Material for this article can be found online at: <https://www.frontiersin.org/articles/10.3389/fonc.2022.923641/full#supplementary-material>

Supplementary Figure 1 | Class discovery *via* consensus clustering to assigned patients into two clusters. (A) Consensus index of clustering models with CDF for $k = 2-9$ (k means cluster count). (B) Consensus clustering matrix for $k = 2$. (C) Consensus clustering model with CDF for $k = 2-9$. (D) Relative change in area under the CDF curve for $k = 2-9$.

Supplementary Figure 2 | Multiple GSEA analysis was used to predict the potential functions and pathways involved in the clusters. (A) The enriched KEGG pathways involved in cluster 1. (B) The enriched KEGG pathways involved in cluster 2.

Supplementary Figure 3 | The coefficients of the 27 IRL signatures evaluated by multivariate Cox regression with LASSO.

Supplementary Figure 4 | Transcription of five IRLs involved in our risk signature. (A–E) The transcription level of (A) LEMD1-AS1, (B) HMGN3-AS1, (C) AP000880.1, (D) AC244517.1, and (E) AC011466.1, differs significantly between the groups. (F–J) RT-qPCR were conducted to validate this difference in clinical samples. The transcription level of IRLs (G) LEMD1-AS1 and (H) AP000880.1 differs significantly between normal and tumor samples.

Supplementary Figure 5 | PCA and alluvial plot are utilized to explore the distribution of patients into risk groups. (A–C) Principal components analysis between the groups in (A) training set, (B) testing set, and (C) the entire set. (D) Alluvial diagram of patients in risk-stratified groups distributed in different gene cluster and survival outcomes.

Supplementary Figure 6 | The transcription level of (A) M6A methylation related genes and (B–D) Mismatch repair genes in high-risk and low-risk group.

2. Sung H, Ferlay J, Siegel RL, Laversanne M, Soerjomataram I, Jemal A, et al. Global Cancer Statistics 2020: GLOBOCAN Estimates of Incidence and Mortality Worldwide for 36 Cancers in 185 Countries. *CA Cancer J Clin* (2021) 71(3):209–49. doi: 10.3322/caac.21660

3. Moiola CP, Lopez-Gil C, Cabrera S, Garcia A, Van Nyen T, Annibali D, et al. Patient-Derived Xenograft Models for Endometrial Cancer Research. *Int J Mol Sci* (2018) 19(8). doi: 10.3390/ijms19082431
4. Njoku K, Chiasserini D, Whetton AD, Crosbie EJ. Proteomic Biomarkers for the Detection of Endometrial Cancer. *Cancers (Basel)* (2019) 11(10). doi: 10.3390/cancers11101572
5. Coussens LM, Werb Z. Inflammation and Cancer. *Nature* (2002) 420 (6917):860–7. doi: 10.1038/nature01322
6. Turnquist C, Ryan BM, Horikawa I, Harris BT, Harris CC. Cytokine Storms in Cancer and COVID-19. *Cancer Cell* (2020) 38(5):598–601. doi: 10.1016/j.ccell.2020.09.019
7. Bulun SE, Yilmaz BD, Sison C, Miyazaki K, Bernardi L, Liu S, et al. Endometriosis. *Endocr Rev* (2019) 40(4):1048–79. doi: 10.1210/er.2018-00242
8. Nallasamy P, Chava S, Verma SS, Mishra S, Gorantla S, Coulter DW, et al. PD-L1, Inflammation, non-Coding RNAs, and Neuroblastoma: Immunology Perspective. *Semin Cancer Biol* (2018) 52(Pt 2):53–65. doi: 10.1016/j.semcancer.2017.11.009
9. Dong P, Xiong Y, Yue J, JBH S, Kobayashi N, Todo Y, et al. Exploring lncRNA-Mediated Regulatory Networks in Endometrial Cancer Cells and the Tumor Microenvironment: Advances and Challenges. *Cancers (Basel)* (2019) 11(2). doi: 10.3390/cancers11020234
10. Dong P, Xiong Y, Yue J, Xu D, Ihira K, Konno Y, et al. Long Noncoding RNA NEAT1 Drives Aggressive Endometrial Cancer Progression via miR-361-Regulated Networks Involving STAT3 and Tumor Microenvironment-Related Genes. *J Exp Clin Cancer Res* (2019) 38(1):295. doi: 10.1186/s13046-019-1306-9
11. Wang L, Zhao S, Mingxin YU. lncRNA NR2F1-AS1 is Involved in the Progression of Endometrial Cancer by Sponging miR-363 to Target SOX4. *Pharmazie* (2019) 74(5):295–300. doi: 10.1691/ph.2019.8905
12. Hu H, Wang Y, Ding X, He Y, Lu Z, Wu P, et al. Long non-Coding RNA XLOC_000647 Suppresses Progression of Pancreatic Cancer and Decreases Epithelial-Mesenchymal Transition-Induced Cell Invasion by Down-Regulating NLRP3. *Mol Cancer* (2018) 17(1):18. doi: 10.1186/s12943-018-0761-9
13. Liu B, Sun L, Liu Q, Gong C, Yao Y, Lv X, et al. A Cytoplasmic NF-kappaB Interacting Long Noncoding RNA Blocks IkappaB Phosphorylation and Suppresses Breast Cancer Metastasis. *Cancer Cell* (2015) 27(3):370–81. doi: 10.1016/j.ccell.2015.02.004
14. Talukdar S, Emdad L, Gogna R, Das SK, Fisher PB. Metabolic Control of Cancer Progression as Novel Targets for Therapy. *Adv Cancer Res* (2021) 152:103–77. doi: 10.1016/bs.acr.2021.06.002
15. Qin S, Mao Y, Wang H, Duan Y, Zhao L. The Interplay Between M6a Modification and Non-Coding RNA in Cancer Stemness Modulation: Mechanisms, Signaling Pathways, and Clinical Implications. *Int J Biol Sci* (2021) 17(11):2718–36. doi: 10.7150/ijbs.60641
16. Felix AS, Weissfeld J, Edwards R, Linkov F. Future Directions in the Field of Endometrial Cancer Research: The Need to Investigate the Tumor Microenvironment. *Eur J Gynaecol Oncol* (2010) 31(2):139–44.
17. Willvonseder B, Stogbauer F, Steiger K, Jesinghaus M, Kuhn PH, Brambs C, et al. The Immunologic Tumor Microenvironment in Endometrioid Endometrial Cancer in the Morphomolecular Context: Mutual Correlations and Prognostic Impact Depending on Molecular Alterations. *Cancer Immunol Immunother* (2021) 70(6):1679–89. doi: 10.1007/s00262-020-02813-3
18. Wilkerson MD, Hayes DN. ConsensusClusterPlus: A Class Discovery Tool With Confidence Assessments and Item Tracking. *Bioinformatics* (2010) 26 (12):1572–3. doi: 10.1093/bioinformatics/btq170
19. Subramanian A, Tamayo P, Mootha VK, Mukherjee S, Ebert BL, Gillette MA, et al. Gene Set Enrichment Analysis: A Knowledge-Based Approach for Interpreting Genome-Wide Expression Profiles. *Proc Natl Acad Sci USA* (2005) 102(43):15545–50. doi: 10.1073/pnas.0506580102
20. Mootha VK, Lindgren CM, Eriksson KF, Subramanian A, Sihag S, Lehar J, et al. PGC-1alpha-Responsive Genes Involved in Oxidative Phosphorylation are Coordinately Downregulated in Human Diabetes. *Nat Genet* (2003) 34 (3):267–73. doi: 10.1038/ng1180
21. Chen B, Khodadoust MS, Liu CL, Newman AM, Alizadeh AA. Profiling Tumor Infiltrating Immune Cells With CIBERSORT. *Methods Mol Biol* (2018) 1711:243–59. doi: 10.1007/978-1-4939-7493-1_12
22. Yoshihara K, Shahmoradgol M, Martinez E, Vegesna R, Kim H, Torres-Garcia W, et al. Inferring Tumour Purity and Stromal and Immune Cell Admixture From Expression Data. *Nat Commun* (2013) 4:2612. doi: 10.1038/ncomms3612
23. Hanzelmann S, Castelo R, Guinney J. GSEA: Gene Set Variation Analysis for Microarray and RNA-Seq Data. *BMC Bioinf* (2013) 14:7. doi: 10.1186/1471-2105-14-7
24. Tibshirani R. The Lasso Method for Variable Selection in the Cox Model. *Stat Med* (1997) 16(4):385–95. doi: 10.1002/(SICI)1097-0258(19970228)16:4<385::AID-SIM380>3.0.CO;2-3
25. Friedman J, Hastie T, Tibshirani R. Regularization Paths for Generalized Linear Models via Coordinate Descent. *J Stat Softw* (2010) 33(1):1–22. doi: 10.18637/jss.v033.i01
26. Saha-Chaudhuri P, Heagerty PJ. Non-Parametric Estimation of a Time-Dependent Predictive Accuracy Curve. *Biostatistics*. (2013) 14(1):42–59. doi: 10.1093/biostatistics/kxs021
27. Xiang M, Feng Y, Wang Y, Wang J, Zhang Z, Liang J, et al. Correlation Between Circulating Interleukin-18 Level and Systemic Lupus Erythematosus: A Meta-Analysis. *Sci Rep* (2021) 11(1):4707. doi: 10.1038/s41598-021-84170-4
28. Dai JJ, Lieu L, Locke D. Dimension Reduction for Classification With Gene Expression Microarray Data. *Stat Appl Genet Mol* (2006) 5. doi: 10.2202/1544-6115.1147
29. Liu TT, Li R, Huo C, Li JP, Yao J, Ji XL, et al. Identification of CDK2-Related Immune Forecast Model and ceRNA in Lung Adenocarcinoma, a Pan-Cancer Analysis. *Front Cell Dev Biol* (2021) 9:682002. doi: 10.3389/fcell.2021.682002
30. Mayakonda A, Lin DC, Assenov Y, Plass C, Koeffler HP. Maftools: Efficient and Comprehensive Analysis of Somatic Variants in Cancer. *Genome Res* (2018) 28(11):1747–56. doi: 10.1101/gr.239244.118
31. Yi L, Huang P, Zou X, Guo L, Gu Y, Wen C, et al. Integrative Stemness Characteristics Associated With Prognosis and the Immune Microenvironment in Esophageal Cancer. *Pharmacol Res* (2020) 161:105144. doi: 10.1016/j.phrs.2020.105144
32. Charoentong P, Finotello F, Angelova M, Mayer C, Efremova M, Rieder D, et al. Pan-Cancer Immunogenomic Analyses Reveal Genotype-Immunophenotype Relationships and Predictors of Response to Checkpoint Blockade. *Cell Rep* (2017) 18(1):248–62. doi: 10.1016/j.celrep.2016.12.019
33. Yang WJ, Soares J, Greninger P, Edelman EJ, Lightfoot H, Forbes S, et al. Genomics of Drug Sensitivity in Cancer (GDSC): A Resource for Therapeutic Biomarker Discovery in Cancer Cells. *Nucleic Acids Res* (2013) 41(D1):D955–61. doi: 10.1093/nar/gks111
34. Shankavaram UT, Varma S, Kane D, Sunshine M, Chary KK, Reinhold WC, et al. CellMiner: A Relational Database and Query Tool for the NCI-60 Cancer Cell Lines. *BMC Genomics* (2009) 10:277. doi: 10.1186/1471-2164-10-277
35. Reinhold WC, Sunshine M, Liu H, Varma S, Kohn KW, Morris J, et al. CellMiner: A Web-Based Suite of Genomic and Pharmacologic Tools to Explore Transcript and Drug Patterns in the NCI-60 Cell Line Set. *Cancer Res* (2012) 72(14):3499–511. doi: 10.1158/0008-5472.CAN-12-1370
36. Tabelow K, Clayden JD, de Micheaux PL, Polzehl J, Schmid VJ, Whitche B. Image Analysis and Statistical Inference in Neuroimaging With R. *Neuroimage*. (2011) 55(4):1686–93. doi: 10.1016/j.neuroimage.2011.01.013
37. Wang Z, Zhang J, Liu Y, Zhao R, Zhou X, Wang H. An Integrated Autophagy-Related Long Noncoding RNA Signature as a Prognostic Biomarker for Human Endometrial Cancer: A Bioinformatics-Based Approach. *BioMed Res Int* (2020) 2020:5717498. doi: 10.1155/2020/5717498
38. Tang H, Wu Z, Zhang Y, Xia T, Liu D, Cai J, et al. Identification and Function Analysis of a Five-Long Noncoding RNA Prognostic Signature for Endometrial Cancer Patients. *DNA Cell Biol* (2019) 38(12):1480–98. doi: 10.1089/dna.2019.4944
39. Vonderheide RH. CD40 Agonist Antibodies in Cancer Immunotherapy. *Annu Rev Med* (2020) 71:47–58. doi: 10.1146/annurev-med-062518-045435
40. Tekpli X, Lien T, Rossevoold AH, Nebdal D, Borgen E, Ohnstad HO, et al. An Independent Poor-Prognosis Subtype of Breast Cancer Defined by a Distinct Tumor Immune Microenvironment. *Nat Commun* (2019) 10(1):5499. doi: 10.1038/s41467-019-13329-5
41. Sun J, Zhang Z, Bao S, Yan C, Hou P, Wu N, et al. Identification of Tumor Immune Infiltration-Associated lncRNAs for Improving Prognosis and Immunotherapy Response of Patients With non-Small Cell Lung Cancer. *J Immunother Cancer* (2020) 8(1). doi: 10.1136/jitc-2019-000110
42. Malta TM, Sokolov A, Gentles AJ, Burzykowski T, Poisson L, Weinstein JN, et al. Machine Learning Identifies Stemness Features Associated With

- Oncogenic Dedifferentiation. *Cell* (2018) 173(2):338–54. doi: 10.1016/j.cell.2018.03.034
43. Zhao P, Li L, Jiang X, Li Q. Mismatch Repair Deficiency/Microsatellite Instability-High as a Predictor for Anti-PD-1/PD-L1 Immunotherapy Efficacy. *J Hematol Oncol* (2019) 12(1):54. doi: 10.1186/s13045-019-0738-1
 44. Lizardo DY, Kuang C, Hao S, Yu J, Huang Y, Zhang L. Immunotherapy Efficacy on Mismatch Repair-Deficient Colorectal Cancer: From Bench to Bedside. *Biochim Biophys Acta Rev Cancer* (2020) 1874(2):188447. doi: 10.1016/j.bbcan.2020.188447
 45. Brooks RA, Fleming GF, Lastra RR, Lee NK, Moroney JW, Son CH, et al. Current Recommendations and Recent Progress in Endometrial Cancer. *CA Cancer J Clin* (2019) 69(4):258–79. doi: 10.3322/caac.21561
 46. Jing X, Peng J, Dou Y, Sun J, Ma C, Wang Q, et al. Macrophage ERalpha Promoted Invasion of Endometrial Cancer Cell by mTOR/KIF5B-Mediated Epithelial to Mesenchymal Transition. *Immunol Cell Biol* (2019) 97(6):563–76. doi: 10.1111/imcb.12245
 47. De Nola R, Menga A, Castegna A, Loizzi V, Ranieri G, Cicinelli E, et al. The Crowded Crosstalk Between Cancer Cells and Stromal Microenvironment in Gynecological Malignancies: Biological Pathways and Therapeutic Implication. *Int J Mol Sci* (2019) 20(10). doi: 10.3390/ijms20102401
 48. Rizvi NA, Hellmann MD, Snyder A, Kvistborg P, Makarov V, Havel JJ, et al. Cancer Immunology. Mutational Landscape Determines Sensitivity to PD-1 Blockade in Non-Small Cell Lung Cancer. *Science* (2015) 348(6230):124–8. doi: 10.1126/science.aaa1348
 49. Liu J, Wang Y, Mei J, Nie S, Zhang Y. Identification of a Novel Immune Landscape Signature for Predicting Prognosis and Response of Endometrial Carcinoma to Immunotherapy and Chemotherapy. *Front Cell Dev Biol* (2021) 9:671736. doi: 10.3389/fcell.2021.671736
 50. Dou Y, Kawaler EA, Cui Zhou D, Gritsenko MA, Huang C, Blumenberg L, et al. Proteogenomic Characterization of Endometrial Carcinoma. *Cell* (2020) 180(4):729–48. doi: 10.1016/j.cell.2020.01.026
 51. Moroney MR, Woodruff E, Qamar L, Bradford AP, Wolsky R, Bitler BG, et al. Inhibiting Wnt/beta-Catenin in CTNNB1-Mutated Endometrial Cancer. *Mol Carcinog* (2021) 60(8):511–23. doi: 10.1002/mc.23308
 52. Chen JJ, Xiao ZJ, Meng X, Wang Y, Yu MK, Huang WQ, et al. MRP4 Sustains Wnt/beta-Catenin Signaling for Pregnancy, Endometriosis and Endometrial Cancer. *Theranostics* (2019) 9(17):5049–64. doi: 10.7150/thno.32097
 53. Ueda T, Furusawa T, Kurahashi T, Tessarollo L, Bustin M. The Nucleosome Binding Protein HMGN3 Modulates the Transcription Profile of Pancreatic Beta Cells and Affects Insulin Secretion. *Mol Cell Biol* (2009) 29(19):5264–76. doi: 10.1128/MCB.00526-09
 54. Koh M, Ahmad I, Ko Y, Zhang Y, Martinez TF, Diedrich JK, et al. A Short ORF-Encoded Transcriptional Regulator. *Proc Natl Acad Sci USA* (2021) 118(4). doi: 10.1073/pnas.2021943118
 55. Gaudet P, Livstone MS, Lewis SE, Thomas PD. Phylogenetic-Based Propagation of Functional Annotations Within the Gene Ontology Consortium. *Brief Bioinform* (2011) 12(5):449–62. doi: 10.1093/bib/bbr042
 56. Li Q, Ge Y, Chen X, Wang L, Xia Y, Xu Z, et al. LEM Domain Containing 1 Promotes Proliferation via Activating the PI3K/Akt Signaling Pathway in Gastric Cancer. *J Cell Biochem* (2019) 120(9):15190–201. doi: 10.1002/jcb.28783
 57. Yuki D, Lin YM, Fujii Y, Nakamura Y, Furukawa Y. Isolation of LEM Domain-Containing 1, a Novel Testis-Specific Gene Expressed in Colorectal Cancers. *Oncol Rep* (2004) 12(2):275–80. doi: 10.3892/or.12.2.275
 58. Ghafouri-Fard S, Ousati Ashtiani Z, Sabah Golian B, Hasheminasab SM, Modarressi MH. Expression of Two Testis-Specific Genes, SPATA19 and LEMD1, in Prostate Cancer. *Arch Med Res* (2010) 41(3):195–200. doi: 10.1016/j.arcmed.2010.04.003
 59. Wattanawaraporn R, Singhilarak T, Nuchprayoon I, Mutirangura A. Hypermethylation of TTC12 Gene in Acute Lymphoblastic Leukemia. *Leukemia* (2007) 21(11):2370–3. doi: 10.1038/sj.leu.2404876
 60. Chen C, Chio CL, Zeng H, Li Y. High Expression of CD56 may be Associated With Favorable Overall Survival in Intermediate-Risk Acute Myeloid Leukemia. *Hematology* (2021) 26(1):210–4. doi: 10.1080/16078454.2021.1880734
 61. Frank M, Kemler R. Protocadherins. *Curr Opin Cell Biol* (2002) 14(5):557–62. doi: 10.1016/s0955-0674(02)00365-4
 62. Linder A, Bauernfried S, Cheng Y, Albanese M, Jung C, Keppler OT, et al. CARD8 Inflammasome Activation Triggers Pyroptosis in Human T Cells. *EMBO J* (2020) 39(19):e105071. doi: 10.15252/embj.2020105071
 63. Grawunder U, Zimmer D, Fugmann S, Schwarz K, Lieber MR. DNA Ligase IV Is Essential for V(D)J Recombination and DNA Double-Strand Break Repair in Human Precursor Lymphocytes. *Mol Cell* (1998) 2(4):477–84. doi: 10.1016/s1097-2765(00)80147-1
 64. Bentley D, Selfridge J, Millar JK, Samuel K, Hole N, Ansell JD, et al. DNA Ligase I Is Required for Fetal Liver Erythropoiesis But Is Not Essential for Mammalian Cell Viability. *Nat Genet* (1996) 13(4):489–91. doi: 10.1038/ng0896-489
 65. Chen X, Ballin JD, Della-Maria J, Tsai MS, White EJ, Tomkinson AE, et al. IIIalpha, IIbeta, and IV Reveal Direct DNA Sensing Ability and Differential Physiological Functions in DNA Repair. *DNA Repair (Amst)* (2009) 8(8):961–8. doi: 10.1016/j.dnarep.2009.06.002
 66. Li D, Li R, Zhang J, Li K, Wu Y. Association Between the LIG1 Polymorphisms and Lung Cancer Risk: A Meta-Analysis of Case-Control Studies. *Cell Biochem Biophys* (2015) 73(2):381–7. doi: 10.1007/s12013-015-0619-3
 67. Hemmi H, Kaisho T, Takeuchi O, Sato S, Sanjo H, Hoshino K, et al. Small Anti-Viral Compounds Activate Immune Cells via the TLR7 MyD88-Dependent Signaling Pathway. *Nat Immunol* (2002) 3(2):196–200. doi: 10.1038/ni758
 68. Soong RS, Song L, Trieu J, Knoff J, He L, Tsai YC, et al. Toll-Like Receptor Agonist Imiquimod Facilitates Antigen-Specific CD8+ T-Cell Accumulation in the Genital Tract Leading to Tumor Control Through IFNgamma. *Clin Cancer Res* (2014) 20(21):5456–67. doi: 10.1158/1078-0432.CCR-14-0344
 69. Schon MP, Schon M. Imiquimod: Mode of Action. *Br J Dermatol* (2007) 157 Suppl 2:8–13. doi: 10.1111/j.1365-2133.2007.08265.x
 70. Matar HE, Almerie MQ, Sampson SJ. Fluphenazine (Oral) Versus Placebo for Schizophrenia. *Cochrane Database Syst Rev* (2018) 6:CD006352. doi: 10.1002/14651858.CD006352.pub3
 71. Abou-Alfa GK, Meyer T, Cheng AL, El-Khoueiry AB, Rimassa L, Ryoo BY, et al. Cabozantinib in Patients With Advanced and Progressing Hepatocellular Carcinoma. *N Engl J Med* (2018) 379(1):54–63. doi: 10.1056/NEJMoa1717002
 72. Schoffski P, Blay JY, Ray-Coquard I. Cabozantinib as an Emerging Treatment for Sarcoma. *Curr Opin Oncol* (2020) 32(4):321–31. doi: 10.1097/CCO.0000000000000644
 73. Choueiri TK, Escudier B, Powles T, Mainwaring PN, Rini BI, Donskov F, et al. Cabozantinib Versus Everolimus in Advanced Renal-Cell Carcinoma. *N Engl J Med* (2015) 373(19):1814–23. doi: 10.1056/NEJMoa1510016

Conflict of Interest: The authors declare that the research was conducted in the absence of any commercial or financial relationships that could be construed as a potential conflict of interest.

Publisher's Note: All claims expressed in this article are solely those of the authors and do not necessarily represent those of their affiliated organizations, or those of the publisher, the editors and the reviewers. Any product that may be evaluated in this article, or claim that may be made by its manufacturer, is not guaranteed or endorsed by the publisher.

Copyright © 2022 Gu, Song, Chen, Wang, Tan and Zhao. This is an open-access article distributed under the terms of the Creative Commons Attribution License (CC BY). The use, distribution or reproduction in other forums is permitted, provided the original author(s) and the copyright owner(s) are credited and that the original publication in this journal is cited, in accordance with accepted academic practice. No use, distribution or reproduction is permitted which does not comply with these terms.



Advances in the Application of Radionuclide-Labeled HER2 Affibody for the Diagnosis and Treatment of Ovarian Cancer

Xianwen Hu¹, Dandan Li², Yujie Fu³, Jiashen Zheng¹, Zelong Feng¹, Jiong Cai^{1*} and Pan Wang^{1*}

¹ Department of Nuclear Medicine, Affiliated Hospital of Zunyi Medical University, Zunyi, China, ² Department of Obstetrics, Zunyi Hospital of Traditional Chinese Medicine, Zunyi, China, ³ Research and Development Department, Jiangsu Yuanben Biotechnology Co., Ltd., Zunyi, China

OPEN ACCESS

Edited by:

Jinhui Liu,
Nanjing Medical University, China

Reviewed by:

Du Wangqi,
Wenzhou Medical University, China
Luca Falzone,
G. Pascale National Cancer Institute
Foundation (IRCCS), Italy

*Correspondence:

Jiong Cai
jiong_cai@163.com
Pan Wang
1298178828@qq.com

Specialty section:

This article was submitted to
Gynecological Oncology,
a section of the journal
Frontiers in Oncology

Received: 11 April 2022

Accepted: 20 May 2022

Published: 15 June 2022

Citation:

Hu X, Li D, Fu Y, Zheng J, Feng Z, Cai J
and Wang P (2022) Advances in the
Application of Radionuclide-Labeled
HER2 Affibody for the Diagnosis and
Treatment of Ovarian Cancer.
Front. Oncol. 12:917439.
doi: 10.3389/fonc.2022.917439

Human epidermal growth factor receptor 2 (HER2) is a highly expressed tumor marker in epithelial ovarian cancer, and its overexpression is considered to be a potential factor of poor prognosis. Therefore, monitoring the expression of HER2 receptor in tumor tissue provides favorable conditions for accurate localization, diagnosis, targeted therapy, and prognosis evaluation of cancer foci. Affibody has the advantages of high affinity, small molecular weight, and stable biochemical properties. The molecular probes of radionuclide-labeled HER2 affibody have recently shown broad application prospects in the diagnosis and treatment of ovarian cancer; the aim is to introduce radionuclides into the cancer foci, display systemic lesions, and kill tumor cells through the radioactivity of the radionuclides. This process seamlessly integrates the diagnosis and treatment of ovarian cancer. Current research and development of new molecular probes of radionuclide-labeled HER2 affibody should focus on overcoming the deficiencies of non-specific uptake in the kidney, bone marrow, liver, and gastrointestinal tract, and on reducing the background of the image to improve image quality. By modifying the amino acid sequence; changing the hydrophilicity, surface charge, and lipid solubility of the affibody molecule; and using different radionuclides, chelating agents, and labeling conditions to optimize the labeling method of molecular probes, the specific uptake of molecular probes at tumor sites will be improved, while reducing radioactive retention in non-target organs and obtaining the best target/non-target value. These measures will enable the clinical use of radionuclide-labeled HER2 affibody molecular probes as soon as possible, providing a new clinical path for tumor-specific diagnosis, targeted therapy, and efficacy evaluation. The purpose of this review is to describe the application of radionuclide-labeled HER2 affibody in the imaging and treatment of ovarian cancer, including its potential clinical value and dilemmas.

Keywords: human epidermal growth factor receptor, ovarian cancer, radionuclide, HER2 affibody, molecular probes

INTRODUCTION

Ovarian cancer is the disease with the highest mortality rate after cervical cancer secondary to female reproductive tract malignant tumors; in 2020, 313,959 new patients with ovarian cancer and 207,252 new deaths from ovarian cancer were reported worldwide. Although ovarian cancer is generally more common in developed countries, studies have shown an increasing incidence in China (1, 2). Several risk factors for ovarian cancer include genetics, reproduction, sex hormones, and lifestyle behaviors (3). Specifically, a family history of ovarian cancer in first- or second-degree relatives, polycystic ovary syndrome, endometriosis, gynecological inflammation, increased estrogen/androgen, high-fat diet, etc. are associated with a high risk of cancer. However, fertility, contraception including the intrauterine device and oral contraceptives, tubal ligation, and breastfeeding can reduce the risk of ovarian cancer (4–14). Ovarian cancer has an insidious onset and lacks specific clinical symptoms in the early stage, and the clinical diagnostic process is relatively unsatisfactory. Approximately 60% of patients with ovarian cancer are in the advanced stage of the disease by the time symptoms are recognized or medical help is sought. Therefore, the prognosis of patients is poor, with a 5-year survival rate of less than 30% (15, 16).

OVERVIEW OF HER2 AND AFFIBODY

Human epidermal growth factor receptor 2 (HER2), also known as receptor tyrosine protein kinase erbB-2, is a member of the epidermal growth factor receptor family (17). The oncogenic mechanisms of HER2 include inhibiting tumor cell apoptosis, increasing tumor cell invasiveness, promoting tumor cell proliferation, and promoting tumor angiogenesis and lymphangiogenesis (18). HER2 is rarely expressed in normal ovarian epithelial cells, but is highly positive in epithelial ovarian cancers, including 45.5% of mucinous carcinomas, 41.7% of clear cell carcinomas, and 17.5% of serous carcinomas (19). Studies confirmed that the positive expression of HER2 is significantly correlated with patient prognosis (20, 21). Therefore, it is significantly important to obtain HER2-positive expression accurately and effectively for the precise diagnosis and targeted therapy of HER2-positive ovarian cancer.

The use of multiple methods to detect the presence of relevant mutations in tumor specimens and the optimal targets of targeted therapy, which are useful for prognosis and treatment, is the best strategy to strengthen and improve patients with ovarian cancer (22–24). Clinically, the state of HER2 expression is often determined by immunohistochemistry (IHC) and nucleic acid fluorescence *in situ* hybridization (FISH) on biopsy tissue (25). IHC uses the principle of specific binding of antigen and antibody, and determines the antigen in tissue cells through a chemical reaction to develop the color of the chromogenic reagent labeled with the antibody. However, the stability of this method is poor, and various technical variables, different antibody sensitivities, and resulting evaluation systems

during the operation may affect the test results (26). FISH is a molecular cytogenetic technique that uses fluorescent probes that bind only to parts of chromosomes with a high degree of sequence complementarity. DNA is analyzed under the microscope by fluorescence detection (25, 26). By using gene-specific DNA probes to determine the copy number of the HER2 gene, the detection results are reliable due to the relative stability of the DNA; however, this method is expensive and technically complicated. Furthermore, the expression of the protein is regulated by many factors; therefore, the HER2 gene is regulated by many factors and the amplification of the HER2 gene is not always consistent with the overexpression of protein (27, 28). In addition, both IHC and FISH are invasive tests, which only reflect the local situation of the biopsy tissue. These tests cannot reflect the HER2 expression of the tumor as a whole and other metastases. Hillig et al. showed that the misdiagnosis rate of HER2 expression measured by IHC or FISH is 20% (29). Single photon emission computed tomography (SPECT) and positron emission tomography (PET) imaging can obtain functional information about the organization of biological chemistry. Advantages of these methods include noninvasiveness, accuracy, and safety. become one of the hot spot of the HER2 receptor positive tumors. The positive rate of HER2 expression in ovarian cancer is low. Although the nuclear medicine molecular probe targeting the HER2 receptor is not suitable for the screening and diagnosis of ovarian cancer directly, it can be used as an important complementary means to IHC or FISH. This method can obtain a general expression of HER2 positive, including primary tumor location, the extent of the tumor invasion into the surrounding tissue, and the detection of metastasis sites. In addition, targeting the HER2 receptor helps clinicians monitor the efficacy of HER2-targeted therapy in patients and facilitates stratified patient studies, laying a solid foundation for the integration of ovarian cancer diagnosis and treatment.

Affibody is an artificial protein molecule with a single-chain structure, and is a new type of protein ligand that evolved from the B segment of the immunoglobulin binding region of *Staphylococcus* protein A, with a relative molecular weight of 6.5 kDa. Affibody has the ability to bind to other proteins (30). SPA is a cell wall protein of type A *Staphylococcus aureus*, containing 7 domains (S, E, D, A, B, C, and X), among which the B domain contains 58 amino acid residues and is the main functional fragment that mediates the binding of SPA to the FC segment of IgG (except IgG3) (31). These amino acid defects constitute three α -helix structures. In 1995, to improve the chemical stability of the affinity body, the Swedish scholar Nord et al. replaced the 29th glycine of the B domain with alanine and renamed it as the Z domain (32). The amino acids at 13 positions in the first and second helices of the Z domain are Q9 (glutamine), Q10 (glutamine), N11 (asparagine), F13 (benzene), Y14 (tyrosine), L17 (leucine), and H18 (histidine) of the first α -helix, and (alanine), E24 (glutamic acid), E25 (glutamic acid), R27 (arginine), N28 (asparagine), Q32 (glutamine), and K35 (lysine) of the second α -helix, which have no obvious effect on the higher-order structure of the Z

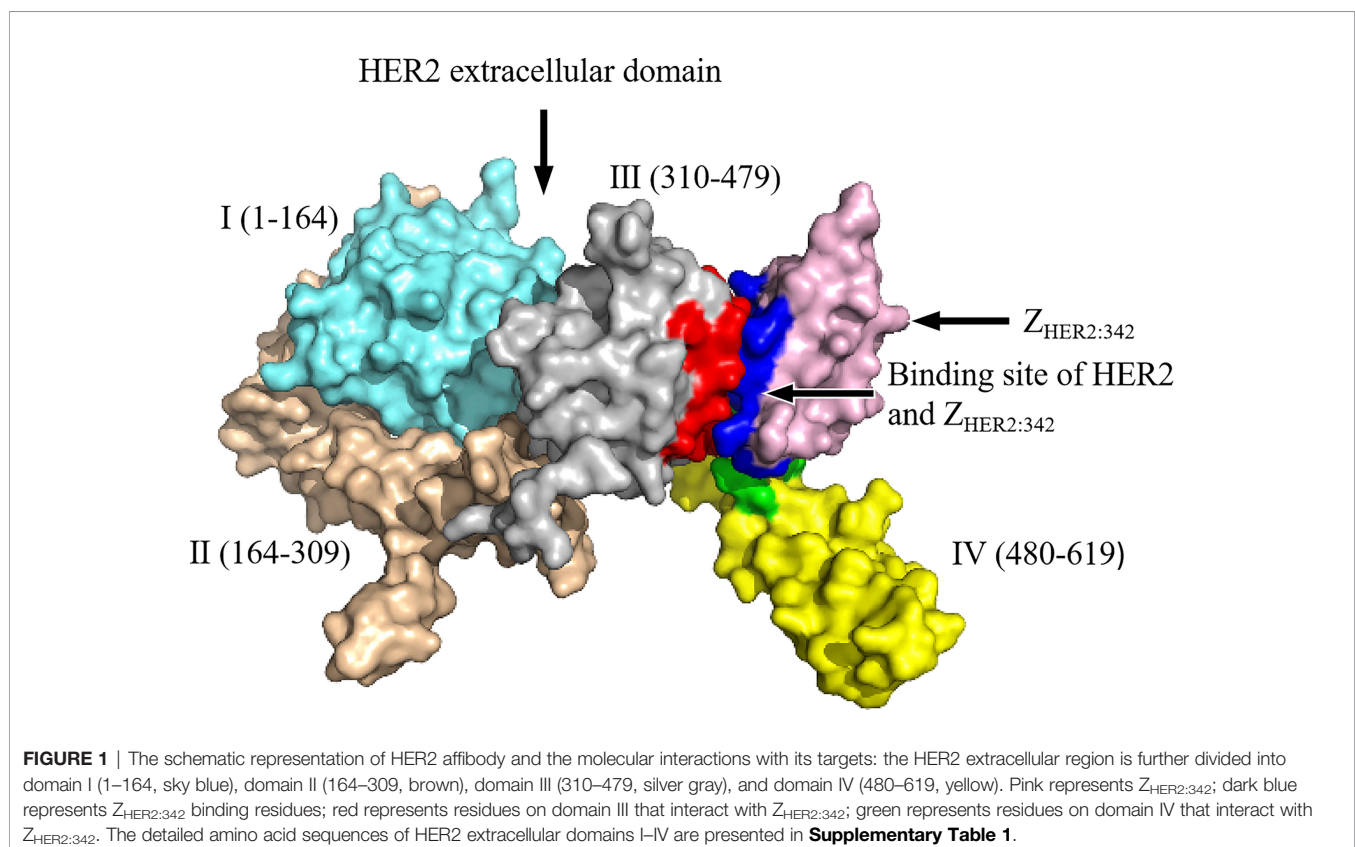
domain. The Z domain retains the binding function of the Fc segment (33). Random replacement of these 13 amino acid codons with degenerate codon NNK (K = G, Guanylate or T, Thymine, including 32 codons and 20 amino acids) can theoretically generate 3,213 gene sequences and 2,013 amino acid sequences; these constitute the affibody library. The affibody library can basically be combined with any protein molecule, and the affinity body of a certain protein molecule can be obtained after screening (32, 34). In addition to HER2, a variety of proteins such as fibrinogen, transferrin, tumor necrosis factor Q, interleukin-8, CD28, human serum albumin, IgA, IgE, IgM, and epidermal growth factor receptor (EGFR) have been discovered, and their affinity is in the range of $\mu\text{mol/L}$ to pmol/L according to the characteristics of the bound proteins and the structure of the affibody (35). Due to the small size and high affinity of HER2 affibody that can specifically bind to HER2 receptor both *in vitro* and *in vivo*, rapid clearance from blood and non-targeted tissues, ease of structural modification, and selectivity for cancer-related targets, this affibody is suitable as a radionuclide molecular probe and has excellent potential for use in the diagnosis and treatment of cancer (36–41). The schematic representation of the HER2 affibody and its interaction with the target molecule, HER2, is shown in **Figure 1**.

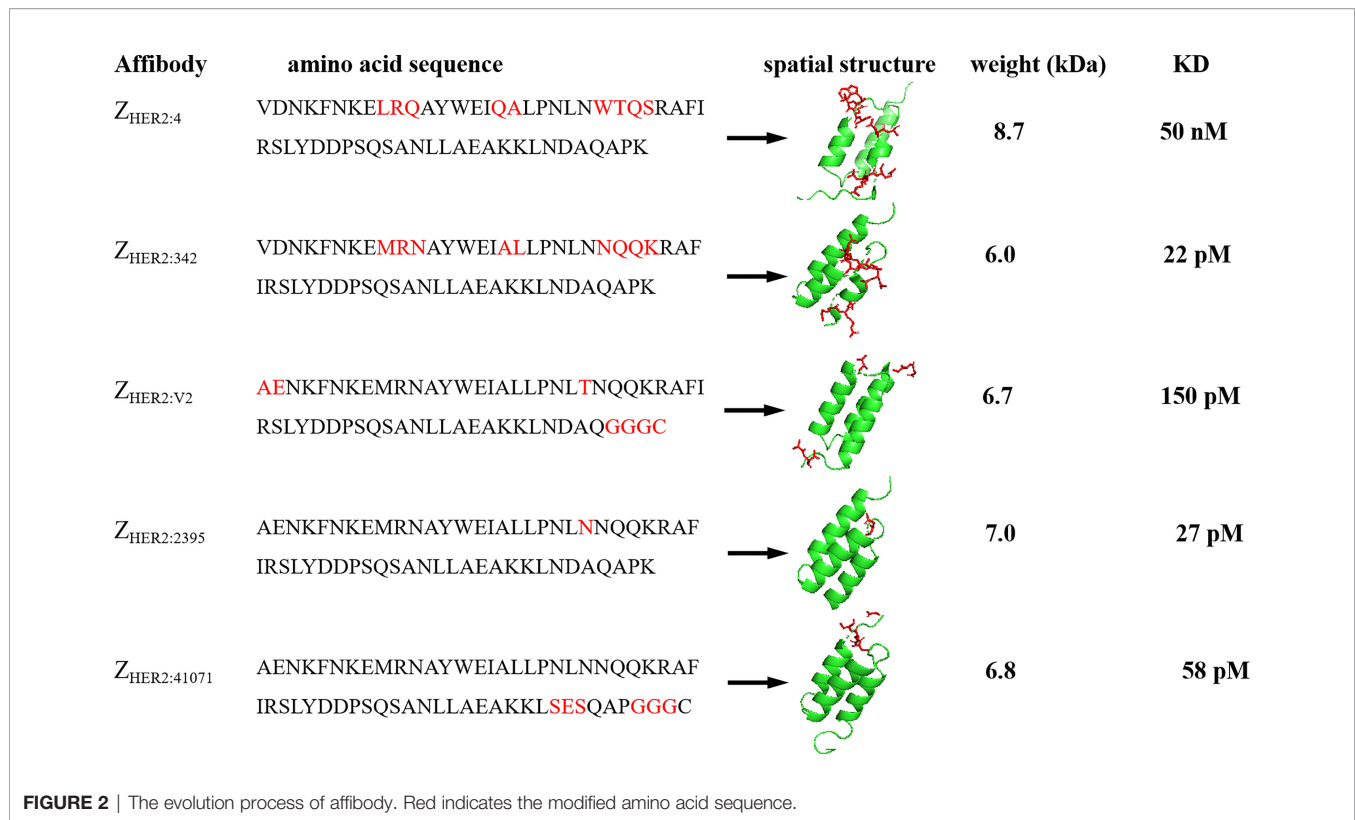
The first-generation HER2 affibody $Z_{\text{HER2:4}}$ has a low affinity; therefore, researchers combined its head and tail to form a dimer ($Z_{\text{HER2:4}}$)₂, and its dissociation equilibrium constant K_D value changed from the original 50 nM to 3 nM, leading to obvious

improvement in its affinity (42, 43). The second-generation HER2 affibody is mainly $Z_{\text{HER2:342}}$, which has a triple-helix structure through modification of the first generation; its affinity is 2,200 times that of the first generation (44). The third-generation affibody is mainly $Z_{\text{HER2:2395}}$, which is made by introducing a cysteine at the carboxy terminus of $Z_{\text{HER2:342}}$ to obtain a unique attachment site, using bifunctional chelators, linking molecules or other thiol-reactive carriers, such as maleimide or iodoacetamide, which can be directionally coupled to this particular cysteine. $Z_{\text{HER2:2395}}$ has an affinity of approximately 27 pM, which is comparable to that of the second generation (45, 46). A recent study reported the replacement of the -NDA-sequence near the C segment of the affibody $Z_{\text{HER2:2395}}$ with the -SES-sequence, which further improved the stability and hydrophilicity of the affibody, resulting in an affinity that is close to $Z_{\text{HER2:2395}}$ (47). The detailed evolution process of the affibody is shown in **Figure 2**.

OVERVIEW OF RADIONUCLIDE-LABELLED HER2 AFFIBODY MOLECULAR PROBES

Molecular probes targeting HER2 affibody can evaluate the expression status of tumor HER2 receptors and predict early efficacy after treatment, and significant progress has been made in the research on the integration of tumor diagnosis and treatment. The main applications of radionuclide-labeled HER2 molecular probes are summarized in **Table 1**.





HER2 Affibody Molecular Probes as SPECT Tracers

[¹¹¹In]: Indium-111 (¹¹¹In) is a pure γ -ray emitter with a half-life of 2.81 days, making it an ideal radionuclide tracer for SPECT imaging. Benzyl-dtpa,-CHX-A³-DTPA (diethylenetriaminepentaacetic acid) and DOTA (1,4,7,10-tetraazacyclodecane-*N,N,N,N*-tetra acetic acid) have been

used as chelating agents for affibody Z_{HER2:342}. When labeled with ¹¹¹In, which showed a good labeling yield (>95%) and a high affinity (21–65 pM), the molecular probe with specific uptake by the SKOV3 ovarian cancer xenograft tumor tissues with high HER2 receptor expression showed high tumor targeting binding properties (48–52). Unfortunately, in addition to tumor uptake of these molecular probes, renal

TABLE 1 | Overview of the major applications of radionuclide-labeled HER2 affibody molecular probes.

Radioisotope	T1/2	Diagnostic/therapy	Representative molecular probes	Study object	First posted	Phase	References
¹¹¹ In	2.81 days	SPECT	¹¹¹ In-ABY-002	Ovarian cancer	05/2006	Preclinical	(48–52)
			¹¹¹ In-DOTA-Z _{HER2:342}	Breast cancer	07/2007	I	(53)
^{99m} Tc	6.02 h	SPECT	¹¹¹ In-Z _{HER2:2395}	Ovarian cancer	08/2008	Preclinical	(49)
			^{99m} Tc-Z _{HER2:342}	Prostate cancer	05/2012	Preclinical	(54)
			^{99m} Tc-Z _{HER2:V2}	Ovarian cancer	12/2006	Preclinical	(55–59)
				Lung cancer	11/2018	Preclinical	(60, 61)
				Ovarian cancer	02/2011	Preclinical	(62, 63)
¹²⁵ I	60 days	SPECT/therapy	^{99m} Tc-Z _{HER2:41071}	Ovarian cancer	03/2021	Preclinical	(47)
			^{99m} Tc-ABH2	Breast cancer	06/2018	I	(64)
			¹²⁵ I-Z _{HER2:4}	Ovarian cancer	06/2005	Preclinical	(42, 43)
¹⁸ F	109.8 min	PET	¹²⁵ I-IPEM-Z _{HER2:2395}	Ovarian cancer	01/2015	Preclinical	(65)
			¹⁸ F-Z _{HER2:342}	Breast cancer	06/2012	Preclinical	(66)
⁶⁸ Ga	68 min	PET		Ovarian cancer	12/2007	Preclinical	(67, 68)
			⁶⁸ Ga-DOTA-MUT-DS	Ovarian cancer	08/2009	Preclinical	(69)
			⁶⁸ Ga-ABY-002	Breast cancer	07/2007	I	(53)
⁶⁴ Cu	12.7 h	PET/therapy	⁶⁸ Ga-ABY-025	Breast cancer	05/2013	I/II	(70, 71)
			⁶⁴ Cu-Z _{HER2:342}	Ovarian cancer	10/2019	Preclinical	(72)
¹⁸⁸ Re	17 h	Therapy	¹⁸⁸ Re-Z _{HER2:V2}	Ovarian cancer	10/2014	Preclinical	(73, 74)
¹⁷⁷ Lu	6.7 days	Therapy	¹⁷⁷ Lu-Z _{HER2:342}	Ovarian cancer	03/2007	Preclinical	(75)

uptake is also high, increasing the potential for renal toxicity. Based on this disadvantage, Honarvar et al. (76) designed a 15-mer HP1 PNA recognition tag and a complementary HP2 hybridization probe ^{111}In -Z_{HER2:342}-SR-HP1 to reduce the uptake of the molecular probe in the kidney. Moreover, a number of studies have used DOTA as a chelating agent to bind to the affibodies Z_{HER2:342min}, Z_{HER2:2395}, and Z_{HER2:2395}-Cys, and then labeled with the radionuclide ^{111}In . This method shows good potential for targeted imaging (77–80). However, one disadvantage of using DOTA as a chelator is that the liver uptake is relatively high. Researchers then compared the results of using DOTAGA (2-[1,4,7,10-Tetraazacyclododecane-4,7,10-tris(t-butyl acetate)]-pentanedioic acid-1t-butyl ester) instead of DOTA as a chelator, and found that the change improved the biodistribution of molecular probes *in vivo*, reducing uptake by the liver (81).

[$^{99\text{m}}\text{Tc}$]: Technetium-99m ($^{99\text{m}}\text{Tc}$) emits γ -rays of 140 keV and has a half-life of 6.02 h. It can be obtained by the ^{99}Mo - $^{99\text{m}}\text{Tc}$ generator and is inexpensive; therefore, it is widely used in clinical and basic research. An early study used the indirect labeling method to add chelating agent maGGG (mercaptoacetyl-glycyl-glycyl-glycyl) to the N-terminal of the affibody Z_{HER2:342}, and successfully labeled affibody Z_{HER2:342} with $^{99\text{m}}\text{Tc}$. The researchers further completed a series of *in vivo* biodistribution and imaging studies, and the results showed that the molecular probe was specifically absorbed by SKOV3 ovarian cancer xenograft tumor with high expression of the HER2 receptor and high targeting ability (79). However, the liver and gastrointestinal tract uptake of this molecular probe is high, thus affecting the detection rate of abdominal lesions. Subsequently, the research team replaced the chelating agent maGGG with maGSG (mercaptoacetyl-glycyl-seryl-glycyl), maG(D-S)G (mercaptoacetyl-glycyl-D-seryl-glycyl), and maSSS (mercaptoacetyl-seryl-seryl-seryl), respectively, and labeled it with $^{99\text{m}}\text{Tc}$. Results showed that when the glycine residue in the chelating agent maSSS was replaced with a hydrophilic serine amino group, the hydrophilic activity of the chelating agent maGGG was increased. Therefore, the uptake of the molecular probe in the liver and gastrointestinal tract was significantly reduced, resulting in a significant increase in the detection rate of abdominal tumor lesions. However, the excretion route was shifted from the liver to the kidney, increasing the potential for kidney toxicity (80). To overcome this shortcoming, the team further optimized the study design and compared the $^{99\text{m}}\text{Tc}$ labeling studies using maGEG (mercaptoacetyl-Gly-Glu-Gly), maEEE (Mercaptoacetyl-Glu-Glu-Glu), maESE (mercaptoacetyl-glutamyl-seryl-glutamyl), maEES (mercaptoacetyl-glutamyl-glutamyl-seryl), maSEE (mercaptoacetyl-seryl-glutamyl-glutamyl), maSKS (mercaptoacetyl-seryl-lysyl-seryl), and maKKK (mercaptoacetyl-trilysyl) as chelators. The results showed that the use of the molecular probes $^{99\text{m}}\text{Tc}$ -maEEE-Z_{HER2:342}, $^{99\text{m}}\text{Tc}$ -maSKS-Z_{HER2:342}, and $^{99\text{m}}\text{Tc}$ -maESE-Z_{HER2:342} with maEEE, maSKS, and maESE as chelators significantly reduced the radioactive uptake in the kidney. In addition, the radioactive uptake of $^{99\text{m}}\text{Tc}$ -maESE-Z_{HER2:342} was found to be the most obvious, further improving the abdominal image quality (55, 56, 81).

Furthermore, other studies introduced a chelating agent at the C-terminus or/and N-terminus of the affibody Z_{HER2:342} for $^{99\text{m}}\text{Tc}$ labeling, and obtained molecular probes $^{99\text{m}}\text{Tc}$ -(HE)₃-Z_{HER2:342}-GGGC, $^{99\text{m}}\text{Tc}$ -Z_{HER2:342}-GGGC, $^{99\text{m}}\text{Tc}$ -Z_{HER2:V2}, etc. The researchers performed *in vivo* biodistribution and imaging studies, and results showed that these molecular probes are stable *in vitro* and *in vivo*, with high specificity and high targeting (82–84).

[^{123}I / ^{125}I]: Iodine-123 (^{123}I) has a half-life of 13.3 h and can emit 159 keV γ rays, which is suitable for SPECT imaging. ^{125}I has a long half-life (59.4 days) and is a convenient replacement nuclide usually used in the development of radioactive iodination technology instead of ^{123}I and ^{124}I (85). An early study used ^{125}I labeling for the affibody (Z_{HER2:4})₂, but SPECT imaging showed high radioactivity retention in the kidney and liver in addition to tumor uptake. This resulted in substandard image quality (86). To address the prevention of affibody destruction by radionuclides upon labeling, further studies were performed with iodobenzoate (PIB) and [4-isothiocyanate-amino]-undecahydro-o-dodecaborate (DABI) as chelators to label affibody molecule Z_{HER2:342} with ^{125}I , and molecular probes ^{125}I -PIB-Z_{HER2:342} and ^{125}I -DABI-Z_{HER2:342} were prepared. Results showed that ^{125}I -PIB-Z_{HER2:342} expressed high contrast imaging and low renal radioretenion of HER2 in the mice bearing SKOV-3 xenografts; however, a disadvantage was that the molecular probe did not bind specifically to the tumor (44, 87). Subsequently, the team used HPEM(4-hydroxyphenyl-ethyl-maleimide) as a chelating agent to design and synthesize the molecular probe ^{131}I / ^{125}I -HPEM-Z_{HER2:342}-C. Compared with the previous molecular probe ^{125}I -PIB-Z_{HER2:342}, HPEM provided a site-specific conjugate for indirect radioiodination of cysteine-containing affibody Z_{HER2:342}, and preserved the specificity of binding to HER2-expressing cells (88). Several studies have shown that the labeling strategy of using HPEM as a chelator further reduces renal uptake, but increases hepatobiliary and gastric uptake; thus, this strategy is detrimental to the detection of abdominal metastases (85, 87, 88). To solve this problem, the HEHEHE sequence was recently introduced into the amino terminal of the affibody, and the molecular probe ^{125}I -PIB-(HE)₃-G₃ was prepared by using PIB as a chelating agent. This process reduces the radioactive retention of the liver and kidney while maintaining the highly specific binding of tumor cells, and enables the obtainment of high contrast imaging of tumors expressing HER2 receptor *in vivo* (89).

HER2 Affibody Molecular Probes as PET Tracers

PET can provide molecular information such as function and metabolism, and has important clinical value in early diagnosis, staging and restaging of tumors, finding primary tumor or metastases, guiding tumor treatment, evaluating treatment efficacy, and predicting recurrence (90). Compared with SPECT imaging, PET imaging has the advantages of high spatial resolution, good sensitivity, and quantification (91). The radionuclide fluorine-18 (^{18}F), gallium-68 (^{68}Ga), copper-64

(^{64}Cu), rhenium-186/188 ($^{186/188}\text{Re}$), and other labeled HER2 affibodies have been used in preclinical research on ovarian cancer, showing good prospects for clinical application (54, 67, 68, 78, 92–97).

[^{18}F]: The half-life of ^{18}F is 109.8 min, and the positron energy produced by ^{18}F is low (average of 0.25 MeV). Its annihilation distance in tissues is short (approximately 2.4 mm), which enables the obtainment of high-resolution images. Therefore, ^{18}F is considered as the most ideal nuclide for PET imaging. An early study used FBO (N-[4-fluorobenzylidene]oxime) as a chelating agent to label the affibody $\text{Z}_{\text{HER2}:477}$ to obtain the molecular probe ^{18}F -FBO- $\text{Z}_{\text{HER2}:477}$. The results of animal PET imaging showed that the molecular probe can specifically bind to the HER2 receptor *in vitro* and *in vivo*, and obvious radionuclide uptake can be seen in the SKOV3 tumor tissue. However, due to the large amount of radioactive retention in the liver and kidney, the molecular probe is not clinically applicable (94). Kramer-Marek et al. used N-[2-(4-fluoro-benzamido)ethyl] maleimide (FBEM) as a chelating agent to prepare the molecular probe ^{18}F -FBEM- $\text{Z}_{\text{HER2}:342}$, and animal PET imaging results showed that the molecular probe had high radiation uptake and high image contrast in mice bearing SKBR3 and SKOV-3 xenografts with high HER2 expression, but no obvious uptake in mice bearing MDA-MB-468 xenografts with low HER2 expression. However, the high radioactive uptake in the kidney and bone also limits its clinical application (67). Recently, researchers have used FET (fluoroethyl-L-tyrosine) as a linker to prepare a molecular probe [^{18}F]FET- $\text{Z}_{\text{HER2}:342}$, and a preclinical study has shown that the molecular probe specifically binds to tumors and has a lower radioactive uptake in the liver. Unfortunately, its radiochemical yield is relatively low (68). Moreover, different methods of ^{18}F labeling for $\text{Z}_{\text{HER2}:2395}$ and $\text{Z}_{\text{HER2}:2891}$ have been reported, but their clinical transformation has been hindered by a large amount of radioactive retention in the kidney or the complex manufacturing process and low yield of molecular probes (62, 63, 73).

[^{68}Ga]: The half-life of ^{68}Ga is 68 min, and the positron decay rate is 89%. ^{68}Ga can be prepared by a ^{68}Ge - ^{68}Ga generator. It is suitable for labeling small molecules that can rapidly distribute *in vivo* and reach the target, and high-quality images can be obtained approximately 1 h after intravenous injection. An early animal study of PET imaging used DOTA as a chelating agent to label the HER2 affibody $\text{Z}_{\text{HER2}:342}$ and the small-molecule protein MUT-DS of HER2, respectively, with ^{68}Ga (69). The results showed that the tumor tissue with high expression of HER2 receptor showed obvious radionuclide aggregation, which was quickly cleared in the blood, with low background and high image quality. However, the disadvantage was that there was also a high radioactive uptake in the kidney. Recently, a number of studies have successively used DOTA, NOTA (1,4,7-triazacyclononane-*N,N,N*-triacetic acid), and NODAGA [1-(1,3-carboxypropyl)-4,7-carboxymethyl-1,4,7-triazacyclononane] as chelating agents to label the affibodies $\text{Z}_{\text{HER2}:51}$, $\text{Z}_{\text{HER2}:2395}$, and $\text{Z}_{\text{HER2}:2891}$, respectively, and performed molecular probe research *in vivo* and *in vitro*. The results showed

that NODAGA as a chelator for ^{68}Ga -labeled synthesis of molecular probes provided the best tumor-to-organ ratio, and was the best chelator for ^{68}Ga -labeled HER2 affibody, indicating excellent prospects for clinical application (81, 92, 93).

[^{64}Cu]: ^{64}Cu can simultaneously release β^- with a maximum energy of 580 keV and β^+ with a maximum energy of 656 keV, which can be used for PET imaging and radionuclide therapy. The half-life of ^{64}Cu is 12.7 h, and it can be produced by nuclear reactors and medical accelerators (98, 99). Researchers first used DOTA as a chelating agent to label the affibody $\text{Z}_{\text{HER2}:477}$ with ^{64}Cu and performed PET imaging studies in tumor-bearing nude mice with high HER2 receptor expression. The results showed that the molecular probe can be significantly taken up by tumor tissue. However, the disadvantage is that there is also a large amount of aggregation in the liver and kidney, and the uptake of radioactivity in liver and kidney is significantly higher than that in tumor tissue, thus affecting the detection of abdominal lesions (100). Subsequently, the research team further introduced cysteine into different positions of the affibody $\text{Z}_{\text{HER2}:342}$ for ^{64}Cu labeling to prepare molecular probes ^{64}Cu -DOTA-Cys- $\text{Z}_{\text{HER2}:342}$, ^{64}Cu -DOTA- $\text{Z}_{\text{HER2}:342}$ (Cys39), and ^{64}Cu -DOTA- $\text{Z}_{\text{HER2}:342}$ -Cys. All three probes showed good affinity and stability in *in vitro* studies, and ^{64}Cu -DOTA-Cys- $\text{Z}_{\text{HER2}:342}$ had the highest affinity and *in vivo* stability. However, the problem of high renal radioactivity retention remained unresolved (72). In addition, some researchers conducted *in vitro* and *in vivo* studies and compared the use of NOTA and NODAGA as chelators for ^{64}Cu labeling of affibodies. The results showed that the tumor-to-organ ratio was higher when NODAGA was used as a chelator than when NOTA was used as a chelator. The disadvantage was that the molecular probes had higher radioactive retention in the kidney and bone marrow (101). Therefore, research of ^{64}Cu -labeled HER2 affibody molecular probe needs to be further optimized and perfected.

[$^{186/188}\text{Re}$]: The two isotopes of rhenium, ^{186}Re and ^{188}Re , can simultaneously emit γ rays and β rays, enabling their use for both imaging and therapy. ^{186}Re is produced by the reactor and has a half-life of 3.72 days. ^{186}Re can emit β rays with a maximum energy of 1.08 MeV and γ rays with an energy of 155 keV at a time. ^{188}Re has a half-life of 17.0 h, can be produced by a $^{188}\text{W}/^{188}\text{Re}$ generator, and can emit β rays with a maximum energy of 2.1 MeV and γ rays with an energy of 137 keV. Orlova et al. (102) first used maGGG and maGSG as chelators to label affibody $\text{Z}_{\text{HER2}:342}$ with ^{186}Re and compared the resulting molecular probe with the $^{99\text{m}}\text{Tc}$ -labeled molecular probe. The results showed that the molecular probe ^{186}Re -maGSG- $\text{Z}_{\text{HER2}:342}$ showed obvious radioactive uptake in the tumors of mice bearing SKOV3 xenografts at 4 h after injection. Compared with the $^{99\text{m}}\text{Tc}$ -labeled molecular probe, the ^{186}Re -labeled molecular imaging probe significantly reduces the renal uptake; its renal uptake is only 1/4 of the $^{99\text{m}}\text{Tc}$ -labeled molecular probe. However, the excretion of molecular probes through the hepatobiliary tract leads to relatively high uptake in the liver, which may affect the detection of liver lesions. Subsequently, the same research team attached different amino acid sequences to the carboxy-terminus to label the affibodies with ^{188}Re and

compared them *in vitro* and *in vivo*. The results showed that the uptake of the molecular probe $^{188}\text{Re-Z}_{\text{HER2:V2}}$ with GGGC sequence linked to the carboxyl terminus was significantly higher than that of any organ tissue (including liver and kidney) at 4 h after injection. Furthermore, the uptake of the kidney was 5 times lower than that of the tumor, indicating that this molecular probe is a promising candidate for imaging and treatment of tumors with high expression of HER2 receptor (73, 74).

In addition, preclinical studies of PET molecular probes labeled to HER2 affibody by radionuclides such as astatine-211 (^{211}At), scandium-44 (^{44}Sc), zirconium-89 (^{89}Zr), and carbon-11 (^{11}C) through different chelating agents in SKOV3 ovarian tumors with high HER2 expression have also been reported in the literature, and the results show good potential for clinical application (103–106).

Radionuclide-Labeled HER2 Affibody as Targeted Therapeutic Probes

Ovarian cancer is traditionally treated with radical tumor resection and platinum-paclitaxel chemotherapy. Most tumors eventually become resistant to cytotoxic chemotherapy, leading to disease recurrence and progression (107). Recent studies have shown significant efficacy of poly (ADP-ribose) polymerase (PARP) inhibitors in patients with epithelial ovarian cancer, especially in patients with germline breast-related cancer antigens 1 and 2 (BRCA1/2) mutations. However, its clinical application value in patients without BRCA1/2 mutation remains controversial (108–110). The HER2 proto-oncogene is closely related to the occurrence of epithelial ovarian cancer; therefore, it provides an ideal target for the treatment of ovarian cancer. Trastuzumab, pertuzumab, olaparib, and lapatinib are widely approved by the Food and Drug Administration (FDA) for the treatment of HER2-positive cancers. However, clinical studies have shown that HER2-positive cancers are prone to become resistant to trastuzumab and pertuzumab; resistance mainly involves crosstalk with heterologous receptors, amplification, and the destruction of binding sites to HER2 receptors (111, 112), which may be related to the abnormal activation of the PI3K-Akt signaling pathway leading to PI3KCA mutation, phosphatase, and tensin homologue loss (113–115). It is estimated that approximately half of patients with HER2-positive metastatic breast cancer do not respond to trastuzumab (116). Lapatinib has shown positive efficacy in patients with HER2-positive ovarian cancer, but its efficacy in patients with ovarian cancer is only 22% to 30% (117, 118). Therefore, many researchers have recently focused on finding new methods and approaches for the comprehensive treatment of ovarian cancer through radioimmunotherapy. To date, many studies have focused on the targeted therapy of a variety of radionuclide-labeled HER2 affibody, including lutetium-177 (^{177}Lu), ^{64}Cu , and yttrium-90 (^{90}Y). Nevertheless, studies have shown that molecular probes of the radionuclide ^{64}Cu and ^{90}Y -labeled HER2 affibody need to be further optimized due to higher radioactive uptake in kidney or bone marrow and longer retention time (100, 119). ^{177}Lu , with a half-life of 6.7 days,

can emit β^- particles with three energies of 498 keV (79.3%), 380 keV (9.1%), and 176 keV (12.2%). Due to its relatively low particle energy, the normal tissue around the lesion is less damaged, making it a very suitable radionuclide for therapy (120). In 2007, Tolmachev et al. first used CHX-A"-DTPA as a chelating agent to label affibody $\text{Z}_{\text{HER2:342}}$ with ^{177}Lu ; the results showed that $^{177}\text{Lu-CHX-A}''\text{-DTPA-ABD-(Z}_{\text{HER2:342}}\text{)}_2$ could prevent the growth of SKOV3 ovarian cancer cells highly expressing the HER2 receptor, compared with the control group injected with PBS and simultaneously injected with non-labeled affibody, $^{177}\text{Lu-CHX-A}''\text{-DTPA-ABD-(Z}_{\text{HER2:342}}\text{)}_2$ blocking group. The survival time of nude mice injected with $^{177}\text{Lu-CHX-A}''\text{-DTPA-ABD-(Z}_{\text{HER2:342}}\text{)}_2$ was significantly prolonged; however, a disadvantage of this affibody is the high radioactive retention in the blood and bone marrow (75). Subsequently, the researchers further linked high-affinity ABD035 to the N-terminus of the affibody $\text{Z}_{\text{HER2:2891}}$ and linked a DOTA derivative maleimide group to the C-terminus, namely, $\text{Z}_{\text{HER2:2891-ABD035-DOTA}}$, and then labeled it with ^{177}Lu to obtain molecular probe $^{177}\text{Lu-ABY-027}$. This was then compared with that of the previous molecular probe $^{177}\text{Lu-CHX-A}''\text{-DTPA-ABD-(Z}_{\text{HER2:342}}\text{)}_2$. The results showed that the uptake of the former in the tumor was twice that of the latter, and the radioactive retention in the liver and kidney was significantly reduced (75). To further improve the radioactive uptake of molecular probes by tumors and reduce the radioactive retention of normal organs such as the kidneys, the research team further optimized the molecular probes in a series of studies in which they conducted comparative evaluations *in vivo* and *in vitro*. The results showed that the molecular probe [^{177}Lu]Lu-HP16, containing 9 nucleic acid bases, has the highest tumor/kidney uptake ratio and is a promising molecular probe for targeted therapy of HER2-positive ovarian cancer (121–123).

Although there are many advantages that make radionuclide-labeled HER2 affibodies particularly suitable for molecular imaging, many challenges and hurdles remain in the development of these affibodies. One disadvantage is that labeling methods can lead to increased lipophilicity, often leading to off-target interactions with normal tissues and binding to blood proteins (124). Another disadvantage may be the bacterial source of the protein scaffold, as repeated use in patient treatment leads to an increased risk of immunogenicity (125).

DISCUSSION

HER2 is found in the cytoplasm of normal cells, mainly in the mitochondrial cristae, with little amounts occurring on the cell membrane; HER2 is found only on the cell membrane in tumor cells. The expression of HER2 in normal ovarian epithelium is very low; however, the expression in epithelial ovarian tumor tissue has been reported to be high at 55 times that of normal ovarian epithelium (126). Epithelial ovarian cancer consists of histological subtypes, which include serous carcinoma (prevalence 75%), mucinous carcinoma (20%), endometrioid carcinoma (2%), and clear cell carcinoma (<1%). Regarding

HER2 positivity, serous (29%) and mucinous carcinomas (38%) had higher positivity than endometrioid (20%) and clear cell carcinomas (23.1%), while the differential expressions of HER2 among different tissue types in epithelial ovarian carcinoma were important biomarkers for prognosis in epithelial ovarian cancer (127).

Fluorodeoxyglucose (FDG) labeled with radionuclide ^{18}F is widely used in clinical practice and has been proved to be highly accurate in the differential diagnosis of benign and malignant ovarian masses (128, 129). However, a study of ^{18}F -FDG PET/CT to evaluate the expression status of HER2 receptor has not been reported. Affibody has high affinity for HER2-expressing tumors, low molecular weight, stable biological activity, and fast blood clearance time (130). Recently, the use of molecular probes from radionuclide-labeled affibody has shown promise in tumor molecular imaging research. However, there are many difficulties in the preparation of molecular probes from radionuclide-labeled HER2 affibody that need to be addressed to enable more effective use in clinical practice. Most notably, research needs to focus on the reduction of non-specific uptake in the liver, kidney, bone marrow, and gastrointestinal tract. To this end, researchers have modified the amino acid sequence to change the molecular surface charge, lipid solubility, and affinity, and used different radionuclides to optimize the labeling method, improving the specific uptake of molecular probes at the tumor

site, reducing the uptake of non-target organs, thereby optimizing the distribution *in vivo*. Moreover, different chelating agents have been introduced into the radionuclide labeling of HER2 affibody. Increasing the hydrophilicity of the chelating agent can reduce the non-specific uptake of the liver, enable the molecular probe to be excreted through the kidney, reduce the uptake of the gastrointestinal tract, and thus reduce the background of the image, increase the target/non-target ratio, and lead to an improved image. To date, more than 20 chelating agents have been introduced into molecular probes for radionuclide-labeled HER2 affibody. The advantages and disadvantages of commonly used chelators are shown in **Table 2**.

The median survival of patients with ovarian cancer has been significantly improved recently through the introduction of novel drug treatments and minimally invasive surgical techniques (22). However, the symptomatology, diagnosis, and treatment of ovarian cancer still pose great challenges. Multidisciplinary cooperation and multiple detection methods are needed to provide gynecological oncologists with as much detailed clinical data as possible to optimally design appropriate treatment plans for each patient (22, 131). HER2 is overexpressed or amplified in various malignancies. Therefore, therapeutic drugs that target the linkage of HER2-positive tumor cells to a peptide with a high affinity for the HER2 receptor should be developed to target a variety of HER2-positive

TABLE 2 | Overview of advantages and disadvantages of commonly used chelators as molecular probes.

Chelating agent	Full name	Representative molecular probes	Metabolic pathways	Benifits	Disadvantages
-maGSG-	mercaptoacetyl-glycyl-seryl-glycyl	$^{99\text{m}}\text{Tc}$ -maGSG- $\text{Z}_{\text{HER2}:342}$	kidney	low liver and gastrointestinal uptake	high renal uptake
-maESE-	mercaptoacetyl-glutamyl-seryl-glutamyl	$^{99\text{m}}\text{Tc}$ -maESE- $\text{Z}_{\text{HER2}:342}$	liver	high affinity; low image background; low renal uptake	relatively high liver uptake
-PIB-	Iodobenzoate	^{125}I -PIB- $\text{Z}_{\text{HER2}:342}$	liver	high affinity; low renal uptake	untargeted uptake
-HPEM-	4-hydroxyphenyl-ethyl-maleimide	$^{131}\text{I}/^{125}\text{I}$ -HPEM- $\text{Z}_{\text{HER2}:342}\text{-C}$	liver	high affinity; low renal uptake	high liver and gastrointestinal uptake
-DOTA-	1,4,7,10-tetraazacyclodecane- <i>N,N,N</i> -tetra acetic acid	^{111}In -DOTA- $\text{Z}_{\text{HER2}:342}$ - pep2 ^{68}Ga -DOTA- $\text{Z}_{\text{HER2}:342\text{min}}$	kidney	high affinity; fast blood clearance; low image background	high renal uptake
-NOTA-	1,4,7-triazacyclononane- <i>N,N,N</i> -triacetic acid	^{68}Ga -NOTA- $\text{Z}_{\text{HER2}:S1}$ ^{64}Cu -NOTA- $\text{Z}_{\text{HER2}:S1}$	kidney	high affinity; low image background	high renal uptake
-FBO-	(<i>N</i> -(4-fluorobenzylidene)oxime)	^{18}F -FBO- $\text{Z}_{\text{HER2}:477}$	liver, kidney	high affinity	high liver and renal uptake
-FBEM-	<i>N</i> -[2-(4-fluoro-benzamido)ethyl] maleimide	^{18}F -FBEM- $\text{Z}_{\text{HER2}:342}$	kidney	high affinity; low liver uptake	high renal and bone uptake
-FET-	fluoroethyl-L-tyrosine	^{18}F FET- $\text{Z}_{\text{HER2}:342}$	kidney	high affinity; low liver uptake	low yield
-NODAGA-	1-(1,3-carboxypropyl)-4,7-carboxymethyl-1,4,7-triazacyclononane	^{68}Ga -NODAGA- $\text{Z}_{\text{HER2}:S1}$ ^{64}Cu -NODAGA- $\text{Z}_{\text{HER2}:S1}$	kidney	high affinity; low image background; low liver uptake	high bone marrow uptake
-maGSG-	mercaptoacetyl-glycyl-seryl-glycyl	^{186}Re -maGSG- $\text{Z}_{\text{HER2}:342}$	liver	high affinity; low renal uptake	high liver uptake
		$^{99\text{m}}\text{Tc}$ -maGSG- $\text{Z}_{\text{HER2}:342}$	kidney	high affinity; low liver uptake	high renal uptake
-maGGG-	mercaptoacetyl-glycyl-glycyl-glycyl	$^{99\text{m}}\text{Tc}$ -maGGG- $\text{Z}_{\text{HER2}:342}$ ^{186}Re -maGGG- $\text{Z}_{\text{HER2}:342}$	not applicable	high affinity; low liver and renal uptake	high image background

malignancies (132). To date, a variety of HER2-targeting therapeutic drugs have been developed, including HER2 addressing therapeutic monoclonal antibodies, nanobodies, and affibodies. Several of these drugs have entered the clinical trial stage, and the results of clinical studies have shown that they benefit patients with HER2-positive breast cancer. However, the study and use of radionuclide-labeled HER2 affibody have been hampered by its short residence time in the blood (133).

In conclusion, the molecular probe of radionuclide-labeled HER2 affibody can accurately evaluate the expression status of HER2 receptor in epithelial ovarian cancer, which provides favorable conditions for the localization, diagnosis of cancer foci, targeted therapy, and prognosis evaluation. The research and development of new molecular probes for nuclear medicine aims to introduce radionuclides into cancer foci in a targeted manner, display systemic lesions, and kill tumor cells through radionuclides' radioactivity. Continued progress will result in improved methods for the integration of the diagnosis and treatment of ovarian cancer. Nuclear medicine imaging technology is an important imaging method for basic and clinical research on malignant tumors. A variety of radionuclide-labeled HER2 affibody molecular probes have been successfully developed and have shown potential in preclinical experimental studies of ovarian cancer, laying a foundation for multi-center clinical trials. In the future, the research and development of HER2 affibody molecular probes will focus on optimizing the labeling method of radionuclides, using different chelating agents, or modifying the amino acid sequence to further improve the specific uptake of molecular probes in tumor sites, while reducing the uptake of non-target organs, especially in the liver, kidney, bone marrow, and gastrointestinal tract. This will optimize the distribution in the body, and the radionuclide-labeled HER2 small-molecule

targeting binding protein can then be used in clinical practice as soon as possible to enable tumor-specific diagnosis, and to promote the evaluation of the therapeutic efficacy of targeted therapy drugs objectively at an early stage.

AUTHOR CONTRIBUTIONS

XH compiled/interpreted resources and was the primary author for majority of the manuscript. DL assisted with manuscript writing. YF assisted with manuscript edits. JZ and ZF developed the conception and overall design of the project/paper. JC and PW provided manuscript editing/revisions and interpretation of resources to include in the paper. All authors contributed to manuscript revision, and read and approved the submitted version.

FUNDING

This study was funded by the National Natural Science Foundation of the People's Republic of China, NSFC (grant number: 81571712), Zunyi Medical College Research Start Fund 2018ZYFY03, and QianKeHe platform talents [2017] (grant number: 5733-035).

SUPPLEMENTARY MATERIAL

The Supplementary Material for this article can be found online at: <https://www.frontiersin.org/articles/10.3389/fonc.2022.917439/full#supplementary-material>

REFERENCES

- Sung H, Ferlay J, Siegel RL, Laversanne M, Soerjomataram I, Jemal A, et al. Global Cancer Statistics 2020: GLOBOCAN Estimates of Incidence and Mortality Worldwide for 36 Cancers in 185 Countries. *CA Cancer J Clin* (2021) 71(3):209–49. doi: 10.3322/caac.21660
- Wang B, Liu SZ, Zheng RS, Zhang F, Chen WQ, Sun XB. Time Trends of Ovarian Cancer Incidence in China. *Asian Pac J Cancer Prev* (2014) 15(1):191–3. doi: 10.7314/APJCP.2014.15.1.191
- Huang Z, Zheng Y, Wen W, Wu C, Bao P, Wang C, et al. Incidence and Mortality of Gynaecological Cancers: Secular Trends in Urban Shanghai, China Over 40 Years. *Eur J Cancer* (2016) 63:1–10. doi: 10.1016/j.ejca.2016.04.016
- Westhoff C. Ovarian Cancer. *Annu Rev Public Health* (1996) 17:85–96. doi: 10.1146/annurev.pu.17.050196.000505
- Hoekstra A, Rodriguez GC. Chemoprevention of Ovarian Cancer. *Cancer Treat Res* (2009) 149:3–34. doi: 10.1007/978-0-387-98094-2_1
- Hanna L, Adams M. Prevention of Ovarian Cancer. *Best Pract Res Clin Obstet Gynaecol* (2006) 20:339–62. doi: 10.1016/j.bpobgyn.2005.10.016
- Shan W, Liu J. Inflammation: A Hidden Path to Breaking the Spell of Ovarian Cancer. *Cell Cycle* (2009) 8:3107–11. doi: 10.4161/cc.8.19.9590
- Toriola AT, Grankvist K, Agborsangaya CB, Lukanova A, Lehtinen M, Surcel HM. Changes in Pre-Diagnostic Serum C-Reactive Protein Concentrations and Ovarian Cancer Risk: A Longitudinal Study. *Ann Oncol* (2011) 22(8):1916–21. doi: 10.1093/annonc/mdq694
- Lin HW, Tu YY, Lin SY, Su WJ, Lin WL, Lin WZ, et al. Risk of Ovarian Cancer in Women With Pelvic Inflammatory Disease: A Population-Based Study. *Lancet Oncol* (2011) 12(9):900–4. doi: 10.1016/S1470-2045(11)70165-6
- Chittenden BG, Fullerton G, Maheshwari A, Bhattacharya S. Polycystic Ovary Syndrome and the Risk of Gynaecological Cancer: A Systematic Review. *Reprod BioMed Online* (2009) 19(3):398–405. doi: 10.1016/S1472-6483(10)60175-7
- Al-Sabbagh M, Lam EW, Brosens JJ. Mechanisms of Endometrial Progesterone Resistance. *Mol Cell Endocrinol* (2012) 358(2):208–15. doi: 10.1016/j.mce.2011.10.035
- Whiteman DC, Siskind V, Purdie DM, Green AC. Timing of Pregnancy and the Risk of Epithelial Ovarian Cancer. *Cancer Epidemiol Biomarkers Prev* (2003) 12(1):42–6.
- Collaborative Group on Epidemiological Studies of Ovarian Cancer, Beral V, Doll R, Hermon C, Peto R, Reeves G. Ovarian Cancer and Oral Contraceptives: Collaborative Reanalysis of Data From 45 Epidemiological Studies Including 23,257 Women With Ovarian Cancer and 87,303 Controls. *Lancet* (2008) 371(9609):303–14. doi: 10.1016/S0140-6736(08)60167-1
- Danforth KN, Tworoger SS, Hecht JL, Rosner BA, Colditz GA, Hankinson SE. Breastfeeding and Risk of Ovarian Cancer in Two Prospective Cohorts. *Cancer Causes Control* (2007) 18(5):517–23. doi: 10.1007/s10552-007-0130-2
- Terry KL, Schock H, Fortner RT, Hüsing A, Fichorova RN, Yamamoto HS, et al. A Prospective Evaluation of Early Detection Biomarkers for Ovarian

- Cancer in the European EPIC Cohort. *Clin Cancer Res* (2016) 22(18):4664–75. doi: 10.1158/1078-0432.CCR-16-0316
16. Mathieu KB, Bedi DG, Thrower SL, Qayyum A, Bast RC Jr. Screening for Ovarian Cancer: Imaging Challenges and Opportunities for Improvement. *Ultrasound Obstet Gynecol* (2018) 51(3):293–303. doi: 10.1002/uog.17557
 17. Schechter AL, Stern DF, Vaidyanathan L, Decker SJ, Drebin JA, Greene MI, et al. The Neu Oncogene: An Erb-B-Related Gene Encoding a 185,000-Mr Tumour Antigen. *Nature* (1984) 312(5994):513–6. doi: 10.1038/312513a0
 18. Connell CM, Doherty GJ. Activating HER2 Mutations as Emerging Targets in Multiple Solid Cancers. *ESMO Open* (2017) 2(5):e000279. doi: 10.1136/esmoopen-2017-000279
 19. Lee ES, Lee Y, Suh D, Kang J, Kim I. Detection of HER-2 and EGFR Gene Amplification Using Chromogenic in-Situ Hybridization Technique in Ovarian Tumors. *Appl Immunohistochem Mol Morphol* (2010) 18(1):69–74. doi: 10.1097/PAL0b013e3181af7d3f
 20. Corkery DP, Le Page C, Meunier L, Provencher D, Mes-Masson AM, Dellea G. PRP4K Is a HER2-Regulated Modifier of Taxane Sensitivity. *Cell Cycle* (2015) 14(7):1059–69. doi: 10.1080/15384101.2015.1007775
 21. Cloven NG, Kyshtobayeva A, Burger RA, Yu IR, Fruehauf JP. In Vitro Chemoresistance and Biomarker Profiles are Unique for Histologic Subtypes of Epithelial Ovarian Cancer. *Gynecol Oncol* (2004) 92(1):160–6. doi: 10.1016/j.ygyno.2003.09.030
 22. Falzone L, Scandurra G, Lombardo V, Gattuso G, Lavoro A, Distefano AB, et al. A Multidisciplinary Approach Remains the Best Strategy to Improve and Strengthen the Management of Ovarian Cancer (Review). *Int J Oncol* (2021) 59(1):53. doi: 10.3892/ijo.2021.5233
 23. Orr B, Edwards RP. Diagnosis and Treatment of Ovarian Cancer. *Hematol Oncol Clin North Am* (2018) 32(6):943–64. doi: 10.1016/j.hoc.2018.07.010
 24. Dilley J, Burnell M, Gentry-Maharaj A, Ryan A, Neophytou C, Apostolidou S, et al. Ovarian Cancer Symptoms, Routes to Diagnosis and Survival - Population Cohort Study in the 'No Screen' Arm of the UK Collaborative Trial of Ovarian Cancer Screening (UKCTOCS). *Gynecol Oncol* (2020) 158(2):316–22. doi: 10.1016/j.ygyno.2020.05.002
 25. Moelans CB, de Weger RA, van der Wall E, van Diest PJ. Current Technologies for HER2 Testing in Breast Cancer. *Crit Rev Oncol Hematol* (2011) 80(3):380–92. doi: 10.1016/j.critrevonc.2010.12.005
 26. Schlüter B, Gerhards R, Strumberg D, Voigtmann R. Combined Detection of Her2/neu Gene Amplification and Protein Overexpression in Effusions From Patients With Breast and Ovarian Cancer. *J Cancer Res Clin Oncol* (2010) 136(9):1389–400. doi: 10.1007/s00432-010-0790-2
 27. Jiang D, Im HJ, Sun H, Valdovinos HF, England CG, Ehlerding EB, et al. Radiolabeled Pertuzumab for Imaging of Human Epidermal Growth Factor Receptor 2 Expression in Ovarian Cancer. *Eur J Nucl Med Mol Imaging* (2017) 44(8):1296–305. doi: 10.1007/s00259-017-3663-y
 28. Schlüter B, Gerhards R, Strumberg D, Voigtmann R. Combined Detection of Her2/neu Gene Amplification and Protein Overexpression in Effusions From Patients With Breast and Ovarian Cancer. *J Cancer Res Clin Oncol* (2010) 136(9):1389–400. doi: 10.1007/s00432-010-0790-2
 29. Hillig T, Thode J, Breinholt MF, Franzmann MB, Pedersen C, Lund F, et al. Assessing HER2 Amplification by IHC, FISH, and Real-Time Polymerase Chain Reaction Analysis (Real-Time PCR) Following LCM in Formalin-Fixed Paraffin Embedded Tissue From 40 Women With Ovarian Cancer. *APMIS* (2012) 120(12):1000–7. doi: 10.1111/j.1600-0463.2012.02929.x
 30. Nilsson B, Moks T, Jansson B, Abrahmsén L, Elmlblad A, Holmgren E, et al. A Synthetic IgG-Binding Domain Based on Staphylococcal Protein a. *Protein Eng* (1987) 1(2):107–13. doi: 10.1093/protein/1.2.107
 31. Braisted AC, Wells JA. Minimizing a Binding Domain From Protein a. *Proc Natl Acad Sci USA* (1996) 93(12):5688–92. doi: 10.1073/pnas.93.12.5688
 32. Nord K, Nilsson J, Nilsson B, Uhlén M, Nygren PA. A Combinatorial Library of an Alpha-Helical Bacterial Receptor Domain. *Protein Eng* (1995) 8(6):601–8. doi: 10.1093/protein/8.6.601
 33. Löfblom J, Feldwisch J, Tolmachev V, Carlsson J, Ståhl S, Frejd FY. Affibody Molecules: Engineered Proteins for Therapeutic, Diagnostic and Biotechnological Applications. *FEBS Lett* (2010) 584(12):2670–80. doi: 10.1016/j.febslet.2010.04.014
 34. Nord K, Gunneriusson E, Ringdahl J, Ståhl S, Uhlén M, Nygren PA. Binding Proteins Selected From Combinatorial Libraries of an Alpha-Helical Bacterial Receptor Domain. *Nat Biotechnol* (1997) 15(8):772–7. doi: 10.1038/nbt0897-772
 35. Nygren PA. Alternative Binding Proteins: Affibody Binding Proteins Developed From a Small Three-Helix Bundle Scaffold. *FEBS J* (2008) 275(11):2668–76. doi: 10.1111/j.1742-4658.2008.06438.x
 36. Jamous M, Haberkorn U, Mier W. Synthesis of Peptide Radiopharmaceuticals for the Therapy and Diagnosis of Tumor Diseases. *Molecules* (2013) 18(3):3379–409. doi: 10.3390/molecules18033379
 37. Weidle UH, Auer J, Brinkmann U, Georges G, Tiefenthaler G. The Emerging Role of New Protein Scaffold-Based Agents for Treatment of Cancer. *Cancer Genomics Proteomics* (2013) 10(4):155–68.
 38. Antunes P, Ginj M, Walter MA. Influence of Different Spacers on the Biological Profile of a DOTA-Somatostatin Analogue. *Bioconjug Chem* (2007) 18(1):84–92. doi: 10.1021/bc0601673
 39. Ståhl S, Gräslund T, Eriksson Karlström A, Frejd FY, Nygren PÅ, Löfblom J. Affibody Molecules in Biotechnological and Medical Applications. *Trends Biotechnol* (2017) 35(8):691–712. doi: 10.1016/j.tibtech.2017.04.007
 40. Baum RP, Prasad V, Müller D, Schuchardt C, Orlova A, Wennborg A, et al. Molecular Imaging of HER2-Expressing Malignant Tumors in Breast Cancer Patients Using Synthetic ¹¹¹In or ⁶⁸Ga Labeled Affibody Molecules. *J Nucl Med* (2010) 51(6):892–97. doi: 10.2967/jnumed.109.073239
 41. Sörensen J, Sandberg D, Sandström M, Wennborg A, Feldwisch J, Tolmachev V, et al. First-In-Human Molecular Imaging of HER2 Expression in Breast Cancer Metastases Using the ¹¹¹In-ABY-025 Affibody Molecule. *J Nucl Med* (2014) 55(5):730–5. doi: 10.2967/jnumed.113.131243
 42. Steffen AC, Wikman M, Tolmachev V, Adams GP, Nilsson FY, Ståhl S, et al. In Vitro Characterization of a Bivalent Anti-HER-2 Affibody With Potential for Radionuclide-Based Diagnostics. *Cancer Biother Radiopharm* (2005) 20(3):239–48. doi: 10.1089/cbr.2005.20.239
 43. Steffen AC, Orlova A, Wikman M, Nilsson FY, Ståhl S, Adams GP, et al. Affibody-Mediated Tumour Targeting of HER-2 Expressing Xenografts in Mice. *Eur J Nucl Med Mol Imaging* (2006) 33(6):631–8. doi: 10.1007/s00259-005-0012-3
 44. Orlova A, Magnusson M, Eriksson TL, Nilsson M, Larsson B, Höiden-Guthenberg I, et al. Tumor Imaging Using a Picomolar Affinity HER2 Binding Affibody Molecule. *Cancer Res* (2006) 66(8):4339–48. doi: 10.1158/0008-5472.CAN-05-3521
 45. Ahlgren S, Orlova A, Rosik D, Sandström M, Sjöberg A, Baastrup B, et al. Evaluation of Maleimide Derivative of DOTA for Site-Specific Labeling of Recombinant Affibody Molecules. *Bioconjug Chem* (2008) 19(1):235–43. doi: 10.1021/bc700307y
 46. Altai M, Perols A, Karlström AE, Sandström M, Boschetti F, Orlova A, et al. Preclinical Evaluation of Anti-HER2 Affibody Molecules Site-Specifically Labeled With ¹¹¹In Using a Maleimide Derivative of NODAGA. *Nucl Med Biol* (2012) 39(4):518–29. doi: 10.1016/j.nucmedbio.2011.10.013
 47. Oroujeni M, Rinne SS, Vorobyeva A, Loftenius A, Feldwisch J, Jonasson P, et al. Preclinical Evaluation of ^{99m}Tc-ZHER2:41071, a Second-Generation Affibody-Based HER2-Visualizing Imaging Probe With a Low Renal Uptake. *Int J Mol Sci* (2021) 22(5):2770. doi: 10.3390/ijms22052770
 48. Tolmachev V, Velikyan I, Sandström M, Orlova A. A HER2-Binding Affibody Molecule Labelled With ⁶⁸Ga for PET Imaging: Direct In Vivo Comparison With the ¹¹¹In-Labelled Analogue. *Eur J Nucl Med Mol Imaging* (2010) 37(7):1356–67. doi: 10.1007/s00259-009-1367-7
 49. Wällberg H, Orlova A. Slow Internalization of Anti-HER2 Synthetic Affibody Monomer ¹¹¹In-DOTA-ZHER2:342-Pep2: Implications for Development of Labeled Tracers. *Cancer Biother Radiopharm* (2008) 23(4):435–42. doi: 10.1089/cbr.2008.0464
 50. Tolmachev V, Nilsson FY, Widström C, Andersson K, Rosik D, Gedda L, et al. ¹¹¹In-Benzyl-DTPA-ZHER2:342, an Affibody-Based Conjugate for In Vivo Imaging of HER2 Expression in Malignant Tumors. *J Nucl Med* (2006) 47(5):846–53.
 51. Rosik D, Orlova A, Malmberg J, Altai M, Varasteh Z, Sandström M, et al. Direct Comparison of ¹¹¹In-Labelled Two-Helix and Three-Helix Affibody Molecules for In Vivo Molecular Imaging. *Eur J Nucl Med Mol Imaging* (2012) 39(4):693–702. doi: 10.1007/s00259-011-2016-5

52. Orlova A, Rosik D, Sandström M, Lundqvist H, Einarsson L, Tolmachev V. Evaluation of [(111/114m)In]CHX-A"-DTPA-ZHER2:342, an Affibody Ligand Conjugate for Targeting of HER2-Expressing Malignant Tumors. *Q J Nucl Med Mol Imaging* (2007) 51(4):314–23.
53. Baum RP, Prasad V, Muller D, Schuchardt C, Orlova A, Wennborg A, et al. Molecular Imaging of HER2-Expressing Malignant Tumors in Breast Cancer Patients Using Synthetic 111In- or 68Ga-Labeled Affibody Molecules. *J Nucl Med* (2010) 51(6):892–7. doi: 10.2967/jnumed.109.073239
54. Altai M, Perols A, Karlström AE, Sandström M, Boschetti F, Orlova A, et al. Preclinical Evaluation of Anti-HER2 Affibody Molecules Site-Specifically Labeled With 111In Using a Maleimido Derivative of NODAGA. *Nucl Med Biol* (2012) 39(4):518–29. doi: 10.1016/j.nucmedbio.2011.10.013
55. Engfeldt T, Orlova A, Tran T, Bruskin A, Widström C, Karlström AE, et al. Imaging of HER2-Expressing Tumours Using a Synthetic Affibody Molecule Containing the 99mtc-Chelating Mercaptoacetyl-Glycyl-Glycyl-Glycyl (MAG3) Sequence. *Eur J Nucl Med Mol Imaging* (2007) 34(5):722–33. doi: 10.1007/s00259-006-0266-4
56. Tran T, Engfeldt T, Orlova A, Sandström M, Feldwisch J, Abrahmsén L, et al. (99m)Tc-maEEE-Z(HER2:342), an Affibody Molecule-Based Tracer for the Detection of HER2 Expression in Malignant Tumors. *Bioconjug Chem* (2007) 18(6):1956–64. doi: 10.1021/bc7002617
57. Engfeldt T, Tran T, Orlova A, Widström C, Feldwisch J, Abrahmsén L, et al. 99mtc-Chelator Engineering to Improve Tumour Targeting Properties of a HER2-Specific Affibody Molecule. *Eur J Nucl Med Mol Imaging* (2007) 34(11):1843–53. doi: 10.1007/s00259-007-0474-6
58. Ekblad T, Tran T, Orlova A, Widström C, Feldwisch J, Abrahmsén L, et al. Development and Preclinical Characterisation of 99mtc-Labeled Affibody Molecules With Reduced Renal Uptake. *Eur J Nucl Med Mol Imaging* (2008) 35(12):2245–55. doi: 10.1007/s00259-008-0845-7
59. Tran TA, Ekblad T, Orlova A, Sandström M, Feldwisch J, Wennborg A, et al. Effects of Lysine-Containing Mercaptoacetyl-Based Chelators on the Biodistribution of 99mtc-Labeled Anti-HER2 Affibody Molecules. *Bioconjug Chem* (2008) 19(12):2568–76. doi: 10.1021/bc800244b
60. Han J, Zhao Y, Zhao X, Ma T, Hao T, Liu J, et al. Therapeutic Efficacy and Imaging Assessment of the HER2-Targeting Chemotherapy Drug ZHER2: V2-Pemetrexed in Lung Adenocarcinoma Xenografts. *Invest New Drugs* (2020) 38(4):1031–43. doi: 10.1007/s10637-019-00876-3
61. Jiao H, Zhao X, Liu J, Ma T, Zhang Z, Zhang J, et al. *In Vivo* Imaging Characterization and Anticancer Efficacy of a Novel HER2 Affibody and Pemetrexed Conjugate in Lung Cancer Model. *Nucl Med Biol* (2019) 68–69:31–9. doi: 10.1016/j.nucmedbio.2018.11.004
62. Wällberg H, Orlova A, Altai M, Hosseinimehr SJ, Widström C, Malmberg J, et al. Molecular Design and Optimization of 99mtc-Labeled Recombinant Affibody Molecules Improves Their Biodistribution and Imaging Properties. *J Nucl Med* (2011) 52(3):461–9. doi: 10.2967/jnumed.110.083592
63. Yang Y, Zhao X, Xing Y, Yu T, Zhang J, Wang J. Preclinical Evaluation of 99mtc Direct Labeling ZHER2:V2 for HER2 Positive Tumors Imaging. *Oncol Lett* (2018) 16(4):5361–66. doi: 10.3892/ol.2018.9279
64. Cai J, Li X, Mao F, Wang P, Luo Y, Zheng K, et al. Non-Invasive Monitoring of HER2 Expression in Breast Cancer Patients With 99mtc-Affibody SPECT/Ct. *Iran J Radiol* (2020) 17(1):e96419. doi: 10.5812/iranradiol.96419
65. Strand J, Nordeman P, Honarvar H, Altai M, Orlova A, Larhed M, et al. Site-Specific Radioiodination of HER2-Targeting Affibody Molecules Using 4-Iodophenethylmaleimide Decreases Renal Uptake of Radioactivity. *ChemistryOpen* (2015) 4(2):174–82. doi: 10.1002/open.201402097
66. Kramer-Marek G, Bernardo M, Kiesewetter DO, Bagci U, Kuban M, Aras O, et al. PET of HER2-Positive Pulmonary Metastases With 18F-ZHER2:342 Affibody in a Murine Model of Breast Cancer: Comparison With 18F-FDG. *J Nucl Med* (2012) 53(6):939–46. doi: 10.2967/jnumed.111.100354
67. Kramer-Marek G, Kiesewetter DO, Martiniova L, Jagoda E, Lee SB, Capala J. [18f]FBEM-Z(HER2:342)-Affibody Molecule-a New Molecular Tracer for *In Vivo* Monitoring of HER2 Expression by Positron Emission Tomography. *Eur J Nucl Med Mol Imaging* (2008) 35(5):1008–18. doi: 10.1007/s00259-007-0658-0
68. Yanai A, Harada R, Iwata R, Yoshikawa T, Ishikawa Y, Furumoto S, et al. Site-Specific Labeling of F-18 Proteins Using a Supplemented Cell-Free Protein Synthesis System and O-2-[18f]Fluoroethyl-L-Tyrosine: [18f]FET-HER2 Affibody Molecule. *Mol Imaging Biol* (2019) 21(3):529–37. doi: 10.1007/s11307-018-1266-z
69. Ren G, Zhang R, Liu Z, Webster JM, Miao Z, Gambhir SS, et al. A 2-Helix Small Protein Labeled With 68Ga for PET Imaging of HER2 Expression. *J Nucl Med* (2009) 50(9):1492–9. doi: 10.2967/jnumed.109.064287
70. Sandstrom M, Lindskog K, Velikyan I, Wennborg A, Feldwisch J, Sandberg D, et al. Biodistribution and Radiation Dosimetry of the Anti-HER2 Affibody Molecule 68Ga-ABY-025 in Breast Cancer Patients. *J Nucl Med* (2016) 57(6):867–71. doi: 10.2967/jnumed.115.169342
71. Sorensen J, Velikyan I, Sandberg D, Wennborg A, Feldwisch J, Tolmachev V, et al. Measuring HER2-Receptor Expression in Metastatic Breast Cancer Using [68Ga]ABY-025 Affibody PET/Ct. *Theranostics* (2016) 6(2):262–71. doi: 10.7150/thno.13502
72. Qi S, Hoppmann S, Xu Y, Cheng Z. PET Imaging of HER2-Positive Tumors With Cu-64-Labeled Affibody Molecules. *Mol Imaging Biol* (2019) 21(5):907–16. doi: 10.1007/s11307-018-01310-5
73. Altai M, Wällberg H, Honarvar H, Strand J, Orlova A, Varasteh Z, et al. 188Re-ZHER2:V2, a Promising Affibody-Based Targeting Agent Against HER2-Expressing Tumors: Preclinical Assessment. *J Nucl Med* (2014) 55(11):1842–8. doi: 10.2967/jnumed.114.140194
74. Altai M, Honarvar H, Wällberg H, Strand J, Varasteh Z, Rosestedt M, et al. Selection of an Optimal Cysteine-Containing Peptide-Based Chelator for Labeling of Affibody Molecules With (188)Re. *Eur J Med Chem* (2014) 87:519–28. doi: 10.1016/j.ejmech.2014.09.082
75. Tolmachev V, Orlova A, Pehrson R, Galli J, Baastrup B, Andersson K, et al. Radionuclide Therapy of HER2-Positive Microxenografts Using a 177Lu-Labeled HER2-Specific Affibody Molecule. *Cancer Res* (2007) 67(6):2773–82. doi: 10.1158/0008-5472.CAN-06-1630
76. Honarvar H, Westerlund K, Altai M, Sandström M, Orlova A, Tolmachev V, et al. Feasibility of Affibody Molecule-Based PNA-Mediated Radionuclide Pretargeting of Malignant Tumors. *Theranostics* (2016) 6(1):93–103. doi: 10.7150/thno.12766
77. Ahlgren S, Orlova A, Wällberg H, Hansson M, Sandström M, Lewsley R, et al. Targeting of HER2-Expressing Tumors Using 111In-ABY-025, a Second-Generation Affibody Molecule With a Fundamentally Reengineered Scaffold. *J Nucl Med* (2010) 51(7):1131–8. doi: 10.2967/jnumed.109.073346
78. Heskamp S, Laverman P, Rosik D, Boschetti F, van der Graaf WT, Oyen WJ, et al. Imaging of Human Epidermal Growth Factor Receptor Type 2 Expression With 18F-Labeled Affibody Molecule ZHER2:2395 in a Mouse Model for Ovarian Cancer. *J Nucl Med* (2012) 53(1):146–53. doi: 10.2967/jnumed.111.093047
79. Tolmachev V, Xu H, Wällberg H, Ahlgren S, Hjertman M, Sjöberg A, et al. Evaluation of a Maleimido Derivative of CHX-A" DTPA for Site-Specific Labeling of Affibody Molecules. *Bioconjug Chem* (2008) 19(8):1579–87. doi: 10.1021/bc800110y
80. Altai M, Varasteh Z, Andersson K, Eek A, Boerman O, Orlova A. *In Vivo* and *In Vitro* Studies on Renal Uptake of Radiolabeled Affibody Molecules for Imaging of HER2 Expression in Tumors. *Cancer Biother Radiopharm* (2013) 28(3):187–95. doi: 10.1089/cbr.2012.1304
81. Westerlund K, Honarvar H, Norrström E, Strand J, Mitran B, Orlova A, et al. Increasing the Net Negative Charge by Replacement of DOTA Chelator With DOTAGA Improves the Biodistribution of Radiolabeled Second-Generation Synthetic Affibody Molecules. *Mol Pharm* (2016) 13(5):1668–78. doi: 10.1021/acs.molpharmaceut.6b00089
82. Lindberg H, Hofström C, Altai M, Honarvar H, Wällberg H, Orlova A, et al. Evaluation of a HER2-Targeting Affibody Molecule Combining an N-Terminal HEHEHE-Tag With a GGGC Chelator for 99mtc-Labeling at the C Terminus. *Tumour Biol* (2012) 33(3):641–51. doi: 10.1007/s13277-011-0305-z
83. Wällberg H, Orlova A, Altai M, Hosseinimehr SJ, Widström C, Malmberg J, et al. Molecular Design and Optimization of 99mtc-Labeled Recombinant Affibody Molecules Improves Their Biodistribution and Imaging Properties. *J Nucl Med* (2011) 52(3):461–9. doi: 10.2967/jnumed.110.083592
84. Yang Y, Zhao X, Xing Y, Yu T, Zhang J, Wang J. Preclinical Evaluation of 99mtc Direct Labeling ZHER2:V2 for HER2 Positive Tumors Imaging. *Oncol Lett* (2018) 16(4):5361–6. doi: 10.3892/ol.2018.9279

85. Strand J, Nordeman P, Honarvar H, Altai M, Orlova A, Larhed M, et al. Site-Specific Radioiodination of HER2-Targeting Affibody Molecules Using 4-Iodophenethylmaleimide Decreases Renal Uptake of Radioactivity. *ChemistryOpen* (2015) 4(2):174–82. doi: 10.1002/open.201402097
86. Steffen AC, Orlova A, Wikman M, Nilsson FY, Ståhl S, Adams GP, et al. Affibody-Mediated Tumour Targeting of HER-2 Expressing Xenografts in Mice. *Eur J Nucl Med Mol Imaging* (2006) 33(6):631–8. doi: 10.1007/s00259-005-0012-3
87. Tran T, Orlova A, Sivaev I, Sandström M, Tolmachev V. Comparison of Benzoate- and Dodecaborate-Based Linkers for Attachment of Radioiodine to HER2-Targeting Affibody Ligand. *Int J Mol Med* (2007) 19(3):485–93. doi: 10.3892/ijmm.19.3.485
88. Tolmachev V, Mume E, Sjöberg S, Frejd FY, Orlova A. Influence of Valency and Labelling Chemistry on *In Vivo* Targeting Using Radioiodinated HER2-Binding Affibody Molecules. *Eur J Nucl Med Mol Imaging* (2009) 36(4):692–701. doi: 10.1007/s00259-008-1003-y
89. Vorobyeva A, Schulga A, Rinne SS, Günther T, Orlova A, Deyev S, et al. Indirect Radioiodination of DARPIn G3 Using N-Succinimidyl-Para-Iodobenzoate Improves the Contrast of HER2 Molecular Imaging. *Int J Mol Sci* (2019) 20(12):3047. doi: 10.3390/ijms20123047
90. Beyer T, Townsend DW, Brun T, Kinahan PE, Charron M, Roddy R, et al. A Combined PET/CT Scanner for Clinical Oncology. *J Nucl Med* (2000) 41(8):1369–79.
91. Vahidfar N, Farzanefar S, Ahmadzadehfar H, Molloy EN, Eppard E. A Review of Nuclear Medicine Approaches in the Diagnosis and the Treatment of Gynecological Malignancies. *Cancers (Basel)* (2022) 14(7):1779. doi: 10.3390/cancers14071779
92. Altai M, Strand J, Rosik D, Selvaraju RK, Eriksson Karlström A, et al. Influence of Nuclides and Chelators on Imaging Using Affibody Molecules: Comparative Evaluation of Recombinant Affibody Molecules Site-Specifically Labeled With ^{68}Ga and ^{111}In via Maleimido Derivatives of DOTA and NODAGA. *Bioconjug Chem* (2013) 24(6):1102–9. doi: 10.1021/bc300678y
93. Strand J, Honarvar H, Perols A, Orlova A, Selvaraju RK, Karlström AE, et al. Influence of Macrocyclic Chelators on the Targeting Properties of (^{68}Ga) -Labeled Synthetic Affibody Molecules: Comparison With (^{111}In) -Labeled Counterparts. *PLoS One* (2013) 8(8):e70028.
94. Cheng Z, De Jesus OP, Namavari M, De A, Levi J, Webster JM, et al. Small-Animal PET Imaging of Human Epidermal Growth Factor Receptor Type 2 Expression With Site-Specific 18F-Labeled Protein Scaffold Molecules. *J Nucl Med* (2008) 49(5):804–13. doi: 10.2967/jnumed.107.047381
95. Iveson PB, Glaser M, Indrevoll B, Shales J, Mantzilas D, Omtvedt L, et al. FASTlab Radiosynthesis of the 18F-Labelled HER2-Binding Affibody Molecule [18F]GE-226. *J Labelled Comp Radiopharm* (2019) 62(14):925–32. doi: 10.1002/jlcr.3789
96. Trousil S, Hoppmann S, Nguyen QD, Kaliszczak M, Tomasi G, Iveson P, et al. Positron Emission Tomography Imaging With 18F-Labeled ZHER2:2891 Affibody for Detection of HER2 Expression and Pharmacodynamic Response to HER2-Modulating Therapies. *Clin Cancer Res* (2014) 20(6):1632–43. doi: 10.1158/1078-0432.CCR-13-2421
97. Heskamp S, Laverman P, Rosik D, Boschetti F, van der Graaf WT, Oyen WJ, et al. Imaging of Human Epidermal Growth Factor Receptor Type 2 Expression With 18F-Labeled Affibody Molecule ZHER2:2395 in a Mouse Model for Ovarian Cancer. *J Nucl Med* (2012) 53(1):146–53. doi: 10.2967/jnumed.111.093047
98. Zinn KR, Chaudhuri TR, Cheng TP, Morris JS, Meyer WA Jr.. Production of No-Carrier-Added ^{64}Cu From Zinc Metal Irradiated Under Boron Shielding. *Cancer* (1994) 73(3 Suppl):774–8. doi: 10.1002/1097-0142(19940201)73:3+<774::AID-CNCR2820731305>3.0.CO;2-L
99. Kim JY, Park H, Lee JC, Kim KM, Lee KC, Ha HJ, et al. A Simple Cu-64 Production and Its Application of Cu-64 ATSM. *Appl Radiat Isot* (2009) 67(7–8):1190–4. doi: 10.1016/j.apradiso.2009.02.060
100. Cheng Z, De Jesus OP, Kramer DJ, De A, Webster JM, Gheysens O, et al. ^{64}Cu -Labeled Affibody Molecules for Imaging of HER2 Expressing Tumors. *Mol Imaging Biol* (2010) 12(3):316–24. doi: 10.1007/s11307-009-0256-6
101. Tolmachev V, Yim CB, Rajander J, Perols A, Karlström AE, Haaparanta-Solin M, et al. Comparative Evaluation of Anti-HER2 Affibody Molecules Labeled With ^{64}Cu Using NOTA and NODAGA. *Contrast Media Mol Imaging* (2017) 2017:8565802. doi: 10.1155/2017/8565802
102. Orlova A, Tran TA, Ekblad T, Karlström AE, Tolmachev V. (186)Re-maSGS-Z (HER2:342), a Potential Affibody Conjugate for Systemic Therapy of HER2-Expressing Tumours. *Eur J Nucl Med Mol Imaging* (2010) 37(2):260–9. doi: 10.1007/s00259-009-1268-9
103. Steffen AC, Almqvist Y, Chyan MK, Lundqvist H, Tolmachev V, Wilbur DS, et al. Biodistribution of ^{211}At Labeled HER-2 Binding Affibody Molecules in Mice. *Oncol Rep* (2007) 17(5):1141–7. doi: 10.3892/or.17.5.1141
104. Honarvar H, Müller C, Cohrs S, Haller S, Westerlund K, Karlström AE, et al. Evaluation of the First ^{44}Sc -Labeled Affibody Molecule for Imaging of HER2-Expressing Tumors. *Nucl Med Biol* (2017) 45:15–21. doi: 10.1016/j.nucmedbio.2016.10.004
105. Xu Y, Wang L, Pan D, Yan J, Wang X, Yang R, et al. Synthesis of a Novel ^{89}Zr -Labeled HER2 Affibody and Its Application Study in Tumor PET Imaging. *EJNMMI Res* (2020) 10(1):58. doi: 10.1186/s13550-020-00649-7
106. Wallberg H, Grafström J, Cheng Q, Lu L, Martinsson Ahlén HS, Samén E, et al. HER2-Positive Tumors Imaged Within 1 Hour Using a Site-Specifically ^{11}C -Labeled Sel-Tagged Affibody Molecule. *J Nucl Med* (2012) 53(9):1446–53. doi: 10.2967/jnumed.111.102194
107. Puglisi F, Minisini AM, De Angelis C, Arpino G. Overcoming Treatment Resistance in HER2-Positive Breast Cancer: Potential Strategies. *Drugs* (2012) 72(9):1175–93. doi: 10.2165/11634000-000000000-00000
108. Loizzi V, Ranieri G, Laforgia M, Gadaleta CD, Gargano G, Kardhashi A, et al. PARP Inhibitors and Epithelial Ovarian Cancer: Molecular Mechanisms, Clinical Development and Future Prospective. *Oncol Lett* (2020) 20(4):90. doi: 10.3892/ol.2020.11951
109. Lavoro A, Scalisi A, Candido S, Zanghi GN, Rizzo R, Gattuso G, et al. Identification of the Most Common BRCA Alterations Through Analysis of Germline Mutation Databases: Is Droplet Digital PCR an Additional Strategy for the Assessment of Such Alterations in Breast and Ovarian Cancer Families? *Int J Oncol* (2022) 60(5):58. doi: 10.3892/ijo.2022.5349
110. Boussios S, Karathanasi A, Cooke D, Neille C, Sadauskaite A, Moschetta M, et al. PARP Inhibitors in Ovarian Cancer: The Route to “Ithaca”. *Diagnostics (Basel)* (2019) 9(2):55. doi: 10.3390/diagnostics9020055
111. Puglisi F, Minisini AM, De Angelis C, Arpino G. Overcoming Treatment Resistance in HER2-Positive Breast Cancer: Potential Strategies. *Drugs* (2012) 72(9):1175–93. doi: 10.2165/11634000-000000000-00000
112. Pernas S, Tolaney SM. HER2-Positive Breast Cancer: New Therapeutic Frontiers and Overcoming Resistance. *Ther Adv Med Oncol* (2019) 11:1758835919833519. doi: 10.1177/1758835919833519
113. Hanker AB, Pfefferle AD, Balko JM, Kuba MG, Young CD, Sánchez V, et al. Mutant PIK3CA Accelerates HER2-Driven Transgenic Mammary Tumors and Induces Resistance to Combinations of Anti-HER2 Therapies. *Proc Natl Acad Sci USA* (2013) 110(35):14372–7. doi: 10.1073/pnas.1303204110
114. Nagata Y, Lan KH, Zhou X, Tan M, Esteva FJ, Sahin AA, et al. PTEN Activation Contributes to Tumor Inhibition by Trastuzumab, and Loss of PTEN Predicts Trastuzumab Resistance in Patients. *Cancer Cell* (2004) 6(2):117–27. doi: 10.1016/j.ccr.2004.06.022
115. Singh JC, Jhaveri K, Esteva FJ. HER2-Positive Advanced Breast Cancer: Optimizing Patient Outcomes and Opportunities for Drug Development. *Br J Cancer* (2014) 111(10):1888–98. doi: 10.1038/bjc.2014.388
116. Slamon DJ, Leyland-Jones B, Shak S, Fuchs H, Paton V, Bajamonde A, et al. Use of Chemotherapy Plus a Monoclonal Antibody Against HER2 for Metastatic Breast Cancer That Overexpresses HER2. *N Engl J Med* (2001) 344(11):783–92. doi: 10.1056/NEJM200103153441101
117. Lui VW, Lau CP, Ho K, Ng MH, Cheng SH, Tsao SW, et al. Anti-Invasion, Anti-Proliferation and Anoikis-Sensitization Activities of Lapatinib in Nasopharyngeal Carcinoma Cells. *Invest New Drugs* (2011) 29(6):1241–52. doi: 10.1007/s10637-010-9470-y
118. Weroha SJ, Oberg AL, Ziegler KL, Dakhil SR, Rowland KM, Hartmann LC, et al. Phase II Trial of Lapatinib and Topotecan (LapTop) in Patients With Platinum-Refractory/Resistant Ovarian and Primary Peritoneal Carcinoma. *Gynecol Oncol* (2011) 122(1):116–20. doi: 10.1016/j.ygyno.2011.03.030
119. Fortin MA, Orlova A, Malmström PU, Tolmachev V. Labelling Chemistry and Characterization of $[^{90}\text{Y}/^{177}\text{Lu}]$ -DOTA-ZHER2:342-3 Affibody

- Molecule, a Candidate Agent for Locoregional Treatment of Urinary Bladder Carcinoma. *Int J Mol Med* (2007) 19(2):285–91. doi: 10.3892/ijmm.19.2.285
120. Pillai MR, Chakraborty S, Das T, Venkatesh M, Ramamoorthy N. Production Logistics of ¹⁷⁷Lu for Radionuclide Therapy. *Appl Radiat Isot* (2003) 59(2-3):109–18. doi: 10.1016/S0969-8043(03)00158-1
 121. Altai M, Westerlund K, Vellea J, Mitran B, Honarvar H, Karlström AE. Evaluation of Affibody Molecule-Based PNA-Mediated Radionuclide Pretargeting: Development of an Optimized Conjugation Protocol and ¹⁷⁷Lu Labeling. *Nucl Med Biol* (2017) 54:1–9. doi: 10.1016/j.nucmedbio.2017.07.003
 122. Westerlund K, Altai M, Mitran B, Konijnenberg M, Oroujeni M, Atterby C, et al. Radionuclide Therapy of HER2-Expressing Human Xenografts Using Affibody-Based Peptide Nucleic Acid-Mediated Pretargeting: *In Vivo* Proof of Principle. *J Nucl Med* (2018) 59(7):1092–8. doi: 10.2967/jnumed.118.208348
 123. Tano H, Oroujeni M, Vorobyeva A, Westerlund K, Liu Y, Xu T, et al. Comparative Evaluation of Novel ¹⁷⁷Lu-Labeled PNA Probes for Affibody-Mediated PNA-Based Pretargeting. *Cancers (Basel)* (2021) 13(3):500. doi: 10.3390/cancers13030500
 124. Tolmachev V, Orlova A. Affibody Molecules as Targeting Vectors for PET Imaging. *Cancers (Basel)* (2020) 12(3):651. doi: 10.3390/cancers12030651
 125. Feldwisch J, Tolmachev V. Engineering of Affibody Molecules for Therapy and Diagnostics. *Methods Mol Biol* (2012) 899:103–26. doi: 10.1007/978-1-61779-921-1_7
 126. Cong J, Liu R, Hou J, Wang X, Jiang H, Wang J. Effects of Trastuzumab on the Proliferation and Apoptosis of Ovarian Cancer Cells. *Neoplasma* (2019) 66(2):240–4. doi: 10.4149/neo_2018_180724N524
 127. Shang AQ, Wu J, Bi F, Zhang YJ, Xu LR, Li LL, et al. Relationship Between HER2 and JAK/STAT-SOCS3 Signaling Pathway and Clinicopathological Features and Prognosis of Ovarian Cancer. *Cancer Biol Ther* (2017) 18(5):314–22. doi: 10.1080/15384047.2017.1310343
 128. Hu X, Liang Z, Zhang C, Wang G, Cai J, Wang P. The Diagnostic Performance of Maximum Uptake Value and Apparent Diffusion Coefficient in Differentiating Benign and Malignant Ovarian or Adnexal Masses: A Meta-Analysis. *Front Oncol* (2022) 12:840433. doi: 10.3389/fonc.2022.840433
 129. Hu X, Li D, Liang Z, Liao Y, Yang L, Wang R, et al. Indirect Comparison of the Diagnostic Performance of ¹⁸F-FDG PET/CT and MRI in Differentiating Benign and Malignant Ovarian or Adnexal Tumors: A Systematic Review and Meta-Analysis. *BMC Cancer* (2021) 21(1):1080. doi: 10.1186/s12885-021-08815-3
 130. Honarvar H, Jokilaakso N, Andersson K, Malmberg J, Rosik D, Orlova A, et al. Evaluation of Backbone-Cyclized HER2-Binding 2-Helix Affibody Molecule for *In Vivo* Molecular Imaging. *Nucl Med Biol* (2013) 40(3):378–86. doi: 10.1016/j.nucmedbio.2012.12.009
 131. Xu T, Wang L, Jia Y, Jia Z, Li Z, Cui S, et al. Long-Term Multidisciplinary Integrative Therapy Management Resulted in Favorable Outcomes for Ovarian Cancer During Pregnancy: A Case Report and Literature Review. *J Ovarian Res* (2019) 12(1):108. doi: 10.1186/s13048-019-0584-3
 132. Siavoshinia L, Jamalan M, Zeinali M, Pourshohod A, Koushki M, Moradipoodeh B, et al. Improvement of Targeted Chemotherapy of HER2-Positive Ovarian Malignant Cell Line by ZHER2-Idarubicin Conjugate: An *In Vitro* Study. *Iran J Pathol* (2021) 16(2):109–18. doi: 10.30699/ijp.2020.120392.2310
 133. Altunay B, Morgenroth A, Beheshti M, Vogt A, Wong NCL, Ting HH, et al. HER2-Directed Antibodies, Affibodies and Nanobodies as Drug-Delivery Vehicles in Breast Cancer With a Specific Focus on Radioimmunotherapy and Radioimmunoimaging. *Eur J Nucl Med Mol Imaging* (2021) 48(5):1371–89. doi: 10.1007/s00259-020-05094-1

Conflict of Interest: Author YF was employed by Jiangsu Yuanben Biotechnology Co., Ltd.

The remaining authors declare that the research was conducted in the absence of any commercial or financial relationships that could be construed as a potential conflict of interest.

Publisher's Note: All claims expressed in this article are solely those of the authors and do not necessarily represent those of their affiliated organizations, or those of the publisher, the editors and the reviewers. Any product that may be evaluated in this article, or claim that may be made by its manufacturer, is not guaranteed or endorsed by the publisher.

Copyright © 2022 Hu, Li, Fu, Zheng, Feng, Cai and Wang. This is an open-access article distributed under the terms of the Creative Commons Attribution License (CC BY). The use, distribution or reproduction in other forums is permitted, provided the original author(s) and the copyright owner(s) are credited and that the original publication in this journal is cited, in accordance with accepted academic practice. No use, distribution or reproduction is permitted which does not comply with these terms.



Controversial Role of the Immune Checkpoint OX40L Expression on Platelets in Breast Cancer Progression

OPEN ACCESS

Edited by:

Jinhui Liu,

Nanjing Medical University, China

Reviewed by:

Dong Li,

University of Kentucky, United States

Takanori So,

University of Toyama, Japan

Nahid Eskandari,

Isfahan University of Medical

Sciences, Iran

*Correspondence:

Stefanie Maurer

stefanie.maurer@mssm.edu

*ORCID:

Kim L. Clar

orcid.org/0000-0003-1454-9830

Helmut R. Salih

orcid.org/0000-0002-6719-1847

Specialty section:

This article was submitted to

Gynecological Oncology,

a section of the journal

Frontiers in Oncology

Received: 11 April 2022

Accepted: 08 June 2022

Published: 08 July 2022

Citation:

Rittig SM, Lutz MS, Clar KL, Zhou Y, Kropp KN, Koch A, Hartkopf AD, Hinterleitner M, Zender L, Salih HR, Maurer S and Hinterleitner C (2022)

Controversial Role of the Immune Checkpoint OX40L Expression on Platelets in Breast

Cancer Progression.

Front. Oncol. 12:917834.

doi: 10.3389/fonc.2022.917834

Susanne M. Rittig^{1,2}, Martina S. Lutz^{3,4}, Kim L. Clar^{3,4†}, Yanjun Zhou^{3,4}, Korbinian N. Kropp⁵, André Koch⁶, Andreas D. Hartkopf^{6,7}, Martina Hinterleitner^{4,8}, Lars Zender^{4,8,9}, Helmut R. Salih^{3,4†}, Stefanie Maurer^{3,4,10*} and Clemens Hinterleitner^{4,8,11}

¹ Department of Hematology, Oncology and Cancer Immunology, Charité – Universitätsmedizin Berlin, Corporate Member of Freie Universität Berlin and Humboldt-Universität zu Berlin, Berlin, Germany, ² Berlin Institute of Health at Charité – Universitätsmedizin Berlin, BIH Biomedical Innovation Academy, BIH Charité (Junior) (Digital) Clinician Scientist Program, Berlin, Germany, ³ Clinical Collaboration Unit Translational Immunology, German Cancer Consortium (DKTK), Department of Internal Medicine, University Hospital Tuebingen, Tuebingen, Germany, ⁴ Cluster of Excellence iFIT (EXC 2180) “Image-Guided and Functionally Instructed Tumor Therapies”, University of Tuebingen, Tuebingen, Germany, ⁵ Department of Hematology, Medical Oncology and Pneumology, University Medical Center of Mainz, Mainz, Germany, ⁶ Department of Obstetrics and Gynecology, University Hospital Tuebingen, Tuebingen, Germany, ⁷ Department of Gynecology and Obstetrics, University Hospital of Ulm, Ulm, Germany, ⁸ Department of Medical Oncology and Pneumology (Internal Medicine VIII), University Hospital Tuebingen, Tuebingen, Germany, ⁹ German Cancer Research Consortium (DKTK), Partner Site Tuebingen, German Cancer Research Center (DKFZ), Heidelberg, Germany, ¹⁰ Precision Immunology Institute, Department of Oncological Sciences, and The Tisch Cancer Institute, Icahn School of Medicine at Mount Sinai, New York, NY, United States, ¹¹ Department of Cancer Biology and Genetics, Memorial Sloan Kettering Cancer Center, New York, NY, United States

In conventional T cells, OX40 has been identified as a major costimulating receptor augmenting survival and clonal expansion of effector and memory T cell populations. In regulatory T cells, (Treg) OX40 signaling suppresses cellular activity and differentiation. However, clinical trials investigating OX40 agonists to enhance anti-tumor immunity, showed only limited success so far. Here we show that platelets from breast cancer patients express relevant levels of OX40L and platelet OX40L (pOX40L) inversely correlates with platelet-expressed immune checkpoint molecules GITRL (pGITRL) and TACI (pTACI). While high expression of pOX40L correlates with T and NK cell activation, elevated pOX40L levels identify patients with higher tumor grades, the occurrence of metastases, and shorter recurrence-free survival (RFS). Of note, OX40 mRNA levels in breast cancer correlate with enhanced expression of anti-apoptotic, immune-suppressive, and tumor-promoting mRNA gene signatures. Our data suggest that OX40L on platelets might play counteracting roles in cancer and anti-tumor immunity. Since pOX40L reflects disease relapse better than the routinely used predictive markers CA15-3, CEA, and LDH, it could serve as a novel biomarker for refractory disease in breast cancer.

Keywords: breast cancer, biomarker, immunotherapy, platelets, prognosis, OX40L

BACKGROUND

Immune checkpoints are crucial parts of inhibitory or activating immune pathways, regulating self-tolerance and immune responses. Particularly in the context of malignant disease, immune-inhibitory receptors including PD-1 or CTLA-4, are triggered to dampen anti-tumor immune responses (1–3). In contrast, co-stimulatory signaling pathways like CD27, CD40, or OX40 have been described to play a crucial role in T cell activation, proliferation, and tumor immune surveillance (4–6). An increasing number of therapeutic strategies have been exploited to block or activate the respective pathways and reinforce anti-tumor immunity (6–9). Strategies to improve co-stimulatory pathways like OX40 have shown promising anti-tumor activity in preclinical mouse models (10–12). The immune checkpoint molecule OX40 is a member of the tumor necrosis factor receptor (TNFR) superfamily. It is expressed on effector T lymphocytes following activation and promotes their differentiation, proliferation, and survival while simultaneously inhibiting the suppressive activity of regulatory T cells (13). Although monoclonal antibodies targeting OX40 are currently being investigated in early clinical trials, a successful translation of the promising preclinical data is still pending (14, 15). Of note, the expression of the cognate ligand (OX40L), also known as tumor necrosis factor superfamily member 4 (TNFSF4) on platelets has been described to be involved in cardiac inflammation and solid tumors (16, 17).

Platelets play a critical role in tumor progression, formation of metastasis, tumor immunosurveillance, and immunotherapy *via* a manifold of mechanisms, including coating of tumor cells, the release of soluble factors, e.g. TGF- β , VEGF, and expression of immunoregulatory molecules like PD-L1, GITRL, CD40L and TACI (18–25). Here we show that the immune checkpoint molecule OX40L is frequently expressed on platelets in breast cancer and is negatively correlated with the expression of the immune checkpoint molecules GITRL and TACI on the platelet surface. In breast cancer, high levels of pOX40L were found to be associated with immune cell activation, higher tumor grades, formation of metastasis, and reduced recurrence-free survival (RFS), indicating that pOX40L might play a controversial role in tumor biology *via* orchestrating immune activation and tumorigenesis. We demonstrate that pOX40L is superior in predicting disease progression compared to routinely used markers in breast cancer.

RESULTS AND DISCUSSION

Expression of OX40L on Platelets Correlates With Immune Cell Activation

Although the expression of several immune checkpoint molecules on platelets has recently been described, their role in cancer is only poorly understood (23–25). In an effort to further investigate the impact of platelet-expressed immune checkpoints in solid tumors, we characterized the concurrent expression of the three TNF members pGITRL (pTNFSF18), pTACI

(pTNFRSF13B), and pOX40L (pTNFSF4) in a cohort of breast cancer patients (**Figure 1A**). Interestingly we found a positive correlation of pGITRL and pTACI, two recently identified platelet-expressed immune checkpoint molecules with predictive value in breast cancer (24, 25). Despite the great homology between OX40 and GITR (26), the ligand of the immune stimulatory co-receptor OX40 on platelets was shown to be negatively correlated with pGITRL and pTACI expression (**Figures 1B,C**). This observation indicates that platelets express a plethora of different immune checkpoint molecules and the platelet immune phenotype (PIP) seems to be specifically regulated, especially in cancer. In a previous study and in line with the different roles of GITR in NK cells and T cells, pGITRL was found to be associated with T cell but inversely correlated with NK cell activation in breast cancer (9, 24, 27). The fact that highest pGITRL level were present in intermediate tumor stages may support the notion that stimulation of T cell derived GITR contributes to tumor immunosurveillance of breast cancer but will lose its impact in furthering tumor progression in later stages. Expression of the receptor TACI on platelets is also specifically upregulated in breast cancer and is inversely correlated with metastasis and advanced tumor stage. It is not yet understood how pTACI may be involved in the (immune) regulation in breast cancer. One could speculate that pTACI induces reverse signaling into ligand-expressing cells such as breast cancer cells (28–30), but the existence of such signaling still warrants proof (31). Additionally, it was found that TACI is expressed on both, macrophages and tumor cells, particularly in breast cancer cases with poor prognosis (30). Thus, another explanation could be a transfer of TACI between platelets and malignant cells - which has been shown for other pathophysiologically relevant molecules like MHC class I and PD-L1 (19, 23) - or immune cells.

It is poorly understood how surface levels of immune regulatory molecules on platelets are regulated. Surface expression of some immunoregulatory molecules like PD-L1 (23) and CD40L (32) for example are dependent on platelet activation. Changed expression levels in breast cancer however, might be regulated *via* trogocytosis, reprogrammed megakaryopoiesis (33) or protein synthesis in platelets which can occur at low levels (34). *In vitro* data show that soluble factors from tumor cells alter megakaryopoiesis in the MEG-01 cell line model and thus the megakaryocyte immunophenotype with regard to GITRL expression. One contributing factor appeared to be TGF- β which is known to be involved in the regulation of GITRL expression on dendritic cells (35). Alike, OX40L is expressed among others on antigen presenting cells where it is upregulated upon antigen presentation and costimulation including interferon gamma (IFN- γ) (36), and following stimulations with prostaglandin E2 (37), IL-18 (38) and thymic stromal lymphopoietin (TSLP) (39). Further studies are needed to study whether these factors also play a role in pOX40L regulation in the context of breast cancer.

Targeting of the co-stimulatory receptor OX40 is recently under evaluation as a novel strategy in cancer immunotherapy, and its expression on CD8+ cytotoxic T cells of breast cancer patients was found to be upregulated upon neo-adjuvant

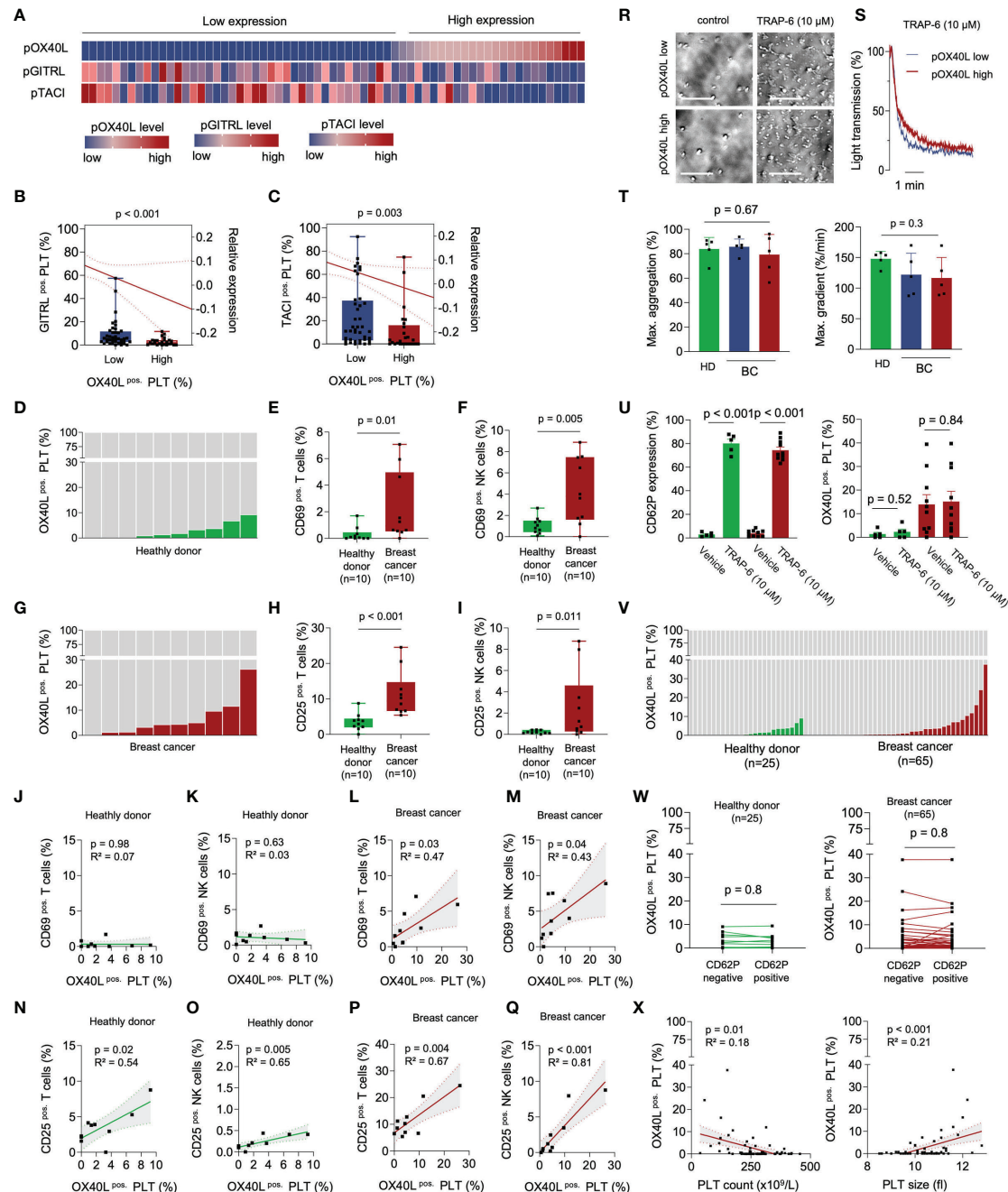


FIGURE 1 | pOX40L in breast cancer patients is associated with a distinct platelet immunophenotype and activation of cytotoxic lymphocytes. **(A–C)** Comparative analysis of the platelet immune checkpoint molecules pOX40L, pTACI and pGITRL (n = 65). The gating strategy used to analyze pOX40L expression on platelets is given in **Supplementary Figure 3**. Co-expression of TACI **(B)** or GITRL **(C)** on pOX40L^{low} and pOX40L^{high} platelets, respectively. **(D–J)** Level of pOX40L in healthy donors **(D)** and breast cancer patients **(G)** and expression of CD69 **(E, F)** and CD25 **(H, I)** on NK cells and T cells of the respective donors (n = 10 each). **(J–Q)** Co-regulation of CD69/CD25 on NK/T cells and pOX40L in healthy donors and breast cancer patients (n = 10 each). **(R–S)** Comparative analysis of platelet activation in the presence or absence of TRAP-6 (10 μM) with regard to pOX40L status. Representative platelet aggregation studies **(R, S)** were performed in pOX40L high and low expressing platelets derived from breast cancer patients. Aggregation studies **(T)** were performed in platelets derived from 5 healthy donors (green) and 10 breast cancer patients (pOX40L low in blue, pOX40L high in red). **(U)** Expression of CD62P and OX40L on platelets from HD and breast cancer patients *ex vivo* (n = 10 each). **(V)** Expression of OX40L on platelets from healthy donors and the complete breast cancer cohort *ex vivo* (n = 25 and n = 65, respectively). **(W)** pOX40L level in healthy donors (HD), (left panel) and breast cancer patients (right panel) with regard to CD62P expression (n = 25 and n = 65, respectively). **(X)** Correlation of pTACI expression and platelet count (left panel) and platelet size (right panel). **(B, C), (E, F), (H, I)** Each dot represents a single patient. Boxes represent median and 25th to 75th percentiles, whiskers are minimum to maximum.

chemotherapy (40). When comparatively analyzing pOX40L and the immunophenotype in a screening cohort of healthy donors and breast cancer patients, we found higher pOX40L levels to be associated with increased T and NK cell activation levels (**Figures 1D–I**). Especially in breast cancer patients, CD69 and CD25 expression on T and NK cells were strongly correlated with the expression of OX40L on platelets (**Figures 1J–Q**). This is particularly interesting since previous studies report on an enlarged CD4⁺ FOXP3⁺ T cells population in breast cancer (41, 42). Yet, further work is required to evaluate whether pOX40L-dependent signaling contributes to the expansion of regulatory T cells. Taking the known immune-activating role of OX40L on other cell types, including B cells, mast cells or endothelial cells into account, our observation might point to pOX40L as a novel and underestimated player mediating immune cell activation and anti-tumor immunity.

Regulation of OX40L on Platelets During Platelet Activation

As it is well established that the platelet surface proteome, as well as the PIP, is modulated *via* platelet activation, we further analyzed pOX40L in the context of platelet reactivity. Platelet aggregometry showed comparable functional capabilities in the presence of the PAR-1 agonist TRAP-6 independent of pOX40L expression (**Figures 1R–T**). This confirms previous data showing that the expression of immune checkpoint molecules on platelets is not associated with platelet reactivity (23, 24). In contrast to previous observations, platelet activation *ex vivo* did not result in an expression change of pOX40L on the platelet surface (**Figure 1U**). Confirming this observation *ex vivo*, we found no significant correlation of pOX40L and CD62P in our entire cohort of healthy donors and breast cancer patients (**Figures 1V, W**). Since pOX40L surface expression seems to be rarely regulated during platelet activation, complex adjustment algorithms to model surface expression *in vivo* are subsequently not required. This highlights pOX40L as a novel putative biomarker candidate in breast cancer. We found that pOX40L, similar to pTACI and pGITRL, was negatively correlated with platelet count and associated with larger platelet size (**Figure 1X**). This might suggest a complex interplay of anti-cancer treatment, platelet regeneration, and tumor homeostasis, resulting in a subsequent chronic inflammatory environment might be involved in PIP regulation, including pOX40L (43, 44).

Regulation of pOX40L Expression During Breast Cancer Progression

In the next step, we studied the association of pOX40L with clinical parameters and disease progression. While pOX40L status was irrespective of the tumor stage (T) and lymph node invasion (N), it was associated with histological grading (G) ($p = 0.03$), whereas most pOX40L^{high} patients were found in the G3 group (**Figures 2A–C**). In line, the proliferation index (Ki67) of tumors and formation of metastasis, which both constitute negative prognostic markers for patients, were directly associated with higher pOX40L levels in breast cancer patients

($p = 0.005$ and $p = 0.008$), respectively (**Figures 2D, E**). Accordingly, with a median time to metastasis (TTM) of 17 months compared to 76 months, recurrence-free survival (RFS) was significantly shorter in patients with a high pOX40L expression compared to patients showing low levels of pOX40L ($p = 0.02$) (**Figure 3F**). Interestingly, this observation seems to be in contrast to the proposed role of pOX40L as an immune-stimulating player promoting anti-tumor effects. Of note, we did not observe any correlation of pOX40L expression and different systemic treatments or number of received treatment regimens (**Supplementary Figure 1 A–C**).

We observed that pOX40L status was inversely correlated with the number of metastatic organs. While patients with high levels of pOX40L showed only one metastatic site, low pOX40L levels were associated with a higher metastatic burden in multiple organs (**Figure 2G**). These findings led to the hypothesis that pOX40L might be involved in tumor immune cell interactions. Interestingly, pOX40L expression was shown to be independent of treatment modality, kind of treatment and number of treatment regimen (**Supplementary Figure 1 A–C**). When analyzing the distribution of metastasis in our cohort we observed that patients with high expression of pOX40L frequently developed lung metastasis (**Figure 2H**). Following this observation, we further investigated putative OX40/OX40L signaling in malignant cells. We correlated OX40 mRNA expression in a TCGA breast cancer data set (TCGA, Firehose Legacy) and gene-expression signatures in breast cancer associated with lung metastasis (45). Remarkably, the main genes involved, e. g. MMP1, MMP2, SPARC, VCMAM1, CXCL1, and CXCR4 were found to be significantly associated in with high OX40 mRNA expression (**Figure 2I**). In addition, these genes clustered with the expression of anti-apoptotic and tumor-promoting factors (**Figures 2I,J**). Finally, we studied whether additional immune checkpoint molecules might be co-regulated with OX40 mRNA in breast cancer cells. We found a strong correlation of OX40 and PD-L1, CD80, CD86, VISTA, HVEM, and TGF β , hypothesizing that OX40 expression on tumor cells might be associated with an immune-inhibitory phenotype (**Figures 2K–P**).

Our data suggest that OX40L and OX40 are expressed on various cell types in the tumor microenvironment, and OX40/OX40L signaling in cancer might be much more complex than previously known. This might be reflected by the limited success of OX40 targeting therapies so far (10–12). As a result, further comprehensive studies investigating both, OX40 signaling in tumor cells and the functional role of pOX40L on platelets are needed. Since expression of OX40 on breast cancer cells has already been shown to be associated with an aggressive cancer phenotype (46), expression of OX40 on tumor tissue as well as determination of pOX40L might be useful to stratify patients who might benefit from an immunotherapy targeting the OX40 pathway.

Since pOX40L is not regulated upon platelet activation and was shown to predict PFS in our cohort, we finally investigated the potential of pOX40L as a prognostic marker in breast cancer. We comparatively analyzed pOX40L expression and commonly used clinical markers (47–49) to predict disease relapse in breast

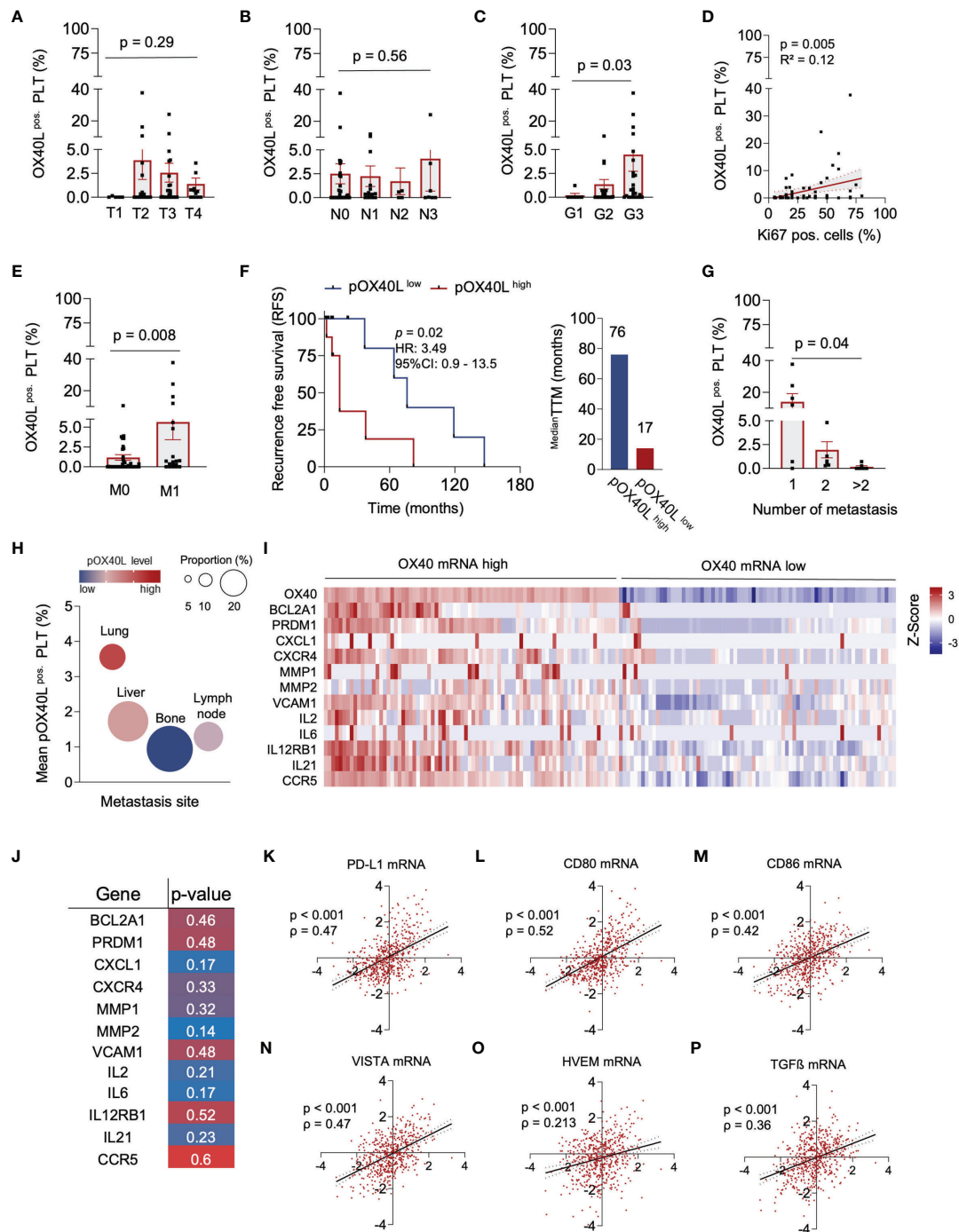


FIGURE 2 | pOX40L predicts disease relapse and metastasis in breast cancer. **(A)** pOX40L expression in different tumor stages (T), (n = 65) **(B)** Association of pOX40L expression and lymph node invasion (N), (n = 65). **(C)** pOX40L level in patients with different tumor grading (G), (n = 65). **(D)** Correlation between pOX40L expression on platelets of 65 BC patients and the Ki67 positive cells (%). **(E)** pOX40L expression in patients with and without metastatic disease (M), (n = 65). **(F)** Kaplan-Meier curves estimates of RFS (months) in patients with a pOX40L > mean (pOX40L^{high} = red) and pOX40L level < mean (pOX40L^{low} = blue), (n = 65). Median time to metastasis (pOX40L^{high} = red, pOX40L^{low} = blue). **(G)** pOX40L expression in patients with different number of metastasis (n = 65). **(H)** Mean expression of pOX40L in different metastatic organs (n = 20). **(I)** Heatmap depicting the relative mRNA level OX40 and a gene set associated with lung metastasis, anti-apoptotic and tumor-promoting signatures in breast tumors (TCGA-Firehose legacy), (n = 65). **(J)** Spearman correlation mRNA gene signatures and OX40 mRNA. **(K-P)** Scatter plot of OX40 mRNA and PD-L1 **(K)**, CD80 **(L)**, CD86 **(M)**, VISTA **(N)**, HVEM **(O)** and TGFβ **(P)** mRNA level in breast cancer. Each dot represents a single patient. **(A-E, G, K-P)** Each dot represents a single patient. **(A-E, G)** Data are mean ± SEM.

cancer (**Figure 3A**). Whereas pOX40L expression, as well as CA15-3, CEA and LDH was independent of the respective subtype (**Figure 3B**; **Supplementary Figures 2A–C**), we observed a positive correlation of pOX40L expression and the conventional tumor markers CEA and LDH (**Figures 3C–E**). This in line with our observation that pOX40L was also associated with higher Ki67 level and higher tumor grading. Of

note, with a sensitivity of 0.78 (95% CI: 0.55 – 0.91) and specificity of 0.77 (95% CI: 0.63 – 0.86) pOX40L showed the highest accuracy in predicting disease relapse (**Figures 3F–K**). Since ER/HER2 status represents an indispensable part of the management of breast cancer patients we additionally analyzed the influence of ER and HER2 status on pOX40L expression in our cohort. Interestingly we didn't observe any correlation of

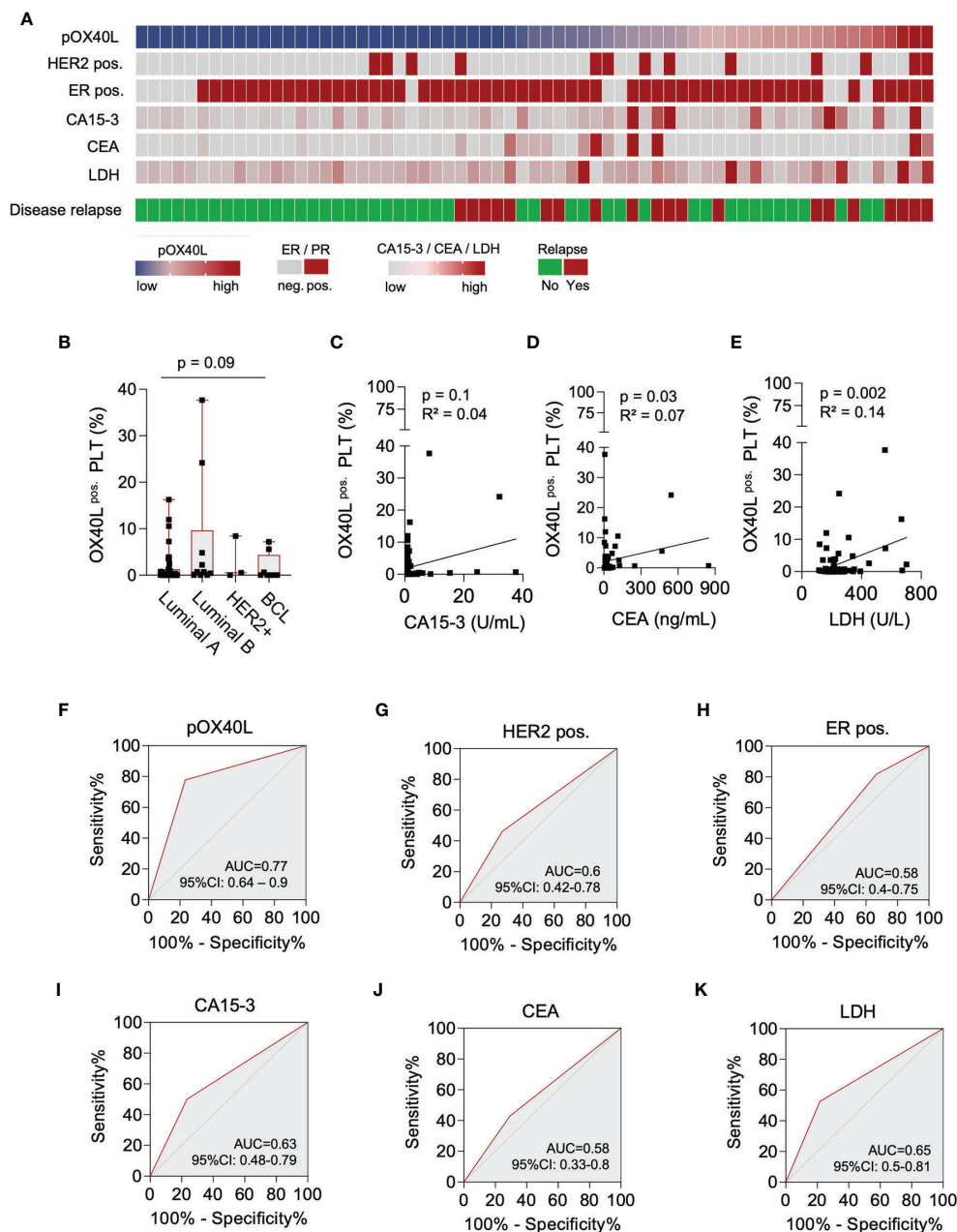


FIGURE 3 | Predictive value of pOX40L in breast cancer relapse. **(A)** Comparative analysis of pOX40L and the clinical markers HER2, ER, CA 15-3, CEA and LDH. **(B)** Association of pOX40L expression and different breast cancer subtypes. **(C–E)** Correlation of pOX40L and conventional tumor marker including CA15-3 **(C)**, CEA **(D)** and LDH **(E)**. **(F–K)** Predictive value of pOX40L **(F)**, HER2 **(G)**, ER **(H)**, CA15-3 **(I)**, CEA **(J)** and LDH **(K)** expression for disease relapse was analyzed using ROC (Area under the ROC curve) analysis.

hormone receptor or HER2 status and expression of OX40L on platelets (**Supplementary Figures 2D, E**). However, taking into account that triple negative and HER2-positive breast cancer patients present the highest levels of tumor infiltrating lymphocytes (TILs) (50), which is prerequisite for the successful use of immunotherapy, pOX40L expression as well as HER2 and hormone receptor status might be useful predictive tools for OX40 agonists. Of note, additional data are needed to further investigate such an approach.

Nevertheless, our exploratory study suffers from some limitations. Due to the fact that we used an exploratory study design our breast cancer cohort constitutes an unequal representation of tumor stages, different treatments and different cycles of various treatment regimens. Even if pOX40L expression seems to be independent of tumor stages, lymph node invasion, treatment modalities and number of treatment regimen (**Supplementary Figures 1A–C**), further consecutive analysis in a balanced, prospective study cohort are needed.

In addition, our exploratory study was not powered to compare the determination of pOX40L with conventional screening methods including mammogram/MRI or determination of CEA or CA15-3. Further prospective data are needed to verify the predictive role of pOX40L in breast cancer. Nevertheless, since high level of pOX40L were associated with a shorter RFS and TTM, determination of pOX40L might be a useful, noninvasive and cost-effective method allowing for longitudinal follow-up analysis. In patients with high levels of pOX40L follow-up care might be intensified and supplemented by specific screening for metastases.

In conclusion, our explorative data not only highlight the prognostic potential of the platelet-expressed immunoregulatory molecule OX40L as a biomarker in breast cancer progression. They further indicate that OX40/OX40L signaling in cancer seems to be complex and might play a controversial role in tumor biology *via* orchestrating immune activation and tumorigenesis, an approach which requires further functional and clinical validation.

MATERIAL AND METHODS

Patients

During 2019–2021, 65 breast cancer patients treated at the Department of Obstetrics and Gynecology and the Department of Medical Oncology and Pneumology were included in our prospective study. The study was approved by IRB (ethics committee of the Faculty of Medicine of the Eberhard Karls Universität Tübingen) and of the University Hospital (13/2007V). Written informed consent in accordance with the Helsinki protocol was given in all cases. The patient characteristics in detail are given in **Supplementary Table 1**.

Reagents

Paraformaldehyde was from Affymetrix (Santa Clara, CA, USA). Anti-OX40L antibodies were from Ancell Corporation (Bayport, MN, USA). Anti-human TACI, anti-human GITRL antibody

and the respective isotype control were from R&D Systems (Minneapolis, MN). CD41a-PECy5, and CD62P-FITC were from BD Pharmingen, CD3-APC/Fire, CD69-PE and CD25-FITC and CD56-PECy7 were obtained from BioLegend. The goat anti-mouse PE conjugate was from Dako (Glostrup, Denmark). Dead cells were excluded using Fixable Aqua (Invitrogen, Carlsbad, CA, USA) after extracellular staining according to the manufacturer's instructions. Bicol Separating Solution was purchased from Biochrom AG (Berlin, Germany).

Platelet Aggregation

Platelet aggregation was analyzed using the four-channel light transmission platelet aggregometer APACT 4004 (Elitech, Puteaux, France) according to the manufacturer's instructions. For platelet activation *ex vivo* 10 μ M of Thrombin Receptor Activator Peptide 6 (TRAP-6) was added to the platelets.

Generation and Preparation of Peripheral Blood Mononuclear Cells (PBMC) and Peripheral Blood Platelets

PBMCs were obtained from patients and healthy donors after informed writing consent. Preparation of PBMCs was performed as previously described (19). Peripheral blood platelets were collected in citrate buffer and briefly centrifuged for 20 min at 120 \times g. For the generation of platelet-rich plasma, platelets were washed with citrate wash buffer (128 mmol/L NaCl, 11 mmol/L glucose, 7.5 mmol/L Na₂HPO₄, 4.8 mmol/L sodium citrate, 4.3 mmol/L NaH₂PO₄, 2.4 mmol/L citric acid, and 0.35% bovine serum albumin).

Flow Cytometry

Flow cytometry was performed as described previously (24). The percentage of positive cells was calculated as follows: “% surface expression obtained with specific antibody” – “% surface expression obtained with isotype control”. T cells were selected by positivity for CD3, and NK cells by a CD56+CD3– phenotype. Platelets were selected by CD41a+ and CD62P– (resting) or CD62P+ (activated).

Statistics

For continuous variables student's t test, Mann-Whitney U test, one-way ANOVA and Kruskal-Wallis test was used. For multiple comparison Dunn's multiple comparison test was used. For categorical data we used chi-squared test or Fisher's exact test. Correlation of pOX40L expression and CD69/CD25 expression on T and NK cells, platelet size and platelet volume as well as Ki67 level and pOX40L expression was analyzed using simple linear regression analysis. Correlation of mRNA expression was performed using simple linear regression analysis. Recurrence free survival (RFS) were calculated using the Kaplan-Meier method. Hazard ratios (HRs) were determined using Cox regression analysis. High pOX40L expression was defined as follows: pOX40L high > mean pOX40L, pOX40L low < mean pOX40L. The predictive value of pOX40L was evaluated by examining the area under the receiver-operator characteristic (ROC) with a confidence interval of 95%. All statistical tests

were considered statistically significant when P was below 0.05. Statistical analysis was performed using GraphPadPrism (v.8.4.0).

DATA AVAILABILITY STATEMENT

The genome dataset presented in this study can be found in online repositories (The Cancer Genome Atlas Database (TCGA), <https://www.cbiportal.org>). The data that support the findings of this study are available from the corresponding author, SM upon reasonable request.

ETHICS STATEMENT

The study was approved by IRB (ethics committee of the Faculty of Medicine of the Eberhard Karls Universität Tuebingen) and of the University Hospital (13/2007V). The patients/participants provided their written informed consent to participate in this study.

AUTHOR CONTRIBUTIONS

CH, SM, LZ, and HS conceived and designed the study. ML, KC, and YZ conducted *in vitro* experiments. AK and AH conducted patient data and sample collection as well as medical evaluation and analysis. SR, MH, KK, SM, and CH analyzed data and performed statistical analyses. SR, CH, and SM prepared figures and tables; SR, SM, and CH wrote the first draft of the manuscript. HS, LZ, and AH contributed to data interpretation and manuscript edit. All authors critically reviewed, read, and approved the final manuscript.

FUNDING

This work was funded by the Deutsche Forschungsgemeinschaft (DFG, German Research Foundation) under Germany's

Excellence Strategy - EXC 2180 - 39090067 and DFG, project number 374031971-TRR 240/project B05. SM was supported by the Institutional Strategy of the University of Tuebingen (Deutsche Forschungsgemeinschaft, ZUK 63) and the Deutsche Forschungsgemeinschaft, MA 8774/1-1. HS was funded by Deutsche Forschungsgemeinschaft, SA1360/7-3, Wilhelm Sander-Stiftung, 2007.115.3, and Deutsche Krebshilfe 70112914. SR is participant in the BIH Charité Clinician Scientist Program funded by the Charité – Universitätsmedizin Berlin, and the Berlin Institute of Health at Charité (BIH).

ACKNOWLEDGMENTS

Flow cytometry sample acquisition was performed on shared instruments of the Flow Cytometry Core Facility Tuebingen.

SUPPLEMENTARY MATERIAL

The Supplementary Material for this article can be found online at: <https://www.frontiersin.org/articles/10.3389/fonc.2022.917834/full#supplementary-material>

Supplementary Figure 1 | Association of pOX40L and breast cancer treatment.

(A) Comparative analysis of pOX40L and different breast cancer subtypes.

(B) Association of pOX40L and endocrine therapy. (C) Correlation of pOX40L and different numbers of treatment regimen.

Supplementary Figure 2 | pOX40L expression in different breast cancer subtypes

Expression of CA15-3 (A), CEA (B) and LDH (C) in different breast cancer subtypes.

(D) pOX40L expression in HER2 positive and negative patients. (E) pOX40L

expression in ER positive vs. ER negative patients. pos. = positive, neg. = negative.

Supplementary Figure 3 | Gating strategy used to analyze pOX40L expression

on platelets pOX40L levels were assessed by flow cytometry. Platelets were defined as CD41a-positive subcellular fragments and specific staining for OX40L level was analyzed in association with the platelet activation marker P-selectin (CD62P). If not indicated otherwise, data reflect pOX40L expression on all CD41+ platelets, i.e. activated (CD62P+) and resting (CD62P-) platelets.

Supplementary Table 1 | Patient characteristics. Other immune checkpoint molecules in parts of this cohort have been published previously (24, 25, 51).

REFERENCES

- McDermott DF, Atkins MB. PD-1 as a Potential Target in Cancer Therapy. *Cancer Med* (2013) 2(5):662–73. doi: 10.1002/cam4.106
- Leach DR, Krummel MF, Allison JP. Enhancement of Antitumor Immunity by CTLA-4 Blockade. *Science* (1996) 271(5256):1734–6. doi: 10.1126/science.271.5256.1734
- Hiam-Galvez KJ, Allen BM, Spitzer MH. Systemic Immunity in Cancer. *Nat Rev Cancer* (2021) 21(6):345–59. doi: 10.1038/s41568-021-00347-z
- Aspeshlagh S, Postel-Vinay S, Rusakiewicz S, Soria J-C, Zitvogel, Aurélien Marabelle, et al. Rationale for Anti-OX40 Cancer Immunotherapy. *Eur J Cancer* (2016) 52:50–66. doi: 10.1016/j.ejca.2015.08.021
- Qin S, Xu L, Yi M, Yu S, Wu K, Luo S. Novel Immune Checkpoint Targets: Moving Beyond PD-1 and CTLA-4. *Mol Cancer* (2019) 18(1):155. doi: 10.1186/s12943-019-1091-2
- Buchan SL, Rogel A, Al-Shamkhani A. The Immunobiology of CD27 and OX40 and Their Potential as Targets for Cancer Immunotherapy. *Blood* (2018) 131(1):39–48. doi: 10.1182/blood-2017-07-741025
- Weiss JM, Wiltout RH. Multifaceted Antitumor Responses to Activating Anti-CD40 Antibody Therapy Combined With Immunomodulatory or Targeted Agents. *Oncimmunology* (2014) 3(8):e954483. doi: 10.4161/21624011.2014.954483
- Ansell SM, Flinn I, Taylor MH, Sikic BI, Brody J, Nemunaitis J, et al. Safety and Activity of Varlilumab, a Novel and First-in-Class Agonist Anti-CD27 Antibody, for Hematologic Malignancies. *Blood Adv* (2020) 4(9):1917–26. doi: 10.1182/bloodadvances.2019001079
- Marin-Acevedo JA, Dholaria B, Soyano AE, Knutson KL, Chumsri S, Lou Y. Next Generation of Immune Checkpoint Therapy in Cancer: New Developments and Challenges. *J Hematol Oncol* (2018) 11(1):39. doi: 10.1186/s13045-018-0582-8

10. Ma Y, Li J, Wang H, Chiu Y, Kingsley CV, Fry D, et al. Combination of PD-1 Inhibitor and OX40 Agonist Induces Tumor Rejection and Immune Memory in Mouse Models of Pancreatic Cancer. *Gastroenterology* (2020) 159(1):306–319.e12. doi: 10.1053/j.gastro.2020.03.018
11. Kuang Z, Pu P, Wu M, Wu Z, Wang L, Li Y, et al. A Novel Bispecific Antibody With PD-L1-Assisted OX40 Activation for Cancer Treatment. *Mol Cancer Ther* (2020) 19(12):2564–74. doi: 10.1158/1535-7163.MCT-20-0226
12. Fromm G, de Silva S, Johannes K, Patel A, Hornblower JC, Schreiber TH. Agonist Redirected Checkpoint, PD1-Fc-OX40L, for Cancer Immunotherapy. *J Immunother Cancer* (2018) 6(1):149. doi: 10.1186/s40425-018-0454-3
13. Croft M. Control of Immunity by the TNFR-Related Molecule OX40 (Cd134). *Annu Rev Immunol* (2010) 28:57–78. doi: 10.1146/annurev-immunol-030409-101243
14. Diab A, Hamid O, Thompson JA, Ros W, Eskens FALM, Doi T, et al. A Phase I, Open-Label, Dose-Escalation Study of the OX40 Agonist Ivuxolimab in Patients With Locally Advanced or Metastatic Cancers. *Clin Cancer Res* (2022) 28(1):71–83. doi: 10.1158/1078-0432.CCR-21-0845
15. Gutierrez M, Moreno V, Heinhuis KM, Olszanski AJ, Spreafico A, Ong M, et al. OX40 Agonist BMS-986178 Alone or in Combination With Nivolumab and/or Ipilimumab in Patients With Advanced Solid Tumors. *Clin Cancer Res* (2021) 27(2):460–72. doi: 10.1158/1078-0432.CCR-20-1830
16. Clar KL, Hinterleitner C, Schneider P, Salih HR, Maurer S. Inhibition of NK Reactivity Against Solid Tumors by Platelet-Derived RANKL. *Cancers (Basel)* (2019) 11(3):277. doi: 10.3390/cancers11030277
17. Liu DM, Yan JC, Wang CP, Chen GH, Ding S, Liu PJ, et al. The Clinical Implications of Increased OX40 Ligand Expression in Patients With Acute Coronary Syndrome. *Clin Chim Acta* (2008) 397(1–2):22–6. doi: 10.1016/j.cca.2008.07.003
18. Gay LJ, Felding-Habermann B. Contribution of Platelets to Tumour Metastasis. *Nat Rev Cancer* (2011) 11(2):123–34. doi: 10.1038/nrc3004
19. Placke T, Örgel M, Schaller M, Jung G, Rammensee HG, et al. Platelet-Derived MHC Class I Confers a Pseudonormal Phenotype to Cancer Cells That Subverts the Antitumor Reactivity of Natural Killer Immune Cells. *Cancer Res* (2012) 72(2):440–8. doi: 10.1158/0008-5472.CAN-11-1872
20. Maurer S, Kropp KN, Klein G, Steinle A, Haen SP, Walz JS, et al. Platelet-Mediated Shedding of NKG2D Ligands Impairs NK Cell Immune-Surveillance of Tumor Cells. *Oncimmunology* (2018) 7(2):e1364827. doi: 10.1080/2162402X.2017.1364827
21. Amirkhosravi A, Amaya M, Desai H, Francis JL. Platelet-CD40 Ligand Interaction With Melanoma Cell and Monocyte CD40 Enhances Cellular Procoagulant Activity. *Blood Coagul Fibrinolysis* (2002) 13(6):505–12. doi: 10.1097/00001721-200209000-00005
22. Lutz MS, Klimovich B, Maurer S, Heitmann JS, Märklin M, Zekri L, et al. Platelets Subvert Antitumor Efficacy of T Cell-Recruiting Bispecific Antibodies. *J Immunother Cancer* (2022) 10(2):e003655. doi: 10.1136/jitc-2021-003655
23. Hinterleitner C, Strähle J, Malenke E, Hinterleitner M, Henning M, Seehawer M, et al. Platelet PD-L1 Reflects Collective Intratumoral PD-L1 Expression and Predicts Immunotherapy Response in Non-Small Cell Lung Cancer. *Nat Commun* (2021) 12(1):7005. doi: 10.1038/s41467-021-27303-7
24. Zhou Y, Heitmann JS, Clar KL, Kropp KN, Hinterleitner M, Engler T, et al. Platelet-Expressed Immune Checkpoint Regulator GITRL in Breast Cancer. *Cancer Immunol Immunother* (2021) 70(9):2483–96. doi: 10.1007/s00262-021-02866-y
25. Hinterleitner C, Zhou Y, Tandler C, Heitmann JS, Kropp KN, Hinterleitner M, et al. Platelet-Expressed TNFRSF13B (TACI) Predicts Breast Cancer Progression. *Front Oncol* (2021) 11:642170. doi: 10.3389/fonc.2021.642170
26. Riccardi C, Ronchetti S, Nocentini G. Glucocorticoid-Induced TNFR-Related Gene (GITR) as a Therapeutic Target for Immunotherapy. *Expert Opin Ther Targets* (2018) 22(9):783–97. doi: 10.1080/14728222.2018.1512588
27. Baltz KM, Krusch M, Baessler T, Schmiedel BJ, Bringmann A, Brossart P, Salih HR. Neutralization of Tumor-Derived Soluble Glucocorticoid-Induced TNFR-Related Protein Ligand Increases NK Cell Anti-Tumor Reactivity. *Blood* (2008) 112(9):3735–43. doi: 10.1182/blood-2008-03-143016
28. Lee WH, Seo D, Lim SG, Suk K. Reverse Signaling of Tumor Necrosis Factor Superfamily Proteins in Macrophages and Microglia: Superfamily Portrait in the Neuroimmune Interface. *Front Immunol* (2019) 10:262. doi: 10.3389/fimmu.2019.00262
29. Lim SG, Kim JK, Suk K, Lee WH. Crosstalk Between Signals Initiated From TLR4 and Cell Surface BAFF Results in Synergistic Induction of Proinflammatory Mediators in THP-1 Cells. *Sci Rep* (2017) 7:45826. doi: 10.1038/srep45826
30. Kampa M, Notas G, Stathopoulos EN, Tsapis A, Castanas E. The TNFSF Members APRIL and BAFF and Their Receptors TACI, BCMA, and BAFFR in Oncology, With a Special Focus in Breast Cancer. *Front Oncol* (2020) 10:827. doi: 10.3389/fonc.2020.00827
31. Eslami M, Schneider P. Function, Occurrence and Inhibition of Different Forms of BAFF. *Curr Opin Immunol* (2021) 71:75–80. doi: 10.1016/j.coi.2021.06.009
32. Cognasse F, Duchez AC, Audoux E, Ebermeyer T, Arthaud CA, Prier A, et al. Platelets as Key Factors in Inflammation: Focus on CD40L/Cd40. *Front Immunol* (2022) 13:825892. doi: 10.3389/fimmu.2022.825892
33. Plantureux L, Mège D, Crescence L, Carminita E, Robert S, Cointe S, et al. The Interaction of Platelets With Colorectal Cancer Cells Inhibits Tumor Growth But Promotes Metastasis. *Cancer Res* (2020) 80(2):291–303. doi: 10.1158/0008-5472.CAN-19-1181
34. Panes O, Matus V, Sáez CG, Quiroga T, Pereira J, Mezzano D. Human Platelets Synthesize and Express Functional Tissue Factor. *Blood* (2007) 109(12):5242–50. doi: 10.1182/blood-2006-06-030619
35. Ni XY, Sui HX, Liu Y, Ke SZ, Wang YN, Gao FG. TGF- β of Lung Cancer Microenvironment Upregulates B7H1 and GITRL Expression in Dendritic Cells and Is Associated With Regulatory T Cell Generation. *Oncol Rep* (2012) 28(2):615–21. doi: 10.3892/or.2012.1822
36. Webb GJ, Hirschfield GM, Lane PJ. OX40, OX40L and Autoimmunity: A Comprehensive Review. *Clin Rev Allergy Immunol* (2016) 50(3):312–32. doi: 10.1007/s12016-015-8498-3
37. Krause P, Bruckner M, Uermösi C, Singer E, Groettrup M, Legler DF. Prostaglandin E(2) Enhances T-Cell Proliferation by Inducing the Costimulatory Molecules OX40L, CD70, and 4-1BBL on Dendritic Cells. *Blood* (2009) 113(11):2451–60. doi: 10.1182/blood-2008-05-157123
38. Maxwell JR, Yadav R, Rossi RJ, Ruby CE, Weinberg AD, Aguila HL, et al. IL-18 Bridges Innate and Adaptive Immunity Through IFN- γ and the CD134 Pathway. *J Immunol* (2006) 177(1):234–45. doi: 10.4049/jimmunol.177.1.234
39. Ito T, Wang YH, Duramad O, Hori T, Delespesse GJ, Watanabe N, et al. TSLP-Activated Dendritic Cells Induce an Inflammatory T Helper Type 2 Cell Response Through OX40 Ligand. *J Exp Med* (2005) 202(9):1213–23. doi: 10.1084/jem.20051135
40. Wesolowski R, Stiff A, Quiroga D, McQuinn C, Li Z, Nitta H, et al. Exploratory Analysis of Immune Checkpoint Receptor Expression by Circulating T Cells and Tumor Specimens in Patients Receiving Neo-Adjuvant Chemotherapy for Operable Breast Cancer. *BMC Cancer* (2020) 20(1):445. doi: 10.1186/s12885-020-06949-4
41. Wang L, Simons DL, Lu X, Tu TY, Solomon S, Wang R, et al. Connecting Blood and Intratumoral Treg Cell Activity in Predicting Future Relapse in Breast Cancer. *Nat Immunol* (2019) 20(9):1220–30. doi: 10.1038/s41590-019-0429-7
42. Sun S, Fei X, Mao Y, Wang X, Garfield DH, Huang O, et al. PD-1(+) Immune Cell Infiltration Inversely Correlates With Survival of Operable Breast Cancer Patients. *Cancer Immunol Immunother* (2014) 63(4):395–406. doi: 10.1007/s00262-014-1519-x
43. Korniluk A, Koper-Lenkiewicz OM, Kamińska J, Kemona H, Dymicka-Piekarska V. Mean Platelet Volume (MPV): New Perspectives for an Old Marker in the Course and Prognosis of Inflammatory Conditions. *Mediators Inflamm* (2019) 2019:9213074. doi: 10.1155/2019/9213074
44. Kraytman M. Platelet Size in Thrombocytopenias and Thrombocytosis of Various Origin. *Blood* (1973) 41(4):587–98. doi: 10.1182/blood.V41.4.587.587
45. Minn AJ, Kang Y, Serganova I, Gupta GP, Giri DD, Doubrovina M, et al. Distinct Organ-Specific Metastatic Potential of Individual Breast Cancer Cells and Primary Tumors. *J Clin Invest* (2005) 115(1):44–55. doi: 10.1172/JCI22320
46. Xie F, Wang Q, Chen Y, Gu Y, Mao H, Zeng W, et al. Costimulatory Molecule OX40/OX40L Expression in Ductal Carcinoma in Situ and Invasive Ductal Carcinoma of Breast: An Immunohistochemistry-Based Pilot Study. *Pathol Res Pract* (2010) 206(11):735–9. doi: 10.1016/j.prp.2010.05.016
47. Ménard S, Fortis S, Castiglioni F, Agresti R, Balsari A. HER2 as a Prognostic Factor in Breast Cancer. *Oncology* (2001) 61 Suppl 2:67–72. doi: 10.1159/000055404

48. Liu D, Wang D, Wu C, Zhang L, Mei Q, Hu G, et al. Prognostic Significance of Serum Lactate Dehydrogenase in Patients With Breast Cancer: A Meta-Analysis. *Cancer Manag Res* (2019) 11:3611–9. doi: 10.2147/CMAR.S199260
49. Shao Y, Sun X, He Y, Liu C, Liu H. Elevated Levels of Serum Tumor Markers CEA and CA15-3 Are Prognostic Parameters for Different Molecular Subtypes of Breast Cancer. *PloS One* (2015) 10(7):e0133830. doi: 10.1371/journal.pone.0133830
50. Loi S, Sirtaine N, Piette F, Salgado R, Viale G, Van Eenoo F, et al. Prognostic and Predictive Value of Tumor-Infiltrating Lymphocytes in a Phase III Randomized Adjuvant Breast Cancer Trial in Node-Positive Breast Cancer Comparing the Addition of Docetaxel to Doxorubicin With Doxorubicin-Based Chemotherapy: BIG 02-98. *J Clin Oncol* (2013) 31(7):860–7. doi: 10.1200/JCO.2011.41.0902
51. Zhou Y, Heitmann JS, Kropp KN, Hinterleitner M, Koch A, Hartkopf AD, et al. Regulation of Platelet-Derived ADAM17: A Biomarker Approach for Breast Cancer? *Diagnostics (Basel)* (2021) 11(7):1188. doi: 10.3390/diagnostics11071188

Conflict of Interest: The authors declare that the research was conducted in the absence of any commercial or financial relationships that could be construed as a potential conflict of interest.

Publisher's Note: All claims expressed in this article are solely those of the authors and do not necessarily represent those of their affiliated organizations, or those of the publisher, the editors and the reviewers. Any product that may be evaluated in this article, or claim that may be made by its manufacturer, is not guaranteed or endorsed by the publisher.

Copyright © 2022 Rittig, Lutz, Clar, Zhou, Kropp, Koch, Hartkopf, Hinterleitner, Zender, Salih, Maurer and Hinterleitner. This is an open-access article distributed under the terms of the Creative Commons Attribution License (CC BY). The use, distribution or reproduction in other forums is permitted, provided the original author(s) and the copyright owner(s) are credited and that the original publication in this journal is cited, in accordance with accepted academic practice. No use, distribution or reproduction is permitted which does not comply with these terms.



OPEN ACCESS

EDITED BY

Shaohua Xu,
Tongji University, China

REVIEWED BY

Shen Yujie,
Fudan University, China
Jianguang Ji,
Lund University, Sweden

*CORRESPONDENCE

Xinyuan Zhao
zhaoxinyuan@ntu.edu.cn
Sen Huang
hl-96@126.com

[†]These authors share first authorship

SPECIALTY SECTION

This article was submitted to
Gynecological Oncology,
a section of the journal
Frontiers in Oncology

RECEIVED 29 May 2022

ACCEPTED 30 June 2022

PUBLISHED 26 July 2022

CITATION

Gu C, Lin C, Zhu Z, Hu L, Wang F,
Wang X, Ruan J, Zhao X and Huang S
(2022) The IFN- γ -related long non-
coding RNA signature predicts
prognosis and indicates immune
microenvironment infiltration in
uterine corpus endometrial carcinoma.
Front. Oncol. 12:955979.
doi: 10.3389/fonc.2022.955979

COPYRIGHT

© 2022 Gu, Lin, Zhu, Hu, Wang, Wang,
Ruan, Zhao and Huang. This is an open-
access article distributed under the
terms of the [Creative Commons
Attribution License \(CC BY\)](#). The use,
distribution or reproduction in other
forums is permitted, provided the
original author(s) and the copyright
owner(s) are credited and that the
original publication in this journal is
cited, in accordance with accepted
academic practice. No use,
distribution or reproduction is
permitted which does not comply with
these terms.

The IFN- γ -related long non-coding RNA signature predicts prognosis and indicates immune microenvironment infiltration in uterine corpus endometrial carcinoma

Chunyan Gu^{1†}, Chen Lin^{2†}, Zheng Zhu^{3†}, Li Hu^{4†},
Fengxu Wang⁵, Xuehai Wang⁵, Junpu Ruan⁵,
Xinyuan Zhao^{5*} and Sen Huang^{1*}

¹Department of Obstetrics and Gynecology, Nantong Haimen People's Hospital, Nantong, China,

²Vectors and Parasitosis Control and Prevention Section, Center of Disease Prevention and Control in Pudong New Area of Shanghai, Shanghai, China, ³Department of Urology, The First Affiliated Hospital of Nanjing Medical University, Nanjing, China, ⁴Department of Medicine, Kangda College of Nanjing Medical University, Lianyungang, China, ⁵Department of Occupational Medicine and Environmental Toxicology, Nantong Key Laboratory of Environmental Toxicology, School of Public Health, Nantong University, Nantong, China

Background: One of the most common diseases that have a negative impact on women's health is endometrial carcinoma (EC). Advanced endometrial cancer has a dismal prognosis and lacks solid prognostic indicators. IFN- γ is a key cytokine in the inflammatory response, and it has also been suggested that it has a role in the tumor microenvironment. The significance of IFN- γ -related genes and long non-coding RNAs in endometrial cancer, however, is unknown.

Methods: The Cancer Genome Atlas (TCGA) database was used to download RNA-seq data from endometrial cancer tissues and normal controls. Genes associated with IFN- γ were retrieved from the gene set enrichment analysis (GSEA) website. Co-expression analysis was performed to find lncRNAs linked to IFN- γ gene. The researchers employed weighted co-expression network analysis (WGCNA) to find lncRNAs that were strongly linked to survival. The prognostic signature was created using univariate Cox regression and least absolute shrinkage and selection operator (LASSO) regression. The training cohort, validation cohort, and entire cohort of endometrial cancer patients were then split into high-risk and low-risk categories. To investigate variations across different risk groups, we used survival analysis, enrichment analysis, and immune microenvironment analysis. The platform for analysis is R software (version X64 3.6.1).

Results: Based on the transcript expression of IFN- γ -related lncRNAs, two distinct subgroups of EC from TCGA cohort were formed, each with different

outcomes. Ten IFN- γ -related lncRNAs were used to build a predictive signature using Cox regression analysis and the LASSO regression, including CFAP58, LINC02014, UNQ6494, AC006369.1, NRAV, BMPR1B-DT, AC068134.2, AP002840.2, GS1-594A7.3, and OLMALINC. The high-risk group had a considerably worse outcome ($p < 0.05$). In the immunological microenvironment, there were also substantial disparities across different risk categories.

Conclusion: Our findings give a reference for endometrial cancer prognostic type and immunological status assessment, as well as prospective molecular markers for the disease.

KEYWORDS

interferon-gamma, bioinformatics, signature, immunology, endometrial carcinoma

Introduction

Endometrial carcinoma generally refers to cancer of the corpus uteri, which is a common malignant tumor of the female reproductive system. Since it has increasingly become the main cause of cancer death, early diagnosis is important. In 2020, the incidence rate of EC ranks sixth in the female population (1). In 2021, cancer statistics reported the estimation, which conjectures the fourth incidence rate and sixth mortality of EC in the United States (2). Citizens of developed countries have a high risk of developing EC owing to obesity and lack of exercise (3). EC could be categorized into type I and type II (3). The former type is usually related to excessive estrogen expression, while the latter is often estrogen-independent, including clear cell carcinoma and serous carcinoma (4). Segmental curettage and endometrial biopsy are efficient diagnostic approaches. Although patients with early-stage endometrial cancer have better results after surgical treatment, there are still some patients who are diagnosed at an advanced stage and lose the opportunity for surgery (5, 6). Moreover, the treatment of estrogen-independent EC and undifferentiated EC remains a challenge (7). The use of immune checkpoint inhibitors and angiogenesis inhibitors has yielded encouraging results in patients with advanced, hormone-independent, or undifferentiated EC (8). However, EC patients also have significant heterogeneity, with different tumor immune reprogramming states and microsatellite instability phenotypes, resulting in varying degrees of response to immunotherapy (9). Therefore, it is necessary to explore the tumor microenvironment of EC to provide a reference for treatment.

Abbreviations: EC, endometrial carcinoma; TCGA, The Cancer Genome Atlas; GSEA, gene set enrichment analysis; WGCNA, weighted gene co-expression network analysis; LASSO, least absolute shrinkage and selection operator; ECM, extracellular matrix; EMT, epithelial–mesenchymal transition.

Interferon- γ (IFN- γ) is common in the tumor microenvironment and body inflammation (10). IFN- γ is produced primarily by T and NK cells in response to various inflammatory or immune stimuli (11). The role of IFN- γ in immune surveillance and immune escape of tumors has been demonstrated. Many studies have indicated an increase in IFN- γ production during immune checkpoint blocking therapy (12). Defects in IFN- γ signaling are associated with resistance to immunotherapy. Thus, IFN- γ plays a key role in the tumor microenvironment (13). On the one hand, it serves as an immunogenicity enhancer *via* upregulating the expression of MHC and genes required in antigen processing (14). On the other hand, IFN- γ could combine with PD-1 on tumor-infiltrating T cells, inhibiting tumor immune regulation (15). Apart from them, researchers had indicated that IFN- γ acts as a regulator of hematopoietic stem cells in both homeostasis and during infection (16). A meta-analysis by Deng et al. (17) also showed the significant relationship between IFN- γ polymorphisms +874 (T/A) and the occurrence risk of aplastic anemia. Additionally, IFN- γ alone could moderately suppress tumor cell growth by inducing apoptosis in, for example, ovarian cancer (18).

Non-coding RNA longer than 200 nt is known as long non-coding RNA (lncRNA), and it is now thought that lncRNA plays a significant role in the development and spread of cancer (19). There is growing evidence that lncRNA can play a role in the regulation of gene expression and transcription at the transcriptional and epigenetic levels, as well as the important regulatory processes of chromatin modification, transcription activation, and genomic imprinting (20). It also plays a role in the development of complex precision in gene expression, as well as tumor growth, apoptosis, invasion, metastasis, and many other biological processes (21). However, the role of IFN- γ -related lncRNAs in endometrial cancer has hardly been studied.

In this study, we explored the significance of IFN- γ -related genes in endometrial carcinoma and constructed prognostic

signatures through comprehensive analysis. With this signature, the prognosis and immune status of patients with endometrial cancer can be well assessed and stratified, thus providing a reference for the diagnosis and treatment of endometrial cancer.

Methods

Data acquisition

The RNA-seq transcriptome data in fragment per kilobase method (FPKM) format and corresponding clinical data of uterine corpus EC (UCEC) patients were extracted from The Cancer Genome Atlas (TCGA) (UCEC tissue samples, 552; normal samples, 23). After clinical information was combined with transcriptome data, 511 tumor samples were obtained. The 511 tumor samples were evenly divided into the training cohort (256 samples) and validation cohort (255 samples), at a 1:1 ratio. Subsequently, these data were collated, annotated, and then collapsed into protein-coding genes and lncRNAs by employing the annotation documents from the GENCODE database. A total of 13,349 lncRNAs were identified (22). The IFN- γ -related genes were obtained from the HALLMARK_INTERFERON_GAMMA_RESPONSE genome of gene set enrichment analysis (GSEA). Subsequently, Pearson's correlation analysis was conducted using the 13,349 lncRNAs and IFN- γ -related genes ($p < 0.001$, correlation coefficient > 0.3). Ultimately, 1,700 IFN- γ -related lncRNAs were screened for follow-up bioinformatics analysis. [Supplementary Table 1](#) shows the clinical data of UCEC patients obtained from TCGA. We used R software to extract the expression of IFN- γ -related lncRNAs for further investigation.

Weighted gene co-expression network analysis

To develop a scale-free co-expression network in EC, genes related to IFN- γ based on the 25th percentile of variance were selected by using the weighted gene co-expression network analysis ('WGCNA') package (23). For all IFN- γ -related genes, during this time, Pearson's correlation and average linkage algorithm were performed, and a weighted adjacency matrix was constructed ($MM_i = |\text{cor}(x(i)), ME|$, where i is the value of each gene) (24). Then, average linkage modules were clustered, and the further dissimilarity of module IFN- γ -related genes was detected.

Establishment and validation of the prediction model

Prognostic IFN- γ -related lncRNAs were screened out *via* univariate Cox regression analysis. Further, a prediction model based on IFN- γ -related lncRNAs expression was established

through least absolute shrinkage and selection operator (LASSO) analysis, and the formula of the prediction model was as follows: Risk score = coef * Exp (lncRNA A) + coef * Exp (lncRNA B) + coef * Expi (lncRNA i) (25).

EC patients were divided into two groups based on the training cohort's median risk score. The group with a greater risk score than the median was labeled as high risk. The rest of them were in the low-risk category. The overall survival (OS) of the two groups was calculated using the Kaplan–Meier (KM) analysis (26), and the reliability of the prediction model was assessed using receiver operating characteristic (ROC) curve analysis (27). The innovative prediction model was verified using the same methodology in the test and entire TCGA cohorts.

Evaluation of the prediction model

GSEA study was performed using the Java GSEA program with 1,000 random permutations to investigate the varied biological activities of the high- and low-risk groups based on IFN- γ -related lncRNAs (28). In accordance with past findings, immune cell infiltration affects the survival and tumor metastasis of patients. The immune cell infiltration of the two groups was investigated using two distinct techniques, the CIBERSORT algorithm (29) and the ssGSEA algorithm (30). The immune cell infiltration of EC patients in different groups was compared using the Wilcoxon test, with a p -value of 0.05 considered statistically significant. Furthermore, the expression of genes related to immunological checkpoints, N^6 -methyladenosine RNA methylation, and the stem cell pathway was calculated in two groups, with a p -value of 0.05 considered statistically significant.

Independent prognostic analysis and construction of a nomogram

Univariate and multivariate Cox regression analyses were conducted to determine if the prediction model we constructed could be used as an independent predictor of survival in EC patients. A nomogram was then constructed based on the independent prognostic factors by the 'rms' package in R software. Calibration curves and ROC curves were used to verify the validity of the prediction model.

Quantitative real-time polymerase chain reaction

The 15 EC patients whose EC tissue and normal uterine tissue were collected for mRNA quantification were then subjected to qRT-PCR analysis. Following the manufacturer's directions, total cellular RNAs were extracted from cells using Trizol Reagent (Invitrogen, Carlsbad, CA, USA). Reverse transcription was done

with the Takara reverse transcription kit (Otsu, Shiga, Japan). Thermo Fisher Scientific (Waltham, MA, USA) provided the QuantiTect SYBR Green PCR Kit and QuantStudio 1 for the real-time polymerase chain reaction (RT-PCR). The $-2^{\Delta\Delta Ct}$ technique was used to determine relative quantification. Each gene's relative messenger RNA (mRNA) expression level was adjusted to that of the mRNA for the enzyme glyceraldehyde-3-phosphate dehydrogenase (GAPDH). The primer sequences used are shown in [Supplementary Table 2](#).

Statistical analysis

R software was used to conduct all statistical analyses (version x64 3.6.1). A *p*-value of less than 0.05 was considered statistically significant.

Result

Our workflow is shown in [Figure 1](#).

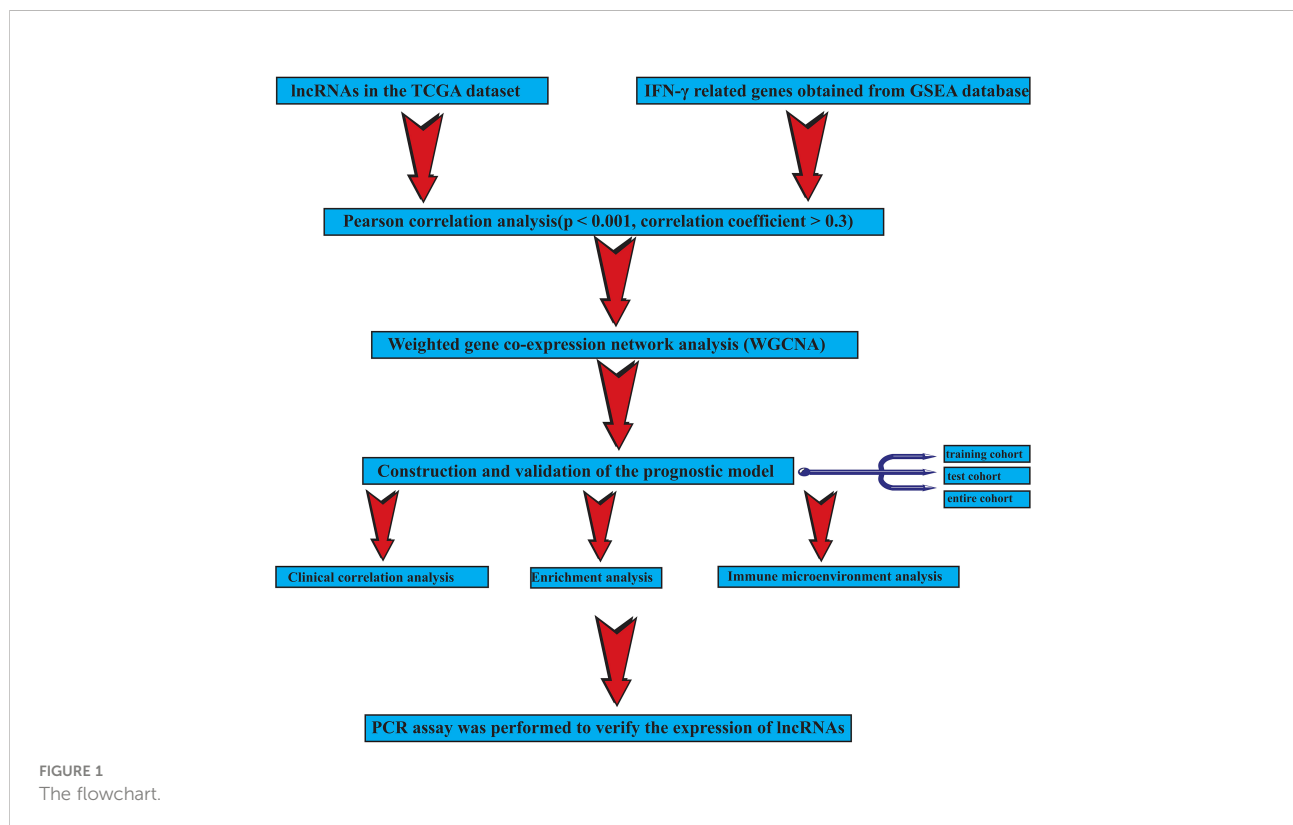
Identification of prognostic interferon gamma-related long non-coding RNAs in endometrial carcinoma

A total of 1,700 IFN- γ -related lncRNAs were obtained by co-expression analysis. Then weighted co-expression network

analysis (WGCNA) was used to screen lncRNAs that were most correlated with clinical traits, i.e., survival time and survival status ([Figure 2A](#)). It was found that as the threshold increased, the R^2 value increased and crossed 0.8. When the number of modules is 8, the model is more stable ([Figure 2B](#)). A total of 8 modules were identified from the co-expression network ([Figures 2C, D](#)). Among all non-gray modules, green, red, and yellow modules have the most significant correlation with survival time and survival status ([Figure 2D](#)). A total of 260 lncRNAs in the green, red, and yellow modules were selected for univariate Cox regression analysis, and 40 lncRNAs were obtained for subsequent cluster analysis (*p*-value < 0.05, [Figure 3A](#)).

Based on the expression of interferon gamma-related long non-coding RNAs, a consensus clustering analysis was performed

Consensus clustering was conducted and indicated that patients in TCGA cohort can be classified into two clusters efficiently ([Figures 3B, C](#)). A sample correlation heatmap was created to depict the relationship between clusters and clinical characteristics ([Figure 3D](#)). KM survival curves demonstrated that cluster 2 had a more significant relationship with a higher



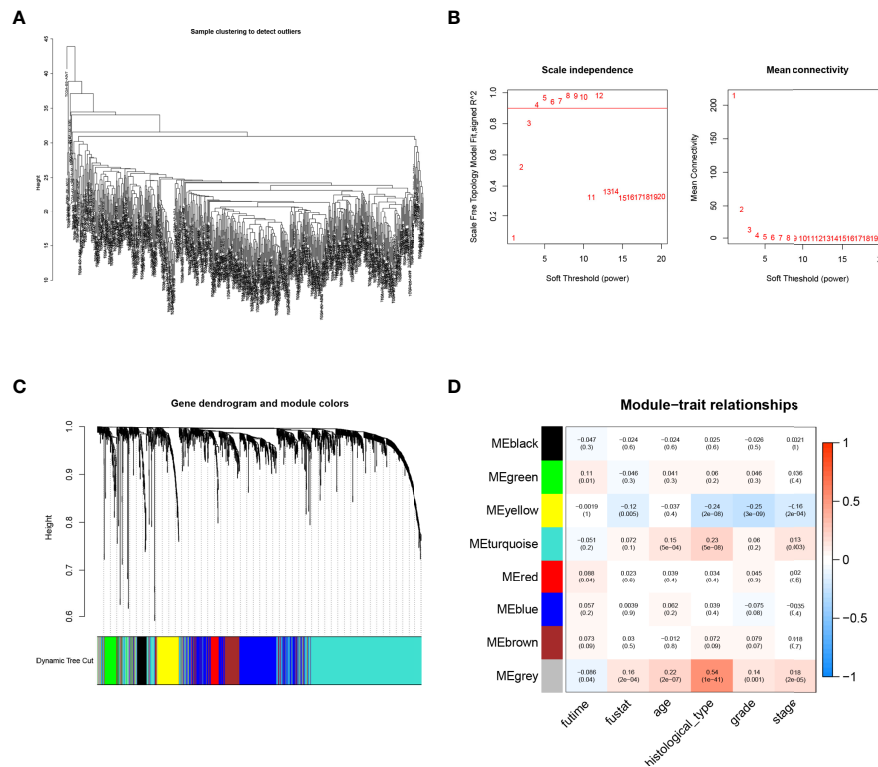


FIGURE 2

Weighted co-expression network analysis (WGCNA). (A) Sample clustering tree. (B) Soft threshold selection. As the threshold increased, the R^2 value increased and crossed 0.8. When the number of modules is 8, the model is more stable. (C, D) Distribution and correlation of each module. Through correlation analysis between different modules and phenotype (survival time and survival status), it was finally found that green, red, and yellow modules were significantly positively correlated with endometrial carcinoma (EC) prognosis.

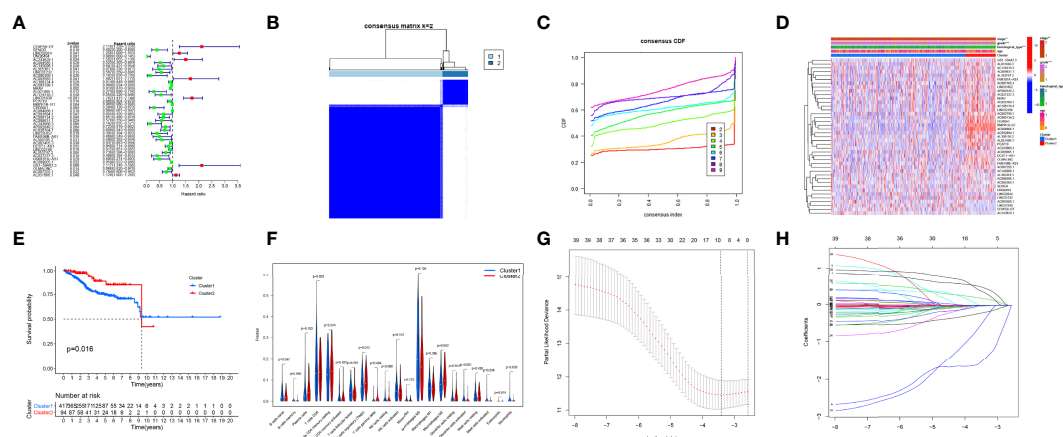


FIGURE 3

Consensus clustering analysis and the construction of the prognostic signature. (A) Univariate Cox regression. (B, C) Endometrial carcinoma (EC) patients of The Cancer Genome Atlas (TCGA) cohort can be classified into two clusters efficiently. (D) Relationship between clusters and clinical characteristics. (E) Cluster 2 had a more significant relationship with higher survival probability (p -value < 0.05). (F) The levels of immune cell infiltration between the two clusters were different. (G, H) Least absolute shrinkage and selection operator (LASSO) regression.

survival probability (p -value < 0.05, Figure 3E). Figure 3F shows the differences in immune cell infiltration between the two clusters.

Establishment and validation of a prediction model based on interferon gamma-related long non-coding RNAs

To avoid overfitting of IFN- γ -related lncRNAs, the LASSO algorithm was utilized to construct a prediction model (Figures 3G, H). We consequently obtained a precise formulation: CFAP58-DT * 0.4686 + LINC02014 * 0.1798 + UNQ6494 * 1.4725 + AC006369.1 * -0.4049 + NRAV * -0.0066 + BMPR1B-DT * -0.0004 + AC068134.2 * -0.0235 + AP002840.2 * -0.1923 + GS1-594A7.3 * 0.3475 + OLMALINC * -0.0112.

Patients in the training cohort were divided into the high- and low-risk groups based on their median risk score, with high-risk patients having a higher proportion of death occurrences (Figure 4). Patients in the high-risk group had lower survival outcomes than those in the low-risk group, according to the

Kaplan–Meier analysis (Figure 4A). The area under the curve (AUC) for 1-year, 3-year, and 5-year OS was 0.717, 0.697, and 0.641, respectively, according to ROC curve analysis (Figure 4B). Figures 3C–E show the survival status of patients and the signature risk score in the low- and high-risk categories. The heatmap clearly illustrated the relationship between the two risk groups and part of the clinical information (Figure 4C). Also, the expression of the prognosis-related risk lncRNAs was demonstrated plainly. CFAP58-DT and LINC02014 were highly expressed in the high-risk group, while UNQ6494, AC006369.1, NRAV, AP002840.2, and OLMALINC were highly expressed in the low-risk group. Similar results observed in the test and entire cohort for validation are shown in Figures 5, 6, indicating a great diagnostic capability of the prediction model.

Correlation between clinical parameters and prediction model

To explore the relationship between clinical parameters and the prediction model, the detailed characteristic distribution of

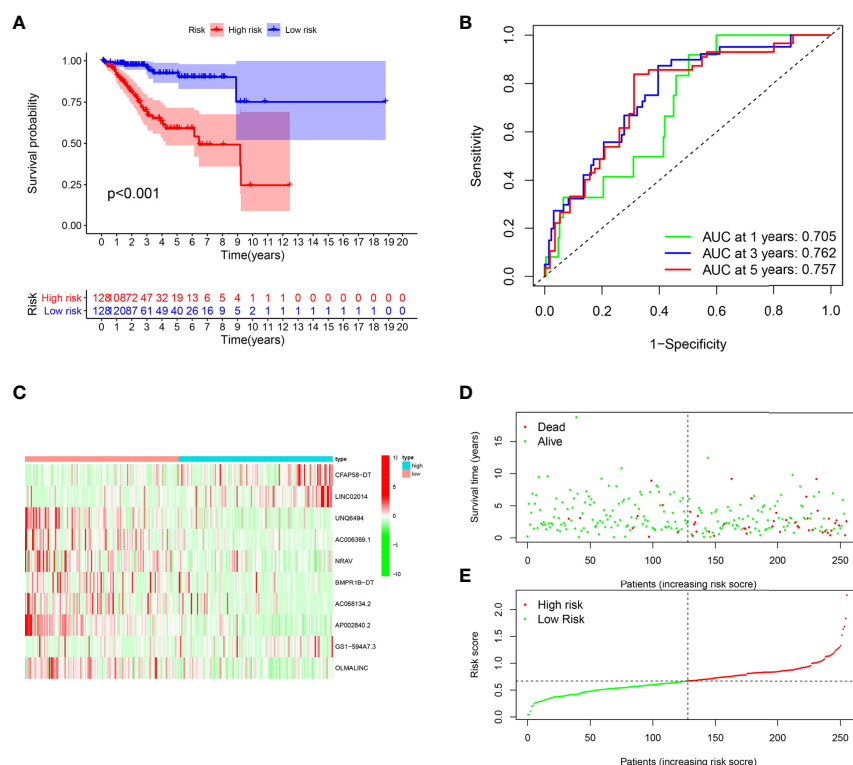


FIGURE 4

Evaluation of the prognostic value of this signature in training cohort. (A) Survival analysis showed a worse prognosis in the high-risk group ($p < 0.001$). (B) The 1-, 3-, and 5-year area under the curve (AUC) values of the signature are 0.705, 0.762, and 0.757, respectively. (C) Expression heatmaps of 10 lncRNAs in signature. (D, E) Survival status and risk score status of training cohort.

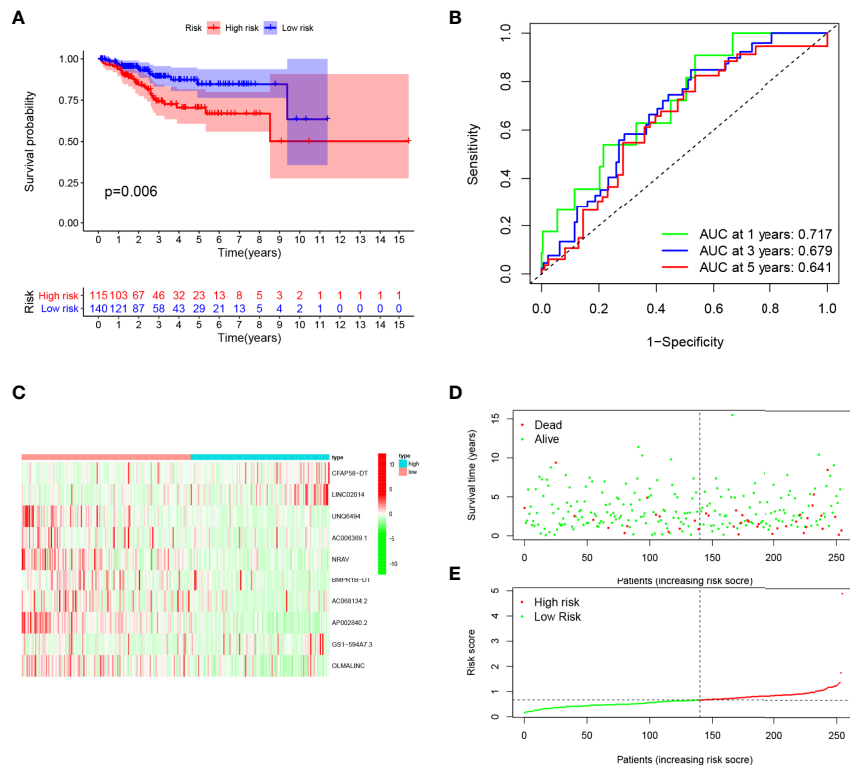


FIGURE 5

Evaluation of the prognostic value of this signature in validation cohort. (A) Survival analysis showed a worse prognosis in the high-risk group ($p = 0.006$). (B) The 1-, 3-, and 5-year area under the curve (AUC) values of the signature are 0.717, 0.679, and 0.641, respectively. (C) Expression heatmaps of 10 lncRNAs in signature. (D, E) Survival status and risk score status of validation cohort.

the two groups is shown in Figure 7A. Specifically, the risk score was significantly different in patients stratified by the clinical factors, including age, grade, histological type, stage, and cluster (Supplementary Figure 1). The Kaplan–Meier survival analysis according to the prognostic signature stratified by clinicopathological factors was further conducted, and the prognostic model could effectively discriminate the prognosis of the patients stratified by different clinical factors (age, grade, histological type, and stage, Figures 7B–I). Accordingly, patients included in the high-risk group have a poor prognosis regardless if they are over 60 or not. Aside from this, the high-risk group showed poor prognostic condition in stage, grade, and pathology subgroups, which indicated the efficiency of the established model in distinguishing the prognosis of EC patients.

Pathway enrichment analysis of genes associated with the high- and low-risk groups

Genes associated with high risk are enriched in axon guidance, cell cycle, DNA replication, extracellular matrix (ECM)–receptor interaction, and proximal tubule bicarbonate reclamation

(Figure 7J), whereas genes associated with low risk are enriched in allograft rejection, autoimmune thyroid disease, chemokine signaling pathway, complement and coagulation cascades, and cytokine–cytokine receptor interaction (Figure 7K).

Immune context of prediction model

It is known that immune cell infiltration affects the survival and tumor metastasis of patients. A violin plot of the immune microenvironment differences demonstrated that the high-risk group had a trend to gain low immune score, stromal score, and estimate score and eventually develop a high-purity tumor (Figures 8A–H). Through the CIBERSORT algorithm and ssGSEA algorithm, the low-risk group showed a higher proportion of immune cells than the high-risk group (Figures 8I–K), which indicates that patients in the high-risk group had a relatively low immune status. We also checked the expression changes of immune checkpoints, which might be indicative of the clinical response of immunotherapies, and we found the patients of the low-risk group had a higher expression of immune checkpoints as compared with the high-risk group (Figure 8). These findings may explain the different overall survival of the two groups. Based

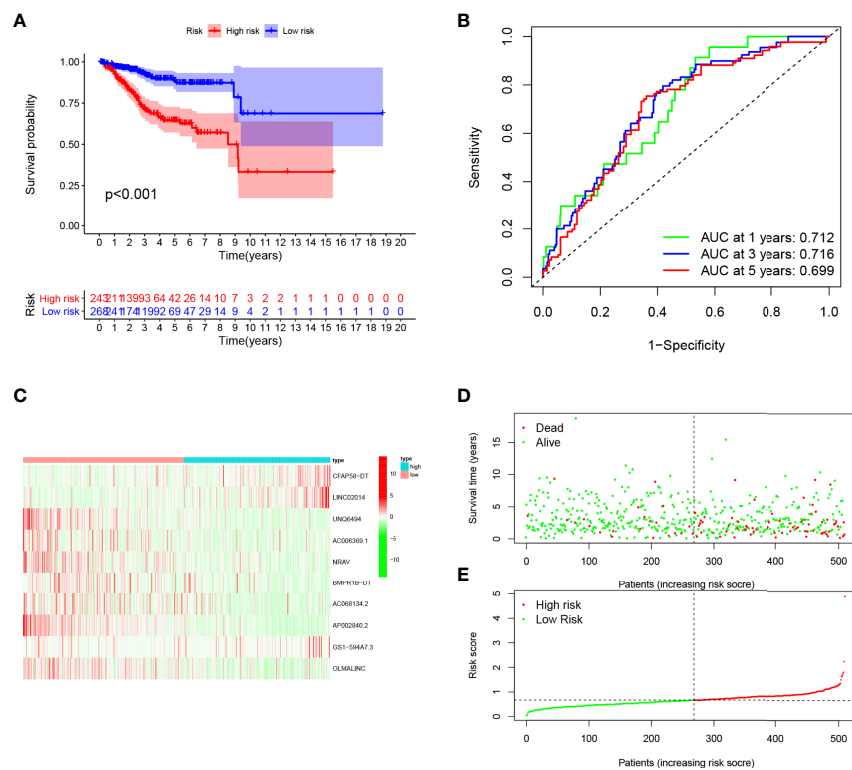


FIGURE 6

Evaluation of the prognostic value of this signature in entire cohort. (A) Survival analysis showed a worse prognosis in the high-risk group ($p < 0.001$). (B) The 1, 3, and 5-year area under the curve (AUC) values of the signature are 0.712, 0.716, and 0.699, respectively. (C) Expression heatmaps of 10 lncRNAs in signature. (D, E) Survival status and risk score status of entire cohort.

on the observation, we performed targeted drug tests on experimental animals and recorded the curative effect of the 16 kinds of drugs (Supplementary Figure 2). TNFRSF9, CD27, CTLA4, BTNL2, CD244, CD200R1, ICOS, HHLA2, CD48, CD28, TNFSF15, CD200, TIGIT, PDCD1, CD40, HAVCR2, TNFSF14, CD86, TMIGD2, CD70, TNFRSF14, CD40LG, LGALS9, TNFRSF4, BTLA, and LAIR1 were expressed significantly differently in the high- and low-risk groups.

Additionally, we screened the expression of N^6 -methyladenosine RNA methylation and stem cell pathway-related genes in the two groups (Supplementary Figures 2B–D). As a result, YTHDF1, YTHDC2, RBM15, and WTAP were observed to have high expression in the high-risk group, which reflected the poor prognosis indirectly.

Independent prognostic analysis and construction of a nomogram based on the established model

Univariate and multivariate Cox regression analyses indicated that the risk score can serve as an independent prognostic factor in EC (Table 1). Further, tests and entire

cohorts were enrolled, and the same results were observed (Tables 2 and 3). Based on the results of independent prognostic analysis, a nomogram was developed for clinical application (Figure 9A). The calibration curves of the nomogram we developed showed a great consistency between the actual observation and the nomogram prediction (Figure 9B). As is shown in Figure 9C, the nomogram achieved a significantly higher c-index value than other clinical factors, meaning a better predictive accuracy for EC.

Moreover, the AUC values of the nomogram for 1-, 3-, and 5-year OS were higher than 0.7 and other clinical factors, indicating that the nomogram was reliable (Figures 9D–F).

PCR was used to verify the expression of long non-coding RNAs in the model in endometrial carcinoma

To further verify our analysis results, PCR experiments were carried out. The results showed that BMP1B-DT and UNQ6494 were significantly upregulated in endometrial carcinoma (Supplementary Figure 3; $p < 0.05$). However, LINC02014 and NRAV were significantly downregulated in

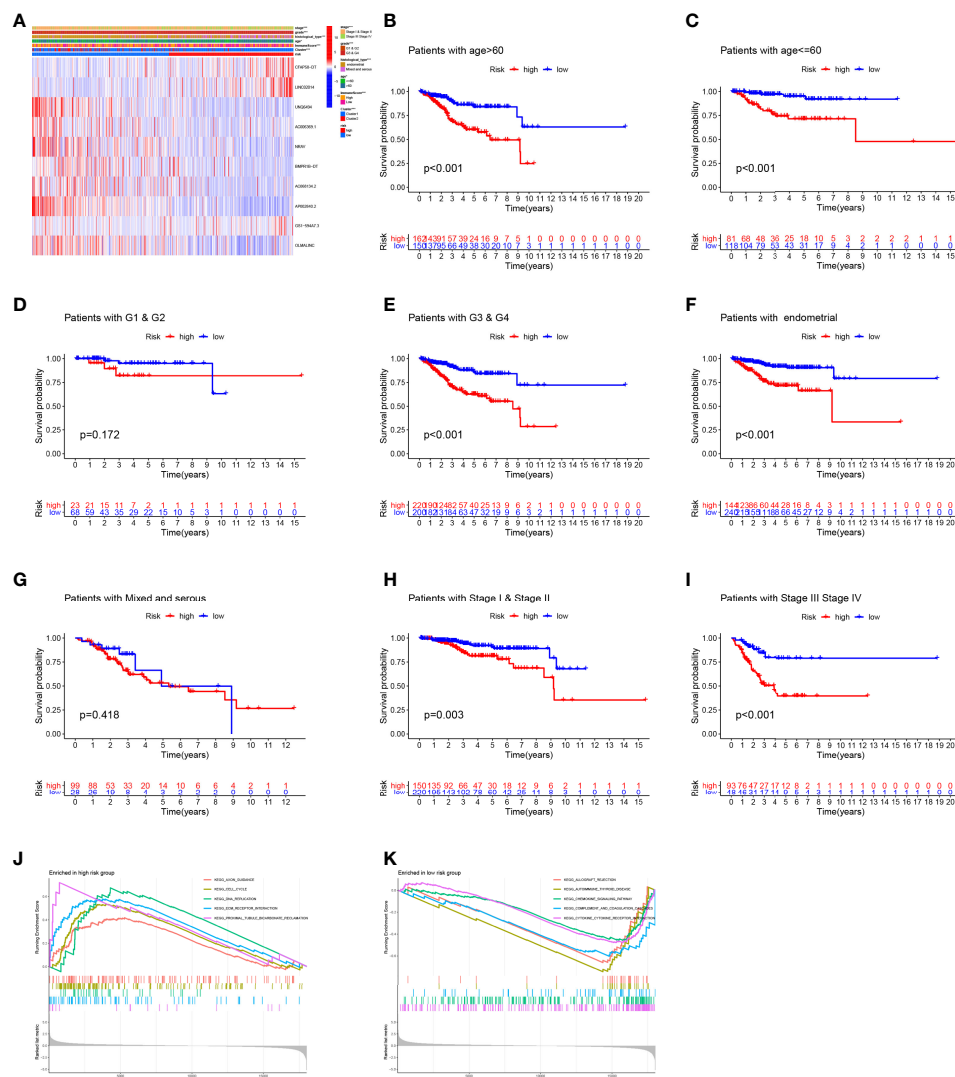


FIGURE 7

Correlation between clinical parameters and prediction signature. (A) The detailed characteristic distribution of two groups. (B–I) The prognostic model could effectively discriminate the prognosis of the patients stratified by different clinical factors (age, grade, histological type, and stage). (J, K) GSEA analysis.

endometrial carcinoma (Supplementary Figure 3; $p < 0.05$). PCR showed no statistical difference in the expression of other lncRNAs.

Discussion

Endometrial cancer is one of the most common malignant tumors of the female reproductive tract, mainly in postmenopausal women, but a number of young women are still affected (31). Patients with early, localized EC who have undergone surgical treatment have a good prognosis, with a 5-year survival rate of more than 80% (32). However, patients with

advanced EC often have lymph node or distant metastasis, poor prognosis, and limited treatment (33). Therefore, it is necessary to explore new biomarkers for prognostic stratification of EC patients and to provide a reference for precise treatment. IFN- γ , one of the most common types of immune cytokines, has been preliminarily elucidated to play a key role in the tumor immune microenvironment (34). However, the prognostic value and mechanisms of IFN- γ -related genes and lncRNAs in EC remain unclear. In-depth exploration is necessary to uncover the role of the IFN- γ pathway in EC. Moreover, endometrial carcinoma is a group of tumors with heterogeneity, including pathogenesis, growth characteristics, treatment response, and prognosis (35). Among them, identifying the prognostic difference in endometrial

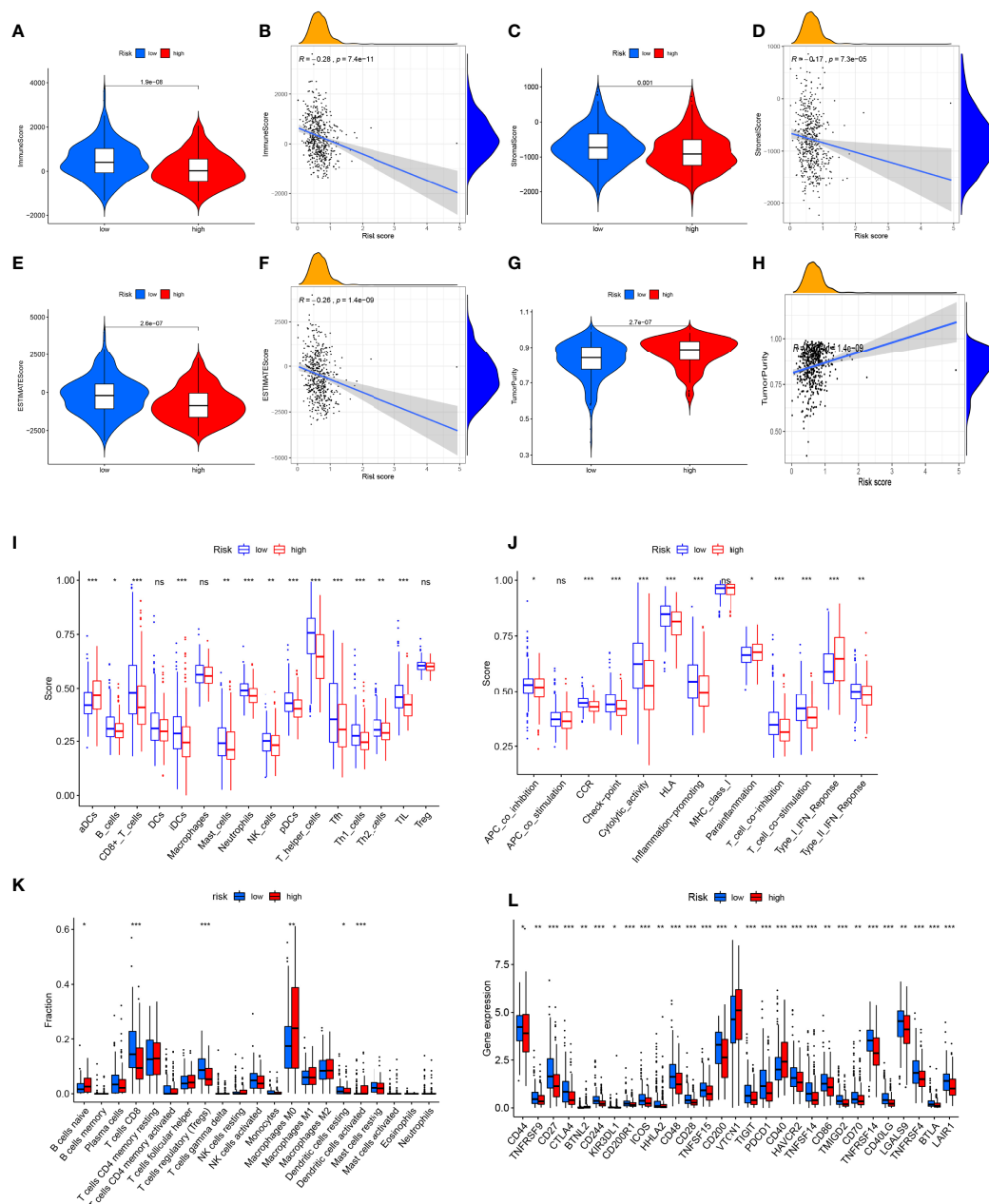


FIGURE 8
Analysis of immune microenvironment. **(A, B)** Immune score was lower in the high-risk group, and there was a significant negative correlation with risk scores. **(C, D)** Stromal score was lower in high-risk group, and there was a significant negative correlation with risk score. The **(E, F)** ESTIMATE score was lower in the high-risk group and significantly negatively correlated with the risk score. **(G, H)** Tumor purity was higher in the high-risk group, and there was a significant positive correlation with risk score. **(I–K)** Analysis of infiltration level of immune cells. **(L)** Expression analysis of immune checkpoint-related genes. * $P < 0.05$, ** $P < 0.01$, *** $P < 0.001$, ns, no significance.

cancer can provide a reference for early intervention and precise treatment (36). Previously, the International Federation of Gynecology and Obstetrics (FIGO) grading based on the degree of differentiation of glands has been widely used in clinical diagnosis and treatment of endometrial cancer and prognosis assessment (37). However, in genomics advances, genomic-based

endometrial cancer typing is becoming more and more attractive (38). Moreover, the identification of genomic instability or microsatellite instability subtypes can provide a reference for immunotherapy (39). Our study establishes the prognostic signature of IFN- γ -related lncRNAs for the first time, in which the grouping of endometrial cancer patients not only can guide

TABLE 1 Independent prognostic analysis of training cohort.

	Univariate analysis				Multivariate analysis			
	HR	HR.95L	HR.95H	p-Value	HR	HR.95L	HR.95H	p-Value
age	2.310787	1.174746	4.54544	0.015244	2.101931	0.997104	4.430943	0.050898
histological type	2.723841	1.540402	4.816476	0.00057	0.995563	0.507416	1.953321	0.989683
grade	4.132983	1.281972	13.32444	0.017508	1.686432	0.477843	5.951856	0.416654
stage	3.370365	1.901033	5.975361	3.20E-05	2.829301	1.467133	5.456181	0.00191
risk Score	6.640916	3.541853	12.45161	3.57E-09	4.685257	2.19568	9.997646	6.50E-05

TABLE 2 Independent prognostic analysis of test cohort.

	Univariate analysis				Multivariate analysis			
	HR	HR.95L	HR.95H	p-Value	HR	HR.95L	HR.95H	p-Value
age	1.358867	0.703253	2.625685	0.361529	NA	NA	NA	NA
histological type	3.430404	1.847279	6.370272	9.49E-05	2.457144	1.307522	4.617558	0.005222
grade	2.714988	0.826275	8.920951	0.099854	NA	NA	NA	NA
stage	5.346375	2.818812	10.14035	2.85E-07	4.087041	2.108869	7.920787	3.04E-05
risk Score	2.56945	1.692921	3.899812	9.29E-06	1.997949	1.201528	3.322268	0.00764

TABLE 3 Independent prognostic analysis of entire TCGA cohort.

	Univariate analysis				Multivariate analysis			
	HR	HR.95L	HR.95H	p-Value	HR	HR.95L	HR.95H	p-Value
age	1.778212	1.112123	2.843245	0.016228	1.566681	0.956845	2.56519	0.074324
histological type	3.043526	2.003172	4.62419	1.84E-07	1.643683	1.039595	2.598794	0.033495
grade	3.363109	1.467057	7.709655	0.004165	1.342176	0.551863	3.264285	0.516335
stage	4.116248	2.699981	6.275414	4.82E-11	3.043751	1.918006	4.830235	2.31E-06
risk Score	3.106371	2.316925	4.164804	3.55E-14	2.532946	1.754055	3.657704	7.15E-07

TCGA, The Cancer Genome Atlas.

prognostic assessment but also can help in understanding the differences in the immune microenvironment.

In this study, we analyzed endometrial cancer data from TCGA database using a variety of bioinformatics methods. First, the interferon gamma-related lncRNAs were divided into a total of eight modules by WGCNA, among which the gray module was most correlated with the interferon gamma phenotype of EC. Subsequently, lncRNAs in the gray module were extracted for further analysis. Consensus clustering analysis found that these lncRNAs could well divide EC patients in TCGA database into two clusters, with significant prognostic differences between the two clusters. Cox regression and LASSO regression were used to construct prognostic signatures. Each patient could be calculated with a risk score = $CFAP58\text{-}DT * 0.4686 + LINC02014 * 0.1798 + UNQ6494 * 1.4725 + AC006369.1 * -0.4049 + NRAV * -0.0066 + BMPR1B\text{-}DT * -0.0004 + AC068134.2 * -0.0235 + AP002840.2 * -0.1923 + GS1\text{-}594A7.3 * 0.3475 + OLMALINC * -0.0112$. This allowed the

value of risk to be assessed for each patient, allowing patients from various cohorts to be separated into the high-risk and low-risk groups, with the high-risk group having a worse prognosis. Varying levels of immune cell infiltration, medication sensitivity, and immunological checkpoint levels were also associated with different risk scores.

The signature we constructed consists of 10 lncRNAs, and many studies have preliminarily explained the role of these 10 lncRNAs in cancer. Sui et al. found that UNQ6494 was a poor prognostic marker for lung adenocarcinoma (40). The role of NRAV in cancer has been repeatedly confirmed. Wang et al. found that NRAV can mediate the activation of the Wnt/ β -catenin signaling pathway to promote the proliferation and invasion of hepatocellular carcinoma (41). Lin et al. discovered that BMPR1B-DT is a prognostic marker of ovarian cancer and is associated with drug sensitivity (42). The role of OLMALINC in osteosarcoma was confirmed by He et al., who found that it was highly correlated with the immune microenvironment of

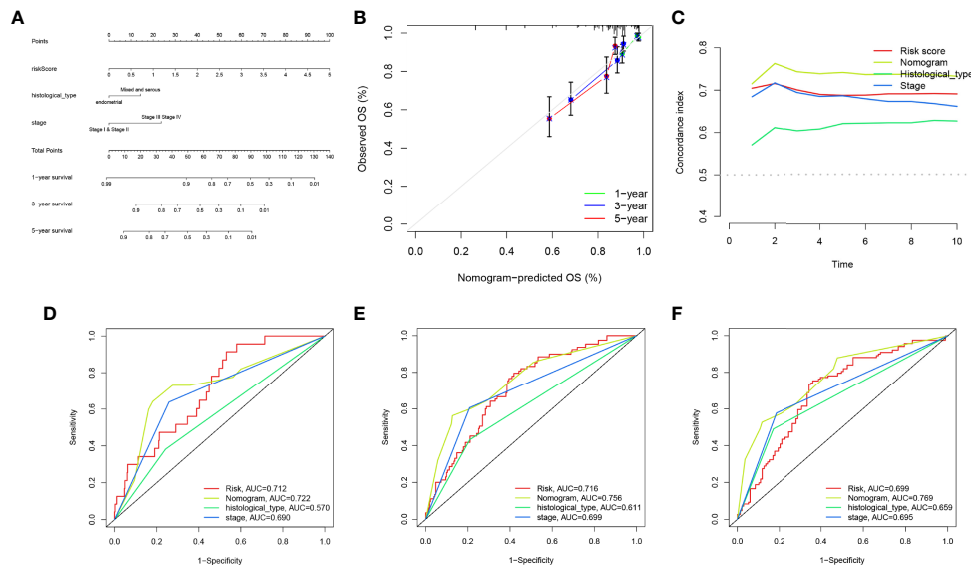


FIGURE 9

Construction and evaluation of the nomogram. (A) The nomogram was developed for clinical application. (B) Calibration curves of the nomogram we developed. (C) The nomogram achieved a significantly higher c-index value than other clinical factors, meaning a better predictive accuracy for endometrial carcinoma (EC). (D–F) The area under the curve (AUC) values of the nomogram for 1-, 3-, and 5-year overall survival (OS) were higher than 0.7 and other clinical factors, indicating that the nomogram was reliable.

osteosarcoma and could assess patient outcomes (43). Our study is the first to reveal the role of the aforementioned lncRNAs in endometrial cancer and their value in the tumor microenvironment.

The development of cancer is associated with the activation of multiple pathways, and the exploration of these key pathways will help to identify vulnerable points of cancer and enable more effective treatment of cancer (44). Our study found that the high-risk group was associated with enrichment of cell cycle, DNA replication, and ECM–receptor interaction pathways, which are highly related to cancer cell replication and growth, which may be one of the reasons for poorer prognosis in the high-risk group. Cancer cells are known to be in a highly active state of metabolism and replication (45). In the process of unlimited replication, cancer cells accumulate a large number of mutations and instabilities, which may be potential therapeutic targets for cancer (46). Through enrichment analysis, we found that the high-risk group was associated with significant enrichment of DNA replication and cell cycle pathways, which may be potentially related to IFN- γ , providing a reference for us to understand its complex crosstalk. The role of ECM-related signaling pathways in cancer is central and variable (47). Dysregulation of ECM in cancer results in adherent junctions, loss of tissue polarity, and epithelial–mesenchymal transition (EMT) (48). Moreover, dysregulation of ECM is also associated with the chronic inflammatory background of cancer, where oversecretion of cytokines stimulates downstream signaling pathways, promotes tumor growth, and mediates the development of drug resistance (49). The activation of the

ECM signaling pathway in the high-risk group may be the underlying mechanism of IFN- γ in regulating endometrial cancer growth, which provides a reference for guiding related treatment.

Currently, several IFN- γ -related signatures have been built. Yan et al. constructed the prognostic signature associated with IFN- γ -activated CD8+ T cells to assess the prognosis and immune response level of melanoma patients using a weighted co-expression network analysis (50). Yao et al. constructed the signature of seven IFN- γ -related lncRNAs to assess prognosis in patients with lung adenocarcinoma, in which the high-risk group had a worse prognosis and was associated with high levels of tumor-promoting immune cells (51). Liu et al. constructed an IFN- γ -related signature in renal clear cell carcinoma, where the high risk score is associated with immunosuppressive microenvironment and drug resistance (52). In addition, there are many new signatures being built in multiple tumors. Liu et al. constructed the signature of mutation-derived genome instability-associated lncRNAs, in which risk score was negatively correlated with prognosis and immune cell infiltration (53). Yuan et al. explored the role of M5C-associated lncRNA in pancreatic ductal adenocarcinoma and found that the M5C-associated signature is a prognostic marker and immune evaluation indicator of pancreatic ductal adenocarcinoma (54). Through in-depth analysis, Gao et al. found that EMT-related lncRNAs constitute a prognostic signature in pancreatic cancer, with a significantly worse prognosis in the high-risk group (55). Liu et al. also

constructed an immune-related lncRNA signature in endometrial cancer through bioinformatics analysis, and different risk scores were associated with different prognoses and immune statuses (56). In contrast to these published studies, our study constructed the prognostic signature of IFN- γ -related lncRNAs for the first time to assess the prognosis and immune microenvironment of endometrial cancer. Our signature has good robustness in evaluating the prognosis of EC, and it can be seen that the prognosis of patients in the high-risk group is significantly worse in the training cohort, validation cohort, and entire cohort. Second, the ROC curve shows that our signature has a high AUC value and good accuracy. Our signature also reveals the immune landscape and differences in drug sensitivity between different risk groups to provide a reference for their treatment.

Conclusion

Our study provides an in-depth analysis of the role of IFN- γ -related lncRNAs in endometrial cancer. The prognostic signature constructed by us can effectively evaluate the prognosis and immune status of patients with endometrial cancer. However, there are limitations to our study, as we lack *in vivo* and *in vitro* experiments to confirm our conclusions. Meanwhile, we lack the validation of cohort from our center, and we will improve it in the future. More studies are expected to explore the significance of IFN- γ in endometrial cancer.

Data availability statement

The datasets presented in this study can be found in online repositories. The names of the repository/repositories and accession number(s) can be found in the article/[supplementary material](#).

Ethics statement

This study was reviewed and approved by Ethics Committee of Nantong Haimen People's Hospital. The patients/participants provided their written informed consent to participate in this study.

References

1. Huvila J, Pors J, Thompson EF, Gilks CB. Endometrial carcinoma: molecular subtypes, precursors and the role of pathology in early diagnosis. *J Pathol* (2021) 253(4):355–65. doi: 10.1002/path.5608
2. Crosbie EJ, Kitson SJ, McAlpine JN, Mukhopadhyay A, Powell ME, Singh N. Endometrial cancer. *Lancet* (2022) 399(10333):1412–28. doi: 10.1016/S0140-6736(22)00323-3

Author contributions

CG designed the study. CG and ZZ were involved in database search and statistical analyses. CG, ZZ, CL, and LH were involved in the writing of the manuscript and its critical revision. CG, XZ, and SH were responsible for the submission of the final version of the paper. All authors approved the final version. All authors agree to be accountable for all aspects of the work.

Funding

This research was supported by the National Natural Science Foundation of China (82173554).

Acknowledgments

We are very grateful for the data provided by databases such as TCGA and GEO.

Conflict of interest

The authors declare that the research was conducted in the absence of any commercial or financial relationships that could be construed as a potential conflict of interest.

Publisher's note

All claims expressed in this article are solely those of the authors and do not necessarily represent those of their affiliated organizations, or those of the publisher, the editors and the reviewers. Any product that may be evaluated in this article, or claim that may be made by its manufacturer, is not guaranteed or endorsed by the publisher.

Supplementary material

The Supplementary Material for this article can be found online at: <https://www.frontiersin.org/articles/10.3389/fonc.2022.955979/full#supplementary-material>

3. Liu J, Cui G, Shen S, Gao F, Zhu H, Xu Y. Establishing a prognostic signature based on epithelial-mesenchymal transition-related genes for endometrial cancer patients. *Front Immunol* (2022) 12:805883. doi: 10.3389/fimmu.2021.805883
4. Makker V, Colombo N, Casado Herráez A, Santin AD, Colomba E, Miller DS, et al. Study 309–keynote-775 investigators. lenvatinib plus pembrolizumab for advanced endometrial cancer. *N Engl J Med* (2022) 386(5):437–48. doi: 10.1056/NEJMoa2108330
5. van den Heerik ASVM, Horeweg N, de Boer SM, Bosse T, Creutzberg CL. Adjuvant therapy for endometrial cancer in the era of molecular classification:

radiotherapy, chemoradiation and novel targets for therapy. *Int J Gynecol Cancer* (2021) 31(4):594–604. doi: 10.1136/ijgc-2020-001822

6. Liu J, Geng R, Ni S, Cai L, Yang S, Shao F, et al. Pyroptosis-related lncRNAs are potential biomarkers for predicting prognoses and immune responses in patients with UCEC. *Mol Ther Nucleic Acids* (2022) 27:1036–55. doi: 10.1016/j.omtn.2022.01.018

7. Blanchard Z, Vahrenkamp JM, Berrett KC, Arnesen S, Gertz J. Estrogen-independent molecular actions of mutant estrogen receptor 1 in endometrial cancer. *Genome Res* (2019) 29(9):1429–41. doi: 10.1101/gr.244780.118

8. Gómez-Raposo C, Merino Salvador M, Aguayo Zamora C, García de Santiago B, Casado Sáenz E. Immune checkpoint inhibitors in endometrial cancer. *Crit Rev Oncol Hematol* (2021) 161:103306. doi: 10.1016/j.critrevonc.2021.103306

9. Raglan O, Kalliala I, Markozannes G, Cividini S, Gunter MJ, Nautiyal J, et al. Risk factors for endometrial cancer: An umbrella review of the literature. *Int J Cancer* (2019) 145(7):1719–30. doi: 10.1002/ijc.31961

10. Schroder K, Hertzog PJ, Ravasi T, Hume DA. IFN- γ : an overview of signals, mechanisms and functions. *J Leukoc Biol* (2004) 75(2):163–89. doi: 10.1189/jlb.0603252

11. Castro F, Cardoso AP, Gonçalves RM, Serre K, Oliveira MJ. IFN- γ at the crossroads of tumor immune surveillance or evasion. *Front Immunol* (2018) 9:847. doi: 10.3389/fimmu.2018.00847

12. Alsapch E, Lussier DM, Schreiber RD. Interferon γ and its important roles in promoting and inhibiting spontaneous and therapeutic cancer immunity. *Cold Spring Harb Perspect Biol* (2019) 11(3):a028480. doi: 10.1101/cshperspect.a028480

13. Ni L, Lu J. Interferon gamma in cancer immunotherapy. *Cancer Med* (2018) 7(9):4509–16. doi: 10.1002/cam4.1700

14. Dunn GP, Old LJ, Schreiber RD. The immunobiology of cancer immunosurveillance and immunoeediting. *Immunity* (2004) 21(2):137–48. doi: 10.1016/j.immuni.2004.07.017

15. Zaidi MR. The IFN- γ paradox in cancer. *J Interferon Cytokine Res* (2019) 39(1):30–8. doi: 10.1089/jir.2018.0087

16. Lobo de Figueiredo-Pontes L, Adamcova MK, Grusanovic S, Kuzmina M, Aparecida Lopes I, Fernandes de Oliveira Costa A, et al. Improved hematopoietic stem cell transplantation upon inhibition of natural killer cell-derived IFN- γ . *Stem Cell Rep* (2021) 16(8):1999–2013. doi: 10.1016/j.stemcr.2021.06.008

17. Deng S, Lin S, Shen J, Zeng Y. The relationship between IFN- γ (IFN- γ) single nucleotide polymorphism +874(T/A) and occurrence risk of aplastic anemia: a meta-analysis. *Hematology* (2020) 25(1):85–90. doi: 10.1080/16078454.2019.1631508

18. Yoo HJ, Byun HJ, Kim BR, Lee KH, Park SY, Rho SB. DAPK1 inhibits NF- κ B activation through TNF- α and IFN- γ -induced apoptosis. *Cell Signal* (2012) 24(7):1471–7. doi: 10.1016/j.cellsig.2012.03.010

19. Peng WX, Koirala P, Mo YY. LncRNA-mediated regulation of cell signaling in cancer. *Oncogene* (2017) 36(41):5661–7. doi: 10.1038/ncr.2017.184

20. Tan YT, Lin JF, Li T, Li JJ, Xu RH, Ju HQ. LncRNA-mediated posttranslational modifications and reprogramming of energy metabolism in cancer. *Cancer Commun (Lond)* (2021) 41(2):109–20. doi: 10.1002/cac2.12108

21. Wang L, Cho KB, Li Y, Tao G, Xie Z, Guo B, et al. (lncrna)-mediated competing endogenous rna networks provide novel potential biomarkers and therapeutic targets for colorectal cancer. *Int J Mol Sci* (2019) 20(22):5758. doi: 10.3390/ijms20225758

22. Blum A, Wang P, Zenklusen JC. SnapShot: TCGA-analyzed tumors. *Cell* (2018) 173(2):530. doi: 10.1016/j.cell.2018.03.059

23. Langfelder P, Horvath S. WGCNA: an R package for weighted correlation network analysis. *BMC Bioinf* (2008) 9:559. doi: 10.1186/1471-2105-9-559

24. Langfelder P, Horvath S. Eigengene networks for studying the relationships between co-expression modules. *BMC Syst Biol* (2007) 1:54. doi: 10.1186/1752-0509-1-54

25. Tibshirani R. The lasso method for variable selection in the cox model. *Stat Med* (1997) 16(4):385–95. doi: 10.1002/(sici)1097-0258(19970228)16:4<385::aid-sim380>3.0.co;2-3

26. Lira RPC, Antunes-Foschini R, Rocha EM. Survival analysis (Kaplan-Meier curves): a method to predict the future. *Arq Bras Oftalmol* (2020) 83(2):VVII. doi: 10.5935/0004-2749.20200036

27. Mandrekari JN. Receiver operating characteristic curve in diagnostic test assessment. *J Thorac Oncol* (2010) 5(9):1315–6. doi: 10.1097/JTO.0b013e3181ec173d

28. Subramanian A, Kuehn H, Gould J, Tamayo P, Mesirov JP. GSEA-p: a desktop application for gene set enrichment analysis. *Bioinformatics* (2007) 23(23):3251–3. doi: 10.1093/bioinformatics/btm369

29. Newman AM, Liu CL, Green MR, Gentles AJ, Feng W, Xu Y, et al. Robust enumeration of cell subsets from tissue expression profiles. *Nat Methods* (2015) 12(5):453–7. doi: 10.1038/nmeth.3337

30. Huang L, Wu C, Xu D, Cui Y, Tang J. Screening of important factors in the early sepsis stage based on the evaluation of ssGSEA algorithm and ceRNA regulatory network. *Evol BioInf Norm Online* (2021) 17:11769343211058463. doi: 10.1177/11769343211058463

31. Aoki Y, Kanao H, Wang X, Yunokawa M, Omatsu K, Fusegi A, et al. Adjuvant treatment of endometrial cancer today. *Jpn J Clin Oncol* (2020) 50(7):753–65. doi: 10.1093/jjco/hyaa071

32. Murali R, Delair DF, Bean SM, Abu-Rustum NR, Soslow RA. Evolving roles of histologic evaluation and Molecular/Genomic profiling in the management of endometrial cancer. *J Natl Compr Canc Netw* (2018) 16(2):201–9. doi: 10.6004/jnccn.2017.7066

33. Kasherman L, Ahrari S, Lheureux S. Dostarlimab in the treatment of recurrent or primary advanced endometrial cancer. *Future Oncol* (2021) 17(8):877–92. doi: 10.2217/fon-2020-0655

34. Al-Rashidi HE, Refaat A, Ahmed E, Hussein DT, Eltantawy FM, Hamed S. Involvement of IFN- γ functional single nucleotide polymorphism +874 T/A (rs2430561) in breast cancer risk. *Saudi J Biol Sci* (2021) 28(11):6289–96. doi: 10.1016/j.sjbs.2021.06.083

35. Boretto M, Maenhoudt N, Luo X, Hennes A, Boeckx B, Bui B, et al. Patient-derived organoids from endometrial disease capture clinical heterogeneity and are amenable to drug screening. *Nat Cell Biol* (2019) 21(8):1041–51. doi: 10.1038/s41556-019-0360-z

36. Yin FF, Zhao LJ, Ji XY, Duan N, Wang YK, Zhou JY, et al. Intra-tumor heterogeneity for endometrial cancer and its clinical significance. *Chin Med J (Engl)* (2019) 132(13):1550–62. doi: 10.1097/CM9.0000000000000286

37. Lewin SN. Revised FIGO staging system for endometrial cancer. *Clin Obstet Gynecol* (2011) 54(2):215–8. doi: 10.1097/GRE.0b013e3182185baa

38. Devor EJ, Gonzalez-Bosquet J, Thiel KW, Leslie KK. Genomic characterization of five commonly used endometrial cancer cell lines. *Int J Oncol* (2020) 57(6):1348–57. doi: 10.3892/ijo.2020.5139

39. Travaglino A, Raffone A, Gencarelli A, Mollo A, Guida M, Insabato L, et al. TCGA classification of endometrial cancer: the place of carcinosarcoma. *Pathol Oncol Res* (2020) 26(4):2067–73. doi: 10.1007/s12253-020-00829-9

40. Sui J, Li YH, Zhang YQ, Li CY, Shen X, Yao WZ, et al. Integrated analysis of long non-coding RNA-associated ceRNA network reveals potential lncRNA biomarkers in human lung adenocarcinoma. *Int J Oncol* (2016) 49(5):2023–36. doi: 10.3892/ijo.2016.3716

41. Wang Q, Tang Y, Ge Y, Zhang S, Zheng M. Long non-coding RNA NRAV enhances proliferation and invasion of hepatocellular carcinoma cells by modulating the wnt/ β -catenin signaling pathway. *Bioengineered* (2022) 13(4):10026–37. doi: 10.1080/21655979.2022.2062977

42. Lin N, Lin JZ, Tanaka Y, Sun P, Zhou X. Identification and validation of a five-lncRNA signature for predicting survival with targeted drug candidates in ovarian cancer. *Bioengineered* (2021) 12(1):3263–74. doi: 10.1080/21655979.2021.1946632

43. He Y, Zhou H, Xu H, You H, Cheng H. Construction of an immune-related lncRNA signature that predicts prognosis and immune microenvironment in osteosarcoma patients. *Front Oncol* (2022) 12:769202. doi: 10.3389/fonc.2022.769202

44. Krishnamurthy N, Kurzrock R. Targeting the wnt/beta-catenin pathway in cancer: Update on effectors and inhibitors. *Cancer Treat Rev* (2018) 62:50–60. doi: 10.1016/j.ctrv.2017.11.002

45. Xie J, Chen L, Tang Q, Wei W, Cao Y, Wu C, et al. A necroptosis-related prognostic model of uveal melanoma was constructed by single-cell sequencing analysis and weighted Co-expression network analysis based on public databases. *Front Immunol* (2022) 13:847624. doi: 10.3389/fimmu.2022.847624

46. Wenzel ES, Singh ATK. Cell-cycle checkpoints and aneuploidy on the path to cancer. *In Vivo* (2018) 32(1):1–5. doi: 10.21873/invivo.11197

47. Xie J, Chen L, Cao Y, Wu D, Xiong W, Zhang K, et al. Single-cell sequencing analysis and weighted Co-expression network analysis based on public databases identified that TNC is a novel biomarker for keloid. *Front Immunol* (2021) 12:783907. doi: 10.3389/fimmu.2021.783907

48. Walker C, Mojares E, Del Rio Hernández A. Role of extracellular matrix in development and cancer progression. *Int J Mol Sci* (2018) 19(10):3028. doi: 10.3390/ijms19103028

49. Karamanos NK, Piperigkou Z, Passi A, Götte M, Rousselle P, Vlodavsky I. Extracellular matrix-based cancer targeting. *Trends Mol Med* (2021) 27(10):1000–13. doi: 10.1016/j.molmed.2021.07.009

50. Yan K, Lu Y, Yan Z, Wang Y. 9-gene signature correlated with cd8-t cell infiltration activated by ifn- γ : a biomarker of immune checkpoint therapy response in melanoma. *Front Immunol* (2021) 12:622563. doi: 10.3389/fimmu.2021.622563

51. Yao B, Wang L, Wang H, Bao J, Li Q, Yu F, et al. Seven interferon gamma response genes serve as a prognostic risk signature that correlates with immune IFN infiltration in lung adenocarcinoma. *Aging (Albany NY)*. (2021) 13(8):11381–410. doi: 10.18632/aging.202831

52. Liu L, Du X, Fang J, Zhao J, Guo Y, Zhao Y, et al. Development of an interferon gamma response-related signature for prediction of survival in clear cell renal cell carcinoma. *J IFN Inflamm Res* (2021), 14:4969–4985. doi: 10.2147/JIR.S334041
53. Liu J, Cui G, Ye J, Wang Y, Wang C, Bai J. Comprehensive analysis of the prognostic signature of mutation-derived genome instability-related lncRNAs for patients with endometrial cancer. *Front Cell Dev Biol* (2022) 10:753957. doi: 10.3389/fcell.2022.753957
54. Yuan H, Liu J, Zhao L, Wu P, Chen G, Chen Q, et al. Prognostic risk model and tumor immune environment modulation of m5c-related lncRNAs in pancreatic ductal adenocarcinoma. *Front Immunol* (2021) 12:800268. doi: 10.3389/fimmu.2021.800268
55. Gao Y, Liu J, Cai B, Chen Q, Wang G, Lu Z, et al. Development of epithelial-mesenchymal transition-related lncRNA signature for predicting survival and immune microenvironment in pancreatic cancer with experiment validation. *Bioengineered* (2021) 12(2):10553–67. doi: 10.1080/21655979.2021.2000197
56. Liu J, Mei J, Wang Y, Chen X, Pan J, Tong L, et al. Development of a novel immune-related lncRNA signature as a prognostic classifier for endometrial carcinoma. *Int J Biol Sci* (2021) 17(2):448–59. doi: 10.7150/ijbs.51207



OPEN ACCESS

EDITED BY

Shaohua Xu,
Tongji University, China

REVIEWED BY

Benjamin Oskar Grabarek,
University of Technology in Katowice,
Poland
Xihu Qin,
Changzhou No.2 People's Hospital,
China
Krisztina Hanley,
Emory University, United States

*CORRESPONDENCE

Sufen Liu
liusufen11978@126.com
Zhongzhi Jia
jiazhongzhi.1998@163.com

[†]These authors have contributed
equally to this work

SPECIALTY SECTION

This article was submitted to
Gynecological Oncology,
a section of the journal
Frontiers in Oncology

RECEIVED 24 May 2022

ACCEPTED 18 July 2022

PUBLISHED 05 August 2022

CITATION

Qiao D, Qin X, Yang H, Liu X, Liu L,
Liu S and Jia Z (2022) Estradiol
mediates the interaction of LINC01541
and miR-429 to promote
angiogenesis of G1/G2
endometrioid adenocarcinoma
in-vitro: A pilot study.
Front. Oncol. 12:951573.
doi: 10.3389/fonc.2022.951573

COPYRIGHT

© 2022 Qiao, Qin, Yang, Liu, Liu, Liu
and Jia. This is an open-access article
distributed under the terms of the
Creative Commons Attribution License
(CC BY). The use, distribution or
reproduction in other forums is
permitted, provided the original
author(s) and the copyright owner(s)
are credited and that the original
publication in this journal is cited, in
accordance with accepted academic
practice. No use, distribution or
reproduction is permitted which does
not comply with these terms.

Estradiol mediates the interaction of LINC01541 and miR-429 to promote angiogenesis of G1/G2 endometrioid adenocarcinoma *in-vitro*: A pilot study

Dan Qiao^{1†}, Xiaoduo Qin^{1†}, Haiyan Yang^{1†}, Xuanton Liu²,
Libing Liu², Sufen Liu^{2*} and Zhongzhi Jia^{3*}

¹Department of Gynecology, Dalian Medical University, Dalian, China, ²Department of Gynecology, Changzhou No. 2 People's Hospital, Changzhou, China, ³Department of Interventional Radiology, Changzhou No. 2 People's Hospital, Changzhou, China

Background: Endometrioid adenocarcinoma (EAC) is the most common subtype of endometrial cancer (EC) and is an estrogen-related cancer. In this study, we sought to investigate the expressions and mechanism of action of 17 β -estradiol (E2) and long noncoding RNA (lncRNA) LINC01541 in G1/G2 EAC samples.

Methods: The expressions of estrogen receptor β (ESR2), LINC01541, miR-200s, and VEGFA were evaluated using real-time PCR in human EAC tissues (n = 8) and adjacent normal tissues (n = 8). Two EC cell lines (Ishikawa and RL95-2) were selected for validation *in vitro*. Bioinformatics analyses and luciferase reporter analyses were performed to verify potential binding sites. qRT-PCR, Western blot, and CCK-8 were used to identify the regulatory mechanisms of related genes in cell biological behavior.

Results: Compared with adjacent normal tissues, LINC01541 and miR-200s family (except miR-200c) were highly expressed in EAC tissues (n=8), while ESR2 and VEGFA were lowly expressed in EAC tissues (**P* < 0.05; ***P* < 0.01). *In vitro*: E2 inhibited the expression of LINC01541 and miR-429 in both cell lines, and estrogen antagonist (PHTPP) could reverse this effect, in addition, PHTPP could promote the proliferation of these two cancer cells, cell transfection LINC01541 also had this effect after overexpression of plasmid and miR-429 mimic. E2 promotes the expression of VEGFA in both cell lines, and PHTPP can also reverse this effect. LINC01541 interacts with miR-429 to promote the expression of each other, and both inhibit the synthesis of VEGFA in EAC cells after overexpression. Through the double validation of bioinformatics analysis and dual fluorescein reporter gene, it was confirmed that miR-429 targets the regulation of VEGFA expression (**P* < 0.05; ***P* < 0.01).

Conclusion: E2 promotes the synthesis of VEGFA by altering the expression levels of LINC01541 and miR-429 in EAC, thereby affecting the angiogenesis process of EAC. Also, E2-mediated LINC01541/miR-429 expression may affect cell migration in EAC. In addition, we identified a reciprocal promotion between LINC01541 and miR-429.

KEYWORDS

endometrioid adenocarcinoma, estradiol, LINC01541, angiogenesis, miR-200s

Introduction

Endometrial cancer (EC) is the sixth most common tumor type and the eleventh most common cause of death in women worldwide, with endometrioid adenocarcinoma (EAC) accounting for 80% of all EC cases and the majority of well and moderately differentiated endometrioid histology (G1/G2). The vast majority of EC cases are in postmenopausal women. Long-term estrogen therapy, premature menarche, delayed menopause, infertility, polycystic ovary syndrome, advanced age, obesity, hypertension, diabetes are all risk factors for EC (1, 2). It is well known that EC is an endocrine-related cancer and that estrogen plays a key role in the occurrence and progression of this disease. Two specific intracellular receptors, estrogen receptor α (ER α) (ESR1) and ER β (ESR2), mediate the biological effects of estrogen, with 17 β -estradiol (E2) acting in the body mainly through ESR2 (3, 4). Research has demonstrated that siRNA-mediated knockdown of ESR2 and treatment with the ESR2 antagonist PHTPP can induce proliferation of HEC-1A (EC cell line) and RL95-2 (EC cell line) cells (5).

Increasingly, studies have shown that long noncoding RNAs (lncRNAs) play a key role in many biological processes (6). One such lncRNA is LOC100505776, also known as LINC01541 (NR_038325.1). Mai and colleagues used the Ishikawa cell line as a tool cell to study endometriosis and found that E2 inhibited the expression of LINC01541 in Ishikawa cells (7). Along similar lines, miRNAs have been found to be dysregulated in many human cancers, acting as tumor promoters or suppressors (8). More specifically, the miR-200s (miR-200a, miR-200b, miR-200c, miR-141, and miR-429) are dysregulated in EC, affecting cell processes such as migration and invasion. Some research has found that the expression of miR-429 is up-regulated in EC tissues versus in adjacent tissues, and other studies have shown that silencing the expression of miR-429 significantly inhibits the growth of HEC-1A and Ishikawa cells (9, 10).

Angiogenesis also plays a vital role in tumor progression (11). Multiple studies have demonstrated that angiogenesis is regulated by vascular endothelial growth factor (VEGF), including VEGFA, VEGFB, VEGFC, VEGFD and VEGFE,

which are part of the dimeric glycoprotein family. These factors are secreted by many types of cells, including cancer cells (12), and research has shown that the expression of VEGF mRNA in uterine tissues is significantly up-regulated after exposure to estradiol treatment (13). Studies have found that VEGFA is a potential target of miR-429 (14, 15). Taken together, we speculate that ESR2 affects the production of VEGFA by regulating the expression of LINC01541 and miR-429 in EAC tissue, and this pathway affects the occurrence and progression of EAC. In this study, we sought to explore the effect of E2 stimulation on Ishikawa and RL95-2 cells, as well as the effects of LINC01541 silencing and overexpression in both cell lines. Ishikawa and RL95-2 cells are estrogen-sensitive and represent a well differentiated EAC cell line and a moderately differentiated adenosquamous carcinoma cell line, respectively (16, 17). We also aimed to investigate the effects of LINC01541 on cell proliferation and VEGFA secretion.

Materials and methods

Patients and tissue collection

This study was approved by the Ethics Committee of our hospital. Patients provided informed consent for tissue sample collection before the study began.

From October 2020 to July 2021, both human EAC tissues and adjacent normal endometrial tissues were collected from 8 patients (mean age: 54.5 ± 5.0 y; tumor grade G1-G2) who underwent total hysterectomy recruited from the Changzhou No. 2 People's Hospital Affiliated to Nanjing Medical University. The clinical information of all patients was shown in Table 1. Formalin-fixed paraffin embedded samples from each tumor were stained with hematoxylin-eosin and evaluated by two pathologists. Inclusion criteria were as follows: 1) patients had not received any hormone therapy in the previous 6 months, 2) patients were diagnosed as EAC (tumor grade G1-G2) according to the International Federation of Gynecology and Obstetrics (FIGO) surgical and pathological criteria. Exclusion criteria were

TABLE 1 Clinicopathological characteristics of the EAC patients included in the study.

Characteristic	All patients n=8	grade G1 n=4	grade G2 n=4
Mean age (y) (range)	54.5 (44-60)	52.5 (44-59)	56.5 (55-60)
BMI (kg/m ²)			
<24.9 (normal)	2 (25.0%)	1 (25.0%)	1 (25.0%)
25.0-29.9 (overweight)	5 (62.5%)	2 (50.0%)	3 (75.0%)
>30.0 (obese)	1 (12.5%)	1 (25.0%)	–
Hypertension			
Yes	3 (37.5%)	1 (25.0%)	2 (50.0%)
No	5 (62.5%)	3 (75.0%)	2 (50.0%)
Diabetes			
Yes	2 (25.0%)	1 (25.0%)	1 (25.0%)
No	6 (75.0%)	3 (75.0%)	3 (75.0%)
FIGO stage			
IA	7 (87.5%)	4 (100%)	3 (75.0%)
IB	1 (12.5%)	–	1 (25.0%)
LVSI			
Yes	1 (12.5%)	–	1 (25.0%)
No	7 (87.5%)	4 (100%)	3 (75.0%)

LVSI, lymphovascular space invasion.

as follows: The patient has other malignant tumors or gynecological diseases other than EC.

Bioinformatics predictions

We used three bioinformatics software programs: RNAhybrid (<https://bibiserv.cebitec.uni-bielefeld.de/rnahybrid>), starBase v3.0 (<https://starbase.sysu.edu.cn/index.php>) and GEPIA (<http://gepia.cancer-pku.cn/detail.php>) to predict the expression of and associations between LINC01541, miR-200s, and VEGFA. The results of each program were screened, and common miRNAs were selected as candidate LINC01541-interacting miRNAs.

Cell line culture and transfection

Ishikawa cells were obtained from Chuan Qiu Biotechnology (catalog number H044, Shanghai, China), RL95-2 cells were obtained from Zhong Qiao Xin Zhou Cell (ZQ0362, Shanghai, China). Neither cell line was contaminated. Ishikawa cells were treated with DMEM medium (C11995500BT, Gibco; Auckland, New Zealand) containing 10% fetal bovine serum (FBS) (10270-106, Gibco) and 1% penicillin/streptomycin (15140122, Gibco). RL95-2 cells were cultured in DMEM/F12 medium (ZQ-604-100, Gibco) mixture supplemented with 10% FBS and 1% penicillin/streptomycin and 10 mg/ml insulin (CSP001-10, Zhong Qiao Xin Zhou Cell). Both cell lines were carried out at 37°C in 5% CO₂ conditions. LINC01541 pCDNA 3.1 overexpression vector, LINC01541-specific siRNA, miR-429 mimic, and miR-429

inhibitor were synthesized by RiboBio (Guangzhou, China) (si-LINC01541: 5'-ATTCAATTGTTTTTAATCCAT-3'; si-NC: 5'-GGCTCTAGAAAAGCCTATGC-3'; has-miR-429 mimic: 5'-UAAUACUGUCUGGUAAAACCGU-3'; mimic negative control: 5'-UUUGUACUACACAAAAGUACUG-3'; has-miR-429 inhibitor: 5'-ACGGUUUUACCAGACAGUAUUA-3'; and inhibitor negative control: 5'-CAGUACUUUUGUGUAGUACAAA-3').

Hormone treatment

E2 (E8875, Sigma-Aldrich; St. Louis, USA) and PHTPP (ESR2 antagonist) (SML1355, Sigma-Aldrich) were dissolved in alcohol. The precultured Ishikawa and RL95-2 cells were then treated with various concentrations of E2 (0 [control], 10⁻⁶ mol/L, 10⁻⁸ mol/L, and 10⁻¹⁰ mol/L) and PHTPP (0 [control], 10⁻³ mol/L, 10⁻⁴ mol/L, and 10⁻⁵ mol/L). After hormone treatment, the cells were incubated with DMEM or DMEM/F12 medium for 24 h. The culture medium was then changed daily.

Cell viability assay

The transfected cells were seeded into a 96-well plate at a density of 5×10³ cells per well. A total of 10 μL of cell counting kit-8 (CCK-8) reagent (CK04, Dojindo, Japan) was added to each well, and the cells were incubated for 1 h at 37°C and 5% CO₂. The OD450 value for each well was detected using an ultramicro microplate spectrophotometer (BioTek Epoch; Santa

Clara, CA, USA). Each group was assayed in triplicate at daily intervals after consecutive seeding for up to 72 or 96 h.

Western blot assay

The Ishikawa and RL95-2 cells were homogenized in radio immunoprecipitation assay (RIPA) buffer (P0013B, Beyotime Biotechnology; Shanghai, China) using a standard method. Protein extracts (30 µg) were then transferred to polyvinylidene difluoride membranes (Millipore; Boston, MA, USA). The membranes were blocked and incubated with antibody for VEGFA (66828-1-Ig, Proteintech; Wuhan, China) (diluted at 1:1000) or Tubulin (200608, ZENBIO; Chengdu, China) (diluted at 1:5000) and then with horseradish peroxidase conjugated secondary antibody (511103, ZENBIO) (diluted at 1:5000). The membranes were developed using chemiluminescence substrate (A38555, Thermo Scientific; Shanghai, China) and exposed to X-ray films.

Total RNA extraction and quantitative real-time polymerase chain reaction

Total RNA was extracted using Trizol reagent (T9108, Takara; Dalian, China), and first-strand cDNA was synthesized using HiScript II Q RT SuperMix for qPCR (+gDNA wiper) (R223, Vazyme; Nanning, China). The qRT-PCR was performed using SYBR-Green Premix (Q131-02/03, Vazyme) with specific PCR primers (RiboBio). The qRT-PCR for miRNAs was performed using miRNA Strand cDNA Synthesis Kit (MR101-02, Vazyme) and miRNA Universal SYBR qPCR Master Mix (MQ101-01/02, Vazyme), respectively. Two primers (h-LINC01541-90bp/h-LINC01541-120bp) were designed for LINC01541; qRT-PCR demonstrated that h-LINC01541-90bp was more efficient, and so this primer was used in subsequent experiments. GAPDH and U6 were used as internal controls. Fold changes were calculated using the $2^{-\Delta\Delta C_t}$ method. RT primer for ESR2, LINC01541 and VEGFA

are premixed random primers. The remaining primer sequences are listed in the Table 2 with the exception of the RiboBio miRNA and U6 primer (including RT primer) sequences, which are confidential to the company.

Luciferase assay

Ishikawa and RL95-2 cells were seeded into a 96-well plate at a density of 1.5×10^4 cells per well. Subsequently, the cells were cotransfected with miR-429 mimic (5'-UAAUACUGUCUG GUAAAACCGU-3')/negative control and wild-type/mutant VEGFA (pmirGLO-h-VEGFA-WT: 5'...CAGTATT...3'/pmirGLO-h-VEGFA-MUT: 5'...GTCATAA...3') (RiboBio). After 48 h of transfection, a dual-luciferase reporter assay was performed according to the manufacturer's instructions (E2920, Promega; Madison, WI, USA). Renilla luciferase activity was used for calibration.

Rescue assay

To further study the relationship between LINC01541 and miR-429, we used Ishikawa and RL95-2 cells for rescue experiments. For the first set of experiments, we established 4 groups: a LINC01541 overexpression group, an miR-429 inhibitor group, a co-culture group (LINC01541 overexpression/miR-429 inhibitor), and a PBS group (control). For the second set of experiments, we then established another 4 groups: a knockdown of LINC01541 group, an miR-429 mimic group, a co-culture group (knockdown of LINC01541/miR-429 mimic), and another PBS group (control). Cells were then cultured in 24-well plates for 24 h for qRT-PCR, in 96-well plates for 24 h/48 h/72 h for CCK-8 analysis, and in 6-well plates for 48 h for Western blot analysis.

Statistical analysis

In this study, GraphPad Prism 8.0.2 software was used to analyze data. All studies were verified by three independent experiments. Student's *t*-test was used to analyze two sets of data, and one-way ANOVA was used to analyze multiple sets of data. Data were expressed as mean \pm SD. *P* values less than 0.05 were used to represent statistical significance.

Results

Bioinformatics prediction and the expression of related genes in EAC tissues

RNAhybrid demonstrated that, with the exception of miR0200c, the miR-200s family was able to bind with

TABLE 2 Primers used in the study.

Primers of genes	Sequences (5'-3')
hESR2-81-F	TTCAAAGAGGGATGCTCACTTC
hESR2-81-R	CCTTCACACGACCAGACTCC
h-LINC01541-90bp-F1	GCTTCCTTGCCCTTTCTCCT
h-LINC01541-90bp-R1	TGAGGCTGGAACAGAGGTT
h-LINC01541-120bp-F2	GAATGAAGCTTTGGGGTGAA
h-LINC01541-120bp-R2	CCCACAAATGCACATCTATCC
hVEGFA-91-F	TCGGGAACCAGATCTCTCAC
hVEGFA-91-R	TCTGTGCGATGGTATGGTGT
GAPDH-F	TGAAGGTCCGAGTCAACGGATTTGGT
GAPDH-R	CATGTGGGCCATGAGGTCCACCAC

LINC01541 (Figure 1A). The starBase v3.0 database also demonstrated this binding ability, as well as increased expression of miR-200s (except miR-200c) in uterine corpus endometrial carcinoma (UCEC) (Figures 1B, C). The expression of VEGFA was found to be down-regulated in UCEC compared with adjacent tissues ($P < 0.05$) (Figure 1D). As shown in Figure 1E, LINC01541 was highly expressed in EAC tissues, suggesting that this could be a prognostic marker. The miR-200s family (with the exception of miR-200c) was also highly expressed in EAC tissues.

E2 regulates the expression of LINC01541 and miR-429 and affects the progress of EAC

E2 (at an optimal concentration of 10^{-8} mol/L) was found to have an inhibitory effect on LINC01541 and miR-429, and PHTPP (at an optimal concentration of 10^{-4} mol/L) was found to reverse this effect in Ishikawa and RL95-2 cells (Figures 2A–F).

E2 slightly inhibited the proliferation of Ishikawa and RL95-2 cells, whereas PHTPP significantly promoted the proliferation of these cells (Figures 3A, B). As expected, both LINC01541 and miR-429 promoted the proliferation of EAC cells (Figures 3C–J), suggesting that the effect of E2 on the proliferation of EAC cells was not mediated by the regulation of LINC01541 and miR-429. Finally, E2 was found to promote the expression of VEGFA, with PHTPP able to reverse this effect (Figure 3K).

The interaction between LINC01541 and miR-429 affects the expression of VEGFA in EAC

qRT-PCR demonstrated that LINC01541 and miR-429 interacted to promote each other's expression (Figure 4). The expression of miR-200a, miR-200b, and miR-141 was down-regulated after LINC01541 interference treatment in Ishikawa (Figure 5A) and RL95-2 (Figure 5B) cells. A mixture of knockdown of LINC01541/miR-429 mimic had an intermediate effect in Ishikawa and RL95-2 cells (Figures 5C–F). In addition, LINC01541 was found to promote cell proliferation, but a mixture of LINC01541 overexpression and miR-429 inhibitor was able to reverse this effect in Ishikawa cells (Figure 6A) and RL95-2 cells (Figure 6B). Similarly, the knockdown of LINC01541 inhibited cell proliferation, but a mixture of LINC01541 knockdown and miR-429 mimic was able to reverse this effect in Ishikawa cells (Figure 6C) and RL95-2 cells (Figure 6D).

Western blot analysis demonstrated that LINC01541 overexpression and miR-429 mimic inhibited the production of VEGFA, whereas knockdown of LINC01541 and miR-429 inhibitor promoted the production of VEGFA (Figures 6E–H).

A mixture of LINC01541 overexpression and miR-429 inhibitor, however, had an intermediate effect on Ishikawa cells (Figure 6E) and RL95-2 cells (Figure 6F). A mixture of knockdown of LINC01541 and miR-429 mimic also had an intermediate effect on Ishikawa (Figure 6G) and RL95-2 (Figure 6H) cells.

Bioinformatics analysis and dual luciferase reporter gene detection suggest that miR-429 targets VEGFA

starBase v3.0 software was used to identify the binding site between miR-429 and VEGFA (Figure 7A). miR-429 mimic was found to inhibit the production of VEGFA, whereas miR-429 inhibitor promoted the production of VEGFA. Dual-luciferase assay demonstrated that RL95-2 cells cotransfected with miR-429 mimic and VEGFA-WT had less luciferase activity than other groups (Figure 7B). These results suggest that VEGFA can directly interact with miR-429.

Discussion

In this study, we demonstrated that the expression levels of ESR2 and VEGFA were decreased in EAC tissue, whereas the expression levels of LINC01541 miR-200s (except miR-200c) were increased. The GEPIA software predicted that VEGFA would be down-regulated in EAC tissue, which was consistent with our finding that VEGFA expression was decreased in G1/G2 EAC specimens. We also found that E2 treatment of EAC cells inhibited the expression of LINC01541 and miR-429, whereas PHTPP treatment had the opposite effect. E2 treatment of EAC cells was found to inhibit the expression of VEGFA. LINC01541 and miR-429 were found to inhibit the expression of VEGFA and promote the proliferation of EAC cells. In addition, the interaction of LINC01541 and miR-429 promoted the expression of both factors. Finally, through the double validation of bioinformatics analysis and dual fluorescein reporter gene, it was confirmed that miR-429 targets the regulation of VEGFA expression. (* $P < 0.05$; ** $P < 0.01$)

EC is the most frequent gynecological cancer in developed countries and its incidence is increasing, the majority of EC cases are estrogen dependent but the mechanisms of estrogen are not completely understood (2). Previous studies have shown that the mRNA and protein expression levels of ESR2 are significantly lower in more than 100 EC specimens than those in normal endometrium (18–20), and we similarly observed decreased expression of ESR2 in EC samples in our analysis. Hu et al. found that knockdown of E2 in Ishikawa cells promoted cell proliferation (21). *In vivo* study has shown that ER including ESR1, ESR2 and G protein-coupled estrogen receptor (GPER) is essential for a normal menstrual cycle. Incorrect expression of ERs can cause EC, ESR1 promotes uterine cell proliferation and

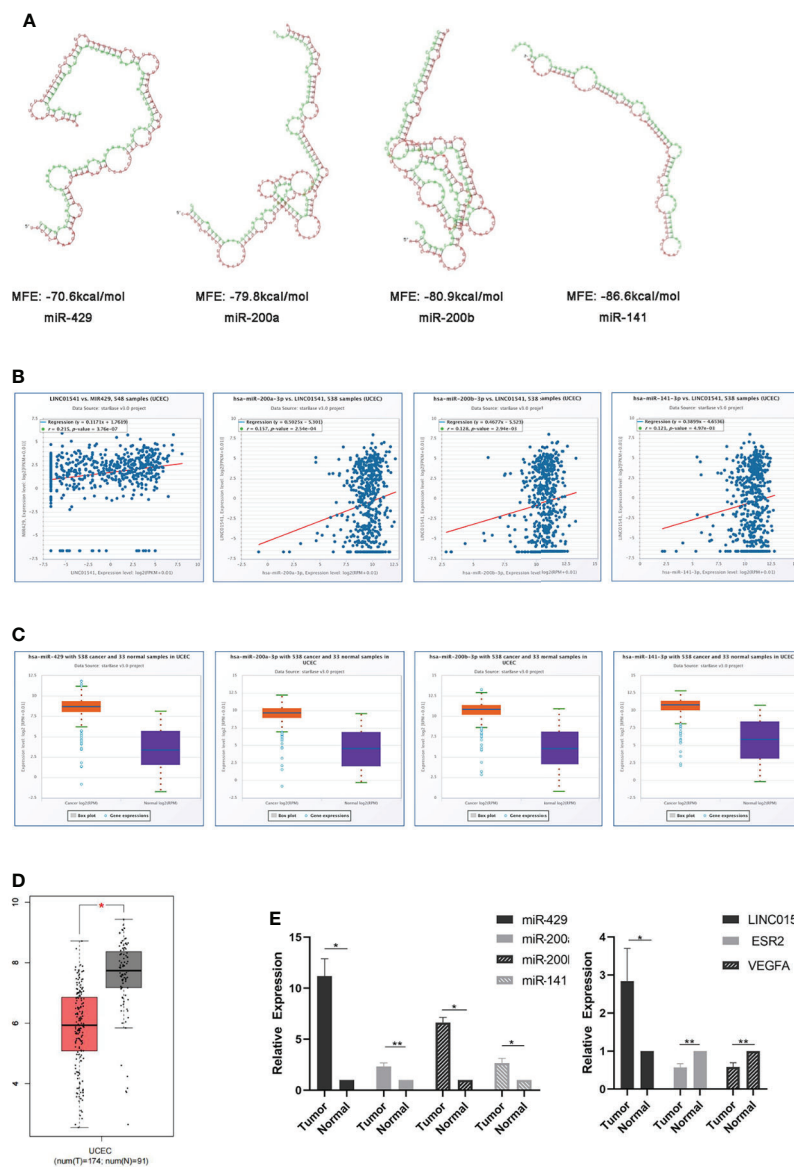


FIGURE 1

Bioinformatics prediction and the expression of related genes in EAC tissue specimens. **(A)** RNAhybrid software demonstrated that miR-429, miR-200a, miR-200b, and miR-141 can bind to LINC01541 (red: LINC01541; green: miRNAs). MFE = minimum free energy (the absolute value of which represents the binding degree of miRNA and target mRNA or lncRNA). **(B)** StarBase v3.0 demonstrated a positive correlation between miR-429 and LINC01541 in UCEC ($P < 0.01$). Other members of the miR-200s family also demonstrated this trend. **(C)** starBase v3.0 demonstrated increased expression of miR-200s (except miR-200c) in UCEC. **(D)** Boxplot demonstrating VEGFA transcriptional expression in UCEC and normal uterus tissues from GEPIA. The red boxes represent UCEC ($n = 174$); the gray boxes represent normal tissue ($n = 91$). The y-axis indicates the log2-transformed gene expression level. **(E)** The expression levels of LINC01541 and miR-200s in G1/G2 EAC tissues ($n = 8$) were significantly higher than those in normal tissue ($n = 8$); however, both ESR2 and VEGFA were decreased in EAC tissue. ($*P < 0.05$; $**P < 0.01$).

increased the risk of EC, while ESR2 has the opposite effects (22). Other research has shown that LINC01541 inhibits VEGFA expression in endometrial stromal cells and that E2 stimulation significantly inhibits the expression of LINC01541, whereas overexpression of LINC01541 attenuates the migration and invasion of endometrial stromal cells induced by E2 (8). Our

findings also support these results. Hormonal therapy is mainly prescribed for fertility preservation with early EC and palliative treatment in patients with advanced or recurrent EC. Studies show that ER pathway activity tests suggest that an active ER pathway may increase sensitivity to EC hormone therapy. High ER pathway activity score (ERPAS) was significantly positively

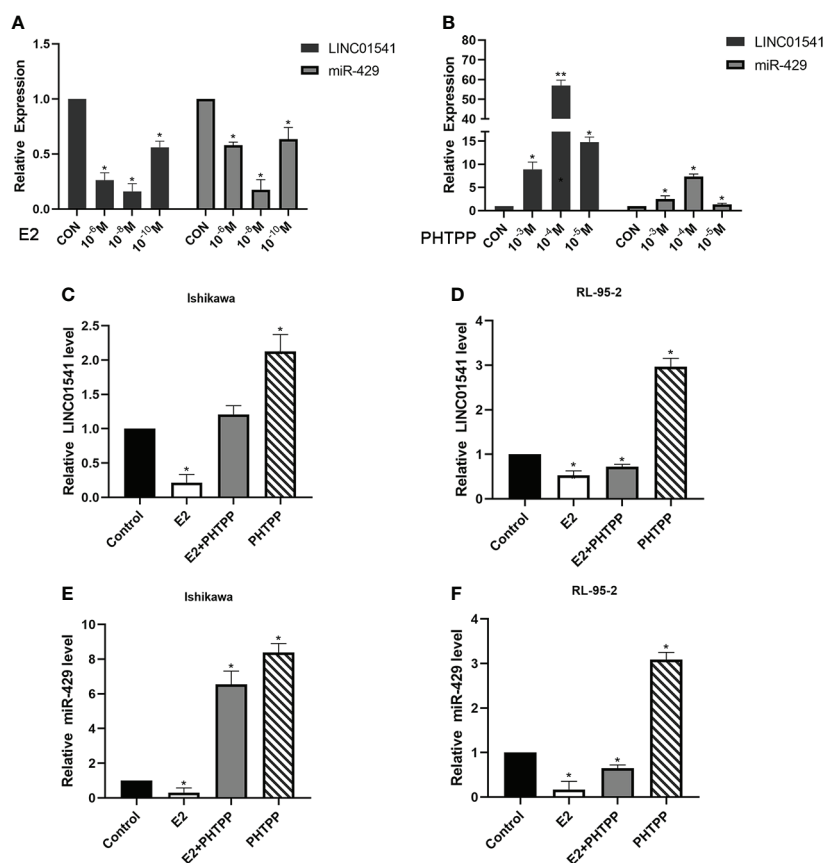


FIGURE 2

qRT-PCR was used to detect the effect of E2 and PHTPP in EAC cells. (A) The down-regulation of LINC01541 and miR-429 was most obvious when the concentration of E2 was 10^{-8} mol/L. (B) The down-regulation of LINC01541 and miR-429 was reversed most obviously when the concentration of PHTPP was 10^{-4} mol/L. (C–F) In Ishikawa and RL95-2 cell lines, E2 inhibited the expression of LINC01541 and miR-429, whereas PHTPP was able to reverse this effect. (* $P < 0.05$; ** $P < 0.01$).

associated with good prognosis and sensitivity to endocrine therapy in EC (23–25).

It is well known that lncRNA can exert its biological function by regulating the expression of miRNA. One group of researchers proposed that lncRNA MT1DP directly binds and stabilizes miR-365 while promoting the expression of miR-365. They found that down-regulation of MT1DP had no effect on the expression of pri-miR-365, suggesting that MT1DP did not regulate miR-365 at the transcriptional level (26, 27). These findings imply that long non-coding RNAs can directly bind and stabilize miRNAs, while promoting the expression of miRNAs, which are consistent with our results. The miR-200 family (miR-200a, miR-200b, miR200c, miR-429, and miR-141) has previously been shown to be up-regulated in EC (28–30). Cui et al. detected 33 EC tissues and 14 endometrial tissue samples and found that miR-141-3p played a positive role in promoting EC cell proliferation (31). Our study did not demonstrate any effect of LINC01541 on pri-miR-429. The specific relationship between LINC01541 and miR-429 needs further study. However, the research results of some scholars have

some enlightenment for us. RNA methylation, similar to DNA or protein modification, is regulated by a variety of regulators, including methyltransferases ('writers'), RNA binding proteins ('readers'), and demethylases ('erasers'). Methylation of N6 adenosine (m6A) is the most common type of RNA modification. Alarcón et al. found that methyltransferase-like 3 (METTL3) methylates pri-miRNAs, and *in vitro* experiments also confirmed the role of m6A markers in promoting pri-miRNA processing. In conclusion, alterations in METTL3 expression may significantly affect miRNA expression in various human cancers (32–34). In addition, m6A-lncRNAs have been proven to be involving in regulating tumorigenesis and m6A is likely to participate in the construction of the lncRNA-miRNA-mRNA (ceRNA) interaction regulatory network (35–37). We hypothesized that the interaction between LINC01541 and miR-429 assessed in our study may therefore be m6A-dependent.

The regulatory relationship between miR-429 and VEGFA has been demonstrated in a variety of cancers and systemic diseases. MiR-429 mimics, on the other hand, have been found

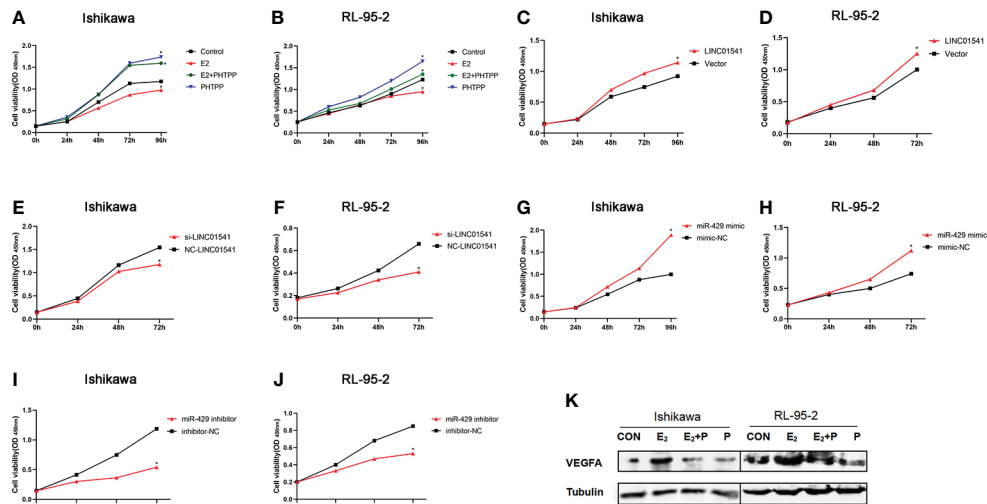


FIGURE 3

CCK-8 and Western blot analysis were used to analyze the effects of treatment. (A, B) In Ishikawa and RL95-2 cells, E2 inhibited cell proliferation, whereas PHTPP and a mixture of PHTPP and E2 promoted cell proliferation. (C, D) Overexpression of LINC01541 promoted proliferation of both cell lines. (E, F) Interfering with the expression of LINC01541 inhibited proliferation of both cell lines. (G, H) Overexpression of miR-429 promoted proliferation of both cell lines. (I, J) Silencing the expression of miR-429 inhibited proliferation of both cell lines. (K) Compared with the control group, E2 promoted the expression of VEGFA, whereas PHTPP inhibited the expression of VEGFA; a mixture of the two had an intermediate effect on VEGFA in Ishikawa and RL95-2 cells. (* $P < 0.05$).

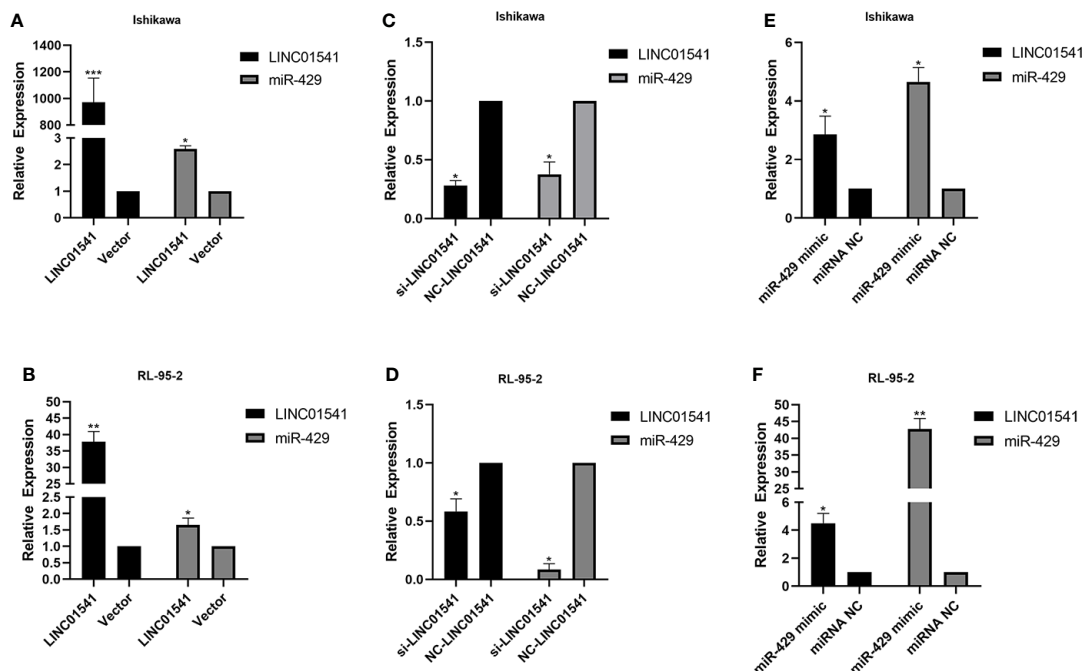


FIGURE 4

LINC01541 and miR-429 were transfected to measure expression. (A, B) After forced overexpression of LINC01541, the expression of LINC01541 and miR-429 were up-regulated in Ishikawa and RL95-2 cells. (C, D) When cells were transfected with LINC01541 siRNA, the expression of LINC01541 and miR-429 was down-regulated. (E, F) After both cells were treated with miR-429 mimics, the expression of LINC01541 and miR-429 was up-regulated. (* $P < 0.05$; ** $P < 0.01$; *** $P < 0.001$).

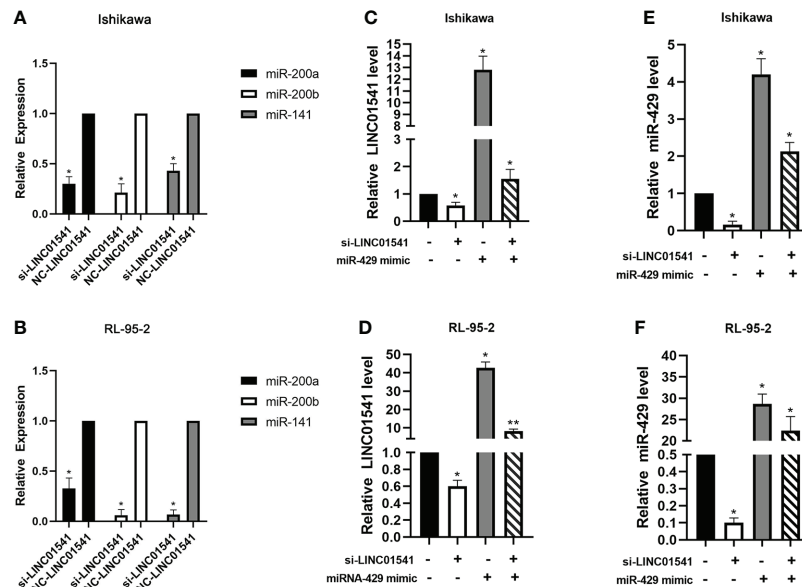


FIGURE 5

QRT-PCR was used to detect the expression of genes after LINC01541/miR-429 treatment. (A, B) Knockdown of LINC01541 was found to inhibit the expression of miR-200a, miR-200b, and miR-141 in Ishikawa and RL95-2 cells. (C–F) A co-culture system was constructed with LINC01541 siRNA and miR-429 mimic, and qRT-PCR was used to further verify the relationship between LINC01541 and miR-429 in Ishikawa and RL95-2 cells. (* $P<0.05$; ** $P<0.01$).

to reduce the expression of VEGF in clear cell renal cell carcinoma cells (38). Chan et al. proposed that VEGFA with high expression levels was negatively correlated with hsa-miR-429, and inhibition of hsa-miR-429 expression stabilized VEGFA expression in urothelial carcinoma (UC) (39). Ye

et al. used bioinformatics analysis software and GEO database to propose miRNA-mRNA pathways such as hsa-miR-429-VEGFA as potential biomarkers for diagnosis and treatment of ovarian cancer (OC) patients (40). Previous research in human umbilical vein endothelial cells has shown that miR-429 can

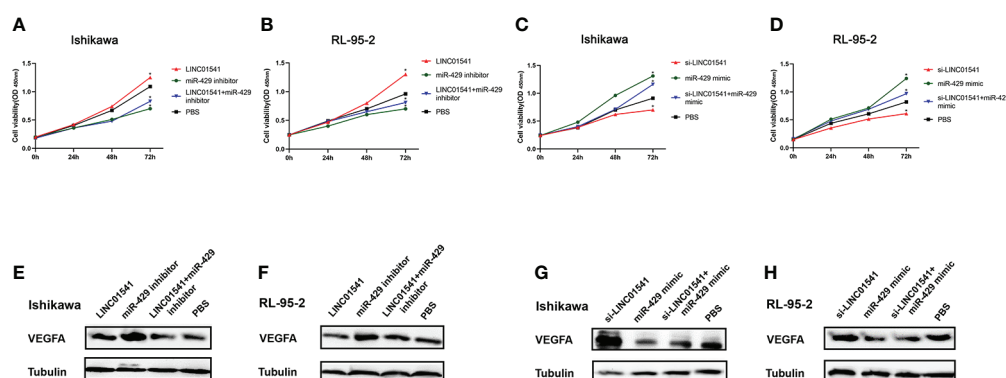


FIGURE 6

Construction of a co-cultivation system after cell transfections. (A, B) CCK-8 used for rescue experiments in Ishikawa and RL95-2 cells demonstrated that LINC01541 promoted cell proliferation, but a mixture of LINC01541 overexpression and miR-429 inhibitor reversed this effect. (C, D) In both cell lines, the knockdown of LINC01541 inhibited cell proliferation, but a mixture of LINC01541 knockdown and miR-429 mimic reversed this effect. (E–H) Western blot analysis demonstrated that LINC01541 and miR-429 inhibited the production of VEGFA. Western blot analysis used for rescue experiments demonstrated that a mixture of LINC01541 overexpression and miR-429 inhibitor had an intermediate effect on both cell lines. Similarly, a mixture of a knockdown of LINC01541 and miR-429 mimic had an intermediate effect on both cell lines. (* $P<0.05$).

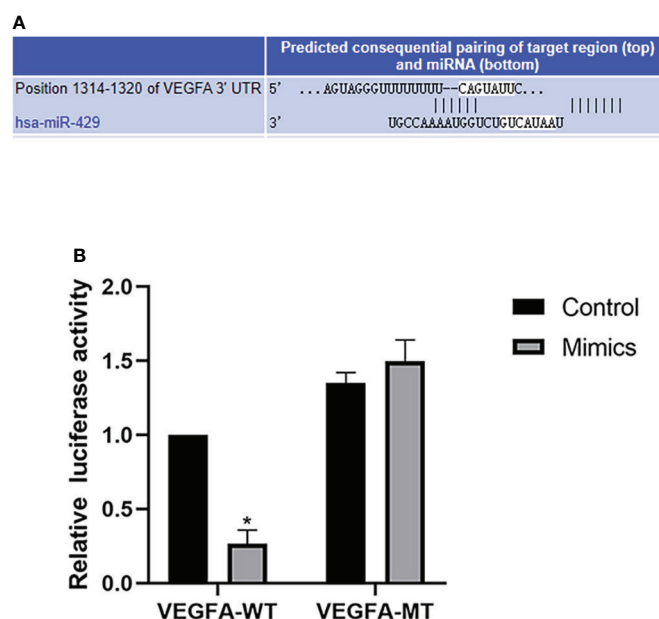


FIGURE 7

Bioinformatics analysis and dual luciferase reporter gene. (A) The binding site of VEGFA and miR-429 was identified with starBase v3.0. (B) Dual-luciferase assay results for RL95-2 cells transfected with wild-type (WT) or mutated (Mut) VEGFA reporters plus miR-429 mimic or mimic-NC molecules for 48 h. * $P < 0.05$.

directly bind to the 3'UTR of VEGFA mRNA to directly regulate its expression (41). In cases of neonatal necrotizing enterocolitis, miR-429/200a/200b and miR-141/200c clusters were found to negatively regulate VEGFA, increasing its expression (14). MiR-429 has been shown to increase the expression of VEGF by promoting the synthesis of hypoxia-inducible factor 1 α (HIF-1 α) in human amniotic mesenchymal stem cells (15).

Gu et al. found that blocking ESR1 or ESR2 can reduce the expression of VEGF and VEGFR in UECC. However, exposure to estrogen accelerated growth and VEGF production in Ishikawa-xenografted nude mice (42). Zhang et al. demonstrated that estrogen-induced angiogenesis appears to occur through induction of various angiogenic factors, such as VEGF and basic fibroblast growth factor (bFGF). Estradiol upregulated mRNA expression and induced protein synthesis of VEGF and bFGF. However, the expression of VEGF and bFGF was blocked by ER inhibitor in estrogen receptor-positive Ishikawa cells (43). One study showed that exogenous therapy with E2 rescues pre-existing advanced heart failure (HF) in mice mainly by regulating ESR2 expression. ESR2 agonists are associated with reduced cardiac fibrosis and increased cardiac angiogenesis (44). In another study, E2 treatment of endometrial stromal cells was demonstrated to be more angiogenic and associated with increased VEGFB protein expression. Meanwhile, these stimulants can be partially eliminated by an estrogen-receptor antagonist (45). In the current study, miR-200s (except miR-200c) were shown to interact with

LINC01541. Because EAC is an estrogen-dependent disease, it is possible that an E2/LINC01541/miR-429/VEGFA axis exists in EAC tissues and that this axis may be a potential therapeutic target.

This study had several limitations. First, the number of samples was also small. Only G1/G2 EAC specimens were collected, and G3 EAC specimens were not included in this study. Secondly, we only conducted CCK-8 experiments to study the effects of 17 β -estradiol, estrogen antagonists, LINC01541 and miR-429 on the proliferation of EAC cell lines, and we can also add Edu experiments and plate cloning experiments. Third, we did not study the effect of related genes on the migration, invasion ability and apoptosis of the two cell lines; Fourth, our current work has not examined the effect of LINC01541 on pri-miR-429, and the specific mechanism of the interaction between LINC01541 and miR-429 needs further study; Finally, we have not conducted *in vivo* experiments, and the findings represent only one phenomenon.

Conclusion

In summary, our results demonstrated that E2 promote the expression of VEGFA by altering LINC01541 and miR-429 expression levels in EAC. We also found that E2-mediated LINC01541/miR-429 expression may affect cell proliferation in EAC. In addition, we identified a reciprocal promotion between

LINC01541 and miR-429. These initial results allow us to understand the angiogenesis of EAC from a new perspective and also suggest that the E2-mediated LINC01541/miR-429/VEGFA axis may serve as a new therapeutic target for EAC. More research is needed to validate the diagnostic potential of these genes in larger studies.

Data availability statement

The original contributions presented in the study are included in the article/supplementary material. Further inquiries can be directed to the corresponding authors.

Ethics statement

The studies involving human participants were reviewed and approved by The Ethics Committee of Changzhou No. 2 People's Hospital. The patients/participants provided their written informed consent to participate in this study.

Author contributions

Conceptualization, ZJ. methodology, SL and ZJ. software, XQ and HY. validation, DQ and XQ. Formal analysis, DQ, HY and XQ. Investigation, LL and XL. Resources, SL. Writing—original draft preparation, DQ. Writing—review and editing, SL

and ZJ. All authors have read and agreed to the final version of the manuscript.

Funding

This study was supported by the hospital level project fund of Changzhou No. 2 People's Hospital (2020K008). The funder had no role in study design, data collection and analysis, decision to publish, or preparation of the manuscript.

Conflict of interest

The authors declare that the research was conducted in the absence of any commercial or financial relationships that could be construed as a potential conflict of interest.

The reviewer XQ declared a shared affiliation with the authors XL, LL, SL and ZJ to the handling editor at the time of review.

Publisher's note

All claims expressed in this article are solely those of the authors and do not necessarily represent those of their affiliated organizations, or those of the publisher, the editors and the reviewers. Any product that may be evaluated in this article, or claim that may be made by its manufacturer, is not guaranteed or endorsed by the publisher.

References

- Erickson LA. Endometrial adenocarcinoma, endometrioid type. *Mayo Clinic Proc* (2018) 93:963–4. doi: 10.1016/j.mayocp.2018.03.017
- Bray F, Ferlay J, Soerjomataram I, Siegel RL, Torre LA, Jemal A. Global cancer statistics 2018: GLOBOCAN estimates of incidence and mortality worldwide for 36 cancers in 185 countries. *CA: A Cancer J Clin* (2018) 68:394–424. doi: 10.3322/caac.21492
- Backes FJ, Walker CJ, Goodfellow PJ, Hade EM, Agarwal G, Mutch D, et al. Estrogen receptor-alpha as a predictive biomarker in endometrioid endometrial cancer. *Gynecol Oncol* (2016) 141:312–7. doi: 10.1016/j.ygyno.2016.03.006
- Rodriguez AC, Blanchard Z, Maurer KA, Gertz J. Estrogen signaling in endometrial cancer: a key oncogenic pathway with several open questions. *Horm CANC* (2019) 10:51–63. doi: 10.1007/s12672-019-0358-9
- Treeck O, Diepolder E, Skrzypczak M, Schüler-Toprak S, Ortmann O. Knockdown of estrogen receptor β increases proliferation and affects the transcriptome of endometrial adenocarcinoma cells. *BMC Cancer* (2019) 19:745. doi: 10.1186/s12885-019-5928-2
- Malik B, Feng F. Long noncoding RNAs in prostate cancer: overview and clinical implications. *Asian J Androl* (2016) 18:568. doi: 10.4103/1008-682X.177123
- Mai H, Wei Y, Yin Y, Huang S, Lin H, Liao Y, et al. LINC01541 overexpression attenuates the 17 β -estradiol-induced migration and invasion capabilities of endometrial stromal cells. *Syst Biol Reprod Med* (2019) 65:214–22. doi: 10.1080/19396368.2018.1549290
- Callegari E, Gramantieri L, Domenicali M, D'Abundo L, Sabbioni S, Negrini M. MicroRNAs in liver cancer: a model for investigating pathogenesis and novel therapeutic approaches. *Cell Death Differ* (2015) 22:46–57. doi: 10.1038/cdd.2014.136
- Humphries B, Yang C. The microRNA-200 family: small molecules with novel roles in cancer development, progression and therapy. *Oncotarget* (2015) 6:6472–98. doi: 10.18632/oncotarget.3052
- Gu Y, Zhou Z. Berberine inhibits the proliferation, invasion and migration of endometrial stromal cells by downregulating miR-429. *Mol Med Rep* (2021) 23:416. doi: 10.3892/mmr.2021.12055
- Wang Y, Wang L, Chen C, Chu X. New insights into the regulatory role of microRNA in tumor angiogenesis and clinical implications. *Mol Cancer* (2018) 17:22. doi: 10.1186/s12943-018-0766-4
- Zhang X, Tang J, Zhi X, Xie K, Wang W, Li Z, et al. miR-874 functions as a tumor suppressor by inhibiting angiogenesis through STAT3/VEGF-a pathway in gastric cancer. *Oncotarget* (2015) 6:1605–17. doi: 10.18632/oncotarget.2748
- Shetty A, Suresh PS. A synergy of estradiol with leptin modulates the long non-coding RNA NEAT1/ mmu-miR-204-5p/IGF1 axis in the uterus of high-fat-diet-induced obese ovariectomized mice. *J Steroid Biochem Mol Biol* (2021) 209:105843. doi: 10.1016/j.jsbmb.2021.105843
- Liu H, Wang Y-B. Systematic large-scale meta-analysis identifies miRNA-429/200a/b and miRNA-141/200c clusters as biomarkers for necrotizing enterocolitis in newborn. *Bioscience Rep* (2019) 39:BSR20191503. doi: 10.1042/BSR20191503
- Ge L, Wang Y, Cao Y, Li G, Sun R, Teng P, et al. MiR-429 improved the hypoxia tolerance of human amniotic cells by targeting HIF-1 α . *Biotechnol Lett* (2018) 40:1477–86. doi: 10.1007/s10529-018-2604-6
- Hevir-Kene N, Rizner TL. The endometrial cancer cell lines ishikawa and HEC-1A, and the control cell line HIEEC, differ in expression of estrogen biosynthetic and metabolic genes, and in androstenedione and estrone-sulfate

metabolism. *Chemico-Biological Interact* (2015) 234:309–19. doi: 10.1016/j.cbi.2014.11.015

17. Way DL, Grosso DS, Davis JR, Surwit EA, Christian CD. Characterization of a new human endometrial carcinoma (RL95-2) established in tissue culture. *In Vitro* (1983) 19:147–58. doi: 10.1007/BF02618053

18. Senol S, Sayar I, Ceyran AB, Ibiloglu I, Akalin I, Firat U, et al. Stromal clues in endometrial carcinoma: Loss of expression of β -catenin, epithelial-mesenchymal transition regulators, and estrogen-progesterone receptor. *Int J Gynecol Pathol* (2016) 35:238–48. doi: 10.1097/PGP.0000000000000233

19. Kasoha M, Dernektzi C, Seibold A, Bohle RM, Takacs Z, Ioan-Iulian I, et al. Crosstalk of estrogen receptors and wnt/ β -catenin signaling in endometrial cancer. *J Cancer Res Clin Oncol* (2020) 146:315–27. doi: 10.1007/s00432-019-03114-8

20. Gibson DA, Simitsidellis I, Collins F, Saunders PTK. Androgens, oestrogens and endometrium: a fine balance between perfection and pathology. *J Endocrinol* (2020) 246:R75–93. doi: 10.1530/JOE-20-0106

21. Hu G, Zhang J, Zhou X, Liu J, Wang Q, Zhang B. Roles of estrogen receptor α and β in the regulation of proliferation in endometrial carcinoma. *Pathol - Res Pract* (2020) 216:153149. doi: 10.1016/j.prp.2020.153149

22. Yu K, Huang Z-Y, Xu X-L, Li J, Fu X-W, Deng S-L. Estrogen receptor function: Impact on the human endometrium. *Front Endocrinol* (2022) 13:827724. doi: 10.3389/fendo.2022.827724

23. Inda MA, Blok EJ, Kuppen PJK, Charehbili A, den Biesen-Timmermans EC, van Brussel A, et al. Estrogen receptor pathway activity score to predict clinical response or resistance to neoadjuvant endocrine therapy in primary breast cancer. *Mol Cancer Ther* (2020) 19:680–9. doi: 10.1158/1535-7163.MCT-19-0318

24. van Weelden WJ, van der Putten LJM, Inda MA, van Brussel A, Snijders MPLM, Schriever LMM, et al. Oestrogen receptor pathway activity is associated with outcome in endometrial cancer. *Br J Cancer* (2020) 123:785–92. doi: 10.1038/s41416-020-0925-4

25. Sieuwerts A M, Inda M A, Smid M, van Ooijen H, van de Stolpe A, Martens JWM, et al. ER and PI3K pathway activity in primary ER positive breast cancer is associated with progression-free survival of metastatic patients under first-line tamoxifen. *Cancers* (2020) 12:802. doi: 10.3390/cancers12040802

26. Gao M, Li C, Xu M, Liu Y, Cong M, Liu S. LncRNA MT1DP aggravates cadmium-induced oxidative stress by repressing the function of Nrf2 and is dependent on interaction with miR-365. *Adv Sci* (2018) 5:1800087. doi: 10.1002/advs.201800087

27. Wang Y, Yang T, Han Y, Ren Z, Zou J, Liu J, et al. LncRNA OTUD6B-AS1 exacerbates as O_3 -induced oxidative damage in bladder cancer via miR-6734-5p-Mediated functional inhibition of IDH2. *Oxid Med Cell Longevity* (2020) 2020:1–22. doi: 10.1155/2020/3035624

28. Donkers H, Hirschfeld M, Weiß D, Erbes T, Jaeger M, Pijnenborg JMA, et al. Usefulness of microRNA detection in the diagnostics of endometrial cancer. *Acta Obstet Gynecol Scand* (2021) 100:1148–54. doi: 10.1111/aogs.14141

29. Guo CM, Liu SQ, Sun MZ. miR-429 as biomarker for diagnosis, treatment and prognosis of cancers and its potential action mechanisms: A systematic literature review. *neo* (2020) 67:215–28. doi: 10.4149/neo_2019_190401N282

30. Donkers H, Bekkers R, Galaal K. Diagnostic value of microRNA panel in endometrial cancer: A systematic review. *Oncotarget* (2020) 11:2010–23. doi: 10.18632/oncotarget.27601

31. Cui Z, An X, Li J, Liu Q, Liu W. LncRNA MIR22HG negatively regulates miR-141-3p to enhance DAPK1 expression and inhibits endometrial carcinoma cells proliferation. *Biomedicine Pharmacotherapy* (2018) 104:223–8. doi: 10.1016/j.biopha.2018.05.046

32. Liu N, Zhou KI, Parisien M, Dai Q, Diatchenko L, Pan T. N 6-methyladenosine alters RNA structure to regulate binding of a low-complexity protein. *Nucleic Acids Res* (2017) 45:6051–63. doi: 10.1093/nar/gkx141

33. Yang Y, Fan X, Mao M, Song X, Wu P, Zhang Y, et al. Extensive translation of circular RNAs driven by N6-methyladenosine. *Cell Res* (2017) 27:626–41. doi: 10.1038/cr.2017.31

34. Li Y, Xiao J, Bai J, Tian Y, Qu Y, Chen X, et al. Molecular characterization and clinical relevance of m6A regulators across 33 cancer types. *Mol Cancer* (2019) 18:137. doi: 10.1186/s12943-019-1066-3

35. Yang D, Qiao J, Wang G, Lan Y, Li G, Guo X, et al. N 6-methyladenosine modification of lincRNA 1281 is critically required for mESC differentiation potential. *Nucleic Acids Res* (2018) 46:3906–20. doi: 10.1093/nar/gky130

36. Li T, Wang T, Jing J, Sun L. Expression pattern and clinical value of key m6A RNA modification regulators in abdominal aortic aneurysm. *JIR* (2021) 14:4245–58. doi: 10.2147/JIR.S327152

37. Lin G, Wang H, Wu Y, Wang K, Li G. Hub long noncoding RNAs with m6A modification for signatures and prognostic values in kidney renal clear cell carcinoma. *Front Mol Biosci* (2021) 8:682471. doi: 10.3389/fmolb.2021.682471

38. Chen D, Li Y, Li Y, Jin L, Su Z, Yu Z, et al. Tumor suppressive microRNA-429 regulates cellular function by targeting VEGF in clear cell renal cell carcinoma. *Mol Med Rep* (2016) 13:1361–6. doi: 10.3892/mmr.2015.4653

39. Chan T-C, Hsing C-H, Shiue Y-L, Huang SK, Hsieh K-L, Kuo Y-H, et al. Angiogenesis driven by the CEBPD-hsa-miR-429-VEGFA signaling axis promotes urothelial carcinoma progression. *Cells* (2022) 11:638. doi: 10.3390/cells11040638

40. Ye G, Feng S, Yang Y, Cao Z, Zhang B, Wang F. Establishment and comprehensive analysis of underlying microRNA-mRNA interactive networks in ovarian cancer. *J Oncol* (2022) 2022:1–13. doi: 10.1155/2022/5120342

41. Bartoszewska S, Rochan K, Piotrowski A, Kamysz W, Ochocka RJ, Collawn JF, et al. The hypoxia-inducible miR-429 regulates hypoxia-inducible factor-1 α expression in human endothelial cells through a negative feedback loop. *FASEB J* (2015) 29:1467–79. doi: 10.1096/fj.14-267054

42. Gu C-J, Xie F, Zhang B, Yang H-L, Cheng J, He Y-Y, et al. High glucose promotes epithelial-mesenchymal transition of uterus endometrial cancer cells by increasing ER/GLUT4-mediated VEGF secretion. *Cell Physiol Biochem* (2018) 50:706–20. doi: 10.1159/000494237

43. Zhang J, Song H, Lu Y, Chen H, Jiang S, Li L. Effects of estradiol on VEGF and bFGF by akt in endometrial cancer cells are mediated through the NF- κ B pathway. *Oncol Rep* (2016) 36:705–14. doi: 10.3892/or.2016.4888

44. Iorga A, Umar S, Ruffenach G, Aryan L, Li J, Sharma S, et al. Estrogen rescues heart failure through estrogen receptor beta activation. *Biol Sex Differ* (2018) 9:48. doi: 10.1186/s13293-018-0206-6

45. Wang Y, Duan H, Wang S, Quan Y, Huang J, Guo Z. Upregulated Talin1 synergistically boosts β -estradiol-induced proliferation and pro-angiogenesis of eutopic and ectopic endometrial stromal cells in adenomyosis. *Reprod Biol Endocrinol* (2021) 19:70. doi: 10.1186/s12958-021-00756-7



OPEN ACCESS

EDITED BY

Shaohua Xu,
Tongji University, China

REVIEWED BY

Yingkun Xu,
Chongqing Medical University, China
Fei Wei,
Nanjing University of Chinese
Medicine, China

*CORRESPONDENCE

Suping Han
hsuper2021@163.com
Xinyuan Zhao
zhaoxinyuan@ntu.edu.cn
Jinxiu Wang
jinxiuwang2022@163.com

[†]These authors have contributed
equally to this work

SPECIALTY SECTION

This article was submitted to
Gynecological Oncology,
a section of the journal
Frontiers in Oncology

RECEIVED 16 July 2022

ACCEPTED 08 August 2022

PUBLISHED 29 August 2022

CITATION

Tang H, Shan J, Liu J, Wang X,
Wang F, Han S, Zhao X and Wang J
(2022) Molecular subtypes, clinical
significance, and tumor immune
landscape of angiogenesis-related
genes in ovarian cancer.
Front. Oncol. 12:995929.
doi: 10.3389/fonc.2022.995929

COPYRIGHT

© 2022 Tang, Shan, Liu, Wang, Wang,
Han, Zhao and Wang. This is an open-
access article distributed under the
terms of the [Creative Commons
Attribution License \(CC BY\)](#). The use,
distribution or reproduction in other
forums is permitted, provided the
original author(s) and the copyright
owner(s) are credited and that the
original publication in this journal is
cited, in accordance with accepted
academic practice. No use,
distribution or reproduction is
permitted which does not comply with
these terms.

Molecular subtypes, clinical significance, and tumor immune landscape of angiogenesis-related genes in ovarian cancer

Haixia Tang^{1†}, Jingsong Shan^{2†}, Juan Liu^{3†}, Xuehai Wang⁴,
Fengxu Wang⁴, Suping Han^{5*}, Xinyuan Zhao^{4*}
and Jinxiu Wang^{1*}

¹Department of Gynecology, Nantong Hospital of Traditional Chinese Medicine, Nantong, China,

²Division of Natural and Applied Sciences, Duke Kunshan University, Kunshan, China, ³Department of Obstetrics and Gynecology, Women's Hospital of Nanjing Medical University, Nanjing Maternity and Child Health Care Hospital, Nanjing, China, ⁴Department of Occupational Medicine and Environmental Toxicology, Nantong Key Laboratory of Environmental Toxicology, School of Public Health, Nantong University, Nantong, China, ⁵Department of Gynecology, The First Affiliated Hospital of Nanjing Medical University, Nanjing, China

Angiogenesis is a physiological process, where new blood vessels are formed from pre-existing vessels through the mechanism called sprouting. It plays a significant role in supporting tumor growth and is expected to provide novel therapeutic ideas for treating tumors that are resistant to conventional therapies. We investigated the expression pattern of angiogenesis-related genes (ARGs) in ovarian cancer (OV) from public databases, in which the patients could be classified into two differential ARG clusters. It was observed that patients in ARGcluster B would have a better prognosis but lower immune cell infiltration levels in the tumor microenvironment. Then ARG score was computed based on differentially expressed genes *via* cox analysis, which exhibited a strong correlation to copy number variation, immunophenoscore, tumor mutation load, and chemosensitivity. In addition, according to the median risk score, patients were separated into two risk subgroups, of which the low-risk group had a better prognosis, increased immunogenicity, and stronger immunotherapy efficacy. Furthermore, we constructed a prognostic nomogram and demonstrated its predictive value. These findings help us better understand the role of ARGs in OV and offer new perspectives for clinical prognosis and personalized treatment.

KEYWORDS

angiogenesis, ovarian cancer, tumor microenvironment, prognostic signature, drug sensitivity

Introduction

Ovarian cancer (OV) is the most common gynecological cancer with the highest mortality rate in the world, accounting for 4.4% of female cancer-related mortality in 2018 (1, 2). Annually, 225,500 new incidences of ovarian cancer are diagnosed worldwide, resulting in 140,200 cancer-specific deaths (2, 3). Due to the heterogeneity of OV, the World Health Organization (WHO) classifies it into several morphological categories based on cell type (4). Despite significant differences in molecular biology and prognosis, they are all treated identically with cytoreductive surgery and platinum/taxane combined chemotherapy (5). Most patients respond favorably to first-line treatment, but most patients relapse and develop chemotherapeutic resistance (6–9). Worse more, OV is insidious with few sentinel symptoms and lack of effective diagnostic strategies (10–12). As result, more than two-thirds patients were diagnosed with a bad prognosis in an advanced stage (13, 14). Many studies have shown that early diagnosis and appropriate treatment can significantly reduce the metastasis and recurrence of OV (11, 15).

Late diagnosis and heterogeneous treatment result in poor clinical outcomes of patients with OV (16). Thus, novel methods of diagnosis and treatment are required. Immunotherapy has been a research hotspot and an essential supplementary cancer treatment method in recent years due to the in-depth understanding of immune recognition and immunomodulatory molecules (17). Molecular subtyping analysis of OV with complex heterogeneity has a promising future due to the development of molecular tools. Researchers around the world are attempting to identify novel biomarkers that combine molecular characteristics with traditional clinicopathological parameters to improve risk stratification systems to predict clinical outcomes and response to immunotherapy (18).

Angiogenesis, one of the hallmarks of cancer, is the formation of new blood vessels from pre-existing ones through a process called sprouting (19). Angiogenesis plays a significant role in supporting tumor growth and progression, where numerous angiogenic factors are often overexpressed (20, 21). Suppression of angiogenesis has been recognized as a promising therapeutic strategy, especially for cancers that are resistant to conventional treatment (22). It is believed that anti-angiogenic therapy could correct anatomical and functional abnormalities in tumor blood vessels through the process called “vascular normalization” (23, 24). Moreover, this may help prevent cancer cells from developing aggressive phenotypes related to hypoxic microenvironments (20, 25). These studies suggest that exploring the molecular characteristics of angiogenesis-related genes (ARGs) can help clarify the causes of OV heterogeneity and provide new prognostic and therapeutic approaches.

Wang, G., et al. analyzed the molecular subtypes of ARG in Glioblastoma multiforme and established a prognostic model to predict the treatment response of patients (26). Based on the 48

ARGs provided in their study, we developed a prognosis prediction model in OV, which reveals the significant value in prognosis, tumor microenvironment, and pharmacological sensitivity. Furthermore, we incorporated the ARG score with the clinical characteristics for clinical outcomes prediction and verified its accurate prediction performance. Our research will provide new concepts for accurate diagnosis and personalized treatment of OV patients.

Methods and materials

OV dataset and reprocessing

Gene expression data and relevant clinical information of OV patients are obtained from the public databases The Cancer Genome Atlas (TCGA) and Gene Expression Omnibus (GEO). In this study, two cohorts, GSE9891 and TCGA-OV, were used for subsequent analysis, where cases without complete clinical data will be excluded to minimize statistical bias. The details of the sample are displayed in Table S1. For differential analysis, FPKM (fragments per kilobase) values of the TCGA-OV cohort were converted to transcripts per kilobase million (27). We combined the TCGA-OV and GSE9891 and corrected the batch effects using the “ComBat” algorithm from the “sva” package (28).

Consensus clustering analysis for ARGs

Forty-eight ARGs were derived from the previous study (26). According to these gene expression profiles, “ConsensusClusterPlus” was constructed for consensus clustering (29), where patients were divided into various molecular subgroups on the basis of gene expression pattern. For the major parameters in the “ConsensusClusterPlus” function, we set the max clusters number (maxK)=9, repeated times (reps)=1000, proportion of items to sample (pItem)=0.8, proportion of features to sample (pFeature)=1, cluster algorithm (clusterAlg)=hc/hierarchical, distance= spearman (29). Subsequently, the principal component analysis (PCA) was performed by the “ggplot2” R package.

Identification of Gene subtypes based on DEGs

Firstly, the R package “limma” was used to investigate the differentially expressed genes (DEGs) between distinct clusters with the standard of adjusted p-value < 0.05 (30). Following that, two different gene subtypes were identified with the consistent clustering algorithm. Gene Ontology (GO) and Kyoto Encyclopedia of Genes and Genomes (KEGG) analyses were

performed to further investigate the enriched molecular pathway (31, 32).

Build prognostic risk signature related to angiogenesis

After data reprocessing, OS-related prognostic OV samples were screened out for further analysis. The TCGA-OV cohort served as the training set, while samples from GSE9891 and the set consisting of the TCGA-OV cohort and GSE9891 served as the testing set to validate the performance of the signature. In the training set, correlations between DEGs and OV survival were determined by univariate Cox regression analysis. The R package “glmnet” was then used to perform the least absolute shrinkage and selection operator (LASSO) regression based on *angiogenesis*-related prognostic genes to minimize the risk of overfitting (33). Formula: $risk\ factor = \sum_{i=1}^n coef_i \times exp_i$ was employed to select candidate genes to build prognostic signature based on ARGs using multivariate Cox analysis. The coef and exp respectively refer to the risk coefficient and gene expression level. The patients were classified into high-risk and low-risk groups according to the median risk score. Subsequently, we used the “survminer” software to conduct the Kaplan–Meier analysis of survival. Receiver operating characteristic (ROC) curves were then used to evaluate the model’s precision. The performance of the model precision was then assessed by plotted ROC curves.

Compared the risk score of different clinical features and stratified analysis

The correlations between risk score and various clinicopathological characteristics (grade, stage, age, fustat, and histological type) were evaluated using univariate and multivariate cox regression analysis, where Table S2 provides clinical details. We conducted univariate and multivariate cox analyses to investigate whether the risk score is a factor independent of other available clinicopathological features. Furthermore, stratified analysis was also conducted to examine the performance of the model based on the clinical characteristics described before.

Assessment of immune infiltration level

Cancers relied on their complex tissue environments for sustained growth, invasion, and metastasis. Moreover, drug resistance and tumor recurrence are intimately associated with the tumor microenvironment (TME) as a potential therapeutic target (34, 35). Gene sets of relevant biological processes were

curated from previous research (36, 37). From the gene expression pattern of these related pathways, the ESTIMATE algorithm conducted through the R package “estimate” can predict the status of TME (38, 39). Differences in immune function between different subgroups were then demonstrated by single-sample gene set enrichment analysis (ssGSEA), which allows the quantitative evaluation of immune cell components derived from complex gene expression data (40, 41). Subsequently, the abundance of 22 tumor immune infiltrating cells (TIIC) in risk groups was quantified by CIBERSORT.

Prediction of immunotherapy response

Immunophenoscore (IPS) was utilized to investigate the immunotherapeutic function of immune cell infiltration scores, which has been validated as a predictor of patient immunotherapy response (42). Higher IPS refers to higher immunogenicity. Tumor mutation burden (TMB) represents the number of mutations per megabase of DNA sequence in a given tumor, which can be used to identify patients who will obtain the greatest benefit from immune checkpoint inhibitors (ICIs) (43, 44). The burden of copy number variation (CNV) gain or loss was evaluated by gene pattern (45).

Drug sensitivity analysis

The half-maximum inhibitory concentration (IC50) was employed to assess the efficacy of chemotherapeutic drugs in OV patients. The CellMiner database served as the drug sensitivity data source, which was created in response to the list of 60 types of cancer cells (NCI-60) compiled by the National Cancer Institute’s Center for Cancer Research (46).

Construction of a nomograph system

To predict the prognosis of OV based on clinical characteristics and risk score, a nomograph system was constructed to measure the OS of 1-, 3- and 5- years through R package “rms” (47). In the nomogram, each variable is assigned a score, and the total score is obtained by adding the scores of all factors to make an accurate prediction. Next, we conducted the area under the curve (AUC) and c-index to evaluate the prediction capacity of the nomogram (48–50).

Statistical analysis

All statistical analyses were conducted in R version 4.1.0 with $P < 0.05$ defined as significant. The difference between the

subgroups was determined by the student t-tests and variance analysis. Spearman and distance correlation analyses were used to compute the correlation coefficients between the expression of ARGs and immune infiltrating cells.

Results

Genetic mutation landscape of ARGs in OV

The analysis process of this study is shown in Figure S1. Firstly, we investigated the different expression pattern of the 48 ARGs in tumor and normal samples within the TCGA-OV dataset (Figure 1A). The string website was then employed to conduct a protein-protein interaction (PPI) analysis of DEGs (Figure 1B). Subsequently, the incidence of CNVs and somatic mutations of ARGs were analyzed in OV, where 47 mutations

occurred in 436 samples with 10.78% somatic mutation. It is observed that VCAN has the highest mutation frequency (2%), followed by COL3A1, COL5A2, and other genes (Figure 1C). Furthermore, we investigated the CNV mutational incident, which had significantly increased in genes like PTK2, S100A4, and APOH but decreased in genes like VCAN, PDGFA, and PGLYRP1 (Figure 1D). Figure 1E displays 48 ARGs' chromosomal locations of the CNV alterations. Among the 48 genes, 27 ARGs presenting significant prognostic values were identified (Figure S2). The above results suggest the potential regulatory role of CNV in ARGs expression, which plays an important role in the development of OV.

Identify ARGclusters in OV

In the angiogenesis network, the ARGs interactions, regulator relationships, and their prognostic significance in

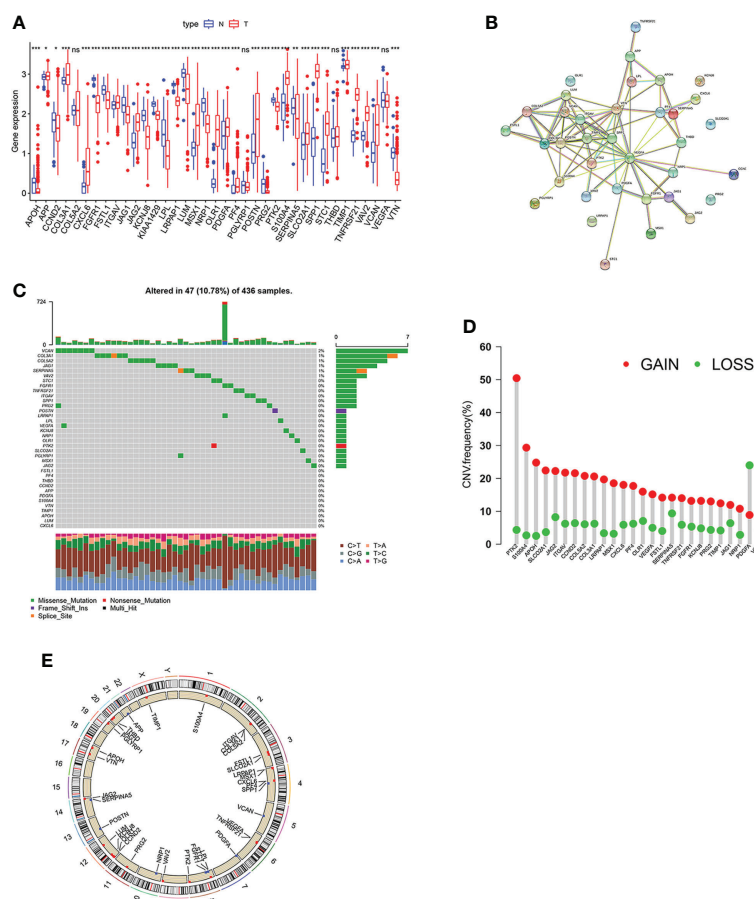


FIGURE 1

Genetic mutation landscape of ARGs in OV. (A) Expression pattern of ARGs in OV and normal tissues. (B) The interactivity of DEGs is revealed by PPI analysis. (C) genetic alternation of ARGs where mutations occurred in 47 of 436 OV patients. (D) CNV gain, loss, and non-CNV frequency in ARGs. (E) The chromosomal distributions of CNV alterations in ARGs. Adjusted p-values were shown as ns, not significant; * $p < 0.05$; ** $p < 0.01$; *** $p < 0.001$.

OV patients were illustrated (Figure 2A). To further analyze the expression features of ARGs in OV, we conducted the consensus clustering analysis, where the patients were classified from $k = 2$ to $k = 9$ (Figure S3). The results revealed that $k=2$ was the optimal clustering variable (Figure 2B). Moreover, PCA analysis also verified the discrepancies between these two ARGclusters (Figure 2C). Between the two ARGclusters, there were 181 differently expressed genes (Figure 2D). Furthermore, a substantial OS time disparity was detected between the two ARGclusters, where patients in ARGcluster B have a higher survival probability ($p=0.003$, Figure 2E). Then we examined the ARGs expression levels and clinicopathological characteristics between the ARGclusters and identified the distinctions (Figure 2F).

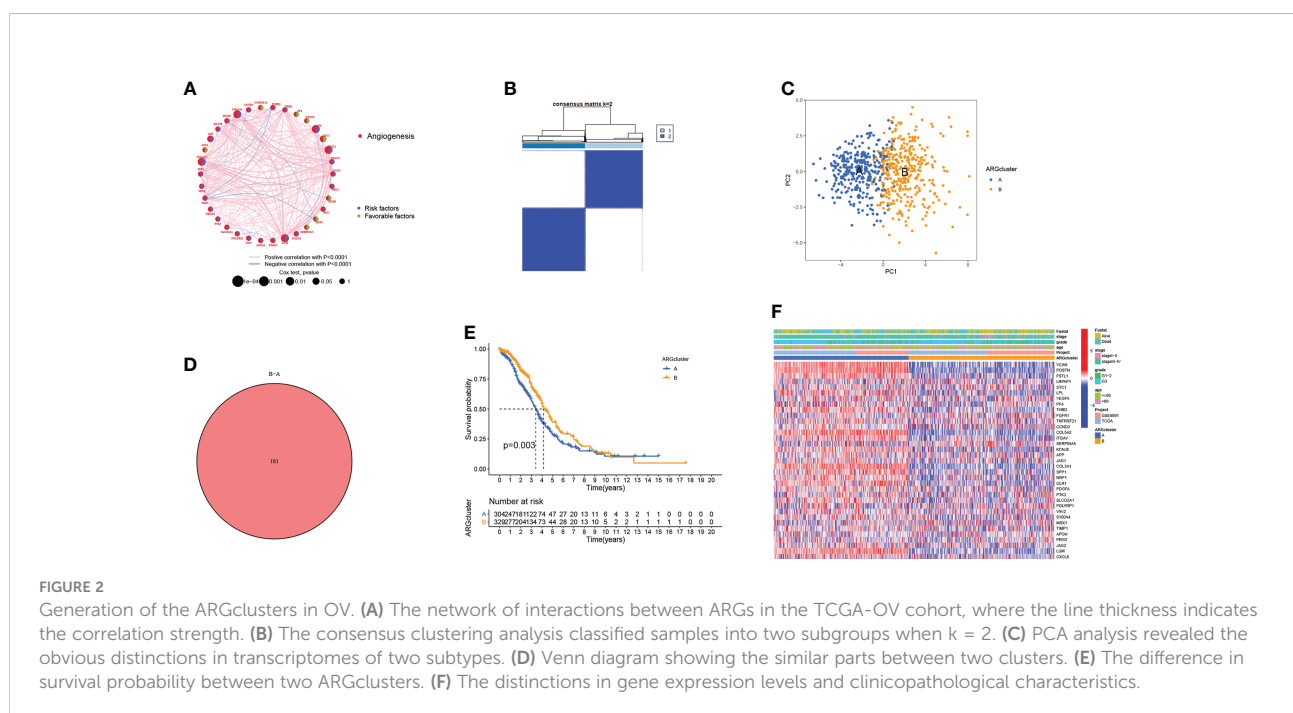
Characteristics of TME in different subtypes

According to the gene set variation analysis between these two ARGclusters, it was observed that cluster A was enriched in cancer-related pathways (like Glioma, Renal cell carcinoma, and Melanoma) and metastasis-related pathways (like focal adhesion, cell adhesion molecule, and ECM receptor interaction) (Figure 3A). Then ssGSEA was employed to explore the immune infiltration levels in these two ARGclusters, where significant enrichment difference was noticed. The enrichment levels of innate and adaptive immune cells were all significantly higher in ARGcluster A (Figure 3B). Subsequently, the correlation between

two ARGclusters and 22 TIICs was determined using CIBERSORT (Figure 3C). We noted that the expression levels of immune checkpoints, PD1, PD-L1, PD-L2, and CTLA4, were all higher in ARGcluster A (Figures 3D–G). Moreover, it was observed that ARGcluster A has higher TME scores (Figures 3H–J). ARGcluster A is usually identified as “hot” tumors characterized by strong immune infiltration levels that will benefit more from the immunotherapy, while ARGcluster B can be characterized as a “cold” tumor with low intensity of immune infiltration and relatively unsuitable for immunotherapy. Furthermore, we explore the correlation between known biological processes and these two ARGclusters, where some immune-related processes like CD8 T effector, antigen processing machinery, and Pan-F-TBRS were prominent in ARGcluster A (Figure 3K). Additionally, ARGclusters A also had markedly higher expression levels of human leukocyte antigen (HLA) related genes (Figure 3L).

Identification of gene subtype based on DEGs

The “limma” package was employed to conduct functional enrichment analysis and screen out the DEGs between two ARGclusters. GO and KEGG analysis revealed that DEGs between two ARGclusters were primarily enriched in immune-related pathways, indicating their importance in the immunological regulation of TME. (Figures 4A, B). Subsequently, univariate COX analysis and consensus clustering analysis were employed to categorize the samples into different



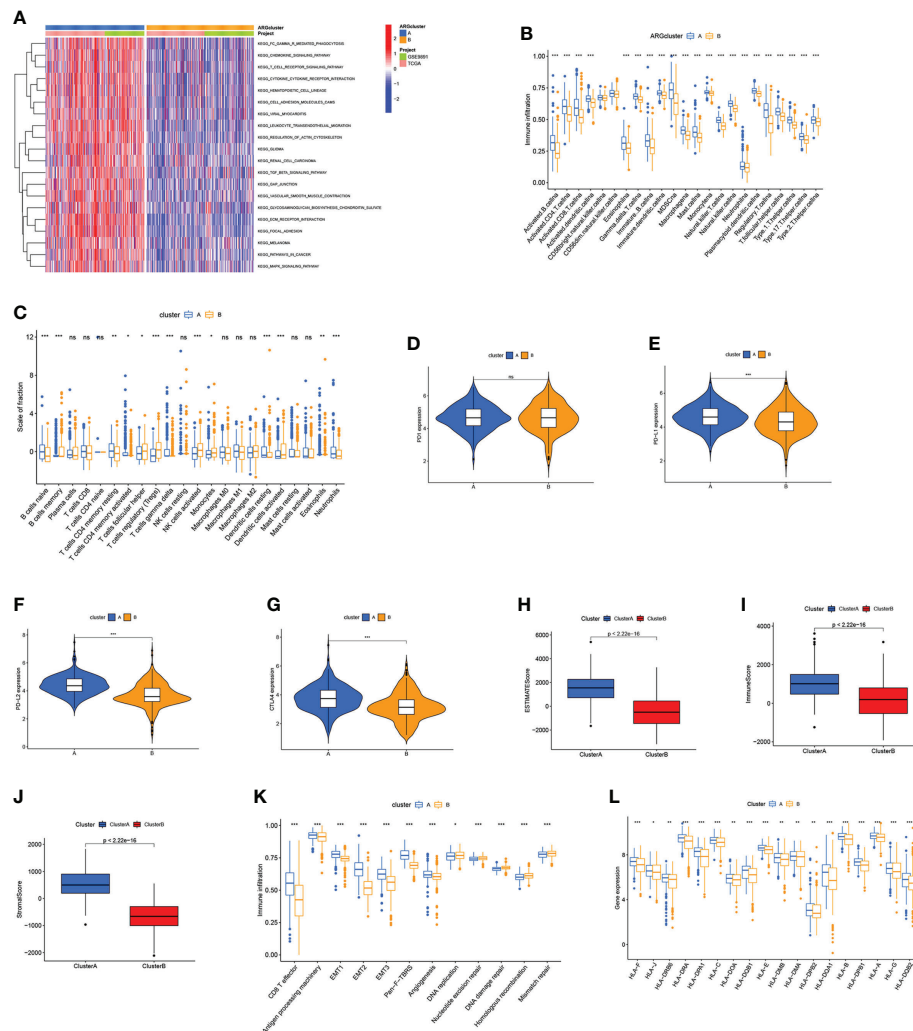


FIGURE 3

Correlations between TME and ARGclusters. (A) GSVA of biological pathways between ARGclusters, where red indicates activation while blue indicates inhibition. (B) The abundance of infiltrating immune cells in two ARGclusters. (C) 22 TIICs were evaluated by the CIBERSORT algorithm in two ARGclusters. (D–G) The expression level of immune checkpoints in two ARGclusters. (H–J) Comparison of TME scores in two ARGclusters. (K) Correlations between known relevant biological processes and two ARGclusters. (L) HLA expression levels in two ARGclusters. Adjusted p-values were shown as ns, not significant; * $p < 0.05$; ** $p < 0.01$; *** $p < 0.001$.

clusters based on the DEGs in OV patients. The results indicated that the clustering effect was the best when $k=2$ (Figure S4). Kaplan-Meier curve demonstrated that patients in gene cluster B had a higher survival probability ($P = 0.002$; Figure 4C). Patients in ARGcluster B are basically patients of gene cluster B, which was associated with better survival status, and early-stage (Figure 4D). The immune infiltration levels in these two gene clusters were investigated by ssGSEA, where gene cluster A has a higher enrichment level of immune cells (Figure 4E). Additionally, the results of CIBERSORT algorithm revealed that gene cluster A was primarily infiltrated by adaptive immune cells like B cells naive and macrophages M1 (Figure 4F). Moreover, the expression of immune checkpoints and TME scores were all higher in gene

cluster A (Figures 4G–M). Gene cluster A also has higher expression levels of HLA related genes and classical biological pathways like CD8 T effector, EMT and Pan-F-TBRs were more prevalent (Figures 4N, O). The above immune signatures indicate that gene cluster A can be defined as a “hot” tumor.

Establish and validate the prognostic model based on ARG score

To estimate the prognosis of individual OV patients, we developed an ARG scoring system based on these DEGs. Figure 5A shows the distributions of the patient in two

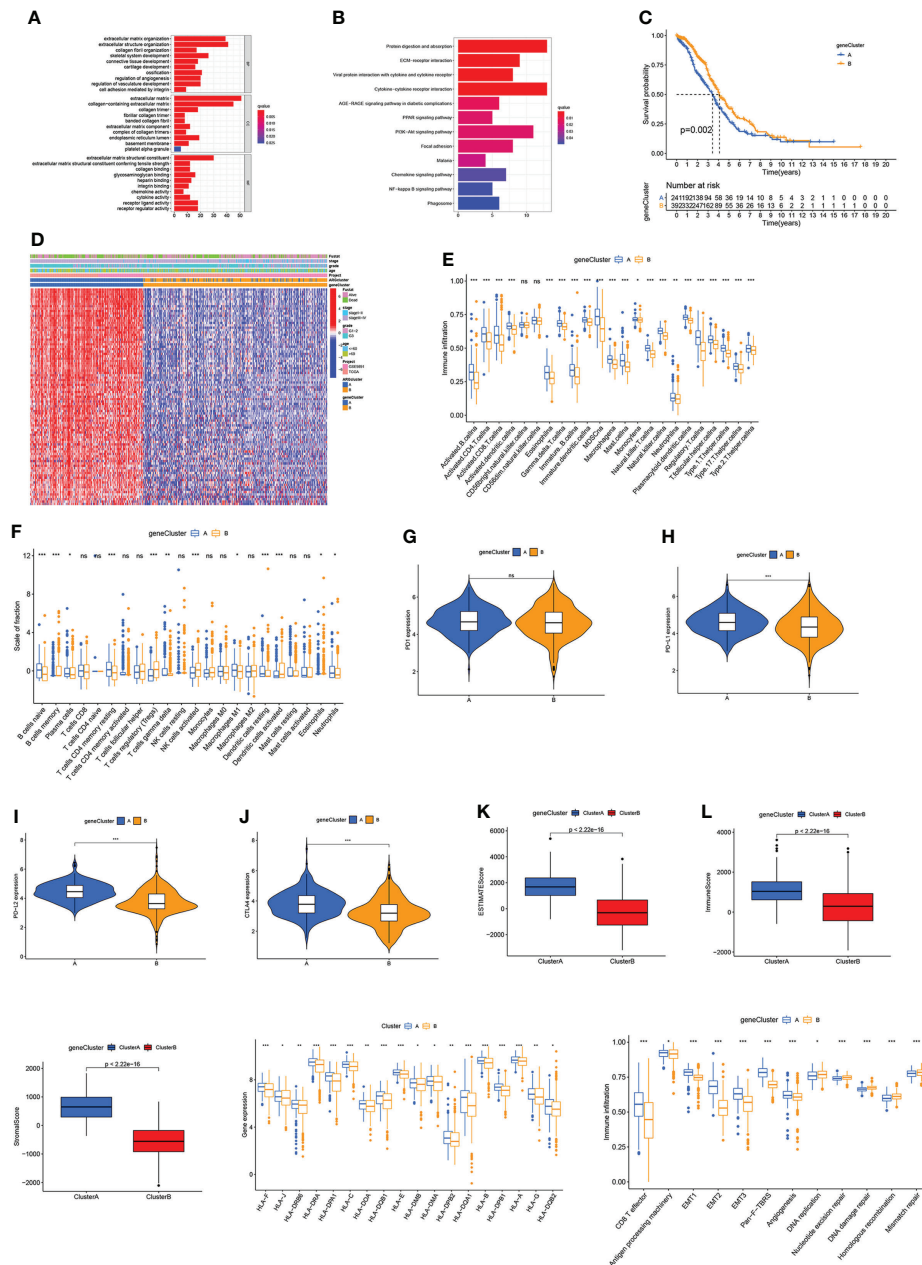


FIGURE 4

Identification of gene subtype based on DEGs. (A, B) GO and KEGG enrichment analysis. (C) Kaplan-Meier curve for OS of OV patients. (D) Correlation between two gene clusters and clinicopathologic features. (E, F) Immune infiltration levels in two gene clusters. (G–J) Immune checkpoints expression levels in two gene clusters. (K–M) HLA expression levels. (N) The scores of immune infiltrations. Adjusted p-values were shown as ns, not significant; *p<0.05; **p<0.01; ***p<0.001.

ARGclusters, two gene clusters, and two risk score groups. To establish the optimal predictive model, LASSO and multivariate cox analysis were performed on the DEGs of 317 samples from the training set (Figure S5). We finally screened out four genes (TENM3, GFRA1, HOXA3, and CXCL13) associated with the OV survival were screened out based on the minimum partial likelihood deviation and multivariate cox regression analysis.

The ARG score can be calculated as following: Risk score = (0.127* expression of TENM3) + (0.1368* expression of GFRA1) + (0.1358* expression of HOXA3) + (-0.1879* expression of CXCL13). It is observed that the risk score of gene cluster B and ARGcluster B was significantly lower (Figures 5B, C). The patients were divided into a high-risk group and a low-risk group based on the median risk score

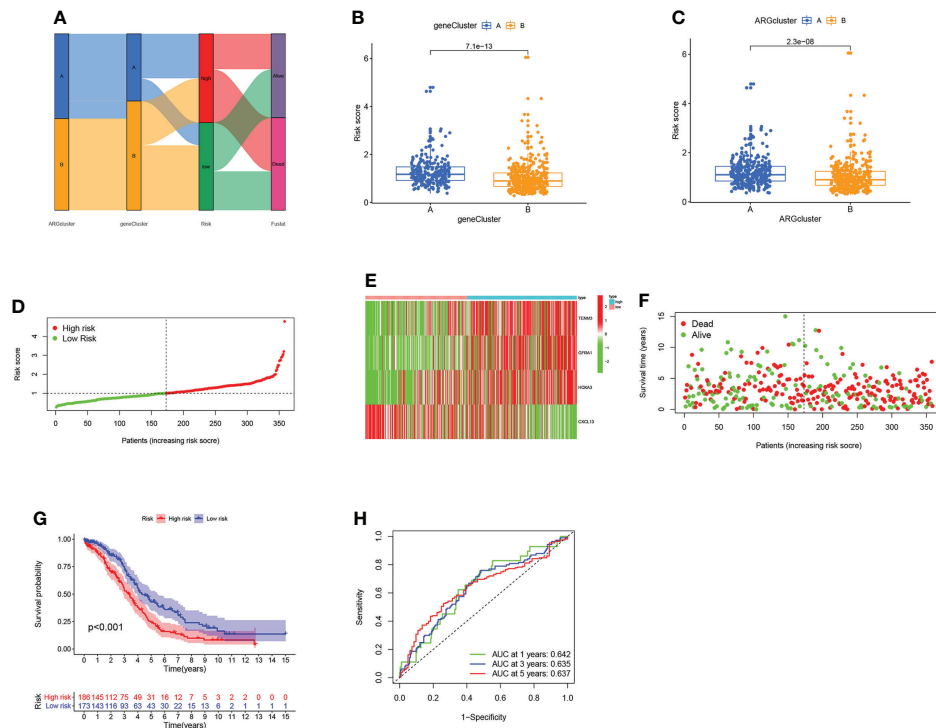


FIGURE 5

Construction of the ARG score in the training set. (A) The dispersion of patients. (B) Difference of the risk score in two gene clusters. (C) Difference of the risk score in two ARGclusters. (D) Distribution of risk scores in two groups. (E) Expression pattern of four ARGs in two groups. (F) The fustat of patients. (G) The comparison of the OS between two groups. (H) The sensitivity and specificity of 1-, 3- and 5-year survival rates were predicted based on ARG scores.

(Figure 5D). Moreover, the expression patterns of four genes in the two groups were shown in the heatmap, and the fustat of patients was shown in the scatter plot (Figures 5E, F). Patients with low-risk scores had better OS performance than those with higher scores ($P < 0.001$; Figure 5G). The AUC values of ROC curves for 1-, 3-, and 5-year survival rates were 0.642, 0.635, and 0.637, respectively (Figure 5H). Then the above results were validated by using the GEO cohort and data set comprised of the GEO cohort and TCGA cohort as the testing set (Figure S6).

Compared the risk score of different clinical characteristics and stratified analysis

The risk scores of individuals with various clinicopathological characteristics were examined to determine their association. It was observed that a higher risk score corresponds to worse fustat status and advanced stage (Figures S7A–D). Subsequently, Cox regression analysis of risk score and clinical characteristics (age, grade, and stage) illustrated that risk score was an independent prognostic factor for OV patients (Table S2). Following that, we conducted the subgroup analysis to validate the prediction

capacity of the signature. As depicted in Figures S7E–J, except for the patients with stage I–II, the survival outcomes of the high-risk score group were worse than that of the low-risk group, regardless of their clinical features.

Estimation of TME based on ARGs

To further investigate the TME status in different subgroups, we utilized GSEA and found that the high-risk group was enriched in some cancer-related pathway and metastasis-related pathway, while the low-risk group was enriched in the pathways related to the immune disease (Figures 6A, B). Following that, ssGSEA revealed that the low-risk group has high immune infiltration levels (Figure 6C). To further investigate the characteristic of these subtypes, we divided 220 TCGA patients into various immune subgroups. C2 is the most prevalent subtype and has the lowest risk score, while C1 has the highest risk score (Figures 6D, E). It was observed that the risk score has negative correlation with estimated scores, immune scores, and stromal scores (Figures 6F–H). After comparing the TME scores of these two groups, we found that the low-risk group has higher estimated scores but lower immune score (Figure 6I). Subsequently, we further investigate the

correlation between DRGs and immune cell abundance. A significant difference in the abundance of innate and adaptive immune cells was observed between the two risk groups (Figures 7A–C). Furthermore, just as Figure 7D illustrates, the ARG score was positively correlated with T cells CD4 memory resting, B cells naive, macrophages M2, mast cells activated, and neutrophils, but the opposite relationship was observed with T cells CD4 memory activated, T cells CD8, T cells gamma delta, T cells follicular helper, macrophages M1 and plasma cells. Then we explored the relationship between the selected ARGs in the prognostic signature and immune cells abundance, where the results indicate that many immune cells like T cells regulatory, T cells gamma delta, and T cells CD4 memory resting were strongly correlated with these genes, especially for the gene CXCL13 and GFRA1 (Figure 7E). Further research indicates that the low-risk group has higher HLA related genes expression levels and higher immune checkpoint expression levels (Figures 7F, G). The six genes selected like CTLA4, HAVCR2, and CD274 were all negatively correlated with the risk score (Figure 7H). Moreover, IPS scores of patients were higher in low-risk groups, which indicates that they have higher immunogenicity (Figures 7I–L). Based on the above findings, it can be inferred that the low-risk group can be characterized as the “hot” tumor mentioned before.

Relationships between ARG score and TMB

Numerous studies have demonstrated that tumor mutation burden (TMB) can be used to predict tumor immune response, thereby identifying patients who may benefit from ICIs (43, 44). Our results revealed that there were no difference between risk and TMB (Figures S8A, B). Subsequently, to further investigate the impact of TMB on OV patients, we analyzed the survival probability in different TMB subgroups. The patients in the L-TMB group present a low survival probability compared with the H-TMB group (Figure S8C). Furthermore, we integrated the TMB and risk score for survival probability analysis, where the group with high TMB and low risk has the highest survival probability, while the group with low TMB and high risk was the lowest (Figure S8D). Next, we assessed the distribution of somatic mutations between two risk score subgroups in the TCGA-OV cohort. The mutation incidence of these two subgroups presented some similarity, where genes like TP53, TTN, MUC16, and CSMD6 all presented high alternations, especially for TP53 and TTN. However, except for the gene TTN, all these major mutated genes showed a higher alternation in the low-risk group (Figures S8E, F)

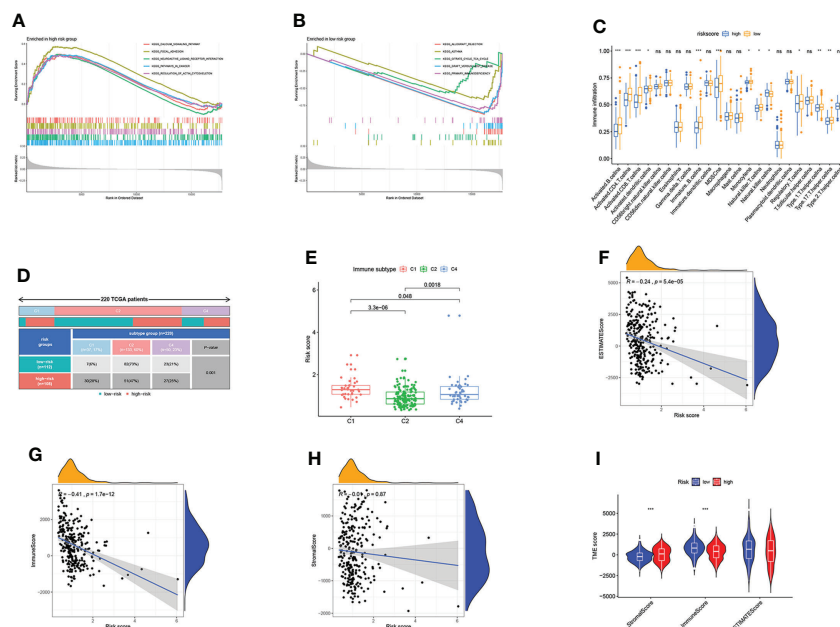


FIGURE 6

Estimation of TME based on ARGs. (A) GSEA of high-risk score group. (B) GSEA of low-risk score group. (C) The difference in immune infiltration levels. (D) 220 TCGA patients were divided into three immune subgroups. (E) Risk scores of three immune subgroups. (F–H) Correlations between risk scores and estimated scores, immune cells, and stromal cells. (I) Comparison of TME scores in two ARG score groups. Adjusted p-values were shown as ns, not significant; * $p < 0.05$; ** $p < 0.01$; *** $p < 0.001$.

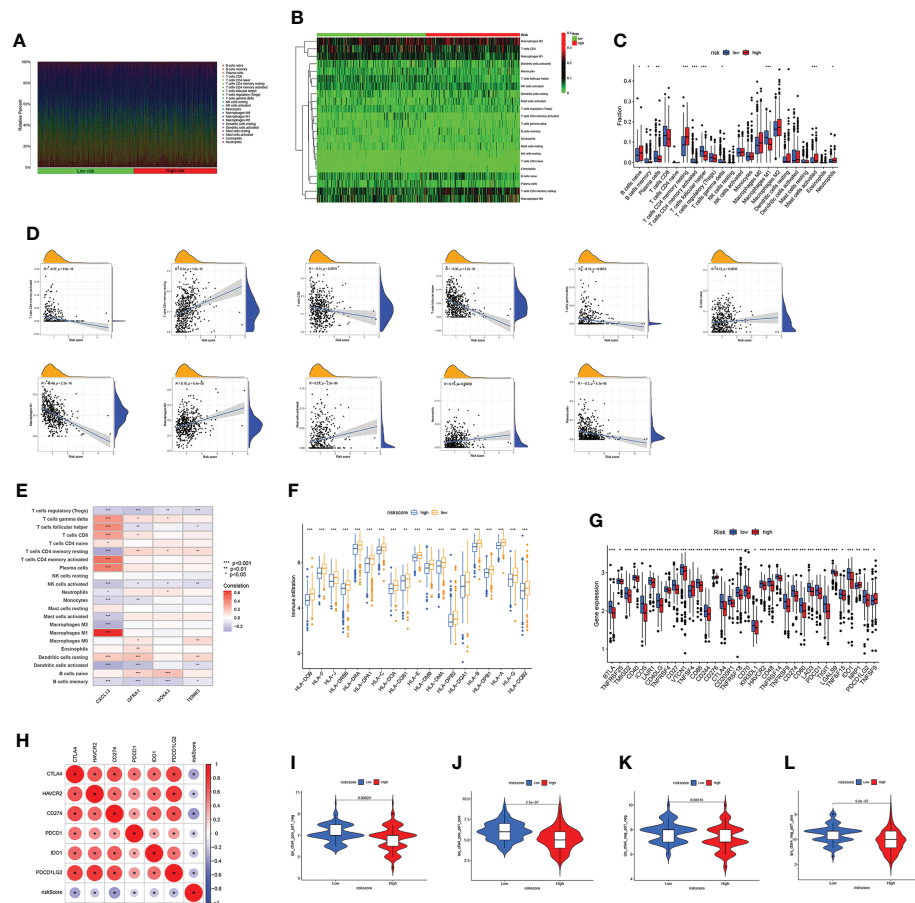


FIGURE 7

*Immune infiltration characteristics of the two subgroups. (A–C) Differences in immune cell abundance. (D) Correlations between risk scores and immune cell abundance. (E) Correlations between selected genes in prognostic model and immune cell abundance. (F) The expression level of HLA in two risk groups. (G) Differential expression of thirty-four immune checkpoints in the two subgroups. (H) Correlations between selected immune checkpoints and risk score. (I–L) The m6Ascore of ips_ctla4_neg_pd1_neg, ips_ctla4_neg_pd1_pos, ips_ctla4_pos_pd1_neg and ips_ctla4_pos_pd1_pos in two subgroups. Adjusted p-values were shown as * $p < 0.05$; ** $p < 0.01$; *** $p < 0.001$.*

Analysis of drug sensitivity

To further examine the efficacy of the ARG score as a marker predicting the therapeutic response of the patients, we calculated the sensitivity of different subgroups of patients to five chemotherapeutic agents commonly used in OV. As depicted in Figure S9A, IC50 values of three chemotherapeutic drugs chosen (gemcitabine, paclitaxel, and vinblastine) were lower in patients of the low-risk group, while the other two (bleomycin and docetaxel) were lower in patients of the high-risk group. Following that, we calculated the correlation between ARGs and different drugs, and the results further verified the associations between the ARGs and drug sensitivity (Figure S9B).

Develop nomograms for survival predicting

Given the important role of the risk score in the prognostic model, we incorporated it with clinical characteristics like age and stage to construct a nomogram, aiming to estimate the clinical outcomes for 1-, 3- and 5- years (Figure 8A). The C-index of the nomogram developed was higher than other models that only consider one clinical feature (Figure 8B). Subsequently, we estimated the AUC values of these models for predicting the clinical outcomes at 1-, 3- and 5- years, where the nomogram has the highest AUC values as we expected, indicating that the nomogram combined ARG risk score, age and stage has a better

prediction performance (Figures 8C–E). The subsequent calibration diagram further validated the accurate prediction performance by comparing it with the actual OS observed (Figure 8F).

ARG model as a new predictor of OV

To further demonstrate the predictive capacity of our model, we examined and compared three previously established OV prognostic models with our own (51–53). To make them comparable, multivariate analysis was employed to calculate the risk value of each dataset with these three published models. The analysis of survival probability revealed that the prognosis of the low-risk patients was much better in all of these three models (Figures S10A–C). However, the ROC curves indicate that the AUC value of our model was higher than these three models (Figures S10D–F). Then the C index was calculated utilizing the restricted mean survival (RMS) package,

where we observed that the C index of our model was 0.621, higher than previously established models (Figure S10G). The above results make us convinced that our model has better prediction performance.

Discussion

OV is a prevalent gynecological malignancy worldwide with the highest mortality (54). Every year, more than 240,000 women are diagnosed with OV, responsible for 150,000 deaths (55). The vast majority of ovarian cancer fatalities are attributable to the chemoresistant and widely metastatic disease in the late stage (56). Worse more, while the majority of patients will respond to first-line chemotherapy, disease recurrence rates remain high and the 5-year survival rate is extremely low (57–59). There is an urgent need for the development of novel therapeutic methods that take advantage

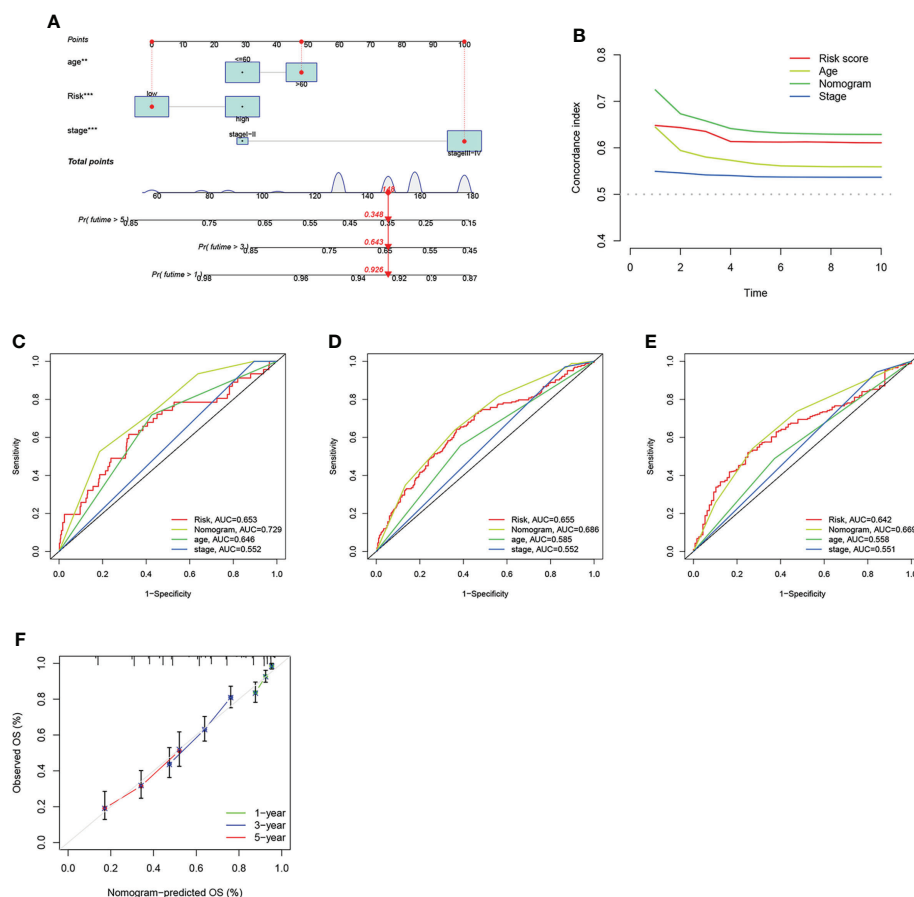


FIGURE 8

Construction and validation of the nomogram. (A) Nomogram constructed for predicting the clinical outcomes at 1-, 3, and 5- years for OV patients. (B) The consistency index of prognosis factors. (C–E) The ROC curves of the nomograms for 1-, 3-, 5- years OS in OV patients. (F) Nomogram calibration curve of 1-, 3-, and 5- years.

of the diverse genetics and unique tumor microenvironment of a patient's cancer. Angiogenesis is a natural and complicated process controlled by various biomolecules produced in the body. Effective suppression of tumor angiogenesis can help halt tumor progression, especially when combined with chemotherapy (60). Moreover, Numerous studies have demonstrated the inextricable link between intrinsic immunity and angiogenesis, and angiogenesis inhibiting may play a crucial role in boosting tumor immunotherapy (61, 62).

Therefore, it is of great significance to explore the role of angiogenesis in tumors, and many studies have established prognostic models to assess prognosis and immune microenvironment in OV (63, 64). The results of our study demonstrated the function of ARGs in (OV), where we screened two distinct molecular subgroups based on 48 ARGs and found that patients in ARGcluster B had superior survival and clinicopathological features. Subsequently, we investigate the feature of TME among these two subgroups, where ARGcluster A has a higher infiltration level of immune cells and is predicted to benefit more from immunotherapy. In addition, ARGs are predominately enriched in immune-related pathways, illustrating their substantial effect on the immunological regulation of TME. Subsequently, two gene clusters were identified based on DEGs, where the results demonstrated the potential of ARGs serving as predictors for the clinical outcomes and immunotherapeutic response of patients. Interestingly, patients in gene cluster A have higher immune infiltration levels, TME scores, and ARG expression levels but worse survival status. Gene cluster A can be identified as a "hot" tumor based on these markers, which corresponds to prior results of ARGclusters, as gene cluster A is an identical subset of the ARGcluster A.

Based on DEGs, we constructed an ARG-based prognostic model for individual OV patients. This model consists of TENM3, GFRA1, HOXA3, and CXCL13. A gene-based query at the Human Protein Atlas revealed the correlation between poor survival and high TENM3 expression in the majority of the examined malignancies, including ovarian, endometrial, and glioma cancer (65). In addition, immunotherapy has been developed in response to the identification of TENM3 as one of the neoantigens expressed in recurrent OV patients (66). GFRA1 plays a crucial role in the formation and maintenance of the nervous system, whose abnormal expression level is frequently observed in numerous cancer cells (67). Mounting evidence revealed the involvement of GFRA1 in the development and progression of tumors (68–70). HOXA3 is a member of the HOX transcription factor family, which regulates gene expression in embryonic development and performs crucial physiological functions. The expression of HOXA3 is associated with the immune system and cancer development, where it has been used as the diagnostic biomarker in various cancer (71–74). As for CXCL13, it has functions in inflammatory, infectious, and immune responses. CXCL13 is involved in the control of cancer

cell phenotypes and play an important role in the progression and metastasis of solid tumor (75). Furthermore, a recent study revealed its function in maintaining the antitumor environment and supported clinical investigation on the combination of CXCL13 and PD-1 blockade therapy for high-grade serous ovarian cancer (76). Accordingly, the ARG score model comprised of these four genes has the potential to predict the clinical outcomes and immunotherapy response of OV patients.

TME refers to the ecosystem around the tumor in the body, which has been considered the crucial determinant in the incident and progression of OV (77, 78). Moreover, previous studies have highlighted TME reactive therapy as a promising strategy for developing accurate cancer-targeted therapies (79, 80). Therefore, we further investigate the TME status in two ARG score subgroups, where the results revealed that patients in the low-risk score group have a high estimated score, immune cells, and stromal cells. Moreover, the ARG score was negatively correlated with the abundance of some innate and adaptive immune cells like CD8+ T cells, T cells follicular helper, Gamma Delta T cells, and macrophages M1. CD8+ T cells often serve as the backbone of cancer immunotherapy for their prominence as anticancer immune response effectors (81, 82). The presence of T follicular helper cells in solid tumor tissue is indicative of a favorable prognosis, which is indispensable for the potent antibody responses of B cells (83). As the bridge between innate and adaptive immune systems, Gamma Delta T cells are involved in various immune responses during the progression of the tumor. Moreover, Gamma Delta T cells have received extensive attention in cancer immunotherapy for their antitumor cytotoxicity and potent cytokine production (84). Macrophage M1 has a pro-inflammatory effect, whose expression is positively correlated to the prognosis of patients with OV (85). Furthermore, some immune-related processes like CD8 T effector, antigen processing machinery, and Pan-F-TBRS were more prevalent in ARGcluster A and gene cluster A. Subsequently, we further investigate the discrepancies in the characteristics of TME and the abundance of 22 TIIC between subgroups, which illustrates the significance of ARGs in the OV progression.

Currently, the only treatment strategy for OV is cytoreductive surgery and platinum/taxane combined chemotherapy. Fortunately, immunotherapy has made great progress in gynecological malignancies, especially for ICIs (86). Moreover, a recent study demonstrated that combining immunotherapy with chemotherapy can considerably enhance treatment efficacy (87). Further research revealed that the low-risk score group has higher HLA and immune checkpoint expression levels. Besides, the high IPS scores in the low-risk score group indicated higher immunogenicity. As for the six genes selected, CTLA4, HAVCR2 and CD274 had a negative correlation to the risk score. All these three genes have been well studied and proved to be important immunotherapeutic targets (88–91). TMB is regarded as a significant immunotherapy

predictor, where multiple tumor instances demonstrated that the TMB score is positively correlated to the immunotherapy outcome, corresponding to our findings (92). The above results demonstrated that the low ARG score group is more suitable for immunotherapy.

The mutation rate of the two ARG score subgroups presented some similarity, where genes like TP53 (>80%), and TTN (>20%) all presented high alternations. These two genes have been demonstrated to play important roles in tumor progression and immune infiltration of TME in previous research (93–95). Nowadays, chemotherapy resistance remains a major challenge in the treatment of ovarian cancer (96). This study further investigated potentially sensitive agents in patients of different ARG score groups, which may help alleviate drug resistance and improve clinical outcomes. It was observed that the IC50 values of three chemotherapeutic drugs (gemcitabine, paclitaxel, and vinblastine) were lower in the low ARG score group, while the other two (bleomycin and docetaxel) were lower in the high ARG score group. Moreover, significant differences in drug sensitivity were detected between the two risk groups, where specific people identified can be treated with drugs of higher sensitivity.

Finally, we incorporated the ARG scores and clinical features like age and stage into a nomogram to illustrate the function of these factors in OV prognosis and thereby improve the clinical application of the ARG score. In this study, three previously established models were selected and their prediction performance was compared (51–53). Nevertheless, current research has limitations. All conclusions are based on the processing and analysis of public database data, but there is a dearth of clinical data and experimental studies to verify the results. Future research into the clinical applicability of the model will necessitate the collection of additional OV cases and the execution of a substantial number of prospective clinical evaluations.

Conclusion

Our comprehensive analysis of ARGs successfully demonstrated its value in the field of TME, prognosis, and clinical characteristics of OV patients. Our study also highlights the value of ARGs in the prognostic model and their potency as the biomarker of the immunotherapy response. Our findings validate the great clinical significance of ARGs and provide new guidance for further research on personalized therapy strategies for OV patients.

Data availability statement

The datasets presented in this study can be found in online repositories. The names of the repository/repositories and accession number(s) can be found in the article/Supplementary Material.

Author contributions

SH, XZ and JW conceived the study and participated in the study design, performance and manuscript writing. HT, JS and JL conducted the bioinformatics analysis. XW and FW revised the manuscript. All authors read and approved the final manuscript.

Acknowledgments

We would like to extend our gratitude to the researchers and study patients for their contributions.

Conflict of interest

The authors declare that the research was conducted in the absence of any commercial or financial relationships that could be construed as a potential conflict of interest.

Publisher's note

All claims expressed in this article are solely those of the authors and do not necessarily represent those of their affiliated organizations, or those of the publisher, the editors and the reviewers. Any product that may be evaluated in this article, or claim that may be made by its manufacturer, is not guaranteed or endorsed by the publisher.

Supplementary material

The Supplementary Material for this article can be found online at: <https://www.frontiersin.org/articles/10.3389/fonc.2022.995929/full#supplementary-material>

SUPPLEMENTARY FIGURE 1
The flow chart of this study.

SUPPLEMENTARY FIGURE 2
Correlation between the OS variations and gene expression level.

SUPPLEMENTARY FIGURE 3
Consensus clustering analysis. (A) Uniform clustering cumulative distribution function (CDF) with the number of clusters k , ranging from 2 to 9. (B) The change of area under CDF curve with k ranging from 2 to 9. (C) Tracking plot of the cluster when $k = 2$.

SUPPLEMENTARY FIGURE 4
Consensus clustering analysis. (A) Uniform clustering cumulative distribution function (CDF) with the number of clusters k , ranging from 2 to 9. (B) The change of area under CDF curve with k ranging from 2 to 9. (C) The samples were classified into two clusters when $k = 2$. (D) Tracking plot of the cluster when $k = 2$.

SUPPLEMENTARY FIGURE 5
Identification of representative candidate prognostic genes. (A, B) The LASSO regression analysis and partial likelihood deviance on the prognostic genes.

SUPPLEMENTARY FIGURE 6

Validation of the prognostic model based on ARG score. The expression patterns of eight genes between the two groups in testing set_GSE9891 (A), testing set_GSE9891+TCGA (B). The median risk score to separate the patients in testing set_GSE9891 (C), testing set_GSE9891+TCGA (D). The fustat of patients in testing set_GSE9891 (E) and testing set_GSE9891+TCGA (F) were shown in a scatter plot. Kaplan–Meier analysis reveals the difference of the survival probability between the two groups in testing set_GSE9891 (G), testing set_GSE9891+TCGA (H). ROC curves were performed to predict the sensitivity and specificity of 1-, 3- and 5-year survival according to the CRG score in testing set_GSE9891 (I), testing set_GSE9891+TCGA (J).

SUPPLEMENTARY FIGURE 7

Clinical correlation analysis and stratified analysis of the model. (A–D) Comparison of risk scores of patients with different ages, fustat, grade and stage. (E–J) Survival analysis of OV patients with various clinical characteristics.

SUPPLEMENTARY FIGURE 8

Analysis of TMB in ARG score groups. (A, B) Relationships between ARG scores and TMB. (C) Analysis of survival probability in different TMB groups. (D) Analysis of survival probability combined TMB and ARG scores. (E, F) The distribution of somatic mutations in two ARG score groups.

SUPPLEMENTARY FIGURE 9

Analysis of drug sensitivity. (A) The difference of bleomycin, docetaxel, gemcitabine, paclitaxel and vinblastine IC50 between high and low risk groups of patients, respectively. (B) Correlation between common drugs and ARGs

SUPPLEMENTARY FIGURE 10

Comparison of our risk model with three published models. (A–C) Analysis of survival probability for three published models. (D–F) ROC curves of three published models. (G) Comparison of the C-index in four models.

References

- Momenimovahed Z, Tiznobaik A, Taheri S, Salehiniya H. Ovarian cancer in the world: Epidemiology and risk factors. *Int J Women Health* (2019) 11:287–99. doi: 10.2147/IJWH.S197604
- Siegel RL, Miller KD, Jemal A. Cancer statistics, 2020. *CA Cancer J Clin* (2020) 70:7–30. doi: 10.3322/caac.21590
- Jemal A, Bray F, Center MM, Ferlay J, Ward E, Forman D, et al. Global cancer statistics. *CA Cancer J Clin* (2011) 61(2):69–90. doi: 10.3322/caac.20107
- Kurman RJ. International Agency for Research on Cancer and World Health Organization. WHO classification of tumours of female reproductive organs. In: *World health organization classification of tumours, 4th*. Lyon: International Agency for Research on Cancer (2014). p. 307.
- Kossai M, Leary A, Scoazec JY, Genestie C. Ovarian cancer: A heterogeneous disease. *Pathobiology* (2018) 85:41–9. doi: 10.1159/000479006
- Herzog TJ, Pothuri B. Ovarian cancer: A focus on management of recurrent disease. *Nat Clin Pract Oncol* (2006) 3:604–11. doi: 10.1038/nclonc0637
- Herzog TJ. Recurrent ovarian cancer: How important is it to treat to disease progression? *Clin Cancer Res* (2004) 10:7439–49. doi: 10.1158/1078-0432.CCR-04-0683
- Lengyel E. Ovarian cancer development and metastasis. *Am J Pathol* (2010) 177:1053–64. doi: 10.2353/ajpath.2010.100105
- Kroeger PT Jr., Drapkin R. Pathogenesis and heterogeneity of ovarian cancer. *Curr Opin Obstet Gynecol* (2017) 29:26–34. doi: 10.1097/GCO.0000000000000340
- Goff B. Symptoms associated with ovarian cancer. *Clin Obstet Gynecol* (2012) 55:36–42. doi: 10.1097/GRF.0b013e3182480523
- Goff BA, Matthews B, Andrilla CH, Miller JW, Trivers KF, Berry D, et al. How are symptoms of ovarian cancer managed? A study of primary care physicians. *Cancer* (2011) 117(19):4414–23. doi: 10.1002/cncr.26035
- Orr B, Edwards RP. Diagnosis and treatment of ovarian cancer. *Hematol Oncol Clin North Am* (2018) 32:943–64. doi: 10.1016/j.hoc.2018.07.010
- Bast RC Jr., Matulonis UA, Sood AK, Ahmed AA, Amobi AE, Balkwill FR, et al. Critical questions in ovarian cancer research and treatment: Report of an American association for cancer research special conference. *Cancer* (2019) 125(12):1963–72. doi: 10.1002/cncr.32004
- Peres LC, Cushing-Haugen KL, Köbel M, Harris HR, Berchuck A, Rossing MA, et al. Invasive epithelial ovarian cancer survival by histotype and disease stage. *J Natl Cancer Inst* (2019) 111:60–8. doi: 10.1093/jnci/djy071
- Reid F, Bhatla N, Oza AM, Blank SV, Cohen R, Adams T, et al. The world ovarian cancer coalition every woman study: Identifying challenges and opportunities to improve survival and quality of life. *Int J Gynecol Cancer* (2021) 31:238–44. doi: 10.1136/ijgc-2019-000983
- Bao M, Zhang L, Hu Y. Novel gene signatures for prognosis prediction in ovarian cancer. *J Cell Mol Med* (2020) 24:9972–84. doi: 10.1111/jcmm.15601
- Odunsi K. Immunotherapy in ovarian cancer. *Ann Oncol* (2017) 28:viii1–7. doi: 10.1093/annonc/mdx444
- McAlpine J, Leon-Castillo A, Bosse T. The rise of a novel classification system for endometrial carcinoma; integration of molecular subclasses. *J Pathol* (2018) 244:538–49. doi: 10.1002/path.5034
- Hanahan D, Weinberg RA. Hallmarks of cancer: The next generation. *Cell* (2011) 144:646–74. doi: 10.1016/j.cell.2011.02.013
- Viallard C, Larrivee B. Tumor angiogenesis and vascular normalization: alternative therapeutic targets. *Angiogenesis* (2017) 20:409–26. doi: 10.1007/s10456-017-9562-9
- Qing X, Xu W, Liu S, Chen Z, Ye C, Zhang Y. Molecular characteristics, clinical significance, and cancer immune interactions of angiogenesis-associated genes in gastric cancer. *Front Immunol* (2022) 13:843077. doi: 10.3389/fimmu.2022.843077
- El-Kenawi AE, El-Remessy AB. Angiogenesis inhibitors in cancer therapy: mechanistic perspective on classification and treatment rationales. *Br J Pharmacol* (2013) 170:712–29. doi: 10.1111/bph.12344
- Jain RK. Normalizing tumor vasculature with anti-angiogenic therapy: A new paradigm for combination therapy. *Nat Med* (2001) 7:987–9. doi: 10.1038/nm0901-987
- Jain RK. Normalization of tumor vasculature: an emerging concept in antiangiogenic therapy. *Science* (2005) 307:58–62. doi: 10.1126/science.1104819
- Jain RK. Antiangiogenesis strategies revisited: from starving tumors to alleviating hypoxia. *Cancer Cell* (2014) 26:605–22. doi: 10.1016/j.ccr.2014.10.006
- Wang G, Hu JQ, Liu JY, Zhang XM. Angiogenesis-related gene signature-derived risk score for glioblastoma: Prospects for predicting prognosis and immune heterogeneity in glioblastoma. *Front Cell Dev Biol* (2022) 10:778286. doi: 10.3389/fcell.2022.778286
- Conesa A, Madrigal P, Tarazona S, Gomez-Cabrero D, Cervera A, McPherson A, et al. A survey of best practices for RNA-seq data analysis. *Genome Biol* (2016) 17:13. doi: 10.1186/s13059-016-0881-8
- Yu K, Lin CJ, Hatcher A, Lozzi B, Kong K, Huang-Hobbs E, et al. PIK3CA variants selectively initiate brain hyperactivity during gliomagenesis. *Nature* (2020) 578:166–71. doi: 10.1038/s41586-020-1952-2
- Wilkerson MD, Hayes DN. ConsensusClusterPlus: A class discovery tool with confidence assessments and item tracking. *Bioinf (Oxford England)* (2010) 26:1572–3. doi: 10.1093/bioinformatics/btq170
- Ritchie ME, Phipson B, Wu D, Hu Y, Law CW, Shi W, et al. Limma powers differential expression analyses for RNA-sequencing and microarray studies. *Nucleic Acids Res* (2015) 43:e47. doi: 10.1093/nar/gkv007
- Chen L, Zhang YH, Wang S, Zhang Y, Huang T, Cai YD. Prediction and analysis of essential genes using the enrichments of gene ontology and KEGG pathways. *PLoS One* (2017) 12:e0184129. doi: 10.1371/journal.pone.0184129
- Liang Y, Ma B, Jiang P, Yang HM. Identification of methylation-regulated differentially expressed genes and related pathways in hepatocellular carcinoma: A study based on TCGA database and bioinformatics analysis. *Front Oncol* (2021) 11:636093. doi: 10.3389/fonc.2021.636093
- Bloniarz A, Liu H, Zhang CH, Sekhon JS, Yu B. Lasso adjustments of treatment effect estimates in randomized experiments. *Proc Natl Acad Sci U.S.A.* (2016) 113(27):7383–90. doi: 10.1073/pnas.1510506113
- Arneth B. Tumor microenvironment. *Med (Kaunas)* (2019) 56(1):15. doi: 10.3390/medicina56010015

35. Quail DF, Joyce JA. Microenvironmental regulation of tumor progression and metastasis. *Nat Med* (2013) 19:1423–37. doi: 10.1038/nm.3394
36. Rosenberg JE, Hoffman-Censits J, Powles T, van der Heijden MS, Balar AV, Necchi A, et al. Atezolizumab in patients with locally advanced and metastatic urothelial carcinoma who have progressed following treatment with platinum-based chemotherapy: A single-arm, multicentre, phase 2 trial. *Lancet* (2016) 387:1909–20. doi: 10.1016/S0140-6736(16)00561-4
37. Senbabaoglu Y, Gejman RS, Winer AG, Liu M, Van Allen EM, de Velasco G, et al. Tumor immune microenvironment characterization in clear cell renal cell carcinoma identifies prognostic and immunotherapeutically relevant messenger RNA signatures. *Genome Biol* (2016) 17:231. doi: 10.1186/s13059-016-1092-z
38. Yoshihara K, Shahmoradgoli M, Martínez E, Vegesna R, Kim H, Torres-García W, et al. Inferring tumour purity and stromal and immune cell admixture from expression data. *Nat Commun* (2013) 4:2612. doi: 10.1038/ncomms3612
39. Wu J, Li L, Zhang H, Zhao Y, Zhang H, Wu S, et al. A risk model developed based on tumor microenvironment predicts overall survival and associates with tumor immunity of patients with lung adenocarcinoma. *Oncogene* (2021) 40:4413–24. doi: 10.1038/s41388-021-01853-y
40. Jiang Y, Chen J, Ling J, Zhu X, Jiang P, Tang X, et al. Construction of a glycolysis-related long noncoding RNA signature for predicting survival in endometrial cancer. *J Cancer* (2021) 12:1431–44. doi: 10.7150/jca.50413
41. Chen B, Khodadoust MS, Liu CL, Newman AM, Alizadeh AA. Profiling tumor infiltrating immune cells with CIBERSORT. *Methods Mol Biol* (2018) 1711:243–59. doi: 10.1007/978-1-4939-7493-1_12
42. Zhou J, Zhang M, Dong H, Wang M, Cheng Y, Wang S, et al. Comprehensive analysis of acetylation-related lncRNAs and identified AC099850.3 as prognostic biomarker in non-small cell lung cancer. *J Oncol* (2021) 2021:4405697. doi: 10.1155/2021/4405697
43. Addeo A, Friedlaender A, Banna GL, Weiss GJ. TMB or not TMB as a biomarker: That is the question. *Crit Rev Oncol Hematol* (2021) 163:103374. doi: 10.1016/j.critrevonc.2021.103374
44. Cristescu R, Mogg R, Ayers M, Albright A, Murphy E, Yearley J, et al. Pan-tumor genomic biomarkers for PD-1 checkpoint blockade-based immunotherapy. *Science* (2018) 362(6411):eaar3593. doi: 10.1126/science.aar3593
45. Waddell N, Pajic M, Patch AM, Chang DK, Kassahn KS, Bailey P, et al. Whole genomes redefine the mutational landscape of pancreatic cancer. *Nature* (2015) 518:495–501. doi: 10.1038/nature14169
46. Reinhold WC, Sunshine M, Liu H, Varma S, Kohn KW, Morris J, et al. CellMiner: A web-based suite of genomic and pharmacologic tools to explore transcript and drug patterns in the NCI-60 cell line set. *Cancer Res* (2012) 72:3499–511. doi: 10.1158/0008-5472.CAN-12-1370
47. Hoshino N, Hida K, Sakai Y, Osada S, Idani H, Sato T, et al. Nomogram for predicting anastomotic leakage after low anterior resection for rectal cancer. *Int J Colorectal Dis* (2018) 33:411–8. doi: 10.1007/s00384-018-2970-5
48. Nie K, Zheng Z, Wen Y, Shi L, Xu S, Wang X, et al. Construction and validation of a TP53-associated immune prognostic model for gastric cancer. *Genomics* (2020) 112:4788–95. doi: 10.1016/j.ygeno.2020.08.026
49. Liu J, Nie S, Wu Z, Jiang Y, Wan Y, Li S, et al. Exploration of a novel prognostic risk signatures and immune checkpoint molecules in endometrial carcinoma microenvironment. *Genomics* (2020) 112:3117–34. doi: 10.1016/j.ygeno.2020.05.022
50. Li L, Liang J, Song T, Yin S, Zeng J, Zhong Q, et al. A nomogram model to predict prognosis of patients with genitourinary sarcoma. *Front Oncol* (2021) 11:656325. doi: 10.3389/fonc.2021.656325
51. Wang R, Ye XH, Zhao XL, Liu JL, Zhang CY. Development of a five-gene signature as a novel prognostic marker in ovarian cancer. *Neoplasia* (2019) 66:343–9. doi: 10.4149/neo_2018_180705N447
52. Yue H, Wang J, Chen R, Hou X, Li J, Lu X. Gene signature characteristic of elevated stromal infiltration and activation is associated with increased risk of hematogenous and lymphatic metastasis in serous ovarian cancer. *BMC Cancer* (2019) 19:1266. doi: 10.1186/s12885-019-6470-y
53. Ye Y, Dai Q, Qi H. A novel defined pyroptosis-related gene signature for predicting the prognosis of ovarian cancer. *Cell Death Discov* (2021) 7:71. doi: 10.1038/s41420-021-00451-x
54. Kuroki L, Guntupalli SR. Treatment of epithelial ovarian cancer. *BMJ* (2020) 371:m3773. doi: 10.1136/bmj.m3773
55. Ferlay J, Soerjomataram I, Dikshit R, Eser S, Mathers C, Rebelo M, et al. Cancer incidence and mortality worldwide: Sources, methods and major patterns in GLOBOCAN 2012. *Int J Cancer* (2015) 136:E359–386. doi: 10.1002/ijc.29210
56. Bilbao M, Aikins JK, Ostrovsky O. Is routine omentectomy of grossly normal omentum helpful in surgery for ovarian cancer? A look at the tumor microenvironment and its clinical implications. *Gynecol Oncol* (2021) 161:78–82. doi: 10.1016/j.ygyno.2020.12.033
57. Cannistra SA. Cancer of the ovary. *N Engl J Med* (2004) 351:2519–29. doi: 10.1056/NEJMra041842
58. Siegel R, Naishadham D, Jemal A. Cancer statistics, 2012. *CA Cancer J Clin* (2012) 62:10–29. doi: 10.3322/caac.20138
59. Torre LA, Trabert B, DeSantis CE, Miller KD, Samimi G, Runowicz CD, et al. Ovarian cancer statistics, 2018. *CA Cancer J Clin* (2018) 68:284–96. doi: 10.3322/caac.21456
60. Rajabi M, Mousa SA. The role of angiogenesis in cancer treatment. *Biomedicines* (2017) 5(2):34. doi: 10.3390/biomedicines5020034
61. Rivera LB, Bergers G. Intertwined regulation of angiogenesis and immunity by myeloid cells. *Trends Immunol* (2015) 36:240–9. doi: 10.1016/j.it.2015.02.005
62. Trenti A, Tedesco S, Boscaro C, Trevisi L, Bolego C, Cignarella A, et al. Estrogen, angiogenesis, immunity and cell metabolism: Solving the puzzle. *Int J Mol Sci* (2018) 19(3):859. doi: 10.3390/ijms19030859
63. Liu J, Meng H, Nie S, Sun Y, Jiang P, Li S, et al. Identification of a prognostic signature of epithelial ovarian cancer based on tumor immune microenvironment exploration. *Genomics* (2020) 112:4827–41. doi: 10.1016/j.ygeno.2020.08.027
64. Liu J, Chen C, Wang Y, Qian C, Wei J, Xing Y, et al. Comprehensive of N1-methyladenosine modifications patterns and immunological characteristics in ovarian cancer. *Front Immunol* (2021) 12:746647. doi: 10.3389/fimmu.2021.746647
65. Rebollo-Jaramillo B, Ziegler A. Teneurin: An integrative molecular, functional, and biomedical overview of their role in cancer. *Front Neurosci* (2018) 12:937. doi: 10.3389/fnins.2018.00937
66. Peppino G, Rui R, Arigoni M, Riccardo F, Iacoviello A, Barutello G, et al. Teneurins: Role in cancer and potential role as diagnostic biomarkers and targets for therapy. *Int J Mol Sci* (2021) 22(5):2321. doi: 10.3390/ijms22052321
67. Kim M, Kim DJ. GFRA1: A novel molecular target for the prevention of osteosarcoma chemoresistance. *Int J Mol Sci* (2018) 19(4):1078. doi: 10.3390/ijms19041078
68. Kim MH, Kim HB, Acharya S, Sohn HM, Jun JY, Chang IY, et al. Ape1/Ref-1 induces glial cell-derived neurotrophic factor (GDNF) responsiveness by upregulating GDNF receptor alpha1 expression. *Mol Cell Biol* (2009) 29:2264–77. doi: 10.1128/MCB.01484-08
69. Li J, Bakhom SF. Expanding the Role of STING in Cellular Homeostasis and Transformation. *Trends Cancer* (2019) 5(4):195–97. doi: 10.1016/j.trecan.2019.02.001
70. He R, Liu P, Xie X, Zhou Y, Liao Q, Xiong W, et al. circGFRA1 and GFRA1 act as ceRNAs in triple negative breast cancer by regulating miR-34a. *J Exp Clin Cancer Res* (2017) 36(1):145. doi: 10.1186/s13046-017-0614-1
71. Al Sadoun H, Burgess M, Hentges KE, Mace KA. Enforced expression of Hoxa3 inhibits classical and promotes alternative activation of macrophages. *In Vitro In Vivo. J Immunol* (2016) 197:872–84. doi: 10.4049/jimmunol.1501944
72. Chojnowski JL, Masuda K, Trau HA, Thomas K, Capecci M, Manley NR. Multiple roles for HOXA3 in regulating thymus and parathyroid differentiation and morphogenesis in mouse. *Development* (2014) 141:3697–708. doi: 10.1242/dev.110833
73. Chojnowski JL, Trau HA, Masuda K, Manley NR. Temporal and spatial requirements for Hoxa3 in mouse embryonic development. *Dev Biol* (2016) 415:33–45. doi: 10.1016/j.ydbio.2016.05.010
74. Mahdipour E, Charnock JC, Mace KA. Hoxa3 promotes the differentiation of hematopoietic progenitor cells into proangiogenic gr-1+CD11b+ myeloid cells. *Blood* (2011) 117:815–26. doi: 10.1182/blood-2009-12-259549
75. Kazanietz MG, Durando M, Cooke M. CXCL13 and its receptor CXCR5 in cancer: Inflammation, immune response, and beyond. *Front Endocrinol (Lausanne)* (2019) 10:471. doi: 10.3389/fendo.2019.00471
76. Yang M, Lu J, Zhang G, Wang Y, He M, Xu Q, et al. CXCL13 shapes immunoreactive tumor microenvironment and enhances the efficacy of PD-1 checkpoint blockade in high-grade serous ovarian cancer. *J Immunother Cancer* (2021) 9(1):e001136. doi: 10.1136/jitc-2020-001136
77. Ghoneum A, Affy H, Salih Z, Kelly M, Said N. Role of tumor microenvironment in the pathobiology of ovarian cancer: Insights and therapeutic opportunities. *Cancer Med* (2018) 7:5047–56. doi: 10.1002/cam4.1741
78. Li BL, Wan XP. Prognostic significance of immune landscape in tumour microenvironment of endometrial cancer. *J Cell Mol Med* (2020) 24:7767–77. doi: 10.1111/jcmm.15408
79. Jia Q, Ge J, Liu W, Zheng X, Chen S, Wen Y, et al. A magnetofluorescent carbon dot assembly as an acidic H₂O₂-driven oxygenator to regulate tumor hypoxia for simultaneous bimodal imaging and enhanced photodynamic therapy. *Adv Mater* (2018) 30(13):e1706090. doi: 10.1073/pnas.1510506113
80. Lin X, Liu S, Zhang X, Zhu R, Chen S, Chen X, et al. An ultrasound activated vesicle of janus au-MnO nanoparticles for promoted tumor penetration and sonodynamic therapy of orthotopic liver cancer. *Angew Chem Int Ed Engl* (2020) 59:1682–8. doi: 10.1002/anie.201912768

81. Raskov H, Orhan A, Christensen JP, Gogenur I. Cytotoxic CD8(+) T cells in cancer and cancer immunotherapy. *Br J Cancer* (2021) 124:359–67. doi: 10.1038/s41416-020-01048-4
82. St Paul M, Ohashi PS. The roles of CD8(+) T cell subsets in antitumor immunity. *Trends Cell Biol* (2020) 30:695–704. doi: 10.1016/j.tcb.2020.06.003
83. Sckisel GD, Mirsoian A, Minnar CM, Crittenden M, Curti B, Chen JQ, et al. Differential phenotypes of memory CD4 and CD8 T cells in the spleen and peripheral tissues following immunostimulatory therapy. *J Immunother Cancer* (2017) 5:33. doi: 10.1186/s40425-017-0235-4
84. Zhao Y, Niu C, Cui J. Gamma-delta (gammadelta) T cells: Friend or foe in cancer development? *J Transl Med* (2018) 16:3. doi: 10.1186/s12967-017-1378-2
85. An Y, Yang Q. MiR-21 modulates the polarization of macrophages and increases the effects of M2 macrophages on promoting the chemoresistance of ovarian cancer. *Life Sci* (2020) 242:117162. doi: 10.1016/j.lfs.2019.117162
86. De Felice F, Marchetti C, Tombolini V, Panici PB. Immune check-point in endometrial cancer. *Int J Clin Oncol* (2019) 24:910–6. doi: 10.1007/s10147-019-01437-7
87. Yang C, Xia BR, Zhang ZC, Zhang YJ, Lou G, Jin W, et al. Immunotherapy for ovarian cancer: Adjuvant, combination, and neoadjuvant. *Front Immunol* (2020) 11:577869. doi: 10.3389/fimmu.2020.577869
88. Rowshanravan B, Halliday N, Sansom DM. CTLA-4: A moving target in immunotherapy. *Blood* (2018) 131:58–67. doi: 10.1182/blood-2017-06-741033
89. Zhai Y, Celis-Gutierrez J, Voisinne G, Mori D, Girard L, Burlet-Schiltz O, et al. Opposing regulatory functions of the TIM3 (HAVCR2) signalosome in primary effector T cells as revealed by quantitative interactomics. *Cell Mol Immunol* (2021) 18:1581–3. doi: 10.1038/s41423-020-00575-7
90. Kelly AD, Murugesan K, Kuang Z, Montesin M, Ross JS, Albacker LA, et al. Pan-cancer landscape of CD274 (PD-L1) rearrangements in 283,050 patient samples, its correlation with PD-L1 protein expression, and immunotherapy response. *J Immunother Cancer* (2021) 9(11):e003550. doi: 10.1136/jitc-2021-003550
91. Qiu Y, Li Z, Pouzoulet F, Vishnu P, Copland JA 3rd, Knutson KL, et al. Immune checkpoint inhibition by anti-PDCD1 (anti-PD1) monoclonal antibody has significant therapeutic activity against central nervous system lymphoma in an immunocompetent preclinical model. *Br J Haematol* (2018) 183:674–8. doi: 10.1111/bjh.15009
92. Liu J, Geng R, Ni S, Cai L, Yang S, Shao F, et al. Pyroptosis-related lncRNAs are potential biomarkers for predicting prognoses and immune responses in patients with UCEC. *Mol Ther Nucleic Acids* (2022) 27:1036–55. doi: 10.1016/j.omtn.2022.01.018
93. Leroy B, Anderson M, Soussi T. TP53 mutations in human cancer: database reassessment and prospects for the next decade. *Hum Mutat* (2014) 35:672–88. doi: 10.1002/humu.22552
94. Xue D, Lin H, Lin L, Wei Q, Yang S, Chen X. TTN/TP53 mutation might act as the predictor for chemotherapy response in lung adenocarcinoma and lung squamous carcinoma patients. *Transl Cancer Res* (2021) 10:1284–94. doi: 10.21037/tcr-20-2568
95. Chauveau C, Rowell J, Ferreiro A. A rising titan: TTN review and mutation update. *Hum Mutat* (2014) 35:1046–59. doi: 10.1002/humu.22611
96. Zamarin D. Novel therapeutics: response and resistance in ovarian cancer. *Int J Gynecol Cancer* (2019) 29:s16–21. doi: 10.1136/ijgc-2019-000456



OPEN ACCESS

EDITED BY
Jinhui Liu,
Nanjing Medical University, China

REVIEWED BY
Xintian Cai,
People's Hospital of Xinjiang Uygur
Autonomous Region, China
Zhongbao Zhou,
Beijing Tiantan Hospital, Capital
Medical University, China

*CORRESPONDENCE
Fei Mao
maofeidoctor@njmu.edu.cn

SPECIALTY SECTION
This article was submitted to
Gynecological Oncology,
a section of the journal
Frontiers in Oncology

RECEIVED 28 July 2022
ACCEPTED 18 August 2022
PUBLISHED 14 September 2022

CITATION
Wang J, Meng F and Mao F (2022)
Single cell sequencing analysis and
transcriptome analysis constructed the
liquid-liquid phase separation(LLPS)-
related prognostic model for
endometrial cancer.
Front. Oncol. 12:1005472.
doi: 10.3389/fonc.2022.1005472

COPYRIGHT
© 2022 Wang, Meng and Mao. This is
an open-access article distributed under
the terms of the [Creative Commons
Attribution License \(CC BY\)](#). The use,
distribution or reproduction in other
forums is permitted, provided the
original author(s) and the copyright
owner(s) are credited and that the
original publication in this journal is
cited, in accordance with accepted
academic practice. No use,
distribution or reproduction is
permitted which does not comply with
these terms.

Single cell sequencing analysis and transcriptome analysis constructed the liquid-liquid phase separation(LLPS)-related prognostic model for endometrial cancer

Jiayang Wang¹, Fei Meng² and Fei Mao^{3*}

¹Department of Radiotherapy, The Affiliated Huaian No. 1 People's Hospital of Nanjing Medical University, Huaian, China, ²Department of Gynaecology, The Affiliated Huaian No. 1 People's Hospital of Nanjing Medical University, Huaian, China, ³Department of Urology, The Affiliated Huaian No. 1 People's Hospital of Nanjing Medical University, Huaian, China

Background: Endometrial cancer is one of the most common gynecological tumors in developed countries. Our understanding of the pathogenesis of endometrial cancer and the changes in the immune microenvironment are still unclear. It is necessary to explore new biomarkers to guide the diagnosis and treatment of endometrial cancer.

Methods: The GEO database was used to download the endometrial cancer single cell sequencing dataset GSE173682. The UCSC database was used to download transcriptome sequencing data. The validation set was the transcriptome dataset GSE119041, which was retrieved from the GEO database. On the DrLLPS website, liquid-liquid phase separation-related genes can be downloaded. Relevant hub genes were found using weighted co-expression network analysis and dimension reduction clustering analysis. Prognostic models were built using Lasso regression and univariate COX regression. Analyses of immune infiltration were employed to investigate the endometrial cancer immunological microenvironment. The expression of model genes in endometrial cancer was confirmed using a PCR test.

Results: We created an LLPS-related predictive model for endometrial cancer by extensive study, and it consists of four genes: EIF2S2, SNRPC, PRELID1, and NDUFB9. Patients with endometrial cancer may be classified into high-risk and low-risk groups based on their risk scores, and those in the high-risk group had significantly worse prognoses ($P < 0.05$). Additionally, there were notable variations in the immunological milieu between the groups at high and low risk. EIF2S2, SNRPC, PRELID1, and NDUFB9 were all up-regulated in endometrial cancer tissues, according to PCR results.

Conclusions: Our study can provide a certain reference for the diagnosis and treatment of endometrial cancer.

KEYWORDS

liquid-liquid phase separation, endometrial cancer, immune microenvironment, single cell sequencing data, transcriptome data

Introduction

The most common disease of the female reproductive system, endometrial cancer, is becoming more common everywhere (1). Both perimenopausal and postmenopausal women are impacted (2). It is difficult to diagnose and treat endometrial cancer because of its high incidence, which is thought to be mostly attributed to obesity (3). Bleeding is a common sign of endometrial cancer after menopause, which helps many people get diagnosed early (4). However, some people continue to experience occult symptoms, which delays diagnosis (5). Surgery is typically avoided because of the poor prognosis and limited therapy options for endometrial cancer in its advanced stages (6). Advanced endometrial cancer cannot be effectively treated with chemotherapy or radiotherapy (7). Therefore, the need for improved prognostic classification systems for endometrial cancer is critical.

Cancer growth-related signals and apoptosis resistance are both activated by a variety of events, including gene mutation, transcriptome alterations, epigenetic modification, and others (8). Liquid-liquid phase separation (LLPS) complicates the etiology of cancer (9). In the past, LLPS was believed to be a frequent occurrence and experimental principle in the fields of physics, chemistry, and pharmacy (10). The development of membraneless organelles and research led to the hypothesis that LLPS controls the synthesis of membraneless agglutinins in healthy living cells, enabling a dynamic and steady reaction (11). LLPS may participate in a variety of signal transduction pathways, epigenetic control of cancer, and cancer genesis (12). On the other hand, it is yet unclear how LLPS affects endometrial cancer. The importance of LLPS in endometrial cancer has to be examined. It's time to examine LLPS's connection to endometrial cancer.

In this study, we studied the involvement of LLPS-related genes in endometrial cancer by single-cell sequencing analysis and transcriptome sequencing analysis, and created a predictive model to estimate the prognosis and immunological status of patients with endometrial cancer. Overall, our study presents novel therapeutic concepts and new biomarkers for endometrial cancer.

Methods

Single cell sequencing data download and processing

GEO (Gene Expression Omnibus) database (<https://www.ncbi.nlm.nih.gov/geo/>) provides many the transcriptome data and single cell sequencing data of the disease. From this database, the single cell sequencing dataset GSE173682 for endometrial cancer was retrieved. The dataset comprised both endometrial and ovarian cancer, and only five endometrial cancer samples were preserved for later analysis. The quality control method was as follows: 1) Genes expressed in less than three cells were deleted. 2) Cells with gene expression between 200 and 3000 were maintained. 3) Cells that retain fewer than 10 percent of mitochondrial genes. Sample and pericellular batch effects were eliminated and samples were combined using the "SCT" approach. The DIMS was set at 1:25, and the TSNE method was utilized to minimize the dimension of samples. K. Peram was 20, random seed was 2021, and all cells were grouped using KNN's approach. Cells were annotated using SingleR's approach.

Transcriptome data downloading and processing

Data from many databases, including TCGA and TARGET, are included in the UCSC database (<https://xena.ucsc.edu/>). GDC TCGA Endometrioid Cancer transcriptome data and clinical information were retrieved *via* the database. Through matching, a total of 533 samples with expression matrices and clinical data were found. The downloaded transcriptome data is HTseq-FPKM. From the GEO database, the endometrial cancer dataset GSE119041 was taken, and it served as an independent external validation cohort. After log2 transformation, transcriptome data were used for future analysis.

Download of LLPS related genes

A significant amount of pertinent LLPS phenotypic correlation gene is sent to the DrLLPS website (<http://llps.biocuckoo.cn/>). This database's list of LLPS-related genes, which includes 3611 genes in total, can be downloaded by choosing the download module.

Single-sample gene set enrichment analysis

Single-sample gene-set enrichment analysis is an extension of the GSEA method, which can compute and obtain enrichment scores for each sample and gene set pairing, showing the degree to which members of a given gene set in the sample are coordinately up-or down-regulated. In this study, we eventually computed and acquired the enrichment fraction of LLPS phenotype in each sample by this analysis method.

Weighted gene co-expression network analysis

Co-expressed genes can be categorized into modules using WGCNA, and the relationship between modules and phenotype can be investigated. This approach was utilized in this investigation to identify genes associated with the LLPS phenotype. The pickSoftThreshold function of the R package "WGCNA" is used to find the best soft field value. Step sizes of 1:10 and 12:20 are set to 1 and 2, respectively. Set deepSplit to 2 and the minimum number of module genes to 100.

Construction and validation of the prognostic model

First, univariate COX regression was used to identify the genes associated with prognosis. After that, the prognosis-related genes were further examined using LASSO regression, with the family set to "Cox" and Maxit set to 1000. The survival differences between the model's high and low risk groups were investigated in the training cohort and validation cohort, as well as whether the model could more accurately classify patients' risk categories.

Immune infiltration analysis

Immunedeconv is a R package that is used on the Timer2.0 website (<http://timer.comp-genomics.org/>) to provide a more accurate measurement of immune infiltration. The findings of

seven different calculation techniques were retrieved from the Timer2 website for each endometrial cancer sample. The variations in immune infiltration between the high and low risk groups in the model were investigated, and the results were displayed using a heat map.

The construction of a nomogram

In order to more correctly assess the prognosis of patients, clinical data and sample models were combined using the R program "Regplot" and then presented as a nomogram.

PCR was used to verify the expression of model genes

The 8 EC patients were chosen between October 2021 and July 2022, and their EC tissue as well as healthy uterine tissue was obtained for mRNA quantification and qRT-PCR testing. This study was approved by the Ethics Committee of Huai 'an First People's Hospital (No.KY-2022-084-01). Total cellular RNAs were isolated from cells using Trizol Reagent per the manufacturer's instructions (Invitrogen, Carlsbad, CA, USA). Using the Takara reverse transcription kit, reverse transcription was completed (Otsu, Shiga, Japan). The QuantiTect SYBR Green PCR Kit and QuantStudio 1 for the real-time polymerase chain reaction were given by Thermo, Waltham, Massachusetts (RT-PCR). Relative quantification was determined using the $-2^{\Delta\Delta Ct}$ method. The relative expression level of each gene's messenger RNA (mRNA) was changed to match the mRNA for the enzyme glyceraldehyde-3-phosphate dehydrogenase (GAPDH). The primer sequence used was as follows: GAPDH: Forward primer: GAATGGGCAGCCGTTAGGAA; Reverse primer: CCCAATACGACCAAATCAGAGA. EIF2S2: Forward primer: AGGTGTAAAGATTGAAAGTGATGTT; Reverse primer: TGTTGTCTTCATCTTCTAGAGCTTC. SNRPC: Forward primer: ACTGCAGTGGAAGGAAACACA; Reverse primer: TGTGAAATGCAGCCGTTGT. PRELID1: Forward primer: GTCTCCAGAGCTGTCCAGGAAT; Reverse primer: TGTCTCAACAAGTGTTTGGGAAGG. NDUF9: Forward primer: GTAATGGCGTTCTTGGCGTC; Reverse primer: TTCAAACCGGGCTCTGGAC.

Statistical analysis

Genes linked to prognosis were screened using a univariate COX analysis. The KM survival analysis was used to evaluate the results for the patients. To compare gene expression between high- and low-risk groups, the wilcox test was employed. Statistics were judged significant at $P < 0.05$.

Results

Single cell sequencing data analysis

Single-cell sequencing data for endometrial cancer were studied. As indicated in Figure 1A, no significant batch effect was seen in the 5 endometrial cancer samples, which were appropriate for additional study. As shown in Figure 1B, all cells were clustered into 22 groups following dimension reduction and clustering. The cells were then further annotated, as shown in Figure 1C, where nine cell types were annotated as fibroblasts, smooth muscle cells, T cells, epithelial cells, endothelial cells, tissue stem cells, macrophage, DC, and NK cells. The percentage of LLPS phenotype in each cell is determined according to the “PercentageFeatureSet” function of Seurat R package, and then separated into high LLPS score group and low LLPS score group according to the median value. As demonstrated in Figure 1D, high LLPS score group is largely distributed in fibroblasts and smooth muscle cells and epithelial cells group. And then differentially expressed genes analysis between the two groups were performed, by setting the conditions as $|\text{avg logFC}| > 1$ and the rectified adj p value $<$

0.05. A total of 2512 differentially expressed genes associated to LLPS in endometrial cancer were found.

WGCNA analysis

Genes associated to LLPS phenotype were further examined at the transcriptome level of endometrial cancer. Firstly, the enrichment fraction of LLPS phenotype in each sample was estimated by ssGSEA algorithm, and then separated into high LLPS group and low LLPS group according to the median value. As shown in Figure 2A, KM survival analysis suggested that the survival prognosis of the high LLPS group was poor. As shown in Figure 2B, when the soft domain value is set to 9, it is discovered that $R^2 > 0.8$, and the data correspond to the power-law distribution, which is suitable for following analysis. Moreover, with the increase in soft domain value, Mean Connectivity tends to stay steady. As indicated in Figure 2C, all genes were clustered into 8 non-grey modules, among which the green module exhibited the highest connection with LLPS score (Figure 2D, $P < 0.05$). Then 1004 genes in the green module were selected out.

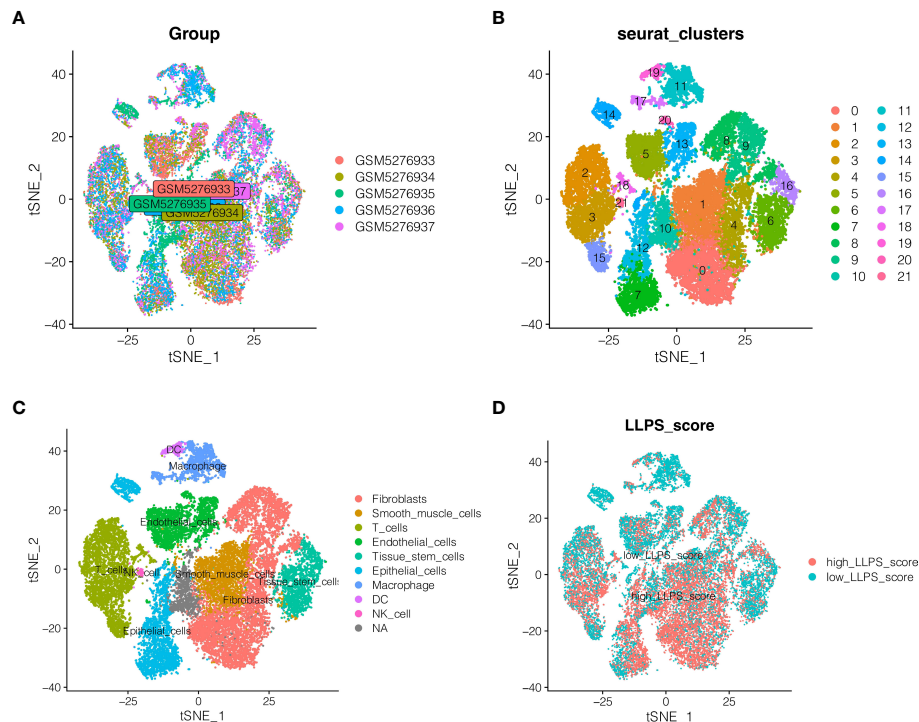


FIGURE 1

Single cell sequencing data analysis. (A) Detection of batch effects. (B) Dimension reduction and clustering. (C) Cell annotation. Nine cell types were annotated as Fibroblasts, Smooth muscle cells, T cells, epithelial cells, endothelial cells, Tissue stem cells, macrophage, DC, and NK cells. (D) Distribution of LLPS score in different cells.

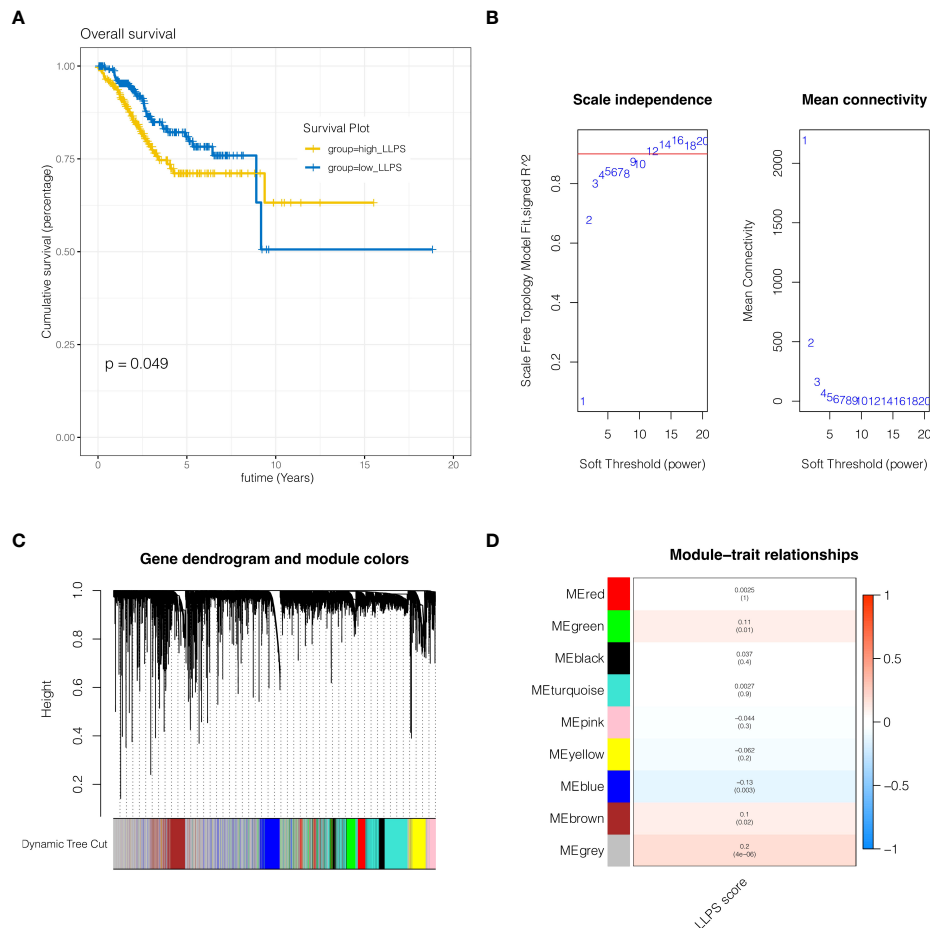


FIGURE 2

WGCNA analysis. (A) KM survival analysis. The survival prognosis of the high LLPS group was poor. (B) When the soft domain value is set to 9, it is discovered that $R^2 > 0.8$, and the data correspond to the power-law distribution, which is suitable for following analysis. (C, D) Clustering of modules. A total of 8 non-grey modules were identified, among which the green module had the strongest correlation with LLPS.

Construction and validation of the prognostic model

To further identify LLPS-related genes in endometrial cancer at the single-cell level and tissue transcriptome sequencing level, 2512 genes obtained by the above single-cell sequencing analysis were intersected with 1004 genes of the green module analyzed by WGCNA, and a total of 158 genes were obtained. In order to further discover genes linked to prognosis, univariate COX analysis was done with $P < 0.05$, and 8 genes related to prognosis in TCGA cohort and GSE119041 dataset were screened. As indicated in Figure 3A, these genes were EIF2S2, SNRPC, PRELID1, NDUFB9, YBX1, ABCF1, AK2 and GNL1. As shown in Figures 3B, C, when the best lambda value was 0.03 using LASSO regression, four genes were included in the model, namely EIF2S2, SNRPC, PRELID1, and NDUFB9. The calculation formula of the model was: riskScore = EIF2S2*

(0.213) + SNRPC *(0.030) + PRELID1 *(0.024) + NDUFB9 *(0.002). (0.002). Then patients were separated into risk high group and risk low group according to the median riskscore value. As shown in Figures 3D, E, in both the training cohort TCGA and the external validation cohort GSE119041, it was observed that the prognosis of the risk high group was poorer than that of the risk low group ($P < 0.05$). As shown in Figures 3F, G, this model can discriminate endometrial cancer patients well in both the training and validation cohorts.

Unsupervised clustering analysis

In TCGA cohort, as shown in Figure 4A, according to the expressions of EIF2S2, SNRPC, PRELID1 and NDUFB9, the R package “ConsensusClusterPlus” was used, clusterAlg was set as

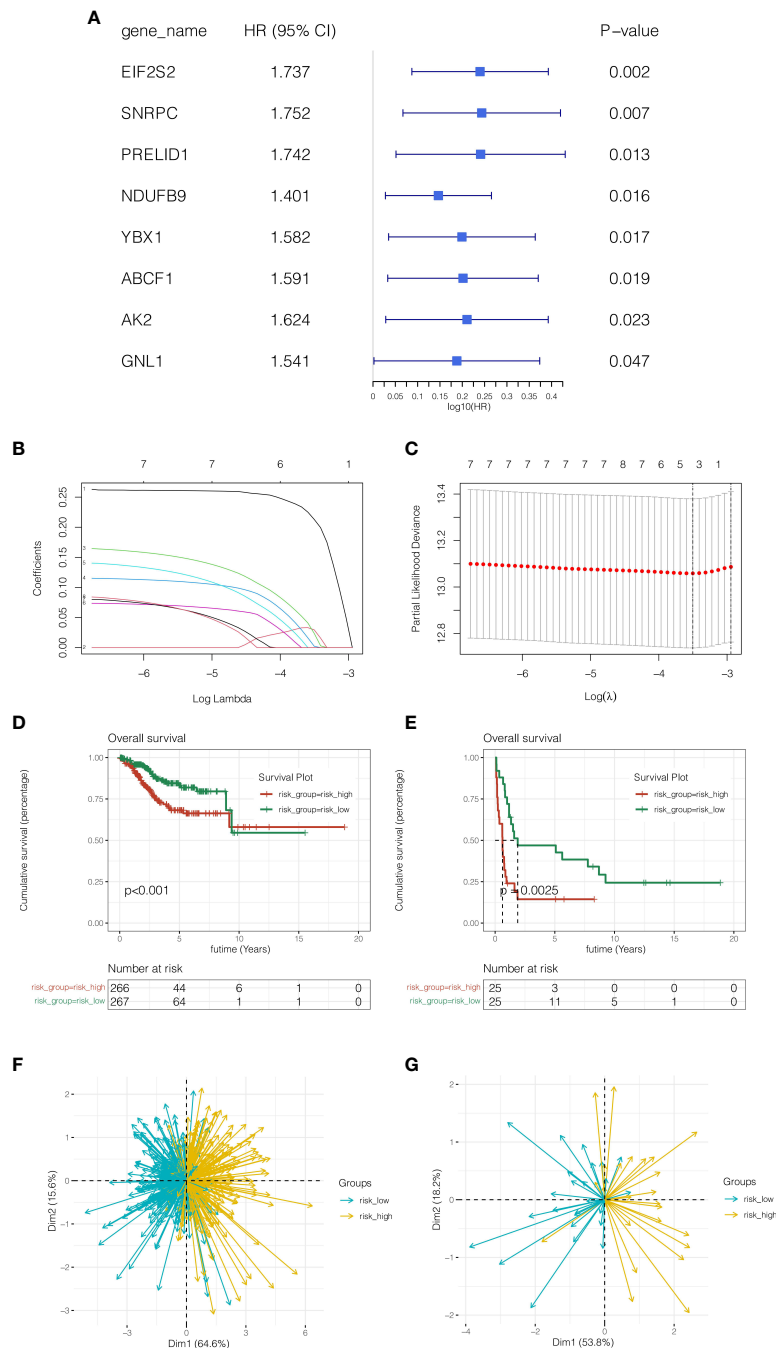


FIGURE 3 Construction and validation of the prognostic model. **(A)** Univariate COX analysis. **(B, C)** LASSO regression, four genes were included in the model, namely EIF2S2, SNRPC, PRELID1, and NDUFB9. **(D, E)** In both the training cohort TCGA and the external validation cohort GSE119041, it was observed that the prognosis of the risk high group was poorer than that of the risk low group ($P < 0.05$). **(F, G)** Principal component analysis. This model can discriminate endometrial cancer patients well in both the training and validation cohorts.

“PAM”, Distance was set as “Euclidean”, the random seed was set as 123456 and unsupervised clustering was done. All endometrial cancer patients were diagnosed with two subgroups, Cluster1 and Cluster2. As demonstrated in

Figure 4B, the prognosis of Cluster2 was poorer than that of Cluster1 ($P < 0.001$). As indicated in Figure 4C, risk high group mostly belongs to Cluster2, and risk low group mainly corresponds to Cluster1.

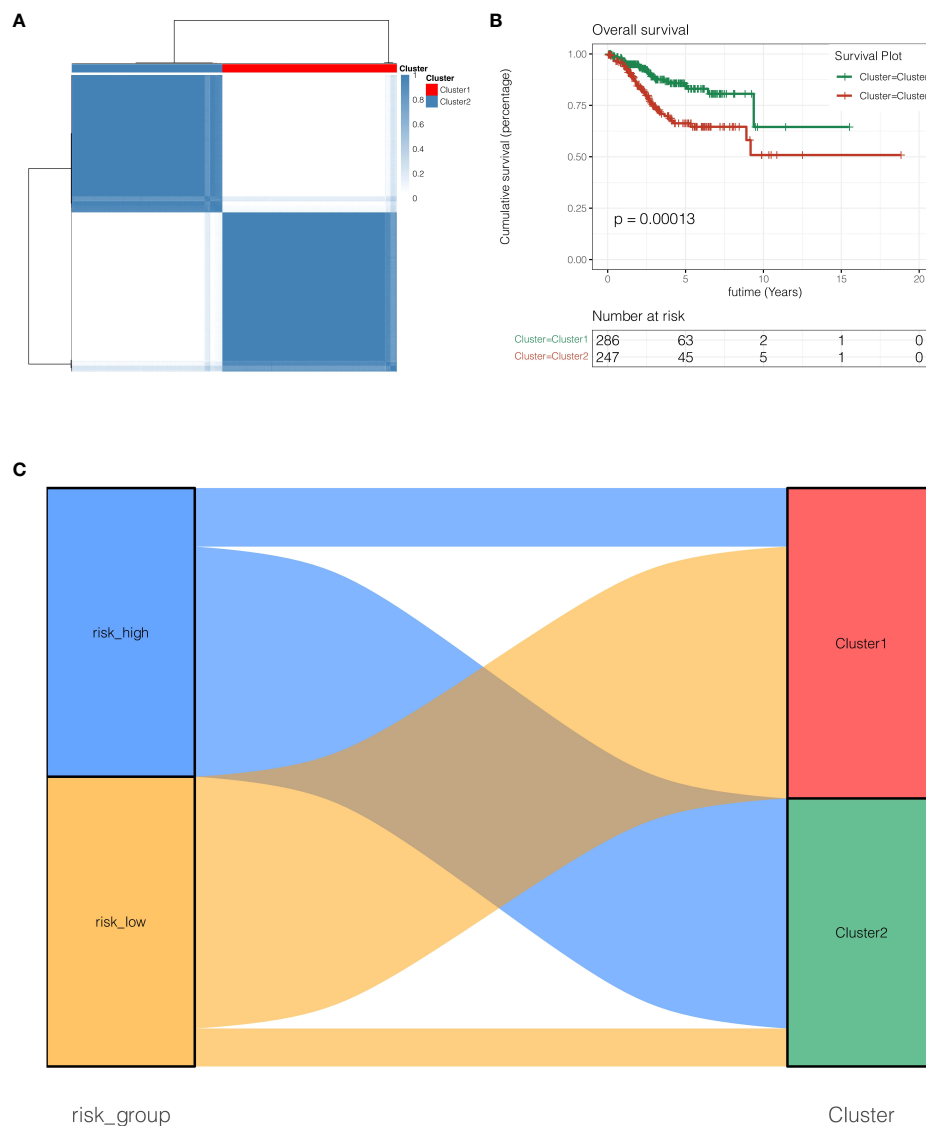


FIGURE 4

Unsupervised clustering analysis. (A) Unsupervised clustering clustered all endometrial cancer patients with two subgroups, Cluster1 and Cluster2. (B) the prognosis of Cluster2 was poorer than that of Cluster1 ($P < 0.001$). (C) Risk high group mostly belongs to Cluster2, and risk low group mainly corresponds to Cluster1.

Expression of model genes in cell subtypes

The expression of the four genes in the model was then studied at the single-cell level. As indicated in Figures 5A–D, EIF2S2 and PRELID1 genes are largely expressed in epithelial cells and endothelial cells, while NDUF9 and SNRPC genes are mainly expressed in epithelial cells, endothelial cells, fibroblasts and smooth muscle cells.

Immune infiltration analysis

To further study the reasons for the difference in prognosis between risk high and risk low groups, correlation analysis of immune infiltration was done. As indicated in Figure 6A, macrophage was found to be relatively infiltrated in the risk high group, whereas T cell was largely infiltrated in the risk low group. As indicated in Figure 6B, tumor necrosis factor (TNF)-related genes were generally significantly expressed in the risk

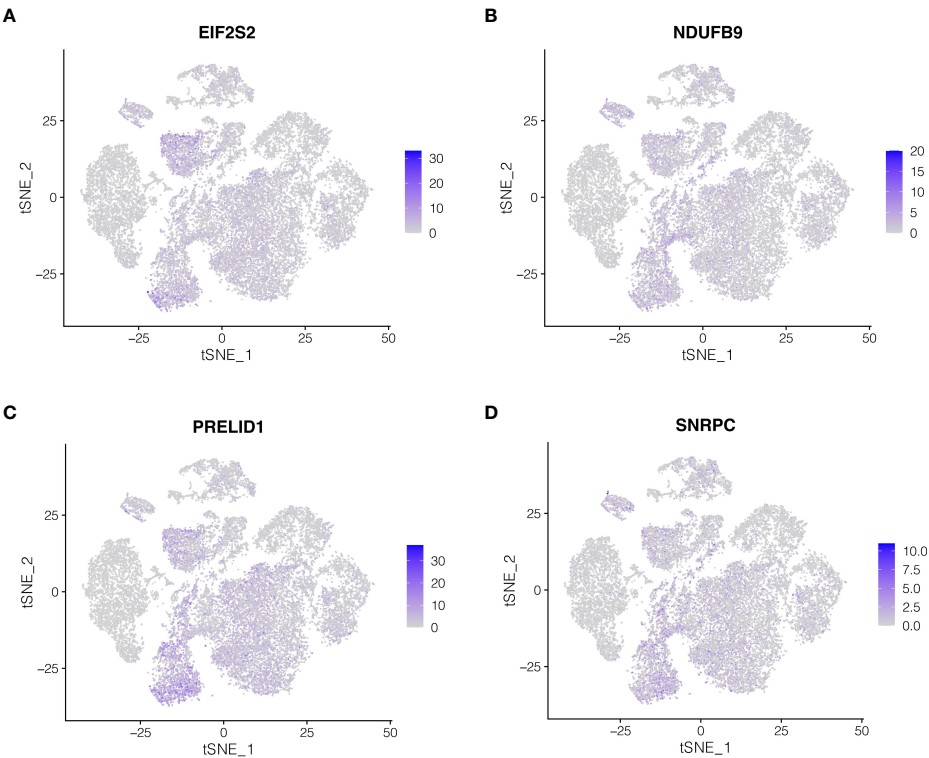


FIGURE 5 (A-D) Expression of model genes in cell subtypes.

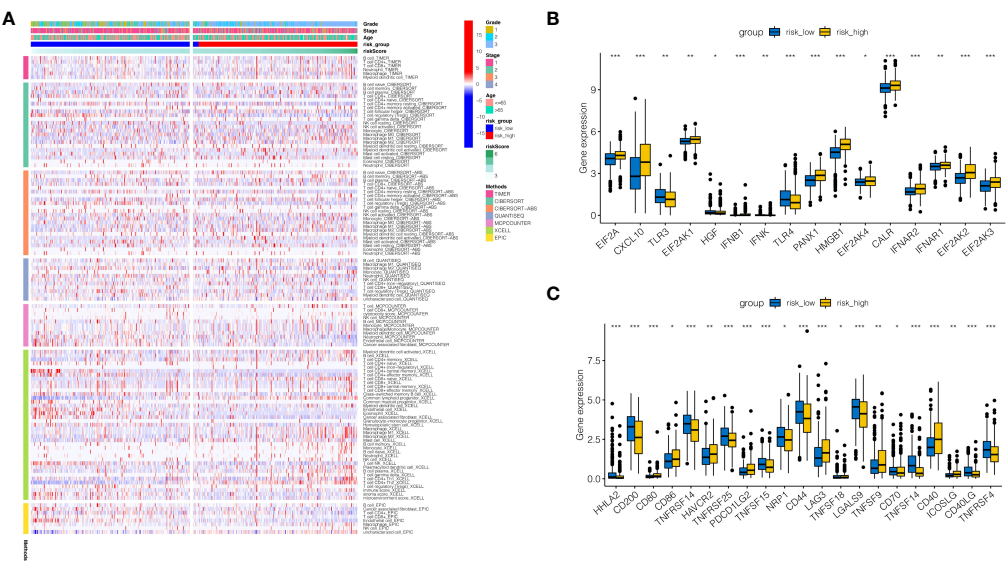


FIGURE 6 Immune infiltration analysis. (A) Immune infiltration landscape in high-risk and low-risk groups. (B) Tumor necrosis factor (TNF)-related genes were generally significantly expressed in the risk high group, such as EIF2A, CXCL10, and TLR3. (C) Immune checkpoint associated genes CD80, CD86, HAVCR2, PDCD1LG2, LAG3, TNFSF9, CD40, and ICOSLG were strongly expressed in RISK HIGH group. HHLA2, CD200, TNFRSF14, TNFRSF25, TNFSF15, NRP1, CD44, LGALS9, CD70, TNFSF14, CD40LG, and TNFRSF4 tended to be strongly expressed in risk low group. *P < 0.05, **P < 0.01, ***P < 0.001.

high group, such as EIF2A, CXCL10, and TLR3. As demonstrated in Figure 6C, immune checkpoint associated genes CD80, CD86, HAVCR2, PDCD1LG2, LAG3, TNFSF9, CD40, and ICOSLG were strongly expressed in RISK HIGH group. HHLA2, CD200, TNFRSF14, TNFRSF25, TNFSF15, NRP1, CD44, LGALS9, CD70, TNFSF14, CD40LG, and TNFRSF4 tended to be strongly expressed in risk low group.

The construction of a nomogram

In order to properly evaluate the prognosis of patients, the clinical data of patients and the risk score of the model were merged. As shown in Figure 7A, the 1, 3, and 5-year death rates of TCGA-BS-A0TE patients were 0.0814, 0.3110, and 0.4000, respectively. As shown in Figure 7B, continuous prognostic ROC analysis showed that the AUC of nomogram in determining the prognosis of patients was steady at around 0.8, which was better than other clinical indicators, such as age, stage and grade. As

shown in Figure 7C, decision curve analysis reveals that patients who make timely therapeutic decisions according to nomogram will benefit more than age, stage and grade.

PCR was used to verify the expression of model genes

Figure 8 displays the PCR findings. SNRPC, PRELID1, EIF2S2, and NDUFB9, four of the model's genes, were discovered to have higher levels of expression in endometrial cancer than in nearby tissues (Figures 8A–D, * $P < 0.05$, ** $P < 0.01$, *** $P < 0.001$).

Discussion

Endometrial cancer is the fourth most prevalent malignancy worldwide and the most common type of gynecologic cancer

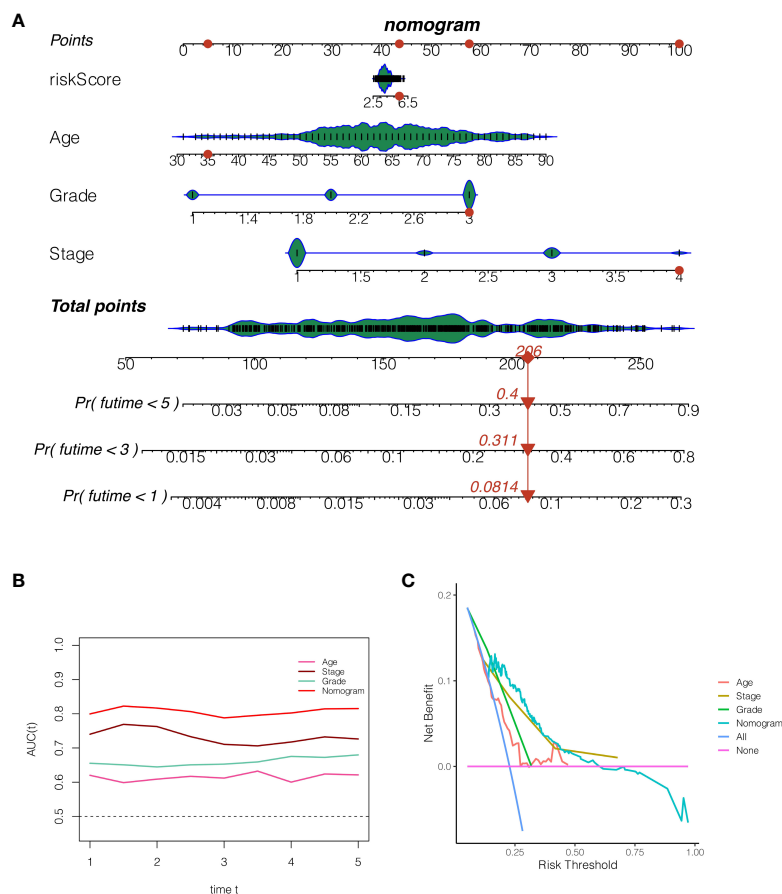


FIGURE 7

The construction of a nomogram. (A) The 1, 3, and 5-year death rates of TCGA-BS-A0TE patients were 0.0814, 0.3110, and 0.4000, respectively. (B) Continuous prognostic ROC analysis showed that the AUC of nomogram in determining the prognosis of patients was steady at around 0.8, which was better than other clinical indicators, such as age, stage and grade. (C) Decision curve analysis.

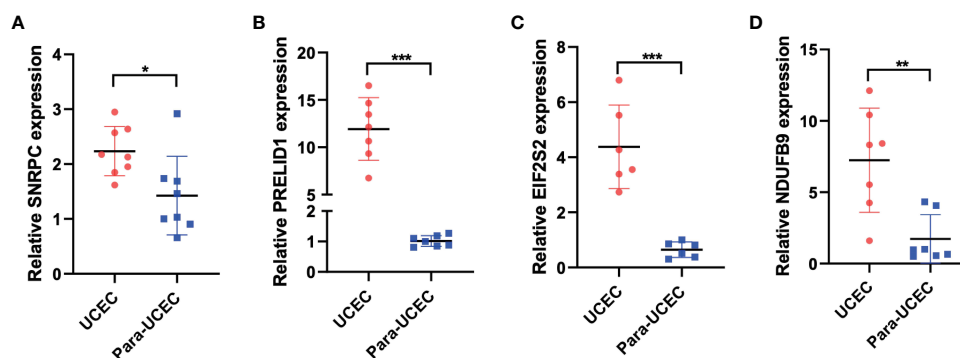


FIGURE 8

PCR was performed to verify the expression of model genes. (A–D) SNRPC, PRELID1, EIF2S2, and NDUFB9 were up-regulated in endometrial carcinoma. * $p < 0.05$; ** $p < 0.01$; *** $p < 0.001$.

harming women's health in affluent countries (13). Although most endometrial cancer patients are detected in the early stage because of vaginal bleeding, some individuals are still recognized late, typically accompanied by recurrence and metastasis, and the prognosis is dismal (14–16). For advanced, metastatic endometrial cancer, therapeutic choices are limited (17). Although developing targeted treatments and immunotherapies have been originally employed in the treatment of advanced endometrial cancer, low drug response and drug resistance are widespread, and many mechanisms of start and progression are still unexplained (18). It is of vital significance to research novel risk assessment methodologies and propose new biomarkers for endometrial cancer. Liquid-liquid phase separation (LLPS) was formerly thought to be involved in the development of membraneless intracellular organelles, and in recent years LLPS have been regarded to be highly relevant for many benign and malignant disorders (19–21). However, the significance of LLPS in endometrial cancer is not fully recognized. This study intends to explore the impact of LLPS-related genes in endometrial cancer.

In this investigation, a multiomics analysis was utilized to determine the expression, heterogeneity, prognostic value, and immunological evaluation value of LLPS-related genes in endometrial cancer. In order to explore the heterogeneity and activation status of LLPS in endometrial cancer, we first categorized endometrial cancer cells into several clusters using single-cell sequencing analysis. Based on this, we scored these cells and separated them into high-LLPS score groups and low-LLPS score groups. Genes that were differentially expressed between the two groups were also discovered. The heterogeneity of LLPS in endometrial cancer may be strongly correlated with these genes. The genes in this module were then believed to be strongly related with LLPS regulation in endometrial cancer after weighted co-expression network analysis (WGCNA) discovered green module that were highly

associated with LLPS in endometrial cancer. By crossing these genes with differentially expressed genes previously discovered by single-cell sequencing research, these genes were recognized as LLPS hub genes in endometrial cancer. These genes served as the foundation for a predictive model that was built using COX regression and Lasso regression and included EIF2S2, SNRPC, PRELID1, and NDUFB9. Endometrial cancer patients were split into high-risk and low-risk groups using this predictive model, with the high-risk group having a noticeably worse prognosis. Unsupervised cluster analysis provides additional evidence of the model's correctness. Between the high-risk group and the low-risk group, there were substantial differences in the amounts of immune cell infiltration and immune checkpoint gene expression, which may be a contributing factor to the different prognoses between the two groups and serve as a guide for immunotherapy.

According to certain studies, the four model genes EIF2S2, SNRPC, PRELID1, and NDUFB9 have significant roles in the development of cancer. The EIF2S2-LINC01600-MYC axis has been linked to the development and progression of tumors, according to Zhang et al (22). SNRPC, according to Zhang et al., can accelerate the development of hepatocellular carcinoma by triggering the epithelial-mesenchymal transition (23). Gillen and colleagues discovered that PRELID1's alternative polyadenylation controls mitochondrial ROS signaling and the development of cancer (24). According to Li et al., down-regulation of NDUFB9 caused breast cancer cells to proliferate and spread by modulating mitochondrial metabolism (25). Our study reveals the role of these genes in endometrial cancer and provides a reference for understanding the role of these genes in regulating LLPS.

The single-cell dataset used in our study, GSE173682, was published in 2021. In that original study, the authors constructed a single-cell landscape of human gynecologic tumors using

single-cell sequencing technology, revealing powerful heterogeneity in human gynecologic tumors (26). On this basis, we further analyzed the sequencing data and further explored the heterogeneity of LLPS in endometrial cancer, which provides a powerful reference for us to understand the pathogenesis and regulatory elements of endometrial cancer.

Currently, several bioinformatics signatures have been constructed in other tumors (27, 28). Qiu et al. constructed the signature of 11 LLPS-related genes in ovarian cancer by bioinformatics analysis, and accurately stratified the prognosis of ovarian cancer patients, among which patients in the high-risk group had significantly worse prognosis (29). And they found that LLPS-related genes were involved in several cancer-related pathways, such as MAPK signaling, cell cycle and DNA replication. Fang et al. constructed a signature composed of six LLPS-related genes in hepatocellular carcinoma by weighted co-expression network analysis and regression analysis to evaluate the prognosis and immune status of patients (30). Compared with these published studies, our study incorporated analysis of single-cell sequencing data and validated our conclusions using PCR assays with clinical samples. Our study can provide a reference for the diagnosis and treatment of endometrial cancer.

Conclusions

We constructed a novel LLPS-related signature in endometrial cancer to assess patient prognosis and immune status. However, we lack corresponding clinical cohort to evaluate the practicality and accuracy of this signature. We will improve it in the future.

Data availability statement

The original contributions presented in the study are included in the article/supplementary material. Further inquiries can be directed to the corresponding author.

References

1. Amant F, Moerman P, Neven P, Timmerman D, Van Limbergen E, Vergote I. Endometrial cancer. *Lancet* (2005) 366(9484):491–505. doi: 10.1016/S0140-6736(05)67063-8
2. Braun MM, Overbeek-Wager EA, Grumbo RJ. Diagnosis and management of endometrial cancer. *Am Fam Physician* (2016) 93(6):468–74.
3. Passarello K, Kurian S, Villanueva V. Endometrial cancer: An overview of pathophysiology, management, and care. *Semin Oncol Nurs* (2019) 35(2):157–65. doi: 10.1016/j.soncn.2019.02.002
4. Yen TT, Wang TL, Fader AN, Shih IM, Gaillard S. Molecular classification and emerging targeted therapy in endometrial cancer. *Int J Gynecol Pathol* (2020) 39(1):26–35. doi: 10.1097/PGP.0000000000000585
5. McDonald ME, Bender DP. Endometrial cancer: Obesity, genetics, and targeted agents. *Obstet Gynecol Clin North Am* (2019) 46(1):89–105. doi: 10.1016/j.ogc.2018.09.006
6. Chang Z, Talukdar S, Mullany SA, Winterhoff B. Molecular characterization of endometrial cancer and therapeutic implications. *Curr Opin Obstet Gynecol* (2019) 31(1):24–30. doi: 10.1097/GCO.0000000000000508

Ethics statement

The studies involving human participants were reviewed and approved by Ethics Committee of Huai 'an First People's Hospital. The patients/participants provided their written informed consent to participate in this study.

Author contributions

JW designed the study. JW and FMe were involved in database search and statistical analyses. JW, FMe and FMA were involved in the writing of manuscript and its critical revision. All authors were responsible for the submission of the final version of the paper. All authors approved the final version. All authors agree to be accountable for all aspects of the work.

Acknowledgments

We are very grateful for data provided by databases such as TCGA, GEO.

Conflict of interest

The authors declare that the research was conducted in the absence of any commercial or financial relationships that could be construed as a potential conflict of interest.

Publisher's note

All claims expressed in this article are solely those of the authors and do not necessarily represent those of their affiliated organizations, or those of the publisher, the editors and the reviewers. Any product that may be evaluated in this article, or claim that may be made by its manufacturer, is not guaranteed or endorsed by the publisher.

7. Clarke MA, Long BJ, Del Mar Morillo A, Arbyn M, Bakkum-Gamez JN, Wentzensen N. Association of endometrial cancer risk with postmenopausal bleeding in women: A systematic review and meta-analysis. *JAMA Intern Med* (2018) 178(9):1210–22. doi: 10.1001/jamainternmed.2018.2820
8. Zhang H, Ji X, Li P, Liu C, Lou J, Wang Z, et al. Liquid-liquid phase separation in biology: Mechanisms, physiological functions and human diseases. *Sci China Life Sci* (2020) 63(7):953–85. doi: 10.1007/s11427-020-1702-x
9. Mehta S, Zhang J. Liquid-liquid phase separation drives cellular function and dysfunction in cancer. *Nat Rev Cancer* (2022) 22(4):239–52. doi: 10.1038/s41568-022-00444-7
10. Nozawa RS, Yamamoto T, Takahashi M, Tachiwana H, Maruyama R, Hirota T, et al. Nuclear microenvironment in cancer: Control through liquid-liquid phase separation. *Cancer Sci* (2020) 111(9):3155–63. doi: 10.1111/cas.14551
11. Lu B, Zou C, Yang M, He Y, He J, Zhang C, et al. Pharmacological inhibition of core regulatory circuitry liquid-liquid phase separation suppresses metastasis and chemoresistance in osteosarcoma. *Adv Sci (Weinh)* (2021) 8(20):e210189. doi: 10.1002/advs.202101895
12. Igelmann S, Lessard F, Ferbeyre G. Liquid-liquid phase separation in cancer signaling, metabolism and anticancer therapy. *Cancers (Basel)* (2022) 14(7):1830. doi: 10.3390/cancers14071830
13. Makker V, MacKay H, Ray-Coquard I, Levine DA, Westin SN, Aoki D, et al. Endometrial cancer. *Nat Rev Dis Primers* (2021) 7(1):88. doi: 10.1038/s41572-021-00330-w
14. Terzic M, Aimagambetova G, Kunz J, Bapayeva G, Aitbayeva B, Terzic S, et al. Molecular basis of endometriosis and endometrial cancer: Current knowledge and future perspectives. *Int J Mol Sci* (2021) 22(17):9274. doi: 10.3390/ijms22179274
15. Luna C, Balcacer P, Castillo P, Huang M, Alessandrino F. Endometrial cancer from early to advanced-stage disease: an update for radiologists. *Abdom Radiol (NY)* (2021) 46(11):5325–36. doi: 10.1007/s00261-021-03220-7
16. Emons G, Vordermark D. Adjuvant treatment for endometrial cancer. *Curr Opin Oncol* (2019) 31(5):404–10. doi: 10.1097/CCO.0000000000000558
17. Sorosky JL. Endometrial cancer. *Obstet Gynecol* (2008) 111(2 Pt 1):436–47. doi: 10.1097/AOG.0b013e318162f690
18. De Felice F, Marchetti C, Tombolini V, Panici PB. Immune check-point in endometrial cancer. *Int J Clin Oncol* (2019) 24(8):910–6. doi: 10.1007/s10147-019-01437-7
19. Meng F, Yu Z, Zhang D, Chen S, Guan H, Zhou R, et al. Induced phase separation of mutant NF2 imprisons the cGAS-STING machinery to abrogate antitumor immunity. *Mol Cell* (2021) 81(20):4147–4164.e7. doi: 10.1016/j.molcel.2021.07.040
20. Rubio K, Dobersch S, Barreto G. Functional interactions between scaffold proteins, noncoding RNAs, and genome loci induce liquid-liquid phase separation as organizing principle for 3-dimensional nuclear architecture: implications in cancer. *FASEB J* (2019) 33(5):5814–22. doi: 10.1096/fj.201802715R
21. Zhang X, Vigers M, McCarty J, Rauch JN, Fredrickson GH, Wilson MZ, et al. The proline-rich domain promotes tau liquid-liquid phase separation in cells. *J Cell Biol* (2020) 219(11):e202006054. doi: 10.1083/jcb.202006054
22. Zhang J, Li S, Zhang L, Xu J, Song M, Shao T, et al. RBP EIF2S2 promotes tumorigenesis and progression by regulating MYC-mediated inhibition via FHIT-related enhancers. *Mol Ther* (2020) 28(4):1105–18. doi: 10.1016/j.yymthe.2020.02.004. Erratum in: *Mol Ther*. 2021 Feb 3;29(2):886.
23. Zhang Y, Qiu J, Zuo D, Yuan Y, Qiu Y, Qiao L, et al. SNRPC promotes hepatocellular carcinoma cell motility by inducing epithelial-mesenchymal transition. *FEBS Open Bio* (2021) 11(6):1757–70. doi: 10.1002/2211-5463.13175
24. Gillen AE, Brechbuhl HM, Yamamoto TM, Kline E, Pillai MM, Hesselberth JR, et al. Alternative polyadenylation of PRELID1Regulates mitochondrial ROS signaling and cancer outcomes. *Mol Cancer Res* (2017) 15(12):1741–51. doi: 10.1158/1541-7786.MCR-17-0010
25. Li LD, Sun HF, Liu XX, Gao SP, Jiang HL, Hu X, et al. Down-regulation of NDUFB9 promotes breast cancer cell proliferation, metastasis by mediating mitochondrial metabolism. *PLoS One* (2015) 10(12):e0144441. doi: 10.1371/journal.pone.0144441
26. Regner MJ, Wisniewska K, Garcia-Recio S, Thennavan A, Mendez-Giraldez R, Malladi VS, et al. A multi-omic single-cell landscape of human gynecologic malignancies. *Mol Cell* (2021) 81(23):4924–4941.e10. doi: 10.1016/j.molcel.2021.10.013
27. Liu J, Cui G, Shen S, Gao F, Zhu H, Xu Y. Establishing a prognostic signature based on epithelial-mesenchymal transition-related genes for endometrial cancer patients. *Front Immunol* (2022) 12:805883. doi: 10.3389/fimmu.2021.805883
28. Liu J, Geng R, Ni S, Cai L, Yang S, Shao F, et al. Pyroptosis-related lncRNAs are potential biomarkers for predicting prognoses and immune responses in patients with UCEC. *Mol Ther Nucleic Acids* (2022) 27:1036–55. doi: 10.1016/j.omtn.2022.01.018
29. Qiu Y, Pan M, Chen X. A liquid-liquid phase separation-related gene signature as prognostic biomarker for epithelial ovarian cancer. *Front Oncol* (2021) 11:671892. doi: 10.3389/fonc.2021.671892
30. Fang ZS, Zhang Z, Liang ZJ, Long ZR, Xiao Y, Liang ZY, et al. Liquid-liquid phase separation-related genes associated with tumor grade and prognosis in hepatocellular carcinoma: A bioinformatic study. *Int J Gen Med* (2021) 14:9671–9. doi: 10.2147/IJGM.S342602



OPEN ACCESS

EDITED BY
Jinhui Liu,
Nanjing Medical University, China

REVIEWED BY
Yuchen Liu,
Shenzhen University, China
Xiao Hu,
University of Chinese Academy of
Sciences, China

*CORRESPONDENCE
Shuguang Zhou
zhoushuguang@ahmu.edu.cn

[†]These authors have contributed
equally to this work and share
first authorship

SPECIALTY SECTION
This article was submitted to
Gynecological Oncology,
a section of the journal
Frontiers in Oncology

RECEIVED 03 August 2022
ACCEPTED 30 August 2022
PUBLISHED 16 September 2022

CITATION
Zhang W, Cao W, Tong Z, Jin Q,
Jiang X, Yang Y, Yao H, Chen G,
Gao W, Zhu Y and Zhou S (2022)
Identification and validation of a
novel necroptosis-related
prognostic signature in cervical
squamous cell carcinoma and
endocervical adenocarcinoma.
Front. Oncol. 12:1011000.
doi: 10.3389/fonc.2022.1011000

COPYRIGHT
© 2022 Zhang, Cao, Tong, Jin, Jiang,
Yang, Yao, Chen, Gao, Zhu and Zhou.
This is an open-access article
distributed under the terms of the
Creative Commons Attribution License
(CC BY). The use, distribution or
reproduction in other forums is
permitted, provided the original
author(s) and the copyright owner(s)
are credited and that the original
publication in this journal is cited, in
accordance with accepted academic
practice. No use, distribution or
reproduction is permitted which does
not comply with these terms.

Identification and validation of a novel necroptosis-related prognostic signature in cervical squamous cell carcinoma and endocervical adenocarcinoma

Weiye Zhang^{1,2†}, Wujun Cao^{3†}, Zhuting Tong^{4†}, Qinqin Jin^{1,2},
Xiya Jiang^{1,2}, Yinting Yang^{1,2}, Hui Yao^{1,2}, Guo Chen^{1,2},
Wei Gao^{1,2}, Yuting Zhu^{1,2} and Shuguang Zhou^{1,2*}

¹Department of Gynecology, Anhui Medical University Affiliated Maternity and Child Healthcare Hospital, Hefei, China, ²Department of Gynecology, Anhui Province Maternity and Child Healthcare Hospital, Hefei, China, ³Department of Clinical Laboratory, Anhui Province Maternity and Child Healthcare Hospital, Hefei, China, ⁴Department of Radiation Oncology, The First Affiliated Hospital of Anhui Medical University, Hefei, China

Background: The purpose of this study was to investigate the prognostic signature of necroptosis-related lncRNAs (NRLs) and explore their association with immune-related functions and sensitivity of the therapeutic drug in cervical squamous cell carcinoma and endocervical adenocarcinoma (CESC).

Methods: UCSC Xena provided lncRNA sequencing and clinical data about CESC, and a necroptosis gene list was obtained from the KEGG database. NRLs were selected by structuring a co-expression network of lncRNAs and necroptosis-related genes. To further screen lncRNAs, we used the univariate Cox regression method, Lasso regression, and multivariate Cox regression. Afterward, an NRL signature was established. We used the xCell algorithm and single-sample gene set enrichment analysis (ssGSEA) to clarify the pertinence between immune infiltration and NRL expressions in CESC patients and explored the relationship between the target lncRNAs and immune-related genes. By leveraging the GDSC database, the therapy-sensitive response of the prognostic signature was forecasted and an experimental validation was performed. We performed GSEA with the aim of recognizing the potential pathway related to the individual prognostic signature.

Results: The two prognostic NRLs (AC009095.1 and AC005332.4) showed significant diversity and constituted the NRL signature. On the grounds of our signature, risk score was an independent element which was bound up with patient outcome (HR = 4.97 CI: 1.87–13.2, P = 0.001). The CESC patients were classified by the median risk score. Immune infiltration analysis revealed significant increases in CD4 + Tcm, eosinophils, epithelial cells, fibroblasts,

NKT, plasma cells, platelets, and smooth muscle in the high-risk group ($P < 0.05$). Target lncRNAs also showed some correlation with NRGs. The estimated IC50 values of bicalutamide, CHIR.99021, and imatinib were lower in the high-risk group. Through the subsequent experimental validation, both AC009095.1 and AC005332.4 were significantly more highly expressed in SiHa than in Hela. AC009095.1 was expressed more highly in SiHa than in HUCEC, but the expression of AC005332.4 was reversed.

Conclusions: This study elucidated that NRLs, as a novel signature, were indispensable factors which can significantly influence the prognosis of patients with CESC and could provide novel clinical evidence to serve as a potential molecular biomarker for future therapeutic targets.

KEYWORDS

long noncoding RNA (lncRNA), necroptosis-related lncRNAs (NRLs), prognostic signature, immune, therapeutic agents, cervical squamous cell carcinoma and endocervical adenocarcinoma (CESC)

Introduction

Cervical squamous cell carcinoma and endocervical adenocarcinoma (CESC) have become two of the most leading cancer types in gynecology all over the world. With the invention of the human papillomavirus (HPV) vaccine, widespread adoption of CESC screening, and advancement in integrated therapy, the incidence of CESC exhibits a downward trend (1). However, even so, CESC continues to be a severe health problem among women and the mortality rates increase worldwide each year (2). Because of the deficiency of specificity and sensitivity, carbohydrate antigen 125 (CA125) and squamous cell carcinoma antigen, which belong to common clinical serum tumor biomarkers, were limited applications in clinical practice. In order to reduce morbidity and improve prognosis, we need neoteric, trustworthy, effective, and non-invasive tumor biomarkers (3).

Necroptosis, as a mode of programmed cell death, is triggered by RIPK1, RIPK3, and MLKL (4). Necroptosis was reported to participate in oncogenesis, cancer immunity, and metastasis (5). In CESC, RETRA (REactivation of Transcriptional Reporter Activity) induces necroptosis and increases ROS production (6), while RIPK3 expression is necessary for PolyIC-induced necroptosis (7). In addition, the low necroptosis process may predict poor prognosis in HPV-positive cervical cancers (8).

Long non-coding RNA (lncRNA) is one of numerous RNAs. Most lncRNAs do not participate in the protein translation process but take part in regulation of the gene expression at the transcriptional or posttranscriptional level (9). There are studies that have detected a close relation between necroptosis and

lncRNAs (10). Necroptosis-related factors are involved in the ischemia-reperfusion process, and their main role is the regulation of programmed necrosis and myocardial injury (11). More recently, necroptosis-related lncRNAs (NRLs) have been extensively explored in predicting prognosis and immunotherapy response in breast cancer (12), colon cancer (13), gastric cancer (14), lung adenocarcinoma (15), and stomach adenocarcinoma (16). However, in fact, it remains to elucidate the potential role of NRLs in CESC.

In our research, we identified necroptosis-related lncRNAs of CESC and developed a risk model, with hopes of contributing helpful insights into the prognostic prediction and potential drug selection of CESC.

Methods and materials

Sample and data acquisition

UCSC Xena (<http://xena.ucsc.edu/>) provided the RNA sequencing (RNA-seq) data about CESC. The expression of normalized genes was detected as a single per million mapped reads per kilobase transcript fragment and \log^2 -based transformation. The inclusion standard was listed as follows: (1) patients diagnosed with CESC; (2) patients with integrated lncRNA data and clinic information. On the basis of the inclusion criteria, 296 patients diagnosed with CESC were incorporated. In addition to that, TCGA database provided integrated clinic information for the patients. When filtrating clinic information, samples were abandoned which were less than 30 days of follow-up. The approval from the ethics

committee was not required because TCGA database supplied all clinical data related to this study and strictly adhered to the publication guidelines of TCGA database (<http://cancergenome.nih.gov/abouttcga/policies/publicationguidelines>).

Extraction of NRGs and lncRNAs

All data for lncRNAs were obtained from the RNA-seq data. Moreover, log₂ transformation was utilized to normalize the total RNA expression data. The necroptosis gene list was obtained from the Kyoto Encyclopedia of Genes and Genomes (KEGG, <https://www.genome.jp/kegg>). Furthermore, the GENCODE (https://www.encodegenes.org/human/release_23.html) database provided NRG information. The pertinence between lncRNAs and NRGs was determined by the Pearson correlation method. The lncRNAs relevant to necroptosis are the square of correlation coefficient $|R^2| > 0.5$ and $P < 0.001$.

Structure of the prognostic signature belonging to the NRLs

First of all, the prognostic value was evaluated by univariate Cox regression. Least Absolute Shrinkage and Selection Operator (Lasso) regression was applied to test the NRLs with $P < 0.01$ from the univariate analysis results. After that, the genes that were screened out by LASSO regression were admitted to a multivariate Cox model to calculate risk scores. We also calculated the risk model calculated as follows:

$$\text{risk scores} = \sum (\beta_i \times \text{Exp}_i)$$

in which β_i refers to the coefficients indicating the weight of each signature and Exp_i indicates the expression of each signature. The patients meeting the inclusion criteria were classified on the basis of the median risk score. The log-rank statistical test was exploited to contrast the survival differences.

Validation of prognostic signature

The individual prognostic signature model was built to validate prognostic features by adopting the Cox regression method. Time-dependent ROC curves were utilized to appraise the efficacy of our signature for predicting prognostic features. Moreover, these methods, which included decision curve analysis (DCA) and calibration curves, were applied to make a thorough inquiry into the accuracy of the signature model. Beyond that, we included demographic data and risk scores into the multivariate Cox regression and tested if they were independent elements which were bound up with patients' prognosis.

Extrapolation of immune-infiltrating cells in CESC

We exploited the R package "xCell" and single-sample gene set enrichment analysis (ssGSEA) with the aim of quantifying the abundance of immune cells in CESC patients. GSEA is a gene set-based enrichment analysis method which first determines the purpose of the analysis and then ranks based on the size of the association of the gene expression data and the phenotype (also understood as changes in expression). ssGSEA permits to define an enrichment score representing gene set absolute enrichment in each sample in a given dataset. ssGSEA was achieved by the R package "GSVA", which estimated the integrated levels of immune cell types. xCell estimated the comprehensive levels of common immune cell types. xCell is an analytical approach on account of the gene signature, which integrates both the RNA-seq and microarray data and integrates the deconvolution approaches and advantages of the gene set enrichment. According to the ssGSEA and xCell instructions, gene expression profiles were prepared and the R package was run. At the same time, permutation was performed by using ssGSEA and xCell signatures. On the other hand, we used CAMOIP (17) (<http://www.camoip.net>) to analyze the association between target lncRNAs and immune-related genes with boxplots using the Mann-Whitney U test.

Prediction of the sensitivity response to therapeutic agents

The sensitivity response to therapeutic agents of CESC patients was forecasted in the light of the data derived from Genomics of Drug Sensitivity in Cancer (GDSC; <https://www.cancerrxgene.org>). The half-maximal inhibitory concentration (IC₅₀) was calculated through the R package "pRRophetic".

Gene set enrichment analysis

GSEA was exploited to discover the distinct enriched term with the aim of recognizing the potential pathway. By using the relevant database, CAMOIP (17) (<http://www.camoip.net>), the CESC patients grouped in line with the expression of the relevant lncRNA, then the enrichment analysis was performed.

Cell lines

SiHa and Hela were human cervical cancer cell lines. SiHa was a cell line of cervical squamous cell carcinoma, and Hela was

a cell line of cervical adenocarcinoma. They were used as the test group. HUCEC was a cell line of normal cervical, and PANC-1 was a cell line of pancreatic cancer. HUCEC cell lines were used as negative control groups and PANC-1 cell lines as a positive control group. All of them were obtained from Shanghai FuHeng Biotechnology company (Shanghai, China). We used DMEM contained with 10% FBS (Gibco, Grand Island, NY) to incubate SiHa and Hela cells. Then, we used RPMI 1640 supplementing 10% FBS (Gibco, Grand Island, NY) to incubate HUCEC and PANC-1 cells. Cells are cultured in an incubator at 37°C with 5% CO₂.

Quantitative real-time polymerase chain reaction

We used TRIzol Reagent (Invitrogen, Carlsbad, CA) to collect and lyse cells. Then, RNA cDNA first-strand synthesis kit (TransGen Biotech, Beijing, China) was utilized to obtain cDNA. Real-time PCR was performed with One Step RT-qPCR Kit (Sangon Biotech, Shanghai, China), and quantitative real-time polymerase chain reaction (qRT-PCR) was carried out as follows: 95°C for 3 min, and then 45 cycles of 95°C for 7 s, 57°C for 10 s, and 72°C for 15 s. The internal reference was the glyceraldehyde-3-phosphate dehydrogenase (GAPDH) gene. Information of primers is shown in Table 1.

Statistical analysis

The survival curve was produced by means of the Kaplan–Meier method, which was detected by log-rank test. The effects, which were of necroptosis-related lncRNA signature and clinicopathological data on prognostic outcomes, were estimated by means of Cox regression and Lasso regression. This study’s statistical analysis was performed by adopting the R language (version 4.1.3 and version 4.2.0). Moreover, the bilateral test had statistical significance with $P \leq 0.01$.

TABLE 1 PCR primers used in this study.

Primer name	Primer type	Primer sequence (5′→3′)
AC009095.1	Forward	GAGAAAGGCESCCTGCATAAGCG
	Reverse	GCESCTAATGGAACTCESCTGCESC
AC005332.4	Forward	AATGCGAGGGCAGCATCAAGT
	Reverse	AGAGAGAGCGAGCGAGTGTA
GAPDH	Forward	GGAGCGAGATCESCCTCESCAAAAT
	Reverse	GGCTGTTGTCTACTTCTCATGG

Results

Reconstruction of a co-expression network of NRGs and lncRNAs

We identified 18,016 lncRNAs in TCGA-CESC, and we obtained 159 genes related to necroptosis. In the NRGs, 133 genes were expressed in TCGA-CESC (Table S1). Furthermore, a lncRNA co-expression network relevant to NRGs was constructed with the aim of identifying the necroptosis-related lncRNAs. Finally, we selected 2,508 lncRNAs associated with necroptosis ($|R^2| > 0.5$ and $P < 0.001$, Table S2).

Appraisal of the prognostic signature relevant to NRLs

There were 36 NRLs meaningful for the patient outcome ($P < 0.01$, Table S3) after the univariate Cox analysis. After Lasso regression, 15 lncRNAs associated with necroptosis were filtrated (Figures 1A, B; Table S4). By using multivariate Cox regression analysis, AC009095.1 and AC005332.4 were discovered to be independent prognostic indicators. Amid two lncRNAs, there was a deleterious prognostic indicator which was named AC009095.1. On the other hand, AC005332.4 was a beneficial prognostic indicator (Table 2). Therefore, we took advantage of these two lncRNAs to set up a signature of NRLs. Moreover, we formulated the risk scores as hereunder mentioned: Risk score = $(0.3857532 \times \text{expression value of AC009095.1} - 0.3954274 \times \text{expression value of AC005332.4})$.

The evaluation of the prognosis by the established signature

By means of the analysis of the survival curves, we could conclude that risk scores were observably relevant to overall survival (OS). Moreover, the high-risk group had shorter OS ($P < 0.001$, log-rank test) (Figure 2). Meanwhile, Cox regression

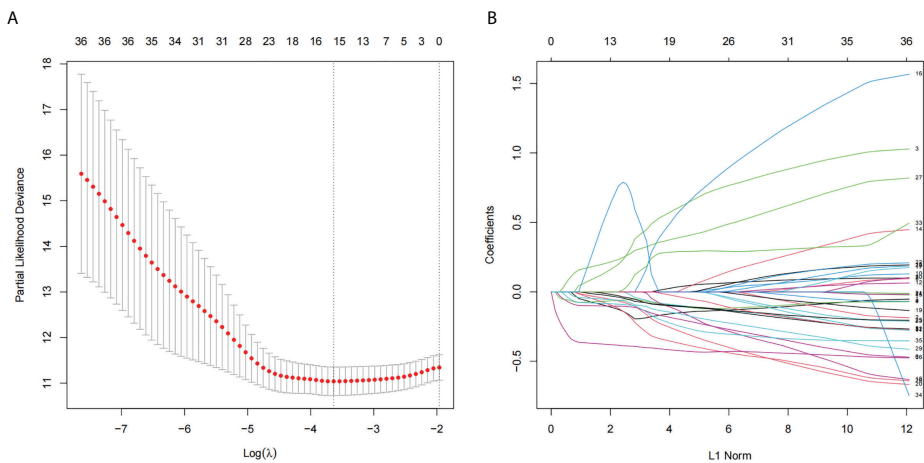


FIGURE 1
The lncRNAs related to necroptosis were screened by using the Lasso: **(A)** Lasso coefficient values for 36 NRLs in CSEC. The vertical dashed line is in the minimal log (lambda) value. **(B)** The overview of Lasso coefficients.

results pointed that risk scores had pivotal differences between the two groups (Figure 3).

Clinical application of the signature relevant to necroptosis-related lncRNAs

Using results from the multivariate Cox regression, it was not difficult to conclude that the Pathologic_N stage and risk score were isolated elements determining prognosis, which were with a HR risk score of 4.97 (95% CI: 1.87–13.2, $P = 0.001$, Figure 4A). Meanwhile, the areas under the ROC curves were respectively 0.735, 0.721, and 0.701, which corresponded to 1, 3, and 5 years of existence (Figure 4B). Beyond these, we also made the nomogram consisting of Pathologic_N staging and risk score. Also, Pathologic_N staging and risk score had the greatest effect on OS of 1, 3, and 5 years for patients with CESC as exhibited in the nomogram (Figure 5A). Furthermore, in comparison with the perfect pattern in the whole cohort, the calibration charts were well forecasted (Figure 5B). The results of DCA of three diverse survival rates also demonstrated that the nomogram had high potential for clinical application (Figures 5C–E).

Immune cell type expression between two groups

The ssGSEA results indicated that 20 immune cells were different in two groups, and all had a higher expression in the group with lower risk scores (Figure 6A). The xCell algorithm results revealed that 32 immune cells were different and the expression of eight immune cells were higher in the group with higher risk scores. They were respectively $CD4^+$ Tcm ($p = 6.49 \times 10^{-3}$), eosinophils ($p = 7.32 \times 10^{-3}$), epithelial cells ($p = 7.45 \times 10^{-3}$), fibroblasts ($p = 1.81 \times 10^{-2}$), NKT ($p = 3.65 \times 10^{-2}$), plasma cells ($p = 1.47 \times 10^{-2}$), platelets ($p = 3.5 \times 10^{-4}$), and smooth muscle ($p = 5.26 \times 10^{-4}$) (Figure 6B).

The expression of immune-related genes in the high- and low-expression groups of target lncRNAs

We used the CAMOIP database to analyze the expression of immune-related genes in different groups of two lncRNAs. After screening, 19 immune-related genes were statistically differently expressed in different groups of two lncRNAs (Figure 7A,

TABLE 2 The results of lncRNAs on account of TCGA CESC data after the multivariate Cox regression.

lncRNA name	Gene name	coef	exp(coef)	se(coef)	Z score	Pr(> z)
AC009095.1	FTL	0.3857532	1.4707216	0.1812545	2.128241	0.03331709
AC005332.4	BCL2	-0.3954274	0.6733922	0.1690220	-2.339502	0.01930946

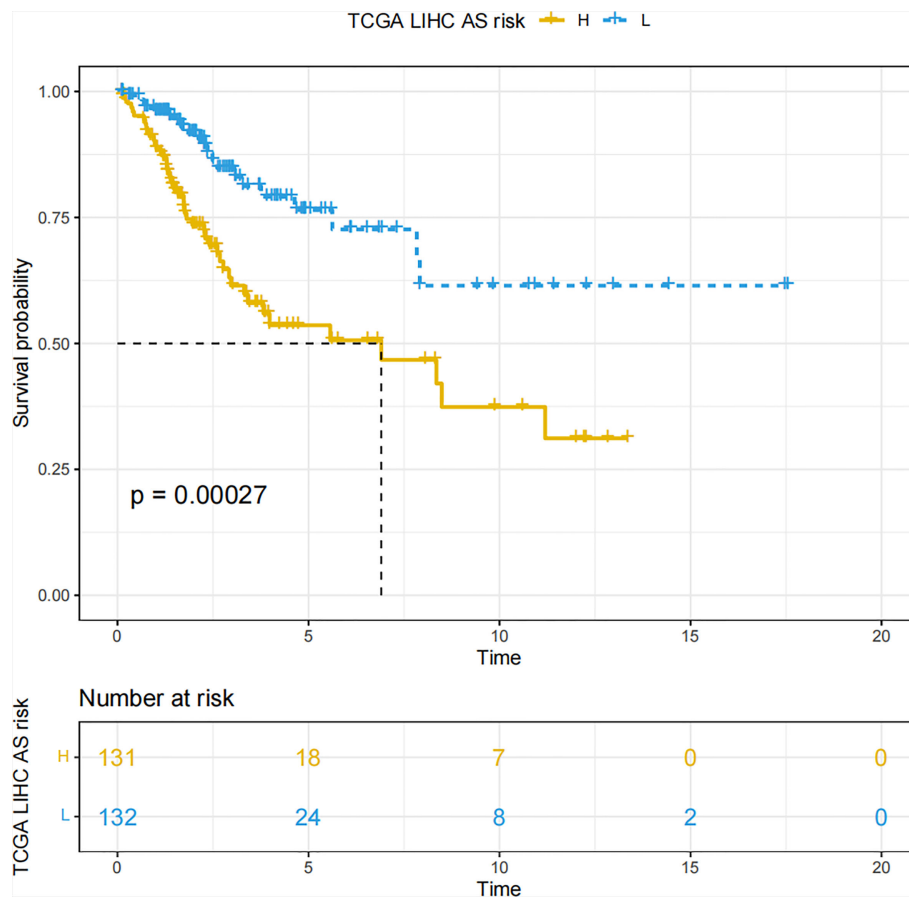


FIGURE 2
The Kaplan–Meier survival curves which are on account of the two NRLs' risk scores.

Figure 7B). These immune genes were ADORA2A, BANK1, BTN3A1, CD68, CD70, CD160, FCRL1, FUCA1, GPR15, HSD17B11, IL12A, MEGF9, TM4SF19, TNFRSF14, TNFSF9, TNFSF15, TRANK1, VEGFA, and VTCN1. It was found that CD68, CD160, TM4SF19, and TNFSF15 were all expressed more highly in the low expression group of two lncRNAs. However, for VEGFA in AC009095.1 groups, the expression was higher in the high expression group, and in AC005332.4 groups, the expression was higher in the low expression group. The remaining immune-related genes were all more highly expressed in the high expression group of two lncRNAs.

The prediction of the signature for response to therapeutic agents

The GDSC database was utilized to foretell the sensitivity reaction to therapeutic agents of the prognostic signature to frequently used therapeutic agents. Between the two groups,

there were 21 therapeutic agents that varied significantly in IC50. The estimated IC50 values of 18 therapeutic agents were higher in the high-risk group (Figure 8A), which incorporated ATRA ($p = 6.760884 \times 10^{-3}$), AZD.2281 ($p = 2.005571 \times 10^{-3}$), bortezomib ($p = 3.735047 \times 10^{-3}$), camptothecin ($p = 1.488292 \times 10^{-3}$), cyclopamine ($p = 9.461664 \times 10^{-3}$), metformin ($p = 1.010847 \times 10^{-8}$), methotrexate ($p = 1.084060 \times 10^{-3}$), MG.132 ($p = 1.134804 \times 10^{-3}$), MK.2206 ($p = 2.074208 \times 10^{-5}$), MS.275 ($p = 2.164303 \times 10^{-3}$), NVP.BEZ235 ($p = 7.133138 \times 10^{-3}$), rapamycin ($p = 7.098552 \times 10^{-3}$), roscovitine ($p = 1.194509 \times 10^{-3}$), salubrinal ($p = 3.341819 \times 10^{-7}$), sunitinib ($p = 4.200432 \times 10^{-4}$), temsirolimus ($p = 5.940194 \times 10^{-5}$), vinblastine ($p = 1.407201 \times 10^{-3}$), and VX.680 ($p = 9.917475 \times 10^{-3}$). On the contrary, the estimated IC50 values of bicalutamide ($p = 1.063005 \times 10^{-4}$), CHIR.99021 ($p = 1.045556 \times 10^{-5}$), and imatinib ($p = 1.654762 \times 10^{-5}$) were lower in the high-risk group (Figure 8B). This implied that bicalutamide, CHIR.99021, and imatinib had stronger sensitivity to patients with higher risk scores. The remaining therapeutic agents indicated stronger sensitivity to patients with lower risk scores.

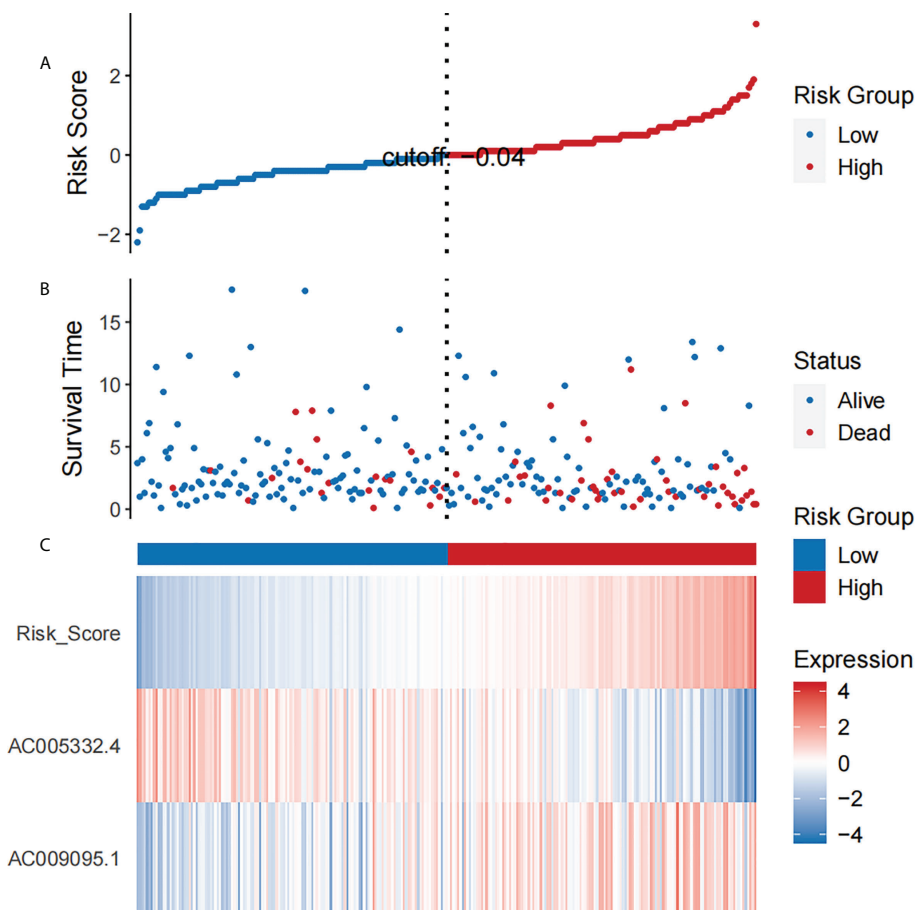


FIGURE 3
The analysis results which belong to CESC patients' NRL signature. **(A)** The risk scores which belong to two groups. **(B)** The CESC patients' survival time. **(C)** Heat map of the expression of the two NRLs and risk scores. The upward trend from low to high levels respectively corresponds to the colors which are from green to red.

Results of the GSEA

The CESC patients were grouped according to lncRNA expression levels in the CAMOIP database. We performed GSEA and obtained the following results. The top 10 pathways with the enrichment scores in the results of enrichment analysis regarding AC009095.1 are respectively termination of O-glycan biosynthesis, O-glycan processing, defective C1GALT1C1-caused Tn polyagglutination syndrome (TNPS), axoneme, oligosaccharide binding, ciliary plasm, defective GALNT3-caused familial hyperphosphatemic tumoral calcinosis (HFTC), defective GALNT12 causes colorectal cancer 1 (CRCS1), O-linked glycosylation of mucins, and axoneme assembly (Figure 9A). The top 10 pathways with the enrichment scores in the results of enrichment analysis regarding AC005332.4 are respectively T-cell receptor complex, immunoglobulin complex, intrinsic component of postsynaptic density membrane, postsynaptic density

membrane, integral component of postsynaptic density membrane, postsynaptic specialization membrane, plasma membrane signaling receptor complex, antigen binding, B-cell receptor signaling pathway, and immunoglobulin complex or circulating (Figure 9B). Subsequently, enrichment analysis was performed again in line with three aspects of functional enrichment analysis, cellular component (GO-CC), molecular function (GO-MF), and biological processes (GO-BP). In terms of biological processes, AC009095.1 was mainly enriched in the oxidative phosphorylation, nonsense-mediated decay, translational initiation, cytoplasmic translation, translation, peptide metabolic process, and the pathways related to RNA catabolism (Figure 10A). AC005332.4 was mainly enriched in keratinization, ribosome biogenesis, cornification, keratinocyte differentiation, epidermal cell differentiation, skin development, adaptive immune response, epidermis development, epithelial cell differentiation, and wound healing (Figure 10B). In terms of molecular function, AC009095.1 was mainly enriched in some of

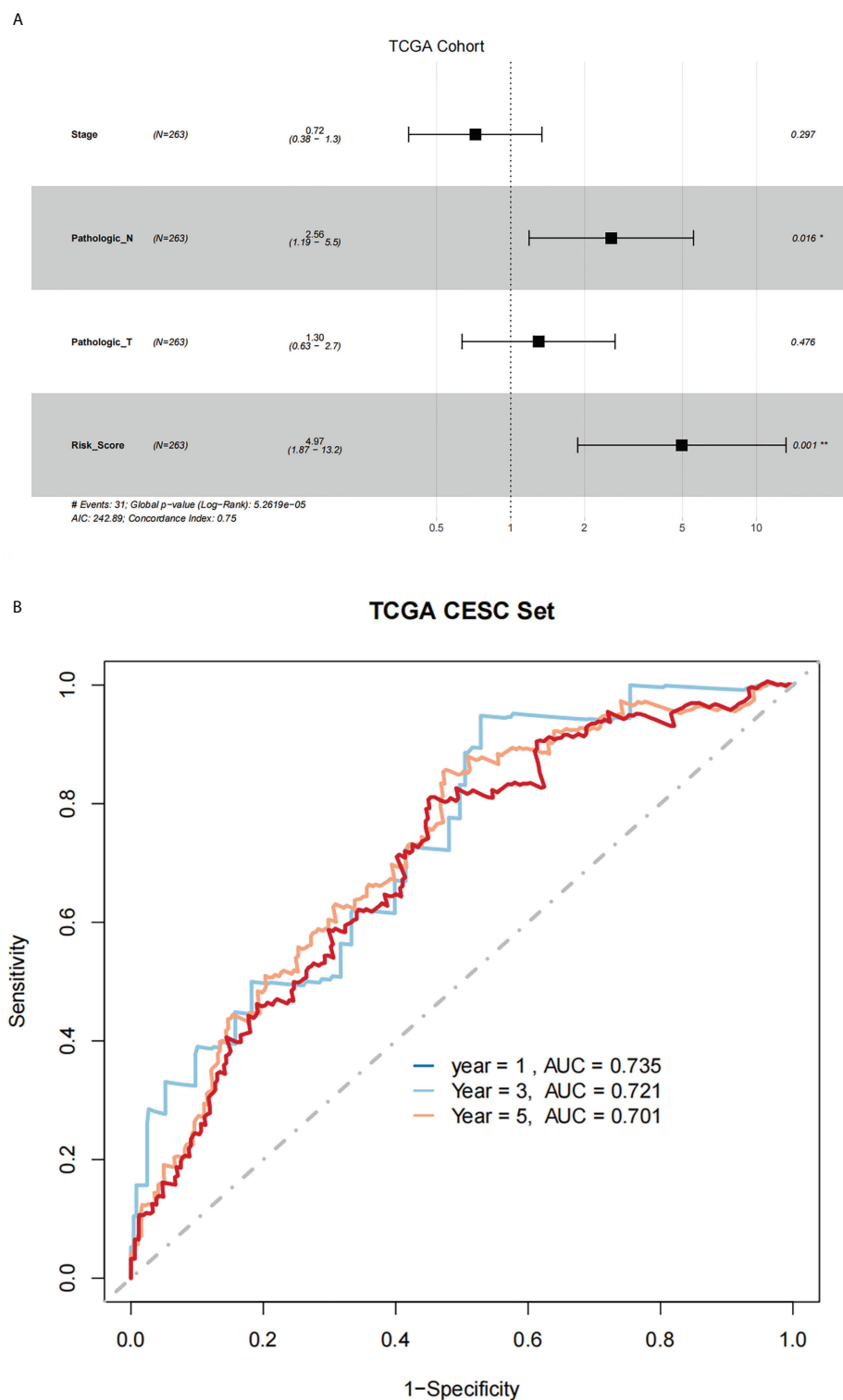


FIGURE 4
There was great predictive performance of the prognostic indicators on the basis of NRLs. **(A)** The forest plots which represented the results of the multivariate Cox regression analysis in CESC. **(B)** The areas were respectively 0.735, 0.721, and 0.701, which were under the ROC curves corresponding to 1, 3, and 5 years of survival.

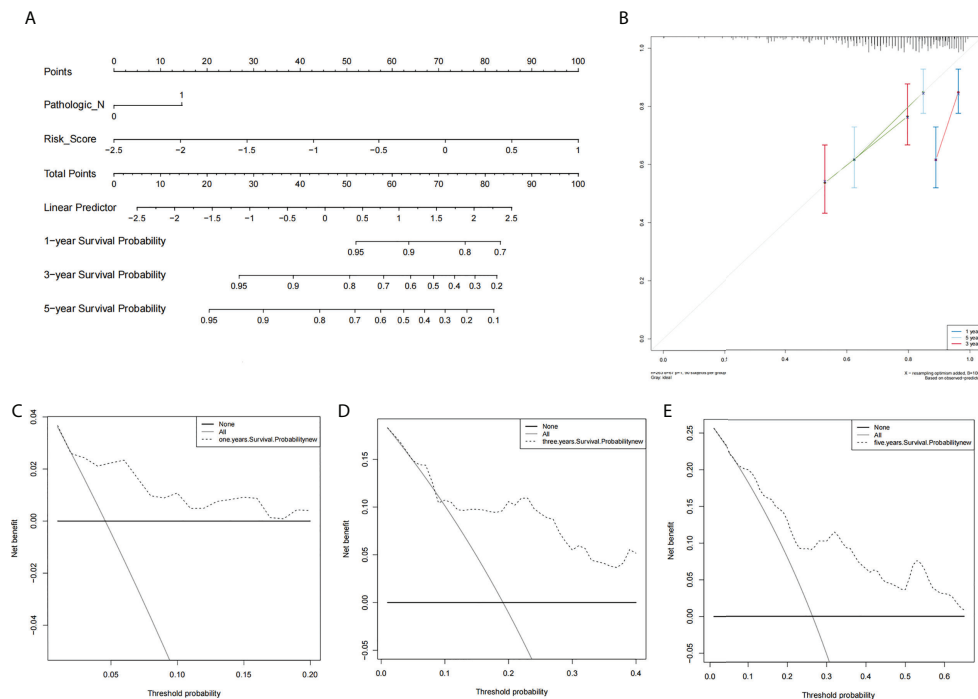


FIGURE 5

The prognostic assessment models in accordance with two lncRNAs related to the necroptosis. (A) The nomogram which consisted of 1-, 3-, and 5-year OS on the basis of the Pathologic_N stage and risk score. (B) The nomogram which predicted the probability of 1-, 3-, or 5-year survival and the calibration plots which were utilized to estimate the consistency between the predictions of the prognostic models and the actual OS. The 45° reference line expresses ideal calibration, in which the predicted probabilities are in accordance with the realistic probabilities. The decision curve analysis (DCA) of 1-year (C), 3-year (D), and 5-year (E) overall survival.

the related pathways of NADH dehydrogenase activity (Figure 10C). AC005332.4 was mainly enriched in the binding to the receptor-associated pathways (Figure 10D). In terms of cellular component, AC009095.1 was mainly enriched on the ribosome-associated pathways (Figure 10E). AC005332.4 was mainly enriched in the T-cell receptor complex, cornified envelope, cytosolic ribosome, ribosomal subunit, ribosome, immunoglobulin complex, receptor complex, and so on (Figure 10F).

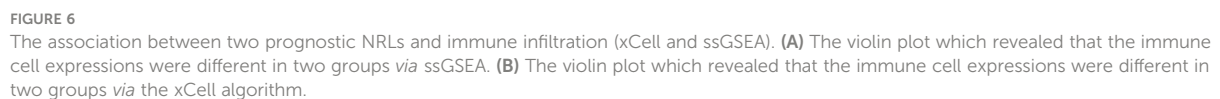
Results of qRT-PCR

We used qRT-PCR to detect the expression of the target lncRNAs in different cell lines. The experimental results indicated that AC009095.1 expression was significantly higher in SiHa cell lines than in the other three cell lines (Figure 11A). AC005332.4 expression was higher in SiHa cell lines than in PANC-1 and Hela cell lines but was slightly lower than in HUCEC cell lines (Figure 11B).

Discussion

Besides breast, colorectal, and lung cancer, CESC is the most common cancer among women (18). In developed countries, the trend of the incidence and mortality of cervical cancer is declining (19), but in underdeveloped countries, it remains high (20). Furthermore, squamous cell carcinoma is the most common type of CESC (21), and only a small proportion of patients with cervical squamous cell carcinoma can be cured with conventional surgery, while a majority of patients develop tumor recurrence and advanced metastases (22–24).

Necroptosis participates in a variety of disease processes (25). Necroptosis has been reported to have different effects in different cancer types. As a mode of death in abnormal cells, necroptosis can abate tumor occurrence. At the same time, necroptosis can also trigger inflammatory responses and promote cancer metastasis as well as immunosuppression (26). Notably, there is little study which is involved in both lncRNA and necroptosis. For example, TRINGS (Tp53-regulated inhibitor of necrosis under glucose starvation) was mentioned



For the purpose of better comprehending the roles of NRLs in the occurrence and development of CESC, first of all, we probed the associated expression of lncRNAs in patients, which were from TCGA database. After that, by using the Pearson analysis, we ascertained the co-expression connection between NRGs and lncRNAs and obtained 2,508 NRLs. Then, after the univariate Cox regression, 36 lncRNAs relevant to necroptosis with prognostic value were selected. After using the Lasso regression method, 15 lncRNAs relevant to necroptosis were identified. Subsequently, there were two NRLs found by further multivariate Cox regression analysis, which were as follows: AC009095.1 and AC005332.4. Next, we calculated the risk

scores for the two lncRNAs relevant to necroptosis and established a signature of lncRNAs relevant to necroptosis. Simultaneously, the patients were grouped in terms of median risk score. Notably, the patients with higher risk scores showed worse prognosis. Moreover, in the high-risk group, AC009095.1 had a higher expression while the result of AC005332.4 was the opposite. Consistent with the above bioinformatic analysis, our experimental results of qRT-PCR demonstrated that AC009095.1 was more highly expressed in Hela and SiHa cell lines compared with PANC-1 (positive control) and HUCEC (negative control) cell lines. AC005332.4 was expressed more highly in both SiHa and Hela than in the positive control, but it was lower than in the negative controls. Therefore, it showed that the two lncRNAs had a vital role in the growth of CESC. Because both were more highly expressed in SiHa than in Hela,

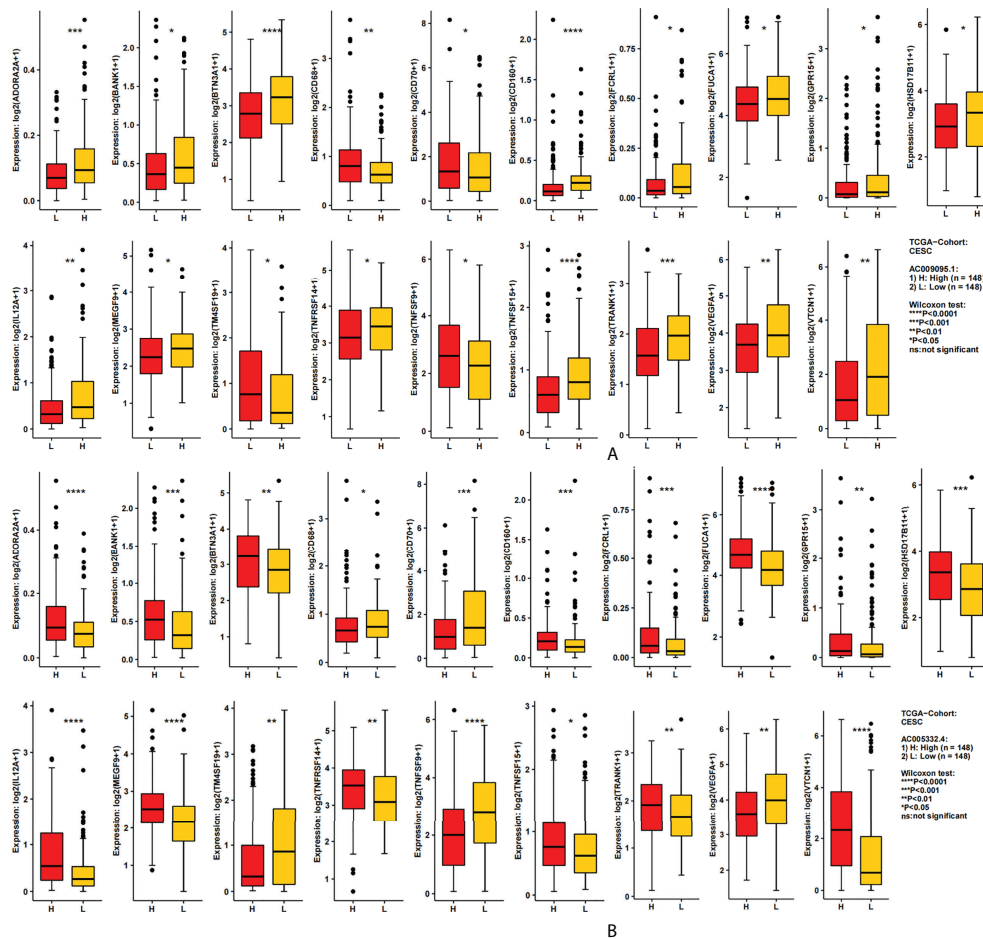


FIGURE 7

The relation between the target lncRNAs and the immune-related genes. (A) Expression of 19 immune-related genes in the AC009095.1 groups. (B) Expression of 19 immune-related genes in the AC005332.4 groups. * $p < 0.05$, ** $p < 0.01$, *** $p < 0.001$, **** $p < 0.0001$.

they may play a more positive role in the development of cervical squamous cell carcinoma. Relative to normal cervical cell lines, the expression of AC009095.1 was higher in cervical cancer cells, while AC005332.4 was the opposite. It was indicated that AC009095.1 may be involved in tumor occurrence and development; however, AC005332.4 may reduce tumor occurrence and development.

Besides, it was proved that our signature owned a favorable prognostic assessment effect in light of the univariate and multivariate Cox regression. Moreover the nomogram displayed that the Pathologic_N stage and risk score had the greatest effect on OS of CESC patients. The areas corresponding to three diverse survival rates were respectively 0.735, 0.721, and 0.701, which were under the ROC curve. This outcome suggested that the signature of risk score had some latent capacity in the aspect of predicting survival. Subsequently, we validated the accuracy of the ideal model according to the calibration curve. In the interest of further exploring the clinic

application of the signature, this study investigated the correlation of the signature by DCA with clinic characteristics, and the consequences demonstrated that our nomogram had great potential for clinic application.

It is complex and difficult to interpret the interaction between tumors and their immune microenvironment, but it is importantly implicated in therapeutic strategies and the development of novel prognostic markers (30). This study clarified the relevance of the expression of lncRNAs relevant to necroptosis AC009095.1 and AC005332.4 and immune infiltration in CESC by using xCell package and ssGSEA. Most importantly, as a result of immune cell infiltration analysis, there was a negative relation between the risk score and aDC, adipocytes, B cells, basophils, CD8⁺ Tcm, CD8⁺ Tem, cDC, DC, HSC, iDC, melanocytes, and so on, whereas CD4⁺ Tcm, eosinophils, epithelial cells, fibroblasts, NKT, plasma cells, platelets, and smooth muscle were increased in the high-risk group. It is reported that B cells have anticancer

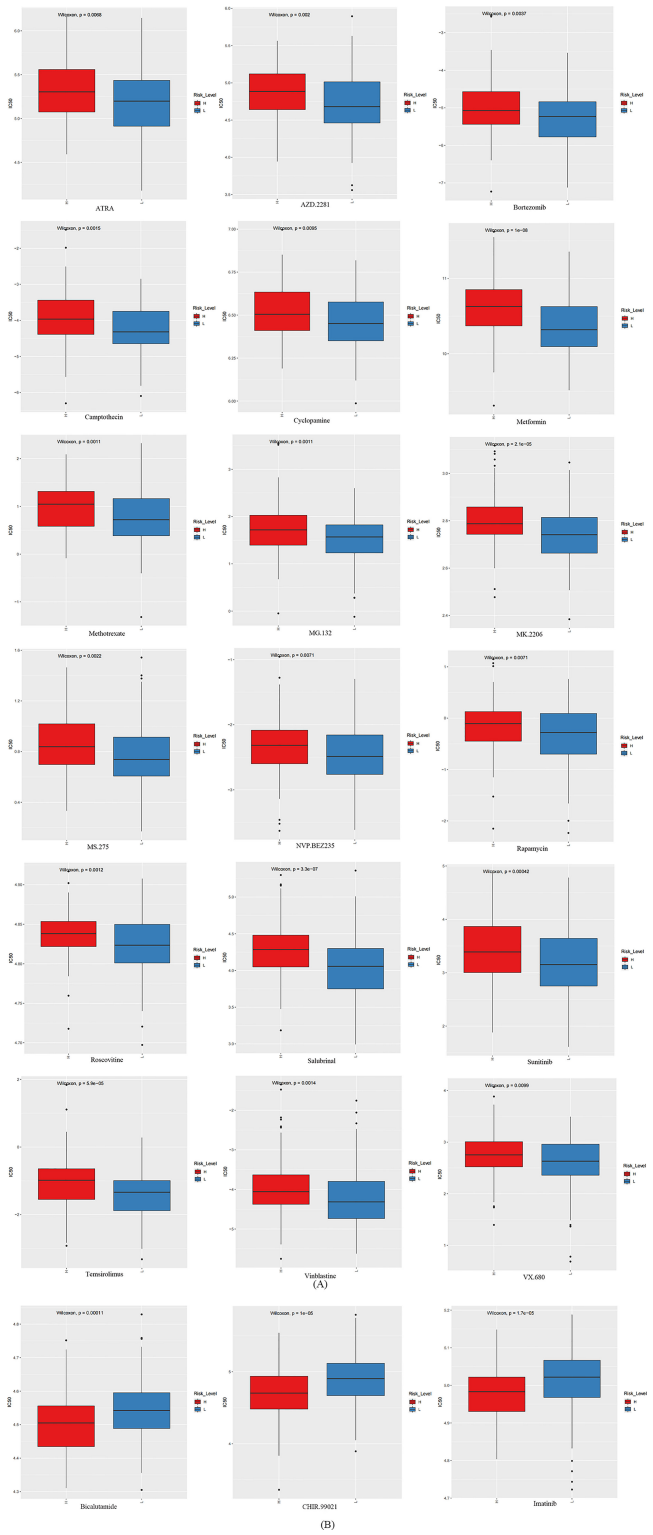


FIGURE 8 The box plots which revealed the IC50 values of 21 therapeutic agents between two groups. **(A)** The estimated IC50 values of 18 therapeutic agents were higher in the group with higher risk scores. **(B)** The estimated IC50 values of three therapeutic agents were higher in the group with lower risk scores.

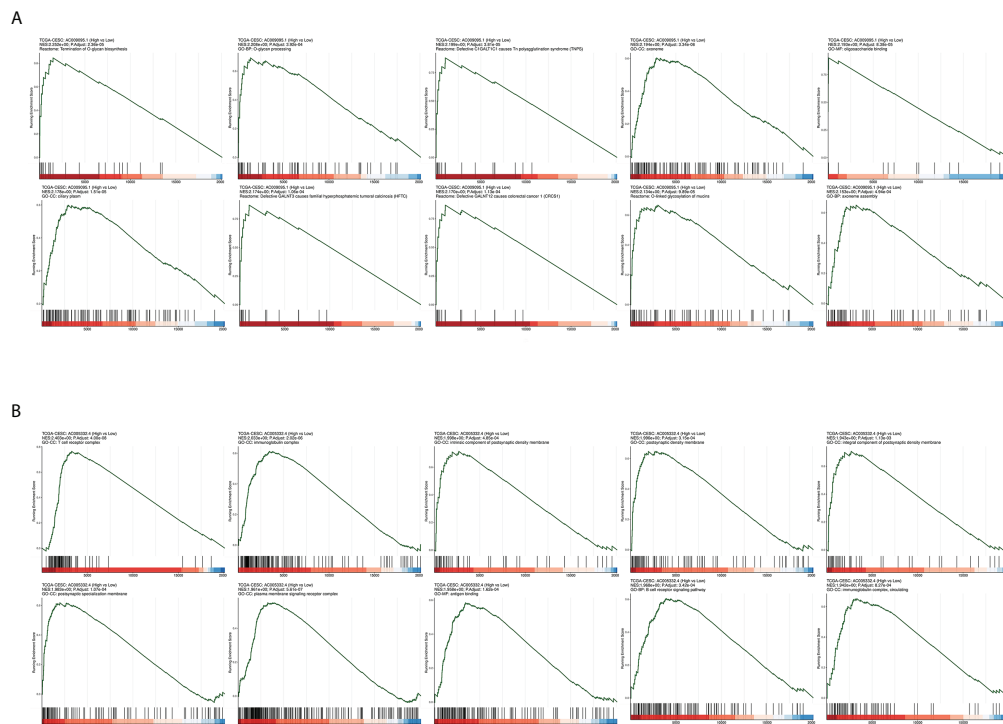


FIGURE 9
Results of GSEA in different groupings of the target lncRNAs in CESC from TCGA database. **(A)** Results of GSEA in groups of AC009095.1. **(B)** Results of GSEA in groups of AC005332.4.

effects in human papillomavirus-associated squamous SCC and have significant beneficial effects on patient prognosis (31). As preclinical evidence from Cao's studies, DCs derived from monocyte activate T cells restrain tumor development by inhibiting tumor cell propagation and accelerating apoptosis. Moreover, tumor cell proliferation is inhibited by cytokines which are secreted by DCs and T cells (32). However, the higher the clinical stage of cervical cancer was, the lower the Th1 level was. It was indicated that Th1 could reduce the development of cervical cancer (33). In another aspect, mDCs and cervical fibroblasts instructed by cocultures of CESC enhanced the tumorigenicity of Th17 cells *in vitro* (34). The cytotoxicity of NKT cells is closely related to the development of cervical cancer. It was found that enhanced tolerance of NKT cells could promote cervical cancer progression (35). It was discovered that thrombocytosis, known as excessive platelets in the blood, was an independent prognostic element in cervical cancer (36). Furthermore, platelets took part in tumor cell extravasation, tumor growth, and metastasis (37). Eosinophils enhanced infiltration of CD8⁺ T cells and normalized tumor vessels to mediate tumor rejection in early animal studies (38). These were in general agreement with our findings. Based on the results of the immunoassay, we found

that overall CD4⁺ T cells were expressed higher in the high-risk group, while CD8⁺ T cells were expressed higher in the low-risk group. Moreover, activated memory CD4⁺ T cells are considered an element of the favorable outcomes about patients with cervical squamous cell carcinoma, whereas resting memory CD4⁺ T cells are considered an element of the adverse outcomes (39). A study of triple-negative breast cancer (TNBC) showed that a high CD4⁺ Tcm enrichment score was associated with worse RFS of patients with TNBC (40). However, the specific role of CD4⁺ Tcm in cervical cancer is not currently clear. In early CESC, CD8⁺ T cells and CD8⁺/CD4⁺ ratio are apparently increased. Both overall survival and disease-free survival are reduced when the CD8⁺/CD4⁺ ratio is below 2, which have been reported in other research studies (41). Moreover, rapid tumor growth and lymph node metastasis are closely related to the reversion of the CD8⁺/CD4⁺ ratio in patients with cervical cancer (42). In a word, in early cervical cancer, the proportion of CD8⁺ T cells was higher than that of CD4⁺ T cells, and it played a relatively important role. When cancer developed further, the proportion of CD4⁺ T cells increased significantly. When the proportion of CD4⁺ T cells was higher than that of CD8⁺ T cells, it indicated that the cancer already had lymph node

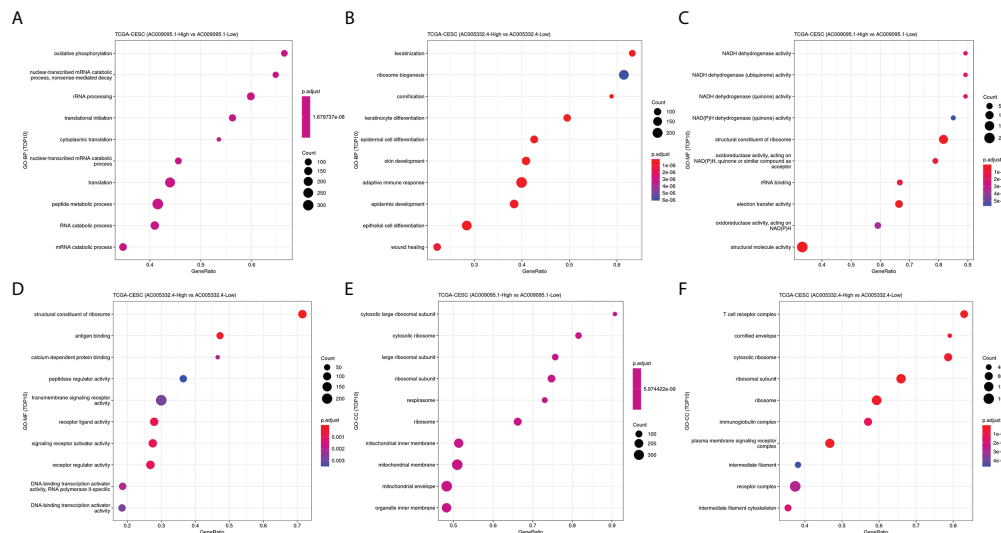


FIGURE 10

Results of GO-BP, GO-MF, and GO-CC. (A) Results of GO-BP in groups of AC009095.1. (B) Results of GO-BP in groups of AC005332.4. (C) Results of GO-MF in groups of AC009095.1. (D) Results of GO-MF in groups of AC005332.4. (E) Results of GO-CC in groups of AC009095.1. (F) Results of GO-CC in groups of AC005332.4.

metastasis associated with immune infiltration. When the ratio gradually decreased, the likelihood of a poor patient prognosis was greater.

With the aim of exploring the relationship between the target lncRNAs and immune-related genes, we divided the target lncRNAs into different groups and analyzed the expression of immune-related genes. It was shown that 19 immune-related genes were statistically differently expressed in different groups. These immune genes were ADORA2A, BANK1, BTN3A1, CD68, CD70, CD160, FCRL1, FUCA1, GPR15, HSD17B11, IL12A, MEGF9, TM4SF19, TNFRSF14, TNFSF9, TNFSF15, TRANK1, VEGFA, and VTCN1. A study has shown that ADORA2A and VTCN1 have a certain relationship with the immune infiltration of CESC (43). In cervical cancer, BTN3A1 overexpression could inhibit the cervical cancer cell phenotype. In other words, BTN3A1 had inhibitory effects on the development of cervical cancer (44). In Ovstad's study, CD160 was also downregulated in the CIN3/AIS lesions (45). The CD68 tumor-associated macrophages in CESC were significantly increased than those in normal tissue or paracarcinoma, and high stromal CD68 tumor-associated macrophages were born on lymph node metastasis (46). The upregulation of FUCA1 in SiHa is shown in Kalliopi's study (47). The IL-12A gene was related to enhanced risk of cervical cancer (48). VEGFA was validated an unfavorable molecules in HPV cervical squamous cell carcinoma (49). The remaining immune-related genes have not been explored in cervical cancer. This is also our next research direction.

Overall, the necroptosis-related signature that we constructed, containing both AC009095.1 and AC005332.4, played a certain role in the immune function. In the immune infiltration analysis, most immune cells were highly infiltrated in the low-risk group. Moreover, the necroptosis-related signature involvement in immune infiltration is more likely achieved through CD4⁺ Tcm, eosinophils, epithelial cells, fibroblasts, NKT, plasma cells, platelets, and smooth muscle. Combined with the results of the enrichment analysis, we could conclude that the major immune role in the necroptosis-related signature is AC005332.4.

In the light of the analysis of the therapeutic agents to the signature we established, we could conclude that three therapeutic agents are more treatment sensitive to the low-risk group. Among them, imatinib is currently considered to own a vital effect in the treatment of CESC but even with paclitaxel more often (50). Bialutamide also has some therapeutic potential in tumors (51), but the therapeutic effect in CESC is still unknown. Thus, it can be seen that the signature we established as well as the prediction of therapeutic drugs have credible evidence.

Furthermore, in the existing studies, we have not found any reports involved in AC009095.1. Of note, the enrichment analysis results showed that AC009095.1 participates in the pathway, and defective GALNT12 causes colorectal cancer 1 (CRCS1), but there is no relevant evidence to support it. AC005332.4 is mostly enriched in pathways related to immunity, such as T-cell receptor complex, immunoglobulin complex, antigen binding, B-cell receptor signaling pathway, and immunoglobulin complex or circulating. This indicates that AC005332.4 is closely related to the immune function (52). Meanwhile, AC005332.4 has also been reported in

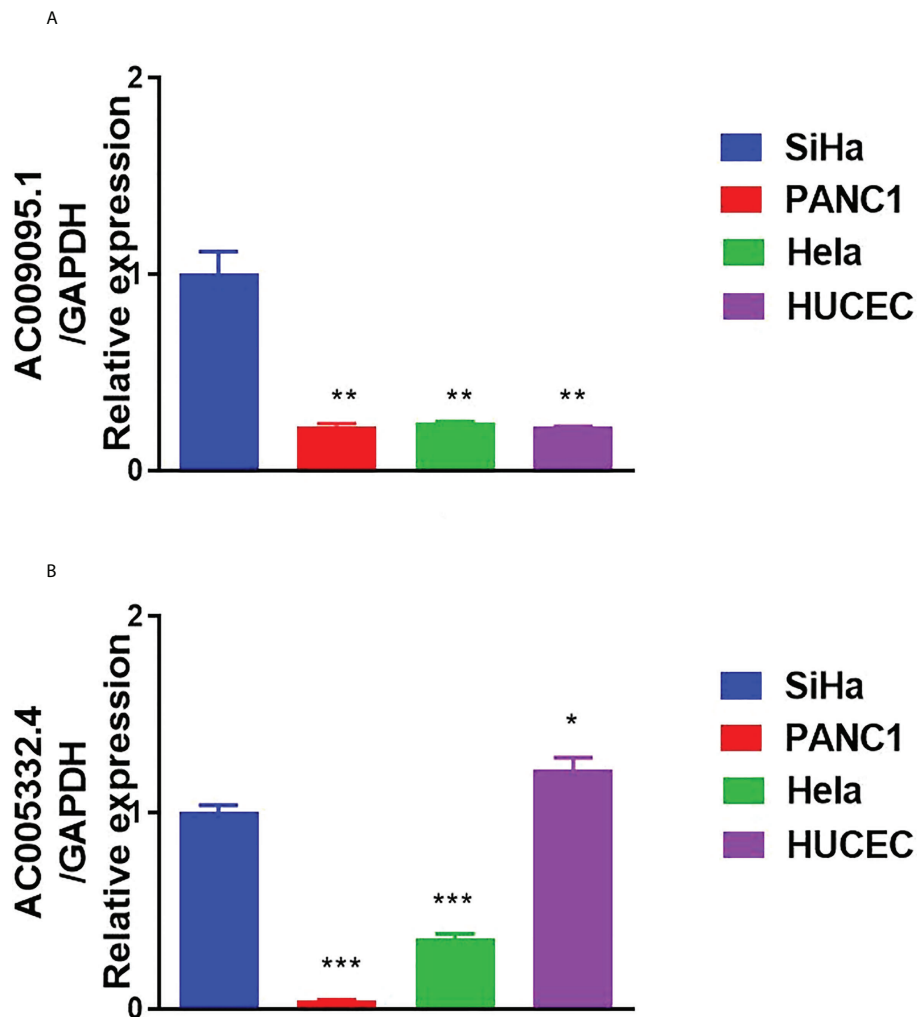


FIGURE 11

Results of qRT-PCR. (A) The expression of AC009095.1 in the four cell lines and AC009095.1 expression were significantly higher in SiHa cell lines than in the other three cell lines. (B) The expression of AC005332.4 in the four cell lines and AC005332.4 expression were higher in SiHa cell lines than in PANC-1 and Hela cell lines but were slightly lower than in HUVEC cell lines. * $p < 0.05$, ** $p < 0.01$, *** $p < 0.001$.

CESC (52), colorectal cancer (53), breast cancer (54), and osteosarcoma (55).

Admittedly, our study has some limitations. First, we did not establish the co-expression network which probably existed in lncRNAs and mRNA. Moreover, the specific molecular mechanisms of the NRLs (AC009095.1 and AC005332.4) have not been verified specifically in the experiments. We also did not perform experiments to verify the selected drug sensitivity. Our sample size was not sufficient, and some of the analysis results may be precise.

By reason of the foregoing, we finally succeeded in constructing the risk score signature in the light of the two necroptosis-related lncRNAs, which was an independent prognostic element in CESC patients. Our study supplied a profound scientific insight of the function of necroptosis in biological traits of malignant tumors. It also advancedly

proposed a double-necroptosis-related lncRNA signature that provides effective and valuable clinic applications for dependable prognostic prediction and individuation therapy of CESC patients. The proposed method improves the prediction accuracy of the target lncRNAs, and these lncRNAs relevant to necroptosis have important implications for prognosis and prediction of therapeutic markers in CESC patients. Therefore, the function of these necroptosis-related lncRNAs of CESC is encouraging enough to warrant advanced exploration.

Data availability statement

Publicly available datasets were analyzed in this study. This data can be found here: The dataset for this study can be found in the

UCSC Xena (<http://xena.ucsc.edu/>), TCGA (<http://cancergenome.nih.gov/abouttcga/policies/publicationguidelines>), KEGG (<https://www.genome.jp/kegg>), GENCODE (https://www.gencodegenes.org/human/release_23.html) and GDSC (<https://www.cancerrxgene.org>).

Author contributions

SZ, GC, and ZT conceived, designed, and supervised the study. WZ, HY, WC, QJ, XJ, and YY drafted the manuscript and performed the data analysis and visualization. WG and YZ collected the data. All authors devoted to data interpretation, manuscript preparation, editing, and review.

Funding

This work was supported by the Applied Medicine Research Project of Hefei Health Commission (Grant No. HWKJ2019-172-14), the Research Fund Project of Anhui Medical University (Grant No. 2020xkj236), and the Natural Science Foundation of Higher Education Institutions of Anhui Province (Grant No. KJ2021A0352).

Acknowledgments

We acknowledge the UCSC Xena, TCGA, KEGG, GENCODE, and GDSC databases for providing their platforms and contributors for uploading their meaningful datasets.

References

1. Sung H, Ferlay J, Siegel RL, Laversanne M, Soerjomataram I, Jemal A, et al. Global cancer statistics 2020: GLOBOCAN estimates of incidence and mortality worldwide for 36 cancers in 185 countries. *CA Cancer J Clin* (2021) 71(3):209–49. doi: 10.3322/caac.21660
2. Bray F, Ferlay J, Soerjomataram I, Siegel RL, Torre LA, Jemal A. Global cancer statistics 2018: GLOBOCAN estimates of incidence and mortality worldwide for 36 cancers in 185 countries. *CA Cancer J Clin* (2018) 68(6):394–424. doi: 10.3322/caac.21492
3. Güzel C, van Sten-Van't Hoff J, de Kok IMCM, Govorukhina NI, Boychenko A, Luider TM, et al. Molecular markers for cervical cancer screening. *Expert Rev Proteomics* (2021) 18(8):675–91. doi: 10.1080/14789450.2021.1980387
4. Gong Y, Fan Z, Luo G, Yang C, Huang Q, Fan K, et al. The role of necroptosis in cancer biology and therapy. *Mol Cancer* (2019) 18(1):100. doi: 10.1186/s12943-019-1029-8
5. Yan J, Wan P, Choksi S, Liu ZG. Necroptosis and tumor progression. *Trends Cancer* (2022) 8(1):21–7. doi: 10.1016/j.trecan.2021.09.003
6. Suchitra M, Poonam Y, Harini L, Priyanshu S, Aravindhan V, Devarajan K. RETRA induces necroptosis in cervical cancer cells through RIPK1, RIPK3, MLKL and increased ROS production. *Eur J Pharmacol* (2022) 920:174840. doi: 10.1016/j.ejphar
7. Schmidt SV, Seibert S, Walch-Rückheim B, Vicinus B, Kamionka EM, Pahne-Zeppenfeld J, et al. Correction: RIPK3 expression in cervical cancer cells

Conflict of interest

The authors declare that the research was conducted in the absence of any commercial or financial relationships that could be construed as a potential conflict of interest.

Publisher's note

All claims expressed in this article are solely those of the authors and do not necessarily represent those of their affiliated organizations, or those of the publisher, the editors and the reviewers. Any product that may be evaluated in this article, or claim that may be made by its manufacturer, is not guaranteed or endorsed by the publisher.

Supplementary material

The Supplementary Material for this article can be found online at: <https://www.frontiersin.org/articles/10.3389/fonc.2022.1011000/full#supplementary-material>

SUPPLEMENTARY TABLE 1

The gene list expressed in CESC related to necroptosis.

SUPPLEMENTARY TABLE 2

The necroptosis-related lncRNAs were screened by a co-expression network.

SUPPLEMENTARY TABLE 3

Univariate Cox results of necroptosis-related lncRNAs.

SUPPLEMENTARY TABLE 4

Lasso regression results of necroptosis-related lncRNAs.

is required for PolyIC-induced necroptosis, IL-1 α release, and efficient paracrine dendritic cell activation. *Oncotarget* (2019) 10(43):4503–4. doi: 10.18632/oncotarget.27066

8. Lin L, Song Y, Chunyi Z. Low necroptosis process predicts poor treatment outcome of human papillomavirus positive cervical cancers by decreasing tumor-associated macrophages M1 polarization. *Gynecol Obstet Invest* (2018) 83(3):259–67. doi: 10.1159/000487434

9. Chi Y, Wang D, Wang J, Yu W, Yang J. Long non-coding RNA in the pathogenesis of cancers. *Cells* (2019) 8(9):1015. doi: 10.3390/cells8091015

10. Jiang N, Zhang X, Gu X, Li X, Shang L. Progress in understanding the role of lncRNA in programmed cell death. *Cell Death Discovery* (2021) 7(1):30. doi: 10.1038/s41420-021-00407-1

11. Wang K, Liu F, Liu CY, An T, Zhang J, Zhou LY, et al. The long noncoding RNA NRF regulates programmed necrosis and myocardial injury during ischemia and reperfusion by targeting miR-873. *Cell Death Differ* (2016) 23(8):1394–405. doi: 10.1038/cdd.2016.28

12. Fangyue C, Jun Y, Min F, Yanmei W, Dongwei S, Yuan S. Necroptosis-related lncRNA to establish novel prognostic signature and predict the immunotherapy response in breast cancer. *J Clin Lab Anal* (2022) 36(4):e24302. doi: 10.1002/jcla.24302

13. Li L, Liu H, Wenzheng C, Guoyang Z, Yebei L, Yukang W, et al. Comprehensive analysis of necroptosis-related long noncoding RNA immune

infiltration and prediction of prognosis in patients with colon cancer. *Front Mol Biosci* (2022) 9:811269. doi: 10.3389/fmolb.2022.811269

14. Zirui Z, Haohan L, Xingyu Z, Deliang F, Xinde O, Jinning Y, et al. Necroptosis-related lncRNAs: Predicting prognosis and the distinction between the cold and hot tumors in gastric cancer. *J Oncol* (2021) 2021:6718443. doi: 10.1155/2021/6718443

15. Yinliang L, Xuehui L, Qi W, Jie C, Xinyue Z, YueSen L, et al. A novel necroptosis-related lncRNA signature predicts the prognosis of lung adenocarcinoma. *Front Genet* (2022) 13:862741. doi: 10.3389/fgene.2022.862741

16. Lianghua L, Leyan L, Li L, Zongfeng F, Qingwen Z, Xufeng S, et al. A necroptosis-related lncRNA-based signature to predict prognosis and probe molecular characteristics of stomach adenocarcinoma. *Front Genet* (2022) 13:833928. doi: 10.3389/fgene.2022.833928

17. Lin A, Qi C, Wei T, Li M, Cheng Q, Liu Z, et al. CAMOIP: a web server for comprehensive analysis on multi-omics of immunotherapy in pan-cancer. *Brief Bioinform* (2022) 9:bbac129. doi: 10.1093/bib/bbac129. Epub ahead of print

18. Arbyn M, Weiderpass E, Bruni L, de Sanjosé S, Saraiya M, Ferlay J, et al. Estimates of incidence and mortality of cervical cancer in 2018: a worldwide analysis. *Lancet Glob Health* (2020) 8(2):e191–203. doi: 10.1016/S2214-109X(19)30482-6

19. Zhang X, Zeng Q, Cai W, Ruan W. Trends of cervical cancer at global, regional, and national level: Data from the global burden of disease study 2019. *BMC Public Health* (2021) 21(1):894. doi: 10.1186/s12889-021-10907-5

20. Hull R, Mbele M, Makhafola T, Hicks C, Wang SM, Reis RM, et al. Cervical cancer in low and middle-income countries. *Oncol Lett* (2020) 20(3):2058–74. doi: 10.3892/ol.2020.11754

21. Siaw SB, Ho YL, Chuanyun X, Zigui C, Paul KSC. Review of the standard and advanced screening, staging systems and treatment modalities for cervical cancer. *Cancers (Basel)* (2022) 14(12):2913. doi: 10.3390/cancers14122913

22. Cohen PA, Jhingran A, Oaknin A, Denny L. Cervical cancer. *Lancet* (2019) 393(10167):169–82. doi: 10.1016/S0140-6736(18)32470-X

23. Fader AN. Surgery in cervical cancer. *N Engl J Med* (2018) 379(20):1955–7. doi: 10.1056/NEJMe1814034

24. Small WJ, Bacon MA, Bajaj A, Chuang LT, Fisher BJ, Harkenrider MM, et al. Cervical cancer: A global health crisis. *Cancer* (2017) 123(13):2404–12. doi: 10.1002/cncr.30667

25. Khoury MK, Gupta K, Franco SR, Liu B. Necroptosis in the pathophysiology of disease. *Am J Pathol* (2019) 190(2):272–85. doi: 10.1016/j.ajpath.2019.10.012

26. Boris S, Lida Y, Julián AJ, Laurens W, Kang H, CMr U, et al. Tumour-cell-induced endothelial cell necroptosis via death receptor 6 promotes metastasis. *Nature* (2016) 536(7615):215–8. doi: 10.1038/nature19076

27. Muhammad RK, Shaoxun X, Zhiyin S, Mian W. The p53-inducible long noncoding RNA TRINGS protects cancer cells from necrosis under glucose starvation. *EMBO J* (2017) 36(23):3483–500. doi: 10.15252/embj.201696239

28. Khan MR, Wu M, Liu G. Tumor-suppressive or tumor-supportive: For p53, that is the question. *Mol Cell Oncol* (2018) 5(3):e1408537. doi: 10.1080/23723556.2017.1408537

29. Tran DDH, Kessler C, Niehus SE, Mahnkopf M, Koch A, Tamura T. Myc target gene, long intergenic noncoding RNA, Linc00176 in hepatocellular carcinoma regulates cell cycle and cell survival by titrating tumor suppressor microRNAs. *Oncogene* (2018) 37(1):75–85. doi: 10.1038/ncr.2017.312

30. Petitprez F, Meylan M, de Reyniès A, Sautès-Fridman C, Fridman WH. The tumor microenvironment in the response to immune checkpoint blockade therapies. *Front Immunol* (2020) 11:784. doi: 10.3389/fimmu.2020.00784

31. Sangwoo SK, Sarek S, Sayuri M, P Dominick S, Ida FP, Loren M, et al. B cells improve overall survival in HPV-associated squamous cell carcinomas and are activated by radiation and PD-1 blockade. *Clin Cancer Res* (2020) 26(13):3345–59. doi: 10.1158/1078-0432.CCR-19-3211

32. Guangming C, Ran C, Chongdong L, Guyu Z, Zhenyu Z. MTBHsp70-exFPR1-pulsed dendritic cells enhance the immune response against cervical cancer. *J Cancer* (2019) 10(25):6364–73. doi: 10.7150/jca.29779

33. Lin W, Zhang HL, Niu ZY, Wang Z, Kong Y, Yang XS, et al. The disease stage-associated imbalance of Th1/Th2 and Th17/Treg in uterine cervical cancer patients and their recovery with the reduction of tumor burden. *BMC Women's Health* (2020) 20:126. doi: 10.1186/s12905-020-00972-0

34. Walch-Rückheim B, Ströder R, Theobald L, Pahne-Zeppenfeld J, Hegde S, Kim YJ, et al. Cervical cancer-instructed stromal fibroblasts enhance IL23 expression in dendritic cells to support expansion of Th17 cells. *Cancer Res* (2019) 79(7):1573–86. doi: 10.1158/0008-5472.CAN-18-1913

35. Zhang Y, Li X, Zhang J, Liang H. Natural killer T cell cytotoxic activity in cervical cancer is facilitated by the LINC00240/microRNA-124-3p/STAT3/MICA axis. *Cancer Lett* (2020) 474:63–73. doi: 10.1016/j.canlet.2019.12.038

36. Juan C, Zhi Z, Qingjian Y, Yu Z, Ronghua Y, Changyan L, et al. The association of pretreatment thrombocytosis with prognosis and clinicopathological significance in cervical cancer: A systematic review and meta-analysis. *Oncotarget* (2017) 8(15):24327–36. doi: 10.18632/oncotarget.15358

37. Monika H, Rebecca LS, David GM, Vahid AK, Anil KS. The platelet lifeline to cancer: Challenges and opportunities. *Cancer Cell* (2018) 33(6):965–83. doi: 10.1016/j.ccell.2018.03.002

38. Grisar-Tal S, Itan M, Klion AD, Munitz A. A new dawn for eosinophils in the tumour microenvironment. *Nat Rev Cancer* (2020) 20(10):594–607. doi: 10.1038/s41568-020-0283-9

39. Wang J, Li Z, Gao A, Wen Q, Sun Y. The prognostic landscape of tumor-infiltrating immune cells in cervical cancer. *BioMed Pharmacother* (2019) 120:109444. doi: 10.1016/j.biopha.2019.109444

40. Deng L, Lu D, Bai Y, Wang Y, Bu H, Zheng H. Immune profiles of tumor microenvironment and clinical prognosis among women with triple-negative breast cancer. *Cancer Epidemiol Biomarkers* (2019) 28(12):1977–85. doi: 10.1158/1055-9965.EPI-19-0469

41. Olga VK, Pavel IK, Ludmila VS, Tatyana OV. T- and NK-cell populations with regulatory phenotype and markers of apoptosis in circulating lymphocytes of patients with CIN3 or microcarcinoma of the cervix: evidence for potential mechanisms of immune suppression. *Infect Agent Cancer* (2017) 12:56. doi: 10.1186/s13027-017-0166-1

42. Lina Z, Zhilei M, Yiqing L, Ting W, Kelian Z, Beibei Z. A review of the research progress in T-lymphocyte immunity and cervical cancer. *Transl Cancer Res* (2020) 9(3):2026–36. doi: 10.21037/tcr.2020.01.33

43. Fang W, Fangfang C, Yangfan F, Deqin C. Clinical significance of TET2 in female cancers. *Front Bioeng Biotechnol* (2022) 10:790605. doi: 10.3389/fbioe.2022.790605

44. Ruxiang C, Ping H. Long noncoding RNA HOXA-AS2 accelerates cervical cancer by the miR-509-3p/BTN3A1 axis. *J Pharm Pharmacol* (2021) 73(10):1387–96. doi: 10.1093/jpp/rgab090

45. Øvestad IT, Engesaeter B, Halle MK, Akbari S, Bicskei B, Lapin M, et al. High-grade cervical intraepithelial neoplasia (CIN) associates with increased proliferation and attenuated immune signaling. *Int J Mol Sci* (2021) 23(1):373. doi: 10.3390/ijms23010373

46. Guo F, Kong W, Zhao G, Cheng Z, Ai L, Lv J, et al. The correlation between tumor-associated macrophage infiltration and progression in cervical carcinoma. *Biosci Rep* (2021) 41(5):BSR20203145. doi: 10.1042/BSR20203145

47. Kalliopi IP, Georgia K, Manousos M, Vasiliki L, Jerome Z, George D, et al. High resolution proteomic analysis of the cervical cancer cell lines secretome documents deregulation of multiple proteases. *Cancer Genomics Proteomics* (2017) 14(6):507–21. doi: 10.21873/cgp.20060

48. de Moura EL, Dos Santos ACM, da Silva DM, Dos Santos BB, Figueredo DS, Moura AWA, et al. Association of polymorphisms in cytokine genes with susceptibility to precancerous lesions and cervical cancer: A systematic review with meta-analysis. *Immunol Invest* (2021) 50(5):492–526. doi: 10.1080/08820139.2020.1778023

49. Meng L, Chen S, Shi G, He S, Wang Z, Shen J, et al. Use of single cell transcriptomic techniques to study the role of high-risk human papillomavirus infection in cervical cancer. *Front Immunol* (2022) 13:907599. doi: 10.3389/fimmu.2022.907599

50. Zhepeng L, Haini C, Fengmei L, Jun W, Shoujin Z, Yijun L, et al. Sequential release of paclitaxel and imatinib from core-shell microparticles prepared by coaxial electrospray for vaginal therapy of cervical cancer. *Int J Mol Sci* (2021) 22(16):8760. doi: 10.3390/ijms22168760

51. Zhao SG, Chen WS, Das R, Chang SL, Tomlins SA, Chou J, et al. Clinical and genomic implications of luminal and basal subtypes across carcinomas. *Clin Cancer Res* (2019) 25(8):2450–7. doi: 10.1158/1078-0432.CCR-18-3121

52. Xu M, Zhang R, Qiu J. A four immune-related long noncoding RNAs signature as predictors for cervical cancer. *Hum Cell* (2022) 35(1):348–59. doi: 10.1007/s13577-021-00654-5

53. Wang XC, Liu Y, Long FW, Liu LR, Fan CW. Identification of a lncRNA prognostic signature-related to stem cell index and its significance in colorectal cancer. *Future Oncol* (2021) 17(23):3087–100. doi: 10.2217/fon-2020-1163

54. Chen Z, Feng R, Kahlert UD, Chen Z, Torres-Dela Roche LA, Soliman A, et al. Construction of ceRNA networks associated with CD8 T cells in breast cancer. *Front Oncol* (2022) 9:883197. doi: 10.3389/fonc.2022.883197

55. He Y, Zhou H, Xu H, You H, Cheng H. Construction of an immune-related lncRNA signature that predicts prognosis and immune microenvironment in osteosarcoma patients. *Front Oncol* (2022) 14:769202. doi: 10.3389/fonc.2022.769202



OPEN ACCESS

EDITED BY

Shaohua Xu,
Tongji University, China

REVIEWED BY

Guochao Nie,
Yulin Normal University, China
David Mutch,
Washington University in
St. Louis, United States

*CORRESPONDENCE

Tiansheng Qin
ogqtsmile@yahoo.com
Weilin Jin
weilinjin@yahoo.com

[†]These authors have contributed
equally to this work

SPECIALTY SECTION

This article was submitted to
Gynecological Oncology,
a section of the journal
Frontiers in Oncology

RECEIVED 24 May 2022

ACCEPTED 31 August 2022

PUBLISHED 23 September 2022

CITATION

Chen F, Qin T, Zhang Y, Wei L, Dang Y,
Liu P and Jin W (2022) Reclassification
of endometrial cancer and
identification of key genes based on
neural-related genes.
Front. Oncol. 12:951437.
doi: 10.3389/fonc.2022.951437

COPYRIGHT

© 2022 Chen, Qin, Zhang, Wei, Dang,
Liu and Jin. This is an open-access
article distributed under the terms of
the [Creative Commons Attribution
License \(CC BY\)](#). The use, distribution
or reproduction in other forums is
permitted, provided the original
author(s) and the copyright owner(s)
are credited and that the original
publication in this journal is cited, in
accordance with accepted academic
practice. No use, distribution or
reproduction is permitted which does
not comply with these terms.

Reclassification of endometrial cancer and identification of key genes based on neural-related genes

Fan Chen^{1†}, Tiansheng Qin^{1*†}, Yigan Zhang^{2†}, Linzhen Wei¹,
Yamei Dang¹, Peixia Liu³ and Weilin Jin^{4*}

¹The First Clinical Medical College of Gansu University of Chinese Medicine (Gansu Provincial Hospital), Lanzhou, China, ²Key Laboratory of RNA Biology, Institute of Biophysics, Chinese Academy of Sciences, Beijing, China, ³Department of Obstetrics and Gynecology, Yuzhong County Hospital of Traditional Chinese Medicine, Lanzhou, China, ⁴Institute of Cancer Neuroscience, Medical Frontier Innovation Research Center, The First Hospital of Lanzhou University, The First Clinical Medical College of Lanzhou University, Lanzhou, China

Endometrial cancer (EC) is the most common gynecologic malignancy, and its incidence has been increasing every year. Nerve signaling is part of the tumor microenvironment and plays an active role in tumor progression and invasion. However, the relationship between the expression of neural-related genes (NRGs) and prognosis in endometrial cancer remains unknown. In this study, we obtained RNA sequencing data of EC from The Cancer Genome Atlas (TCGA). Endometrial cancer was classified into two subtypes based on the expression of neural-associated genes (NRGs), with statistical differences in clinical stage, pathological grading, and prognosis. A prognostic prediction model was established by LASSO-Cox analysis, and the results showed that high expression of NRGs was associated with poor survival prognosis. Further, CHRM2, GRIN1, L1CAM, and SEMA4F were found to be significantly associated with clinical stage, immune infiltration, immune response, and important signaling pathways in endometrial cancer. The reclassification of endometrial cancer based on NRG expression would be beneficial for future clinical practice. The genes CHRM2, GRIN1, L1CAM, and SEMA4F might serve as potential biomarkers of EC prognosis.

KEYWORDS

Endometrial cancer, nerve-cancer crosstalk, immune infiltration, biomarker, neural-related genes (NRGs)

Introduction

In 2020, endometrial cancer has been the sixth most frequent cancer in women worldwide, with 417,000 new cases and 97,000 deaths (1, 2). Although the incidence has leveled off in recent years, it still has been increasing at a rate of 1% per year, making it one of the few human cancers with a rising fatality rate (3). The choice of surgery, radiation, hormonal and/or chemotherapy, immunotherapy, and targeted therapy depend on the stage of the disease.

The tumor microenvironment is composed of neuronal cells, tumor cells, fibroblasts, and immune cells. Cancer cells can generate electroactive tissue by connecting with neural synapses, which drives cancer cells to migrate and develop (4, 5). Active crosstalk between nerves and tumor cells was first observed in prostate and gastric cancers (6, 7), but its role in endometrial cancer remains largely unknown. Perineural infiltration is a new metastatic pathway in endometrial cancer. Endometrial cancer cells have been found to migrate along the neuropil *in vitro*, which is associated with DRG and also a risk factor for perineural infiltration (8). Through cytokinesis, sympathetic nerve endings in the uterus release norepinephrine, adenosine triphosphate (ATP), and other molecules with oxytocic and contractile properties. Uterine parasympathetic fibers primarily release acetylcholine to regulate myometrium activity (9). Furthermore, estrogen and progesterone play important roles in reshaping uterine innervation in response to cyclical changes from puberty to menopause.

Using comprehensive genomic analysis of TCGA, Talhouk et al. classified endometrial cancers into four different subgroups: POLE, microsatellite instability, low copy number, and high copy number (10). Clinically, TCGA molecular typing is practical, useful, and beneficial in predicting the prognosis of patients. Here, we reclassified endometrial carcinoma based on the expression of NRGs. The research on the nerve and endometrial cancer crosstalk can assist the identification of the treatment targets for endometrial cancer. As a result, we found two subgroups related to prognosis by clustering endometrial cancer patients in TCGA data based on NRGs. To find prognosis-associated genes, a prognostic model of neural-associated genes was created. In this study, we investigated the relationship between NRGs and endometrial cancer prognosis, clinical staging, pathological grading, signaling pathways, immune infiltration, and immune response in the hopes of assisting future research.

Materials and methods

Source and processing of data sets

The Cancer Genome Atlas (TCGA) database (<https://Portal.gdc.cancer.gov/repository>) was used to obtain raw data

from 552 endometrial cancer patients (11). In addition, clinical endometrial cancer data was retrieved, including survival time, survival status, age, grade, and stage information. 42 NRGs were identified from a previous comprehensive review (12).

Consensus clustering

The chi-square test and the R language package were used to examine the correlations between clustering and clinical features (13). The “ConsensusClusterPlus” package was used to separate endometrial cancer cases into two subgroups (14). The packages “survival” and “survminer” provided survival analysis between subtypes. The “ggplot2” package was used to identify genetic differences between typings (15), while the “pheatmap” tool was used to create heatmaps. The `prcomp` function in the statistics package was used to perform principal component analysis (PCA) (16).

Differential expression analysis

The R package Limma (v3.40.2) was used to study mRNA differential expression (17). Adjusted p-values (FDR) were analyzed in TCGA to correct for false-positive results. The screening conditions for differentially expressed mRNA were $|\log_2FC| \geq 1$ and $FDR < 0.05$. Determining the cutoff value by the median is the most commonly used method for determining the cutoff value. Similarly, the cut-off value is determined by the interquartile range. High GRIN1/L1CAM expression (top 25%) and low GRIN1/L1CAM expression (bottom 25%) were defined. Since the total expression of CHRM2/SEMA4F was relatively low, 50% was used as the cutoff for high and low expression of both genes. The LASSO regression algorithm was used for feature selection, and 10-fold cross validation was used (18).

Enrichment analysis and ssGSEA analysis

GO enrichment analysis (19) and KEGG enrichment analysis (20) were done by using R packages ClusterProfiler (21). The Cox regression analysis was performed to identify prognostic genes significantly associated with overall survival (OS) in patients with endometrial cancer ($p < 0.01$) (22). Survival curves were constructed using the R packages “survival” and “survminer”. ROC curves were made using the R packages “survivalROC” and “timeROC”. We collected some functional pathways and calculated the functional pathway scores according to the ssGSEA algorithm.

Analysis of immune infiltrates

The CIBERSORT (23) and EPIC (24) in the R package “immunedeconv” (<https://grst.github.io/immunedeconv>) were

used to analyze immune infiltrates of different subtypes. It was also visualized using the R package (v4.0.3) ggplot2 and pheatmap (15).

Analyses of immune checkpoint genes

The correlation of neural-related gene expression with 8 commonly used immune checkpoint genes (CD274, CTLA4, HAVCR2, LAG3, PDCD1, PDCD1LC2, SIGLEC15 and TIGIT) was analyzed and visualized using the R package (v4.0.3) ggplot2 (15) and pheatmap.

Algorithm for Predicting Immune Responses

Treatment response to immune checkpoint inhibitors can be predicted using the TIDE algorithm (25).

Stemness analysis

The stemness of mRNA was evaluated using the OCLR method (26).

Statistical analysis

All statistical analyses were performed in R software (v4.0.3) and were statistically significant at $P < 0.05$.

Results

Identification of EC subtypes based on neural-related genes

We obtained EC data from the TCGA database to explore the relationship between 42 neural-related genes and endometrial cancer. To identify the subtypes, we used the R package ConsensusCluster Plus and two clusters showed up in the result: cluster I (C1) and cluster II (C2) (Figures 1A–C). C1 and C2 were found to be well split into two subgroups using principal component analysis (Figure 1D). From the retrospective 10-year clinical follow-up study, the overall survival (OS) rates of the two groups were statistically different ($P < 0.05$), with C1 having a greater OS than C2 (Figure 1E). In addition, there was a statistically significant difference between C1 and C2 in terms of clinical staging and pathological grading ($P < 0.05$). (Figure 2) (Table 1).

Differential expression analysis and enrichment analysis of C1 and C2

We used the R package Limma to search differentially expressed genes (DEGs) in C1 and C2, with $FC > 2$ and $P < 0.05$ as screening criteria. When compared to C2, C1 showed 209 up-regulated DEGs and 325 down-regulated DEGs. In C1, 24 DEGs were down-regulated (e.g. SEMA4F), 8 DEGs were up-regulated (e.g. ADRB2), and 10 DEGs were unregulated (e.g. GDNF) compared to C2 (Figures 3A, B, S1). To investigate the activated or suppressed signaling pathways in C1 and C2, KEGG and GO analyses were used (Figures 3C, D). KEGG analysis showed that compared to C2, C1 displayed the activation of tumor suppressor pathways like estrogen signaling pathway, ferroptosis, IL-17 signaling pathway, and amino acid metabolic pathway, with the suppression of cancer-associated signaling pathways such as gastric cancer, basal cell carcinoma, Wnt signaling pathway, and neurotransmission. Also, C1 demonstrated the inhibition of multisystem diseases such as cardiomyopathy, hepatitis C, cushing's syndrome, human papillomavirus infection, and pathogenic escherichia coli infection. In addition, C1 inhibited lipolysis in adipocytes and oxytocin signaling pathway associated with endometrial carcinogenesis (Figure 3C). GO analysis suggested that compared to C2, C1 induced activation of the processes including humoral immune response and antibacterial humoral response, with the inhibition of synapse organization, neuron projection guidance, modulation of chemical synaptic transmission, extracellular matrix organization, cell–cell adhesion, which are generally recognized to be key processes that promote cancer growth and metastasis (Figure 3D).

Immune status analysis of C1 and C2

We used the immunedeconv R package to assess immune infiltration of C1 and C2. the CIBERSORT showed that there were statistically significant differences between C1 and C2 in B cell naive ($P < 0.05$), CD8+ T cells ($P < 0.001$), T cell CD4+ memory activated ($P < 0.01$), T cell regulation (Tregs) ($P < 0.001$), myeloid dendritic cell resting ($P < 0.001$), myeloid dendritic cell activated ($P < 0.001$), and neutrophil ($P < 0.01$), indicating that C2 exhibited stronger immunosuppression compared to C1 (Figure 4A). The EPIC further confirmed that C1 and C2 showed stronger immunosuppression in terms of T cell CD4+ ($P < 0.01$) and T cell CD8+ ($P < 0.001$) with statistically significant differences (Figure 4B). We also used the ggplot2 and pheatmap R packages to analyze the ICG of both EC subtypes, and the study showed that CTLA4, HAVCR2, PDCD1, and TIGIT expression were increased in C1 ($P < 0.001$) compared to C2 (Figure 4C), implying that immunotherapy may be more effective. Furthermore, we utilized the TIDE algorithm to predict cancer immune response, and the findings revealed that the C2

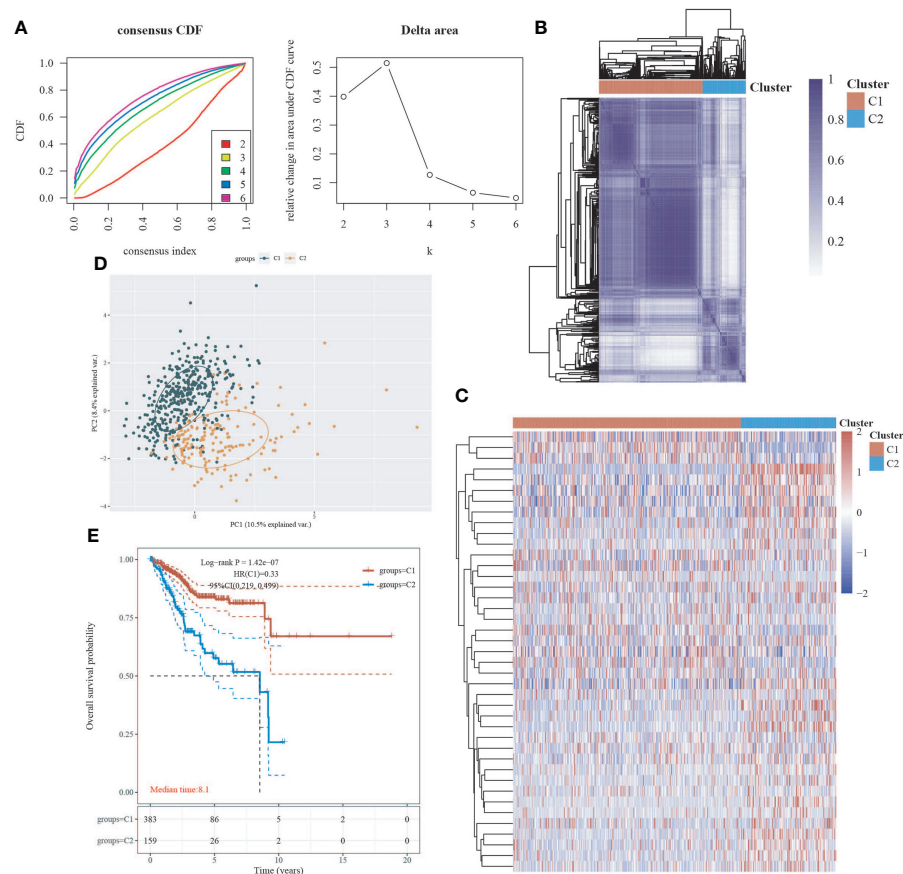


FIGURE 1

Classification of EC subtypes based on neural-related genes (NRGs). (A) Cumulative distribution function (CDF) curve and delta area curve of consensus clustering. (B) Heatmap of consensus clustering. Rows and columns represent samples, and different colors represent different categories. (C) Heatmap of neural-related gene expression in different subtypes of EC. High expression is represented by red, whereas low expression is represented by blue. (D) Principal component analysis (PCA) is a method of analyzing data. (E) Survival curves based on the Kaplan-Meier method. Different subgroups' overall survival curves.

group had a higher TIDE score than the C1 group, with a significant difference ($P=7e-05$), indicating that the C1 group may benefit more from immune checkpoint inhibitor therapy (ICBs) (Figure 4D). The OCLR algorithm revealed that C2 had a greater stemness index than C1, with a statistical difference ($P=0.0017$), indicating that the C2 group had a higher degree of cancer progression, which could help identify novel targets for anticancer drugs (Figure 4E).

Prognostic analysis of neural-related gene expression in EC

Using the LASSO regression technique, we attempted to determine a link between NRGs and EC prognosis. High expression of neurologically linked genes was shown to be associated with a poor prognosis ($P<0.05$) (Figures 5A-D). The expression of 42 NRGs may be a prognostic biomarker for EC

patients: the area under the curve (AUC) for 1 year, 3 years, and 5 years was 0.689, 0.693, and 0.653 respectively (Figure 5E). Individual prognostic analysis revealed that four of the 42 NRGs were statistically different and linked with EC prognosis ($P<0.01$) (Figure 5F). CHRM2 and GRIN1 were shown to be positively related to EC prognosis, while L1CAM and SEMA4F were found to be adversely related (Figure 5F). These results suggest that the expression of neural-related genes including CHRM2, GRIN1, L1CAM, and SEMA4F may be potential biomarkers of EC prognosis.

Correlation of CHRM2/GRIN1/L1CAM/SEMA4F expression with clinical characteristics

Based on RNA sequencing (RNA seq) and clinical data from the TCGA database, we divided the expression of CHRM2,

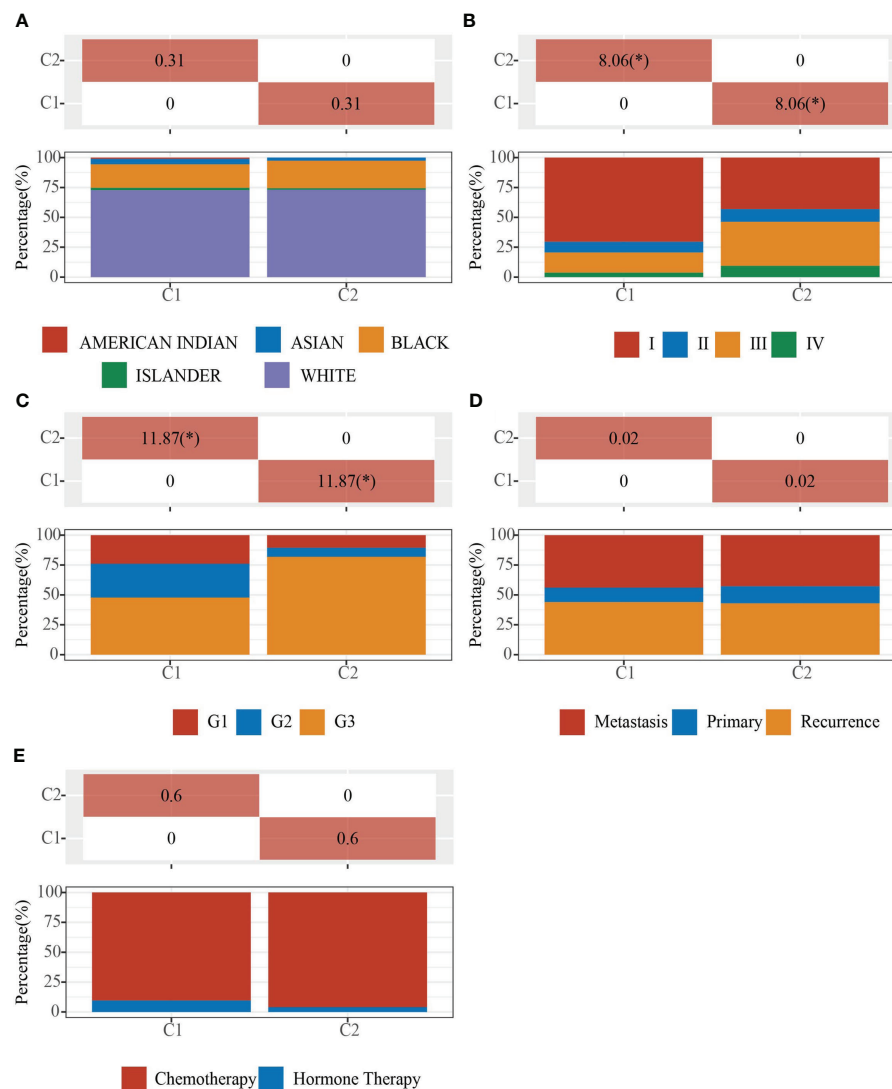


FIGURE 2
Clinical characteristics of C1 and C2. Demonstration of the proportion of different clinical features in different subgroups. **(A)** Ethnicity. **(B)** Stage. **(C)** Grade. **(D)** Primary, Recurrence and Metastasis. **(E)** Chemotherapy and Hormone Therapy. The * means that the difference in clinical features between the two groups is statistically significant ($p < 0.05$).

GRIN1, L1CAM, and SEMA4F into high and low expression groups, and defined the cutoff points for high expression of GRIN1 and L1CAM (top 25%) and low expression of GRIN1 and L1CAM (bottom 25%). Because the total expression of CHRM2 and SEMA4F was low, the cut-off point for high and low expression of both genes was set at 50%. The results showed that the high expression of CHRM2 was negatively correlated with EC grading and staging (Figure S2A) (Table 2); the high expression of GRIN1 was negatively correlated with EC grading and staging (Figure S2B) (Table 3); the high expression of L1CAM was positively correlated with EC tumor grading and staging (Figure S2C) (Table 4); the high expression of SEMA4F

was positively correlated with EC tumor grading and staging (Figure S2D) (Table 5).

The biological significance of CHRM2/GRIN1/L1CAM/SEMA4F in EC

We classified the EC data in the TCGA database into groups based on the expression levels of four neural-related genes: CHRM2, GRIN1, L1CAM, and SEMA4F, and performed GO and KEGG analyses on each group. The definitions of high and low expression were the same as those mentioned previously.

TABLE 1 Clinical characteristics of C1 and C2.

C1 vs. C2		Characteristics	C1	C2	P-value
Status	Alive		339	113	7.00E-07
	Dead		44	47	
Age	Mean (SD)		62.3 (11.5)	67.9 (9.1)	0
	Median [MIN, MAX]		62 [31,89]	67 [39,90]	
Gender	FEMALE		383	160	0.495
Race	AMERICAN INDIAN		4		
	ASIAN		16	4	
	BLACK		71	35	
	ISLANDER		7	2	
	WHITE		261	111	
Stage	I		3		8.76E-09
	IA		136	31	
	IB		111	33	
	IC		20	5	
	II		21	11	
	IIA		4	2	
	IIB		9	4	
	III		1	1	
	IIIA		22	18	
	IIIB		5	1	
	IIIC		18	14	
	IIIC1		10	12	
	IIIC2		9	13	
	IV		3	1	
	IVA		2	1	
	IVB		9	13	
Grade	G1		89	9	7.96E-15
	G2		108	12	
	G3		183	131	
new_tumor_event_type	High Grade		3	8	0.953
	Metastasis		22	15	
	Primary		6	5	
Radiation_therapy	Recurrence		22	15	1
	Non-radiation		12	7	
History_of_neoadjuvant_treatment	Radiation		19	12	1
	Neoadjuvant		1	1	
Therapy_type	No neoadjuvant		382	159	0.251
	Chemotherapy		95	73	
	Chemotherapy:		1	1	
	Chemotherapy::Other. specify in notes:Targeted Molecular therapy		1		
	Chemotherapy:Hormone Therapy		1	5	
	Chemotherapy:Targeted Molecular therapy		2	2	
	Hormone Therapy		10	3	

We gathered some functional pathways and used the ssGSEA algorithm to calculate functional pathway scores.

In the EC with high CHRM2 expression, 92 genes were upregulated and 24 genes were downregulated ($FC > 2$, $P < 0.05$) (Figures 6A, B). Compared with the CHRM2 low expression

group, the CHRM2 highly-expressed group contained upregulation of tumor-promoting pathways including endometrial cancer, Wnt signaling pathway, and estrogen signaling pathway. It also inhibits endometrial carcinogenesis and metastasis by activating the PPAR signaling system,

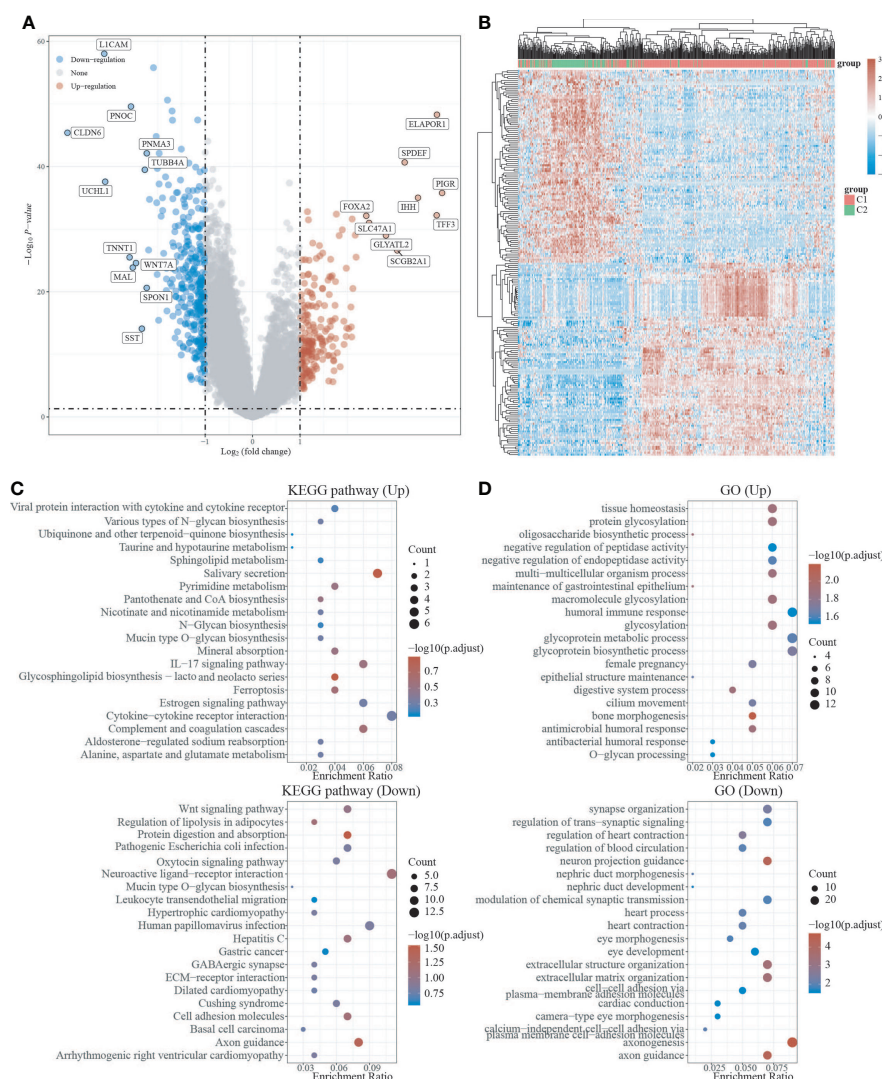


FIGURE 3

Differential expression and enrichment analysis of C1 and C2. **(A)** Volcano plots of C1 and C2 differentially expressed genes. Blue represents genes with high expression, red represents genes with low expression, and gray represents genes without differential expression. **(B)** Heat map of differential expression. **(C)** C1 activates or suppresses the KEGG pathway when compared to C2. **(D)** C1 activates or suppresses the GO pathway in comparison to C2.

suppressing the cAMP signaling pathway, cell adhesion molecules, vasculogenesis, amino acid synthesis and metabolism, and mucin-type O-glycan biosynthesis, among other things (Figures 6C, D). ssGSEA analysis showed that the CHRM2 gene was negatively associated with cellular response to hypoxia, tumor proliferation signature, DNA repair, G2M checkpoint, MYC targets, IL-10 anti-inflammatory signaling pathway, DNA replication, and positively associated with EMT markers, ECM-related genes, angiogenesis, TGFB, collagen formation (Figure 7).

In the EC with high GRIN1 expression, 465 genes were upregulated and 264 genes were downregulated (FC>2, P<0.05) (Figures S3A, S3B). Compared with the GRIN1 low expression

group, the GRIN1 high expression group inhibited the Wnt signaling pathway, signaling pathway regulating pluripotency of stem cells, cell adhesion molecules, hepatocellular carcinoma, and gastric cancer. Activation of cancer-related signaling pathways: p53 signaling pathway, cAMP signaling pathway, AMPK signaling pathway, breast cancer, and prostate cancer (Figures S3C, S3D). ssGSEA analysis showed that GRIN1 was negatively associated with cellular response to hypoxia, tumor proliferation signature, apoptosis, DNA repair, G2M checkpoint, inflammatory response, MYC targets, TGFB, IL-10 anti-inflammatory signaling pathway, DNA replication, collagen formation, and ECM degradation (Figure S4A).

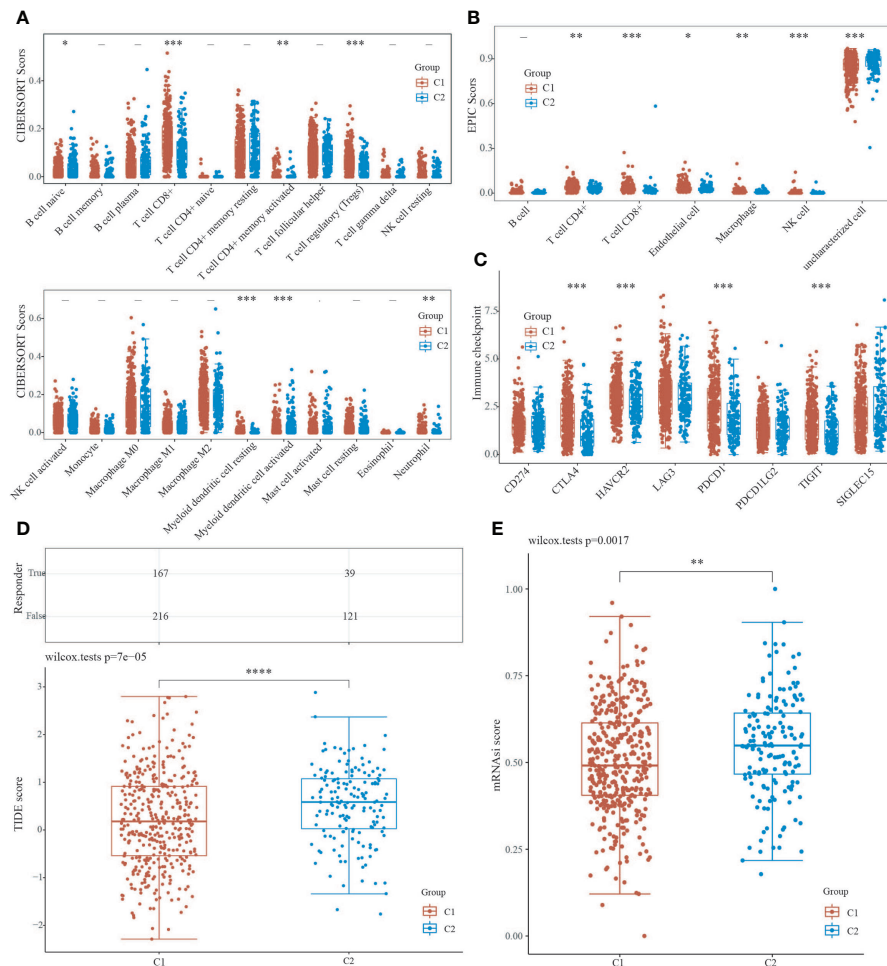


FIGURE 4

Analysis of C1 and C2 immune infiltration, immunological response, and stemness. (A, B) CIBERSORT and EPIC scores reveal a difference in immune cell infiltration between C1 and C2. (C) Immune checkpoint-associated genes are expressed differently in C1 and C2. (D) TIDE scores for C1 and C2 groups were compared using the TIDE algorithm for predicting cancer immune response. (E) The difference in stemness index between C1 and C2 as calculated by the OCLR method. (* $P < 0.05$, ** $P < 0.01$, *** $P < 0.001$, **** $P < 0.0001$).

In the EC with high L1CAM expression, 568 genes were upregulated and 493 genes were downregulated ($FC > 2$, $P < 0.05$) (Figures S5A, S5B). Compared with the L1CAM low expression group, the L1CAM highly-expressed group is consisted of upregulation of tumor-promoting pathways including PI3K-Akt signaling pathway, MAPK signaling pathway, cell adhesion molecules, and synapse organization. The p53 signaling pathway, Wnt signaling pathway, estrogen signaling pathway, and endometrial cancer pathway were inhibited (Figures S5C, S5D). ssGSEA analysis showed that L1CAM positively connected with cellular response to hypoxia, tumor proliferation signature, DNA repair, G2M checkpoint, MYC targets, TGFB, IL-10 anti-inflammatory signaling pathway, DNA replication, collagen production, and ECM degradation. reactive oxygen species (ROS) upregulation of genes was found to be negatively linked (Figure S4B).

In the EC with high SEMA4F expression, 11 genes were upregulated and 62 genes were downregulated ($FC > 2$, $P < 0.05$) (Figures S6A, S6B). Compared to the SEMA4F low expression group, The SEMA4F high expression group activated multiple diseases of neurodegeneration, Parkinson's disease, and Alzheimer's disease while inhibiting the IL-17 signaling pathway, chemical carcinogenesis, protein-coupled receptor signaling pathway, axoneme assembly, and acute inflammatory response (Figures S6C, S6D). ssGSEA analysis showed that SEMA4F was negatively correlated with tumor inflammation signature, ECM-related gene, angiogenesis, apoptosis, inflammatory response, P53 pathway, IL-10 anti-inflammatory signaling pathway, genes up-regulated by reactive oxygen species (ROS), tumor proliferation signature, DNA Repair, G2M checkpoint, MYC targets, TGFB, and DNA replication (Figure S4C).

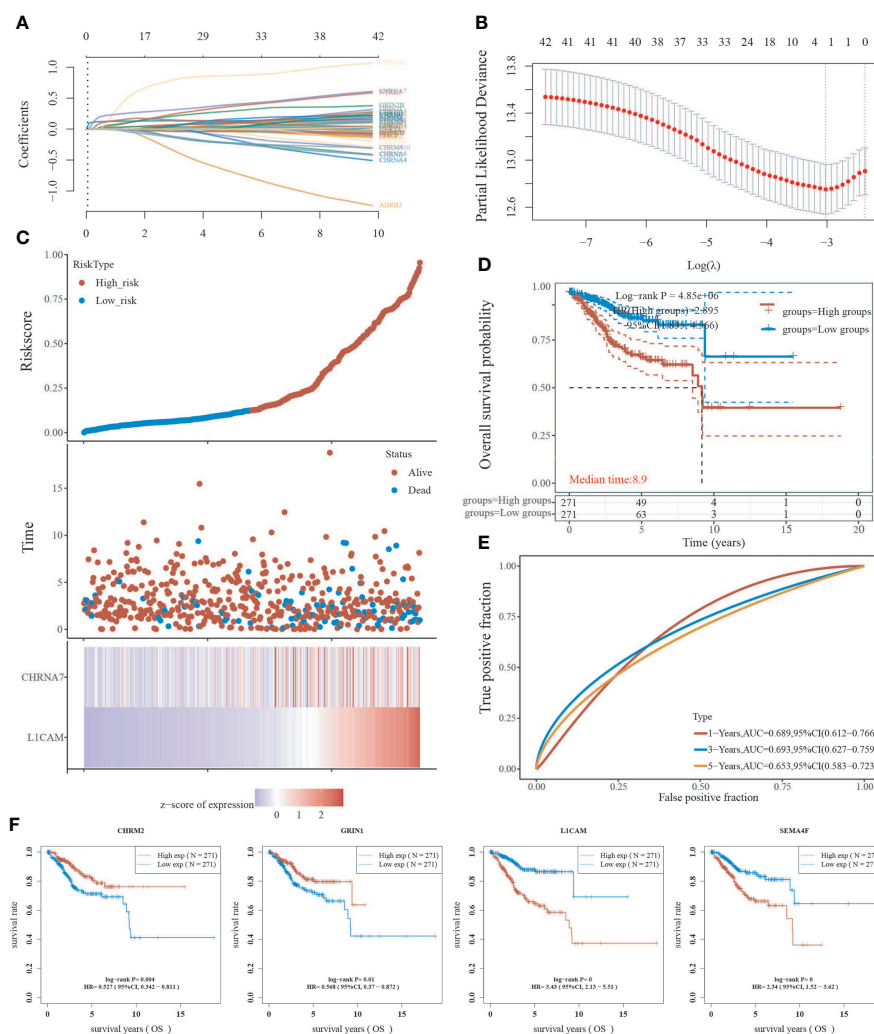


FIGURE 5

Analysis of neural-associated gene expression in EC for prognosis. (A) Coefficients of 42 neural-associated genes represented by λ parameter. (B) LASSO COX regression model was used to draw the partial likelihood deviance versus $\log(\lambda)$. (C) The correlation between risk and survival. A curve, scatter plot, and heatmap are all used to represent the data. (D) Curves of overall survival for high and low risk groups. (E) The receiver operating characteristic (ROC) analysis of risk scores. At 1, 3, and 5 years, the area under the curve (AUC) was 0.900, 0.919, and 0.939, respectively. (F) A univariate Cox analysis was used to look for genes linked to endometrial cancer prognosis.

The findings imply that the genes CHRM2, GRIN1, L1CAM, and SEMA4F in EC have pro- or oncogenic effects as a result of the combined activity of several signaling pathways influencing tumor growth.

Correlation between CHRM2/GRIN1/L1CAM/SEMA4F expression and immune infiltration, immune response and stemness

We used the immunedeconv R package to obtain immune infiltration data for high/low expression of CHRM2, GRIN1,

L1CAM, and SEMA4F in EC. In this research, the CIBERSORT and EPIC algorithms were applied.

The CIBERSORT algorithm showed that high expression of CHRM2 was positively correlated with T cell CD4+ memory resting ($P < 0.05$) and T cell regulatory (Tregs) ($P < 0.001$), myeloid dendritic cell resting ($P < 0.05$), mast cell activated ($P < 0.001$), and mast cell resting ($P < 0.05$), while it was negatively correlated with NK cell activated ($P < 0.05$), and macrophage M1 ($P < 0.05$) were negatively correlated (Figure 8A). The EPIC algorithm showed that high expression of CHRM2 was positively correlated with T cell CD4+ ($P < 0.001$), T cell CD8+ ($P < 0.001$), and endothelial cell ($P < 0.001$), but negatively correlated with macrophage ($P < 0.05$) (Figure 8B).

TABLE 2 Clinical characteristics of CHRM2 high expression group and CHRM2 low expression group.

	Characteristics	CHRM2 High	CHRM2 Low	P-value
Status	Alive	240	212	0.003
	Dead	32	59	
Age	Mean (SD)	62.8 (10.9)	65.2 (11.3)	0.015
	Median [MIN, MAX]	62 [34,90]	66 [31,90]	
Gender	FEMALE	272	271	0.11
Race	AMERICAN INDIAN	2	2	
	ASIAN	13	7	
	BLACK	43	63	
	ISLANDER	5	4	
Stage	WHITE	201	171	0.001
	I	2	1	
	IA	88	79	
	IB	79	65	
	IC	14	11	
	II	22	10	
	IIA	2	4	
	IIB	8	5	
	III		2	
	IIIA	21	19	
	IIIB	1	5	
	IIIC	10	22	
	IIIC1	9	13	
	IIIC2	6	16	
	IV	1	3	
	IVA	1	2	
	IVB	8	14	
Grade	G1	66	32	6.79E-07
	G2	75	45	
	G3	130	184	
	High Grade	1	10	
new_tumor_event_type	Metastasis	21	16	0.489
	Primary	6	5	
	Recurrence	16	21	
Radiation_therapy	Non-radiation	2	17	0.005
	Radiation	17	14	
History_of_neoadjuvant_treatment	No neoadjuvant	272	269	0.477
	Neoadjuvant		2	
Therapy_type	Chemotherapy	69	99	0.55
	Chemotherapy:Other. specify in notes:Targeted Molecular therapy	1		
	Chemotherapy:Hormone Therapy	2	4	
	Chemotherapy:Targeted Molecular therapy	2	2	
	Hormone Therapy	7	6	
	Chemotherapy:		2	

The CIBERSORT algorithm showed that high GRIN1 expression was positively correlated with T cell CD8+ ($P<0.01$), T cell regulatory (Tregs) ($P<0.001$), and NK cell resting ($P<0.01$) compared to low GRIN1 expression ($P<0.001$), while it was

negatively correlated with B cell plasma ($P<0.05$), NK cell activated ($P<0.05$), macrophage M2 ($P<0.05$), and myeloid dendritic cell activated ($P<0.05$) (Figure S7A). The EPIC algorithm showed that high expression of GRIN1 was positively

TABLE 3 Clinical characteristics of GRIN1 high expression group and GRIN1 low expression group.

	Characteristics	GRIN1 High	GRIN1 Low	P-value
Status	Alive	123	103	0.002
	Dead	13	33	
Age	Mean (SD)	62 (11.2)	66.4 (9.7)	0.001
	Median [MIN, MAX]	62 [34,89]	67 [33,90]	
Gender	FEMALE	136	136	0.031
Race	ASIAN	4	5	
	BLACK	18	35	
	ISLANDER	1	2	
	WHITE	106	82	
	AMERICAN INDIAN		1	
pTNM_stage	I	2		0.008
	IA	44	35	
	IB	47	28	
	IC	5	2	
	II	8	6	
	IIA	2	1	
	IIB	3	3	
	III	1	1	
	IIIA	8	14	
	IIIC	7	10	
	IIIC1	3	10	
	IIIC2	1	11	
	IV	1	1	
	IVA	2	1	
	IVB	2	11	
	IIIB		2	
Grade	G1	32	10	7.52E-09
	G2	40	13	
	G3	64	110	
	High Grade		3	
new_tumor_event_type	Metastasis	10	14	0.946
	Primary	3	5	
	Recurrence	8	10	
Radiation_therapy	Non-radiation	5	4	1
	Radiation	8	7	
History_of_neoadjuvant_treatment	No neoadjuvant	136	135	
	Neoadjuvant		1	
Therapy_type	Chemotherapy	35	63	0.278
	Hormone Therapy	4	2	
	Chemotherapy:		2	
	Chemotherapy:Hormone Therapy		1	
	Chemotherapy:Targeted Molecular therapy		1	

correlated with T cell CD4+ ($P<0.001$), T cell CD8+ ($P<0.001$), endothelial cell ($P<0.05$), but negatively correlated with macrophage ($P<0.01$) (Figure S7B).

The CIBERSORT algorithm showed that high L1CAM expression was positively correlated with T cell follicular helper ($P<0.01$), NK cell activated ($P<0.01$), macrophage M1

($P<0.001$), and myeloid dendritic cell activated ($P<0.01$), while it was negatively correlated with T cell CD8+ ($P<0.05$), T cell CD4 + memory resting ($P<0.05$), T cell regulatory (Tregs) ($P<0.001$), NK cell resting ($P<0.01$), macrophage M2($P<0.05$), myeloid dendritic cell resting ($P<0.001$) and neutrophil ($P<0.05$) (Figure S8A). The EPIC algorithm showed that high

TABLE 4 Clinical characteristics of L1CAM high expression group and L1CAM low expression group.

	Characteristics	L1CAM High	L1CAM Low	P-value
Status	Alive	97	125	1.17E-05
	Dead	39	11	
Age	Mean (SD)	68.4 (9.1)	61.2 (11.3)	0
	Median [MIN, MAX]	68 [49,90]	61 [34,87]	
Gender	FEMALE	136	136	0.474
Race	AMERICAN INDIAN	1	1	
	ASIAN	4	6	
	BLACK	39	28	
	ISLANDER	1	2	
	WHITE	80	94	
Stage	I		1	3.33E-08
	IA	23	50	
	IB	24	44	
	IC	5	6	
	II	11	6	
	IIA	4		
	IIB	3	5	
	IIIA	12	10	
	IIIB	2	1	
	IIIC	13	6	
	IIIC1	11	2	
	IIIC2	14	2	
	IV	1		
	IVA	2	1	
	IVB	11	2	
	G1	2	40	
	G2	8	49	
	G3	119	46	
Grade	High Grade	7	1	1.37E-21
	Metastasis	11	6	
	Primary	1	3	
new_tumor_event_type	Recurrence	14	8	0.313
	Non-radiation	9	5	
	Radiation	10	6	
Radiation_therapy	Non-radiation	9	5	1
	Radiation	10	6	
History_of_neoadjuvant_treatment	Neoadjuvant	1		0.042
	No neoadjuvant	135	136	
Therapy_type	Chemotherapy	74	31	0.042
	Chemotherapy:	1	1	
	Chemotherapy:Hormone Therapy	3		
	Chemotherapy:Targeted Molecular therapy	2	2	
	Hormone Therapy	1	5	
	Chemotherapy::Other. specify in notes:Targeted Molecular therapy		1	

expression of L1CAM was positively correlated with B cell (P<0.05) and with T cell CD4+ (P<0.001) and T cell CD8+ (P<0.001), but endothelial cell (P<0.01) negatively (Figure S8B).

The CIBERSORT algorithm showed that high SEMA4F expression was positively correlated with B cell naive (P<0.01),

myeloid dendritic cell resting (P<0.01), myeloid dendritic cell activated (P<0.001), and mast cell activated (P<0.05), while it was negatively correlated with T cell CD8+ (P<0.001), T cell CD4+ memory activated (P<0.01), T cell regulatory (Tregs) (P<0.001) and neutrophil (P<0.05) (Figure S9A). The EPIC algorithm

TABLE 5 Clinical characteristics of SEMA4F high expression group and SEMA4F low expression group.

	Characteristics	SEMA4F High	SEMA4F Low	P-value
Status	Alive	212	240	0.001
	Dead	60	31	
Age	Mean (SD)	65.2 (11.2)	62.8 (10.9)	0.013
	Median [MIN, MAX]	64 [33,90]	63 [31,87]	
Gender	FEMALE	272	271	0.043
Race	ASIAN	6	14	
	BLACK	60	46	
	ISLANDER	3	6	
	WHITE	187	185	
	AMERICAN INDIAN		4	
Stage	I	1	2	0.035
	IA	81	86	
	IB	59	85	
	IC	13	12	
	II	21	11	
	IIA	4	2	
	IIB	7	6	
	III	1	1	
	IIIA	19	21	
	IIIB	4	2	
	IIIC	20	12	
	IIIC1	14	8	
	IIIC2	11	11	
	IV	2	2	
	IVA	3		
	IVB	12	10	
Grade	G1	26	72	2.97E-07
	G2	56	64	
	G3	182	132	
	High Grade	8	3	
new_tumor_event_type	Metastasis	24	13	0.825
	Primary	6	5	
	Recurrence	23	14	
Radiation_therapy	Non-radiation	15	4	0.155
	Radiation	17	14	
History_of_neoadjuvant_treatment	No neoadjuvant	272	269	
	Neoadjuvant		2	
Therapy_type	Chemotherapy	91	77	0.428
	Chemotherapy:	1	1	
	Chemotherapy:Hormone Therapy	3	3	
	Chemotherapy:Targeted Molecular therapy	1	3	
	Hormone Therapy	4	9	
	Chemotherapy::Other. specify in notes:Targeted Molecular therapy		1	

showed that high expression of SEMA4F was positively correlated with T cell CD4+ ($P<0.01$), but macrophage ($P<0.01$) and NK cell ($P<0.001$) negatively (Figure S9B).

In addition, we analyzed the correlation between ICG and the expression of CHRM2, GRIN1, L1CAM, and SEMA4F. CHRM2

expression was positively correlated with CTLA4 ($P<0.05$) and SIGLEC15 ($P<0.01$) (Figure 8C); GRIN1 expression was positively correlated with CTLA4 ($P<0.05$), while negatively correlated with PDCCD1LG2 ($P<0.01$) (Figure S7C); L1CAM expression was positively correlated with CD274 ($P<0.05$), LAG3 ($P<0.001$) and

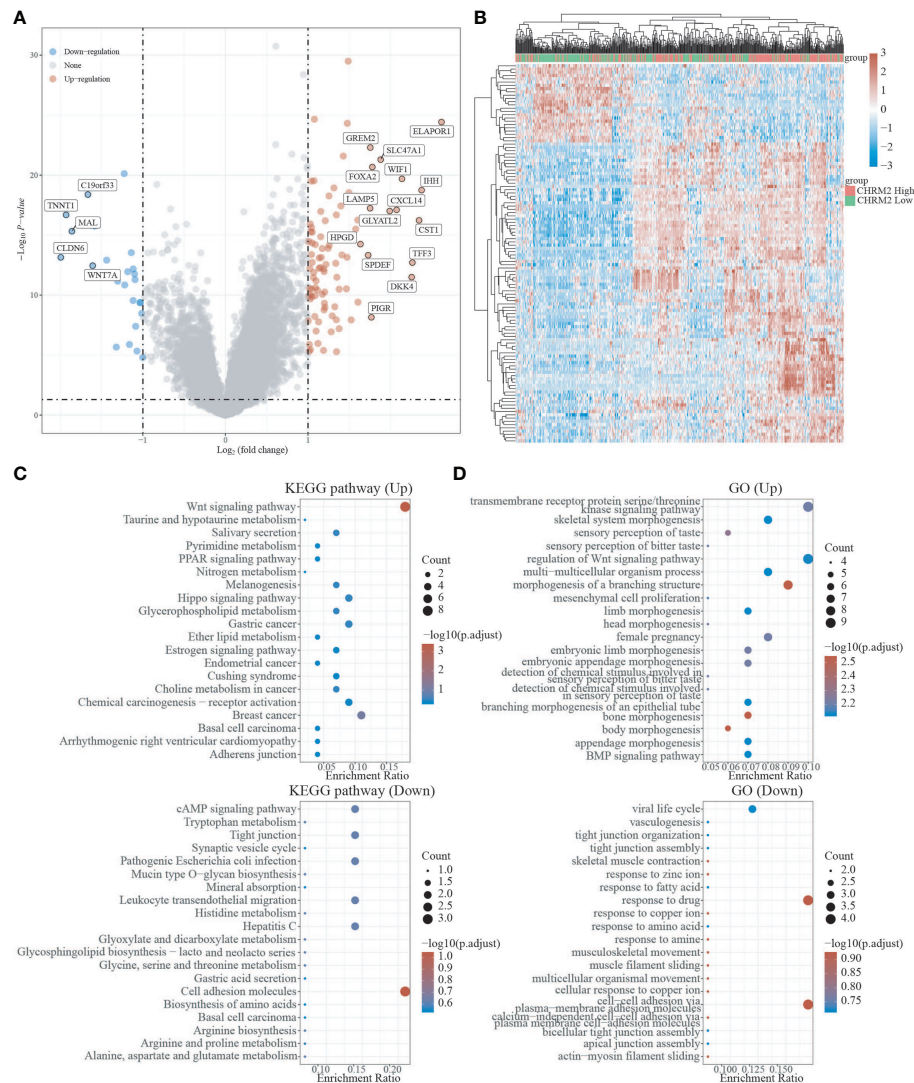


FIGURE 6
Differential expression and enrichment analysis of CHRM2 high and low expression groups. **(A)** The volcano plot shows the differential gene expression of CHRM2 high expression group and CHRM2 low expression group was drawn with fold-change values and adjusted P. **(B)** Differential gene expression showed by heatmap (only 50 genes were displayed because of the large quantity of the genes); **(C, D)** KEGG and GO analysis showed the upregulated/downregulated pathways of the CHRM2 high expression group compared with the low expression group. When $P < 0.05$ or $FDR < 0.05$ is considered to be enriched to a meaningful pathway.

PDCD1LG2 ($P < 0.05$), while negatively correlated with CTLA4 ($P < 0.001$) (Figure S8C). SEMA4F was positively correlated with HAVCR2 ($P < 0.01$), LAG3 ($P < 0.001$), PDCD1 ($P < 0.001$) and TIGIT ($P < 0.01$) (Figure S8C), while negatively correlated with CTLA4 ($P < 0.001$), HAVCR2 ($P < 0.01$), LAG3 ($P < 0.05$), PDCD1 ($P < 0.001$), TIGIT ($P < 0.001$) and SIGLEC15 ($P < 0.05$) (Figure S9C). The TIDE algorithm revealed that high expression of CHRM2, and L1CAM was linked to poor immune response (Figures 8D, S8D), whereas high expression of GRIN1 was linked to a positive immunological response (Figure S7D). Stem cell scores were lower in the high expression group of CHRM2 (Figure 8E) and

GRIN1 (Figure S7E) than in the low expression group, according to Spearman correlation analysis of OCLR scores, while the inverse was true for L1CAM (Figure S8E) and SEMA4F (Figure S9E).

Gene landscape of CHRM2/GRIN1/L1CAM/SEMA4F

We obtained mutational, transcriptomic, and clinical data of EC patients from the TCGA database and found the highest

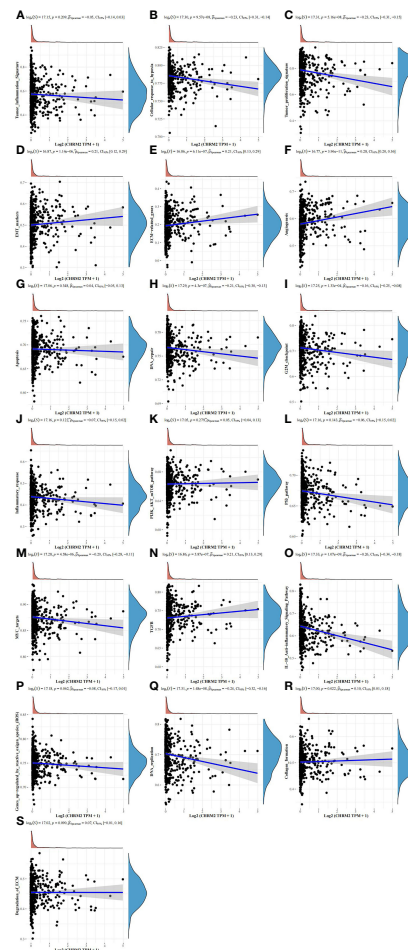


FIGURE 7

Analysis of the correlation between CHRM2 and 19 pathways using the Spearman, ssGSEA algorithm. (Statistically significant difference at $P < 0.05$). (A, G, J–L, P, S) The ssGSEA analysis showed that the CHRM2 gene was not statistically correlated with tumor inflammation signature, apoptosis, inflammatory response, PI3K-AKT-MTOR pathway, p53 pathway, gene up-regulated by reactive oxygen species (ROS) and degradation of ECM. (B, C, H, I, M, O, Q) CHRM2 gene was negatively associated with cellular response to hypoxia, tumor proliferation signature, DNA repair, G2M checkpoint, MYC targets, IL-10 anti-inflammatory signaling pathway and DNA replication. (D–F, N, R) CHRM2 gene was positively associated with EMT markers, ECM-related genes, angiogenesis, TGFβ and collagen formation.

rate of PETN mutations in EC (57%), with varying degrees of mutations in neuro-oncology-related genes CHRM2, GRIN1, L1CAM, and SEMA4F: L1CAM (9%), SEMA4F (6%), CHRM2 (5%), and GRIN1 (3%) (Figure 9). The differences between GRIN1 and tumor mutational load (TMB) and microsatellite instability (MSI) were statistically significant, while L1CAM was negatively connected with TMB and SEMA4F was positively correlated with MSI. The findings imply that GRIN1, L1CAM, and SEMA4F are closely linked to immunotherapy and can respond to immunotherapy characteristics (Figure 10).

Discussion

In the tumor microenvironment, neurons are critical biological components. Denervation and regulation of neurotransmitters for tumor treatment have become hot topics of research in recent years (27). Tumors select neuronal programs to promote their development and progression. The frequency of endometrial cancer has been increasing each year as is the number of patients with endometrial cancer brain metastases (28). Although nerve-cancer crosstalk influences tumor growth, the etiology is yet unknown (7).

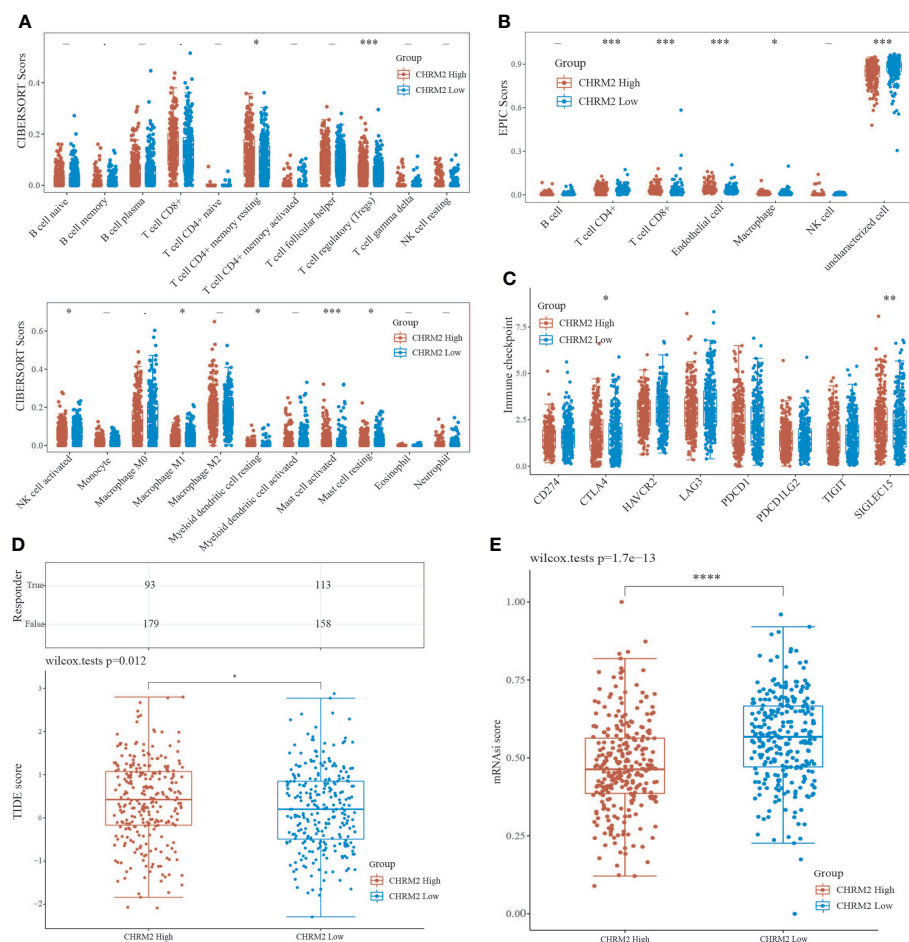


FIGURE 8

An analysis of immune infiltration, immunological response, and stemness in two groups with high and low CHRM2 expression. (A, B) Comparison of CHRM2 high expression group and CHRM2 low expression group in immune infiltration obtained with CIBERSORT and EPIC algorithm; The horizontal axis represents different immune cells, the vertical axis represents the immune scores (*P<0.05, ***P<0.001). (C) Comparison immune checkpoint genes expression in CHRM2 high expression group and CHRM2 low expression group; The horizontal axis represents different immune checkpoint genes, the vertical axis represents the expression level (*P<0.05, **p<0.01). (D) Statistical table of immune response and the distribution of immune response scores of the different groups in predict results. (*P<0.05). (E) Comparison of CHRM2 high expression group and CHRM2 low expression group in stemness was exhibited by mRNAiQ score with OCLR algorithm (****p<0.0001).

The identification of cancer subgroups based on gene expression has proven useful in clinical settings, such as endometrial cancer molecular staging (29). Based on NRGs, we classified endometrial cancer into two subtypes: C1 and C2. Prognosis, clinical-stage, pathological grading, and immunological status were all statistically different between the two subtypes. In comparison to C2, C1 had a lower clinical stage and pathological grade, a better prognosis, better immune activation, stronger immune checkpoint gene expression, and

was more suited to immunotherapy. In addition, there were statistical differences in enriched pathways and biological processes between C1 and C2. These data support the link between neural-related genes and endometrial cancer, and they suggest that using NRGs to classify EC subtypes could be clinically effective.

A prognostic model was constructed by LASSO-Cox, and CHRM2, GRIN1, L1CAM, and SEMA4F were identified as EC prognostic-related genes. CHRM2 is a gene encoding muscarinic

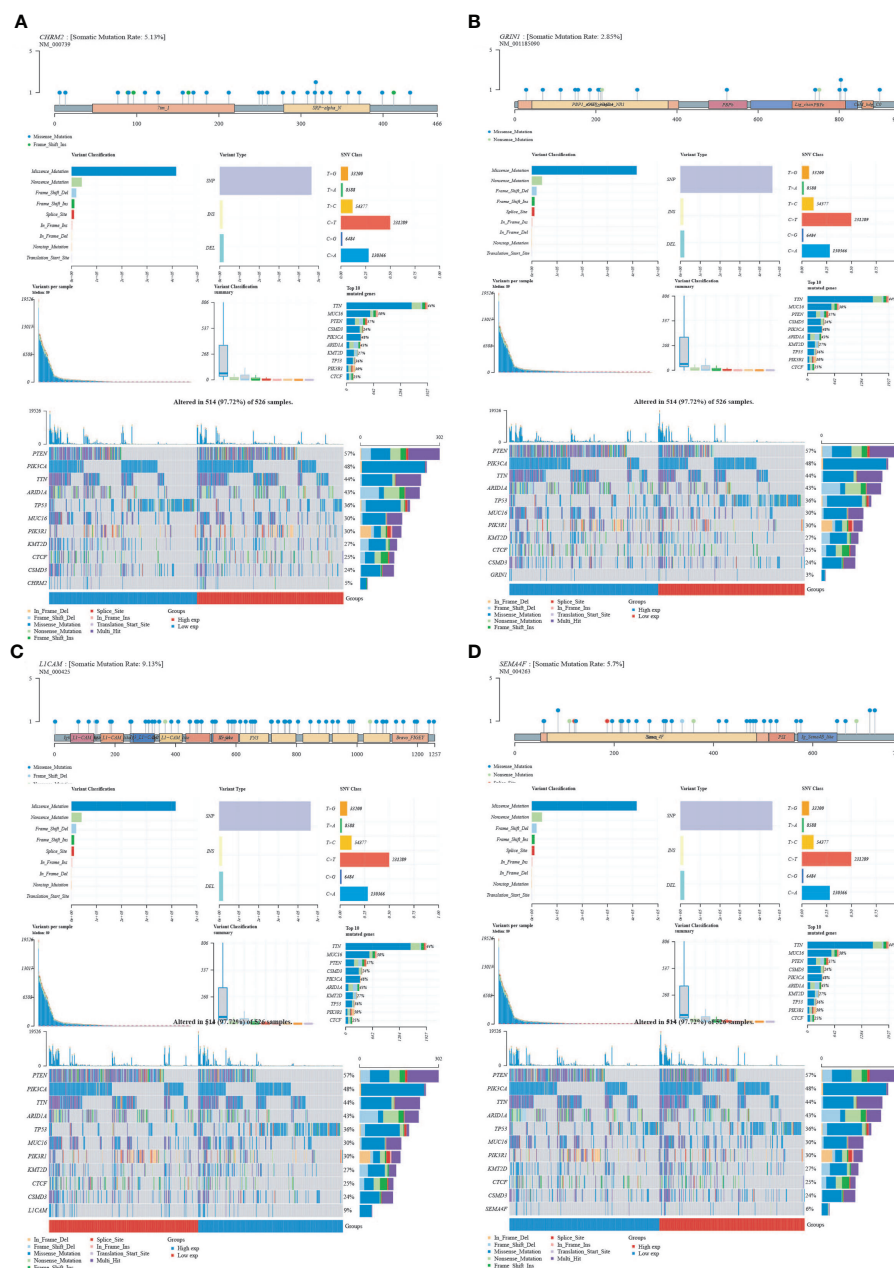


FIGURE 9
Mutational landscape of CHRM2, GRIN1, L1CAM and SEMA4F. (A) CHRM2. (B) GRIN1. (C) L1CAM. (D) SEMA4F.

receptor (mAChR) on neuronal cell membranes, which affects cholinergic activity by influencing the transcription level, mRNA stability, and affinity of the receptor (30). Previous studies have found that CHRM2 is enriched in the PI3K-Akt signaling pathway and its methylation rate rises as a progression of gastric cancer (31). CHRM2 inhibits the invasion and migration of non-small cell lung cancer through the M2R/ERK/Akt/NF- κ B axis (32). In the central nervous system (CNS), glutamate receptor subunit 1 (GRIN1) is essential for synaptic transmission and plasticity (33). GRIN1 mutations are linked to schizophrenia, neurodevelopmental delay, epilepsy, and glioma, but no other tumors are linked to them (34–36). For the first time, our findings reveal that CHRM2 and GRIN1 play significant roles in endometrial cancer and are positively related to endometrial cancer prognosis. L1 cell adhesion molecule (L1CAM) is a membrane glycoprotein of the immunoglobulin family (37). Consistent with previous findings, L1CAM plays a key role in EC cancer cell migration and adhesion (38). Furthermore, we discovered that L1CAM was linked to immune cell infiltration and ICG (CD274, LAG3, PDCD1LG2, CTLA4), and we hypothesized that L1CAM may have a regulatory role in the tumor microenvironment, influencing tumor growth and metastasis. SEMA4F is a membrane-bound glycoprotein of the signaling element receptor family that has been linked to cancer in prior research, including being associated to breast cancer development (39), axonogenesis and neurogenesis in prostate cancer (40), and glioma prognosis (41). We propose that SEMA4F is a key

regulator of tumor growth, angiogenesis, migration, and apoptosis and that it plays a role in endometrial cancer.

In summary, our study reveals the relevance of neural-related genes to endometrial cancer. Our findings suggest that EC reclassification based on neural-related genes is expected to be translated into clinical applications. The genes CHRM2, GRIN1, L1CAM, and SEMA4F, which are prognostically associated with endometrial cancer, play important roles in immune cell infiltration, immune response and stem cell relevance, clinical features, enriched pathways, and immunotherapy, and are potential biomarkers for EC with significant clinical translational potential. Further investigation can be considered to quantify the indicators through tissue specimens and animal experiments to validate them for greater application in the treatment of tumors.

Data availability statement

The original contributions presented in the study are included in the article/[Supplementary Material](#). Further inquiries can be directed to the corresponding authors.

Author contributions

FC and YZ did the analysis. FC wrote the paper. YD and PL did the data sorting and charting. TQ and WJ conceived the paper. All authors contributed to the article and approved the submitted version.

Funding

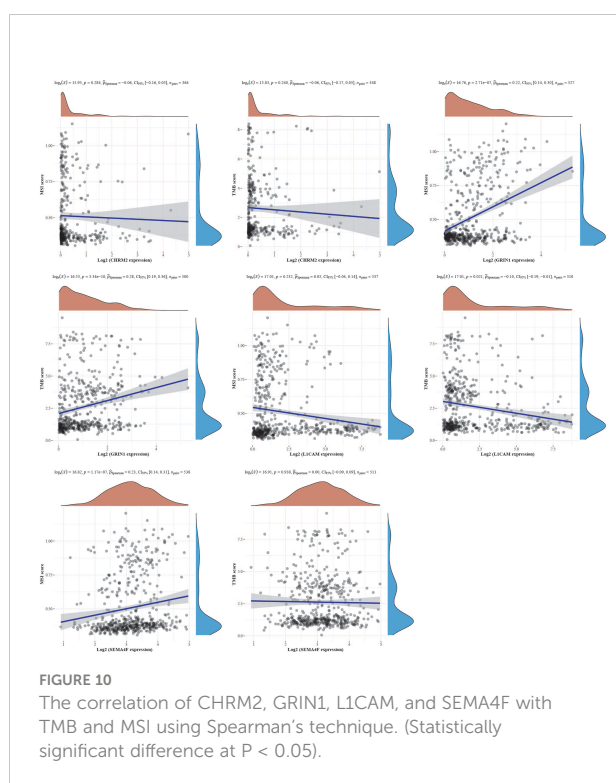
This work was in part supported by the Innovation and Entrepreneurship Talent Project of Lanzhou (2020-RC-52) and the “Innovation Fund” for graduate students of the First Clinical Medical College of Gansu University of Chinese Medicine (LCCX2021011).

Acknowledgments

We apologize to those colleagues whose important work could not be cited due to space constraints.

Conflict of Interest

The authors declare that the research was conducted in the absence of any commercial or financial relationships that could be construed as a potential conflict of interest.



Publisher's note

All claims expressed in this article are solely those of the authors and do not necessarily represent those of their affiliated organizations, or those of the publisher, the editors and the reviewers. Any product that may be evaluated in this article, or claim that may be made by its manufacturer, is not guaranteed or endorsed by the publisher.

Supplementary material

The Supplementary Material for this article can be found online at: <https://www.frontiersin.org/articles/10.3389/fonc.2022.951437/full#supplementary-material>

SUPPLEMENTARY FIGURE 1

Comparison of differential expression of 42 neural-related genes between C1 and C2.

SUPPLEMENTARY FIGURE 2

Comparison of the clinical characteristics of the two groups with high and low expression of CHRM2, GRIN1, L1CAM and SEMA4F. (A) CHRM2. (B) GRIN1. (C) L1CAM. (D) SEMA4F.

SUPPLEMENTARY FIGURE 3

Differential expression and enrichment analysis of GRIN1 high expression group and GRIN1 low expression group.

SUPPLEMENTARY FIGURE 4

The connection of GRIN1, L1CAM, and SEMA4F with 19 pathways was investigated using the Spearman, ssGSEA algorithm. (S4A) GRIN1. (A) GRIN1. (B) L1CAM. (C) SEMA4F.

SUPPLEMENTARY FIGURE 5

Differential expression and enrichment analysis of L1CAM high expression group and L1CAM low expression group.

SUPPLEMENTARY FIGURE 6

Differential expression and enrichment analysis of SEMA4F high expression group and SEMA4F low expression group.

SUPPLEMENTARY FIGURE 7

Analysis of immune infiltration, immunological response, and stemness in two groups with high and low GRIN1 expression.

SUPPLEMENTARY FIGURE 8

Analysis of immune infiltration, immunological response, and stemness in two groups with high and low L1CAM expression.

SUPPLEMENTARY FIGURE 9

Analysis of immune infiltration, immunological response, and stemness in two groups with high and low SEMA4F expression.

References

1. Siegel RL, Miller KD, Fuchs HE, Jemal A. Cancer statistics, 2021. *CA: Cancer J Clin* (2021) 71:7–33. doi: 10.3322/caac.21654
2. Sung H, Ferlay J, Siegel RL, Laversanne M, Soerjomataram I, Jemal A, et al. Global cancer statistics 2020: GLOBOCAN estimates of incidence and mortality worldwide for 36 cancers in 185 countries. *CA: Cancer J Clin* (2021) 71:209–49. doi: 10.3322/caac.21660
3. Xia C, Dong X, Li H, Cao M, Sun D, He S, et al. Cancer statistics in China and united states, 2022: profiles, trends, and determinants. *Chin Med J* (2022) 135:584–90. doi: 10.1097/CM9.0000000000002108
4. Faulkner S, Jobling P, March B, Jiang CC, Hondermarck H. Tumor neurobiology and the war of nerves in cancer. *Cancer Discovery* (2019) 9:702–10. doi: 10.1158/2159-8290
5. Silverman DA, Martinez VK, Dougherty PM, Myers JN, Calin GA, Amit M. Cancer-associated neurogenesis and nerve-cancer cross-talk. *Cancer Res* (2021) 81:1431–40. doi: 10.1158/0008-5472.CAN-20-2793
6. Magnon C, Hall SJ, Lin J, Xue X, Gerber L, Freedland SJ, et al. Autonomic nerve development contributes to prostate cancer progression. *Sci (New York N.Y.)* (2013) 341:1236361. doi: 10.1126/science.1236361
7. Zhao C-M, Hayakawa Y, Kodama Y, Muthupalani S, Westphalen CB, Andersen GT, et al. Denervation suppresses gastric tumorigenesis. *Sci Trans Med* (2014) 6:250ra115. doi: 10.1126/scitranslmed.3009569
8. Ni T, Huang T, Gu S-L, Wang J, Liu Y, Sun X, et al. DRG neurons promote perineural invasion of endometrial cancer via GluR2. *J Cancer* (2020) 11:2518–28. doi: 10.7150/jca.40055
9. Español P, Luna R, Soler C, Caruana P, Altés-Arranz A, Rodríguez F, et al. Neural plasticity of the uterus: New targets for endometrial cancer? *Women's Health (London England)* (2022) 18:17455057221095537. doi: 10.1177/17455057221095537
10. Talhouk A, McConechy MK, Leung S, Li-Chang HH, Kwon JS, Melnyk N, et al. A clinically applicable molecular-based classification for endometrial cancers. *Br J Cancer* (2015) 113:299–310. doi: 10.1038/bjc.2015.190
11. Liu J, Lichtenberg T, Hoadley KA, Poisson LM, Lazar AJ, Cherniack AD, et al. An integrated TCGA pan-cancer clinical data resource to drive high-quality survival outcome analytics. *Cell* (2018) 173:400–16.e11. doi: 10.1016/j.cell.2018.02.052
12. Zhang Y-G, Jin M-Z, Zhu X-R, Jin W-L. Reclassification of hepatocellular cancer with neural-related genes. *Front In Oncol* (2022) 12:877657. doi: 10.3389/fonc.2022.877657
13. Giorgi FM, Ceraolo C, Mercatelli D. The r language: An engine for bioinformatics and data science. *Life (Basel Switzerland)* (2022) 12:648. doi: 10.3390/life12050648
14. Wilkerson MD, Hayes DN. ConsensusClusterPlus: a class discovery tool with confidence assessments and item tracking. *Bioinf (Oxford England)* (2010) 26:1572–3. doi: 10.1093/bioinformatics/btq170
15. Villanueva RAM, Chen ZJ. Ggplot2: Elegant graphics for data analysis (2nd Ed.). *Measurement: Interdiscip Res Perspect* (2019) 17:160–7. doi: 10.1080/15366367.2019.1565254
16. David CC, Jacobs DJ. Principal component analysis: a method for determining the essential dynamics of proteins. *Methods In Molecular Biology (Clifton, N.J.)* (2014) 1084:193–226. doi: 10.1007/978-1-62703-658-0_11
17. Ritchie ME, Phipson B, Wu D, Hu Y, Law CW, Shi W, et al. Limma powers differential expression analyses for RNA-sequencing and microarray studies. *Nucleic Acids Res* (2015) 43:e47. doi: 10.1093/nar/gkv007
18. Friedman J, Hastie T, Tibshirani R. Regularization paths for generalized linear models via coordinate descent. *J Stat Software* (2010) 33:1–22. doi: 10.18637/jss.v033.i01
19. Ashburner M, Ball CA, Blake JA, Botstein D, Butler H, Cherry JM, et al. Gene ontology: tool for the unification of biology. *Gene Ontology Consortium. Nat Genet* (2000) 25:25–9. doi: 10.1038/75556
20. Kanehisa M, Goto S. KEGG: kyoto encyclopedia of genes and genomes. *Nucleic Acids Res* (2000) 28:27–30. doi: 10.1093/nar/28.1.27
21. Yu G, Wang L-G, Han Y, He Q-Y. clusterProfiler: an r package for comparing biological themes among gene clusters. *Omics J Integr Biol* (2012) 16:284–7. doi: 10.1089/omi.2011.0118
22. Abd ElHafeez S, D'Arrigo G, Leonardis D, Fusaro M, Tripepi G, Roumeliotis S. Methods to analyze time-to-Event data: The cox regression analysis. *Oxid Med Cell Longevity* (2021) 2021:1302811. doi: 10.1155/2021/1302811
23. Newman AM, Liu CL, Green MR, Gentles AJ, Feng W, Xu Y, et al. Robust enumeration of cell subsets from tissue expression profiles. *Nat Methods* (2015) 12:453–7. doi: 10.1038/nmeth.3337

24. Racle J, Gfeller D. EPIC: A tool to estimate the proportions of different cell types from bulk gene expression data. *Methods In Mol Biol (Clifton N.J.)* (2020) 2120:233–48. doi: 10.1007/978-1-0716-0327-7_17
25. Jiang P, Gu S, Pan D, Fu J, Sahu A, Hu X, et al. Signatures of T cell dysfunction and exclusion predict cancer immunotherapy response. *Nat Med* (2018) 24:1550–8. doi: 10.1038/s41591-018-0136-1
26. Malta TM, Sokolov A, Gentles AJ, Burzykowski T, Poisson L, Weinstein JN, et al. Machine learning identifies stemness features associated with oncogenic dedifferentiation. *Cell* (2018) 173:338–54. doi: 10.1016/j.cell.2018.03.034
27. Sartori R, Hagg A, Zampieri S, Armani A, Winbanks CE, Viana LR, et al. Perturbed BMP signaling and denervation promote muscle wasting in cancer cachexia. *Science Translational Medicine* (2021) 13:eay9592. doi: 10.1126/scitranslmed.aay9592
28. Bhambhani HP, Zhou O, Cattle C, Taiwo R, Diver E, Hayden Gephart M. Brain metastases from endometrial cancer: Clinical characteristics, outcomes, and review of the literature. *World Neurosurg* (2021) 147:e32–9. doi: 10.1016/j.wneu.2020.11.087
29. Vermij L, Smit V, Nout R, Bosse T. Incorporation of molecular characteristics into endometrial cancer management. *Histopathology* (2020) 76:52–63. doi: 10.1111/his.14015
30. Luo X, Kranzler HR, Zuo L, Zhang H, Wang S, Gelernter J. CHRM2 variation predisposes to personality traits of agreeableness and conscientiousness. *Hum Mol Genet* (2007) 16:1557–68. doi: 10.1093/hmg/ddm104
31. Wang J, Ding Y, Wu Y, Wang X. Identification of the complex regulatory relationships related to gastric cancer from lncRNA-miRNA-mRNA network. *J Cell Biochem* (2020) 121:876–87. doi: 10.1002/jcb.29332
32. Zhao Q, Yue J, Zhang C, Gu X, Chen H, Xu L. Inactivation of M2 AChR/NF- κ B signaling axis reverses epithelial-mesenchymal transition (EMT) and suppresses migration and invasion in non-small cell lung cancer (NSCLC). *Oncotarget* (2015) 6:29335–46. doi: 10.18632/oncotarget.5004
33. Nishimura N, Kumaki T, Murakami H, Enomoto Y, Katsumata K, Toyoshima K, et al. Arthrogryposis multiplex congenita with polymicrogyria and infantile encephalopathy caused by a novel variant. *Hum Genome Variation* (2020) 7:29. doi: 10.1038/s41439-020-00116-8
34. Krzystanek M, Asman M, Witecka J, Palasz A, Wiaderkiewicz R. Selected single-nucleotide variants in GRIN1, GRIN2A, and GRIN2B encoding subunits of the NMDA receptor are not biomarkers of schizophrenia resistant to clozapine: exploratory study. *Pharmacol Rep PR* (2021) 73:309–15. doi: 10.1007/s43440-020-00165-4
35. Allen AS, Berkovic SF, Cossette P, Delanty N, Dlugos D, Eichler EE, et al. *De novo* mutations in epileptic encephalopathies. *Nature* (2013) 501:217–21. doi: 10.1038/nature12439
36. Yang A, Wang X, Hu Y, Shang C, Hong Y. Identification of hub gene GRIN1 correlated with histological grade and prognosis of glioma by weighted gene coexpression network analysis. *BioMed Res Int* (2021) 2021:4542995. doi: 10.1155/2021/4542995
37. Altevogt P, Doberstein K, Fogel M. L1CAM in human cancer. *Int J Cancer* (2016) 138:1565–76. doi: 10.1002/ijc.29658
38. Bednarikova M, Vinklerova P, Gottwaldova J, Ovesna P, Hausnerova J, Minar L, et al. The clinical significance of DJ1 and L1CAM serum level monitoring in patients with endometrial cancer. *J Clin Med* (2021) 10. doi: 10.3390/jcm10122640
39. Gabrovská PN, Smith RA, Tiang T, Weinstein SR, Haupt LM, Griffiths LR. Semaphorin-plexin signalling genes associated with human breast tumorigenesis. *Gene* (2011) 489:63–9. doi: 10.1016/j.gene.2011.08.024
40. Ayala GE, Dai H, Powell M, Li R, Ding Y, Wheeler TM, et al. Cancer-related axonogenesis and neurogenesis in prostate cancer. *Clin Cancer Res an Off J Am Assoc For Cancer Res* (2008) 14:7593–603. doi: 10.1158/1078-0432.CCR-08-1164
41. Shergalis A, Bankhead A, Luesakul U, Muangsins N, Neamati N. Current challenges and opportunities in treating glioblastoma. *Pharmacol Rev* (2018) 70:412–45. doi: 10.1124/pr.117.014944



OPEN ACCESS

EDITED BY

Jinhui Liu,
Nanjing Medical University, China

REVIEWED BY

Baohong Liu,
Lanzhou Veterinary Research Institute,
(CAAS), China
Zhichao Cheng,
Xuzhou Medical University, China
Runsang Pan,
Guizhou Medical University, China

*CORRESPONDENCE

Hui Li
lihui_1973@126.com
Yu-kun Li
yukun_li@foxmail.com

[†]These authors have contributed
equally to this work

SPECIALTY SECTION

This article was submitted to
Gynecological Oncology,
a section of the journal
Frontiers in Oncology

RECEIVED 17 August 2022

ACCEPTED 15 September 2022

PUBLISHED 05 October 2022

CITATION

Zhang J, Li Y, Fan T-y, Liu D, Zou W-d,
Li H and Li Y-k (2022) Identification of
bromodomain-containing proteins
prognostic value and expression
significance based on a genomic
landscape analysis of ovarian serous
cystadenocarcinoma.
Front. Oncol. 12:1021558.
doi: 10.3389/fonc.2022.1021558

COPYRIGHT

© 2022 Zhang, Li, Fan, Liu, Zou, Li and
Li. This is an open-access article
distributed under the terms of the
[Creative Commons Attribution License](#)
(CC BY). The use, distribution or
reproduction in other forums is
permitted, provided the original
author(s) and the copyright owner(s)
are credited and that the original
publication in this journal is cited, in
accordance with accepted academic
practice. No use, distribution or
reproduction is permitted which does
not comply with these terms.

Identification of bromodomain-containing proteins prognostic value and expression significance based on a genomic landscape analysis of ovarian serous cystadenocarcinoma

Juan Zhang^{1†}, Yan Li^{1†}, Ting-yu Fan², Dan Liu¹, Wen-da Zou¹,
Hui Li^{1*} and Yu-kun Li^{1*}

¹Department of Assisted Reproductive Centre, Zhuzhou Central Hospital, Xiangya Hospital Zhuzhou Central South University, Central South University, Zhuzhou, China, ²Hunan Province Key Laboratory of Tumor Cellular and Molecular Pathology, Cancer Research Institute, University of South China, Hengyang, China

Background: Ovarian serous cystadenocarcinoma (OSC), a common gynecologic tumor, is characterized by high mortality worldwide. Bromodomain (BRD)-containing proteins are a series of evolutionarily conserved proteins that bind to acetylated Lys residues of histones to regulate the transcription of multiple genes. The ectopic expression of BRDs is often observed in multiple cancer types, but the role of BRDs in OSC is still unclear.

Methods: We performed the differential expression, GO enrichment, GSEA, immune infiltration, risk model, subtype classification, stemness feature, DNA alteration, and epigenetic modification analysis for these BRDs based on multiple public databases.

Results: Most BRDs were dysregulated in OSC tissues compared to normal ovary tissues. These BRDs were positively correlated with each other in OSC patients. Gene alteration and epigenetic modification were significant for the dysregulation of BRDs in OSC patients. GO enrichment suggested that BRDs played key roles in histone acetylation, viral carcinogenesis, and transcription coactivator activity. Two molecular subtypes were classified by BRDs for OSC, which were significantly correlated with stemness features, m6A methylation, ferroptosis, drug sensitivity, and immune infiltration. The risk model constructed by LASSO regression with BRDs performed moderately well in prognostic predictions for OSC patients. Moreover, BRPF1 plays a significant role in these BRDs for the development and progression of OSC patients.

Conclusion: BRDs are potential targets and biomarkers for OSC patients, especially BRPF1.

KEYWORDS

ovarian serous cystadenocarcinoma, bioinformatic analysis, bromodomain-containing proteins, epigenetic modification, histone modification regulators

Introduction

Ovarian serous cystadenocarcinoma (OSC) ranks eighth in terms of most commonly diagnosed and lethal mortality overall for gynecological oncology, resulting in all kinds of family problems and a huge social burden (1). Molecular medicine has devoted enormous resources to examining signaling pathways and the underlying molecular mechanisms of signalling (2, 3). In spite of this, the mortality rate for OSC is still high, and the five-year survival rate for women with advanced OSC is lower than 50% (2). Therefore, finding biomarkers and therapeutic targets that are effective in diagnosing and treating this malignancy is of great significance.

Bromodomains (BRDs), a group of evolutionarily conserved protein–protein interaction modules, can specifically recognize acetylated lysine (Kac)_{1,2} residues in histone tails and other substrates to epigenetically regulate gene transcription (4). As epigenetic readers, BRDs are also involved in gene fusions, resulting in the generation of diverse and frequent oncogenic proteins (4, 5). The sequence and structural similarities of BRD-containing proteins have led to their classification into eight subfamilies (5). According to a previous study, all BRDs have a distinct secondary structure with a left-handed four-helix bundle connected by two loops (ZA and BC) (6). The ZA and BC loops form a hydrophobic pocket, which coordinates acetylated lysine at the end of the histone tail (6). Tyr1125, Tyr1167, and Asn1168 are at the center of the acetyllysine binding pocket, and they serve as the most conserved residues (6). BRD subfamily I has four members, CECR2 (a chromatin remodeling factor) (7), BPTF (a transcription factor) (8), KAT2A (a Histone acetyl transferase) (9) and KAT2B (a Histone acetyl transferase) (9). Subfamily II includes 4 transcription factors, BRD2/3/4 (10–12) and BRDT (13), and a chromatin remodeling factor, BAZ1A (14). BAZ1B (15), BRWD3 (16), PHIP (17), BRWD1 (18), CREBBP (19), EP300 (19) and BRD8 (20) belong to subfamily III. The subfamily IV members includes 7 transcription factors, ATAD2 (21), ATAD2B (22), BRD1 (23), BRPF1 (24), BRPF3 (25), BRD7 (26) and BRD9 (27). Subfamily V includes SP140 (28), SP140L (29), SP100 (30), SP110 (31), TRIM24 (32), TRIM33 (33), TRIM66 (34), BAZ2A (35) and BAZ2B (7). Subfamily VI has a histone methyltransferase (MLL) (36) and

a transcriptional regulator E3 SUMO ligase (TRIM28) (36). BRD subfamily VII has four transcriptional regulators, including TAF1 (37), TAF1L (38), ZMYND8 (39) and ZMYND11 (40). Subfamily VIII was including 3 chromatin remodeling factors, SMARCA2/4 (41, 42) and PB1 (43), and a methyltransferase, ASH1L (44). The dysregulation of these BRDs plays an important role in the development of inflammatory, autoimmune, and cancer diseases (45–48). However, the biological function and prognostic significance of these BRDs for OSC progression are still poorly understood.

To elucidate the roles of these BRDs in the development and progression of OSC, we utilized The Cancer Genome Atlas (TCGA) database to confirm the mRNA levels of BRDs in OSC. Then, we also confirmed the DNA alteration level of BRDs by the cBioPortal database. Subsequently, we used the STRING database to construct a PPI network. Next, we predicted the biological functions and molecular pathways of BRDs in OSCs based on the DAVID database. Moreover, we performed subtype classification and LASSO modelling to further elucidate the functions and prognostic value of these BRDs in OSC progression based on the TCGA database. Finally, we found that BRPF1 was a significant BRG in the development of OSC. The BRPF1, as a subunit of the MOZ histone acetyltransferase (HAT), recognizes acetylated histones, such as H2AK5ac, H4K12ac, H3K14ac, H4K8ac, and H4K5ac (49). Moreover, several studies have reported that abnormal BRPF1 expression plays an important role in many cancer types, including liver cancer (50), medulloblastoma (51), and leukemia (52). But the role of BRPF1 in OSC progression is still unclear. Therefore, we further confirmed the effect of BRPF1 inhibition on OSC cell proliferation, glucose homeostasis and Wnt pathway activation. The research strategy is showed in Figure 1.

Methods

Bioinformatic expression analysis

We used the Cancer Genome Atlas (TCGA) (<https://www.cancer.gov/tcga>) database to confirm the mRNA levels of BRDs

in 376 OSC patients (53), which contains clinical parameters, DNA alteration, and mRNA expression data for multiple cancer types. The Clinical Proteomic Tumor Analysis Consortium (CPTAC) database (<https://proteomics.cancer.gov/programs/cptac>) (54), an important protein expression database for many cancers, and the Human Protein Atlas (HPA) database (<https://www.proteinatlas.org/>) (55), an excellent protein expression database for cancer patients by IHC staining, were utilized to confirm BRPF1 protein expression and location in OSC patients. The Cancer Cell Line Encyclopedia (CCLE) database (<https://sites.broadinstitute.org/ccle>) was used to confirm the levels of BRPF1 in multiple OSC cancer cell lines. The database could prompt which cell lines was suitable for further cell experiment (56). The GTEX database (<https://www.gtexportal.org/>) was utilized to determine the mRNA levels of BRDs in 88 normal ovary samples (57). TIMER database (<https://cistrome.shinyapps.io/timer/>) was a systematical website for confirming the immune cell abundances by TIMER algorithm, including B cells, CD4+ T cells, CD8+ T cells, Macrophages, Neutrophils, and Dendritic cells which was used to confirm the correlation between immune infiltration and BRPF1 (58).

DNA alteration analysis

The cBioPortal database (<http://www.cbioportal.org/>) was an open-access, open-source resource for elucidated cancer molecular profiles and clinical attributes, which was utilized to detect DNA alterations in BRDs in OSC patients (59).

PPI network construction and GO enrichment

PPI network construction of 42 BRDs was based on the STRING database (<https://cn.string-db.org/>), which was an excellent website for constructing PPI network *via* utilizing proteomics and genomics data (60). The GO and KEGG enrichment analyses were based on the Database for Annotation, Visualization and Integrated Discovery (DAVID) database (<https://david.ncifcrf.gov/>) for these BRDs (61). LinkedOmics database (<https://linkedomics.org/>) was a nice website tool to confirm the expression, correlation, and gene functions of BRD-related genes in OSC patients, which was based on the TCGA database (62).

Subtype classification

The “proportion of ambiguous clustering” (PAC) measure quantifies the middle segment. It is defined as the fraction of sample pairs with consensus indices falling in the interval $(u_1, u_2) \in [0, 1]$, where u_1 is a value close to 0 and u_2 is a value close to 1 (for instance $u_1 = 0.1$ and $u_2 = 0.9$). A low value of PAC indicates a flat middle segment, and a low rate of discordant assignments across permuted clustering runs. We can infer the optimal number of clusters by the K value having the lowest PAC. Using the ConsensusClusterPlus package of R, 1000 iterations were used to evaluate cluster stability. Moreover, four-fifths of the total sample was drawn 100 times, $\text{clusterAlg} = 'hc'$, $\text{innerLinkage} = 'ward D2'$. Clustering heatmaps were generated using the ‘pheatmap’ package

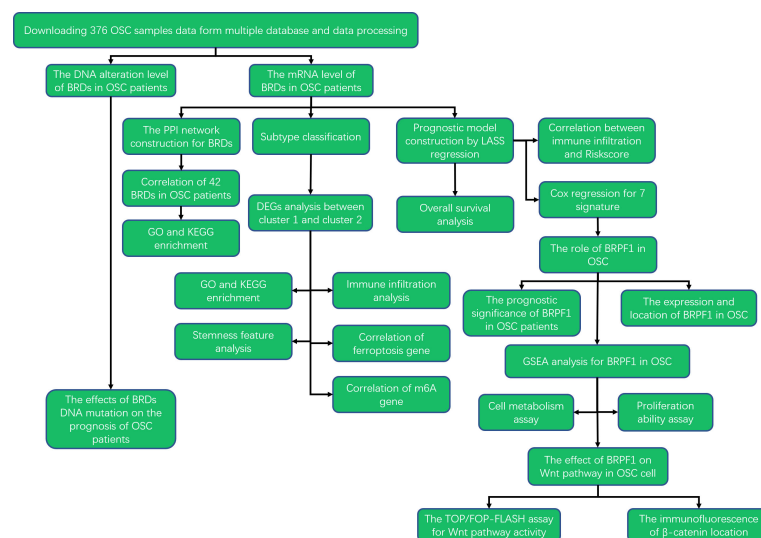


FIGURE 1
Flow chart of the study.

in R. A hierarchical clustering algorithm and heatmaps were drawn using the R package pheatmap v1.0.12. Heatmaps of gene expression were only used when SD > 0.1 was used. Then we used the GO and KEGG enrichment analysis to obtain the molecular functions between different clusters. Immune infiltration, stemness features, and drug sensitivity analysis were carried out to compare the molecular properties between two clusters. All statistics were performed using the R package.

Prognostic model construction

Prognostic model can be used to study the prognosis of a series of genes on a tumor samples, based on the lasso or multivariable cox iterative regression method for dimension reduction and build a prognosis model (model contains the number of genes will not necessarily equal to input the number of genes) or directly through the multi-factors cox model building (model contains gene number is equal to input the number of genes, Note the number of input genes). The model is a RiskScore formula containing multiple genes. Each gene has a weight. Negative numbers represent the gene as a protective gene, while positive numbers represent the gene as a dangerous gene. The difference between Signature and nomogram prognostic models is that the former can only include genetic factors, while the latter can include clinical factors. After converting count data to TPM and normalizing the data \log_2 (TPM+1), normalized transcription data were used to calculate gene expression on the basis of \log_2 (TPM+1). In addition, missing and incomplete samples were deleted when clinical information was merged. Next, there were 376 OSC samples for subsequent analysis. The survival difference between groups was compared using the log-rank test. We evaluated the predictive accuracy of the risk score in all datasets using time-dependent ROC curve analysis (v 0.4). The LASSO regression algorithm was utilized for feature selection, 10-fold cross-validation was used, and the R package glmnet was used for the analysis. The R software ggstatsplot package was used to draw the correlations between gene expression and immune score. To visualize differentially expressed genes, the “pheatmap” package in R software was used. The RiskScore formula = \sum (the expression amount of each gene multiplied by the corresponding coefficient). According to the median risk score, we divided the patients into two groups. All statistics were performed using the R package. A p value <0.05 was considered statistically significant.

Stemness and immune infiltration analysis

The detailed bioinformatic methods are described in our previous article (63).

Cell culture and transfection

Human ovarian cancer cells (SKOV3) were purchased from the American Type Culture Collection (ATCC, VA, USA) and cultured in DMEM containing 10% (v/v) foetal bovine serum (FBS; Gibco, Invitrogen, Carlsbad, CA, USA) and 1% penicillin/streptomycin (GIBCO, CA, USA). All cells were incubated at 37°C and 5% CO₂ (2). BRPF1 shRNA and empty vector plasmids were purchased from HonourGene (Changsha, China). For transient cell transfection, SKOV3 cells were seeded in 6-well plates and transfected with 3 µg empty vector and 3 µg BRPF1 shRNA plasmid using Lipofectamine 3000 (Invitrogen, Carlsbad, CA, USA) according to the protocol to establish a cell line with BRPF1 knockdown.

Proliferation analysis

For MTT analysis, five thousand SKOV3 cells were seeded into 96-well plates for 24, 48, and 72 hours. In the subsequent step, the cells were treated with 0.5% MTT solution (5 mg/ml, Sigma-Aldrich; Merck KGaA) for 4 hours. Then, the MTT solution was removed, and DMSO was added. Cell numbers were calculated from an absorbance measurement at 490 nm. For EdU analysis, cell proliferation was evaluated with an EdU kit (RiboBio, Guangzhou, China). All assays were repeated three times.

ATP, glucose, LD, and ROS measurements

An ATP assay kit (NJJCBIO, A095-1-1) was used to confirm the ATP level. A glucose kit (glucose oxidase method) (NJJCBIO, A154-1-1) was used to confirm the glucose level. A lactic acid assay (NJJCBIO, A019-2-1) kit was utilized to measure the lactic acid level. A reactive oxygen species assay kit (NJJCBIO, E004-1-1) was utilized to measure the ROS level. In these experiments, the OD values were measured at wavelengths of 505 nm (for glucose), 525 nm (for ROS), 530 nm (for lactic acid) and 636 nm (for ATP) after the reagents were mixed step by step according to the protocol.

Immunofluorescence

Cells were fixed for 5 minutes in 100% methanol, followed by permeabilization for 5 minutes in PBS with 0.1% Triton X-100. Then, the cells were incubated in 10% normal goat serum for 1 h to block nonspecific protein-protein interactions. Then, the cells were incubated with the antibody anti-β-catenin (Abcam, ab32572, 1:250) overnight. Following primary

antibody incubation, a secondary antibody (Abcam, ab150079 1 µg/ml) was used to label the cells. Two hours later, 0.1% DAPI was used to stain the nucleus for 15 min. Images were detected by confocal microscopy (Leica, Jena, Germany).

Dual-luciferase reporter gene

M50 Super 8x TOPFlash (VT8105) plasmid and M51 Super 8X FOPFlash (TOPFlash Mutant; VT8196) plasmid were purchased from Ubo Bio. Vector plasmid and M50 Super 8X TOPFlash were cotransfected into SKOV3 cells at a transfection ratio of 10:1, which was used as the control group of TOPFlash. BRPF1 shRNA and M50 Super 8X TOPFlash were cotransfected into SKOV3 cells at a transfection ratio of 10:1, which were used as the BRPF1 knockdown group of TOPFlash. Vector plasmid and M51 Super 8X FOPFlash were cotransfected into SKOV3 cells at a transfection ratio of 10:1, which were used as the control group of FOPFlash. BRPF1 shRNA and M51 Super 8X FOPFlash were cotransfected into SKOV3 cells at a transfection ratio of 10:1, which were used as the BRPF1 knockdown group of FOPFlash. Each group had 3 auxiliary wells. After successful transfection, substrate was added, and luciferase activity was measured..

Western blot

Please refer to our previous article for specific methods (64). In brief, the extracted proteins were collected, denatured, and electrophoresed through a 10% SDS-polyacrylamide gel. The samples were loaded, and electrophoresis was performed for 80 min followed by transfer to PVDF membranes and blocking in 5% skimmed milk at 37°C. After shaking for 2 h, the membranes were incubated with primary antibodies (BRPF1, Abcam, Cat. No. ab282024, 1:500 dilution; beta-actin, Abcam, Cat. No. ab6276, 1:1,000 dilution) at 4°C overnight with shaking. The membranes were then incubated in secondary antibodies (conjugated goat antirabbit IgG; CWBIO, Cat. No. CW0103S, 1:2,000 dilution) at room temperature for 2 h and washed in TBST three times for 15 min. Then, the membranes were incubated in Super Signal ECL-HRP detection reagent (ComWin Biotech) for 1 min followed by exposure to film in a visualizer.

Statistical analysis

All statistical analyses were performed in the R language. All statistical tests were bilateral, and $P < 0.05$ was considered statistically significant.

Results

Ectopic expression of BRDs in OSC patients

First, we confirmed the expression of these BRDs in OSC tissue samples compared to normal ovary tissue samples based on TCGA and GTEx databases. The results showed that BRDs of subfamily I were decreased in OSC samples (Figure 2A). BRD2 was significantly decreased, but BRD4 was significantly increased in OSC samples in BRD subfamily II (Figure 2B). Both genes of BRD subfamily III were decreased in OSC samples (Figure 2C). The members of BRD subfamily IV, ATAD2B, BRD1, BRPF1, and BRD9, were downregulated, but ATAD2 was increased in OSC tissues (Figure 2D). In BRD subfamily V, the expression levels of SP140L, SP140, SP100, SP110, TRIM24, TRIM66, BAZ2A and BAZ2B were significantly reduced, but TRIM33 expression was markedly enhanced (Figure 2E). KMT2A, a subfamily VI gene, was significantly decreased in OSC samples (Figure 2F). In BRD subfamily VII, TAF1, TAF1L and ZMYND11 were significantly decreased, but ZMYND8 was markedly increased in OSC samples (Figure 2G). The members of BRDs of subfamily VIII, ASH1L, PBRM1 and SMARCA2, were significantly decreased, but SMARCA4 was significantly increased in OSC samples compared to normal tissue samples (Figure 2H). These results indicated that the ectopic expression of BRDs might be involved in the development and progression of OSC.

DNA alterations of BRDs in OSCs

Next, we confirmed the DNA alterations of these BRDs in OSC samples based on the cBioPortal database. These BRDs all have different levels of DNA mutations in OSC samples, such as CECR2 (2.7%), BPTF (4%), KAT2A (1.4%), KAT2B (2.2%), BRD2 (6%), BRD3 (2.6%), BRD4 (17%), BRDT (3%), BAZ1A (2.1%), BAZ1B (4%), BRWD3 (1.9%), PHIP (2.4%), BRWD1 (2.6%), CREBBP (5%), EP300 (2.5%), BRD8 (2.1%), ATAD2 (35%), ATAD2B (3%), BRD1 (12%), BRPF1 (3%), BRPF3 (6%), BRD7 (1.4%), BRD9 (14%), SP140L (1.5%), SP140 (1.9%), SP100 (2.2%), SP110 (1.9%), TRIM24 (11%), TRIM33 (2.4%), TRIM66 (0.7%), BAZ2A (2.6%), BAZ2B (5%), KMT2A (4%), TRIM28 (4%), ZMYND8 (11%), TAF1 (2.6%), TAF1L (1.5%), ZMYND11 (8.8%), ASH1L (11%), PBRM1 (2.2%), SMARCA2 (9%), and SMARCA4 (12%) (Figure 3A). The overall survival analysis showed that the DNA alteration group of these OSC patients had a favorable prognosis compared to the non-DNA alteration group (Figure 3B). Moreover, the types of DNA alterations included amplification, deep deletion, multiple alterations, mutation, and structural variants (Figure 3C).

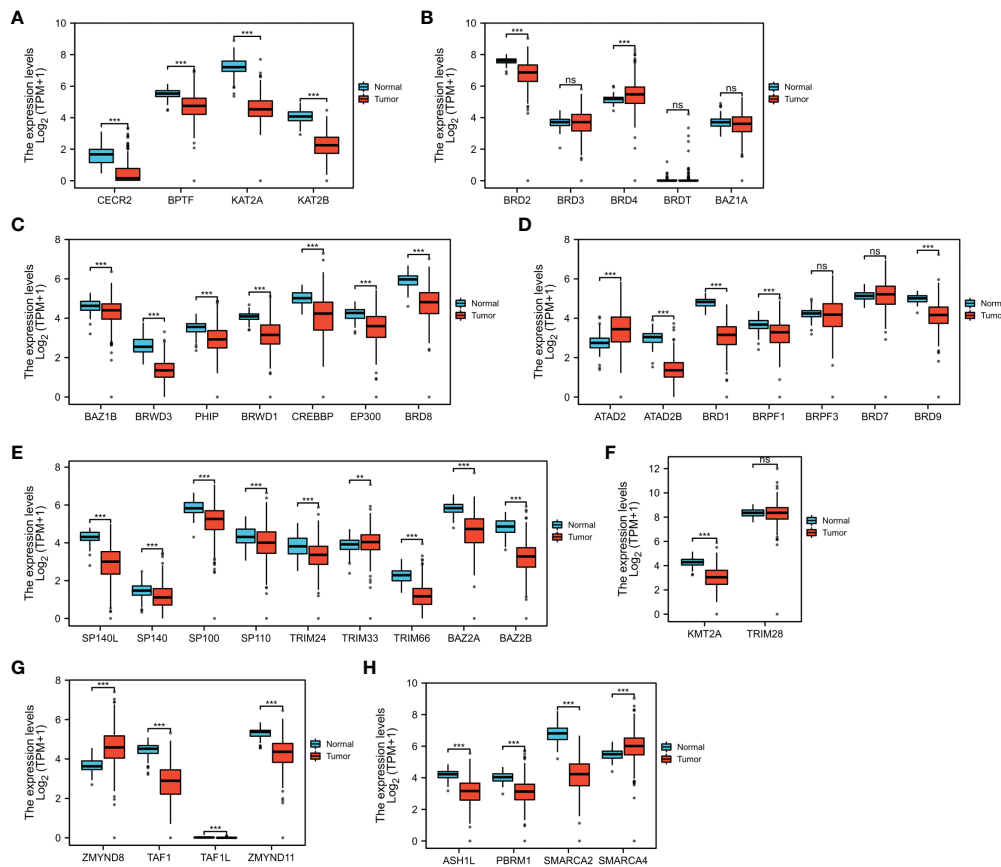


FIGURE 2

BRD mRNA levels in the OSC. The mRNA levels of BRD subfamilies I (A)/II (B)/III (C)/IV (D)/V (E)/VI (F)/VII (G)/VIII (H) in OSC samples and normal ovary samples based on TCGA and GETx databases. ns > 0.05; **p < 0.01; ***p < 0.001.

Possible molecular functions of BRDs in OSC

To further elucidate the possible molecular functions of BRDs in OSC progression, we constructed a PPI network for these BRDs based on the STRING database (Figure 4A). Furthermore, we analyzed the correlations among these BRDs in OSC patients based on the TCGA database OSC dataset (Figure 4B). We also found that these BRDs were enriched in covalent chromatin modification, histone modification, internal protein amino acid acetylation, internal peptidyl-lysine acetylation, and histone acetylation for biological progression terms (Figure 4C); in nuclear chromatin, acetyltransferase complex, protein acetyltransferase complex, histone acetyltransferase complex, and SWI/SNF superfamily type complex for cellular component terms (Figure 4D); and in histone binding, modification-dependent protein binding, acetylation-dependent protein binding, lysine-acetylated histone binding, and transcription coactivator activity for molecular function terms (Figure 4E). Moreover, KEGG

analysis indicated that these genes were also enriched in viral carcinogenesis, human T-cell leukemia virus 1 infection, the thyroid hormone signaling pathway and the Notch signaling pathway (Figure 4F). We also confirmed each BRDs functions in OSC progression based on LinkedOmics database, which indicated that these BRDs were mostly involved in metabolic process, growth, chromatin binding, molecular transducer activity, and lipid binding (Supplemental Figure 1). These results indicated that these BRDs might collaboratively drive viral carcinogenesis by epigenetic regulation, especially histone acetylation to drive OSC progression.

Classification of BRD subtypes in OSC

To further refine the potential role of BRDs in OSC, we used the ConsensusClusterPlus R package to identify OSC patients from the TCGA database into two subtypes based on the 42 BRDs, which classify 234 cases into Cluster 1 and 142 cases into Cluster 2 (Figure 5A). Moreover, the 127 differentially expressed

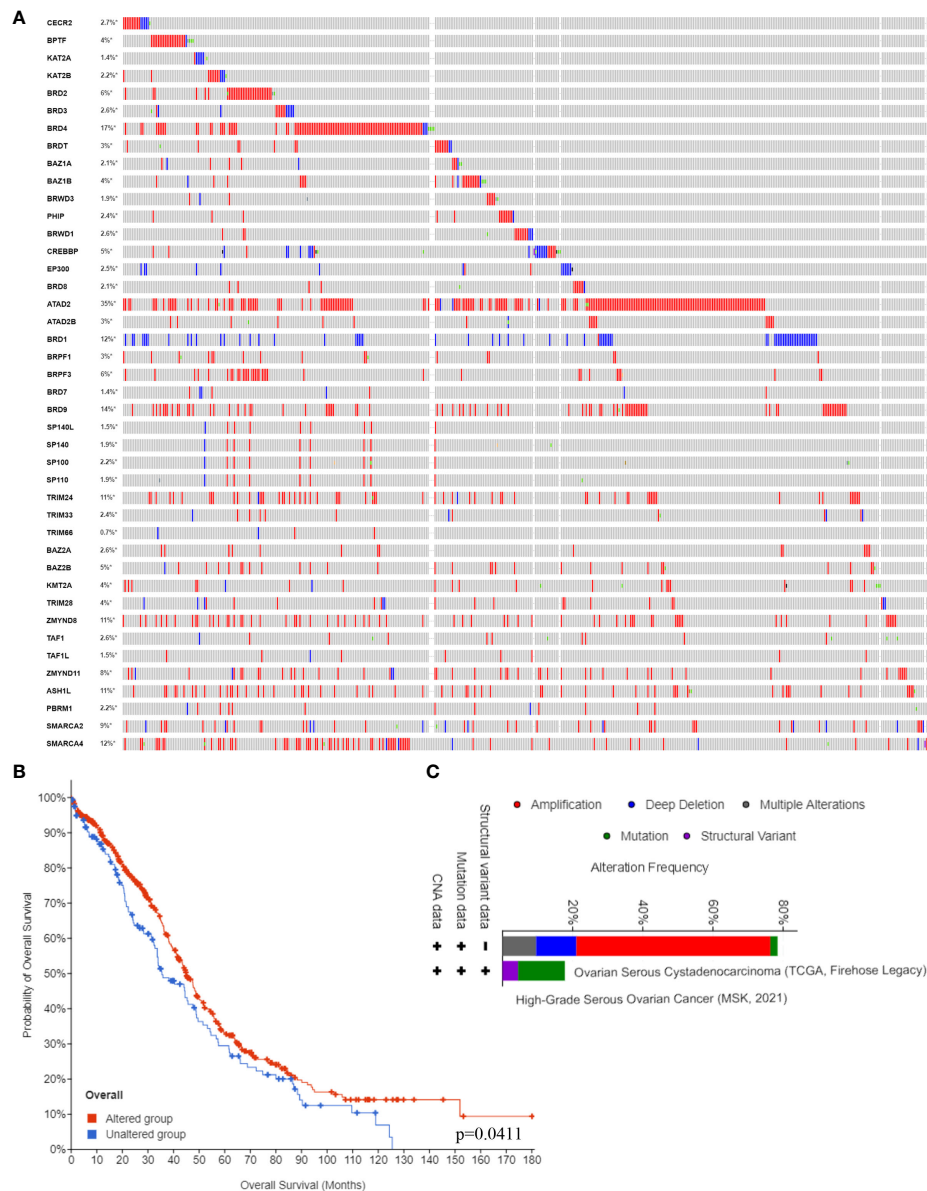


FIGURE 3

BRD DNA alteration levels in the OSC. (A) The DNA alteration levels of BRDs in OSC samples and normal ovary samples based on the cBioPortal database. (B) The overall survival analysis of OSC patients with or without BRD DNA alterations. (C) The types of BRG alterations in OSC samples based on the cBioPortal database. * $p < 0.05$.

genes (DEGs) from Cluster 1 compared to Cluster 2 are shown in Figures 5B, C. GO and KEGG enrichment analyses indicated that these DEGs were enriched in the thyroid hormone signalling pathway, parathyroid hormone synthesis, secretion and actin, the PI3K-Akt signalling pathway, the Notch signalling pathway, the NOD-like receptor signalling pathway, and lysine degradation for KEGG terms (Figure 5D) and enriched in the type I interferon signalling pathway, transcription initiation from RNA polymerase II promoter, stem cell population maintenance, response to type I interferon, positive regulation

of growth, and histone modification (Figure 5E), which indicated that the DEGs might play key roles in OSC progression by driving immune infiltration and stemness maintenance. Therefore, we further confirmed the effects of these DEGs on immune infiltration in OSC patients in different clusters. The results showed that the levels of CD8+ T cells, CD4+ memory-activated T cells, M1 macrophages, and resting mast cells were increased in Cluster 1, but T follicular helper cells and activated myeloid dendritic cells were decreased in Cluster 1 compared to Cluster 2 (Figures 5F, G). The immune

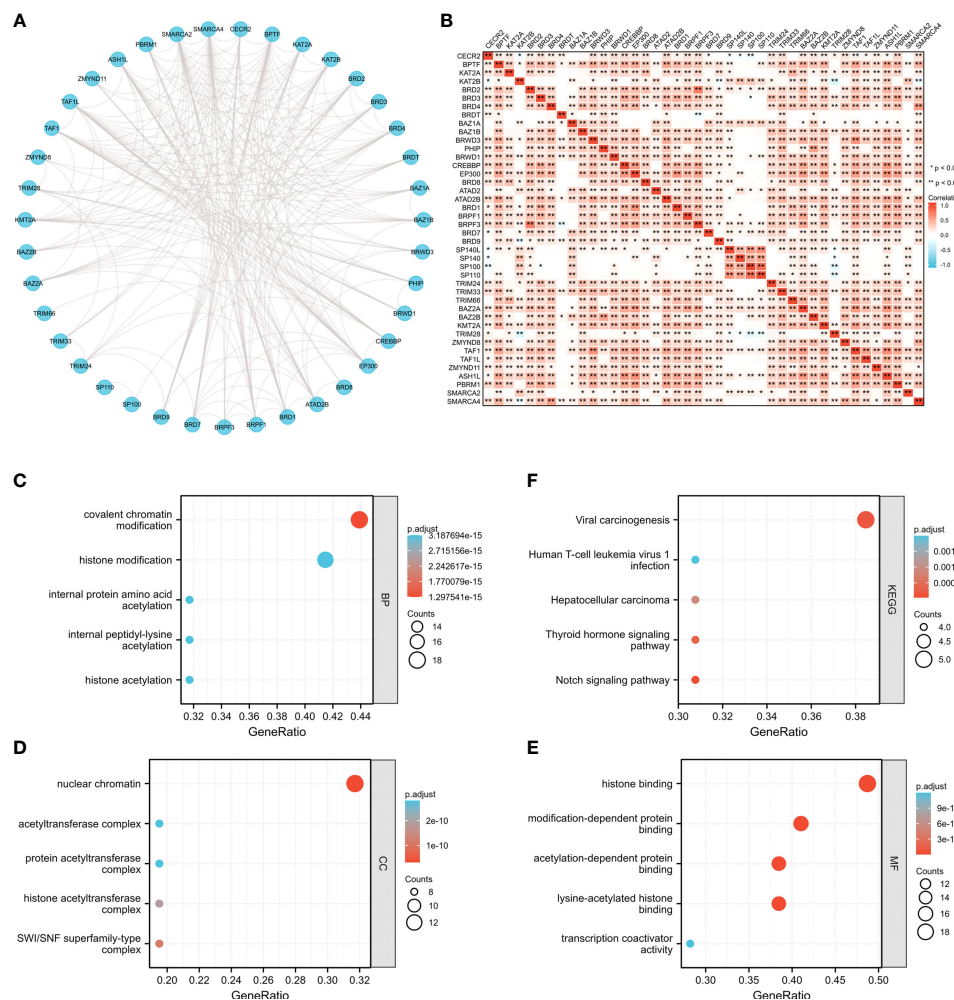


FIGURE 4

The potential molecular functions of BRDs in OSC. (A) PPI network construction for BRDs based on the STRING database. (B) Correlation analysis among the 42 BRGs based on the TCGA database OSC datasets. (C) GO enrichment of BRG genes for BP terms. (D) GO enrichment of BRG genes for CC terms. (E) GO enrichment of BRG genes for MF terms. (F) KEGG enrichment of BRG genes. * $p < 0.05$; ** $p < 0.01$.

checkpoints were decreased in Cluster 1 compared to Cluster 2, including CD274, CTKA4, HAVCR2, LAG3, PDCD1, PDCD1LG2, TIGIT, and SIGLEC15 (Figure 5H). Moreover, stemness analysis indicated that the level of stemness was higher in Cluster 1 than in Cluster 2 (Figure 5I). The drug sensitivity analysis showed that the effect of cisplatin and paclitaxel was significantly sensitivity in Cluster 1 than Cluster 2, but the effect of 5-Fu was more sensitivity in Cluster 2 compared to Cluster 1 (Figure 5J). We also found differential expression of ferroptosis genes, including CDKN1A, HSPA5, EMC2, SLC7A11, NFE2L2, HSPB1, GPX4, FANCD2, CISD1, SLC1A5, TFRC, RPL8, NCOA4, LPCAT3, GLS2, DPP4, CS, CARS1, ATP5MC3, ALOX15, ACSL4 and ATL1, between Cluster 1 and Cluster 2 (Figure 6A). Moreover, we found that

the correlation network of these ferroptosis genes in Cluster 1 samples (Figure 6B) was markedly different compared to Cluster 2 samples (Figure 6C). The expression levels of m6A methylation genes, including METTL3, METTL14, WTAP, VIRMA, RBM15, RBM15B, ZC3H13, YTHDC1, YTHDC2, YTHDF3, YTHDF1, YTHDF2, HNRNPC, IGF2BP1, IGF2BP2, IGF2BP3, RBMX, HNRNPA2B1, FTO and ALKBH5, also showed significant differences in Cluster 1 compared to Cluster 2 (Figure 7A). The correlations of these m6A genes were also markedly different in Cluster 1 compared to Cluster 2 (Figures 7B, C). These results indicated that BRDs might drive immune infiltration, stemness maintenance, ferroptosis and m6A methylation to regulate the development and progression of OSC.

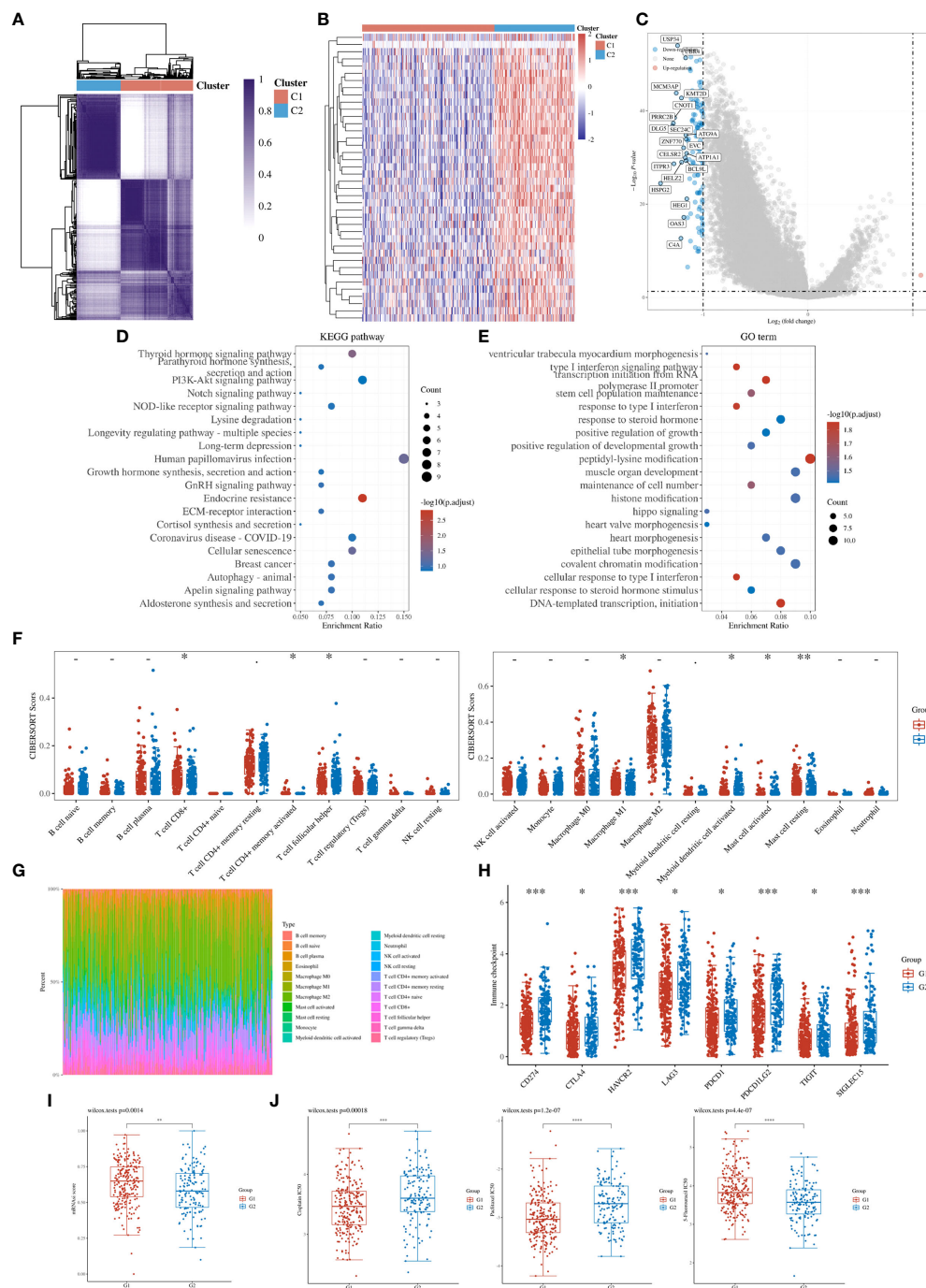


FIGURE 5

Stratification of OSCs based on the expression of BRDs. **(A)** Heatmap depicting consensus clustering solution for BRDs based on the TCGA database OSC dataset. **(B)** Heatmap of DEGs based on Cluster 1 compared to Cluster 2. **(C)** Volcano plot of DEGs. **(D)** KEGG enrichment of DEGs. **(E)** GO enrichment of DEGs. **(F)** Immune cell expression distribution for Cluster 1 compared to Cluster 2. **(G)** The percentage abundances of different immune cell types in each sample. **(H)** Heatmap of immune checkpoint-related gene expression for Cluster 1 and Cluster 2. **(I)** The stemness score for Cluster 1 and Cluster 2. **(J)** The drug sensitivity analysis for cisplatin, paclitaxel, and 5-Fu in Cluster 1 and Cluster 2. (G1 is the group of the Cluster 1 for OC patients. G2 is the group of the Cluster 2 for OC patients.) * $p < 0.05$; ** $p < 0.01$; *** $p < 0.001$; **** $p < 0.0001$.

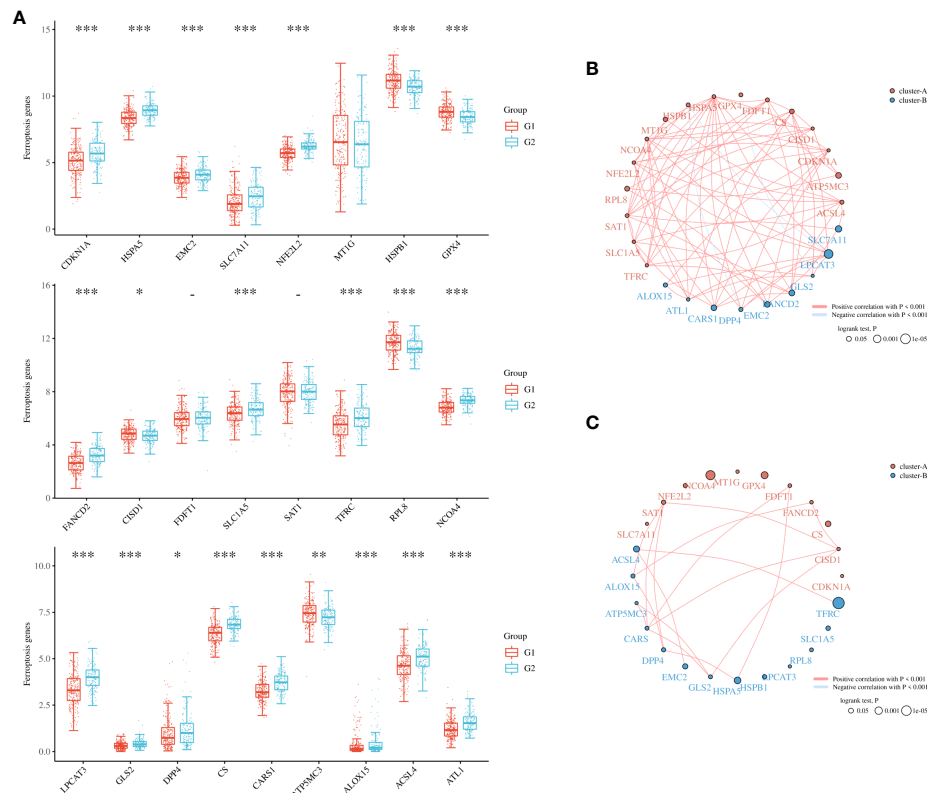


FIGURE 6

Ferroptosis levels in different subgroups of OSC. (A) Heatmap of ferroptosis-related genes in Cluster 1 and Cluster 2. (B) Network construction of ferroptosis-related genes in Cluster 1 samples. (C) Network construction of ferroptosis-related genes in Cluster 2 samples. (G1 is the group of the Cluster 1 for OC patients. G2 is the group of the Cluster 2 for OC patients.) * $p < 0.05$; ** $p < 0.01$; *** $p < 0.001$.

Identification of the BRD signature in OSC

To further clarify the prognostic significance of BRDs in each OSC patient, we used LASSO regression to construct the risk model ($\lambda_{\min}=0.0381$), and 7 signatures were confirmed. Risk score= $(-0.1228)*BRD2+(0.0055)*BRD4+(-0.0525)*PHIP+(0.0277)*BRD1+(0.3124)*BRPF1+(-0.0815)*SP140+(-0.0987)*TRIM24$ (Figure 8A, B). The risk score, status, and 7 signature expression profiles of the high- and low-risk groups are shown in Figure 8C. The overall survival analysis suggested that the OSC patients in the high-risk group had an unfavorable prognosis compared to those in the low-risk group (Figure 8D). The AUC values at 1, 3, and 5 years were 0.517, 0.577, and 0.663, respectively (Figure 8E). Moreover, we found that the risk score was significantly and negatively correlated with the levels of B cells and CD8+ T cells but positively correlated with NK cells (Figure 9). Furthermore, Uni-Cox regression indicated that BRPF1 was a significant risk factor for BRD (Figure 10A), while Multi-Cox regression suggested that BRD2, BRPF1, SP140, and TRIM24 were

significant BRDs in OSC patient's OS (Figure 10B). Moreover, Uni-Cox regression indicated that BRPF1 was a significant risk factor for BRD (Figure 10C), while Multi-Cox regression suggested that BRD2, BRPF1, and SP140 were significant BRDs in OSC patient's DSS (Figure 10D). We further combined the mRNA levels of these BRDs to construct a nomogram to predict the survival probability of patients at 1, 3, and 5 years for OS and DSS. The nomogram suggested that the prognostic prediction of the mRNA level of BRPF1 was better than those of BRD2, SP140, and TRIM24 in OS (Figure 10E), and the BRPF1 mRNA level was also better than BRD2 and SP140 in DSS (Figure 10F). These results indicated that BRDs had significant prognostic value for OSC patients, especially BRPF1.

The role of BRPF1 in OSC

To confirm the role of BRPF1 in OSC progression, we used the CPTAC database to confirm BRPF1 protein expression in OSC patients, which indicated that the protein expression of

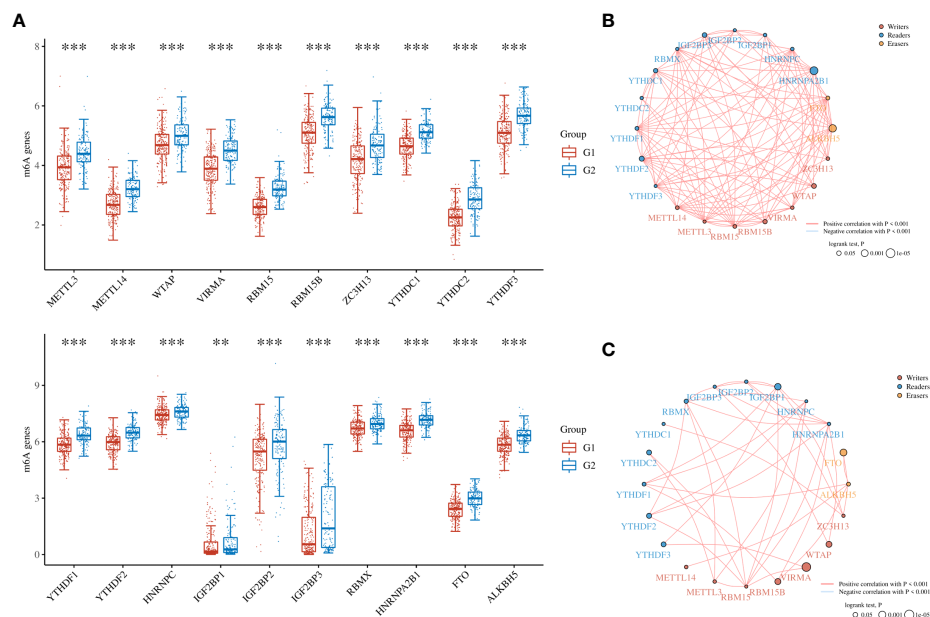


FIGURE 7

The m6A levels in different subgroups of OSC. (A) Heatmap of m6A-related genes in Cluster 1 and Cluster 2. (B) The network construction of m6A-related genes in Cluster 1 samples. (C) The network construction of m6A-related genes in Cluster 2 samples. (G1 is the group of the Cluster 1 for OC patients. G2 is the group of the Cluster 2 for OC patients.) ** $p < 0.01$; *** $p < 0.001$.

BRPF1 was not significantly changed in OSC samples and normal ovary samples (Figure 11A). We further confirmed the cellular localization of BRPF1 in OSC samples based on the HPA database, which showed that BRPF1 was located in the cell nucleus in normal ovary samples but located in the nucleus and cytoplasm in OSC samples (Figure 11B). These results indicated that cytosolic translocation of BRPF1 might be an important step in carcinogenesis. Moreover, overall survival and disease-specific survival analyses indicated that a high level of BRPF1 could induce a poor prognosis in OSC patients (Figures 11C, D). The GSEA indicated that BRPF1 might have multiple molecular functions, such as immunoregulatory interactions between lymphoid and nonlymphoid cells, HDAC deacetylation of histones, degradation of DVL, the Wnt pathway, and mitochondrial translation (Figure 11E). To further verify the molecular functions of BRPF1 in OSC cells, we used the CCLE database to confirm the expression of BRPF1 in OSC cell lines, and we chose SKOV3 to carry out the experiment (Figure 11F).

SKOV3 cells were transfected with three BRPF1 shRNAs, and western blotting indicated that BRPF1 shRNA#1 had the strongest inhibitory effect on BRPF1 expression in SKOV3 cells (Figure 12A). MTT analysis indicated that BRPF1 inhibition could suppress the viability of OSC cells (Figure 12B). EdU analysis also showed that BRPF1 knockdown reduced the proliferation ability of OSC cells (Figure 12C). Based on the GSEA results, we further examined the effect of BRPF1 on cell metabolism (Figure 11E). The results indicated that BRPF1

knockdown decreased the consumption of glucose and the production of ATP and lactic acid but increased ROS production in OSC cells (Figures 12D-G). We also detected the effect of BRPF1 inhibition on the Wnt pathway, which indicated that BRPF1 knockdown could inhibit β -catenin nuclear translocation and Wnt pathway activity (Figure 12H, I). These results indicated that BRPF1 could promote cell proliferation, anaerobic metabolism and the Wnt pathway.

Finally, we confirmed the molecular functions of BRPF1 in immune infiltration, which indicated that high expression of BRPF1 was negatively and significantly correlated with the expression of some immune checkpoints, including CD274, CTLA4, HAVCR2, PDCD1LG2 and SIGLEC15, in OSC patients (Figure 13A). Moreover, BRPF1 was positively correlated with naive B cells but negatively correlated with neutrophils (Figures 13B, C). The CNV analysis indicated that the CD8+ T cell infiltration level was significantly decreased in OSC patients with arm-level deletion of BRPF1 (Figure 13D). The expression of BRPF1 significantly and negatively correlated with macrophage (Figure 13E). Moreover, the protein structure analysis indicated that BRPF1 had multiple function domains, such as EPL1, PHD, zf-HC5HC2H, Bromodomain and PWWP domain. The BRPF1 protein modification include phosphorylation, acetylation and methylation, which may regulate the activity of BRPF1 (Figure 13F). Taken together, BRPF1 might influence cancer immune infiltration to regulate OSC development and progression.

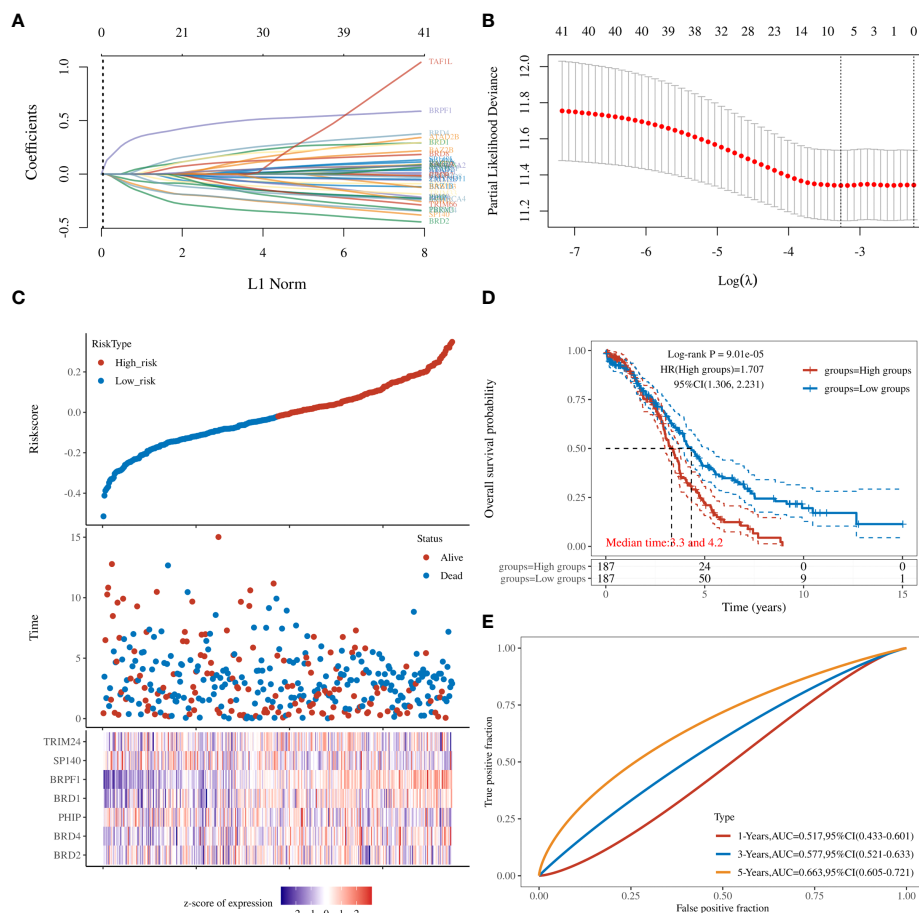


FIGURE 8

Prognostic signature of OSC patients. (A) Prognostic signature construction by LASSO Cox analysis. (B) The lambda is represented in the abscissa, and the coefficients are represented in the ordinate. (C) The risk score, survival time, and signature expression profiles in OSC patients. (D) The overall survival analysis between the high- and low-risk OSC patient groups. (E) ROC curves for survival time in OSC patients.

Discussion

In this study, we confirmed the mRNA levels of 42 BRDs in OSC patient samples based on TCGA database. These BRDs were differently dysregulated in OSC tissues. Nowadays, BRDs are regarded as a kind of emerging clinical therapeutic targets, and inhibiting any of BRDs activation or expression can be a small molecule inhibitor as emerging epigenetic therapies for cancer (65). Ectopic expression of these BRDs has been confirmed in different cancer types, including bladder cancer (66), diffuse large B-cell lymphoma (67), colorectal cancer (68), liver cancer (50), gastric cancer (69), cervical cancer (70), and breast cancer (71). We further confirmed the DNA alteration levels of these BRDs in OSC patients based on the cBioPortal database, indicating that BRDs were frequently mutated, especially in amplification in OSC patients. A previous study also found that multiple BRDs were altered in different cancer

types, such as cervical cancer (72), esophageal squamous cell carcinoma (73), triple-negative breast cancer (74), and diffuse large B-cell lymphoma (75). These results suggested that dysregulation and alteration of BRDs were involved in the occurrence, development and progression of OSC.

To identify the potential functions of BRDs in OSC progression, we found that these BRDs might synergistically exert pathophysiological effects by PPI network construction and correlation analysis in OSC progression, mediating multiple molecular functions, especially histone acetylation, covalent chromatin modification, and viral carcinogenesis. Takao Fujisawa and his colleagues indicated that BRDs selectively recognize and bind to acetylated histone Lys residues to epigenetically regulate gene transcription, and these BRDs are frequently and obviously dysregulated in cancer progression (4). Zaware N et al. found that BRDs could regulate chromatin-templated gene transcription, DNA

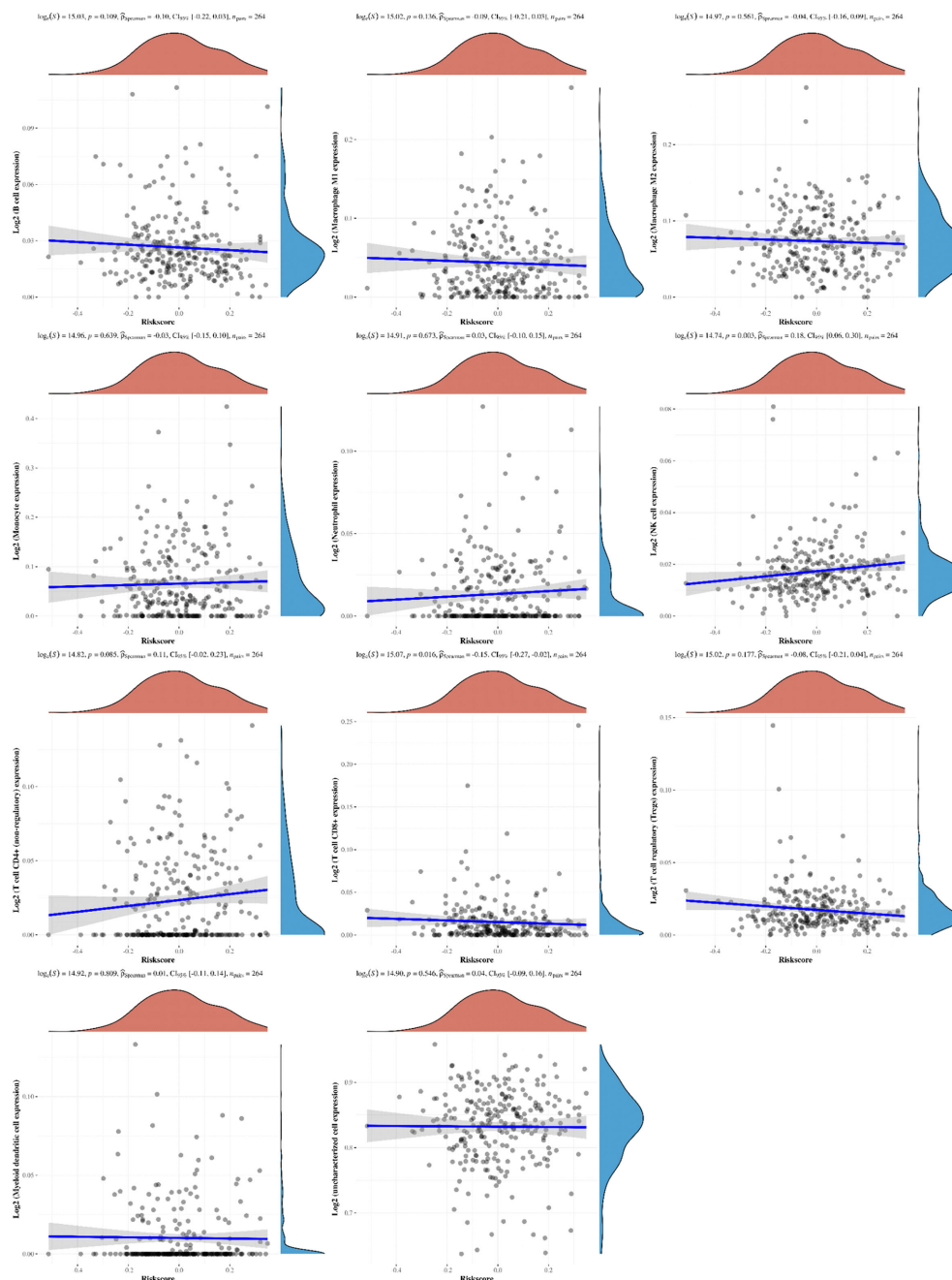


FIGURE 9

The correlations between the RiskScore and different immune cell infiltrations. The associations among the RiskScore and infiltration of different immune cells, including B cells, M1 macrophages, M2 macrophages, monocytes, neutrophils, NK cells, CD4+ T cells, CD8+ T cells, Treg cells, myeloid dendritic cells, and uncharacterized cells.

replication, repair and recombination by driving protein–protein interactions and promoting carcinogenesis (65). Cai et al. found that BRD1 inhibition could attenuate the function of sulfatide to reduce H3K9/14 acetylation and repress the occupancy of histone acetyltransferase binding to ORC1 (HBO1) and monocytic leukemia zinc finger (MOZ) in the

promoter of the integrin αV gene in liver cancer cells, reducing migration and invasion (76). Therefore, these BRDs might synergistically promote OSC carcinogenesis to drive histone acetylation.

To further confirm the role of BRDs in OSC progression, we divided OSC patient samples into two subtypes based on these

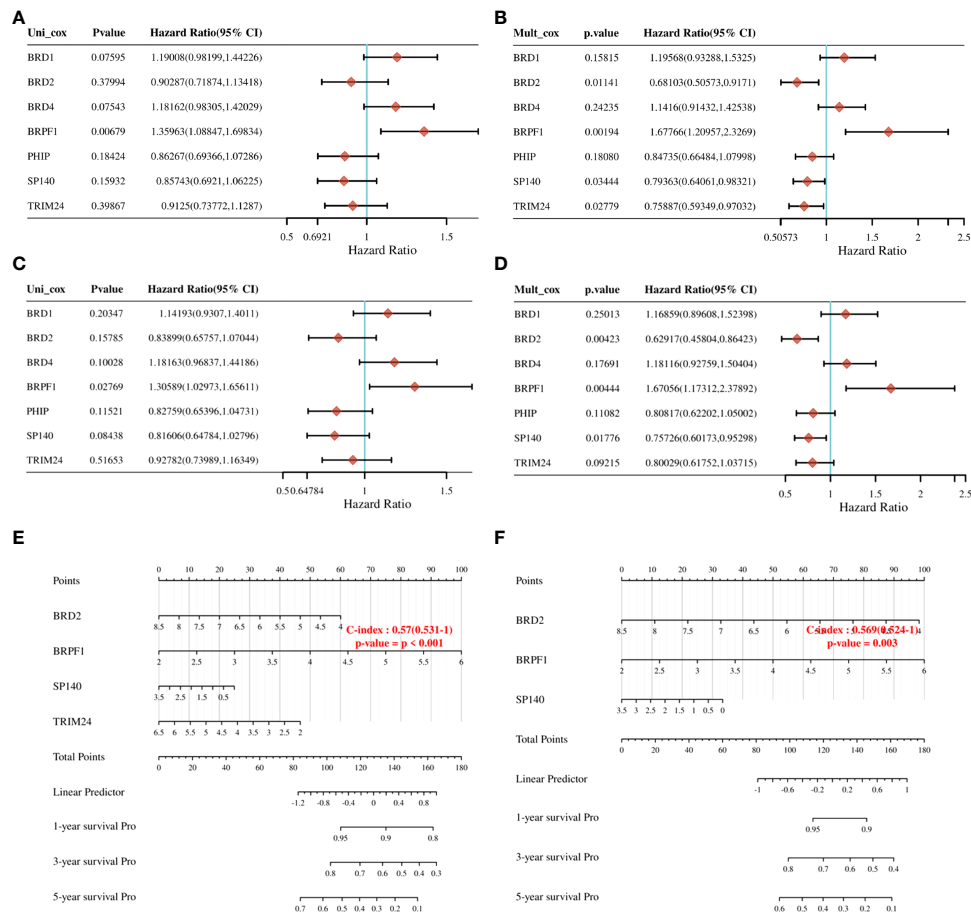


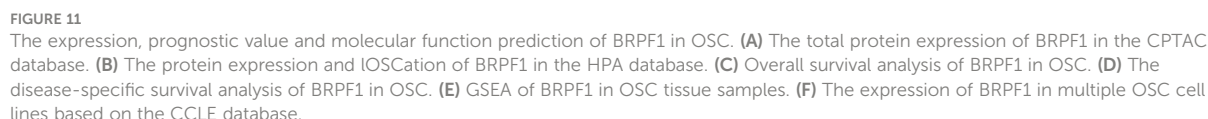
FIGURE 10

Prognostic value of seven expression signatures in OSC. (A) Prognostic values of seven signatures shown by forest plot of hazard ratios by Uni-Cox analysis for OS. (B) Prognostic values of seven signatures shown by forest plot of hazard ratios by Multi-Cox analysis for OS. (C) Prognostic values of seven signatures shown by forest plot of hazard ratios by Uni-Cox analysis for DSS. (D) Prognostic values of seven signatures shown by forest plot of hazard ratios by Multi-Cox analysis for DSS. (E) Nomogram survival prediction chart for predicting OS rates at 1, 3, and 5 years. (F) Nomogram survival prediction chart for predicting DSS rates at 1, 3, and 5 years.

42 BRDs. We found that the DEGs in Cluster 1 compared to Cluster 2 were enriched in response to type I interferon, peptidyl lysine modification, histone modification, cellular response to type I interferon and multiple signaling pathways. Moreover, we found that there were significant differences in immune infiltration, stemness maintenance, ferroptosis scores, and m6A levels between the two subgroups. Previous studies have indicated that ferroptosis plays a significant role in regulating immune infiltration in cancer progression (77, 78). Zhao et al. found that NCOA4 could mediate ferroptosis, relying on the coordination of BRD4 and CDK9 (79). Chen et al. also found that BRD4/8/9 were significantly correlated with immune infiltration in hepatocellular carcinoma (80). Zhu and his colleagues found that EP300 mutation could induce antitumor immunity and upregulate TMB in bladder cancer (66). Taken together, these results indicated that BRDs might regulate

immune infiltration by driving ferroptosis. Furthermore, Patrycja et al. found a significant correlation between distinct BRDs and stemness maintenance in 27 solid cancer types (81). Hao and his colleagues found that EP300 could induce an increase in ALKBH5 expression to reduce the m6A level of FOXM1 mRNA by upregulating H3K27ac, resulting in enhanced FOXM1 mRNA levels and EMT cascade activation in melanoma (82). Zeng et al. found that EP300 could epigenetically upregulate RBM15 to accelerate clear cell renal cell carcinoma growth, metastasis and macrophage infiltration by driving CXCL11 mRNA m6A modification (83). These results indicated that BRDs might maintain cancer stemness by directly driving histone acetylation and indirectly regulating m6A methylation.

Next, we explored the prognostic value of these BRDs in OSC patients. We constructed a prognostic model by LASSO



and CD8+ T cells but positively correlated with NK cells, which indicated that the effect of BRDs on OSC prognosis might be attributed to the influence of immune infiltration, especially in B cells, CD8+ T cells, and NK cells. In a previous study, BRD4 was identified as a biomarker for predicting poor prognosis for

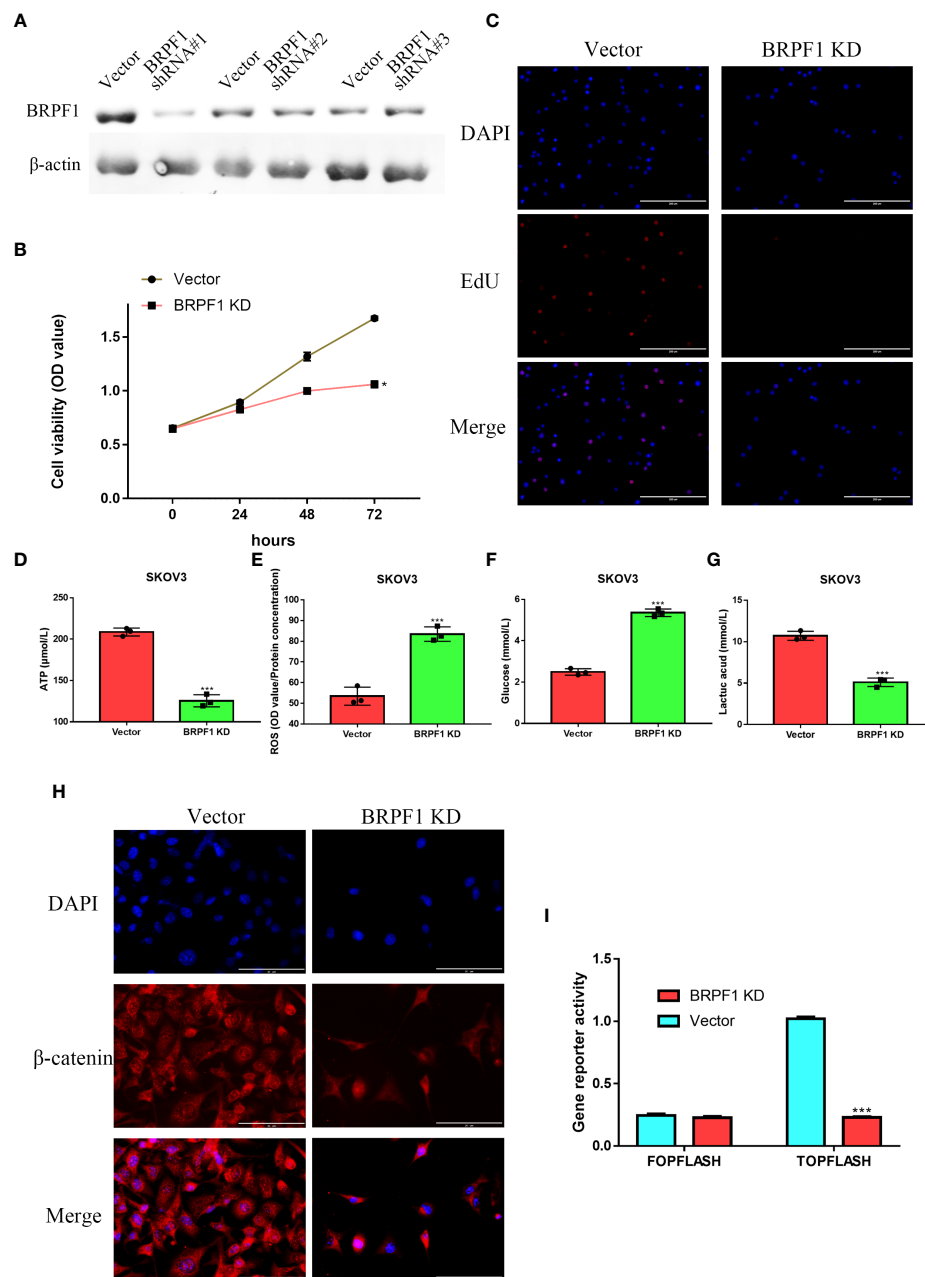


FIGURE 12

The effect of BRPF1 inhibition in SKOV3 cell lines. (A) The effects of BRPF1 shRNA#1/2/3 on SKOV3 cell lines. (B) The effect of BRPF1 knockdown on the viability of SKOV3 cells by MTT assay. (C) The effect of BRPF1 inhibition on SKOV3 cell proliferation by EdU analysis. (D) The effect of BRPF1 inhibition on SKOV3 cell ATP production. (E) The effect of BRPF1 inhibition on SKOV3 cell ROS production. (F) The effect of BRPF1 inhibition on SKOV3 cell glucose consumption. (G) The effect of BRPF1 inhibition on SKOV3 cell lactic acid production. (H) The effect of BRPF1 knockdown on the I/Oscation of β-catenin. (I) The effect of BRPF1 knockdown on Wnt pathway activity by a dual-luciferase reporter. * $p < 0.05$; *** $p < 0.001$.

prostate cancer patients (84, 85). BRD1 was significantly correlated with an unfavorable prognosis in colorectal cancer patients (68). PHIP is regarded as an important biomarker for cutaneous melanoma (86) and breast cancer (87). BRPF1 in urine is considered a potential marker of prostate cancer (88).

SP140 might be a biomarker in head and neck squamous cell carcinoma (89). TRIM24 is a possible prognostic marker for prostate cancer (90), head and neck squamous cell carcinomas (91) and breast cancer (92). However, whether these indicators can be used as prognostic markers independently for OSC is still

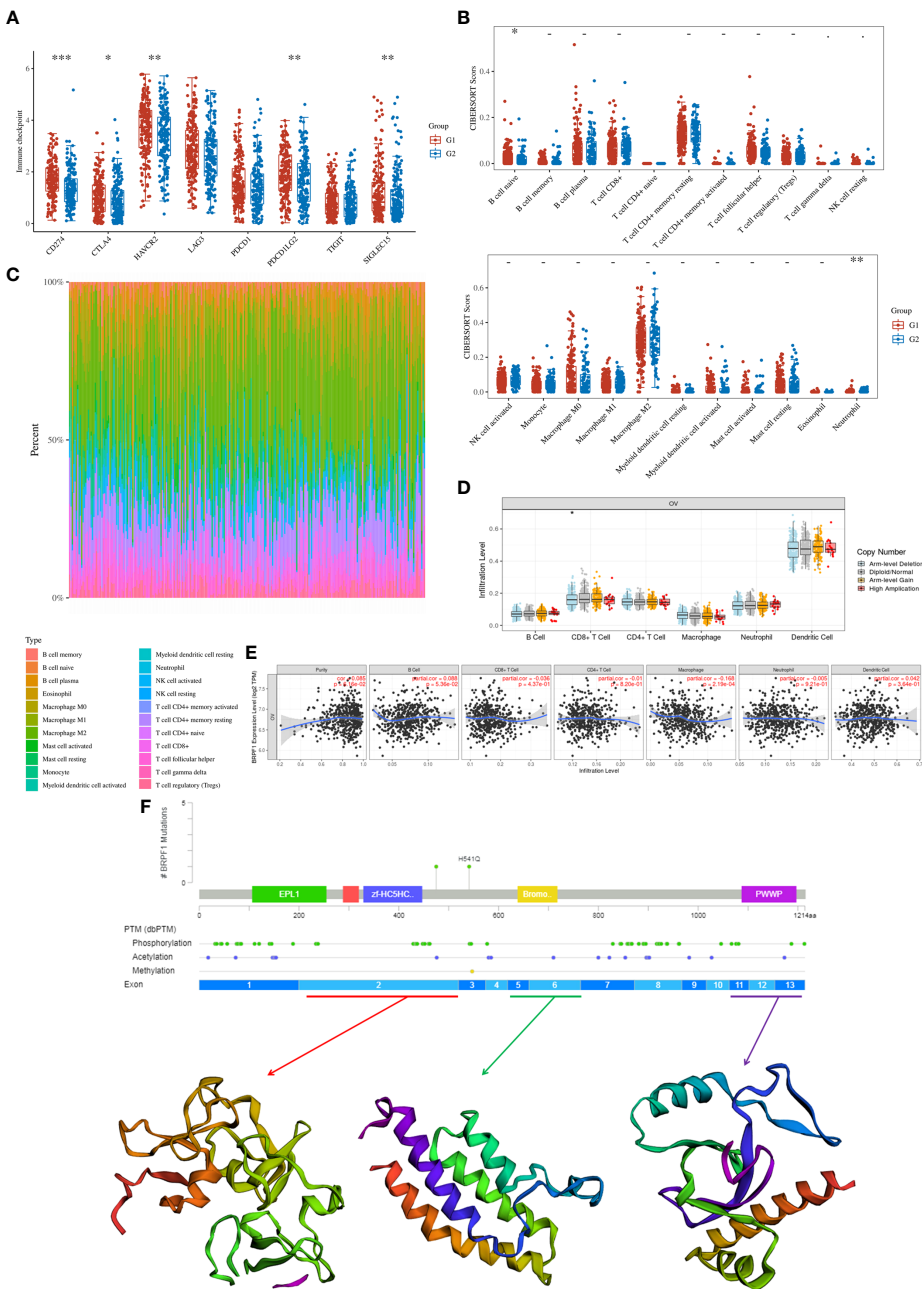


FIGURE 13
The role of BRPF1 in OC immune infiltration. **(A)** Immune cell expression distribution for the OC patients with high expression of BRPF1 compared to the OC patients with low expression of BRPF1. **(B)** The percentage abundances of different immune cell types in each sample. **(C)** Heatmap of immune checkpoint-related gene expression for the OC patients with high expression of BRPF1 compared to the OC patients with low expression of BRPF1. **(D)** The CNV analysis between BRPF1 alteration and immune infiltration based on TIMER database. **(E)** The expression level of BRPF1 and immune infiltration based on TIMER database. **(F)** The protein secondary structure of BRPF1 and the tertiary structure of BRPF1 protein for exon 1, exons 5-6, and exons 11-13. (G1 is the group of the OC patients with high expression of BRPF1. G2 is the group of the OC patients with low expression of BRPF1.) * $p < 0.05$; ** $p < 0.01$; *** $p < 0.001$.

unclear. We further confirmed that BRPF1 had a better prognostic significance than the other 6 signatures by Uni-Cox or Multi-Cox analysis. Our further results suggest that BRPF1 has obvious cytosolic aggregation in OSC tissue samples, which

indicated that it might bind directly to cytosolic proteins. GSEA also indicated that BRPF1 might drive Wnt pathway activation, mitochondrial translation and immune infiltration in OSCC. Moreover, we found that BRPF1 knockdown inhibited OSC cell

proliferation, cell glycometabolism, and Wnt signalling activation. Shima H and his colleagues found that BRPF1 interacts with MOZ to activate the HOX pathway and promote the progression of acute myeloid leukemia (52). Cheng et al. found that BRPF1 interacts with the MOZ/MORF complex to acetylate H3K14, resulting in E2F2 and EZH2 activation and upregulation to promote liver cancer progression (50). Alberto-Aguilar DR et al. found that the ascites of OSC patients could modulate the fucosylation of BRPF1 to promote OSC development (93). These results suggested that BRPF1, as a highly conserved oncogene, might play equally important oncogenic roles in different cancers. Taken together, these results suggest that BRPF1 inhibition suppresses the nuclear translocation of β -catenin and further inactivates the Wnt pathway in OSC. Moreover, BRPF1 had a significant correlation with immune infiltration, especially in naïve B cells and neutrophils, which indicated that BRPF1 not only promoted metabolic reprogramming and proliferation of OSCs in an epigenetic manner but also affected the progression of OSCs by affecting immune infiltration.

Conclusion

In this study, we confirmed the expression, function, and prognostic significance of 42 BRDs in OSC. Subtype classification also indicated the effects of these BRDs on OSC cell immune infiltration, stemness maintenance, ferroptosis and m6A methylation. Moreover, we found that BRPF1 knockdown could inhibit OSC cell proliferation, glycometabolism, and Wnt pathway activation, indicating that BRPF1 might be a potential therapeutic target and prognostic marker for OSC patients.

Data availability statement

The original contributions presented in the study are included in the article/Supplementary Material. Further inquiries can be directed to the corresponding authors.

References

1. Bray F, Ferlay J, Soerjomataram I, Siegel RL, Torre LA, Jemal A. Global cancer statistics 2018: GLOBOCAN estimates of incidence and mortality worldwide for 36 cancers in 185 countries. *CA Cancer J Clin* (2018) 68(6):394–424. doi: 10.3322/caac.21492
2. Miller KD, Siegel RL, Lin CC, Mariotto AB, Kramer JL, Rowland JH, et al. Cancer treatment and survivorship statistics, 2016. *CA Cancer J Clin* (2016) 66(4):271–89. doi: 10.3322/caac.21349
3. Varshney S, Stanley P. Multiple roles for O-glycans in notch signalling. *FEBS Lett* (2018) 592(23):3819–34. doi: 10.1002/1873-3468.13251
4. Fujisawa T, Filippakopoulos P. Functions of bromodomain-containing proteins and their roles in homeostasis and cancer. *Nat Rev Mol Cell Biol* (2017) 18(4):246–62. doi: 10.1038/nrm.2016.143
5. Filippakopoulos P, Qi J, Picaud S, Shen Y, Smith WB, Fedorov O, et al. Selective inhibition of BET bromodomains. *Nature* (2010) 468(7327):1067–73. doi: 10.1038/nature09504
6. Sanchez R, Zhou MM. The role of human bromodomains in chromatin biology and gene transcription. *Curr Opin Drug Discovery Devel.* (2009) 12(5):659–65.
7. Jones MH, Hamana N, Nezu J, Shimane M. A novel family of bromodomain genes. *Genomics* (2000) 63(1):40–5. doi: 10.1006/geno.1999.6071
8. Li H, Ilin S, Wang W, Duncan EM, Wysocka J, Allis CD, et al. Molecular basis for site-specific read-out of histone H3K4me3 by the BPTF PHD finger of NURF. *Nature* (2006) 442(7098):91–5. doi: 10.1038/nature04802

Author contributions

JZ, and YL analyzed the data. T-yF used online tools. DL and W-dZ designed the project. JZ wrote the paper. HL and Y-kL revised the manuscript and designed the experiment. All authors contributed to the article and approved the submitted version.

Funding

The present study was supported by the Natural Science Foundation of HuNan Province (2021JJ50070).

Conflict of interest

The authors declare that the research was conducted in the absence of any commercial or financial relationships that could be construed as a potential conflict of interest.

Publisher's note

All claims expressed in this article are solely those of the authors and do not necessarily represent those of their affiliated organizations, or those of the publisher, the editors and the reviewers. Any product that may be evaluated in this article, or claim that may be made by its manufacturer, is not guaranteed or endorsed by the publisher.

Supplementary material

The Supplementary Material for this article can be found online at: <https://www.frontiersin.org/articles/10.3389/fonc.2022.1021558/full#supplementary-material>

SUPPLEMENTARY FIGURE 1

The gene functional enrichment analysis for each BRDs based on LinkedOmics database.

9. Yang XJ, Ogryzko VV, Nishikawa J, Howard BH, Nakatani Y. A p300/CBP-associated factor that competes with the adenoviral oncoprotein E1A. *Nature* (1996) 382(6589):319–24. doi: 10.1038/382319a0
10. LeRoy G, Rickards B, Flint SJ. The double bromodomain proteins Brd2 and Brd3 couple histone acetylation to transcription. *Mol Cell* (2008) 30(1):51–60. doi: 10.1016/j.molcel.2008.01.018
11. Lamonica JM, Deng W, Kadauke S, Campbell AE, Gamsjaeger R, Wang H, et al. Bromodomain protein Brd3 associates with acetylated GATA1 to promote its chromatin occupancy at erythroid target genes. *Proc Natl Acad Sci U S A*. (2011) 108(22):E159–168. doi: 10.1073/pnas.1102140108
12. Floyd SR, Pacold ME, Huang Q, Clarke SM, Lam FC, Cannell IG, et al. The bromodomain protein Brd4 insulates chromatin from DNA damage signalling. *Nature* (2013) 498(7453):246–50. doi: 10.1038/nature12147
13. Gaucher J, Boussouar F, Montellier E, Curtet S, Buchou T, Bertrand S, et al. Bromodomain-dependent stage-specific male genome programming by brdt. *EMBO J* (2012) 31(19):3809–20. doi: 10.1038/emboj.2012.233
14. Poot RA, Dellaire G, Hülsman BB, Grimaldi MA, Corona DF, Becker PB, et al. HuCHRAC, a human ISWI chromatin remodelling complex contains hACF1 and two novel histone-fold proteins. *EMBO J* (2000) 19(13):3377–87. doi: 10.1093/emboj/19.13.3377
15. Cavellán E, Asp P, Percipalle P, Farrants AK. The WSTF-SNF2h chromatin remodeling complex interacts with several nuclear proteins in transcription. *J Biol Chem* (2006) 281(24):16264–71. doi: 10.1074/jbc.M600233200
16. Müller P, Kutteneuler D, Gesellchen V, Zeidler MP, Boutros M. Identification of JAK/STAT signalling components by genome-wide RNA interference. *Nature* (2005) 436(7052):871–5. doi: 10.1038/nature03869
17. Podcheko A, Northcott P, Bikopoulos G, Lee A, Bommarreddi SR, Kushner JA, et al. Identification of a WD40 repeat-containing isoform of PHIP as a novel regulator of beta-cell growth and survival. *Mol Cell Biol* (2007) 27(18):6484–96. doi: 10.1128/MCB.02409-06
18. Pattabiraman S, Baumann C, Guisado D, Eppig JJ, Schimenti JC, de la Fuente R. Mouse BRWD1 is critical for spermatid postmeiotic transcription and female meiotic chromosome stability. *J Cell Biol* (2015) 208(1):53–69. doi: 10.1083/jcb.201404109
19. Kalkhoven E. CBP and p300: HATs for different occasions. *Biochem Pharmacol* (2004) 68(6):1145–55. doi: 10.1016/j.bcp.2004.03.045
20. Cai Y, Jin J, Tomomori-Sato C, Sato S, Sorokina I, Parmely TJ, et al. Identification of new subunits of the multiprotein mammalian TRRAP/TIP60-containing histone acetyltransferase complex. *J Biol Chem* (2003) 278(44):42733–6. doi: 10.1074/jbc.C300389200
21. Ciró M, Prosperini E, Quarto M, Grazini U, Walfridsson J, McBlane F, et al. ATAD2 is a novel cofactor for MYC, overexpressed and amplified in aggressive tumors. *Cancer Res* (2009) 69(21):8491–8. doi: 10.1158/0008-5472.CAN-09-2131
22. Leachman NT, Brellier F, Ferralli J, Chiquet-Ehrismann R, Tucker RP. ATAD2B is a phylogenetically conserved nuclear protein expressed during neuronal differentiation and tumorigenesis. *Dev Growth Differ* (2010) 52(9):747–55. doi: 10.1111/j.1440-169X.2010.01211.x
23. Mishima Y, Miyagi S, Saraya A, Negishi M, Endoh M, Endo TA, et al. The Hbo1-Brd1/Brp2 complex is responsible for global acetylation of H3K14 and required for fetal liver erythropoiesis. *Blood* (2011) 118(9):2443–53. doi: 10.1182/blood-2011-01-331892
24. Laue K, Daujat S, Crump JG, Plaster N, Roehl HH, Kimmel CB, et al. The multidomain protein Brpf1 binds histones and is required for hox gene expression and segmental identity. *Development* (2008) 135(11):1935–46. doi: 10.1242/dev.017160
25. Feng Y, Vlassis A, Roques C, Lalonde ME, González-Aguilera C, Lambert JP, et al. BRPF3-HBO1 regulates replication origin activation and histone H3K14 acetylation. *EMBO J* (2016) 35(2):176–92. doi: 10.15252/emboj.201591293
26. Kaeser MD, Aslanian A, Dong MQ, Yates JR3rd, Emerson BM. BRD7, a novel PBAF-specific SWI/SNF subunit, is required for target gene activation and repression in embryonic stem cells. *J Biol Chem* (2008) 283(47):32254–63. doi: 10.1074/jbc.M806061200
27. Kadoch C, Hargreaves DC, Hodges C, Elias L, Ho L, Ranish J, et al. Proteomic and bioinformatic analysis of mammalian SWI/SNF complexes identifies extensive roles in human malignancy. *Nat Genet* (2013) 45(6):592–601. doi: 10.1038/ng.2628
28. Zong RT, Das C, Tucker PW. Regulation of matrix attachment region-dependent, lymphocyte-restricted transcription through differential localization within promyelocytic leukemia nuclear bodies. *EMBO J* (2000) 19(15):4123–33. doi: 10.1093/emboj/19.15.4123
29. Fraschilla I, Jeffrey KL. The speckled protein (SP) family: Immunity's chromatin readers. *Trends Immunol* (2020) 41(7):572–85. doi: 10.1016/j.it.2020.04.007
30. Yordy JS, Moussa O, Pei H, Chaussabel D, Li R, Watson DK. SP100 inhibits ETS1 activity in primary endothelial cells. *Oncogene* (2005) 24(5):916–31. doi: 10.1038/sj.onc.1208245
31. Bloch DB, Nakajima A, Gulick T, Chiche JD, Orth D, de La Monte SM, et al. Sp110 localizes to the PML-Sp100 nuclear body and may function as a nuclear hormone receptor transcriptional coactivator. *Mol Cell Biol* (2000) 20(16):6138–46. doi: 10.1128/MCB.20.16.6138-6146.2000
32. Tsai WW, Wang Z, Yiu TT, Akdemir KC, Xia W, Winter S, et al. TRIM24 links a non-canonical histone signature to breast cancer. *Nature* (2010) 468(7326):927–32. doi: 10.1038/nature09542
33. Dupont S, Zacchigna L, Cordenonsi M, Soligo S, Adorno M, Rugge M, et al. Germ-layer specification and control of cell growth by ectoderm, a Smad4 ubiquitin ligase. *Cell* (2005) 121(1):87–99. doi: 10.1016/j.cell.2005.01.033
34. Khetchoumian K, Teletin M, Mark M, Lerouge T, Cerviño M, Oulad-Abdelghani M, et al. TIF1delta, a novel HP1-interacting member of the transcriptional intermediary factor 1 (TIF1) family expressed by elongating spermatids. *J Biol Chem* (2004) 279(46):48329–41. doi: 10.1074/jbc.M404779200
35. Zhou Y, Schmitz KM, Mayer C, Yuan X, Akhtar A, Grummt I. Reversible acetylation of the chromatin remodelling complex NoRC is required for non-coding RNA-dependent silencing. *Nat Cell Biol* (2009) 11(8):1010–6. doi: 10.1038/ncb1914
36. Milne TA, Briggs SD, Brock HW, Martin ME, Gibbs D, Allis CD, et al. MLL targets SET domain methyltransferase activity to hox gene promoters. *Mol Cell* (2002) 10(5):1107–17. doi: 10.1016/S1097-2765(02)00741-4
37. Kimura J, Nguyen ST, Liu H, Taira N, Miki Y, Yoshida K. A functional genome-wide RNAi screen identifies TAF1 as a regulator for apoptosis in response to genotoxic stress. *Nucleic Acids Res* (2008) 36(16):5250–9. doi: 10.1093/nar/gkn506
38. Wang PJ, Page DC. Functional substitution for TAF(II)250 by a retroposed homolog that is expressed in human spermatogenesis. *Hum Mol Genet* (2002) 11(19):2341–6. doi: 10.1093/hmg/11.19.2341
39. Gong F, Chiu LY, Cox B, Aymard F, Clouaire T, Leung JW, et al. Screen identifies bromodomain protein ZMYND8 in chromatin recognition of transcription-associated DNA damage that promotes homologous recombination. *Genes Dev* (2015) 29(2):197–211. doi: 10.1101/gad.252189.114
40. Masselink H, Bernards R. The adenovirus E1A binding protein BS69 is a corepressor of transcription through recruitment of n-CoR. *Oncogene* (2000) 19(12):1538–46. doi: 10.1038/sj.onc.1203421
41. Batsché E, Yaniv M, Muchardt C. The human SWI/SNF subunit brm is a regulator of alternative splicing. *Nat Struct Mol Biol* (2006) 13(1):22–9. doi: 10.1038/nsmb1030
42. Rada-Iglesias A, Bajpai R, Swigut T, Brugmann SA, Flynn RA, Wysocka J. A unique chromatin signature uncovers early developmental enhancers in humans. *Nature* (2011) 470(7333):279–83. doi: 10.1038/nature09692
43. Xue Y, Canman JC, Lee CS, Nie Z, Yang D, Moreno GT, et al. The human SWI/SNF-b chromatin-remodeling complex is related to yeast rsc and localizes at kinetochores of mitotic chromosomes. *Proc Natl Acad Sci USA*. (2000) 97(24):13015–20. doi: 10.1073/pnas.240208597
44. Kanellopoulou C, Gilpatrick T, Kilaur G, Burr P, Nguyen CK, Morawski A, et al. Reprogramming of polycomb-mediated gene silencing in embryonic stem cells by the miR-290 family and the methyltransferase Ash1l. *Stem Cell Rep* (2015) 5(6):971–8. doi: 10.1016/j.stemcr.2015.10.001
45. Muller S, Filippakopoulos P, Knapp S. Bromodomains as therapeutic targets. *Expert Rev Mol Med* (2011) 13:e29. doi: 10.1017/S1462399411001992
46. Belkina AC, Denis GV. BET domain co-regulators in obesity, inflammation and cancer. *Nat Rev Cancer*. (2012) 12(7):465–77. doi: 10.1038/nrc3256
47. Shi J, Vakoc CR. The mechanisms behind the therapeutic activity of BET bromodomain inhibition. *Mol Cell* (2014) 54(5):728–36. doi: 10.1016/j.molcel.2014.05.016
48. Wang CY, Filippakopoulos P. Beating the odds: BETs in disease. *Trends Biochem Sci* (2015) 40(8):468–79. doi: 10.1016/j.tibs.2015.06.002
49. Lloyd JT, Glass KC. Biological function and histone recognition of family IV bromodomain-containing proteins. *J Cell Physiol* (2018) 233(3):1877–86. doi: 10.1002/jcp.26010
50. Cheng CL, Tsang FH, Wei L, Chen M, Chin DW, Shen J, et al. Bromodomain-containing protein BRPF1 is a therapeutic target for liver cancer. *Commun Biol* (2021) 4(1):888. doi: 10.1038/s42003-021-02405-6
51. Aiello G, Ballabio C, Ruggeri R, Fagnocchi L, Anderle M, Morassut I, et al. Truncated BRPF1 cooperates with smoothed to promote adult shh medulloblastoma. *Cell Rep* (2019) 29(12):4036–4052.e4010. doi: 10.1016/j.celrep.2019.11.046
52. Shima H, Yamagata K, Aikawa Y, Shino M, Koseki H, Shimada H, et al. Bromodomain-PHD finger protein 1 is critical for leukemogenesis associated with

- MOZ-TIF2 fusion. *Int J Hematol* (2014) 99(1):21–31. doi: 10.1007/s12185-013-1466-x
53. Tomczak K, Czerwinski P, Wiznerowicz M. The cancer genome atlas (TCGA): an immeasurable source of knowledge. *Contemp Oncol (Pozn)*. (2015) 19(1A):A68–77. doi: 10.5114/wo.2014.47136
54. Whiteaker JR, Halusa GN, Hoofnagle AN, Sharma V, MacLean B, Yan P, et al. CPTAC assay portal: A repository of targeted proteomic assays. *Nat Methods* (2014) 11(7):703–4. doi: 10.1038/nmeth.3002
55. Uhlen M, Zhang C, Lee S, Sjostedt E, Fagerberg L, Bidkhorji G, et al. A pathology atlas of the human cancer transcriptome. *Science* (2017) 357(6352). doi: 10.1126/science.aan2507
56. Nusinow DP, Szpyt J, Ghandi M, Rose CM, McDonald ER3rd, Kalocsay M, et al. Quantitative proteomics of the cancer cell line encyclopedia. *Cell* (2020) 180(2):387–402.e316. doi: 10.1016/j.cell.2019.12.023
57. Consortium G. The genotype-tissue expression (GTEx) project. *Nat Genet* (2013) 45(6):580–5. doi: 10.1038/ng.2653
58. Li T, Fan J, Wang B, Traugh N, Chen Q, Liu JS, et al. TIMER: A web server for comprehensive analysis of tumor-infiltrating immune cells. *Cancer Res* (2017) 77(21):e108–10. doi: 10.1158/1538-7445.AM2017-108
59. Cerami E, Gao J, Dogrusoz U, Gross BE, Sumer SO, Aksoy BA, et al. The cBio cancer genomics portal: An open platform for exploring multidimensional cancer genomics data. *Cancer Discovery* (2012) 2(5):401–4. doi: 10.1158/2159-8290.CD-12-0095
60. Szklarczyk D, Morris JH, Cook H, Kuhn M, Wyder S, Simonovic M, et al. The STRING database in 2017: Quality-controlled protein-protein association networks, made broadly accessible. *Nucleic Acids Res* (2017) 45(D1):D362–d368. doi: 10.1093/nar/gkw937
61. Dennis G Jr., Sherman BT, Hosack DA, Yang J, Gao W, Lane HC, et al. DAVID: Database for annotation, visualization, and integrated discovery. *Genome Biol* (2003) 4(5):P3. doi: 10.1186/gb-2003-4-5-p3
62. Vasaikar SV, Straub P, Wang J, Zhang B. LinkedOmics: analyzing multi-omics data within and across 32 cancer types. *Nucleic Acids Res* (2018) 46(D1):D956–d963. doi: 10.1093/nar/gkx1090
63. Zhang J, Li Y, Zou J, Lai C-t, Zeng T, Peng J, et al. Comprehensive analysis of the glutathione s-transferase mu (GSTM) gene family in ovarian cancer identifies prognostic and expression significance. *Front Oncol* (2022) 12. doi: 10.3389/fonc.2022.968547
64. Zeng J, Li YK, Quan FF, Zeng X, Chen CY, Zeng T, et al. Propofol-induced miR-125a-5p inhibits the proliferation and metastasis of ovarian cancer by suppressing LIN28B. *Mol Med Rep* (2020) 22(2):1507–17. doi: 10.3892/mmr.2020.11223
65. Zaware N, Zhou MM. Bromodomain biology and drug discovery. *Nat Struct Mol Biol* (2019) 26(10):870–9. doi: 10.1038/s41594-019-0309-8
66. Zhu G, Pei L, Li Y, Gou X. EP300 mutation is associated with tumor mutation burden and promotes antitumor immunity in bladder cancer patients. *Aging (Albany NY)*. (2020) 12(3):2132–41. doi: 10.18632/aging.102728
67. Huang YH, Cai K, Xu PP, Wang L, Huang CX, Fang Y, et al. CREBBP/EP300 mutations promoted tumor progression in diffuse large b-cell lymphoma through altering tumor-associated macrophage polarization via FBXW7-NOTCH-CCL2/CSF1 axis. *Signal Transduct. Target Ther* (2021) 6(1):10. doi: 10.1038/s41392-020-00437-8
68. Li Z, Wang J, Ji Y, Song F. Expression characteristics and clinical correlations of BRD1 in colorectal cancer samples. *Technol Cancer Res Treat* (2021) 20:15330338211039678. doi: 10.1177/15330338211039678
69. Nayak A, Roy AD, Rout N, Singh SP, Bhattacharyya A, Roychowdhury A. HIF1 α -dependent upregulation of ATAD2 promotes proliferation and migration of stomach cancer cells in response to hypoxia. *Biochem Biophys Res Commun* (2020) 523(4):916–23. doi: 10.1016/j.bbrc.2019.12.130
70. Ni M, Li J, Zhao H, Xu F, Cheng J, Yu M, et al. BRD4 inhibition sensitizes cervical cancer to radiotherapy by attenuating DNA repair. *Oncogene* (2021) 40(15):2711–24. doi: 10.1038/s41388-021-01735-3
71. Liu B, Liu X, Han L, Chen X, Wu X, Wu J, et al. BRD4-directed super-enhancer organization of transcription repression programs links to chemotherapeutic efficacy in breast cancer. *Proc Natl Acad Sci U S A*. (2022) 119(6). doi: 10.1073/pnas.2109133119
72. Yoshimoto Y, Sasaki Y, Murata K, Noda SE, Miyasaka Y, Hamamoto J, et al. Mutation profiling of uterine cervical cancer patients treated with definitive radiotherapy. *Gynecol. Oncol* (2020) 159(2):546–53. doi: 10.1016/j.ygyno.2020.08.020
73. Gao YB, Chen ZL, Li JG, Hu XD, Shi XJ, Sun ZM, et al. Genetic landscape of esophageal squamous cell carcinoma. *Nat Genet* (2014) 46(10):1097–102. doi: 10.1038/ng.3076
74. Bemanian V, Noone JC, Sauer T, Touma J, Vetvik K, Söderberg-Naucler C, et al. Somatic EP300-G211S mutations are associated with overall somatic mutational patterns and breast cancer specific survival in triple-negative breast cancer. *Breast Cancer Res Treat* (2018) 172(2):339–51. doi: 10.1007/s10549-018-4927-3
75. Nie M, Du L, Ren W, Joung J, Ye X, Shi X, et al. Genome-wide CRISPR screens reveal synthetic lethal interaction between CREBBP and EP300 in diffuse large b-cell lymphoma. *Cell Death Dis* (2021) 12(5):419. doi: 10.1038/s41419-021-03695-8
76. Cai QQ, Dong YW, Qi B, Shao XT, Wang R, Chen ZY, et al. BRD1-mediated acetylation promotes integrin α V gene expression *Via* interaction with sulfatide. *Mol Cancer Res* (2018) 16(4):610–22. doi: 10.1158/1541-7786.MCR-17-0527
77. Wang W, Green M, Choi JE, Gijón M, Kennedy PD, Johnson JK, et al. CD8(+) T cells regulate tumour ferroptosis during cancer immunotherapy. *Nature* (2019) 569(7755):270–4. doi: 10.1038/s41586-019-1170-y
78. Tang R, Xu J, Zhang B, Liu J, Liang C, Hua J, et al. Ferroptosis, necroptosis, and pyroptosis in anticancer immunity. *J Hematol Oncol* (2020) 13(1):110. doi: 10.1186/s13045-020-00946-7
79. Zhao Y, Li J, Guo W, Li H, Lei L. Periodontitis-level butyrate-induced ferroptosis in periodontal ligament fibroblasts by activation of ferritinophagy. *Cell Death Discovery* (2020) 6(1):119. doi: 10.1038/s41420-020-00356-1
80. Chen YR, Ouyang SS, Chen YL, Li P, Xu HW, Zhu SL. BRD4/8/9 are prognostic biomarkers and associated with immune infiltrates in hepatocellular carcinoma. *Aging (Albany NY)*. (2020) 12(17):17541–67. doi: 10.18632/aging.103768
81. Czerwinski P, Jaworska AM, Włodarczyk NA, Cisek M, Karwacka M, Lipowicz J, et al. The association between bromodomain proteins and cancer stemness in different solid tumor types. *Int J Cancer*. (2022) 150(11):1838–49. doi: 10.1002/ijc.33937
82. Hao L, Yin J, Yang H, Li C, Zhu L, Liu L, et al. ALKBH5-mediated m(6)A demethylation of FOXM1 mRNA promotes progression of uveal melanoma. *Aging (Albany NY)*. (2021) 13(3):4045–62. doi: 10.18632/aging.202371
83. Zeng X, Chen K, Li L, Tian J, Ruan W, Hu Z, et al. Epigenetic activation of RBM15 promotes clear cell renal cell carcinoma growth, metastasis and macrophage infiltration by regulating the m6A modification of CXCL11. *Free Radic Biol Med* (2022) 184:135–47. doi: 10.1016/j.freeradbiomed.2022.03.031
84. Shafran JS, Jafari N, Casey AN, Györfy B, Denis GV. BRD4 regulates key transcription factors that drive epithelial-mesenchymal transition in castration-resistant prostate cancer. *Prostate Cancer Prostatic Dis* (2021) 24(1):268–77. doi: 10.1038/s41391-020-0246-y
85. Shafran JS, Andrieu GP, Györfy B, Denis GV. BRD4 regulates metastatic potential of castration-resistant prostate cancer through AHNK. *Mol Cancer Res* (2019) 17(8):1627–38. doi: 10.1158/1541-7786.MCR-18-1279
86. Bezrookove V, Nosrati M, Miller JR3rd, De Semir D, Dar AA, Vosoughi E, et al. Role of elevated PHIP copy number as a prognostic and progression marker for cutaneous melanoma. *Clin Cancer Res* (2018) 24(17):4119–25. doi: 10.1158/1078-0432.CCR-18-0791
87. Pérez-Pena J, Páez R, Nieto-Jiménez C, Sánchez VC, Galan-Moya EM, Pandiella A, et al. Mapping bromodomains in breast cancer and association with clinical outcome. *Sci Rep* (2019) 9(1):5734. doi: 10.1038/s41598-019-41934-3
88. Solé C, Goicoechea I, Goñi A, Schramm M, Armesto M, Arestin M, et al. The urinary transcriptome as a source of biomarkers for prostate cancer. *Cancers (Basel)*. (2020) 12(2). doi: 10.3390/cancers12020513
89. Song Y, Pan Y, Liu J. The relevance between the immune response-related gene module and clinical traits in head and neck squamous cell carcinoma. *Cancer Manag Res* (2019) 11:7455–72. doi: 10.2147/CMAR.S201177
90. Offermann A, Roth D, Hupe MC, Hohensteiner S, Becker F, Joerg V, et al. TRIM24 as an independent prognostic biomarker for prostate cancer. *Urol Oncol* (2019) 37(9):576.e571–576.e510. doi: 10.1016/j.urolonc.2019.05.006
91. Klapper L, Idel C, Kuppler P, Jagomast T, von Bernuth A, Bruchhage KL, et al. TRIM24 expression as an independent biomarker for prognosis and tumor recurrence in HNSCC. *J Pers Med* (2022) 12(6). doi: 10.3390/jpm12060991
92. Ma L, Yuan L, An J, Barton MC, Zhang Q, Liu Z. Histone H3 lysine 23 acetylation is associated with oncogene TRIM24 expression and a poor prognosis in breast cancer. *Tumour Biol* (2016) 37(11):14803–12. doi: 10.1007/s13277-016-5344-z
93. Alberto-Aguilar DR, Hernández-Ramírez VI, Osorio-Trujillo JC, Gallardo-Rincón D, Toledo-Leyva A, Talamás-Rohana P. Ascites from ovarian cancer induces novel fucosylated proteins. *Cancer Microenviron*. (2019) 12(2-3):181–95. doi: 10.1007/s12307-019-00227-z



OPEN ACCESS

EDITED BY

Shaohua Xu,
Tongji University, China

REVIEWED BY

Xiangyu Sui,
Fudan University, China
Yi Huang,
School of Medicine, University of
Pittsburgh, United States

*CORRESPONDENCE

Yongmei Yin
ymyin@njmu.edu.cn
Wei Li
real.lw@163.com

[†]These authors have contributed to
this work equally

SPECIALTY SECTION

This article was submitted to
Gynecological Oncology,
a section of the journal
Frontiers in Oncology

RECEIVED 04 July 2022

ACCEPTED 29 September 2022

PUBLISHED 13 October 2022

CITATION

Zeng T, Xu H, Liu Y, Sun C, Yang F,
Liang Y, Huang X, Fu Z, Li W and Yin Y
(2022) High rate of epidermal
growth factor receptor-mutated
primary lung cancer in patients with
primary breast cancer.
Front. Oncol. 12:985734.
doi: 10.3389/fonc.2022.985734

COPYRIGHT

© 2022 Zeng, Xu, Liu, Sun, Yang, Liang,
Huang, Fu, Li and Yin. This is an open-
access article distributed under the
terms of the [Creative Commons
Attribution License \(CC BY\)](https://creativecommons.org/licenses/by/4.0/). The use,
distribution or reproduction in other
forums is permitted, provided the
original author(s) and the copyright
owner(s) are credited and that the
original publication in this journal is
cited, in accordance with accepted
academic practice. No use,
distribution or reproduction is
permitted which does not comply with
these terms.

High rate of epidermal growth factor receptor-mutated primary lung cancer in patients with primary breast cancer

Tianyu Zeng^{1†}, Hai Xu^{2†}, Yincheng Liu^{3†}, Chunxiao Sun¹,
Fan Yang¹, Yan Liang¹, Xiang Huang¹, Ziyi Fu^{1,4},
Wei Li^{1*} and Yongmei Yin^{1*}

¹Department of Oncology, the First Affiliated Hospital of Nanjing Medical University, Nanjing, China,

²Department of Radiology, the First Affiliated Hospital of Nanjing Medical University, Nanjing, China,

³Department of Plastic Surgery, the First Affiliated Hospital of Nanjing Medical University,
Nanjing, China, ⁴Nanjing Maternal and Child Health Medical Institute, Obstetrics and Gynecology
Hospital Affiliated of Nanjing Medical University, Nanjing, China

Background: With increased survival in breast cancer, resulting from advances in treatment, patients incur the possibility of subsequent primary malignancies, especially lung cancer. The aim of this study was to assess the frequency of CT-detected pulmonary ground-glass nodules and lung cancer following breast cancer diagnosis, the associations between breast cancer and lung cancer, the pathological features of double primary cancer, and the status of epidermal growth factor receptor (EGFR) mutations in second primary lung cancer.

Methods: Clinical data from more than 9000 individuals who were diagnosed with primary breast cancer at Jiangsu Province Hospital (Jiangsu, China) between January 2008 and December 2021 were retrospectively analyzed.

Results: Of the 9179 patients, 6512 underwent diagnostic CT, 55 (0.8%) were diagnosed with a second primary lung cancer, which accounted for approximately 18.4% of the pulmonary ground-glass nodules (GGNs) detected. The incidence was higher than in the general female population (standardized incidence ratio 1.4 [95% confidence interval (CI): 1.25-1.55]). Patients who experienced a second primary lung cancer exhibited a significantly higher rate of EGFR mutation (78.5%) than those with lung adenocarcinoma alone, with most exhibiting low-grade malignancy, older age, estrogen receptor negativity, low Ki67, and no lymph node metastasis.

Conclusions: Breast cancer patients, especially those with low-grade malignancy, were at high risk for developing primary lung cancer. For isolated GGN in patients with high-risk factors, clinicians should insist on close follow-up. Furthermore, EGFR may play an important role in primary lung adenocarcinomas and breast cancer.

KEYWORDS

neoplasms, multiple primary, breast neoplasms, lung neoplasms, epidermal growth factor receptor

Introduction

Breast cancer and lung cancer are the two most frequently diagnosed malignancies, have the highest morbidity, and are the leading causes of cancer-related deaths in women worldwide (1). Advances in treatment and improved surgical techniques have extended the lifespan of breast cancer patients. However, with this prolonged survival, the risk of a second primary cancer has also increased. Approximately 10% of breast cancer patients experience another malignancy within 10 years after diagnosis, 5% of which are lung cancers (2, 3).

What also warrants attention is that the number of women with a double primary cancer may also be increased. The most frequently observed second primary cancers in breast cancer patients are hematological tumors, melanomas, and cancers of the digestive tract, female reproductive system, lung, thyroid, ovary, and urinary tract (4–8). Many studies have demonstrated that a second primary cancer is associated with a lower survival rate (9, 10). However, little is known about secondary lung cancers that follow breast cancer. Although several epidemiological studies have investigated lung cancer secondary to breast cancer (11–15), assessed high-risk factors (16–19) for double primary malignancies, and examined the directional associations of estrogen receptor (ER) status (16) in second lung cancers, the clinical characteristics of primary lung cancer following breast cancer have not been comprehensively described. Therefore, this study aimed to evaluate breast cancer patients with a second primary lung cancer to explore the clinicopathological characteristics of primary lung cancer after breast cancer and to analyze the related associations of breast cancer with primary lung cancer, especially the mutation of EGFR in lung cancer, which may provide new insights for more precise treatment of tumors.

Materials and methods

Study population

A review of medical charts at the Jiangsu Province Hospital (Jiangsu, China) revealed 9179 patients with pathologically

confirmed breast cancer between January 2008 and December 2021. During this period, 6512 consecutive patients underwent diagnostic chest computed tomography (CT), and ground-glass nodules (GGNs) were detected in 1195. Among them, 403 patients had complete clinical data about clinicopathological characteristics. Retrospective analysis of these patients' medical records revealed a total of 55 patients with histologically confirmed lung cancer. Clinical information, including pathology and immunohistochemistry of cancer tissues, EGFR status, date of GGN detection, and cancer stage, was collected. All the CT images were evaluated by two senior radiologists retrospectively.

Follow-up

All patients were evaluated at 3- or 4-month intervals by chest CT. CT findings, including lesion size and radiological features, were confirmed by at least two radiologists. Imaging characteristics were visually classified into four subgroups: pure GGN (pGGN), mixed GGN (mGGN), subsolid GGN (ssGGN), and solid GGN (sGGN).

Statistical analysis

Statistical analysis was performed using SPSS version 21.0 (IBM Corporation, Armonk, NY, USA). Measurement data are expressed as mean \pm standard deviation, and the t-test was used for comparison between groups. The chi-squared test was used for categorical variables, and Fisher's exact test was used for data in which more than 20% of cells had expected frequencies < 5 . The correlation of breast cancer factors with primary lung cancer was analyzed using logistic regression analysis. The standardized incidence ratio (SIR) of lung cancer in patients with breast cancer was then calculated by dividing the number of observed cases by the number of expected cases in the general Chinese population. P-values < 0.05 were considered to be statistically significant.

The study was approved by the Ethics Committee of the First Affiliated Hospital of Nanjing Medical University. Clinical data were collected from patients after obtaining informed consent.

Results

The incidence of primary lung cancer in patients with primary breast cancer

A total of 9179 patients with breast cancer were eligible for analysis. Considering that only 6512 underwent diagnostic CT, GGNs were detected in 1195 (18.4%), and a definitive diagnosis of lung cancer was made in 55 (0.8%). Based on the incidence of cancer in China in 2015 (20), higher rates of second primary lung cancer occurred among breast cancer patients compared with the general female population (SIR 1.4 [95% CI 1.25–1.55]).

Clinicopathological characteristics of patients with double primary cancers

The clinicopathological characteristics of patients with breast cancer, including age, family history of malignancy, tumor size, histological type, lymph node metastasis, and clinical grade, are summarized in Table 1. Patients who experienced a second primary lung cancer were more likely to be older ($p = 0.04$). Patients with ER-negative breast cancer ($p = 0.01$), low Ki67 ($p = 0.01$), and no lymph node metastasis ($p = 0.01$) were more likely to develop a second primary lung cancer. There were no statistically significant differences in the other characteristics.

Of the 55 patients, 54 (98.2%) had lung adenocarcinoma and 1 (1.8%) had small cell lung cancer. Among these patients, EGFR status in lung tissue was assessed in 28, with an EGFR mutation rate of 78.5% ($n = 22$) (Figure 1). We analyzed the relationship between EGFR mutation and breast cancer subtype and found that ER-positive patients were more likely to have EGFR mutations (Table 2A, Figure 2). The progesterone receptor, human epidermal growth factor 2 (HER2), and Ki67 status had no statistically significant correlation with EGFR status (Tables 2B–D).

We performed immunohistochemistry on 20 lung tumors. All patients were diagnosed as ER-negative, 95% ($n = 19$) had wild-type anaplastic lymphoma kinase (ALK), and 85% ($n = 17$) exhibited low Ki67 ($< 30\%$).

CT imaging

Of the 55 patients with primary breast cancer and lung cancer who underwent CT, pGGNs were reported in 54.5% ($n = 30$), whereas mGGNs were found in 32.7% ($n = 18$), sGGNs in 10.9% ($n = 6$), and ssGGN in 1.8% ($n = 1$). The average tumor size among all patients was 14.2 mm (range, 4–29 mm).

All patients with wild type EGFR ($n = 6$) exhibited pGGNs. Among patients with EGFR mutations, 7 (31.8%) had pGGNs,

10 (45.5%) had mGGNs, and 5 (22.7%) had sGGNs (Table 3A; $p = 0.012$).

At the first follow-up CT, the majority of patients (63% [$n = 34$]) exhibited no changes in GGN size. GGN regression at the first follow-up was observed in 1 patient who underwent endocrine therapy. Thirteen patients (46.4%) with EGFR mutation exhibited stable lesions at the first follow-up (Table 3A), but without statistical difference (Table 3B; $p = 0.136$).

Sites and intervals of double primary cancer

Upon initial review of the 55 patients with double primary malignancy, 22 (40%) exhibited tumors on the same side, 32 (58.2%) had contralateral cancer (lung cancer occurring on the side opposite to the breast cancer), and 1 (1.8%) exhibited bilateral breast cancer. As shown in Table 4, the chi-square value was 3.422 ($P = 0.064$).

The interval from breast cancer surgery to diagnosis of lung cancer ranged from 0–420 months, with a mean of 35 ± 13.0 months. Notably, 50 patients were first diagnosed with breast cancer, 3 had breast cancer and lung cancer discovered at the same time, and only 2 developed lung cancer before breast cancer.

Discussion

Metastasis of breast cancer to the lungs is relatively common in clinical practice (21). Therefore, in breast cancer patients who exhibit pulmonary nodules, lung metastasis is often the first diagnosis considered. However, a certain number of patients with breast cancer and primary lung cancer experience complications of solitary pulmonary nodules. Therefore, it is necessary to understand the frequency of primary lung cancer in breast cancer patients.

To address the deficiency of information regarding the development of a second primary cancer following breast cancer, we retrospectively reviewed data from the Jiangsu Province Hospital to analyze all patients with breast cancer and second primary lung cancer, as well as those with breast cancer diagnosed as a second primary cancer after lung cancer, between 2008 and 2021. Our research provides further evidence demonstrating that the occurrence of lung cancer is closely related to the development of breast cancer, especially lung adenocarcinoma with EGFR mutation. As breast cancer patients live longer, there is an increased possibility of developing subsequent primary lung cancer owing to underlying genetic or other factors (22). An interesting phenomenon in our study was the higher frequency of second lung cancer in patients with low-grade malignancies, which

TABLE 1 Clinicopathological characteristics of breast cancer patients.

Variable	BC-LC	BC-GGN	p-value	SIR
Age, years			0.0407	
≤ 50	22	204		0.45
> 50	33	144		2.19
Family history of malignancy			0.2439	
Yes	16	248		2.46
No	38	94		1.47
Unknown	1	6		0.08
Tumor size			0.2430	
≤ 2 cm	36	85		1.19
>2 cm	19	263		2.77
Estrogen receptor			0.0101	
Positive	42	171		1.03
Negative	13	177		2.11
Progesterone receptor			0.0133	
Positive	29	157		1.08
Negative	26	191		1.04
HER2			0.1697	
Positive	19	105		1.32
Negative	36	243		0.93
Ki67			0.0109	
<30%	33	114		1.79
≥30%	17	152		1.02
Unknown	5	82		0.95
Lymph node metastasis			0.0136	
Yes	11	169		1.07
No	44	179		2.19
Grade			0.1799	
1-2	41	245		3.04
3	14	103		0.93
History of smoking			0.4633	
Yes	2	18		1.05
No/Unknown	53	330		0.99
Radiotherapy			0.7714	
Yes	31	186		0.99
None/Unknown	24	162		1.16

Data are presented as n unless otherwise indicated.

BC, breast cancer; HER2, human epidermal growth factor receptor 2; LC, lung cancer; SIR, standardized incidence ratio.

differed from our expectations. Breast cancer patients who were older, had ER-negative cancer, had a low Ki67 index, and displayed no lymph node metastasis exhibited a significantly higher rate of development of a second primary lung cancer. The characteristics of second lung cancer were strikingly similar: 100% were ER-negative, 95% had wild-type ALK, and 85% exhibited low Ki67 (<30%). Further, most patients had stable nodules at the first follow-up. We speculate that low malignancy contributes to longer survival times in cancer patients, and, given that the mean interval of diagnosis of double primary cancers was 35 ± 13.0 months, this was sufficient to permit the development of a second primary lung cancer.

Many previous studies have reported that second primary lung cancer rates are significantly higher in breast cancer patients than in patients with other primary cancers (10, 18, 22), which is consistent with the results of our study. The incidence of secondary primary lung cancer in breast cancer patients may have previously been higher, as there was no pathological diagnosis in the remaining 345 patients with stable GGNs. Chest CT at regular intervals could result in increased detection of pulmonary nodules. Further, the occurrence of stable GGN may be related to common risk factors, including genetics, heredity, hormones, and environmental factors. Previous studies have reported that

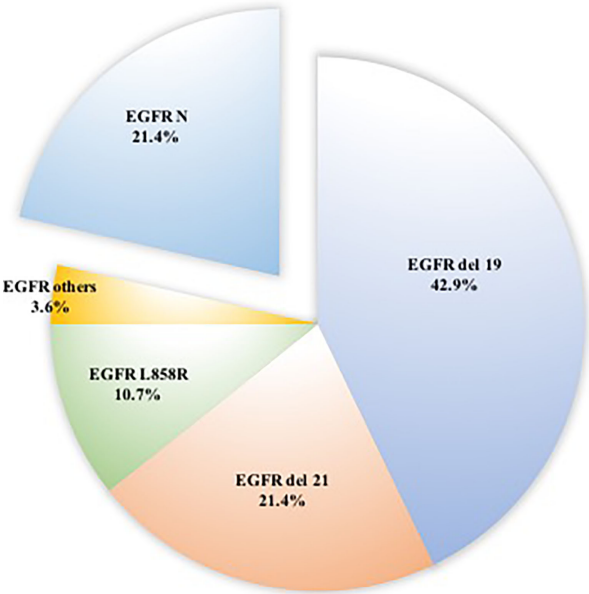


FIGURE 1
Distributions of 22 patients with EGFR mutation in surgically resected ground-glass nodules.

TABLE 2A Correlation of EGFR mutation of lung cancer and ER status of breast cancer.

No.		ER		Total
		Negative	Positive	
EGFR	Wild-type	3	3	6
	Mutated	0	22	22
Total		3	25	28

Fisher’s exact test, $p = 0.006$.
EGFR, epidermal growth factor receptor; ER, estrogen receptor.

TABLE 2B Correlation of EGFR mutation and PR status of breast cancer.

No.		PR		Total
		Negative	Positive	
EGFR	Wild-type	4	2	6
	Mutated	7	15	22
Total		11	17	28

Fisher’s exact test, $p = 0.174$.
EGFR, epidermal growth factor receptor; PR, progesterone receptor.

TABLE 2C Correlation of EGFR mutation and HER2 status of breast cancer.

No.		HER2		Total
		Negative	Positive	
EGFR	Wild-type	3	3	6
	Mutated	7	15	22
Total		10	18	28

Fisher's exact test, $p = 0.634$.
EGFR, epidermal growth factor receptor; HER2, human epidermal growth factor receptor 2.

TABLE 2D Correlation of EGFR mutation and Ki67 expression of breast cancer.

No.		Ki67		Total
		<30%	≥30%	
EGFR	Wild-type	4	2	6
	Mutated	13	9	22
Total		17	11	28

Fisher's exact test, $p = 0.73$.
EGFR, epidermal growth factor receptor.

breast cancer patients who undergo radiotherapy (17, 23), smokers (24), and those treated with chemotherapy (13) have a higher possibility of developing secondary lung cancer.

Nevertheless, the higher risk for developing lung cancer in patients with primary breast cancer cannot be explained merely by regular follow-up. An interesting finding of our study was that the rate of EGFR mutation was as high as 75.6%, which is almost twice that in patients with non-small cell lung cancer without another primary cancer (25). This phenomenon has not been reported in previous studies. These observations suggest that EGFR signaling may play a crucial role in the development of concurrent lung and breast cancers. Several studies have reported that overexpression of EGFR is common in breast

cancer patients and is associated with decreased survival (26–29). Moreover, previous reports have indicated that ER signaling plays an important role in primary lung cancer following breast cancer, and that activation of ER signaling occurs through EGFR/HER-1, thus confirming a correlation between ER expression and EGFR mutation (30–35). Patients with an acquired resistance to EGFR antagonists may, therefore, benefit from antiestrogen therapy (14). Moreover, EGFR and HER2 are members of the human epidermal growth factor receptor family, which are type I transmembrane growth factor receptors that activate intracellular signaling pathways and are major determinants of human cancer (36). According to previous studies, overexpression of EGFR is associated with

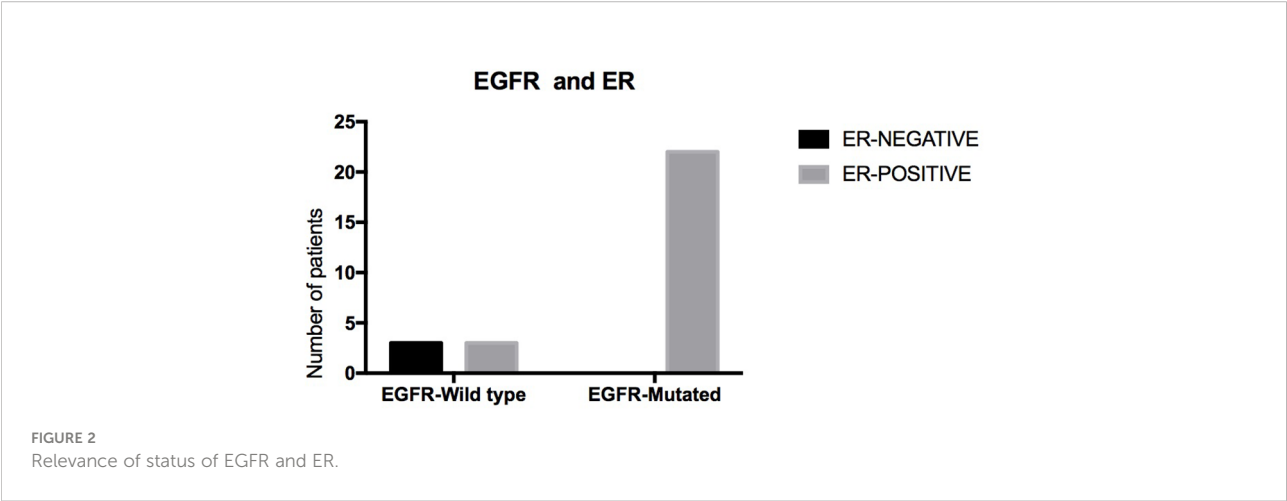


TABLE 3A Correlation of EGFR and type of GGN.

No.		GGN			Total
		pGGN	mGGN	sGGN	
EGFR	Wild-type	6	0	0	6
	Mutated	7	10	5	22
Total		13	10	5	28

Fisher's exact test, $p = 0.012$.

EGFR, epidermal growth factor receptor; GGN, ground glass nodules; pGGN, pure GGN; mGGN, mixed GGN; sGGN, solid GGN.

TABLE 3B Correlation of EGFR and change in CT imaging of first time to follow up.

No.		Change in CT		Total
		Stable lesion	Lesion progression	
EGFR	Wild-type	6	0	6
	Mutated	13	9	22
Total		19	9	28

Fisher's exact test, $p = 0.136$.

EGFR, epidermal growth factor receptor; CT, computed tomography.

TABLE 4 Site of spontaneous breast and lung cancer lesions.

No.		Lung cancer		Total
		Left	Right	
Breast cancer	Left	9	20	29
	Right	14	11	29
Total		23	31	54

Chi-square 3.42 $p = 0.064$.

apoptosis, angiogenesis, and formation of tumor vessels. Therefore, EGFR mutation may provide clues of a common etiological pathway between primary lung adenocarcinoma and breast cancer (37, 38).

Patients with a second primary lung cancer were less likely to have pGGNs and more likely to have sGGNs, and those with EGFR mutations exhibited a similar trend ($P = 0.05$). Analysis of the correlation between CT image patterns and gene mutations demonstrated no statistical significance. Similarly, most of the GGNs had not changed in size at the first follow-up. Unexpectedly, the lesion in one of the patients who underwent endocrine therapy shrunk, consistent with a previous report that breast cancer patients with second primary lung cancers who are treated with antiestrogen therapy exhibit longer cancer-specific survival (14, 34).

There were several limitations to the present study, the first of which was its retrospective, as opposed to prospective, design. Second, random variation and low statistical power resulted from the limited number of patients. Finally, the lack of long-term follow-up prevented us from observing more cancer-

related events and assessing cancer-specific survival. The next step is to further follow up the patient, collect more clinical samples, and conduct basic research to explore its underlying mechanisms.

Conclusions

We observed that women diagnosed with breast cancer demonstrated an increased risk of second primary lung cancer. The present study is the first to report a higher rate of EGFR mutations in second primary lung cancer, which may play an important role in the development of double primary breast and lung cancer. This is an interesting clinical finding that can further the exploration of the mechanism behind elevated EGFR expression in patients with primary breast cancer and the mechanism of EGFR expression in lung cancer and breast cancer, paving the way for development of new drugs. Based on the results of the current research, we recommend that breast cancer patients who exhibit high-risk factors be closely followed.

EGFR-targeted treatment represents an alternative option for these patients.

Data availability statement

The original contributions presented in the study are included in the article/supplementary material. Further inquiries can be directed to the corresponding authors.

Author Contributions

TZ: Conceptualization, data curation, formal analysis, software, writing-original draft, and writing-review and editing. HX: Conceptualization, data curation, formal analysis, writing-original draft, and writing-review and editing. YiL: Conceptualization, data curation, formal analysis, writing-original draft, and writing-review and editing. CS: Data curation, formal analysis, and writing-review and editing. FY: Data curation, and writing-review and editing. YaL: Data curation and writing-review and editing. XH: Formal analysis and writing-review and editing. ZF: Formal analysis and writing-review and editing. WL: Conceptualization, formal analysis, and writing-review and editing. YY: Conceptualization, formal analysis, funding acquisition and writing-review and editing. All authors contributed to the article and approved the submitted version.

Funding

This study was financially supported by the National Key Research and Development Program of China (ZDZX2017ZL-

01), High-level innovation team of Nanjing Medical University (JX102GSP201727), Wu Jieping Foundation (320.6750.17006), Key medical talents (ZDRCA2016023), 333 Project of Jiangsu Province (BRA2017534 and BRA2015470), The collaborative innovation center for tumor individualization focuses on open topics (JX21817902/008), Postgraduate Research&Practice Innovation Program of Jiangsu Province (SJCX21_0625) and Project of China key research and development program precision medicine research (2016YFC0905901).

Acknowledgments

The authors would like to thank Lei Wang for excellent technical support and Professor Xichun Hu for critically reviewing the manuscript.

Conflict of interest

The authors declare that the research was conducted in the absence of any commercial or financial relationships that could be construed as a potential conflict of interest.

Publisher's note

All claims expressed in this article are solely those of the authors and do not necessarily represent those of their affiliated organizations, or those of the publisher, the editors and the reviewers. Any product that may be evaluated in this article, or claim that may be made by its manufacturer, is not guaranteed or endorsed by the publisher.

References

1. Sung H, Ferlay J, Siegel RL, Laversanne M, Soerjomataram I, Jemal A, et al. Global cancer statistics 2020: GLOBOCAN estimates of incidence and mortality worldwide for 36 cancers in 185 countries. *CA Cancer J Clin* (2021) 71(3):209–49. doi: 10.3322/caac.21660
2. Hayat MJ, Howlader N, Reichman ME, Edwards BK. Cancer statistics, trends, and multiple primary cancer analyses from the surveillance, epidemiology, and end results (SEER) program. *Oncologist* (2007) 12(1):20–37. doi: 10.1634/theoncologist.12-1-20
3. Mariotto AB, Rowland JH, Ries LA, Scoppa S, Feuer EJ. Multiple cancer prevalence: a growing challenge in long-term survivorship. *Cancer Epidemiol Biomarkers Prev* (2007) 16(3):566–71. doi: 10.1158/1055-9965.EPI-06-0782
4. Utada M, Ohno Y, Hori M, Soda M. Incidence of multiple primary cancers and interval between first and second primary cancers. *Cancer Sci* (2014) 105(7):890–6. doi: 10.1111/cas.12433
5. Molina-Montes E, Requena M, Sanchez-Cantalejo E, Fernandez MF, Arroyo-Morales M, Espin J, et al. Risk of second cancers cancer after a first primary breast cancer: a systematic review and meta-analysis. *Gynecol Oncol* (2015) 136(1):158–71. doi: 10.1016/j.ygyno.2014.10.029
6. Marcu LG, Santos A, Bezak E. Risk of second primary cancer after breast cancer treatment. *Eur J Cancer Care (Engl)* (2014) 23(1):51–64. doi: 10.1111/ecc.12109
7. Molina-Montes E, Pollan M, Payer T, Molina E, Davila-Arias C, Sanchez MJ. Risk of second primary cancer among women with breast cancer: A population-based study in Granada (Spain). *Gynecol Oncol* (2013) 130(2):340–5. doi: 10.1016/j.ygyno.2013.04.057
8. Bao S, Jiang M, Wang X, Hua Y, Zeng T, Yang Y, et al. Nonmetastatic breast cancer patients subsequently developing second primary malignancy: A population-based study. *Cancer Med* (2021) 10(23):8662–72. doi: 10.1002/cam4.4351
9. Miller KD, Nogueira L, Mariotto AB, Rowland JH, Yabroff KR, Alfano CM, et al. Cancer treatment and survivorship statistics, 2019. *CA Cancer J Clin* (2019) 69(5):363–85. doi: 10.3322/caac.21565
10. Lee KD, Chen SC, Chan CH, Lu CH, Chen CC, Lin JT, et al. Increased risk for second primary malignancies in women with breast cancer diagnosed at young age: a population-based study in Taiwan. *Cancer Epidemiol Biomarkers Prev* (2008) 17(10):2647–55. doi: 10.1158/1055-9965.EPI-08-0109
11. Oya H, Murayama E, Okino M. [Primary lung cancer found following mastectomy for breast cancer]. *Kyobu Geka* (1968) 21(7):510–4.
12. Salomon R, Lopez-Velez R, Pasquau F, Lafuente J, Gallar P. [Lung cancer as a second primary cancer in patients with breast cancer. presentation of 4 cases]. *Rev Clin Esp* (1983) 169(1):51–4.

13. He KW, Wei W, Liu ZY, Song X, Zhuo PY, Ma QH, et al. [Clinicopathological features of second primary lung cancer and pulmonary metastasis in patients with breast cancer]. *Zhonghua Zhong Liu Za Zhi* (2018) 40(3):201–5. doi: 10.3760/cma.j.issn.0253-3766.2018.03.008
14. Hsu LH, Feng AC, Kao SH, Liu CC, Tsai SY, Shih LS, et al. Second primary lung cancers among breast cancer patients treated with anti-estrogens have a longer cancer-specific survival. *Anticancer Res* (2015) 35(2):1121–7.
15. Kerendi F, Gal A, Corvera JS, Halkos ME, Miller JL. Characteristics of second primary lung malignancy in patients with known breast cancer. *South Med J* (2009) 102(3):269–74. doi: 10.1097/SMJ.0b013e318197fec6
16. Schonfeld SJ, Curtis RE, Anderson WF, Berrington de Gonzalez A. The risk of a second primary lung cancer after a first invasive breast cancer according to estrogen receptor status. *Cancer Causes Control* (2012) 23(10):1721–8. doi: 10.1007/s10552-012-0054-3
17. Grantzau T, Thomsen MS, Vaeth M, Overgaard J. Risk of second primary lung cancer in women after radiotherapy for breast cancer. *Radiother Oncol* (2014) 111(3):366–73. doi: 10.1016/j.radonc.2014.05.004
18. Watanabe S, Ochi H, Kobayashi Y, Tsugane S, Arimoto H, Kitagawa K. Frequency of multiple primary cancers and risk factors for lung and breast cancer patients. *Princess Takamatsu Symp* (1987) 18:275–82.
19. Huang YJ, Huang TW, Lin FH, Chung CH, Tsao CH, Chien WC. Radiation therapy for invasive breast cancer increases the risk of second primary lung cancer: A nationwide population-based cohort analysis. *J Thorac Oncol* (2017) 12(5):782–90. doi: 10.1016/j.jtho.2017.01.021
20. Chen W, Zheng R, Baade PD, Zhang S, Zeng H, Bray F, et al. Cancer statistics in China, 2015. *CA Cancer J Clin* (2016) 66(2):115–32. doi: 10.3322/caac.21338
21. Tarutinov VI, Bukavin AS, Skliar S. [Prognostic criteria of breast cancer metastasis to the lungs]. *Klin Khir* (1995) 1995(5):10–2. doi: 10.1007/s12245-010-0249-x
22. Wang R, Yin Z, Liu L, Gao W, Li W, Shu Y, et al. Second primary lung cancer after breast cancer: A population-based study of 6,269 women. *Front Oncol* (2018) 8:427. doi: 10.3389/fonc.2018.00427
23. Struikmans H, Aarts MJ, Jobsen JJ, Koning CC, Poortmans PM, Louwman MW, et al. [Trends in the use of primary radiotherapy for cancer in the Netherlands in patients with breast, prostate, rectal and lung tumours]. *Ned Tijdschr Geneesk* (2012) 156(12):A4426.
24. Kaufman EL, Jacobson JS, Hershman DL, Desai M, Neugut AI. Effect of breast cancer radiotherapy and cigarette smoking on risk of second primary lung cancer. *J Clin Oncol* (2008) 26(3):392–8. doi: 10.1200/JCO.2007.13.3033
25. Wei B, Yang K, Zhao J, Chang Y, Ma Z, Dong B, et al. Quantification of EGFR mutations in primary and metastatic tumors in non-small cell lung cancer. *J Exp Clin Cancer Res* (2014) 33:5. doi: 10.1186/1756-9966-33-5
26. Levva S, Kotoula V, Kostopoulos I, Manousou K, Papadimitriou C, Papadopoulou K, et al. Prognostic evaluation of epidermal growth factor receptor (EGFR) genotype and phenotype parameters in triple-negative breast cancers. *Cancer Genomics Proteomics* (2017) 14(3):181–95. doi: 10.21873/cgp.20030
27. Siziopikou KP, Cobleigh M. The basal subtype of breast carcinomas may represent the group of breast tumors that could benefit from EGFR-targeted therapies. *Breast* (2007) 16(1):104–7. doi: 10.1016/j.breast.2006.09.003
28. Burness ML, Grushko TA, Olopade OI. Epidermal growth factor receptor in triple-negative and basal-like breast cancer: promising clinical target or only a marker? *Cancer J* (2010) 16(1):23–32. doi: 10.1097/PPO.0b013e3181d24fc1
29. Alanazi IO, Khan Z. Understanding EGFR signaling in breast cancer and breast cancer stem cells: Overexpression and therapeutic implications. *Asian Pac J Cancer Prev* (2016) 17(2):445–53. doi: 10.7314/APJCP.2016.17.2.445
30. Siegfried JM, Stabile LP. Estrongen steroid hormones in lung cancer. *Semin Oncol* (2014) 41(1):5–16. doi: 10.1053/j.seminoncol.2013.12.009
31. Stabile LP, Lyker JS, Gubish CT, Zhang W, Grandis JR, Siegfried JM. Combined targeting of the estrogen receptor and the epidermal growth factor receptor in non-small cell lung cancer shows enhanced antiproliferative effects. *Cancer Res* (2005) 65(4):1459–70. doi: 10.1158/0008-5472.CAN-04-1872
32. Stabile LP, Rothstein ME, Cunningham DE, Land SR, Dacic S, Keohavong P, et al. Prevention of tobacco carcinogen-induced lung cancer in female mice using antiestrogens. *Carcinogenesis* (2012) 33(11):2181–9. doi: 10.1093/carcin/bgs260
33. Nose N, Sugio K, Oyama T, Nozoe T, Uramoto H, Iwata T, et al. Association between estrogen receptor-beta expression and epidermal growth factor receptor mutation in the postoperative prognosis of adenocarcinoma of the lung. *J Clin Oncol* (2009) 27(3):411–7. doi: 10.1200/JCO.2008.18.3251
34. Garon EB, Pietras RJ, Finn RS, Kamranpour N, Pitts S, Marquez-Garban DC, et al. Antiestrogen fulvestrant enhances the antiproliferative effects of epidermal growth factor receptor inhibitors in human non-small-cell lung cancer. *J Thorac Oncol* (2013) 8(3):270–8. doi: 10.1097/JTO.0b013e31827d525c
35. Mazieres J, Rouquette I, Lepage B, Milia J, Bouchet L, Guibert N, et al. Specificities of lung adenocarcinoma in women who have never smoked. *J Thorac Oncol* (2013) 8(7):923–9. doi: 10.1097/JTO.0b013e3182904dfb
36. Yarden Y, Sliwkowski MX. Untangling the ErbB signalling network. *Nat Rev Mol Cell Biol* (2001) 2(2):127–37. doi: 10.1038/35052073
37. Althuis MD, Fergenbaum JH, Garcia-Closas M, Brinton LA, Madigan MP, Sherman ME. Etiology of hormone receptor-defined breast cancer: a systematic review of the literature. *Cancer Epidemiol Biomarkers Prev* (2004) 13(10):1558–68. doi: 10.1158/1055-9965.1558.13.10
38. Yeh J, Chun J, Schwartz S, Wang A, Kern E, Guth AA, et al. Clinical characteristics in patients with triple negative breast cancer. *Int J Breast Cancer* (2017) 2017:1796145. doi: 10.1155/2017/1796145



OPEN ACCESS

EDITED BY

Shaohua Xu,
Tongji University, China

REVIEWED BY

Xuehai Wang,
Nantong University, China
Ting Ye,
Guangdong Pharmaceutical
University, China

*CORRESPONDENCE

Xiaopeng Shen
shenxiaopeng_cn@ahnu.edu.cn

[†]These authors have contributed
equally to this work

SPECIALTY SECTION

This article was submitted to
Gynecological Oncology,
a section of the journal
Frontiers in Oncology

RECEIVED 30 August 2022

ACCEPTED 17 October 2022

PUBLISHED 31 October 2022

CITATION

Shen X, Wang C, Li M, Wang S, Zhao Y,
Liu Z and Zhu G (2022) Identification
of CD8+ T cell infiltration-related
genes and their prognostic values in
cervical cancer.
Front. Oncol. 12:1031643.
doi: 10.3389/fonc.2022.1031643

COPYRIGHT

© 2022 Shen, Wang, Li, Wang, Zhao, Liu
and Zhu. This is an open-access article
distributed under the terms of the
[Creative Commons Attribution License](#)
(CC BY). The use, distribution or
reproduction in other forums is
permitted, provided the original
author(s) and the copyright owner(s)
are credited and that the original
publication in this journal is cited, in
accordance with accepted academic
practice. No use, distribution or
reproduction is permitted which does
not comply with these terms.

Identification of CD8+ T cell infiltration-related genes and their prognostic values in cervical cancer

Xiaopeng Shen^{1*†}, Chunguang Wang^{1†}, Meng Li^{1†},
Sufen Wang², Yun Zhao¹, Zhongxian Liu¹ and Guoping Zhu¹

¹College of Life Sciences, Anhui Normal University, Wuhu, Anhui, China, ²Department of Pathology, The First Affiliated Hospital of Wannan Medical College, Wuhu, Anhui, China

Cervical cancer is a female-specific cancer with relatively high morbidity and mortality. As known to all, immune cell infiltrations in the cancer microenvironment are closely related to the cancer diagnosis and prognosis. Here we revealed that the CD8+ T cell infiltration was significantly upregulated in cervical cancer versus normal cervix uteri samples. Through univariate and multivariate cox analyses, we discovered that the CD8+ T cell infiltration was the only independent beneficial factor for the prognosis of cervical cancer. To explore the genes associated with the CD8+ T cell infiltration in cervical cancer, we performed the WGCNA analysis on the differentially expressed genes (DEGs) of cervical cancer versus normal cervix uteri tissues. As a result, 231 DEGs were found to be associated with CD8+ T cell infiltration in cervical cancer. Subsequently, with the Cytoscape analysis, we identified 105 hub genes out of the 231 DEGs. To further explore the genes that might be responsible for the prognosis of cervical cancer, we performed a univariate cox analysis followed by a LASSO assay on the 105 hub genes and located four genes (IGSF6, TLR10, FCRL3, and IFI30) finally. The four genes could be applied to the prediction of the prognosis of cervical cancer, and relatively higher expression of these four genes predicted a better prognosis. These findings contributed to our understanding of the prognostic values of CD8+ T cell infiltration and its associated genes in cervical cancer and thus might benefit future immune-related therapies.

KEYWORDS

CD8+ T cells, cervical cancer, prognosis, IGSF6, TLR10, FCRL3, IFI30

Introduction

Cervical cancer, which primarily arises from the cervix, is the fourth most common and death-causing cancer in women worldwide (1). According to recent Global Cancer statistics, there were about 604,000 new cases and 342,000 deaths of cervical cancer in 2020 (2). The incidence and mortality of cervical cancer were both significantly higher in developing countries, which were 7–10 and 18 times exceeding these in developed countries, respectively (2). Human papillomavirus (HPV) is believed to be the primary cause of cervical cancer. Over 90% of squamous cervical cancer were diagnosed to be HPV positive (3). Thus, the application of the HPV vaccine largely constrained the incidence of cervical cancer in developed countries, but not in developing countries due to the limited vaccination rate (4, 5). Conventional therapy approaches against cervical cancer include surgery, radiation, chemotherapy, targeted drug therapy, and immunotherapy (6–9). Besides these, many efforts have been made to apply Chimeric Antigen Receptor T-Cell (CAR-T) immunotherapy to the therapy against cervical cancer (10–12). The overall therapy outcomes are closely associated with therapy strategies designed based on the specific gene profiles of each individual.

Immune cell infiltration in cancer is an indispensable microenvironmental factor that has been widely applied to prognosis prediction and immunotherapy (13–15). The infiltrations of activated B cells, memory effector T cells, eosinophils, and plasmacytoid dendritic cells were shown to be associated with a better prognosis in cervical cancer (16). The composition of immune cell infiltration might even allocate cervical cancer patients into different subtypes that displayed distinct prognostic outcomes, thus implying the importance of immune cell infiltration (17). Moreover, some therapy strategies, for example, neoadjuvant chemotherapy, work at least partially by reprogramming the immune microenvironment of cervical cancer (17). Some genes have been reported to manipulate the immune cell infiltrations in certain cancers and thus serve as prognostic biomarkers, such as TREM2, HSF1, and GIMAP4 (18–20). Nevertheless, the role of activated CD8⁺ T cells in the prognosis of cervical cancer and the genes that are associated with CD8⁺ T cells remains uncertain.

In this study, we evaluated the changes in immune cell infiltration of cervical cancer versus normal tissues. We found that the CD8⁺ T cell infiltration was the only independent beneficial factor for the prognosis of cervical cancer. Four genes (IGSF6, TLR10, FCRL3, and IFI30) were found to be CD8⁺ T cell infiltration-related genes. The four genes could be applied to the prediction of cervical cancer prognosis.

Materials and methods

General information of datasets

The clinical information and RNA sequencing (RNA-seq) data of the Cervical Squamous Cell Carcinoma and Endocervical Adenocarcinoma (CESC) were downloaded from The Cancer Genome Atlas (TCGA), which included 306 cervical cancer tissues and 3 normal control samples (termed TCGA-CESC cohort). The clinical information of the TCGA-CESC cohort was shown in Table 1. The data of 10 normal cervical tissue samples were downloaded from the Genotype Tissue Expression (GTEx) database. When analyzing the data from TCGA and GTEx together, we directly downloaded a merged expression matrix of these two datasets from the UCSC Xena database instead. The GSE151666 dataset in the Gene Expression Omnibus (GEO) database, which included the RNA-seq data of 68 pre-treatment primary cervical cancer samples, was used as a validation cohort. The expression matrixes retrieved from the TCGA and GTEx databases were in count format, while the expression matrix from the GSE151666 dataset was in FPKM format.

RNA-seq data processing and differentially expressed gene determination

Differentially expressed genes (DEGs) were determined by the “DESeq” software. The adjusted P value ≤ 0.01 and $|\log_2(\text{FoldChange})| > 2$ were used as the cutoff criteria. The gene ontology (GO) analysis was performed using the “clusterProfile” package in R (version 4.1.0) and the Kyoto Encyclopedia of Genes and Genomes (KEGG) analysis was performed at The Database for Annotation, Visualization and Integrated Discovery (DAVID) platform (<https://david.ncifcrf.gov/>). P value < 0.05 was used as the significance threshold. GO results were plotted with the “GOplot” package in R, while KEGG results were plotted using the “ggplot2” package in R.

CIBERSORT analysis

The CIBERSORT analysis was performed to determine immune cell infiltrations as described previously (21). The results of the CIBERSORT analysis included the relative infiltration levels of B cells (naïve B cells, memory B cells, and plasma cells), T cells (CD8⁺ T cells, naïve CD4 T cells, resting

TABLE 1 Clinical characteristics of the TCGA-CESC cohort.

Characteristics	Patients (N = 306)	
	N	%
Gender		
Female	306	100%
Stage		
I	162	52.90%
II	69	22.50%
III	46	15.00%
IV	22	7.20%
NA	7	2.30%
T		
T1	140	45.80%
T2	72	23.50%
T3	21	6.90%
T4	10	3.30%
TIS	1	0.30%
TX	17	5.60%
NA	45	14.70%
N		
N0	134	43.80%
N1	61	19.90%
NX	66	21.60%
NA	45	14.70%
M		
M0	116	37.90%
M1	11	3.60%
MX	129	42.20%
NA	50	16.30%
Race		
American Indian or Alaska Native	7	2.30%
Asian	20	6.50%
Black or African American	31	10.10%
Native Hawaiian or other pacific islander	2	0.70%
white	210	68.60%
NA	36	11.80%
Age		
≤50	188	61.40%
> 50	118	38.60%
Vital status		
ALIVE	233	76.10%
DEAD	73	23.90%
Survival time		
Long(>5years)	47	15.40%
Short(<5years)	259	84.60%

TCGA, The Cancer Genome Atlas; CESC, cervical squamous cell carcinoma and endocervical adenocarcinoma; NA, not applicable.

memory CD4⁺ T cells, activated memory CD4⁺ T cells, follicular helper T cells, regulatory T cells, and gamma delta T cells), NK cells (resting NK cells and activated NK cells), monocytes, macrophages (M0 macrophages, M1 macrophages,

and M2 macrophages), dendritic cells (resting dendritic cells and activated dendritic cells), mast cells (resting mast cells and activated mast cells), eosinophils, neutrophils. P value < 0.05 was used as the significance threshold.

Weighted gene co-expression network analysis (WGCNA)

The DEGs between normal and cervical cancer groups in the TCGA-CESC cohort were subjected to WGCNA, which was performed using the “WGCNA” package in R. We used 0.9 as the cutoff for the scale-free fit index and obtained soft-thresholding power = 2 with the pickSoftThreshold function in the “WGCNA” package. By setting the soft-thresholding power = 2, the DEGs were allocated into 15 modules, which were visualized in a cluster dendrogram. The correlation values and significances between the modules and immune cell infiltrations were calculated and displayed in heatmaps.

Protein-protein interaction analysis

The protein-protein interaction was analyzed in the STRING database (<https://cn.string-db.org/>) and plotted with the Cytoscape software. The hub genes in the protein-protein interaction network were determined by 12 algorithms in the cytoHubba of Cytoscape, respectively, which were Betweenness, BottleNeck, Closeness, ClusteringCoefficient, Degree, DMNC, EcCentricity, EPC, MCC, MNC, Radiality, and stress. The shared hub genes by all 12 algorithms were considered to be the candidate hub genes, which were determined and plotted with the “UpSetR” package in R.

Univariate and multivariate Cox analysis

To evaluate the clinical significance of cervical cancer infiltrated immune cells, univariate and multivariate Cox analyses were performed with the “coxph” function in the “survival” package. As to the clinical significance of the hub genes determined by the WGCNA and Cytoscape, univariate Cox analysis was performed with the “survival” package in R. P value < 0.05 was used as the cutoff to select significant gene candidates, which were then subjected to the least absolute shrinkage and selection operator (LASSO) analysis. The LASSO analysis was performed using the “glmnet” package in R to further filter the genes that significantly affected the prognosis of cervical cancer.

Receiver Operating Characteristic (ROC) analysis

The expressions of selected genes along with the overall survival data of the TCGA-CESC cohort were used to evaluate the predictive values of these genes in the prognosis of cervical cancer. The ROC curve and areas under the ROC curve (AUC) were generated by the “timeROC” package in R.

Overall survival (OS) analysis

291 patients in the TCGA-CESC cohort, whose OS was larger than zero, were included in the OS analysis. The OS was examined by log-rank and Kaplan-Meier plots. When studying the impacts of target genes on the OS, the patients were equally divided into two groups (i.e. “high” versus “low”) based on their median expressions. The OS curves were plotted with the “survival” and “survminer” packages in R. P value < 0.05 was considered to be significant.

Immunohistochemical staining

Tumor and para-carcinoma tissues of cervical cancer were embedded in paraffin and then sectioned. Immunohistochemical staining was performed using an Immunohistochemistry Kit (Sangon Biotech, Cat# D601037) according to the manufacturer's instructions. In brief, slides were first dewaxed with xylene and rehydrated with gradient ethanols. Subsequently, the slides were subjected to antigen retrieval with citrate solution in boiling water. The slides were then blocked with bovine serum albumin (BSA) and incubated with primary antibodies overnight. After that, the slides were incubated with HRP-conjugated secondary antibodies and then reacted with the DAB solution in the kit. Finally, the slides were incubated with hematoxylin. The staining results were observed with a Leica DMi8 fluorescence microscope. The antibodies used in this study were as follows: IGSF6 mAb (Santa Cruz, Cat# sc-377053), TLR10 mAb (Santa Cruz, Cat# sc-293300), FCRL3 mAb (Santa Cruz, Cat# sc-365706), IFI30 mAb (Santa Cruz, Cat# sc-393507), and Goat Anti-Mouse HRP secondary antibody (biosharp, Cat# BL001A). The cervical cancer samples used in this study were obtained with written informed consent from patients. Our study was approved by the Ethics Committee of Anhui Normal University.

Results

Identification of immune cell infiltrations in cervical cancer

We downloaded the RNA-seq data of the TCGA-CESC cohort along with normal cervix uteri samples from the GTEx database. To investigate the immune cell infiltrations in normal cervix uteri and cervical cancer, we performed a CIBERSORT analysis on the RNA-seq data. Among the 22 infiltrated immune cell types, activated dendritic cells, resting dendritic cells, M0 and M1 macrophages, resting NK cells, regulatory T cells, follicular helper T cells, activated memory CD4+ T cells, CD8+ T cells, and memory B cells were significantly upregulated, while resting mast cells, M2 macrophages, monocytes, activated NK cells, resting memory CD4+ T cells, and naïve B cells were significantly downregulated. (Figures 1A, B) The infiltrated immune cells were differentially correlated with each other. (Figure 1C) Among these, naïve B cells were positively related to plasma cells but negatively related to memory B cells, implying the diverse B cell trends in cervical cancer. CD8+ T cells were negatively correlated with naïve CD4+ T cells and M0 macrophages but positively correlated with follicular helper T cells.

CD8+ T cell infiltration was associated with the prognosis of cervical cancer

To determine which immune infiltrations were associated with the prognosis of cervical cancer, we performed both univariate and multivariate Cox regression analyses on the TCGA-CESC cohort. The result of univariate cox analysis suggested that the infiltration of activated NK cells, M0 macrophages, activated mast cells, and neutrophils were hazard factors for the overall survival (OS) of cervical cancer patients, while the CD8+ T cells and M2 macrophages were beneficial factors for the OS. (Figure 2A) Moreover, multivariate cox analysis suggested that the CD8+ T cells and resting dendritic cells were independent beneficial factors affecting the OS of cervical cancer. (Figure 2B) It was worth noting that the infiltration of resting dendritic cells was not a significant factor in the univariate cox analysis (Figure 2A), though it was significant in the multivariate cox analysis (Figure 2B). Thus, we focused on the CD8+ T cell infiltration in subsequent studies. We next plotted the relative levels of the CD8+ T cell infiltration in normal cervix uteri and cervical cancer at different histological stages. The CD8+ T cell infiltration was gradually elevated at stages I and II compared to normal ones but dropped at stages

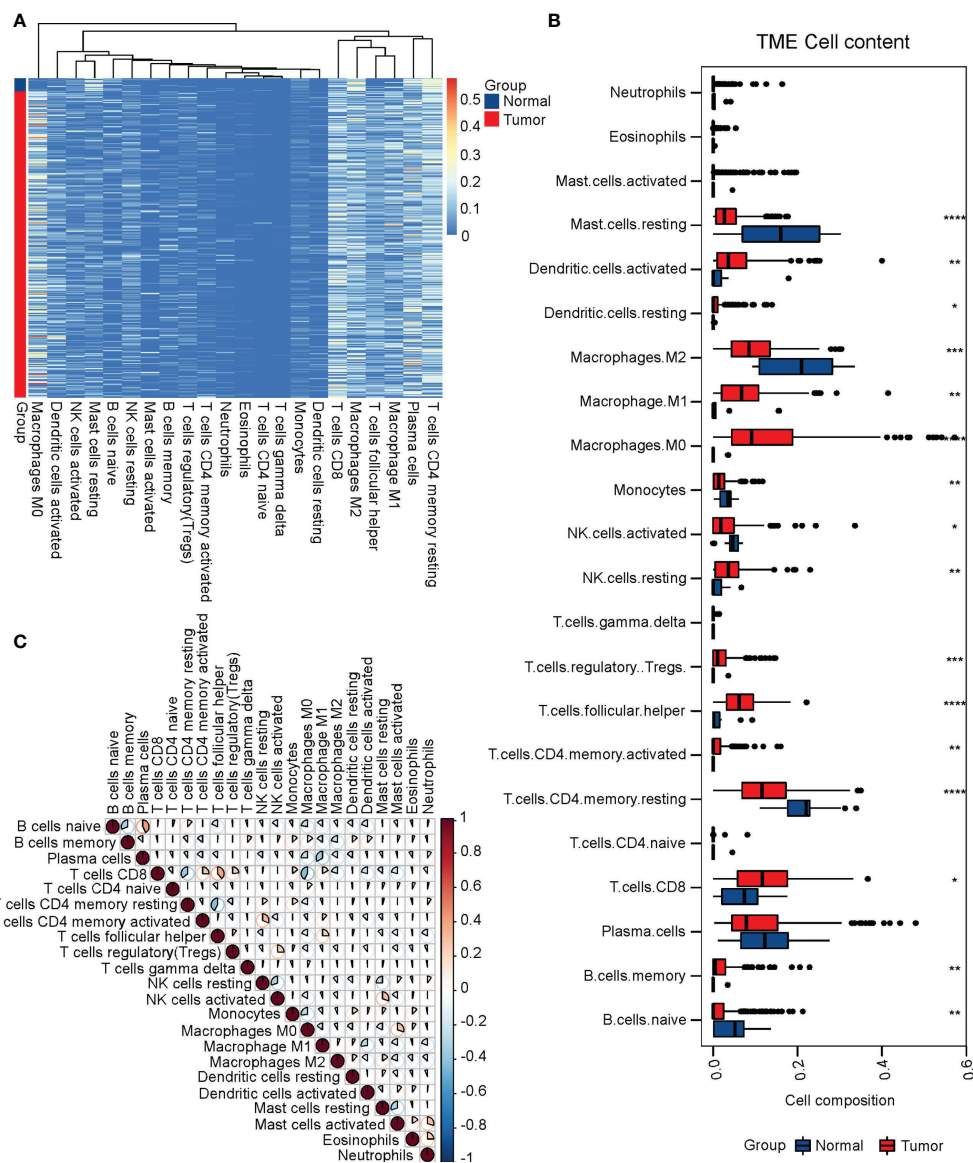


FIGURE 1

Identification of immune cell infiltrations in cervical cancer. To evaluate immune cell infiltrations, we performed a CIBERSORT analysis on the TCGA-CESC cohort along with normal cervix samples from the GTEx. (A) The heatmap of immune cell infiltrations in normal and cervical cancer groups. (B) The relative levels of immune cell infiltrations in normal and cervical cancer groups. (C) The correlation of immune cell infiltrations in normal and cervical cancer groups. * $P < 0.05$; ** $P < 0.01$; *** $P < 0.001$; **** $P < 0.0001$.

III and IV compared to stage II. (Figure 2C) The mean level of CD8+ T cell infiltration at stages III and IV was significantly lower than that of stages I and II. (Figure 2D) By dividing the TCGA-CESC cohort into two groups based on the level of CD8+ T cell infiltration, we found that the patients with a higher CD8+ T cell infiltration showed a remarkable improvement in their OS ($P=0.0024$). (Figure 2E) Therefore, the CD8+ T cell infiltration, which was first elevated at the initial stages of cervical cancer and

then dropped at later stages, was an independent beneficial factor for the OS of cervical cancer.

The altered DEGs, biological processes, and pathways in cervical cancer

We next studied the differentially expressed genes (DEGs) in cervical cancer compared to normal tissues. We performed a

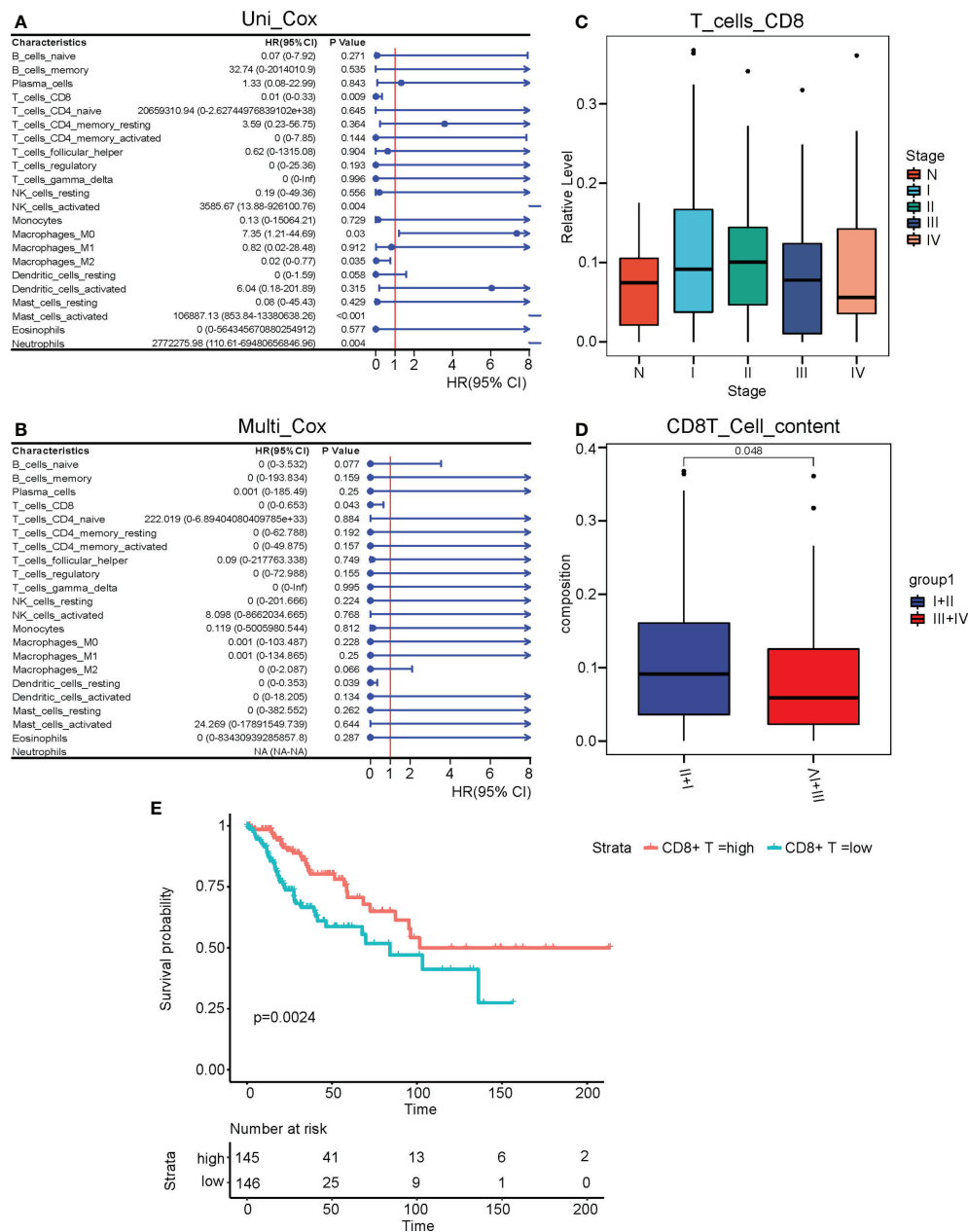


FIGURE 2

CD8+ T cell infiltration was associated with the prognosis of cervical cancer. (A) Univariate and (B) multivariate Cox regression analyses performed on the infiltrated immune cells in the TCGA CESC cohort. (C) The relative levels of CD8+ T cell infiltrations at different clinical stages of cervical cancer. (D) The relative levels of CD8+ T cell infiltrations at stages III and IV versus stages I and II. (E) The survival curve of cervical cancer patients with high and low levels of CD8+ T cell infiltrations. N, Normal; I, stage I; II, stage II; III, stage III; IV, stage IV; I+II, stage I and II; III+IV, stage III and IV.

DEG analysis using the “DESeq2” package in R on the merged RNA-seq data of the cervix uteri in the GTEx and the TCGA-CESC cohort. $|\log_2(\text{FoldChange})| > 2$ and adjusted P value < 0.01 was used as the cutoff. As a result, we identified 2111 upregulated and 2160 downregulated DEGs. (Figure 3A) We plotted a heatmap on the top altered 50 upregulated and 50

downregulated DEGs. (Figure 3B) Next, we performed gene ontology (GO) analyses on the upregulated and downregulated DEGs, respectively. The GO terms enriched with the upregulated DEGs included leukocyte-mediated immunity, lymphocyte-mediated immunity, positive regulation of leukocyte activation, immune response-regulating signaling

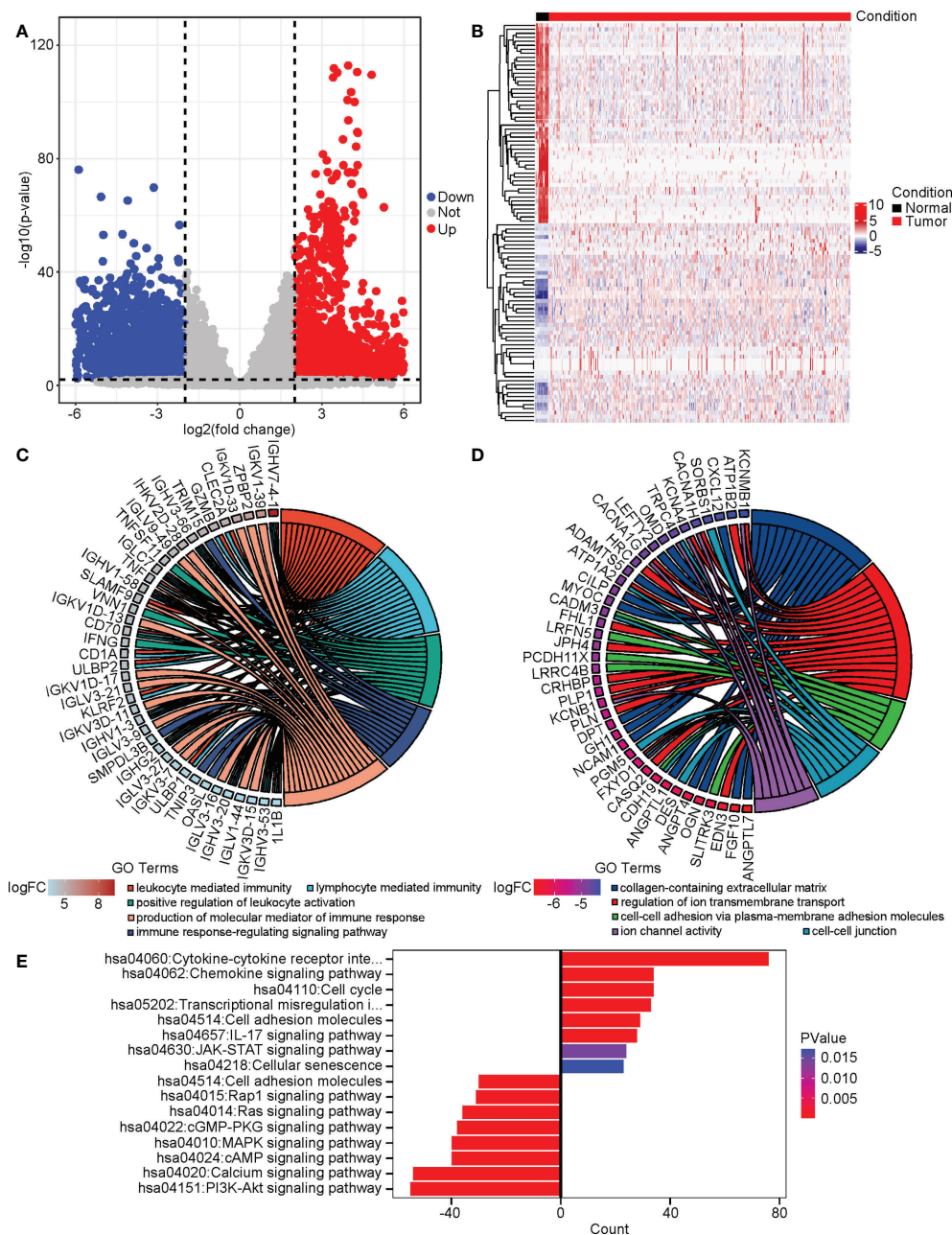


FIGURE 3
The altered DEGs, biological processes, and pathways in cervical cancer. We analyzed the DEGs between cervical cancer and normal tissues and then performed GO and KEGG analyses on these DEGs. (A) The volcano plot of DEGs. (B) The heatmap of the top 50 upregulated and downregulated DEGs. (C) The upregulated GO terms and their associated DEGs. (D) The downregulated GO terms and their associated DEGs. (E) The altered KEGG pathways.

pathway, and production of molecular mediator of the immune response. (Figure 3C) As to the downregulated DEGs, the GO terms included collagen-containing extracellular matrix, regulation of ion transmembrane transport, cell-cell adhesion via plasma-membrane adhesion molecules, cell-cell junction,

and ion channel activity. (Figure 3D) KEGG analysis suggested that the cytokine/chemokine-involved pathways, JAK-STAT signaling, and cell cycle were promoted, while cell adhesion, PI3K-AKT, calcium, cAMP, etc. related pathways were repressed. (Figure 3E)

Next, we performed a Protein-Protein Interaction network assay on the 231 DEGs in the WGCNA MEBrown module. (Figure 5A) We determined hub genes using 12 different algorithms, which were Betweenness, stress, ClusteringCoefficient, DMNC, BottleNeck, Closeness, Degree, EcCentricity, EPC, MCC, MNC, and Radiality. Collectively, there were 105 hub genes shared by all the 12 algorithms, which were focused on in subsequent studies. (Figure 5B)

We performed a univariate Cox analysis to test the association between the 105 hub genes and the OS of cervical cancer. As a result, 18 genes significantly affected the cervical cancer prognosis. (Figure 6A) To further refine the genes, we performed LASSO analysis on these 18 candidate genes and finally got 4 genes, which were IGSF6, TLR10, FCRL3, and IFI30. (Figures 6B, C)

The four CD8+ T cell-related genes were upregulated in cervical cancer and associated with prognosis

The four genes derived from the LASSO test (Figures 6B, C) were all upregulated in cervical cancer. (Figure 7A) They were closely and positively correlated with the CD8+ T cell infiltration. (Figure 7B) Except for TLR10, high expressions of these genes all predicted a better OS. (Figures 7C–F) To validate the immune infiltration pattern, the expressions of IGSF6, TLR10, FCRL3, and IFI30, and the correlation between them, we downloaded the GSE151666 dataset from the GEO database as a validation cohort, which included 68 cervical cancer patients. GTEx normal cervix uteri samples were used as a control. Consistently, the expressions of IGSF6, TLR10, FCRL3, and IFI30 were upregulated in cervical cancer in the validation cohort. (Figure 8A) By CIBERSORT analysis, naïve B cells, CD8+ T cells, regulatory T cells, activated dendritic cells, activated mast cells, and eosinophils were significantly upregulated, while M2 macrophages and resting mast cells were downregulated. (Figure 8B) The four factors also showed close and positive correlations with the CD8+ T cell infiltration. (Figure 8C) To validate the expressions of IGSF6, TLR10, FCRL3, and IFI30 in cervical cancer, we performed immunohistochemistry against these genes, respectively. In line with the results from the transcriptomics, we identified stronger expressions of IGSF6, TLR10, FCRL3, and IFI30 in cervical cancer tissues compared to normal tissues. (Figure 9)

The four CD8+ T cell-related genes could be a predictive factor for the prognosis of cervical cancer

As the expressions of IGSF6, TLR10, FCRL3, and IFI30 were all upregulated in cervical cancer and the higher expressions of IGSF6, FCRL3, and IFI30 predicted better prognosis, we asked if

the combination of these four genes was associated with the risks of cervical cancer. We first performed cox analysis on the TCGA-CESC cohort and equally divided the patients using the cutoff of -0.01 for the risk scores. (Figure 10A) Agreeing with this, the high-risk group included a relatively higher number of deaths, while the low-risk group displayed a relatively longer survival time. (Figure 10B) The expressions of all these four factors were remarkably lower in the high-risk group. (Figure 10C) To evaluate the predictive value in the prognosis of cervical cancer, we performed a ROC analysis with the expressions of these four factors in the TCGA-CESC cohort. The AUCs for 1, 3, 5, -year ROC curve were 0.757, 0.684, and 0.622, respectively. (Figure 10D)

Discussion

Cervical cancer is among the top threats to the health and lives of females. Immune cell infiltrations in the cancer microenvironment have been proven to be an important factor in both diagnosis and prognosis prediction. In this study, we found that the CD8+ T cell infiltration was significantly upregulated in cervical cancer versus normal cervix uteri samples. Through univariate and multivariate cox analyses, we confirmed that the CD8+ T cell infiltration was an independent beneficial factor for the prognosis of cervical cancer. Next, we performed WGCNA on the DEGs of cervical cancer and identified the hub genes using the Cytoscape software, which might be associated with the CD8+ T cell infiltration. Subsequently, we performed univariate cox and LASSO analyses on the hub genes and got four genes (IGSF6, TLR10, FCRL3, and IFI30) finally. The four genes could be applied to the prediction of the prognosis of cervical cancer, and the higher expression of the four genes suggested lower risks for cervical cancer patients.

Immune cell infiltrations in cancer serve as a crucial tumor microenvironment factor that mediates tumor metabolism, immunotherapy outcome, and cancer prognosis prediction (13–15). Although the infiltration of activated B cells, memory effector T cells, eosinophils, and plasmacytoid dendritic cells have been reported to be associated with a better prognosis of cervical cancer (16), the effect of CD8+ T cell infiltration in cervical cancer was previously uncertain. We here discovered that the CD8+ T cell infiltration was significantly upregulated in cervical cancer compared to normal cervix uteri tissues in both the TCGA-CESC and GSE151666 cohorts. With univariate and multivariate cox analyses, we found that the CD8+ T cell infiltration was an independent beneficial factor for the prognosis of cervical cancer. These results suggested that the CD8+ T cell infiltration was evoked upon the occurrence of cervical cancer and served a protective role aimed at eliminating such tumor cells, which agreed with its role in cellular immunity. We determined the CD8+ T cell infiltration in cervical cancer at

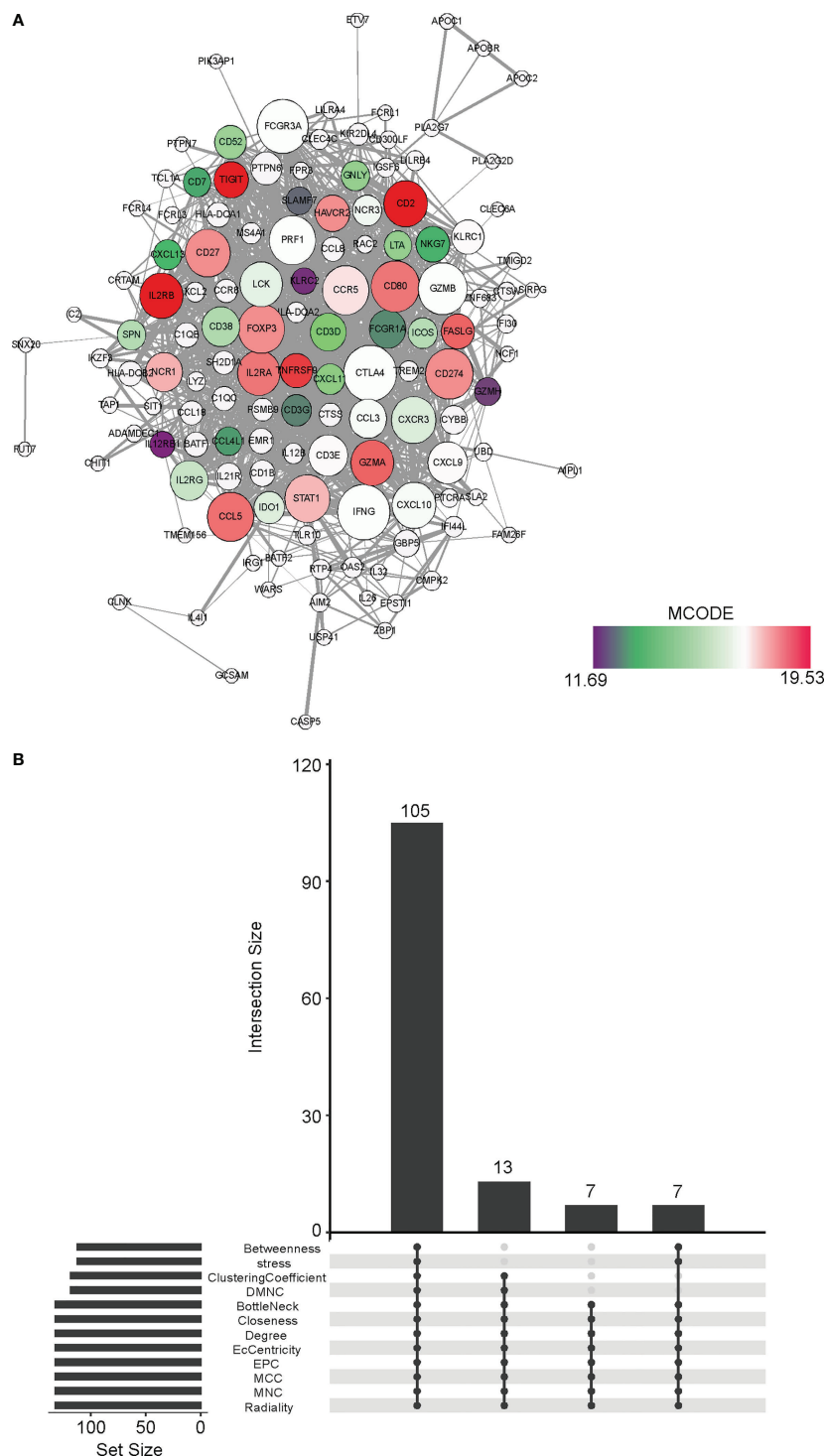


FIGURE 5 Identification of hub genes in the CD8+ T cell infiltration-related MEbrown module **(A)** The Protein-Protein Interaction of the DEGs belonging to the MEbrown module in WGCNA. The network was generated by the Cytoscape software. **(B)** The shared hubs genes determined by 12 different algorithms, which were Betweenness, stress, ClusteringCoefficient, DMNC, BottleNeck, Closeness, Degree, EcCentricity, EPC, MCC, MNC, and Radiality.

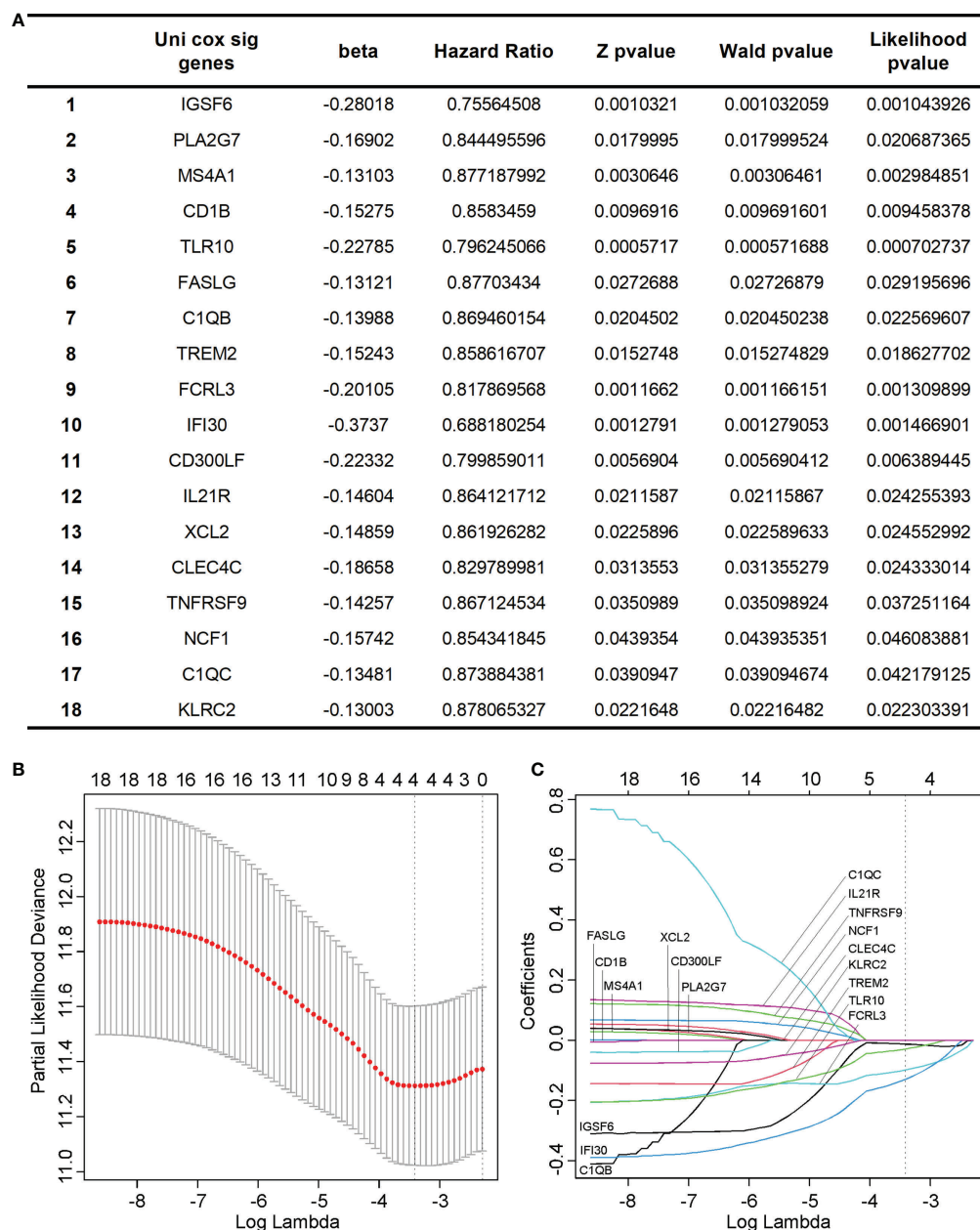


FIGURE 6

Identification of key hub genes significantly associated with the prognosis of cervical cancer. (A) We identified 18 hub genes that significantly affected the cervical cancer prognosis using univariate Cox analysis. (B, C) we performed LASSO analysis on the 18 candidate genes and finally got 4 genes, which were IGSF6, TLR10, FCRL3, and IFI30.

different histological stages. We found that the CD8+ T cell infiltration was truly upregulated at the early stages (I&II) of cervical cancer compared to normal tissues but significantly decreased at late stages (III&IV). It should be noted that although the CD8+ T cell infiltration level was elevated at early stages, these CD8+ T cells could not properly target tumor cells due to the immunosuppressive microenvironment within tumors. This also implied that the therapy against the

immunosuppressive microenvironment at the early stages of cervical cancer might achieve better outcomes. As to the level decrease of the CD8+ T cell infiltration at late stages, a possible reason was that the overall immune system in the body was debilitated.

We also analyzed the DEGs in cervical cancer versus normal cervix uteri tissues. As a result, we identified 2111 upregulated and 2160 downregulated DEGs. We performed GO analyses on

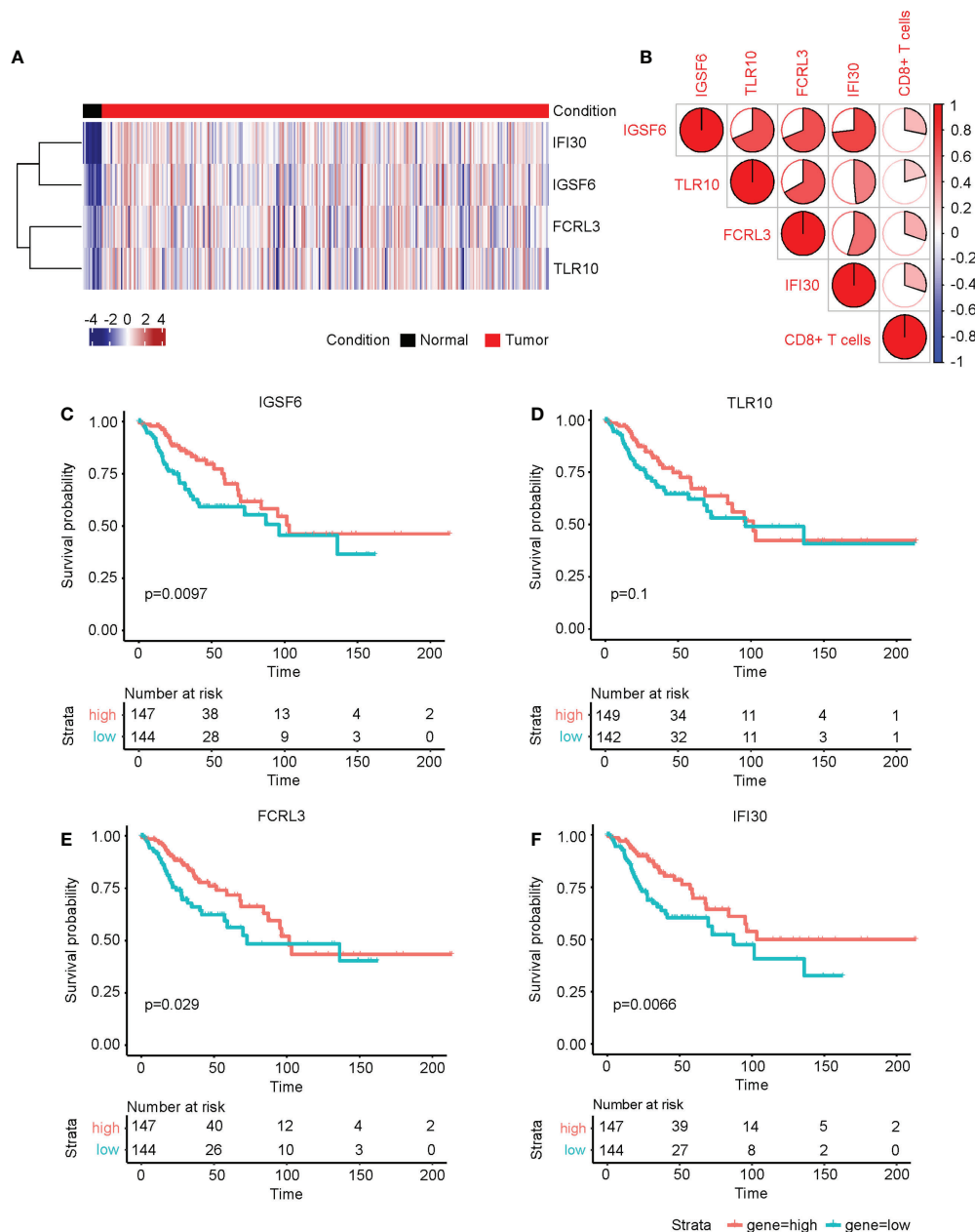


FIGURE 7

The four CD8+ T cell-related genes were upregulated in cervical cancer and associated with prognosis. (A) The heatmap of the relative levels of IGSF6, TLR10, FCRL3, and IFI30 in normal and cervical cancer tissues. (B) The correlations of IGSF6, TLR10, FCRL3, IFI30, and CD8+ T cell infiltration. The overall survival curves of (C) IGSF6, (D) TLR10, (E) FCRL3, and (F) IFI30 in cervical cancer.

the upregulated and downregulated DEGs, respectively. In line with the immune cell infiltration analysis, the processes, such as leukocyte-mediated immunity, lymphocyte-mediated immunity, positive regulation of leukocyte activation, immune response-regulating signaling pathway, and production of molecular mediator of the immune response, were enriched in the upregulated DEGs. Likewise, the cytokine/chemokine-involved pathways were enriched in the KEGG pathway analysis of the

upregulated DEGs. These results suggested that the upregulated DEGs in cervical cancer were involved in the regulation of immune cell infiltration, implying a necessity of revealing immune infiltration-related DEGs.

WGCNA is a powerful tool to locate candidate gene clusters (modules) that were related to external sample traits, for example, immune cell infiltrations here (22). We here adopted WGCNA to search for the genes that might be responsible for the CD8+ T cell

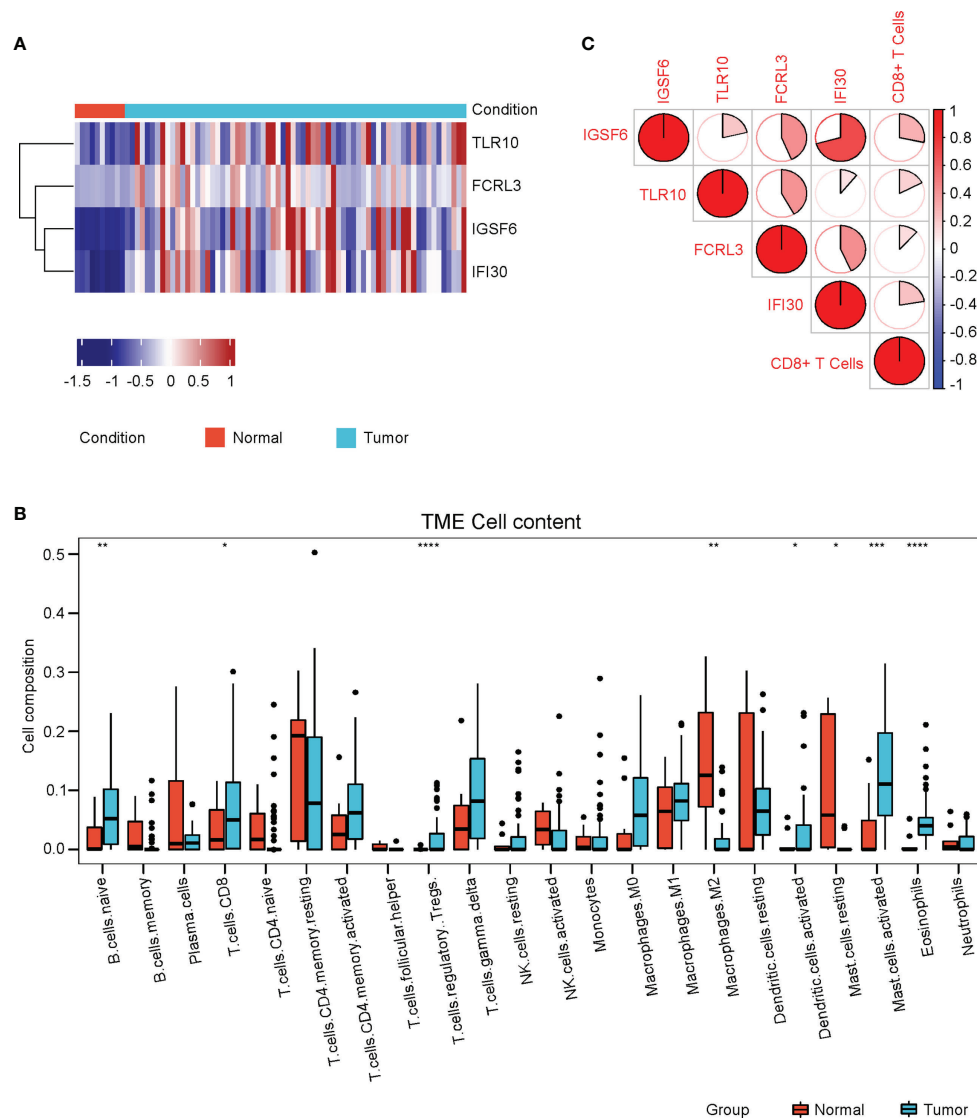


FIGURE 8

Validation of immune cell infiltrations and gene profile in the validation cohort. (A) The heatmap of the relative levels of IGSF6, TLR10, FCRL3, and IFI30 in normal and cervical cancer tissues in the validation cohort. (B) The relative levels of immune cell infiltrations in normal and cervical cancer groups in the validation cohort. (C) The correlations of IGSF6, TLR10, FCRL3, IFI30, and CD8+ T cell infiltration in the validation cohort.

* $P < 0.05$; ** $P < 0.01$; *** $P < 0.001$; **** $P < 0.0001$.

infiltration changes in cervical cancer. As a result, we found that the 231 genes belonging to the brown module showed the highest correlation with the CD8+ T cell infiltration. To further filter the genes, we performed a protein-protein interaction analysis using the Cytoscape. By exploring hub genes using 12 different algorithms, we got 105 candidate hub genes. We next tested if these candidate hub genes were associated with the prognosis of cervical cancer. By univariate Cox and LASSO analyses, we finally got 4 genes (IGSF6, TLR10, FCRL3, and IFI30) that were closely correlated with both the CD8+ T cell infiltration and the prognosis of cervical cancer. The identification of diagnostic and prognostic

biomarkers has brought significant advances to the clinical treatments of certain cancer types, for example, pancreatic ductal adenocarcinoma (PDAC). Currently discovered diagnostic biomarkers of PDAC include glycoproteins (23, 24), microRNAs (25), circulating tumor DNA, circulating tumor cells (26), and metabolomics (27). Some biomarkers have also been applied into guiding drug usage. For instance, the expression of human ENT1 was revealed as an important predictor for the responses to gemcitabine, a chemotherapy drug, in PDAC (28). Given more than 90% of PDAC patients retained KRAS mutations, people have made attempts to use KRAS mutations as the biomarkers for the

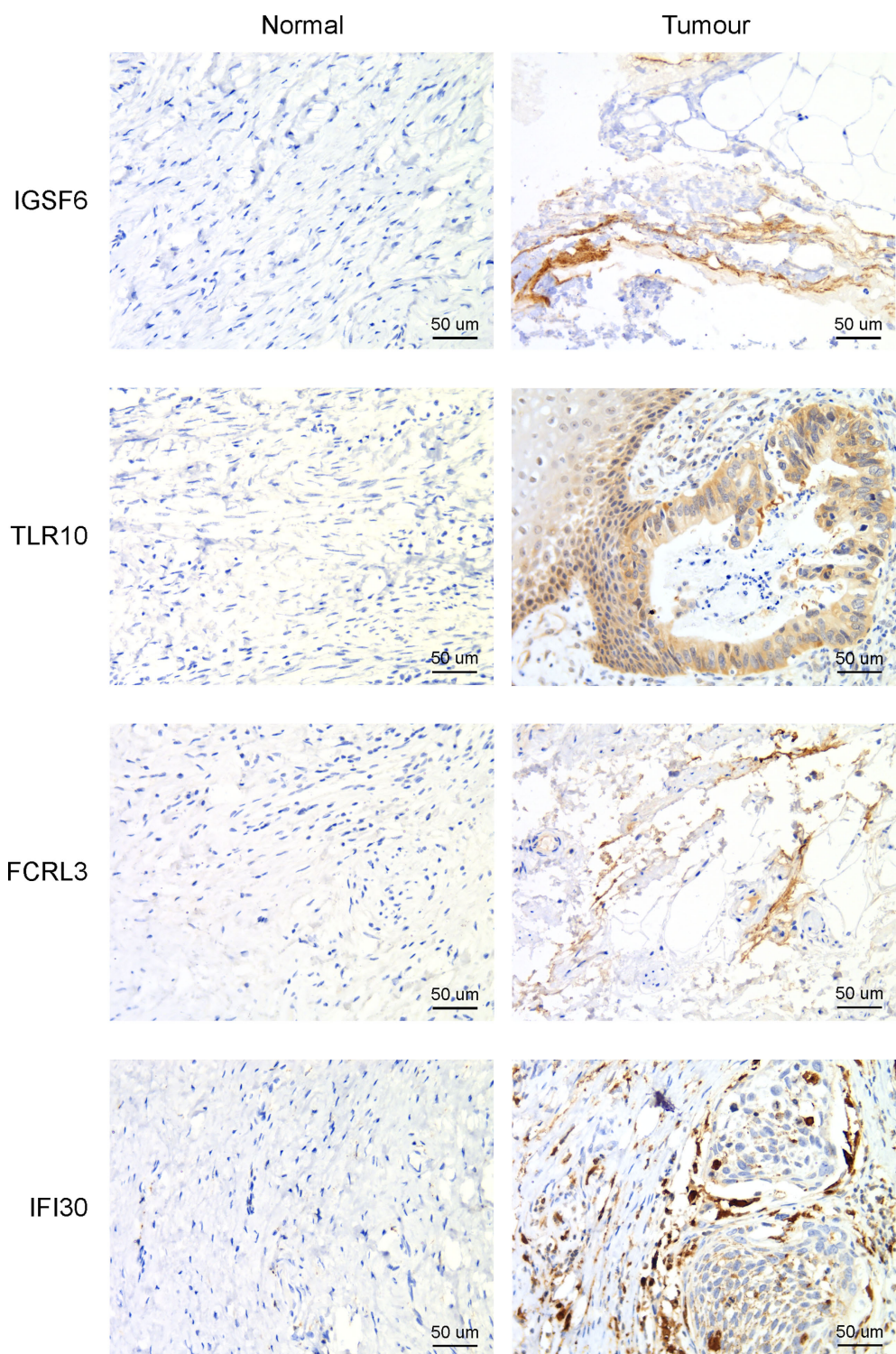


FIGURE 9
Immunohistochemistry to detect the four CD8+ T cell-related genes in cervical cancer and adjacent normal tissues.

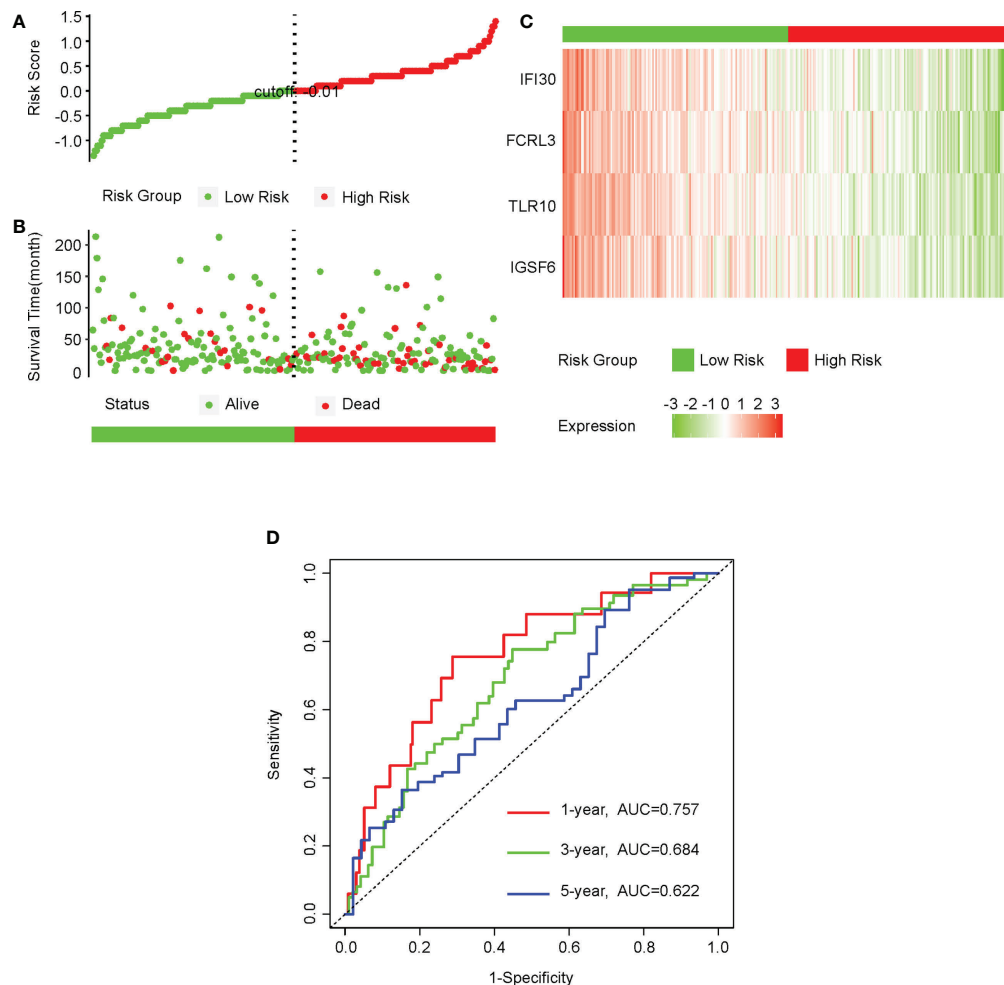


FIGURE 10

The four CD8+ T cell-related genes could be a predictive factor for the prognosis of cervical cancer. (A) We first performed a cox analysis on the CESC-TCGA cohort and equally divided the patients into low- and high-risk groups using the cutoff of -0.01 for the risk score. (B) The distributions of survival time of patients in the low- and high-risk groups. (C) The heatmap of the relative levels of IGSF6, TLR10, FCRL3, and IFI30 in the low- and high-risk groups. (D) The ROC curves showing the predictive value of the combinations of IGSF6, TLR10, FCRL3, and IFI30 in the prognosis of cervical cancer.

determination of using KRAS-target antibody drugs (29). Based on these facts, we thought that the discovery of the 4 novel genes (IGSF6, TLR10, FCRL3, and IFI30) in cervical cancer might shed light on the clinical treatments of cervical cancer as well.

IGSF6 was reported to be involved in the immune regulations of atherosclerosis (30) and inflammatory bowel disease (31). TLR10 is the only member of Toll-like receptors that exerts anti-inflammatory function. TLR10 could compete for the binding of stimulatory TLRs with other TLRs and activate PI3K/Akt pathway to express IL-1Ra (32). A recent study showed that TLR10 was upregulated, thus promoting immune infiltration in breast cancer, and played an important role in tumor development (33). FCRL3 was documented to be involved in many autoimmune diseases (34). FCRL3 was able to promote

IL-10 expression through the MAPK pathway in B cells (35). Meanwhile, FCRL3 contributed to the activation of B cells, while suppressing the differentiation of plasma cells (36). IFI30 has been known as a prognosis factor for many cancers, such as glioma (37, 38) and breast cancer (39). GILT, the protein encoded by IFI30, was shown to enhance the T cells mediated immune surveillance against tumor cells, implying its druggable potential in tumor therapy (40). Despite the known roles of the above four genes in regulating immune processes, the detailed mechanism of how the four genes manipulated the CD8+ T cell infiltration warrants further investigation. Apart from this, an intriguing notion is that the four genes (IGSF6, TLR10, FCRL3, and IFI30) were also upregulated in cervical cancer compared to normal tissues (Figures 7A, 8A), while their high expressions

predicted better prognosis (Figures 7C–F, 9A–C). The profiles of the four genes highly resemble the CD8+ T cell infiltration, which agreed with their correlation tests (Figures 7B, 8C). A possible explanation was that these genes were also evoked upon tumorigenesis and cooperated with CD8+ T cell infiltration, aiming at eliminating the tumor cells within the body. Under the circumstance in which the expressions of these four genes were relatively lower, the prognosis would be worse. The combination of the four genes could serve as the prediction tool for the prognosis of cervical cancer.

Data availability statement

Publicly available datasets were analyzed in this study. This data can be found here: GEO (GSE151666) and The Cancer Genome Atlas (TCGA).

Ethics statement

The studies involving human participants were reviewed and approved by the Ethics Committee of Anhui Normal University. The patients/participants provided their written informed consent to participate in this study.

Author contributions

Conceptualization, XS, CW, and ML; Methodology, XS, CW, and ML; Software, XS and CW; Investigation, XS, CW, ML, SW, YZ, ZL, and GZ; Writing – original draft, XS; Writing – review and editing, XS; Visualization, XS, CW, and SW; Supervision, XS; Project administration, XS; Funding acquisition, XS. All authors contributed to the article and approved the submitted version.

Funding

This work was supported by the National Natural Science Foundation of China (No. 31701289), Anhui Provincial Natural Science Foundation (No. 2208085MH209, 1808085QH234),

Anhui Provincial Funding Scheme to Outstanding Innovative Programs by Returned Scholars (No. 2019LCX003), Anhui Provincial Key Laboratory of Molecular Enzymology and Mechanism of Major Diseases (No. fzm202001), Educational Commission of Anhui Province of China (No. KJ2017A319, KJ2019A0498, KJ2020A0058, KJ2020A0087), Key Projects for Young and Middle-Aged People from Wannan Medical College (No. WK2021ZF08), and the Foundation for High-level Talents in Higher Education of Anhui Province of China and Funds from the Anhui Normal University (No. 2017XJJ38, start-up funds to XS).

Acknowledgments

We thank the platforms and resources provided by Anhui Provincial Key Laboratory of Molecular Enzymology and Mechanism of Major Diseases, Anhui Provincial Engineering Research Centre for Molecular Detection and Diagnostics, Anhui Provincial Key Laboratory of the Conservation and Exploitation of Biological Resources, and Key Laboratory of Biomedicine in Gene Diseases and Health of Anhui Higher Education Institutes.

Conflict of interest

The authors declare that the research was conducted in the absence of any commercial or financial relationships that could be construed as a potential conflict of interest.

Publisher's note

All claims expressed in this article are solely those of the authors and do not necessarily represent those of their affiliated organizations, or those of the publisher, the editors and the reviewers. Any product that may be evaluated in this article, or claim that may be made by its manufacturer, is not guaranteed or endorsed by the publisher.

References

1. Torre LA, Islami F, Siegel RL, Ward EM, Jemal A. Global cancer in women: Burden and trends. *Cancer Epidemiol Biomarkers Prev* (2017) 26(4):444–57. doi: 10.1158/1055-9965.EPI-16-0858
2. Sung H, Ferlay J, Siegel RL, Laversanne M, Soerjomataram I, Jemal A, et al. Global cancer statistics 2020: GLOBOCAN estimates of incidence and mortality worldwide for 36 cancers in 185 countries. *CA Cancer J Clin* (2021) 71(3):209–49. doi: 10.3322/caac.21660
3. Bosch FX, Manos MM, Munoz N, Sherman M, Jansen AM, Peto J, et al. Prevalence of human papillomavirus in cervical cancer: a worldwide perspective. *Int Biol study cervical Cancer (IBSCC) Study Group J Natl Cancer Inst* (1995) 87(11):796–802. doi: 10.1093/jnci/87.11.796
4. Crosbie EJ, Einstein MH, Franceschi S, Kitchener HC. Human papillomavirus and cervical cancer. *Lancet* (2013) 382(9895):889–99. doi: 10.1016/S0140-6736(13)60022-7
5. Ferlay J, Soerjomataram I, Dikshit R, Eser S, Mathers C, Rebelo M, et al. Cancer incidence and mortality worldwide: sources, methods and major patterns in GLOBOCAN 2012. *Int J Cancer* (2015) 136(5):E359–86. doi: 10.1002/ijc.29210
6. Baalbergen A, Veenstra Y, Stalpers L. Primary surgery versus primary radiotherapy with or without chemotherapy for early adenocarcinoma of the uterine cervix. *Cochrane Database Syst Rev* (2013) 1:CD006248. doi: 10.1002/14651858.CD006248.pub3

7. Chemoradiotherapy for Cervical Cancer Meta-analysis C. Reducing uncertainties about the effects of chemoradiotherapy for cervical cancer: Individual patient data meta-analysis. *Cochrane Database Syst Rev* (2010) 1: CD008285. doi: 10.1002/14651858.CD008285
8. Mauricio D, Zeybek B, Tymon-Rosario J, Harold J, Santin AD. Immunotherapy in cervical cancer. *Curr Oncol Rep* (2021) 23(6):61. doi: 10.1007/s11912-021-01052-8
9. Tewari KS, Sill MW, Long HJ3rd, Penson RT, Huang H, Ramondetta LM, et al. Improved survival with bevacizumab in advanced cervical cancer. *N Engl J Med* (2014) 370(8):734–43. doi: 10.1056/NEJMoa1309748
10. Zhang Y, Li X, Zhang J, Mao L. Novel cellular immunotherapy using NKG2D CAR-T for the treatment of cervical cancer. *BioMed Pharmacother* (2020) 131:110562. doi: 10.1016/j.biopha.2020.110562
11. Zheng J, Huang J, Ma W, Yang W, Hu B. The antitumor activity of CAR-T-PD1 cells enhanced by HPV16mE7-pulsed and SOCS1-silenced DCs in cervical cancer models. *Cancer Manag Res* (2021) 13:6045–53. doi: 10.2147/CMAR.S321402
12. He Y, Li XM, Yin CH, Wu YM. Killing cervical cancer cells by specific chimeric antigen receptor-modified T cells. *J Reprod Immunol* (2020) 139:103115. doi: 10.1016/j.jri.2020.103115
13. Zhou R, Zhang J, Zeng D, Sun H, Rong X, Shi M, et al. Immune cell infiltration as a biomarker for the diagnosis and prognosis of stage I–III colon cancer. *Cancer Immunol Immunother* (2019) 68(3):433–42. doi: 10.1007/s00262-018-2289-7
14. Xu Y, Lan S, Zheng Q. Prognostic significance of infiltrating immune cell subtypes in invasive ductal carcinoma of the breast. *Tumori* (2018) 104(3):196–201. doi: 10.5301/tj.5000624
15. Bense RD, Sotiriou C, Piccart-Gebhart MJ, Haanen J, van Vugt M, de Vries EGE, et al. Relevance of tumor-infiltrating immune cell composition and functionality for disease outcome in breast cancer. *J Natl Cancer Inst* (2017) 109(1):djw192. doi: 10.1093/jnci/djw192
16. Yu S, Li X, Zhang J, Wu S. Development of a novel immune infiltration-based gene signature to predict prognosis and immunotherapy response of patients with cervical cancer. *Front Immunol* (2021) 12:709493. doi: 10.3389/fimmu.2021.709493
17. Zhang Y, Yu M, Jing Y, Cheng J, Zhang C, Cheng L, et al. Baseline immunity and impact of chemotherapy on immune microenvironment in cervical cancer. *Br J Cancer* (2021) 124(2):414–24. doi: 10.1038/s41416-020-01123-w
18. Cheng X, Wang X, Nie K, Cheng L, Zhang Z, Hu Y, et al. Systematic pan-cancer analysis identifies TREM2 as an immunological and prognostic biomarker. *Front Immunol* (2021) 12:646523. doi: 10.3389/fimmu.2021.646523
19. Chen F, Fan Y, Cao P, Liu B, Hou J, Zhang B, et al. Pan-cancer analysis of the prognostic and immunological role of HSF1: A potential target for survival and immunotherapy. *Oxid Med Cell Longev* (2021) 2021:5551036. doi: 10.1155/2021/5551036
20. Xu F, Shen J, Xu S. Integrated bioinformatical analysis identifies GIMAP4 as an immune-related prognostic biomarker associated with remodeling in cervical cancer tumor microenvironment. *Front Cell Dev Biol* (2021) 9:637400. doi: 10.3389/fcell.2021.637400
21. Newman AM, Liu CL, Green MR, Gentles AJ, Feng W, Xu Y, et al. Robust enumeration of cell subsets from tissue expression profiles. *Nat Methods* (2015) 12(5):453–7. doi: 10.1038/nmeth.3337
22. Langfelder P, Horvath S. WGCNA: an R package for weighted correlation network analysis. *BMC Bioinf* (2008) 9:559. doi: 10.1186/1471-2105-9-559
23. Goonetilleke KS, Siriwardena AK. Systematic review of carbohydrate antigen (CA 19-9) as a biochemical marker in the diagnosis of pancreatic cancer. *Eur J Surg Oncol* (2007) 33(3):266–70. doi: 10.1016/j.ejso.2006.10.004
24. Nazli O, Bozdog AD, Tansug T, Kir R, Kaymak E. The diagnostic importance of CEA and CA 19-9 for the early diagnosis of pancreatic carcinoma. *Hepatogastroenterology* (2000) 47(36):1750–2.
25. Yonemori K, Kurahara H, Maemura K, Natsugoe S. MicroRNA in pancreatic cancer. *J Hum Genet* (2017) 62(1):33–40. doi: 10.1038/jhg.2016.59
26. Riva F, Dronov OI, Khomenko DI, Huguet F, Louvet C, Mariani P, et al. Clinical applications of circulating tumor DNA and circulating tumor cells in pancreatic cancer. *Mol Oncol* (2016) 10(3):481–93. doi: 10.1016/j.molonc.2016.01.006
27. Mayerle J, Kalthoff H, Reszka R, Kamlage B, Peter E, Schniewind B, et al. Metabolic biomarker signature to differentiate pancreatic ductal adenocarcinoma from chronic pancreatitis. *Gut* (2018) 67(1):128–37. doi: 10.1136/gutjnl-2016-312432
28. Farrell JJ, Elsaleh H, Garcia M, Lai R, Ammar A, Regine WF, et al. Human equilibrative nucleoside transporter 1 levels predict response to gemcitabine in patients with pancreatic cancer. *Gastroenterology* (2009) 136(1):187–95. doi: 10.1053/j.gastro.2008.09.067
29. Hong DS, Fakih MG, Strickler JH, Desai J, Durm GA, Shapiro GI, et al. KRAS(G12C) inhibition with sotorasib in advanced solid tumors. *N Engl J Med* (2020) 383(13):1207–17. doi: 10.1056/NEJMoa1917239
30. Shen Y, Xu LR, Tang X, Lin CP, Yan D, Xue S, et al. Identification of potential therapeutic targets for atherosclerosis by analysing the gene signature related to different immune cells and immune regulators in atheromatous plaques. *BMC Med Genomics* (2021) 14(1):145. doi: 10.1186/s12920-021-00991-2
31. Bates EE, Kissenpfennig A, Peronne C, Mattei MG, Fossiez F, Malissen B, et al. The mouse and human IGSF6 (DORA) genes map to the inflammatory bowel disease 1 locus and are embedded in an intron of a gene of unknown function. *Immunogenetics* (2000) 52(1–2):112–20. doi: 10.1007/s002510000259
32. Fore F, Budipranama M, Destiawan RA. TLR10 and its role in immunity. *Handb Exp Pharmacol* (2022) 276:161–74. doi: 10.1007/164_2021_541
33. Shi S, Xu C, Fang X, Zhang Y, Li H, Wen W, et al. Expression profile of tolllike receptors in human breast cancer. *Mol Med Rep* (2020) 21(2):786–94. doi: 10.3892/mmr.2019.10853
34. Yang Y, Su X, Zhang K, Zhou R. The fc receptor-like 3 gene polymorphisms and susceptibility to autoimmune diseases: an updated meta-analysis. *Autoimmunity* (2013) 46(8):547–58. doi: 10.3109/08916934.2013.835804
35. Cui X, Liu CM, Liu QB. FCRL3 promotes IL-10 expression in b cells through the SHP-1 and p38 MAPK signaling pathways. *Cell Biol Int* (2020) 44(9):1811–9. doi: 10.1002/cbin.11373
36. Li FJ, Schreeder DM, Li R, Wu J, Davis RS. FCRL3 promotes TLR9-induced b-cell activation and suppresses plasma cell differentiation. *Eur J Immunol* (2013) 43(11):2980–92. doi: 10.1002/eji.201243068
37. Jiang W, Zheng F, Yao T, Gong F, Zheng W, Yao N. IFI30 as a prognostic biomarker and correlation with immune infiltrates in glioma. *Ann Transl Med* (2021) 9(22):1686. doi: 10.21037/atm-21-5569
38. Liu X, Song C, Yang S, Ji Q, Chen F, Li W. IFI30 expression is an independent unfavourable prognostic factor in glioma. *J Cell Mol Med* (2020) 24(21):12433–43. doi: 10.1111/jcmm.15758
39. Fan Y, Wang X, Li Y. IFI30 expression predicts patient prognosis in breast cancer and dictates breast cancer cells proliferation via regulating autophagy. *Int J Med Sci* (2021) 18(14):3342–52. doi: 10.7150/ijms.62870
40. Li H, Wang Y, Ma M, Hu L, Zhang X, Xin L, et al. GILT in tumor cells improves T cell-mediated anti-tumor immune surveillance. *Immunol Lett* (2021) 234:1–12. doi: 10.1016/j.imlet.2021.04.001



OPEN ACCESS

EDITED BY
Jinhui Liu,
Nanjing Medical University, China

REVIEWED BY
Yongsheng Yu,
Shanghai University, China
Shangxiang Chen,
Sun Yat-sen University, China

*CORRESPONDENCE
Le Zhang
zhanglelssh@163.com
Hang Zhou
zhouhang@zmu.edu.cn
Feng Jiang
dxyjiang@163.com

[†]These authors have contributed
equally to this work

SPECIALTY SECTION
This article was submitted to
Gynecological Oncology,
a section of the journal
Frontiers in Oncology

RECEIVED 28 August 2022
ACCEPTED 24 October 2022
PUBLISHED 09 November 2022

CITATION
Guo C, He Y, Chen L, Li Y, Wang Y,
Bao Y, Zeng N, Jiang F, Zhou H and
Zhang L (2022) Integrated
bioinformatics analysis and
experimental validation reveals fatty
acid metabolism-related prognostic
signature and immune responses for
uterine corpus endometrial carcinoma.
Front. Oncol. 12:1030246.
doi: 10.3389/fonc.2022.1030246

COPYRIGHT
© 2022 Guo, He, Chen, Li, Wang, Bao,
Zeng, Jiang, Zhou and Zhang. This is an
open-access article distributed under
the terms of the [Creative Commons
Attribution License \(CC BY\)](https://creativecommons.org/licenses/by/4.0/). The use,
distribution or reproduction in other
forums is permitted, provided the
original author(s) and the copyright
owner(s) are credited and that the
original publication in this journal is
cited, in accordance with accepted
academic practice. No use,
distribution or reproduction is
permitted which does not comply with
these terms.

Integrated bioinformatics analysis and experimental validation reveals fatty acid metabolism-related prognostic signature and immune responses for uterine corpus endometrial carcinoma

Chenrui Guo^{1†}, Yan He^{2†}, Leiming Chen^{3†}, Yuan Li^{4†},
Yajun Wang¹, Yunlei Bao⁵, Ni Zeng⁶, Feng Jiang^{5*},
Hang Zhou^{1*} and Le Zhang^{7*}

¹Department of Abdominal Oncology, The Second Affiliated Hospital of Zunyi Medical University, Zunyi, China, ²Department of Gynecology, Shidong Hospital, Shidong Hospital Affiliated to University of Shanghai For Science and Technology, Shanghai, China, ³Department of Laboratory Medicine, Obstetrics and Gynecology Hospital of Fudan University, Shanghai, China, ⁴Department of Dermatology, The Fifth People's Hospital of Hainan Province, Haikou, China, ⁵Department of Neonatology, Obstetrics and Gynecology Hospital of Fudan University, Shanghai, China, ⁶Department of Dermatology, Affiliated Hospital of Zunyi Medical University, Zunyi, China, ⁷Department of Anesthesiology, Obstetrics and Gynecology Hospital of Fudan University, Shanghai, China

Background: Uterine corpus endometrial carcinoma (UCEC) is the third most common gynecologic malignancy. Fatty acid metabolism (FAM) is an essential metabolic process in the immune microenvironment that occurs reprogramming in the presence of tumor signaling and nutrient competition. This study aimed to identify the fatty acid metabolism-related genes (FAMGs) to develop a risk signature for predicting UCEC.

Methods: The differentially expressed FAMGs between UCEC samples and controls from TCGA database were discovered. A prognostic signature was then constructed by univariate, least absolute shrinkage and selection operator (LASSO) and multivariate Cox regression analyses. Based on the median risk score, UCEC samples were categorized into high- and low-FAMGs groups. Kaplan-Meier (K-M) curve was applied to determine patients' overall survival (OS). The independent prognostic value was assessed by uni- and multivariate analyses. The associations between the risk score and immune status, immune score, and drug resistance were evaluated. Quantitative Real-time PCR (qRT-PCR) was utilized to confirm FAMGs expression levels in UCEC cells.

Results: We built a 10-FAMGs prognostic signature and examined the gene mutation and copy number variations (CNV). Patients with a high-FAMGs had a worse prognosis compared to low-FAMGs patients in TCGA train and test sets.

We demonstrated that FAMGs-based risk signature was a significant independent prognostic predictor of UCEC. A nomogram was also created incorporating this risk model and clinicopathological features, with high prognostic performance for UCEC. The immune status of each group was varied, and immune score was higher in a low-FAMGs group. HLA-related genes such as DRB1, DMA, DMB, and DQB2 had higher expression levels in the low-FAMGs group. Meanwhile, high-FAMGs patients were likely to response more strongly to the targeted drugs Bortezomib, Foretinib and Gefitinib. The qRT-PCR evidence further verified the significant expression of FAMGs in this signature.

Conclusions: A FAMGs-based risk signature might be considered as an independent prognostic indicator to predict UCEC prognosis, evaluate immune status and provide a new direction for therapeutic strategies.

KEYWORDS

uterine corpus endometrial carcinoma, fatty acid metabolism, risk signature, immune status, prognosis

Introduction

Uterine corpus endometrial carcinoma (UCEC), a frequent gynecological malignant tumor, has been rapidly increasing in recent years. According to the 2022 cancer statistics, there were an estimated 65,950 cases and 12,550 deaths from uterine corpus cancer in United State (1). In China, it is estimated that the number of new cases was 84,520, and deaths were 17,543 of UCEC in young women (2). It, therefore, remains a major public health issue around the world. Despite surgery, chemotherapy, radiotherapy and brachytherapy currently employed to UCEC intervention, there are still considerable numbers of women with more aggressive lesions whose prognosis is dismal (3). A reliable prognosis assessment is the foundation of effective therapy. However, the present predictive system based on clinical, pathological, imaging, and biological features are insufficient to interpret the progressive and prognostic heterogeneity of UCEC (4). Consequently, exploring effective biomarkers to identify individuals with a high risk of recurrence is helpful for precise therapy.

Tumor growth is deeply reliant on the tumor microenvironment (TME), which is characterized by hypoxia, acidity, and nutrition deprivation because tumor cell proliferation is faster than angiogenesis (5). Consequently, tumor cells displayed distinctive metabolic properties from normal cells to handle a variety of adverse situations *via* a metabolic reprogramming process that supports their growth and survival once the carcinogenic signal is blocked (6). lipid metabolism is one of three primary energy metabolisms of cells, of which fatty acid metabolism (FAM) is a critical metabolic pathway and plays an important role in cancer pathophysiology (7). Specifically, the fatty acid in particular aids cancer cells in not only

maintaining membrane biosynthesis but also supplying a major energy source during metabolic pressure. The FAM pattern tends to be different among various cells and tissues. Previous studies have shown that certain expression patterns of fatty acid metabolism-related genes (FAMGs) were connected with proliferation, prognosis, and immunity of glioma, colorectal cancer, or breast cancer (8–11). However, the pattern of FAMGs in UCEC has not been explored.

As bioinformatic technology develops, numerous approaches have been employed to define meaningful biomarkers (12, 13). In this study, the potential value of FAM in UCEC samples obtained from TCGA database was evaluated by using bioinformatics. We analyzed the differential expression of FAMGs, and selected genes strongly correlated with UCEC prognosis to develop a FAMGs-based risk signature. A scoring system was created to evaluate the probability of survival, as well as immune status and drug sensitivity of UCEC. This risk model offered a novel insight on UCEC prognosis and therapeutic options.

Materials and methods

Data sources

A total of 539 UCEC and 35 normal endometrial cases were retrieved from TCGA database (<https://portal.gdc.cancer.gov/>). Patients were allocated to TCGA training or test cohort in a 1:1 ratio at random. FAM gene sets, including *KEGG FAM pathways*, *Hallmark FAM genes*, and *Reactome FAM genes*, were acquired from the MSigDB v7.4. A total of 309 FAMGs

were finally ascertained after removing the overlapping genes (14).

Construction and verification of a prognostic signature

The DEGs linked to FAM between UCEC, and normal tissues were screened by R “limma” package (15), with $|\log FC| > 0$ and FDR-adjusted $P < 0.05$. Upon these FAM-DEGs, the overall survival (OS) related genes with $P < 0.05$ were selected by using a univariate cox analysis. Then, candidate FAMGs were confirmed by using the least absolute shrinkage and selection operator (LASSO) and multivariate cox regression analysis via R “glmnet” packages (16).

The risk score is computed by using this formula: $\text{risk score} = \sum_{i=1}^n (\text{coef}_i \times \text{Gene}_i)$, where Gene_i denotes the expression level of gene i and coef_i denote the regression coefficient of gene i . Based on median risk score, UCEC patients were divided into a low- or high-FAMGs group in TCGA training or test set. The log-rank test was utilized to compare the difference in survival status between two groups via R “rms” package. Kaplan-Meier (K-M) analysis of OS or PFS was performed via R “survival” package. To reflect the predictive power of risk model, we plotted the time-dependent receiver operating characteristic (ROC) curve and area under the curve (AUC) for 1-year, 3-year, and 5-year OS via R “timeROC” package (17).

Gene Ontology (GO) (18) and Kyoto Encyclopedia of Genes and Genomes (KEGG) (19) functional enrichment analysis of FAMGs in UCEC were conducted by R “ClusterProfiler” package, where $P < 0.05$ indicates a statistical difference.

Establishment of a FAMGs-related nomogram

To verify the independence of the FAMGs-based risk signature, we ran uni- and multivariate cox analyses on risk score and other clinical factors. Then, using the above variables, we established a FAMGs-related clinicopathologic nomogram via R “rms”, “nomogramEx”, and “regplot” packages (20). Then, ROC and calibration curves were utilized to examine the accuracy and discrimination of the nomogram.

Assessment of immune status and drug sensitivity

The association between tumor immune microenvironment (TIME) and this prognostic signature was further assessed. The single-sample gene-set enrichment analysis (ssGSEA) was utilized

to quantify the immune activity in high- and low-FAMGs groups. Tumor Immune Dysfunction and Exclusion (TIDE) algorithm was conducted to evaluate the tumor immune escape in two groups based on FAMGs. ESTIMATE algorithm was used to determine the TME score via R software. The expressions of HLA-genes between high- and low-FAMGs group were further compared. To investigate differences in therapeutic effects of small-molecule drugs between two groups, we calculated the half-maximal inhibitory concentration (IC50) values of drugs commonly for UCEC treatment via R “pRRophetic” package [21 from].

Cell culture and qRT-PCR

Human endometriosis cell line hEM15A and UCEC cell AN3A were cultured in DMEM with 10% FBS in a 5% CO₂ incubator at 37°C. Total RNA was extracted by utilizing Trizol reagent (Invitrogen, USA), then cDNAs were generated with a HiScript Synthesis kit (Vazyme, China). Quantitative real-time PCR (qRT-PCR) was completed by utilizing the Fast SYBR Green Master Mix (Roche, USA) on a StepOnePlus Real-Time PCR system (Applied Biosystems, USA). Primer sequences in our work are described in Table S1.

Results

Landscape of FAMGs expression in UCEC

There are 554 UCEC and 35 normal samples retrieved from TCGA dataset. Differentially expressed FAMGs between tumor and normal were presented in a heat map (Figure 1A). The volcanic diagram displayed 100 up-regulated FAMGs and 106 down-regulated FAMGs (Figure 1B). Principal component analysis (PCA) was applied to evaluate sample heterogeneity, and the results showed a significant difference (Figure 1C). We also included more normal samples from GTEx database (n=78) to verify this difference (Figure S1). 131 up-regulated FAMGs and 103 down-regulated FAMGs were found. Most of the different FAMGs overlapped. These suggested that FAMGs might have a potential ability to differentiate normal patients from UCEC.

Identification of prognostic FAMGs and genomic variance analysis

Firstly, 206 differentially expressed FAMGs were subjected to univariate Cox analysis, and 28 prognosis-related genes were identified with a $P < 0.05$ (Figure 2A). Next, LASSO and multiple Cox analyses were utilized to shrink the range of FAMGs. At last, 10 FAMGs including upregulated PECR, OLAH, ACOT11, ACAT2,

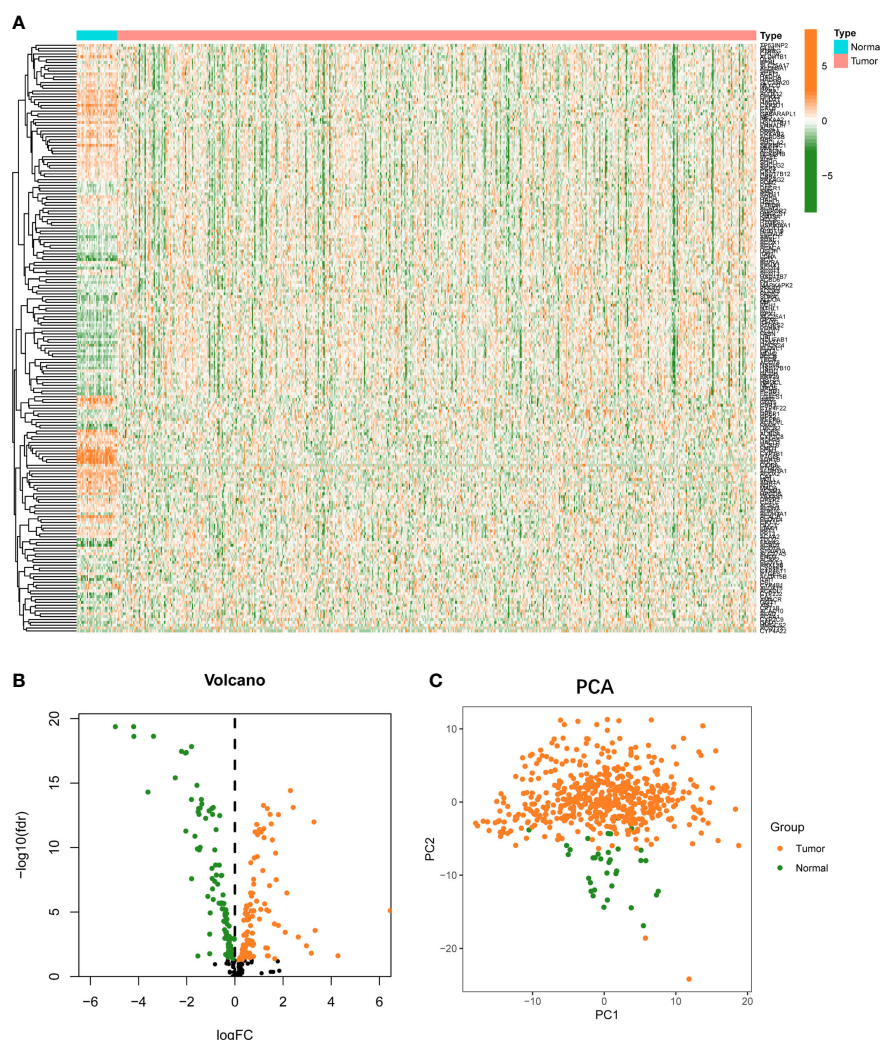


FIGURE 1

Landscape of FAMGs expressions in UCEC and normal endometrial tissues. (A) Heatmap for 309 FAMGs in TCGA cohort. (B) Volcano plot for different expressions of FAMGs. (C) PCA analysis for FAMGs to distinguish tumors ($n = 554$) from normal samples ($n = 35$). FAMGs fatty acid metabolism-related genes. UCEC: Uterine corpus endometrial carcinoma. PCA: principal component analysis.

NUDT19, PTGIS, and downregulated GPX1, ADH5, PTGR1, ACADS were identified for prognostic risk model (Figures 2B, C).

The incidence of somatic mutation of FAMGs in UCEC patients was calculated from TCGA cohort. There are 64/518 (12.36%) UCEC patients who experienced mutations of these 10 FAMGs, with a frequency from 0 to 3% (Figure 2D). Among them, ACOT11, ACADS, PECR, PTGR1, PTGIS, OLAH had 3% mutation frequency, followed by ACAT2, ADH5, NUDT19, while GPX1 did not have any mutations. Next, we investigated the CNV of FAMGs and found its prevalence in these 10 FAMGs. The location of CNV changes of the FAMGs on each of their respective chromosomes was shown in Figure 2E. Among them, NUDT19, PTGIS, ACOT11, OLAH, PTGR1,

and ADH5 exhibited widespread CNV gain, while GPX1, ACADS ACAT2, and PECR had CNV loss (Figure 2F).

Construction and validation of FAMGs-based risk signature

Based on FAMGs median risk score, UCEC patients were categorized into high- and low-FAMGs groups in TCGA training cohort, test cohort and total cohort (Figures 3A). The proportion of alive patients in high-FAMGs group was less than that of low-FAMGs patients among these datasets (Figure 3B). The distribution of these 10 FAMGs expression levels UCEC

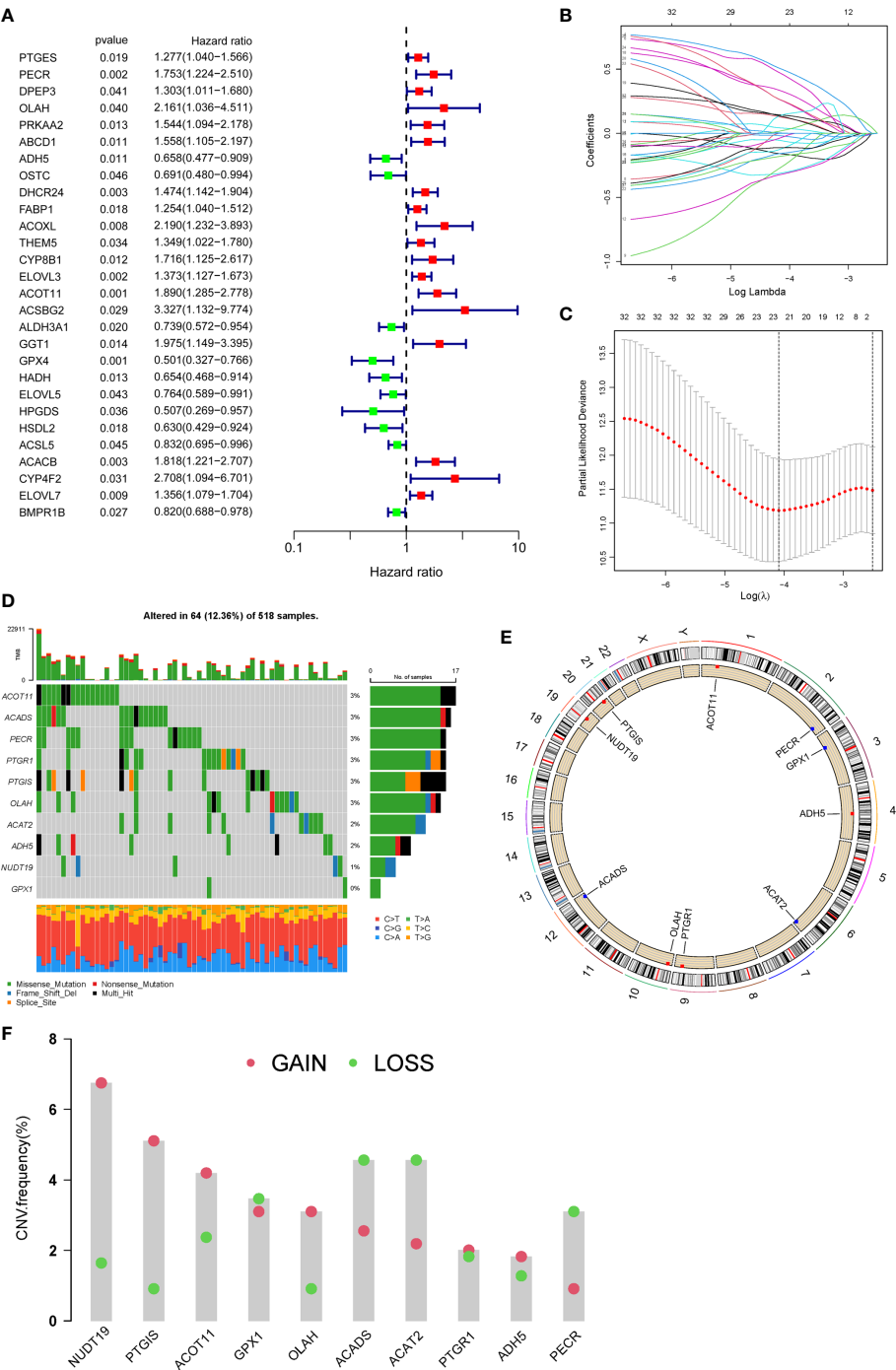


FIGURE 2 Identification of prognostic FAMGs and their characteristic analysis. **(A)** Forrest plot of 28 FAMGs related with prognosis by univariate regression analysis. **(B)** LASSO regression analysis. **(C)** Partial likelihood deviance for LASSO regression. **(D)** Profiles of genetic mutation in UCEC patients. **(E)** CNV alteration of FAMGs on chromosomes. **(F)** Frequencies of CNV gain, loss, and non-CNV among FAMGs. FAMGs: fatty acid metabolism-related genes. LASSO: least absolute shrinkage and selection operator. UCEC: Uterine corpus endometrial carcinoma. CNV: copy number variation. .

patients was shown in a heatmap (Figure 3C). K-M curve revealed that low-FAMGs patients' OS was considerably longer than high-FAMGs patients among these cohorts (Figure 3D), as did their PFS time (Figure S2).

Functional annotation

Further, we identified 835 differentially expressed genes between high- and low-FAMGs groups. To examine the possible biological properties in UCEC, we conducted a functional enrichment analysis of these genes. GO analysis showed that signaling receptor activator activity, tubulin binding, tubulin binding and fatty acid synthase activity were significantly enriched in biological processes (Figure S3A).

KEGG revealed the enrichment in microtubule-based movement, cilium assembly, cilium movement and pattern specification process (Figure S3B).

Independent prognostic value of FAMGs-based risk signature

To elucidate whether FAMGs-based risk signature is an independent prognostic indicator for UCEC, uni- and multivariate Cox analyses were carried out in TCGA total set. As shown in Figure 4A, age ($P = 0.021$), histological type ($P < 0.001$), stage ($P < 0.001$), grade ($P < 0.001$), and risk score ($P = 0.024$) had significant correlation with OS. Multivariate Cox analysis (Figure 4B) showed that age ($P = 0.013$), stage ($P <$

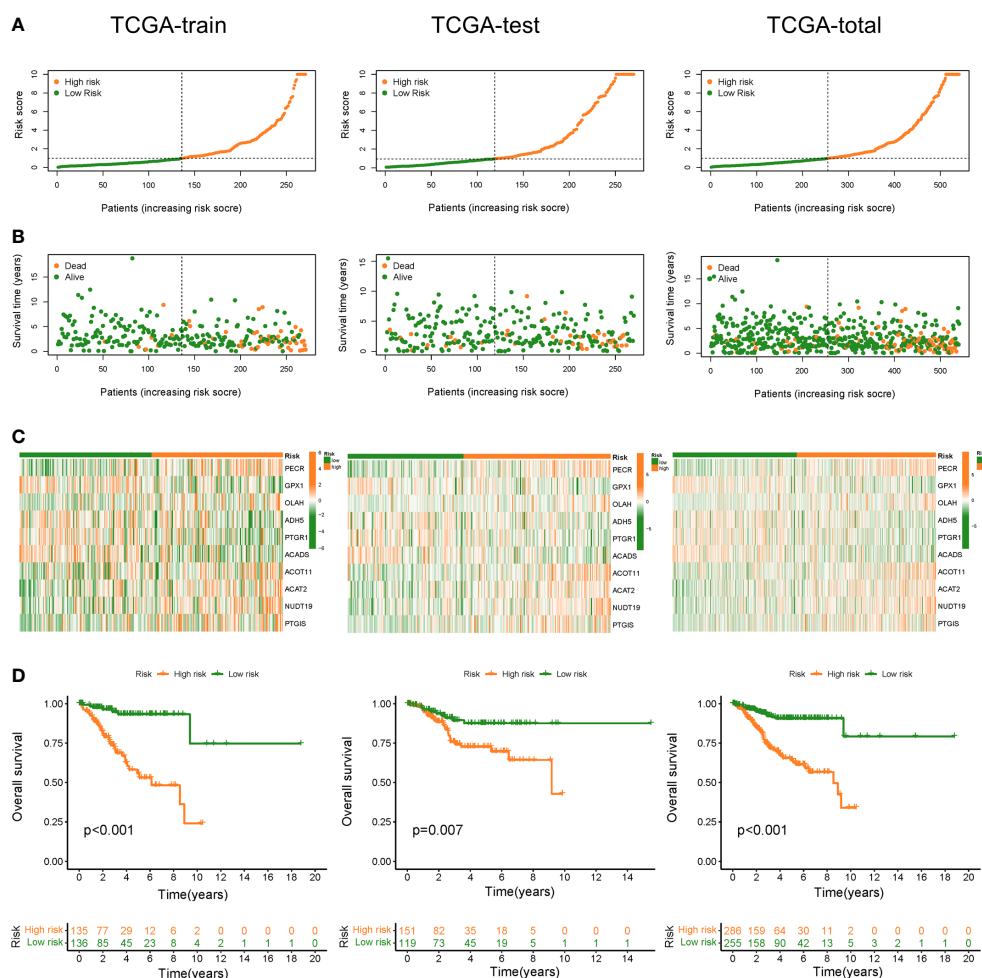


FIGURE 3 Construction and validation of FAMGs-based risk signature in TCGA train set, test set and total set. (A) Distribution of risk score in high- and low- FAMGs groups. (B) Dot plot of survival status with increasing risk score. (C) Heat map of FAMGs expressions in two groups. (D) K-M curve for patients' OS. FAMGs: fatty acid metabolism-related genes. K-M: Kaplan-Meier. OS: overall survival.

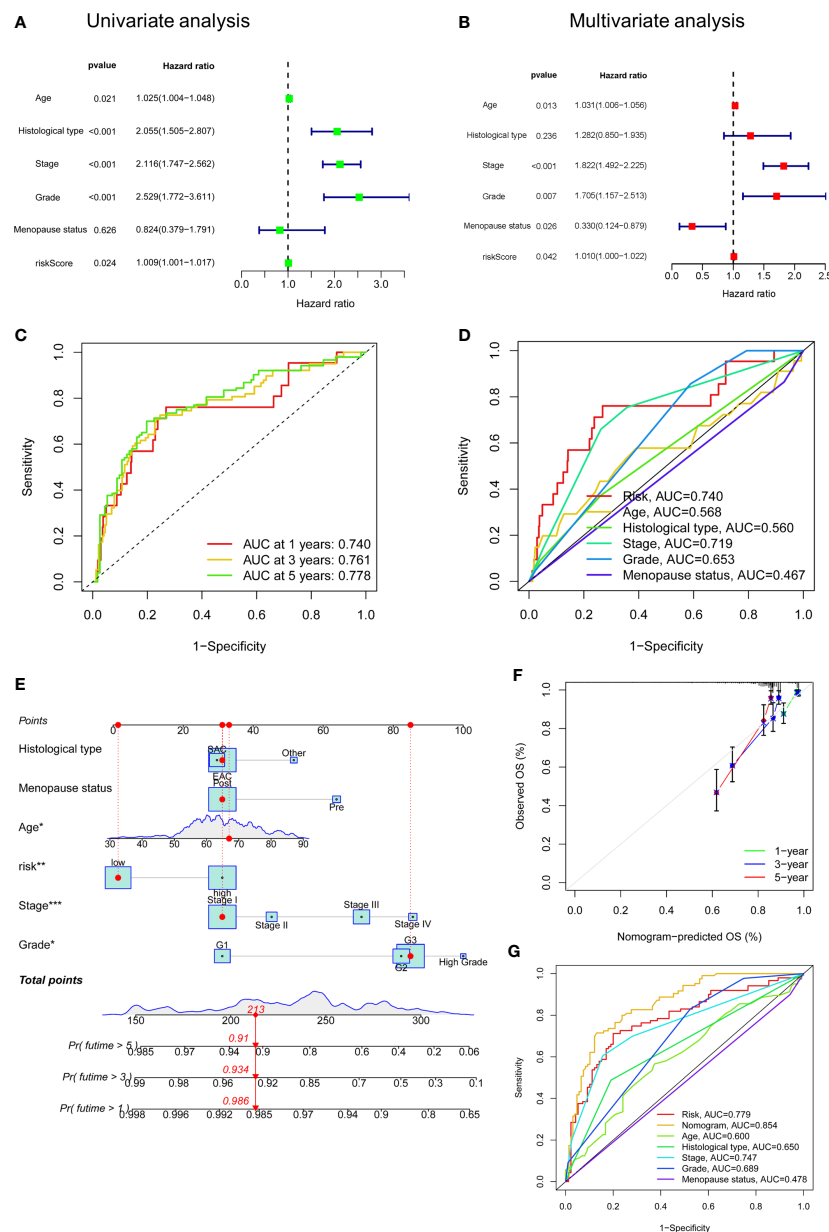


FIGURE 4

Independent prognostic value of risk score and a nomogram construction. (A) Univariate Cox analysis of risk score and clinicopathologic parameters. (B) Multivariate Cox analysis. (C) A nomogram of risk score for 1-, 3- and 5- years' OS. (D) ROC curves of risk score, age, histological type, stage, grade, menopause status. (E) A Nomogram consisting of risk score, age, grade, stage, histological type, and menopause status. (F) Calibration curves for patients' OS at 1, 2, and 3 years. (G) ROC curves for the nomogram and clinicopathologic factors. ROC: receiver operating characteristic. OS: overall survival.

0.001), grade ($P = 0.007$) and menopause status ($P = 0.026$) and risk score ($P = 0.042$) were related to OS. We then performed a time-dependent ROC curve to test this risk model's predicting ability and accuracy (Figure 4C). The result showed that AUC of the 1-, 3-, or 5-year OS was 0.740, 0.761, 0.778, respectively.

Importantly, the AUC value for this risk model was 0.740, which was higher than that for the age (0.568), histological type (0.560), and stage (0.719) (Figure 4D). These results indicated that our FAMGs-based risk signature exhibited a great independent predictive value in UCEC.

Establishment of FAMGs-related nomogram

A nomogram integrating the risk model, age, grade, stage, histological type, and menopause status was created to predict UCEC patients' OS (Figure 4E). By summing the point for each prognostic factor, a total point was generated for each patient, and higher total points meant a worse outcome. The calibration plot showed a close agreement with the ideal model, demonstrating the nomogram's perfect stability and discrimination (Figure 4F). ROC curve showed that this nomogram (AUC = 0.854) had a superior predictive ability than a separate parameter, such as age (AUC = 0.600), stage (AUC = 0.747), or risk model (AUC = 0.779) (Figure 4G).

Prognostic power of FAMGs in UCEC patients

We examined the prognostic power of FAMGs-based risk signature for UCEC patients under different clinicopathological factors, including age, grade, histological type, menopause status

and stage. K-M analysis for each subgroup revealed that low-FAMGs patients have longer OS than high-FAMGs patients, no matter their age, grade, and stage, as is the same situation in patients with EAC or post-menopause (Figure 5). These suggested that FAMGs-based risk signature has strong predictive power in most populations with different clinical features.

Analysis of immune microenvironment

We further evaluate the relationship between TIME and this prognostic signature. Immune status of low- and high-FAMGs patients revealed some degree of heterogeneity (Figure 6A). In addition, high-FAMGs group had a lower TIDE score compared with low-FAMGs group (Figure 6B). Regarding the TME score, high-FAMGs patients had lower immune scores, and ESTIMATE score than low-FAMGs patients, but no significant difference in Stromal score between two groups (Figure 6C). Furthermore, we observed that high-TMB (tumor mutational burden) was linked to a better OS ($P < 0.001$, Figure 6D). We then combined FAMGs with TMB to divide patients into high-TMB/low-risk, low-TMB/low-risk, high-TMB/high-risk, and low-TMB/high-risk groups.

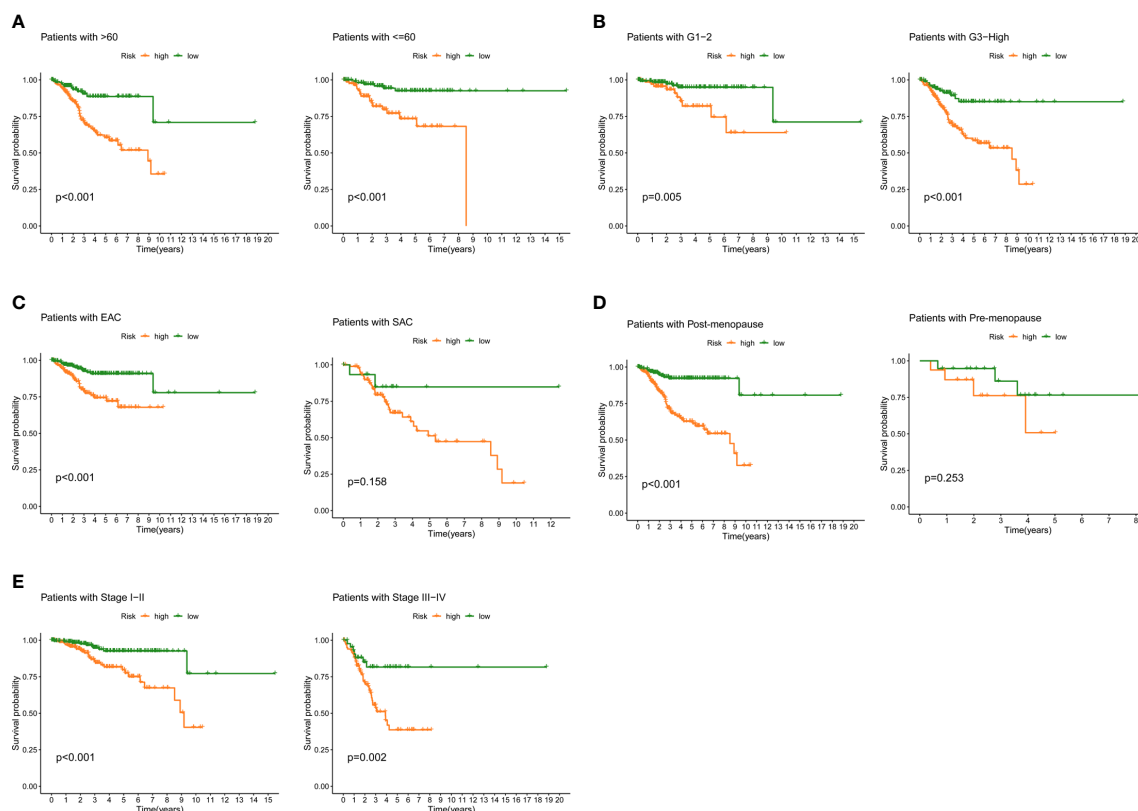
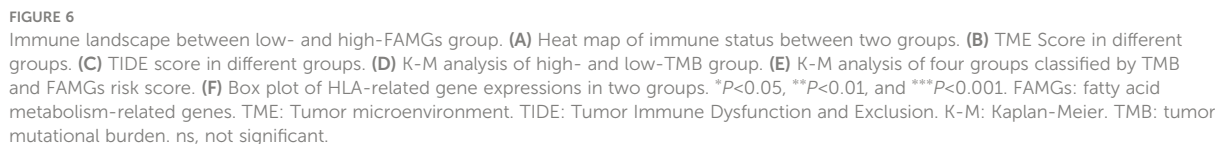


FIGURE 5

Prognostic power in different clinical subgroups. K-M curve analyses for patient subgroups, including (A) age, (B) grade, (C) histological type, (D) menopause, (E) stage. K-M: Kaplan-Meier.



targeted drugs. As shown in [Figures 7A-C](#), low-FAMGs samples had greater IC50 values of Bortezomib, Foretinib and Gefitinib compared with high-FAMGs patients. Moreover, the risk score is inversely correlated with drug sensitivity ([Figures 7D-F](#)). These results suggested that high-FAMGs patients were more responsive to Bortezomib, Foretinib and Gefitinib.

Validation of FAMGs expression

To further validate the expression of FAMGs in this signature, we performed a qRT-PCR experiment to detect the

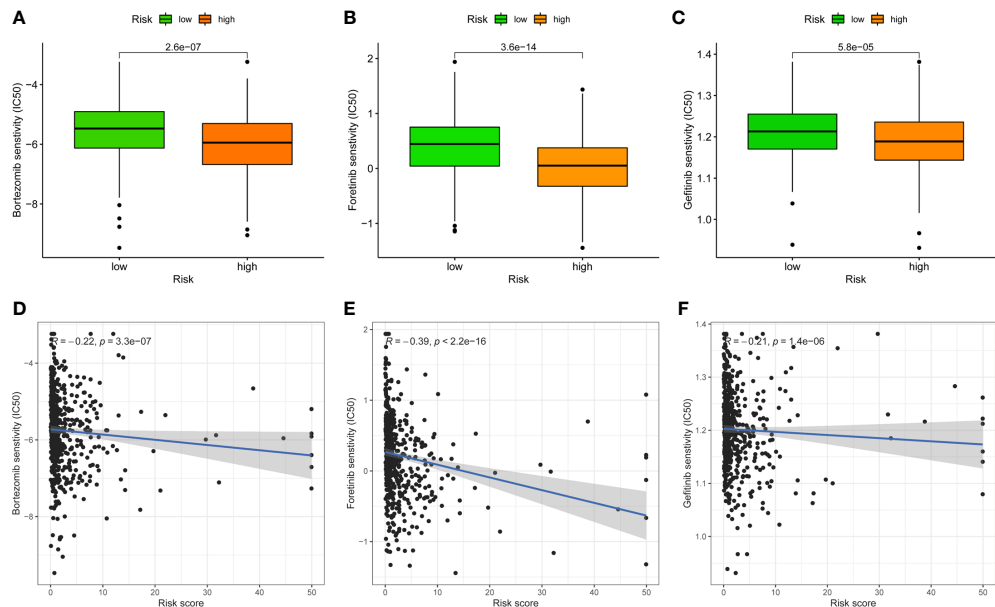


FIGURE 7
Effect of FAMGs-based risk signature in targeted UCEC therapy. (A–C) Comparison of therapeutic sensitivity between low- and high-FAMGs groups. (D–F) Relationship of risk score and estimated IC50 value. FAMGs: fatty acid metabolism-related genes. UCEC: Uterine corpus endometrial carcinoma. IC50: half-maximal inhibitory concentration.

difference between UCEC cells and normal endometrial cells. As expected, the expressions of PECR, OLAH, ACOT11, ACAT2, NUDT19 and PTGIS were upregulated, whereas GPX1, ADH5, PTGR1 and ACADS were downregulated ($P < 0.05$) in UCEC cells compared to normal cells (Figure 8). These were consistent with the above bioinformatic results.

Discussion

UCEC is one of the most prevalently diagnosed gynecologic malignancy and ranks sixth among female tumors worldwide (22). In recent years, UCEC incidence and mortality have been increased with a younger trend. Early-stage UCEC could be

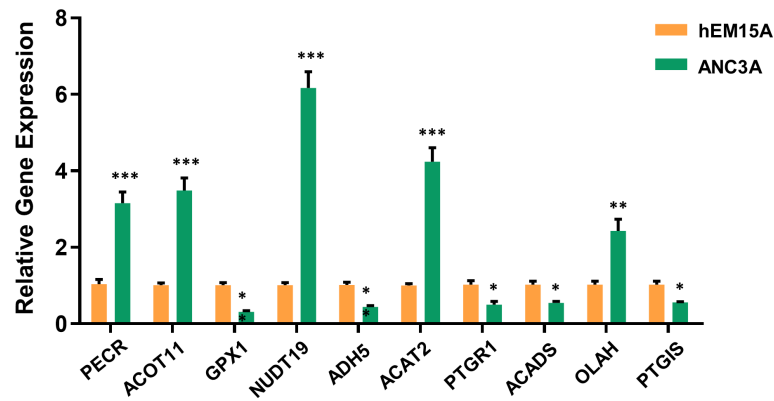


FIGURE 8
Validation of 10-FAMGs expression levels between UCEC cells and controls. * $P < 0.05$, ** $P < 0.01$, and *** $P < 0.001$. FAMGs: fatty acid metabolism-related genes. UCEC: Uterine corpus endometrial carcinoma.

surgically removed followed by chemoradiotherapy, with a 5-year survival rate of up to 90% (23). Nevertheless, advanced-stage patients at a high risk of recurrence had a worse prognosis, some prospective trials have attempted to identify these patients to develop effective adjuvant therapy (24–26), but to date, no interventions have been proven to improve OS. Traditional clinicopathological parameters are insufficient for precisely forecasting the outcome of UCEC, as patients in same clinical stage may exhibit distinct clinical features (27). As a result, the discovery of novel biomarkers for the prognosis and therapy of UCEC has become an urgent clinical issue to be resolved.

It is widely recognized that a major cause of the development of UCEC is obesity (28), which is linked to fatty acid oxidation, synthesis, accumulation and metabolic regulation. Additionally, a majority of FAMGs are known to be tightly related to malignancy and prognosis of cancers. The evidence supports a potent prognostic value of FAMGs for UCEC patients. The advent of bioinformatics has allowed us to examine the specific pattern of FAMGs for UCEC. In our study, a prognostic signature with 10 FAMGs was designed to predict UCEC patients' survival time based on TCGA cohort. Among them, the expression levels of six genes (PECR, OLAH, ACOT11, ACAT2, NUDT19, PTGIS) were significantly upregulated and 4 genes (GPX1, ADH5, PTGR1, ACADS) were downregulated in UCEC samples compared to normal tissues, which have been validated by PCR experiment. Substantial evidence revealed that most of these FAMGs functioned as oncogenes or tumor-suppressor genes in various cancers (29–36). We also determined the prevalence of genetic mutation in UCEC samples, as well as CNV alterations. These confirmed the significant effect of fatty acid metabolism on UCEC malignant progression. Furthermore, a scoring system was created to identify and verify the prognostic value of FAMGs-based risk signature, allowing for the effective risk categorization of UCEC. High-FAMGs UCEC patients had a worse OS or PFS compared with low-FAMGs group. Importantly, FAMGs-based risk signature exhibited great accuracy and independence in predicting UCEC' prognosis than other factors. In addition, a nomogram integrating our signature and patient characteristics was created as a superior tool to predict the survival of UCEC. We also discovered that this signature offered predictive value for different subgroup of patients with specific clinical characteristics. These findings indicated that FAMGs-based risk signature may be a reliable predictor of UCEC.

Tumor development is heavily reliant on the TME, which is complex milieu comprising cancer, stromal and immune cells, as well as microvessels and various chemicals (37). In TME, there are diverse regulatory mechanisms that promote immune tolerance and immune escape, in addition to loss of antigen presentation and upregulation of immune checkpoints, also including cellular metabolic reprogramming. Tumor

metabolism not only modulates the signaling for tumorigenesis and survival, but also an antitumor immune response by releasing intermediate metabolites to affect the expression of immune molecules (38). FAM is a vital metabolic route involved in the immune response, which contains anabolic and catabolic activities for energy homeostasis, as well as metabolites generation that keeps cell membrane structure and function, stores energy and allows cross-talk between tumor and immune cells (39).

In our study, the effect of FAMGs in the risk signature on UCEC TME was further investigated. Patients with low- and high-FAMGs displayed remarkably different immune status. Following processing by ESTIMATE algorithm, it was discovered that low-FAMGs group had a higher estimate score relative to high-FAMGs group, indicating this risk signature may be able to function as a new immune indicator in UCEC. Then, TIDE technique was applied to anticipate clinical response to immune checkpoints and suggested that high-FAMGs patients were more effective to immunotherapy. We continue to investigate the TMB of UCEC patients. The results showed that patients with higher TMB possessed a better prognosis than those with lower TMB. Similar findings have been observed in other cancers (40–42), highlighting the possibility that TMB might serve as a prognostic marker for guiding more efficient immunotherapeutic approaches (43). By combining with FAMGs risk score, patients with low-TMB/high-FAMGs had the lowest survival probability than other groups. In addition, given the importance of HLA-related genes to immune system (44), we compared their expression levels in high- and low-FAMGs group, and found that most of these genes were generally increased in low-FAMGs group. Moreover, the resistance and sensitivity of common targeted drugs were measured to evaluate the prognostic ability of this risk model for therapeutic outcomes. These findings proved that FAMGs-based risk signature was associated with immune status and tumor treatment of UCEC.

Nevertheless, our study also has several limitations. First, the research was completely performed based on TCGA database, but lacked external cohorts for validation. Second, the regulatory mechanism of fatty acid metabolism in UCEC TIME warrants further investigation. Third, the value of FAMGs-based risk signature for clinical application requires multi-center, large sample trials to be processed.

In conclusion, we identified significant FAMGs in UCEC and constructed a FAMGs-based risk signature to predict the patients' prognosis using systematic bioinformatic analyses. Patients with high-FAMGs had a worse prognosis than low-FAMGs patients. This signature might be regarded as an independent indicator to estimate the survival time, immune response and treatment effect. This study provided us a new understanding and direction on the evolution of FAMGs in UCEC.

Data availability statement

The datasets presented in this study can be found in online repositories. The names of the repository/repositories and accession number(s) can be found in the article/Supplementary Material.

Author contributions

CG, YH, LC, and YL designed this work. YW, YB, and NZ analyzed the data, FJ and HZ wrote this manuscript. LZ edited and revised the manuscript. All authors contributed to the article and approved the submitted version.

Funding

This research was supported by Hainan Province Clinical Medical Center.

Acknowledgments

The authors gratefully acknowledge the Cancer Genome Atlas (TCGA) database, which made the data available. The

authors also thank Hainan Province Clinical Medical Center for research support.

Conflict of interest

The authors declare that the research was conducted in the absence of any commercial or financial relationships that could be construed as a potential conflict of interest.

Publisher's note

All claims expressed in this article are solely those of the authors and do not necessarily represent those of their affiliated organizations, or those of the publisher, the editors and the reviewers. Any product that may be evaluated in this article, or claim that may be made by its manufacturer, is not guaranteed or endorsed by the publisher.

Supplementary material

The Supplementary Material for this article can be found online at: <https://www.frontiersin.org/articles/10.3389/fonc.2022.1030246/full#supplementary-material>

References

1. Siegel RL, Miller KD, Fuchs HE, Jemal A. Cancer statistics, 2022. *CA Cancer J Clin* (2022) 72:7–33. doi: 10.3322/caac.21708
2. Xia C, Dong X, Li H, Cao M, Sun D, He S, et al. Cancer statistics in China and united states, 2022: profiles, trends, and determinants. *Chin Med J (Engl)* (2022) 135:584–90. doi: 10.1097/CM9.00000000000002108
3. Lu KH, Broadus RR. Endometrial cancer. *N Engl J Med* (2020) 383:2053–64. doi: 10.1056/NEJMra1514010
4. Lee YY, Choi MC, Park JY, Suh DH, Kim JW. Major clinical research advances in gynecologic cancer in 2020. *J Gynecol Oncol* (2021) 32:e53. doi: 10.3802/jgo.2021.32.e53
5. Hinshaw DC, Shevde LA. The tumor microenvironment innately modulates cancer progression. *Cancer Res* (2019) 79:4557–66. doi: 10.1158/0008-5472.CAN-18-3962
6. Xia L, Oyang L, Lin J, Tan S, Han Y, Wu N, et al. The cancer metabolic reprogramming and immune response. *Mol Cancer* (2021) 20:28. doi: 10.1186/s12943-021-01316-8
7. Munir R, Liseć J, Swinnen JV, Zaidi N. Too complex to fail? targeting fatty acid metabolism for cancer therapy. *Prog Lipid Res* (2022) 85:101143. doi: 10.1016/j.plipres.2021.101143
8. Qi Y, Chen D, Lu Q, Yao Y, Ji C. Bioinformatic profiling identifies a fatty acid metabolism-related gene risk signature for malignancy, prognosis, and immune phenotype of glioma. *Dis Markers* (2019) 2019:3917040. doi: 10.1155/2019/3917040
9. Ding C, Shan Z, Li M, Chen H, Li X, Jin Z. Characterization of the fatty acid metabolism in colorectal cancer to guide clinical therapy. *Mol Ther Oncolytics* (2021) 20:532–44. doi: 10.1016/j.omto.2021.02.010
10. Tang Y, Tian W, Xie J, Zou Y, Wang Z, Li N, et al. Prognosis and dissection of immunosuppressive microenvironment in breast cancer based on fatty acid metabolism-related signature. *Front Immunol* (2022) 13:843515. doi: 10.3389/fimmu.2022.843515
11. Jiang F, Luo F, Zeng N, Mao Y, Tang X, Wang J, et al. Characterization of fatty acid metabolism-related genes landscape for predicting prognosis and aiding immunotherapy in glioma patients. *Front Immunol* (2022) 13:902143. doi: 10.3389/fimmu.2022.902143
12. Lu L, Hu Y, Wang C, Jiang F, Wu C. Methylation and expression of the exercise-related TLR1 gene is associated with low grade glioma prognosis and outcome. *Front Mol Biosci* (2021) 8:747933. doi: 10.3389/fmolb.2021.747933
13. Jiang F, Hu Y, Liu X, Wang M, Wu C. Methylation pattern mediated by m (6)A regulator and tumor microenvironment invasion in lung adenocarcinoma. *Oxid Med Cell Longev* (2022) 2022:2930310. doi: 10.1155/2022/2930310
14. Zhang S, Chang W, Wu H, Wang YH, Gong YW, Zhao YL, et al. Pan-cancer analysis of iron metabolic landscape across the cancer genome atlas. *J Cell Physiol* (2020) 235:1013–24. doi: 10.1002/jcp.29017
15. Ritchie ME, Phipson B, Wu D, Hu Y, Law CW, Shi W, et al. Limma powers differential expression analyses for RNA-sequencing and microarray studies. *Nucleic Acids Res* (2015) 43:e47. doi: 10.1093/nar/gkv007
16. Engebretsen S, Bohlin J. Statistical predictions with glmnet. *Clin Epigenet* (2019) 11:123. doi: 10.1186/s13148-019-0730-1
17. Mandrekar JN. Receiver operating characteristic curve in diagnostic test assessment. *J Thorac Oncol* (2010) 5:1315–6. doi: 10.1097/JTO.0b013e3181ec173d
18. Pomaznoy M, Ha B, Peters B. GOnet: a tool for interactive gene ontology analysis. *BMC Bioinf* (2018) 19:470. doi: 10.1186/s12859-018-2533-3
19. Kanehisa M, Furumichi M, Tanabe M, Sato Y, Morishima K. KEGG: new perspectives on genomes, pathways, diseases and drugs. *Nucleic Acids Res* (2017) 45:D353–353D361. doi: 10.1093/nar/gkw1092
20. Park SY. Nomogram: An analogue tool to deliver digital knowledge. *J Thorac Cardiovasc Surg* (2018) 155:1793. doi: 10.1016/j.jtcvs.2017.12.107
21. Geleher P, Cox N, Huang RS. pRRophetic: an R package for prediction of clinical chemotherapeutic response from tumor gene expression levels. *PloS One* (2014) 9:e107468. doi: 10.1371/journal.pone.0107468

22. Sung H, Ferlay J, Siegel RL, Laversanne M, Soerjomataram I, Jemal A, et al. Global cancer statistics 2020: GLOBOCAN estimates of incidence and mortality worldwide for 36 cancers in 185 countries. *CA Cancer J Clin* (2021) 71:209–49. doi: 10.3322/caac.21660
23. McEachron J, Marshall L, Zhou N, Tran V, Kanis MJ, Gorelick C, et al. Evaluation of survival, recurrence patterns and adjuvant therapy in surgically staged high-grade endometrial cancer with retroperitoneal metastases. *Cancers (Basel)* (2021) 13:2052. doi: 10.3390/cancers13092052
24. Matei D, Filiaci V, Randall ME, Mutch D, Steinhoff MM, DiSilvestro PA, et al. Adjuvant chemotherapy plus radiation for locally advanced endometrial cancer. *N Engl J Med* (2019) 380:2317–26. doi: 10.1056/NEJMoa1813181
25. Randall ME, Filiaci V, McMeekin DS, von Gruenigen V, Huang H, Yashar CM, et al. Phase III trial: Adjuvant pelvic radiation therapy versus vaginal brachytherapy plus Paclitaxel/Carboplatin in high-intermediate and high-risk early stage endometrial cancer. *J Clin Oncol* (2019) 37:1810–8. doi: 10.1200/JCO.18.01575
26. van den Heerik A, Horeweg N, de Boer SM, Bosse T, Creutzberg CL. Adjuvant therapy for endometrial cancer in the era of molecular classification: radiotherapy, chemoradiation and novel targets for therapy. *Int J Gynecol Cancer* (2021) 31:594–604. doi: 10.1136/ijgc-2020-001822
27. Zhou C, Li C, Yan F, Zheng Y. Identification of an immune gene signature for predicting the prognosis of patients with uterine corpus endometrial carcinoma. *Cancer Cell Int* (2020) 20:541. doi: 10.1186/s12935-020-01560-w
28. Hoy AJ, Nagarajan SR, Butler LM. Tumour fatty acid metabolism in the context of therapy resistance and obesity. *Nat Rev Cancer* (2021) 21:753–66. doi: 10.1038/s41568-021-00388-4
29. Liang C, Wang X, Zhang Z, Xiao F, Feng H, Ma Q, et al. ACOT11 promotes cell proliferation, migration and invasion in lung adenocarcinoma. *Transl Lung Cancer Res* (2020) 9:1885–903. doi: 10.21037/tlcr-19-509
30. Weng M, Zhang H, Hou W, Sun Z, Zhong J, Miao C. ACAT2 promotes cell proliferation and associates with malignant progression in colorectal cancer. *Oncotargets Ther* (2020) 13:3477–88. doi: 10.2147/OTT.S238973
31. Lan C, Wang Y, Su X, Lu J, Ma S. LncRNA LINC00958 activates mTORC1/P70S6K signalling pathway to promote epithelial-mesenchymal transition process in the hepatocellular carcinoma. *Cancer Invest* (2021) 39:539–49. doi: 10.1080/07357907.2021.1929282
32. Dai D, Chen B, Feng Y, Wang W, Jiang Y, Huang H, et al. Prognostic value of prostaglandin I₂ synthase and its correlation with tumor-infiltrating immune cells in lung cancer, ovarian cancer, and gastric cancer. *Aging (Albany NY)* (2020) 12:9658–85. doi: 10.18632/aging.103235
33. Zhao Y, Wang H, Zhou J, Shao Q. Glutathione peroxidase GPX1 and its dichotomous roles in cancer. *Cancers (Basel)* (2022) 14:2560. doi: 10.3390/cancers14102560
34. Li N, Li N, Wen S, Li B, Zhang Y, Liu Q, et al. HSP60 regulates lipid metabolism in human ovarian cancer. *Oxid Med Cell Longev* (2021) 2021:6610529. doi: 10.1155/2021/6610529
35. Xue L, Zhu Z, Wang Z, Li H, Zhang P, Wang Z, et al. Knockdown of prostaglandin reductase 1 (PTGR1) suppresses prostate cancer cell proliferation by inducing cell cycle arrest and apoptosis. *Biosci Trends* (2016) 10:133–9. doi: 10.5582/bst.2016.01045
36. Wu Q, Yan T, Chen Y, Chang J, Jiang Y, Zhu D, et al. Integrated analysis of expression and prognostic values of acyl-CoA dehydrogenase short-chain in colorectal cancer. *Int J Med Sci* (2021) 18:3631–43. doi: 10.7150/ijms.63953
37. Anderson NM, Simon MC. The tumor microenvironment. *Curr Biol* (2020) 30:R921–921R925. doi: 10.1016/j.cub.2020.06.081
38. Martinez-Reyes I, Chandel NS. Cancer metabolism: looking forward. *Nat Rev Cancer* (2021) 21:669–80. doi: 10.1038/s41568-021-00378-6
39. Wang Y, Wang Y, Ren Y, Zhang Q, Yi P, Cheng C. Metabolic modulation of immune checkpoints and novel therapeutic strategies in cancer. *Semin Cancer Biol* (2022) 86:542–65. doi: 10.1016/j.semcancer.2022.02.010
40. Guan X, Xu ZY, Chen R, Qin JJ, Cheng XD. Identification of an immune gene-associated prognostic signature and its association with a poor prognosis in gastric cancer patients. *Front Oncol* (2020) 10:629909. doi: 10.3389/fonc.2020.629909
41. Li P, Hao S, Ye Y, Wei J, Tang Y, Tan L, et al. Identification of an immune-related risk signature correlates with immunophenotype and predicts anti-PD-L1 efficacy of urothelial cancer. *Front Cell Dev Biol* (2021) 9:646982. doi: 10.3389/fcell.2021.646982
42. Pei JP, Zhang CD, Yusupu M, Zhang C, Dai DQ. Screening and validation of the hypoxia-related signature of evaluating tumor immune microenvironment and predicting prognosis in gastric cancer. *Front Immunol* (2021) 12:705511. doi: 10.3389/fimmu.2021.705511
43. Romero D. TMB is linked with prognosis. *Nat Rev Clin Oncol* (2019) 16:336. doi: 10.1038/s41571-019-0206-4
44. Paulson KG, Voillet V, McAfee MS, Hunter DS, Wagener FD, Perdicchio M, et al. Acquired cancer resistance to combination immunotherapy from transcriptional loss of class I HLA. *Nat Commun* (2018) 9:3868. doi: 10.1038/s41467-018-06300-3



OPEN ACCESS

EDITED BY
Jinhui Liu,
Nanjing Medical University, China

REVIEWED BY
Lei Lei Liang,
Chinese Academy of Medical Sciences
and Peking Union Medical College,
China
Renyuan Zhang,
Thermo Fisher Scientific, United States

*CORRESPONDENCE
Bei Lin
linbei88@hotmail.com
Xiao Li
lixiaoj@163.com

SPECIALTY SECTION
This article was submitted to
Gynecological Oncology,
a section of the journal
Frontiers in Oncology

RECEIVED 02 September 2022
ACCEPTED 15 November 2022
PUBLISHED 01 December 2022

CITATION
Li S, Hu Y, Liu O, Li X and Lin B
(2022) Prognostic biomarker
MCP-4 triggers epithelial-
mesenchymal transition *via* the p38
MAPK pathway in ovarian cancer.
Front. Oncol. 12:1034737.
doi: 10.3389/fonc.2022.1034737

COPYRIGHT
© 2022 Li, Hu, Liu, Li and Lin. This is an
open-access article distributed under
the terms of the [Creative Commons
Attribution License \(CC BY\)](https://creativecommons.org/licenses/by/4.0/). The use,
distribution or reproduction in other
forums is permitted, provided the
original author(s) and the copyright
owner(s) are credited and that the
original publication in this journal is
cited, in accordance with accepted
academic practice. No use,
distribution or reproduction is
permitted which does not comply
with these terms.

Prognostic biomarker MCP-4 triggers epithelial-mesenchymal transition *via* the p38 MAPK pathway in ovarian cancer

Siting Li^{1,2}, Yuexin Hu^{1,2}, Ouxuan Liu^{1,2}, Xiao Li^{1,2*} and Bei Lin^{1,2*}

¹Department of Obstetrics and Gynecology, Shengjing Hospital of China Medical University, Shenyang, China, ²Key Laboratory of Maternal-Fetal Medicine of Liaoning Province, Key Laboratory of Obstetrics and Gynecology of Higher Education of Liaoning Province, Shenyang, China

Background: Monocyte chemoattractant protein-4 (MCP-4/CCL13) is a proinflammatory factor that is overexpressed in various malignant tumors and may play an important role in tumor progression and metastasis. However, its role and mechanism of action in ovarian cancer remains unknown.

Methods: Immunohistochemistry (IHC) was performed to detect the expression of MCP-4 in ovarian cancer tissues, and the effect of MCP-4 on patient survival and prognosis was analyzed. Overexpression and suppression of MCP-4 in ovarian cancer cell lines were then established, and their effects on cell invasion, migration, and apoptosis were studied. ES-2 cell lines were employed to establish a peritoneal dissemination model in nude mice. Western blotting was performed to detect the expression of epithelial mesenchymal transition (EMT) markers and the p38 mitogen-activated protein kinase (p38 MAPK) signaling pathway.

Results: MCP-4 was highly expressed in ovarian cancer tissues and its expression level was related to the prognosis of patients with ovarian cancer. MCP-4 overexpression promoted the migration and invasion of ovarian cancer cells but inhibited apoptosis. MCP-4 overexpression increased the expression of MMP-2, MMP-9, N-cadherin, vimentin and Bcl2/Bax and decreased the expression of E-cadherin. MCP-4 overexpression increased the phosphorylation of the p38 MAPK pathway. The inhibition of MCP-4 expression indicated an opposite trend. *In vivo* experiments have also confirmed that MCP-4 overexpression can promote metastasis of ovarian cancer.

Conclusion: MCP-4 promotes ovarian cancer progression through the p38 MAPK signaling pathway, and may be a potential biomarker and therapeutic target for ovarian cancer.

KEYWORDS

p38 MAPK signaling pathway, apoptosis, EMT, ovarian cancer, MCP-4

Introduction

Ovarian cancer has the highest death rate among gynecological malignancies, with a five-year survival rate of less than 50% (1). Due to the lack of typical clinical symptoms in the early stages of ovarian cancer, patients are often diagnosed at an advanced stage, when the tumor is difficult to remove completely (2). Despite urgent clinical needs and substantial research efforts, the mainstream treatment of ovarian cancer remains cytoreductive surgery and adjuvant chemotherapy, without much recent progress (3). This further contributes to the fact that ovarian cancer remains a challenge. Therefore, pathogenesis identification of ovarian cancer and new treatment strategies are crucial for improving the survival rate of patients with ovarian cancer.

The human *MCP-4/CCL13* gene is found in the q11.2 segment of chromosome 17, within the chemotactic chemokine (CC) gene cluster (17q11-32), including three exons, two introns, and regulatory sequences near the 5' upstream region. MCP-4 can bind to chemokine receptors CCR1, CCR2, CCR3, and CCR5 and has chemotactic effects on multiple immune cells, including monocytes, eosinophils, basophils, macrophages, T cells, B cells, and dendritic cells (DCs) (4, 5). In addition, MCP-4 is involved in processes such as eosinophil degranulation, histamine release from basophils, expression of adhesion molecules, and cytokine secretion from epithelial, endothelial, and muscle cells (6). Previous studies on MCP-4 have mainly focused on inflammatory diseases, however, more recent studies have reported that the expression of MCP-4 is increased in colorectal (7) and gastric cancers (8), which are associated with the development of malignant tumors. The expression of MCP-4 in ovarian cancer and its effect on malignant biological behavior have not yet been reported.

In this study, the expression of MCP-4 in ovarian tissue was detected by immunohistochemistry, and its relationship with clinicopathological parameters was evaluated. Additionally, the prognoses of patients with ovarian cancer were analyzed. *In vivo* and *in vitro* models of MCP-4 overexpression and inhibition were established. The role of MCP-4 in the EMT process in ovarian cancer was explored as well as the mechanism of MCP-4 in ovarian cancer occurrence and development. These findings suggest that MCP-4 can potentially be used as an indicator of ovarian cancer, which can be used for diagnosis and prognosis. Finally, these findings provide new research directions for targeted therapy regimens against ovarian cancer.

Materials and methods

Specimen source and clinical data

All 147 paraffin-embedded ovarian tissue samples were obtained from surgical inpatients at the Shengjing Hospital,

China Medical University, between 2008 and 2019. The study was approved by the Ethics Committee of the Shengjing Hospital, China Medical University, and all patients provided informed and signed consent. The ovarian malignancy specimens were primary epithelial ovarian tumors, and the patients had not received radiotherapy, chemotherapy, or hormone therapy before surgery. The clinicopathological data of all cases were complete. All tissue sections were diagnosed by experienced pathologists at Shengjing Hospital, China Medical University. The total tissue sections consisted of 9 cases of normal ovarian tissue, 12 cases of benign tumors, 21 cases of ovarian epithelial borderline tumors, and 105 cases of ovarian epithelial malignant tumors. The ages of all patients ranged from 19 to 79 years, with an average of 53 years. All the patients ranged in age from 19 to 79 years, with an average age of 52. The mean ages of patients with normal ovaries, benign tumors, borderline tumors, and malignant tumors were 53 years (34 - 76 years), 47 years (35 - 61 years), 47 years (24 - 79 years) and 55 years (19 - 78 years old), respectively. There were no significant differences between the groups ($P > 0.05$). According to the pathological type, a total of 105 malignant ovarian epithelial tumors were divided into 71 cases of serous carcinoma, 10 cases of mucinous carcinoma, 13 cases of endometrioid carcinoma, and 11 cases of clear cell carcinoma. According to the degree of tumor cell differentiation, the total samples were divided into 54 cases of poorly differentiated carcinoma, 24 cases of moderately differentiated carcinoma, and 28 cases of well-differentiated carcinoma. According to the International Federation of Gynecology and Obstetrics (FIGO, 2014), 28 cases were classified as stage I, 10 cases as stage II, 62 cases as stage III, and six cases as stage IV. According to the absence of lymph node metastasis, 31 patients with lymph node metastasis, 67 without lymph node metastasis, and 8 without lymph node dissection were observed.

Immunohistochemistry

Paraffin-embedded ovarian tissues were cut into 5 μ m serial sections. An immunohistochemical ultrasensitive TM SP (mouse/rabbit) kit (Cat# KIT-9720, MaiXin, China) was used to detect the expression of MCP-4. The rabbit MCP-4 polyclonal antibody was diluted 1:200 (Cat# 820372, ZEN BIO, China). Other reagents and instruments were provided by the Central Laboratory of the Shengjing Hospital, China Medical University. Staining was performed according to the manufacturer instructions on the SP kit. Positive reactions were defined by the presence of brownish-yellow granular deposits in the cell membrane and cytoplasm. A comprehensive score was calculated based on the intensity of staining and the proportion of stained cells. The samples were divided into no staining (0 points), light yellow (1 point), brown-yellow (2 points), and brown (3 points) according to the intensity of

staining. The percentage of colored cells was divided into <5% (0 points), 5%–25% (1 point), 26%–50% (2 points), 51%–75% (3 points), and 76%–100% (4 points). The two items were multiplied by the final scores: 0–2 points (–), 3–4 points (+), 5–8 points (++), and 9–12 points (+++). Based on these scores, 0–4 points were defined as the low-expression group and 5–12 points as the high-expression group. Each sample was scored independently by two observers, with a third observer when disagreement arose.

Cell culture

Ovarian cancer cell lines (Caov3, ES-2) and human ovarian surface epithelial cell line (HOSEpiC) were purchased from the Cell Bank of the Chinese Academy of Sciences (Shanghai Institute of Biochemistry and Cell Biology, Shanghai, China). Caov3 is a cell line with epithelial morphology isolated in 1976 from the ovary of a 54-year-old, White, female ovarian adenocarcinoma patient. ES-2 is a cell line exhibiting fibroblast-like morphology that was isolated from the ovary of a 47-year-old, Black, female clear cell carcinoma patient. The Caov3 and HOSEpiC cells were cultured in RPMI1640 medium containing 10% fetal bovine serum (FBS). The ES-2 cells were cultured in McCoy's5A medium containing 10% FBS. Cells were cultured at 37°C, 5% CO₂, and saturated humidity.

Cell transfection and establishment of stably transfected cell lines

The Caov3 and ES-2 cells in the logarithmic growth phase were inoculated into six-well plates a day before transfection. MCP-4 siRNA and negative control siRNA (GenePharma, China) were transfected into cells using the liposome method (Lipo3000, Cat# L3000015, GIBCO, Invitrogen, USA). The sequence of MCP-4 siRNA is: sense: 5'-GAAAGUCUCUGCAGUGCUUTT-3', antisense: 5'-AAGCACUGCAGAGACUUUCTT-3'. The sequence of its negative control is: sense: 5'-UUCUCCGAACGUGUCACGUTT-3', antisense: 5'-ACGUGACACGUUCGGAGAA TT-3'. Following 48h transfection, cells were collected for real-time quantitative polymerase chain reaction (RT-qPCR), western blotting, and biological assays. Caov3 and ES-2 cells were transfected with lentivirus-mediated vector of MCP-4 (Lot# LV61110906, HANBIO, China) or negative control (Lot# LV61110905, HANBIO, China) to establish MCP-4 overexpression or negative control cell lines. The procedure of transfections was conducted according to the manufacturer's instructions. The volume of lentivirus to be transfected was calculated according to the infection values of different cells, the number of cells at the time of transfection and the lentivirus titer. 2 µg of polybrene (2mg/ml, Lot# 20211015, Hanbio, China) was added to the culture medium to improve transfection efficiency.

After transfection for 48h, stable transfected cells were further screened by puromycin (2 µg/ml, Lot# 20211011, Hanbio, China).

RT-PCR

Total cellular RNA was extracted using TRIzol (Cat# 9109, Takara Bio, Inc., Shiga, Japan), and the purity and concentration of RNA were determined using UV spectrophotometry. A one-step TB Green PrimeScript RT-PCR kit (Cat# 066A Takara Bio, Inc., Shiga, Japan) was used to reverse transcribe RNA into complementary DNA (cDNA), which was then used as a template for DNA amplification. Reverse transcription conditions were as follows: reverse transcription at 42°C for 5 min, heating at 95°C for 10 s. Amplification conditions: denaturation at 95°C for 5 s and 60°C for 30 s, for a total of 40 cycles. MCP-4 primer sequence: Forward: 5'-GCACTCAACGTCCCCTCTAC-3', Reverse: 5'-TTCTCCTTTGGGTCAGCACA-3'. GAPDH primer sequence: Forward: 5'-ACAACCTTTGGTATCGTGGAAGG-3', Reverse: 5'-GCCATCAGCCACAGTTTC-3'. The PCR was performed using a 7500 Fast Real-Time PCR system. Data were analyzed using the 2^{-ΔΔCT} method.

Western blotting

RIPA cell lysis buffer was used to lyse cells at 4°C for 30 min, followed by centrifugation at 12000× g, 4°C for 30 min. The supernatant was collected, and the protein concentration was determined by the BCA method. The 5× loading buffer (Cat# cw0027S, CWVBIO, China) was added to each sample and denatured at 100°C for 10 min. Protein samples were separated by 10% sodium dodecyl sulfate-polyacrylamide gel electrophoresis (SDS-PAGE) and transferred to polyvinylidene difluoride (PVDF) membranes (Cat# IPVH00010, Millipore, USA). Membranes were blocked with 5% nonfat milk for 2 h and incubated with primary antibodies overnight at 4°C. The primary antibodies we used were as follows: MCP-4 (1:1000, Cat# DF9911, Affinity, USA), BCL2 (1:2000, Cat# 12789-1-AP, Proteintech, China), BAX (1:1000, Cat# AF0120, Affinity, China), MMP2 (1:1000, Cat# 10373-2-AP, Proteintech, China), MMP9 (1:500, Cat# 10375-2-AP, Proteintech, China), E-cadherin (1:2000, Cat# 20874-1-AP, Proteintech, China), N-cadherin (1:2000, Cat# 22018-1-AP, Proteintech, China), vimentin (1:2000, Cat# 10366-1-AP, Proteintech, China), p38 MAPK (1:1000, Cat# 8690, Cell Signaling Technology, USA), p-p38 MAPK (1:1000, Cat# 4511, Cell Signaling Technology, USA), and GAPDH (1:2000, Cat# TA-08, ZSGB-BIO, China). The membranes were washed three times with tris-buffered saline tween (TBST) the next day, followed by incubation with a horseradish peroxidase-labeled secondary antibody (1:2000, ZSGB-BIO, China) for 2 h. After washing three times with

TBST, the proteins were detected with western blot chemiluminescence horseradish peroxidase (HRP) substrate (Cat# WBKLS0500, Millipore, Billerica, MA, USA) to detect protein expression, and an Amersham Imager 680 (AI680) ultrasensitive luminometer was used for imaging.

Invasion test

Invasion ability was assessed by Transwell assay in a 24-well culture plate. Matrigel (Cat# 356234, BD Biosciences, USA) and serum-free medium were mixed at a ratio of 1:7.5 and 70 μ L was added to the upper chamber of each transwell chamber (Cat# 3422, Corning, USA) and incubated for 4 h at 37°C. A total of 200 μ L of serum-free cell suspension (2×10^5 /mL) was added to the upper chamber and 500 μ L of RPMI1640 or McCoy's5A medium containing 20% FBS was added to the lower chamber. After incubation at 37°C and 5% CO₂ for 48 h, the cells were fixed with 4% paraformaldehyde for 30 min. The cells were then washed with PBS and stained with 0.1% crystal violet for 30 min. Cells in the upper chamber were gently wiped with a cotton swab. The stained cells were observed and counted under a microscope. At least three random fields were taken photographs for each chamber.

Wound healing test

A marker was used to mark the back of the 6-well plate every 0.5–1 cm, with at least 3 horizontal lines for each hole. Single-cell suspensions were prepared from cells in the logarithmic growth phase and seeded in 6-well plates. When cell fusion reached 90%, the plate was gently scraped with a 200 μ L pipette tip. The scratch lines should be perpendicular to the horizontal lines. The cells were washed twice with PBS and cultured in serum-free medium. The wound-healing ability of the cells was observed and photographed under a microscope at 0 and 24 h.

Apoptosis detection using flow cytometry

The Annexin-V-APC/7AAD (Cat# KGA1025, KeyGEN Biotech, China) double staining method was used to detect apoptosis in ovarian cancer cell lines overexpressing MCP-4, and the Annexin V-FITC/PI (Cat# KGA107, KeyGEN Biotech, China) double staining method was used to detect apoptosis when MCP-4 expression was inhibited. Each group contained a blank control and two types of staining. A blank and single staining control for both dyes were set up for each group. The cells were digested with ethylenediaminetetraacetic acid (EDTA)-free trypsin to obtain a single-cell suspension. Centrifugation (2000 rpm) was performed for 5 min, and the

supernatant was removed. A total of 500 μ L of $1 \times$ Annexin V binding buffer (1×10^6 cell number/mL) was added to resuspend the cells, and 5 μ L Annexin V-APC binding mixture (Annexin V-FITC binding mixture) and 5 μ L 7AAD dye (PI dye) were added. After incubation for 15 min in the dark, cell apoptosis was detected using BD FACSDiva software (Cat# 352054, BD Biosciences, USA).

Nude mouse xenograft model

Twelve 4-week-old female BALB/cA-nu nude mice, purchased from Beijing Huafukang Biosciences (Beijing, China), were maintained in specific pathogen-free conditions. Control vector/MCP-4-overexpressed ES-2 cells (5×10^6) cells were suspended in 150 μ L of PBS and injected subcutaneously into the left flank of mice ($n = 6$). The changes of body weight and abdominal girth were recorded every 4 days. All the mice were sacrificed after 25 days. The animal study was approved by the Institutional Animal Research Committee of China Medical University.

Bioinformatics analysis

RNA-seq data in TPM (transcripts per million reads) format from The Cancer Genome Atlas (TCGA) database (<https://portal.gdc.cancer.gov/>) and the Genotype-Tissue Expression (GTEx) database (<https://gtexportal.org/>) were downloaded. 379 ovarian cancer samples were from TCGA, and 88 normal ovarian tissues samples from the GTEx. Data standardization and log₂ transformation were performed for expression comparison between the samples. R software (version 3.6.3) was operated for statistical analysis and visualization. Two datasets (GSE38666 (9) and GSE18520 (10)) were downloaded from the Gene Expression Omnibus (GEO) database (<https://ncbi.nlm.nih.gov/geo/>). The GSE18520 dataset included 10 normal ovarian epithelial tissues and 53 cases of ovarian epithelial high-grade serous tumors, whereas the GSE38666 dataset included 12 normal ovarian epithelial tissues and 18 ovarian epithelial malignant tumors. These datasets were processed and calibrated, and MCP-4 expression data were extracted using R software (version 3.6.3). The ggplot2 package (version 3.3.3) was used to draw differential expression box plots. GSEA version 4.1.0 software (<http://software.broadinstitute.org/gsea/index.jsp>) was operated for functional enrichment analysis of the Kyoto Encyclopedia of Genes and Genomes (KEGG) using the data from the TCGA database. The parameters of gene set parameters and run enrichment tests were set as follows. The “c2.cp.kegg.v7.4.symbols.gmt” was chosen as the gene sets database. The permutations value was set to 1000 for computing normalized enrichment score (NES). Signaling

pathways with a false discovery rate (FDR) q -value < 0.05 was recognized with significant enrichment. Normalized P -value < 0.05 was used to select the enriched signaling pathways when q -value > 0.05 .

Statistical analysis

Data were analyzed using SPSS (version 23.0, IBM Corporation, USA), and graphs were constructed using GraphPad Prism software (version 8.0). All data are presented as mean \pm standard deviation. Differences between two groups were compared using the chi-square test and t -test, and differences between more than two groups were compared using analysis of variance. Kaplan–Meier and log-rank tests were used for survival analysis. Univariate and multifactorial Cox regression models were used to analyze the risk factors affecting prognosis. Two-sided $P < 0.05$ was considered statistically significant (*, $P < 0.05$; **, $P < 0.01$; ***, $P < 0.001$).

Results

Expression and clinical significance of MCP-4 in ovarian tissues

Immunohistochemical results showed that MCP-4 was mainly expressed in the cell membrane and cytoplasm (Figure 1A). The positive and high expression rates of MCP-4 in the ovarian cancer group (91.43% (96/105) and 75.24% (26/105)) were significantly higher than those in the borderline group (57.14% (12/21) and 19.05% (4/21)) (both $P < 0.05$), benign group (41.67% (5/12) and 8.33% (1/12)) (both $P < 0.05$), and normal ovarian tissues (44.44% (4/9) and 0.00% (0/9)) (both $P < 0.05$) (Table 1). In ovarian borderline tumor tissues, the positive and high expression rates of MCP-4 were higher (57.14% (12/21) and 19.05% (4/21), respectively) than in the benign group (41.67% (5/12) and 8.33% (1/12), respectively) (both $P > 0.05$) and the normal group (44.44% (4/9) and 0.00% (0/9), respectively) (both $P > 0.05$) (Table 1). The IHC scores for MCP-4 expression are shown in Figure 1B. Analysis of normal ovarian tissue data downloaded from the GTEx database and ovarian cancer datasets downloaded from TCGA database showed that the expression of MCP-4 was significantly higher in ovarian epithelial serous cystadenocarcinoma than in normal ovarian tissues ($P < 0.05$) (Figure 1G). In addition, the downloaded datasets GSE18520 (Figure 1H) and GSE38666 (Figure 1I) from GEO also showed the same results (both $P < 0.05$).

According to the IHC results, 105 ovarian cancer samples were divided into the MCP-4 high expression group (+++/++) and MCP-4 low expression group (+/-). The relationship between MCP-4 expression and clinicopathological parameters

is shown in Table 2. High expression of MCP-4 was significantly correlated with the late International Federation of Gynecology and Obstetrics (FIGO) stage ($P < 0.05$). The high expression rate of MCP-4 in the late FIGO stage (stage III–IV) was 83.08%, which was significantly higher than that in the early FIGO stage (stage I–II) (62.50%). However, the expression of MCP-4 was not correlated with age, histological grade, lymph node metastasis, or pathological type ($P > 0.05$). A total of 105 ovarian cancer patients were followed up until April 1, 2021. Kaplan–Meier survival analysis showed that the overall survival of ovarian cancer patients with high MCP-4 expression was significantly shorter than that of patients with low MCP-4 expression ($P < 0.05$) (Figure 1D). FIGO stage ($P < 0.05$) (Figure 1E) and lymph node metastasis ($P < 0.05$) (Figure 1F) were significantly correlated with the overall survival.

Cox regression analysis of the relationship between different clinicopathological parameters and the prognosis of patients with ovarian cancer univariate Cox regression analysis showed that high MCP-4 expression, advanced FIGO stage, and lymph node metastasis were risk factors affecting the prognosis of patients with ovarian cancer (all $P < 0.05$) (Table 3). Multivariate Cox regression analysis showed that high MCP-4 expression and advanced FIGO stage were independent risk factors affecting patient prognosis (all $P < 0.05$) (Table 3). The results of Cox regression analysis were visualized using forest plots (Figures 2A, B). These results suggest that elevated expression of MCP-4 in ovarian cancer tissues is associated with poor prognosis and that high expression of MCP-4 may serve as an independent risk factor for predicting the prognosis of patients with ovarian cancer.

MCP-4 promotes invasion, migration, and EMT of ovarian cancer cells

The expression of MCP-4 in normal ovarian epithelial cells (HOSEpiC) and two ovarian cancer cell lines (Caov3, ES-2) was examined. The results indicated that the expression of MCP-4 in the Caov3 and ES-2 cell lines was higher than that in HOSEpiC cells (Figure 1C).

Overexpression of Caov3 and ES-2 cell lines of MCP-4 were constructed by lentiviral transfection, and inhibition cell lines of MCP-4 were constructed by siRNA transfection. RT-PCR and western blotting confirmed increased/decreased mRNA and protein levels of MCP-4 in overexpression/inhibition cell lines (Figures 3A–D).

To investigate the effect of MCP-4 on the migration and invasion abilities of ovarian cancer cells, we performed invasion and wound healing tests. The results showed that the overexpression of MCP-4 significantly enhanced the invasive ability of Caov3 and ES-2 cells ($P < 0.05$) (Figure 4A), whereas the inhibition of MCP-4 expression decreased the invasive ability of ovarian cancer cells ($P < 0.05$) (Figure 4B). After MCP-4

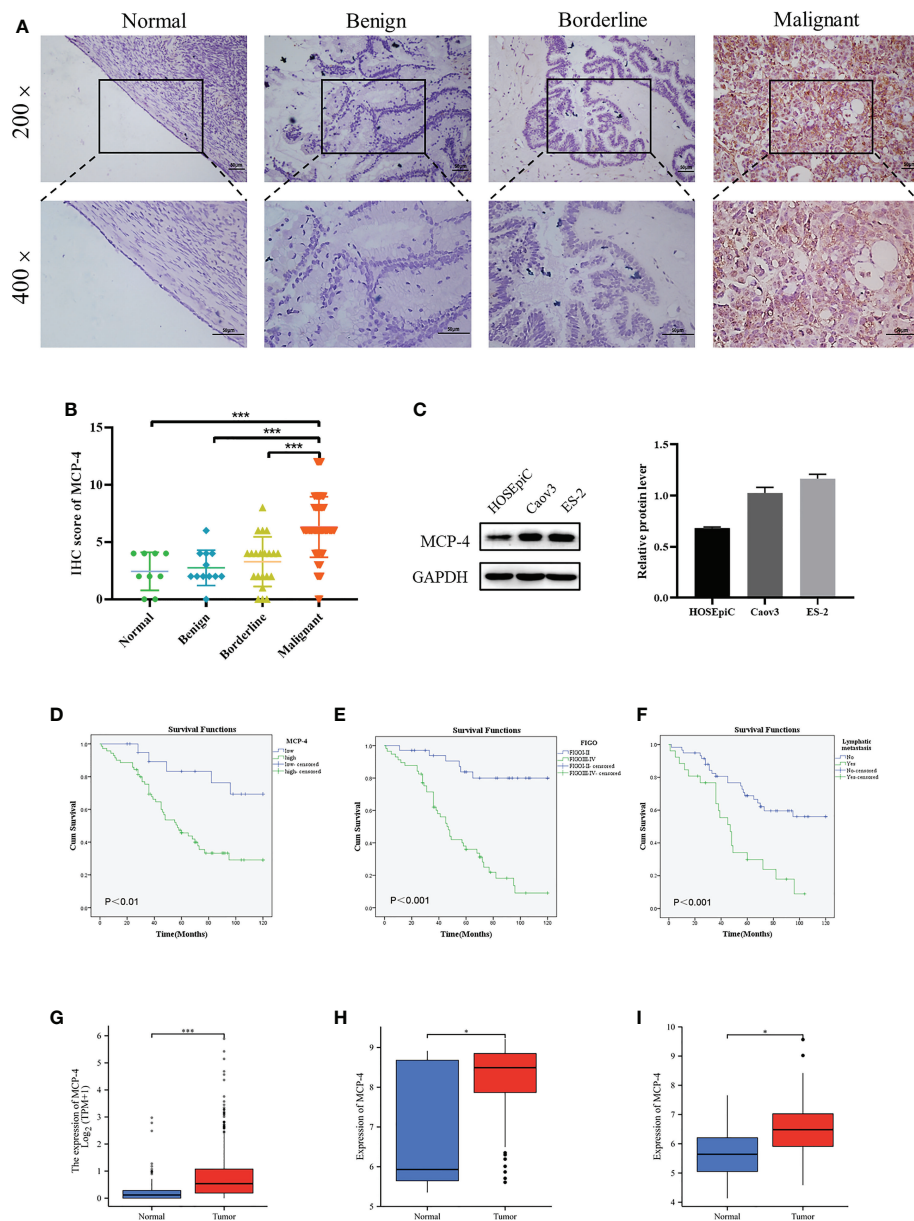


FIGURE 1

High MCP-4 expression in patients with ovarian cancer associated with poor prognosis. **(A)** MCP-4 expression in ovarian tissue samples (x200 and x400, scale bar = 50 μ m): ovarian normal tissue (n = 9), ovarian benign tumor (n = 12), ovarian borderline tumor (n = 21), ovarian malignant tumor (n = 105). **(B)** Immunostaining scores of MCP-4 in normal ovarian tissues, benign, borderline, and malignant tumors. **(C)** Representative images and quantitation of the western blotting showed that the protein expression of MCP-4 in the normal ovary epithelial cells (HOSepIC) and ovarian cancer cell lines (Caov3 and ES-2) (n = 3). GAPDH was used as an internal control. **(D–F)** Overall survival analysis according to MCP-4 expression, FIGO stage and lymph node metastasis. Box plots show MCP-4 mRNA expression in the normal tissues (blue plot) and ovarian tumor (red plot) from TCGA database **(G)**, GSE18520 datasets **(H)**, and GSE38666 datasets **(I)**. Data are presented as mean \pm SD. * P < 0.05; *** P < 0.001.

overexpression, the wound healing speed of Caov3 and ES-2 cells was significantly higher than that of the control group (P < 0.05) (Figure 4C). In addition, when MCP-4 was overexpressed, the levels of N-cadherin, vimentin, MMP-2, and MMP-9 also increased, and the level of E-cadherin decreased (Figure 4E).

Overexpression of MCP-4 promotes epithelial mesenchymal transition in ovarian cancer. An opposite trend was observed when MCP-4 expression was inhibited (Figures 4D, F). These results confirm that MCP-4 can promote the invasion, migration, and EMT of ovarian cancer cells.

TABLE 1 Expression of MCP-4 in different types of ovarian tissue.

Group	n	Low		High		Positive	High positive
		(-)	(+)	(++)	(+++)	rate (%)	rate (%)
Normal	9	5	4	0	0	44.44	0.00
Benign	12	7	4	1	0	41.67	8.33
Borderline	21	9	8	4	0	57.14 ^{a,b}	19.05 ^{c,d}
Malignant	105	9	17	58	21	91.43 ^{e,f}	75.24 ^{g,h}

^aNormal vs. Borderline ($P = 0.002$); ^bBenign vs. Borderline ($P = 0.061$); ^cNormal vs. Borderline ($P = 0.060$); ^dBenign vs. Borderline ($P = 0.031$); ^eNormal vs. Malignant ($P < 0.001$); ^fBenign vs. Malignant ($P = 0.001$); ^gNormal vs. Malignant ($P < 0.001$); ^hBenign vs. Malignant ($P = 0.001$).

TABLE 2 Relationship between MCP-4 expression and clinicopathological parameters of ovarian epithelial malignant tumors.

Items	n	Low		High		High positive	P-value
		(-)	(+)	(++)	(+++)	rate (%)	
FIGO stage							<0.05
I-II	40	0	15	19	6	62.50	
III-IV	65	0	11	39	15	83.08	
Differentiation							>0.05
Well-Moderate	51	0	15	31	5	70.59	
Poorly	54	0	11	27	16	79.63	
Lymph node metastasis							>0.05
Yes	30	0	9	14	7	70.00	
No	67	0	17	39	11	74.63	
Unknown	8	0	0	5	3	100.00	
Pathological subtype							>0.05
Serous	71	0	18	40	13	74.65	
Mucinous	10	0	4	6	0	60.00	
Endometrioid	13	0	3	8	2	76.92	
Clear cell carcinoma	11	0	1	4	6	90.91	

TABLE 3 Cox regression analysis of overall survival of ovarian epithelial malignant tumors.

Variables	Univariate analysis			Multivariate analysis		
	HR	95% CI of HR	P-value	HR	95% CI of HR	P-value
MCP-4 expression (low vs high)	3.740	1.466-9.541	0.006	3.621	1.346-9.742	0.011
Age (<60 vs ≥60 years)	1.605	0.896-2.876	0.112			
FIGO stage (I-II vs III-IV)	7.788	3.250-18.666	0.000	5.589	2.111-14.802	0.001
Differentiation (well-moderate vs poor)	1.148	0.649-2.032	0.635			
Lymph node metastasis (no vs yes)	3.093	1.672-5.721	0.000	1.650	0.844-3.227	0.144

MCP-4 inhibits apoptosis of ovarian cancer cells

Flow cytometry results showed that compared with the control group, the overall apoptosis rate of Caov3 and ES-2 cells was significantly reduced after MCP-4 overexpression ($P < 0.05$) (Figure 5A), and when MCP-4 expression was inhibited, the apoptosis rate was significantly increased ($P < 0.05$)

(Figure 5B). Western blotting showed that the expression of anti-apoptotic protein BCL2 was upregulated, the expression of pro-apoptotic protein BAX was downregulated in the MCP-4 overexpression group, and the ratio of BCL2/BAX was significantly increased ($P < 0.05$) (Figure 5D). The results of MCP-4 inhibited expression group showed contradictory results ($P < 0.05$) (Figure 5E). These results indicate that MCP-4 could inhibit the apoptosis of ovarian cancer cells.

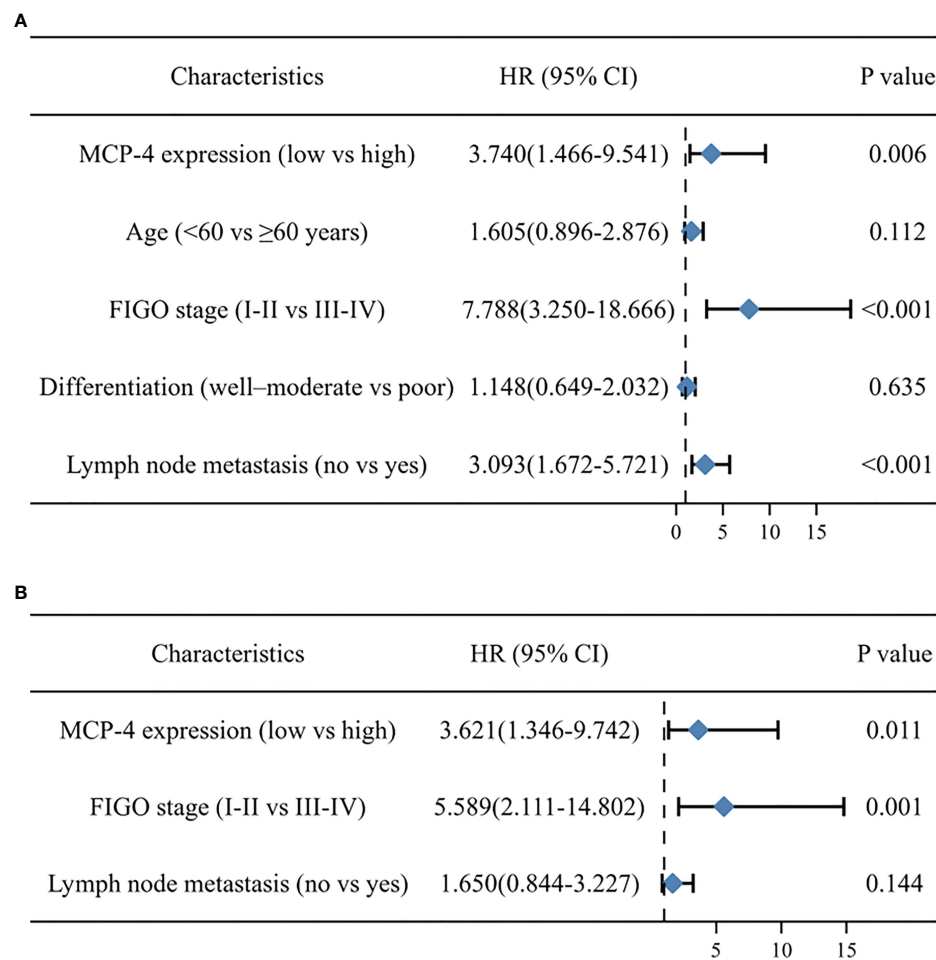


FIGURE 2
Forest map based on univariate (A) and multivariate (B) cox regression analyses.

MCP-4 activates p38 MAPK signaling pathways

The ovarian serous cystadenocarcinoma dataset downloaded from TCGA database was divided into the MCP-4 high-expression group and MCP-4 low-expression group according to the median, followed by GSEA enrichment analysis. These results suggest that MCP-4 is associated with pathways in cancer, cell adhesion molecules, apoptosis, and MAPK signaling pathway, which is consistent with the above experimental results that MCP-4 promotes migration and invasion and inhibits apoptosis in ovarian cancer cell lines (Figure 5C). Western blotting confirmed that MCP-4 activated the p38 MAPK signaling pathway. Overexpression of MCP-4 increased the expression of phosphorylated p38 MAPK (Thr180/Tyr182) ($P < 0.05$) (Figure 5D), whereas inhibition of MCP-4 decreased the expression of phosphorylated p38 MAPK ($P <$

0.05) (Figure 5E). However, the expression level of total p38 MAPK remained unchanged.

MCP-4 promotes metastasis in a nude mouse peritoneal xenograft tumor model

MCP-4 overexpressing and control cells were intraperitoneally injected into nude mice. On the 25th day after intraperitoneal inoculation, nude mice were sacrificed and dissected. In order to objectively evaluate the metastasis ability regulated by MCP-4, all the metastatic nodules were collected, and the results showed that the number of metastatic nodules in the MCP-4-overexpression group were significantly higher than those in the control group (Figures 6A, B). These data indicates that MCP-4 significantly promotes

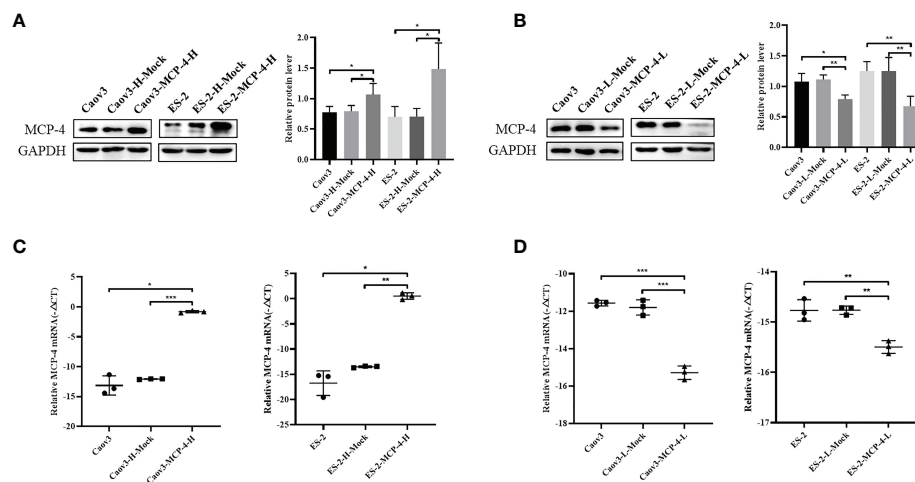


FIGURE 3

The protein and mRNA expression of MCP-4 in the overexpression/inhibition groups. (A, B) Representative images and quantitation of the western blotting showed that the protein expression of MCP-4 in the overexpression/knockdown groups ($n = 3$). GAPDH was used as an internal control. (C, D) The relative MCP-4 mRNA expression in the overexpression/inhibition groups ($n = 3$). Data are presented as mean \pm SD. * $P < 0.05$; ** $P < 0.01$; *** $P < 0.001$.

tumor metastasis, and plays an important role in the malignant process of ovarian cancer.

Discussion

Ovarian cancer is a common gynecological malignancy in women, and its incidence is second only to that of cervical and endometrial cancers. Intraperitoneal spread, extraperitoneal spread, and chemotherapy resistance are the main reasons for the low survival rate of ovarian cancer patients (1). The overall five-year survival rate of patients with advanced epithelial ovarian cancer (EOC) is approximately 30%. However, the overall five-year survival rate for patients diagnosed earlier is greater than 70% (11). Therefore, there is an urgent issue to explore rapid ovarian cancer biomarkers with high sensitivity and specificity.

Chemokines are the largest subfamily of cytokines and can be further subdivided into four major groups based on the position of the first two cysteine residues in their amino acid sequences: CC-chemokines, CXC-chemokines, C-chemokines, and CX3C-chemokines (12). Chemokines play important roles in inflammation, infection, internal environmental homeostasis, and tumor development and progression (13). MCP-4 is a member of the chemokine CC family. It has an α -helix at the carboxyl-terminus, two disulfide bonds near the amino-terminus, and three antiparallel β -sheets in the middle. It has a structure like other CC-chemokines and has high homology with MCP-1, MCP-2, and MCP-3 (14). Studies have found that the expression of MCP-4 is elevated in various diseases, such as

asthma (15), nephritis (16), atherosclerosis (17), atopic dermatitis (18), and rheumatoid arthritis (19). Furthermore, it is involved in the immune response by recruiting inflammatory cells at the inflammation site. Recent studies have revealed that MCP-4 plays an important role in tumorigenesis.

OY et al. (7) reported that the expression of MCP-4 was elevated in colorectal cancer serum and correlated with poor prognosis, which could be used as a biomarker for distant metastasis and recurrence of colorectal cancer. The expression of MCP-4 is significantly higher in *Helicobacter pylori*-positive gastric cancer tissues than in normal gastric tissues (8). To date, no study has reported the expression and mechanism of MCP-4 in ovarian cancer. In this study, we confirmed that MCP-4 expression is elevated in ovarian cancer using IHC. Data from the TCGA and GEO databases further confirmed this result. The expression of MCP-4 was correlated with an advanced FIGO stage. Kaplan–Meier analysis showed that the overall survival of patients with high MCP-4 expression was significantly shorter. Cox analysis showed that MCP-4 was an independent risk factor affecting the prognosis of patients with ovarian cancer. In addition, western blotting confirmed that MCP-4 expression was higher in ovarian cancer cell lines than in normal ovarian epithelial cells. Therefore, MCP-4 may play an important role in ovarian cancer and be a predictor of ovarian cancer prognosis.

In our study, when MCP-4 was overexpressed in Caov3 and ES-2 cell lines, the expression of MMP-2 and MMP-9 were upregulated. EMT-related proteins, such as N-cadherin and vimentin, were increased, while E-cadherin was decreased. The opposite trend was observed when siRNA was used to inhibit the expression of MCP-4. In addition, we found that the apoptosis

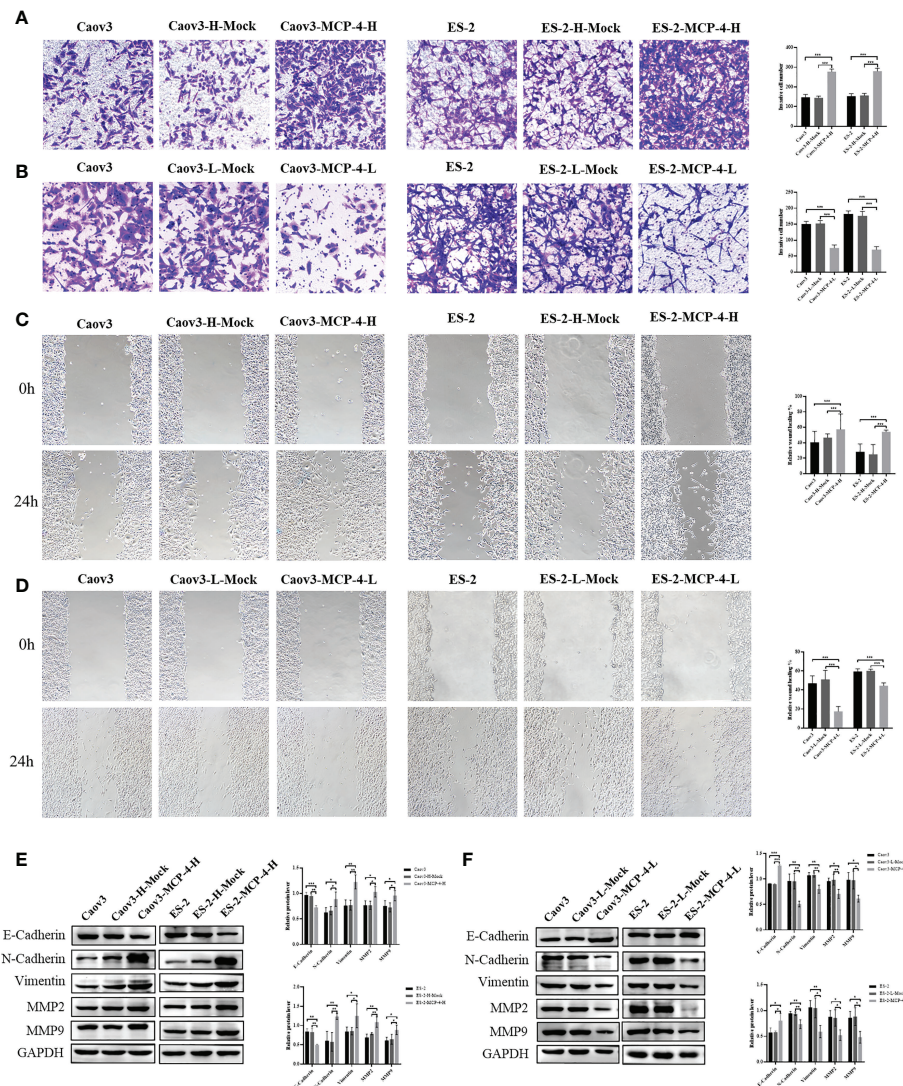


FIGURE 4

MCP-4 promoted invasion, migration, and EMT in ovarian cancer cells. (A) Overexpression of MCP-4 promoted invasion of Caov3 and ES-2 cell lines ($n = 9$; $\times 200$) (B) Inhibition of MCP-4 expression suppressed ovarian cancer cells invasion ($n = 9$; $\times 200$). (C) Overexpression of MCP-4 promoted migration of Caov3 and ES-2 cell lines ($n = 9$; $\times 100$) (D) Inhibition of MCP-4 expression suppressed ovarian cancer cells migration ($n = 9$; $\times 100$). (E, F) Representative images and quantitation of the western blotting showed that the protein expression of E-cadherin, N-cadherin, vimentin, MMP2, and MMP9 in the MCP-4 overexpression/inhibition groups ($n = 3$). GAPDH was used as an internal control. Data are presented as mean \pm SD. * $P < 0.05$; ** $P < 0.01$; *** $P < 0.001$.

rate of ovarian cancer cells decreased when MCP-4 was overexpressed and increased when MCP-4 was inhibited. These results suggest that MCP-4 promotes malignant behavior in ovarian cancer cells. FB et al. (20) analyzed key immune-related proteins in fine-needle aspiration (FNA) biopsy samples from patients with breast cancer ($n = 25$) and benign lesions ($n = 32$). They found that MCP-4 was differentially expressed in breast cancer and benign lesions, and that there was a clear correlation with Ki67 expression. Thus, MCP-4 may promote the progression of breast cancer. AA et al. (21) analyzed the cytokine expression profiles of metastasis-derived colorectal

cancer cell lines and cell lines derived from primary colorectal cancer and found that the expression level of MCP-4 was higher in metastatic colorectal cancer cell lines, suggesting that MCP-4 may be associated with colorectal cancer metastasis. OY et al. (7) examined the serum concentration of MCP-4 in colorectal cancer patients and showed that high concentrations of MCP-4 were significantly associated with old age, advanced T-stage, distant metastasis, and UICC stage. MCP-4 is an independent prognostic factor affecting disease-free survival and overall survival in colorectal cancer. These studies suggest that MCP-4 plays an important role in the development of various malignant

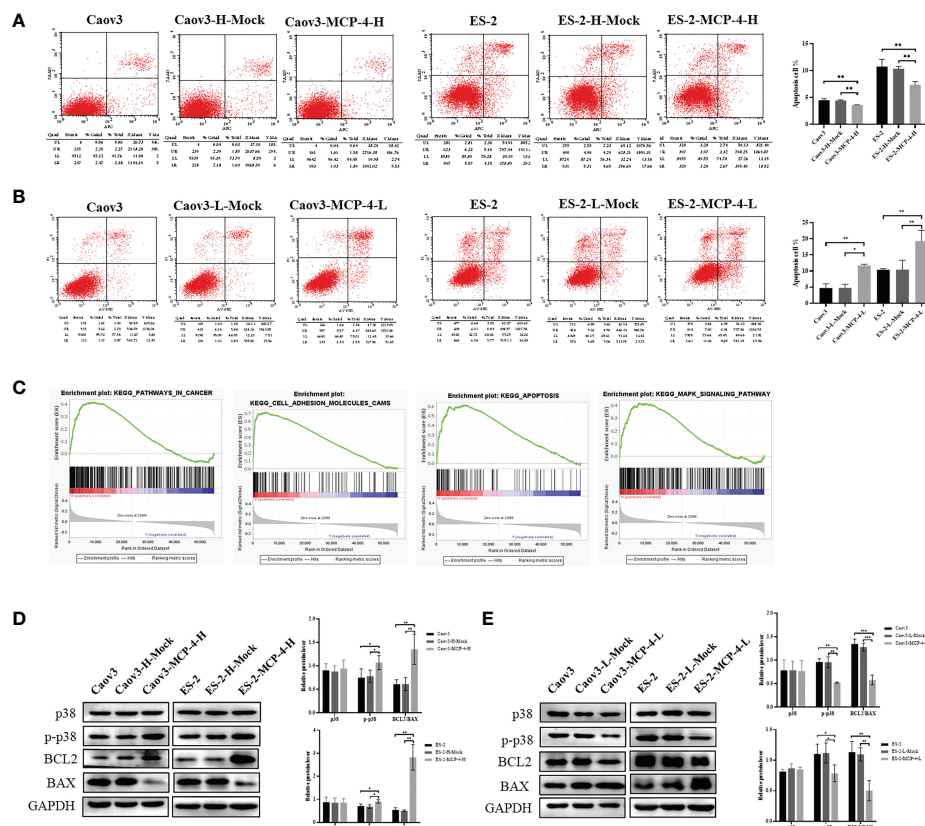


FIGURE 5

MCP-4 decreased cell apoptosis and activated the p38 MAPK signaling pathway. (A) Overexpression of MCP-4 decreased cell apoptosis of Caov3 and ES-2 cell lines (B) Inhibition of MCP-4 expression increased ovarian cancer cells apoptosis. (C) GSEA analysis of MCP-4 related enrichment gene sets. KEGG_PATHWAYS_IN_CANCER (NES = 1.64, P-value = 0.024, FDR = 0.059); KEGG_APOPTOSIS (NES = 2.20, P-value = 0.000, FDR = 0.000); KEGG_CELL_ADHESION_MOLECULES_CAMS (NES = 2.39, P-value = 0.000, FDR = 0.000); KEGG_MAPK_SIGNALING_PATHWAY (NES = 1.69, P-value = 0.012, FDR = 0.046) (D, E) Representative images and quantitation of the western blotting showed that the protein expression of p38 MAPK, p-p38 MAPK, BCL2, and BAX in the MCP-4 overexpression/inhibition groups (n = 3). GAPDH was used as an internal control. Data are presented as mean \pm SD. * P < 0.05; ** P < 0.01; *** P < 0.001.

tumors. Therefore, it is of great significance to investigate the expression and mechanism of MCP-4 in ovarian cancer.

To further explore the mechanisms by which MCP-4 affects the malignant biological behavior of ovarian cancer cells, we performed gene set enrichment analysis using GSEA software and found that MCP-4 is associated with cell adhesion molecules, apoptosis, cancer pathways, and MAPK signaling pathways. Traditional MAPKs include four major categories: ERK1/2, JNK, p38 MAPK, and ERK5 (22). They can be activated by a variety of growth factors or cytokines, thereby regulating a variety of cellular activities, including cell proliferation, differentiation, apoptosis, invasion, and hematopoiesis (23–25). Studies have confirmed that the p38 MAPK signaling pathway is often overactivated in malignant tumors and plays an important role in the malignant progression of ovarian cancer (26–28). ZJ et al. (29) found that galectin-1 enhanced ovarian cancer cell metastasis and EMT by promoting activation of the p38 MAPK/JNK signaling pathway. The combination of p38 MAPK

inhibitors inhibits the growth and metastasis of olaparib-resistant ovarian cancer cells (30). p38 MAPK inhibitors combined with gemcitabine carboplatin improve progression-free survival (PFS) in patients with recurrent platinum-sensitive ovarian cancer (31). MCP-4 is a member of the CC-chemokine family and shares 67% sequence homology with MCP-1 (32). LJ et al. (33) showed that MCP-1 can upregulate the expression of p-MEK, p-ERK, p-p38 MAPK, and p-JNK and promote the invasion and migration of osteosarcoma cells by activating the c-Raf/MAPK/AP-1 signaling pathway. Previous studies have also confirmed that MCP-1 is associated with p38 MAPK phosphorylation in breast cancer cells (34). In ovarian cancer, MCP-1 secreted by tumor-associated mesothelial cells activates the p38 MAPK signaling pathway and promotes migration and invasion of ovarian cancer cells (35). These studies suggest that MCP-1 plays an important role in the tumor microenvironment of ovarian cancer, and may be related to the activation of the p38 MAPK signaling pathway. The mechanism of action of MCP-1

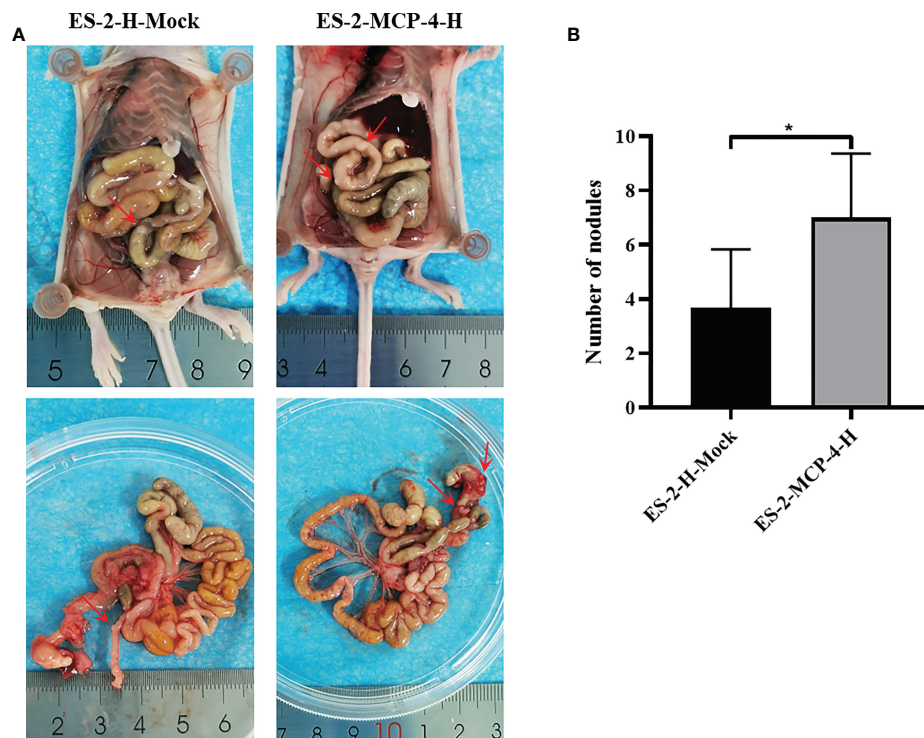


FIGURE 6
MCP-4 promotes metastasis in a nude mouse peritoneal xenograft tumor model. **(A)** After being sacrificed, dissemination of tumor in nude mice was assessed, and the metastasis nodules were marked by red arrows. **(B)** Average number of the peritoneal tumor nodules of each group were quantified ($n = 6$). Data are presented as mean \pm SD. * $P < 0.05$.

in malignancy has been extensively investigated, but it is still unclear how MCP-4 mediates malignant progression of ovarian cancer. Therefore, we examined the changes in the p38 MAPK signaling pathway in ovarian cancer cell lines with MCP-4 overexpression or inhibition. The results showed that overexpression of MCP-4 increased the expression of phosphorylated p38 MAPK, whereas total p38 MAPK expression did not change. The inhibition of MCP-4 expression in ovarian cancer cells showed the opposite trend. We have previously shown that MCP-4 promotes invasion, migration and EMT in ovarian cancer cells. In conclusion, MCP-4 may contribute to the malignant biology of ovarian cancer by activating the p38 MAPK signaling pathway.

In malignant tumors, tumor cells are considered one of the main sources of chemokines, and cells in the tumor stroma produce chemokines in response to stimulation (36). Under the action of specific chemokines, different types of immune cells migrate into the tumor microenvironment and regulate tumor immunity. In addition, chemokines can target non-immune cells in the tumor microenvironment, such as tumor cells and vascular endothelial cells, to influence tumor cell proliferation, invasion, migration, angiogenesis, and other malignant biological behaviors (37). Chemokines also promote

communication among tumor cells, immune cells, mesenchymal cells, and endothelial cells, which play an important role in the development and metastasis of malignant tumors (38, 39). Our study confirmed that MCP-4 is upregulated in ovarian cancer and can promote cell invasion, migration and tumor metastasis. However, whether stromal cells, such as cancer-associated fibroblasts and cancer-associated mesothelial cells, can also express MCP-4 in ovarian cancer and its effects in the progression of ovarian cancer needs to be further investigated.

Conclusion

In conclusion, we demonstrated for the first time that MCP-4 is overexpressed in ovarian cancer and is associated with poor prognosis. MCP-4 promotes ovarian cancer cell invasion, migration, and EMT and inhibits apoptosis. These malignant biological behaviors mediated by MCP-4 are related to the activation of the p38MAPK signaling pathway. Comprehensively elucidating the function of MCP-4 and its mechanism of action in ovarian cancer is important for identifying molecular markers for early diagnosis, targeted therapy, and prognosis evaluation.

Data availability statement

The original contributions presented in the study are included in the article/supplementary material. Further inquiries can be directed to the corresponding authors.

Ethics statement

The studies involving human participants were reviewed and approved by Ethics Committee of Shengjing Hospital Affiliated to China Medical University. The patients/participants provided their written informed consent to participate in this study. The animal study was reviewed and approved by Ethics Committee of Shengjing Hospital Affiliated to China Medical University.

Author contributions

SL, YH, XL, and BL conceived and designed the experiments. SL performed the experiments. OL and XL performed data mining and analysis. SL and XL contributed to writing the manuscript. XL helped modify the manuscript. All authors contributed to the article and approved the submitted version.

References

1. Torre LA, Trabert B, DeSantis CE, Miller KD, Samimi G, Runowicz CD, et al. Ovarian cancer statistics, 2018. *CA Cancer J Clin* (2018) 68(4):284–96. doi: 10.3322/caac.21456
2. Wang Z, Meng F, Zhong Z. Emerging targeted drug delivery strategies toward ovarian cancer. *Adv Drug Delivery Rev* (2021) 178:113969. doi: 10.1016/j.addr.2021.113969
3. Kuroki L, Guntupalli SR. Treatment of epithelial ovarian cancer. *BMJ* (2020) 371:m3773. doi: 10.1136/bmj.m3773
4. Korbecki J, Kojder K, Simińska D, Bohatyrewicz R, Gutowska I, Chlubek D, et al. CC chemokines in a tumor: A review of pro-cancer and anti-cancer properties of the ligands of receptors CCR1, CCR2, CCR3, and CCR4. *Int J Mol Sci* (2020) 21(21):8412. doi: 10.3390/ijms21218412
5. Griffith JW, Sokol CL, Luster AD. Chemokines and chemokine receptors: positioning cells for host defense and immunity. *Annu Rev Immunol* (2014) 32:659–702. doi: 10.1146/annurev-immunol-032713-120145
6. Mendez-Enriquez E, Garcia-Zepeda EA. The multiple faces of CCL13 in immunity and inflammation. *Inflammopharmacology* (2013) 21(6):397–406. doi: 10.1007/s10787-013-0177-5
7. Okugawa Y, Toiyama Y, Mohri Y, Tanaka K, Kawamura M, Hiro J, et al. Elevated serum concentration of monocyte chemoattractant protein 4 (MCP-4) as a novel non-invasive prognostic and predictive biomarker for detection of metastasis in colorectal cancer. *J Surg Oncol* (2016) 114(4):483–9. doi: 10.1002/jso.24335
8. Ellmark P, Ingvarsson J, Carlsson A, Lundin BS, Wingren C, Borrebaeck CA. Identification of protein expression signatures associated with helicobacter pylori infection and gastric adenocarcinoma using recombinant antibody microarrays. *Mol Cell Proteomics* (2006) 5(9):1638–46. doi: 10.1074/mcp.M600170-MCP200
9. Huang C, Clayton EA, Matyunina LV, McDonald LD, Benigno BB, Vannberg F, et al. Machine learning predicts individual cancer patient responses to therapeutic drugs with high accuracy. *Sci Rep* (2018) 8(1):16444. doi: 10.1038/s41598-018-34753-5
10. Mok SC, Bonome T, Vathipadiekal V, Bell A, Johnson ME, Wong KK, et al. A gene signature predictive for outcome in advanced ovarian cancer identifies a survival factor: microfibril-associated glycoprotein 2. *Cancer Cell* (2009) 16(6):521–32. doi: 10.1016/j.ccr.2009.10.018
11. Dochez V, Caillon H, Vaucel E, Dimet J, Winer N, Ducarme G. Biomarkers and algorithms for diagnosis of ovarian cancer: CA125, HE4, RMI and ROMA, a review. *J Ovarian Res* (2019) 12(1):28. doi: 10.1186/s13048-019-0503-7
12. Hughes CE, Nibbs RJB. A guide to chemokines and their receptors. *FEBS J* (2018) 285(16):2944–71. doi: 10.1111/febs.14466
13. Ozga AJ, Chow MT, Luster AD. Chemokines and the immune response to cancer. *Immunity* (2021) 54(5):859–74. doi: 10.1016/j.immuni.2021.01.012
14. Barinka C, Prahl A, Lubkowski J. Structure of human monocyte chemoattractant protein 4 (MCP-4/CCL13). *Acta Crystallogr D Biol Crystallogr* (2008) 64(Pt 3):273–8. doi: 10.1107/S0907444907066164
15. Ghebre MA, Pang PH, Diver S, Desai D, Bafadhel M, Haldar K, et al. Biological exacerbation clusters demonstrate asthma and chronic obstructive pulmonary disease overlap with distinct mediator and microbiome profiles. *J Allergy Clin Immunol* (2018) 141(6):2027–36. doi: 10.1016/j.jaci.2018.04.013
16. Komatsuda A, Wakui H, Iwamoto K, Harada M, Okumoto Y, Sawada K. Gene expression profiling of peripheral blood mononuclear cells from patients with minimal change nephrotic syndrome by cDNA microarrays. *Am J Nephrol* (2008) 28(4):539–47. doi: 10.1159/000114098
17. Gentili A, Zaibi MS, Alomar SY, De Vuono S, Ricci MA, Alaeddin A, et al. Circulating levels of the adipokines monocyte chemoattractant protein-4 (MCP-4), macrophage inflammatory protein-1 β (MIP-1 β), and eotaxin-3 in severe obesity and following bariatric surgery. *Horm Metab Res* (2016) 48(12):847–53. doi: 10.1055/s-0042-108731
18. Lang CCV L, Renert-Yuval Y, Del Duca E, Pavel AB, Wu J, Zhang N, et al. Immune and barrier characterization of atopic dermatitis skin phenotype in Tanzanian patients. *Ann Allergy Asthma Immunol* (2021) 127(3):334–41. doi: 10.1016/j.anai.2021.04.023

Funding

This work was supported by National Natural Science Foundation of China (No. 82173130), Key R&D Guidance Plan Project in Liaoning Province (2019JH8/10300022), and Beijing Kanghua Foundation for the Development of Traditional Chinese and Western Medicine Gynecological Oncology Special Research Fund (KH-2021-LLZX-010).

Conflict of interest

The authors declare that the research was conducted in the absence of any commercial or financial relationships that could be construed as a potential conflict of interest.

Publisher's note

All claims expressed in this article are solely those of the authors and do not necessarily represent those of their affiliated organizations, or those of the publisher, the editors and the reviewers. Any product that may be evaluated in this article, or claim that may be made by its manufacturer, is not guaranteed or endorsed by the publisher.

19. Lee EJ, Lilja S, Li X, Schäfer S, Zhang H, Benson M. Bulk and single cell transcriptomic data indicate that a dichotomy between inflammatory pathways in peripheral blood and arthritic joints complicates biomarker discovery. *Cytokine* (2020) 127:154960. doi: 10.1016/j.cyt.2019.154960
20. Franzén B, Alexeyenko A, Kamali-Moghaddam M, Hatschek T, Kanter L, Ramqvist T, et al. Protein profiling of fine-needle aspirates reveals subtype-associated immune signatures and involvement of chemokines in breast cancer. *Mol Oncol* (2019) 13(2):376–91. doi: 10.1002/1878-0261.12410
21. Abajo A, Bitarte N, Zarate R, Boni V, Lopez I, Gonzalez-Huarriz M, et al. Identification of colorectal cancer metastasis markers by an angiogenesis-related cytokine-antibody array. *World J Gastroenterol* (2012) 18(7):637–45. doi: 10.3748/wjg.v18.i7.637
22. You Z, Liu SP, Du J, Wu YH, Zhang SZ. Advancements in MAPK signaling pathways and MAPK-targeted therapies for ameloblastoma: A review. *J Oral Pathol Med* (2019) 48(3):201–5. doi: 10.1111/jop.12807
23. Pua LJW, Mai CW, Chung FF, Khoo AS, Leong CO, Lim WM, et al. Functional roles of JNK and p38 MAPK signaling in nasopharyngeal carcinoma. *Int J Mol Sci* (2022) 23(3):1108. doi: 10.3390/ijms23031108
24. Zhang D, Guo H, Feng W, Qiu H. LAMC2 regulated by microRNA-125a-5p accelerates the progression of ovarian cancer via activating p38 MAPK signalling. *Life Sci* (2019) 232:116648. doi: 10.1016/j.lfs.2019.116648
25. Peluso I, Yarla NS, Ambra R, Pastore G, Perry G. MAPK signalling pathway in cancers: Olive products as cancer preventive and therapeutic agents. *Semin Cancer Biol* (2019) 56:185–95. doi: 10.1016/j.semcancer.2017.09.002
26. Yu Y, Li H, Xue B, Jiang X, Huang K, Ge J, et al. SDF-1/CXCR7 axis enhances ovarian cancer cell invasion by MMP-9 expression through p38 MAPK pathway. *DNA Cell Biol* (2014) 33(8):543–9. doi: 10.1089/dna.2013.2289
27. Siu MKY, Jiang YX, Wang JJ, Leung THY, Ngu SF, Cheung ANY, et al. PDK1 promotes ovarian cancer metastasis by modulating tumor-mesothelial adhesion, invasion, and angiogenesis via $\alpha 5\beta 1$ integrin and JNK/IL-8 signaling. *Oncogenesis* (2020) 9(2):24. doi: 10.1038/s41389-020-0209-0
28. Kang K, Wang Y. Sevoflurane inhibits proliferation and invasion of human ovarian cancer cells by regulating JNK and p38 MAPK signaling pathway. *Drug Des Devel Ther* (2019) 13:4451–60. doi: 10.2147/DDDT.S223581
29. Zhu J, Zheng Y, Zhang H, Liu Y, Sun H, Zhang P. Galectin-1 induces metastasis and epithelial-mesenchymal transition (EMT) in human ovarian cancer cells via activation of the MAPK JNK/p38 signalling pathway. *Am J Transl Res* (2019) 11(6):3862–78.
30. Chen X, Chen Y, Lin X, Su S, Hou X, Zhang Q, et al. The drug combination of SB202190 and SP600125 significantly inhibit the growth and metastasis of olaparib-resistant ovarian cancer cell. *Curr Pharm Biotechnol* (2018) 19(6):506–13. doi: 10.2174/1389201019666180713102656
31. Vergote I, Heitz F, Buderath P, Powell M, Sehouli J, Lee CM, et al. A randomized, double-blind, placebo-controlled phase 1b/2 study of ralimetinib, a p38 MAPK inhibitor, plus gemcitabine and carboplatin versus gemcitabine and carboplatin for women with recurrent platinum-sensitive ovarian cancer. *Gynecol Oncol* (2020) 156(1):23–31. doi: 10.1016/j.ygyno.2019.11.006
32. Dalgard C, Eidelman O, Jozwik C, Olsen CH, Srivastava M, Biswas R, et al. The MCP-4/MCP-1 ratio in plasma is a candidate circadian biomarker for chronic post-traumatic stress disorder. *Transl Psychiatry* (2017) 7(2):e1025. doi: 10.1038/tp.2016.285
33. Liu JF, Chen PC, Chang TM, Hou CH. Monocyte chemoattractant protein-1 promotes cancer cell migration via c-Raf/MAPK/AP-1 pathway and MMP-9 production in osteosarcoma. *J Exp Clin Cancer Res* (2020) 39(1):254. doi: 10.1186/s13046-020-01756-y
34. Wang LP, Cao J, Zhang J, Wang BY, Hu XC, Shao ZM, et al. The human chemokine receptor CCRL2 suppresses chemotaxis and invasion by blocking CCL2-induced phosphorylation of p38 MAPK in human breast cancer cells. *Med Oncol* (2015) 32(11):254. doi: 10.1007/s12032-015-0696-6
35. Yasui H, Kajiyama H, Tamauchi S, Suzuki S, Peng Y, Yoshikawa N, et al. CCL2 secreted from cancer-associated mesothelial cells promotes peritoneal metastasis of ovarian cancer cells through the P38-MAPK pathway. *Clin Exp Metastasis* (2020) 37(1):145–58. doi: 10.1007/s10585-019-09993-y
36. Yoshimura T. The chemokine MCP-1 (CCL2) in the host interaction with cancer: a foe or ally? *Cell Mol Immunol* (2018) 15(4):335–45. doi: 10.1038/cmi.2017.135
37. Nagarsheth N, Wicha MS, Zou W. Chemokines in the cancer microenvironment and their relevance in cancer immunotherapy. *Nat Rev Immunol* (2017) 17(9):559–72. doi: 10.1038/nri.2017.49
38. Singh AJ, Gray JW. Chemokine signaling in cancer-stroma communications. *J Cell Commun Signal* (2021) 15(3):361–81. doi: 10.1007/s12079-021-00621-7
39. Hussain S, Peng B, Cherian M, Song JW, Ahirwar DK, Ganju RK. The roles of stroma-derived chemokine in different stages of cancer metastases. *Front Immunol* (2020) 11:598532. doi: 10.3389/fimmu.2020.598532

Frontiers in Oncology

Advances knowledge of carcinogenesis and tumor progression for better treatment and management

The third most-cited oncology journal, which highlights research in carcinogenesis and tumor progression, bridging the gap between basic research and applications to improve diagnosis, therapeutics and management strategies.

Discover the latest Research Topics

See more →

Frontiers

Avenue du Tribunal-Fédéral 34
1005 Lausanne, Switzerland
frontiersin.org

Contact us

+41 (0)21 510 17 00
frontiersin.org/about/contact

